COMPARISON OF CANCER RISK ESTIMATES FROM INTERNALIZED UPTAKES OF ENVIRONMENTAL RADIONUCLIDES BASED ON A CHRONIC EXPOSURE

A Thesis

By

AUTUMN ELIZABETH KALINOWSKI

Submitted to the Graduate and Professional School of
Texas A&M University
in partial fulfillment of the requirements for the degree of

MASTER OF SCIENCE

Chair of Committee,	Shaheen A. Dewji
Committee Members,	John Ford
	Susan Bloomfield
	Pavel Tsvetkov
Head of Department,	Michael Nastasi

August 2021

Major Subject: Nuclear Engineering

ABSTRACT

The ICRP quantity effective dose, *E*, is used as an "approximate indicator of possible risk" for uniform exposures.[1] Application of a scaling factor allows *E* to be directly compared to Federal Guidance Report (FGR) risks. With sex- and age-averaged tissue-weights informing *E*, potential exists for non-negligible under- or overestimations of risk, especially for a chronic exposure. Comparison of the FGR risk and ICRP calculated committed effective doses (CED) coefficient generated by the Dose and Risk Calculation (DCAL) software reveals a typical underestimation of the risk via CED for acute exposures. For chronic exposure comparisons, a substantial difference was seen. This comparison was repeated for updated ICRP *Publication 103* data and revealed a similar issue when estimating risk via CED, indicating a need for increased age-specificity in calculating *E* to increase approximation accuracy and better inform radiation protection guidance based upon calculations of *E* for chronic exposures.

DEDICATION

I would like to dedicate this work to my family, without whom I would never have been able to complete this work. Thank you for you continued support and assistance in the pursuance of my dream. Your guidance and teachings have prepared me for the long road ahead. I love you more than words can describe.

ACKNOWLEDGEMENTS

Firstly, I would like to extend my gratitude to Dr. Pavel Tsvetkov. Upon entering graduate school, my plan moving forward was fuzzy at best. His direction led me to my committee chair, Dr. Dewji, who has helped me to experience and accomplish more in the past three years than I could have ever hoped. It is with her guidance that I have been able to forge a path for myself, opening doors that I did not even know existed. I would also like to thank my committee member, Dr. John Ford, for introducing me to the world of the biological effects of radiation, opening more opportunities to me than I could have ever imagined when I first joined Texas A&M.

Through this project, I have had the pleasure of meeting Dr. David Pawel of EPA, who has been a guiding force over the course of this project. Your expertise and kindness are beyond measure, and I am forever grateful. I would also like to thank Dr. Keith Eckerman, for his insight into my work on this project, and guidance for when things seem to refuse to work properly. As well, I extend my gratitude to Dr. Michael Bellamy for helping to get my programs off the ground, and to Dr. Derek Jokisch for his assistance in data acquisition used to inform the latter half of this work.

And finally, my family, whose constant support has seen me through the darkest of times. Dad, I could not have done this without your technical expertise. You have taught me so much. Mom, your unwavering support and confidence continuously kept me going when all I wanted to do was stop. And my brothers, who even through all our challenges, have stayed by my side. I love you all.

CONTRIBUTORS AND FUNDING SOURCES

Contributors

This work was supported by a Texas A&M thesis committee comprised of Dr. Shaheen A. Dewji, Dr. John Ford, and Dr. Pavel Tsvetkov of the Nuclear Engineering Department as well as Dr. Susan Bloomfield of the Health and Kinesiology Department.

Funding Sources

No external funding was received for the completion of this research and thesis.

TABLE OF CONTENTS

Page

LIST OF FIGURES

Page

LIST OF TABLES

Page

1. INTRODUCTION

As the use of radioactive materials has become more prevalent in nuclear energy, medicine, and security applications, evaluating the health effects associated with exposures to radioactive material have continued to be of increasing interest. An ongoing objective associated with evaluation of the effects of radiation has been to develop refined models and improving the evaluated associated cancer risks corresponding to exposures, with one application of informing regulatory recommendations. Guidance for radiation protection recommendations in the U.S. has stemmed from the Environmental Protection Agency's (EPA) Federal Guidance Report (FGR) series to reflect scientific consensus on appropriate models and underlying data for dose and risk coefficients for both internal and external exposure to members of the public, as well as occupational and medical exposures.[2]

Current guidance in FGR 13 (1999)[2] outlines cancer risk models, usage patterns, and metabolic models for over 800 radionuclides. However, FGR 13 was published over 20 years ago, and newer models and recommendations published by bodies, such as the International Commission on Radiological Protection (ICRP), must be harnessed to update the cancer risk coefficients and the corresponding regulatory values and protection metrics such as effective dose.[2] To improve upon limitations with models reflected in FGR 13, an updated approach considering age- and sex-specific biokinetic and dosimetric models must be evaluated to provide a paradigm to evaluate cancer risk. This approach can be expanded to consider limits on the concentration of radionuclides in the environment due to a lifetime exposure. Current models developed in the Biological Effects of Ionizing Radiation VII (BEIR VII) report provide a model of cancer risk calculation in which risk is a function on age-specific variables.[3] A paper written by Brenner pushes for an age-specific replacement for effective dose as a term coined "effective

risk" for use specifically in a medical setting. This quantity is essentially the same as effective dose, calculated in the same manner, save that the ICRP tissue-weights are replaced by the age-specific factors developed in the BEIR VII reports. The purpose of this is to yield a term that is more representative of the impact of the age of exposure on the calculation of effective dose, and the subsequent comparison to risk, and is therefore potentially less prone to misuse in both a public and medical setting.[3] Such a manner of calculation has the potential to be extrapolated to committed dose calculations and acute exposure effective dose calculations to reflect the effect of age on the calculation of these values; something that is not currently considered in effective dose calculations.

More specifically, the models describe how the risk per unit dose is modified by age.[4] This analysis of risk can then be compared to radiation protection metrics, here known as committed effective dose (CED), to determine the limits of its utility as a radiation protection metric. In the proposed work, the age-specific patterns of the absorbed dose rates were characterized, along with the corresponding risk per unit dose with respect to the radionuclide. From these characterizations, the potential ramifications, such as an over- or under-estimation of the true risk due to a chronic exposure to the members of the public through the use of sex-nonspecific quantities such as CED, can be analyzed and quantified. The impact of the proposed work is to better inform radiation protection guidance for environmental exposures to radiation to members of the public by bringing to light the potential ineffectiveness of the approximate comparison between CED and the true risk. Such ineffectiveness is due in part to the lack of age-specificity intrinsic to effective dose, particularly for chronic exposures.

Federal radiological protection guidance utilizes the value of effective dose, *E*, as a concise term to ensure that federal limits implemented are sufficiently protective in regards to radiation

exposure to members of the public. It is used as a singular, concise value to approximately represent the possible risk to an individual due to an exposure. In terms of chronic exposures, current models of effective dose do not reflect the age-specificity of tissue absorbed dose. That is, while radiation-induced cancer risk models reflect the age dependency of the risk per unit dose based on absorbed tissue doses, effective dose instead employs age-independent and sex-averaged tissue and radiation-weighting factors in combination with organ absorbed doses to compute a protective quantity for radiation protection that is determined to be adequately protective of all sexes and ages. In the case of a chronic exposure, there is potential for CED based on the calculated effective doses to over- or underestimate the true lifetime risk, defined as the FGR developed lifetime risk, to the public from an environmental exposure due to the lack of age-specificity inherent in the calculation of effective dose.

The backbone of risk calculation and effective dose calculation is use of the quantity absorbed dose, *D*. Understanding the radionuclide-specific patterns of absorbed dose due to a lifetime environmental internal exposure provides a deeper insight into radiogenic cancer risk to the individual. The calculation of these absorbed dose rates to inform these calculations has changed with iterations of ICRP reference models depicting improving biokinetic designs that more accurately represent the behavior or radionuclides in the body after ingestion or inhalation. The most current biokinetic models and dosimetric data differ from the biokinetic models utilized to calculate the reported values in FGR 13, and a detailed analysis of the variations in dose rate patterns from both generations of data investigated within this report will emphasize the importance of both biokinetic and dosimetric models, as well as modifying functions used to calculate risk between data generations. The behavior of absorbed dose rates for both acute and chronic exposures varies with both radionuclide and age at exposure, and a characterization of this

variation will inform the efficacy of using effective dose as a gauge of true risk to the individual. Taking all this into account, an investigation will be conducted herein for both dataset generations to emphasize the potential areas of concern for the CED comparison to the FGR 13 calculated risk for both acute and chronic exposures.

2. BACKGROUND AND LITERATURE REVIEW

2.1. Fundamental Dose Quantities

The fundamental protection quantity for prospective radiation regulatory guidance and retrospective dose assessment for demonstrating compliance with regulation is effective dose *E*, as defined by the ICRP in its updated recommendations in 2007.[5] The definition of a protection quantity, as defined by ICRP *Publication 103*, is one such that can be used to quantify the extent of exposure of the human body to ionizing radiation from both whole- and partial-body external irradiations and intakes of radionuclides.[4] These protection quantities are not directly measurable, and instead rely on computation of fundamental physical quantities to determine absorbed dose, D_T.

Effective dose, in units of sieverts (Sv), is defined as the tissue-weighted sum of equivalent doses in all specified organs and tissues of the body, as defined by Equation 1:

$$E = \sum_T w_T H_T \qquad \text{EQ. 1}$$

where H_T is the equivalent dose in an organ or tissue *T*; w_T is the tissue-weighting factor, a mean age- and sex-averaged value defined by ICRP to determine the sensitivity of a tissue to radiation which considers factors including morbidity, mortality, possible loss of quality of life, and years of life lost. In essence, it is a weight of the total health detriment. Tissue weights are based on the respective values of relative radiation detriment and represent individual organ and tissue contribution to radiation detriment from stochastic effects.[6] The summation of all tissue weights is equal to 1, allowing for a uniform whole-body dose distribution to yield an effective dose numerically equal to the sum of the weighted equivalent doses in each organ and tissue of the body.[5, 6]

Table 1. ICRP defined tissue-weighting factors for *Publication 26*, *Publication 60*, and *Publication 103*.[6]

Tissue	Tissue-weighting factor, w_T		
	1977 *Publication 26*	1991 *Publication 60*[c]	2007 *Publication 103*
Bone Surfaces	0.03	0.01	0.01
Bladder		0.05	0.04
Breast	0.15	0.05	0.12
Colon		0.12	0.12
Gonads	0.25	0.20	0.08[d]
Liver		0.05	0.04
Lungs	0.12	0.12	0.12
Oesophagus		0.05	0.04
Red Bone Marrow	0.12	0.12	0.12
Skin		0.01	0.01
Stomach		0.12	0.12
Thyroid	0.03	0.05	0.04
Remainder	0.30[a]	0.05	0.12[b]
Brain			0.01
Salivary Glands			0.01

[a]Remainder is comprised of the 5 most highly irradiated other organs and tissues, each with a w_T=0.06.
[b]14 specified tissues, including adrenals, extrathoracic tissue, gall bladder, heart, kidneys, lymphatic nodes, muscle, oral mucosa, pancreas, prostate, small intestine, spleen, thymus, uterus/cervix
[c]Developed from a reference population of equal numbers of both sexes and wide range of ages. Apply to either sex, workers, and the whole population
[d]Is applied to the mean of the doses to the testes and the ovaries

Where tissue-weighting factors represent relative radiation detriment based on radiosensitivity of organs and tissues, effective dose is proportional to the radiobiological detriment.[3] Effective dose is therefore a value used as an approximation of possible risk. It is also used for setting and controlling regulatory dose limits by combining doses from both internal emitters and external radiation fields into a single quantity. It can be used to manage the stochastic risk, the risk of developing a stochastic effect as a function of radiation exposure, to a reference population; however, it is not intended to represent the stochastic health risk to an individual due to exposures.[1] Rather, it is used in prospectively to establish regulation and in retrospective analysis to demonstrate compliance with established protections.[5, 6] Effective dose uses sex-

averaged quantities of absorbed dose, derived from dosimetric models of ICRP-defined Reference Persons.[6, 7]

For the protection quantity equivalent dose, H_T, the dose in a tissue or organ constitutes an element of the effective dose and is defined as:

$$\boldsymbol{H_T = \sum_R w_R D_{T,R}} \quad \text{EQ. 2}$$

where $D_{T,R}$ is the mean absorbed dose (Gy) to the tissue T from radiation type R, and w_R is the radiation-weighting factor, a dimensionless age- and sex-independent quantity which is used to modify tissue absorbed doses in order to reflect the relative biological effectiveness (RBE) of high-LET radiations in comparison to photon radiation.[5, 6] This factor allows for an appropriate comparison of equivalent low-LET dose with the same level of biological effectiveness as a corresponding high-LET dose.[4]

Table 2. ICRP *Publication 60* defined radiation-weighting factors. [6]

Radiation type	Radiation weighting factor, w_R
Photons	1
Electrons and muons	1
Protons and charged pions	2
Alpha particles, fission fragments, heavy ions	20
Neutrons	A continuous function of neutron energy

Dosimetric and biokinetic models are combined with radionuclide-specific decay data, such as data from ICRP *Publication 38* and its update *Publication 107*, to create internal dose coefficients.[8, 9] Internal dose coefficients are computed for six reference ages for both the ICRP *Publication 60* and *Publication 103* methodologies: 100 days, 1, 5, 10, and 15 years, and adult (age of maturity), which is age 20 for all radionuclides that do not seek out bones, and age 25 years

for radionuclides that seek bones, such as ^{90}Sr.[10] For current guidance, while geriatric models are able to be leveraged for geriatric specific studies, it is common practice to assume a constant age-averaged population from age of maturity to death, in which the geriatrics are a part of that averaging. At each of these ages, an age-specific regional integrated activity is calculated by:

$$\widetilde{\boldsymbol{A}}(\boldsymbol{r_s}, \boldsymbol{\tau}) = \int_{\boldsymbol{t_0}}^{\boldsymbol{t_0+\tau}} \boldsymbol{A_s}(\boldsymbol{t})\boldsymbol{dt} \qquad \text{EQ. 3}$$

where t_0 is the time of intake, τ is the commitment period, $A_s(t)$ is the activity in Bq as a function of time in the source region, and $\tilde{A}(r_s, \tau)$ is the total number of transformations occurring in the source region over the commitment period.[7] From this, the internal dose coefficient, reported in units of Sv·Bq^{-1}, can be calculated by the use of a further age-specific calculation:

$$\widetilde{\boldsymbol{a}}(\boldsymbol{r_s}, \boldsymbol{\tau}) = \frac{\widetilde{\boldsymbol{A}}(\boldsymbol{r_s}, \boldsymbol{\tau})}{\boldsymbol{A_{intake}}} = \int_{\boldsymbol{t_0}}^{\boldsymbol{t_0+\tau}} \boldsymbol{a_s}(\boldsymbol{t})\boldsymbol{dt} \qquad \text{EQ. 4}$$

$$a_s(t) = \frac{A_s(t)dt}{A_{intake}} \qquad \text{EQ. 5}$$

where A_{intake} is the total intake activity at the time of intake, $a_s(t)$ is the activity in the source region per unit activity intake, and $\tilde{a}(r_s, \tau)$ is the number of nuclear transformations in a source region per unit activity intake.[7] Here, a unit intake of 1 Bq is typically used, as it renders the division of intake activity trivial.[7] From this activity of the target region, sex-specific committed equivalent dose coefficients to specific target tissues can be calculated through the S-coeffecient, a value defining the radiation-weighted dose to a target tissue per nuclear transformation occurring in a source region, and is depending on the energy and type of emission. It also depends on the yield per nuclear transformation and the specific absorbed fraction (SAF) corresponding to the radiation type from the source region that is deposited in the target region.[7, 10] Further expanding

the committed equivalent dose coefficient through the application of tissue-weighting factors over all tissues yields the sex-averaged committed effective dose coefficient.

2.2. Biokinetic and Dosimetric Models

Biokinetic models calculate the total number of transformations that occur within specific tissues, organs, or body regions over a given period of time. This value is a function of the physical half-life of the radionuclide ingested as well as the biological removal rate from the body, a combination of which yields the effective half-life.[7] This is accomplished by determining the time-integrated activity in each source region, as previously mentioned. A dosimetric model can then be applied to determine the energy deposited in all organs and tissues important to the source region, which allows for the calculation of committed absorbed dose in the target regions, based on the determined decays and depositions.[7, 10]

2.2.1. Development of the ICRP Biokinetic Models

ICRP *Publication 30* brought forth the development of systemic biokinetic models, also known as retention-function models. These models were first-order compartmental models with one-directional flow.[10] Simple and streamlined, this type of model broke up the organs and tissues of the Reference Person into regions which were then further broken down into compartments. For inhalation, the respiratory system is divided into three distinct regions: the nasal passage (N-P), the trachea and bronchial tree (T-B), and the pulmonary parenchyma (P), each of which are further broken down into two to four compartments individually associated with a particular pathway of clearance with a half-time of *T* days.[10]. For each region, deposition after inhalation depends upon the physical and chemical properties of the aerosol radionuclides inhaled. The activity median aerodynamic diameter (AMAD) of the particle will determine which region the particle is deposited in, and is assumed for models in ICRP *Publication 30* to be 1 micrometer.[10] Retention

of the deposited materials within the pulmonary region is classified by three categories, D, W, and Y, which are defined as half-time ranges of less than 10 days, 10 to 100 days, and greater than 100 days respectively.[10] These half-times, the time it takes for half of the radionuclide to be expelled from the body, are dependent upon the chemical form and metabolic data of the radionuclide.

Ingestion of radioactive materials is handled by separating the gastrointestinal (GI) tract into four separate target tissues, each of which is considered to be its own compartment.[11] First-order kinetics determine how particles will translocate within these compartments. The dosimetric models to calculate the activity and coefficients within this compartment model are therefore based on these first-order kinetic equations. The activity of the fraction of the ingested activity is followed through the entire body, compartment to compartment, before being excreted. In these models, there is no differentiation between forms of excreta.[10]

While these models are simple and streamlined, and therefore easy to comprehend and apply, their simplicity limits them greatly. The one-directional flow does not realistically model the movements of radionuclides in the body as a function of time, nor do they explicitly consider feedback of activity from tissues into the blood, as they describe only the initial distribution of the inhaled or ingested radionuclide.[10] The simplicity of the models fits the intended use of the calculation of dose per intake coefficients for prospective study, but are not adequately applicable to retrospective analysis.[10] The models presented in ICRP *Publication 30* are namely limited by the lack of data on the human metabolism, and the behavior of radionuclides within the body. Figure 1 below depicts ICRP *Publication 30's* one directional flow systemic biokinetic model.

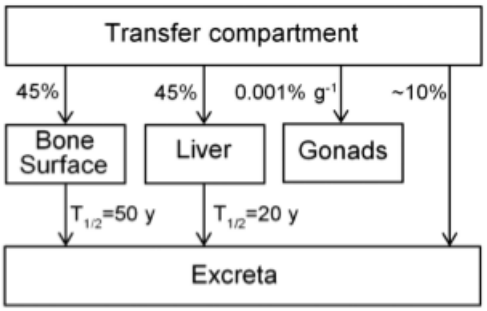

Figure 1. ICRP Publication 30 biokinetic model depicting one-directional flow without recirculation or feedback**.** [10, 11]

The ICRP *Publication 72* series tackles the age-specific systemic biokinetic models for members of the public from an inhalation or ingestion of radionuclides for 31 selected radionuclides, acting as replacements for the ICRP *Publication 30* series of models.[12] In comparison to ICRP *Publication 30*, the models are similar. The models are still compartmental and physiologically based; however, they take into consideration explicit excretion. That is, the GI tract and the urinary tract are considered individually, rather than just as "excreta," as was done in ICRP *Publication 30*, allowing for the separate assessment of dose to both the urinary bladder and the colon.[10-12] This is appropriate, as ICRP *Publication 60* assigned a tissue-weighting factor to both regions; therefore, modeling was adapted to reflect this.[13] As well, the systemic tissues and fluids are further divided into five compartments, and account for the feedback into the blood, and can be seen in Figure 2 below.

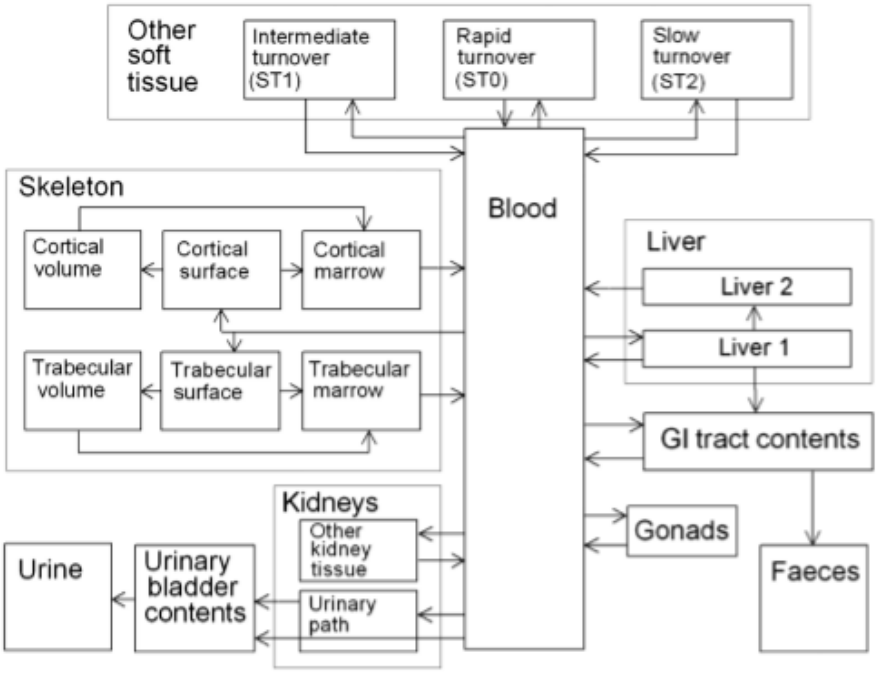

Figure 2. ICRP *Publication 72* series model for bone-surface seeking radionuclides [10, 12]

These paths are more realistic; however, they are only applied for a handful of 'bone-surface-seeking' elements. This bone-seeking model is further adapted for calcium, strontium, barium, lead, radium, and uranium, as they seek the bone volume, not just the bone surface, as seen in Figure 3, below.[10] That is, they integrate into the interior of the bone where there are increased retention times of the radionuclide, rather than simply depositing on the surface.

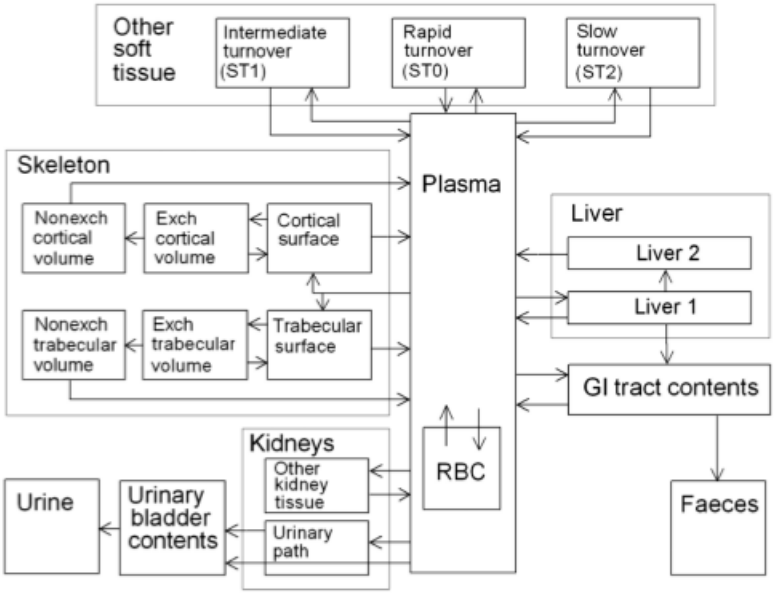

Figure 3. ICRP *Publication 72* bone-volume-seeking modified biokinetic model. [7, 9]

For inhalation, specifically, ICRP *Publication 72* reflects a new set of models for the Human Respiratory Tract (HRT) of a Reference Person.[12] Established in ICRP *Publication 66* documentation, this new model defines clearance from the respiratory tract regions through three pathways: the anterior nose through extrinsic means, the particle transport to the GI tract and lymph nodes, and the absorption into the bodily fluids such as blood.[12, 14] For inhaled materials, the retention classifications were changed beginning in ICRP *Publication 71* to Type F (fast), Type M (moderate), and Type S (slow), corresponding to the retention classes in ICRP *Publication 30*.[11, 15]

The physiologically descriptive models established in the ICRP *Publication 72* series hold a number of advantages over the traditional *ICRP Publication 30* retention-function models. Such advantages include the ability to supplement radiobiological data with physiologically reasonable assumptions, providing a basis for extrapolation beyond established radiobiological databases with regards to subgroups of the population and times outside the observation time, an easier

extrapolation from animal to human data, and an easier extrapolation to varied chemical forms of an element. As well, it visualizes the link between circulating bodily fluids and the tissues they are in contact with, allows for the modeling of daughter radionuclides from decay that happens within the body, and is easily adapted to add further compartments to increase complexity and accuracy as the application of the model deems necessary.[10] The model, however, is not without its drawbacks, as the compartmental model still compromises on biological realism in regards to practical considerations. That is, the inadequacy of some information on biokinetic processes for both well-known and lesser-known radionuclides diminishes the accuracy of the model. Therefore, the compartments should be interpreted as a net result of bodily processes, rather than a specific process themselves.[10] Furthermore, a more complex model is more difficult and expensive to implement.[12]

Current improvements in biokinetic and dosimetric modeling using ICRP *Publication 103* methodologies are reflected in the ICRP *Publication 130* series, known as the Occupation Intake of Radionuclides (OIR) series.[10] While these models are specific to occupational workers, *Publication 103* methodologies are awaiting application to the ICRP *Publication 72* as an analogue to the OIR series for the public in the Environmental Intake of Radionuclides (EIR) series. The models contained within ICRP *Publication 130* are designed to further replace the models developed in *Publication 30* and *68*.[10] In a similar fashion to ICRP *Publication 72*, the Human Respiratory Tract Model (HRTM) developed in ICRP *Publication 66* was revised and adopted for the inhalation coefficient modeling for non-systemic portions of the body.[12, 14] For systemic circulation, a similar model to the ICRP *Publication 72* series was applied, simply on a more limited scale, still including explicit removal paths, but allowing for modification for specific elements.[10]

The biokinetic models for the respiratory and alimentary tracts used in ICRP *Publication 130* allow for the definition of movement of the inhaled or ingested radionuclide which can then be used to determine the absorption into the blood stream. Akin to ICRP *Publication 66*, the inhaled particles are deposited in the lung compartment, with removal happening through absorption into the blood and removal via the GI tract.[10, 14] As with ICRP *Publication 72*, solubility types F, M, and S based on the chemical form of the radionuclide are still used, with altered values for rapid dissolution fractions and dissolutions rates. Type F is quantified by total, 100% absorption within a half-time of 10 minutes in the bronchial (BB), bronchiolar (bb), and alveolar-interstitial regions (AI). Type M requires only 10% absorption in a 10-minute half-time, with a 90% half-time of 140 days. Finally, Type S is classified by only a 0.1% absorption within a 10-minute half-time and a 99.9% half-time of 7,000 days.[10] A Type V, or very fast, is also used, defined as 100% absorption instantaneously. These absorptions act as a direct injection into the blood.[10] More realistic clearance from the nasal passages were also developed.

Biokinetic models for ingestion utilize the Human Alimentary Tract Model (HATM) model developed in ICRP *Publication 100*, with revisions reflecting an increased knowledge on the biokinetics of radionuclides within the human body.[10], [16] These models are linked with the respiratory tract models, as the GI portion assists in clearing radionuclides from the respiratory tract. For ingested nuclides that are more readily absorbed through the GI tract, an f_1 value is assigned as the fraction of the ingested element directly absorbed to the body fluids.[17] As well, deposition in the esophagus after respiration leads to ingestion through swallowing.[10]

2.2.2. Development of Dosimetric Models

Biokinetics are only part of the picture when it comes to defining dose coefficients. Dosimetric models are also necessary. ICRP *Publication 130* utilizes revised decay data from

ICRP *Publication 107* and the reference computational phantoms for both males and females of ICRP *Publication 110*. These phantoms, called voxel phantoms, are based on medical imaging.[18] Monte Carlo codes were also employed to derive energy deposition in the phantoms.[10] For ingestion, explicit dosimetric models can be applied to each of the target regions within the alimentary tract. These dosimetric models take into consideration doses from radionuclides in the contents of the region as well as mucosal retention of radionuclides.[10] The calculation of the dose coefficients can be summarized with the following steps. Firstly, biokinetic models are used to calculate the activity in each source region per unit intake as a function of time. This value is then used to determine the sex-specific absorbed dose per unit intake to each target tissue. From here, the values can be used to determine any dose coefficient or dose rate coefficient related value (e.g., committed effective dose coefficient, risk coefficient).[7]

2.2.3. Exposure Categories

ICRP defines categories of exposure into three potential types: occupational, public, and medical.[6] Occupational exposures consist of individuals who incur an exposure as a result of their work while operating under reasonable operations of their facility, and are the focus of the ICRP *Publication 130* OIR series. The safety of individuals who fall into this category is the responsibility of their employer, who should take reasonable precautions and protective measures to reduce potential exposures, and fall in line with radiological protection regulations of the workplace.[6] Public exposures are defined as any exposure of the public that fall outside of occupational or medical exposures. The largest contributor to these exposures comes from natural sources, such as radionuclides that exist in nature, without human intervention.[6] Some of these sources, such as radon gas, can and should be mitigated to reduce potential exposures. Finally, medical exposures consist of diagnostic, interventional, and therapeutic processes. This can

include x-rays, CT scans, radiotherapy, fluoroscopy, and more. These exposures are considered planned exposures, and are justified by comparing the risk incurred by the patient from the exposure with the risk to the patient if left untreated.[6]

2.2.4. Exposure Pathways

When looking at risk from a radiation exposure, there are two types of exposure, internal and external. For the purpose of this report, the focus will be on internal exposures. Internal exposures stem from either inhalation, ingestion, injection, or uptake of a radionuclide through an open wound. For the purpose of this report, only inhalation and ingestion pathways will be considered.[6] The method of radionuclide intake is important due to the usage factor, which determines the amount of a radionuclide that an individual will either inhale or ingest at various ages through life.

In considering internal radionuclide exposures from inhalation and ingestion pathways, usage rates for the intakes of radionuclides must be considered. The scenarios of radionuclide intake into the body stem from the amount of air, water, or food that is taken into the body over a period of time. In the proposed work, intake via inhalation and intake via the ingestion of water will be considered. These values are dependent upon age and sex, and are typically depicted as being the value established on the date at which the individual ages one year.[2] Table 3 contains FGR 13 relevant usage values for males and females for the three environmental media of interest. Values also exist for the intake of radionuclide via ingestion of cow's milk; however, this is outside the scope of this study and therefore has not been included.[2]

Table 3. Sex- and age-specific usage rates for environmental media. [2]

	air		Water		Food	
Age of Exposure	Male ($m^3 d^{-1}$)	Female ($m^3 d^{-1}$)	Male ($L d^{-1}$)	Female ($L d^{-1}$)	Male ($kcal d^{-1}$)	Female ($kcal d^{-1}$)
0	2.9	2.9	0.191	0.188	478	470
1	5.2	5.2	0.223	0.216	791	752
5	8.8	8.8	0.542	0.499	1566	1431
10	15.3	15.3	0.725	0.649	1919	1684
15	20.1	15.7	0.9	0.712	2425	1828
20	22.2	17.7	1.137	0.754	2952	1927
50	22.2	17.7	1.643	1.119	2570	1758
75	22.2	17.7	1.564	1.179	1990	1508

Figure 4, taken from FGR 13, depicts the general trends seen for inhalation of radionuclides as well as intake of radionuclides via tap water with respect to age for both males and females.[2] ICRP *Publication 66* investigated multiple factors affecting intake of air, including lung capacity with respect to age, as well as tissue type and effects of smoking on lung capacity.[14]

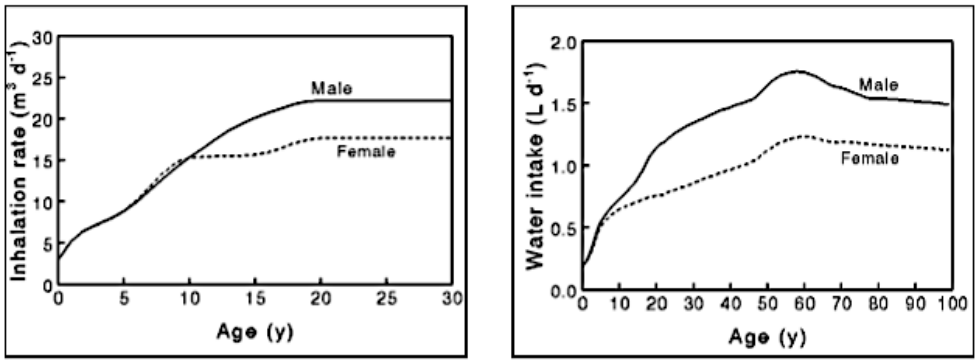

Figure 4. Inhalation and water intake usage rates for males and females with respect to age of intake defined by the 1977-1978 Nationwide Food Consumption Survey of the U.S. Department of Agriculture. [1]

Inhaled radionuclides were considered according to solubility categories; Type F, Type M, and Type S, which represent the fast, medium, and slow solubility rates within the lungs, respectively. These rates are based on the particulate chemical form of the inhaled material.[2] For this solubility type, there is very little absorption from the anterior (ET_1) or posterior (ET_2)

passages, BB, or bb regions, and only 10% of the AI deposition reaches the bodily fluids. For each absorption type, anything that remains unabsorbed is eventually cleared by the GI tract through particle transport.[15]

To establish age-specific intake and usage rates for ingested tap water, the 1977-1978 Nationwide Food Consumption Survey of the U.S. Department of Agriculture was conducted.[19] This includes drinking water, water added to beverages, as well as water that is added to foods during preparation. The values determined here in analysis by Ershow and Cantor in 1989 were not sex-specific so, to determine the sex-specific values, the assumption was made that the ratio of water usage between males and females was the same as for the usage of food consumed.[19, 20]

2.3. Radionuclide Biokinetics

Biokinetics are inherently specific to each individual element. Typically, radionuclides are broken up into two groups: bone-seekers and non-bone-seekers. Bone-seekers are radionuclides that behave in a manner similar to calcium and therefore end up integrated into the bone matrix. This group contains the radionuclides of strontium, americium, uranium, and plutonium. This chemical behavior thereby ensures that the radionuclide seeks the bones, and the longer physical half-life insures integration into the bone matrix. The bone-seeking radionuclides of interest in this work include only ^{90}Sr and ^{235}U. The non-bone-seeking radionuclides of interest include tritium, ^{131}I, and ^{137}Cs.

2.3.1. ^{90}Sr

Strontium, after an ingestion by adults, is 15 to 45% absorbed by the body, depending on a number of factors.[21] Such factors include fasting or low levels of calcium, magnesium, and phosphorus in the body and a diet high in milk and vitamin D content.[22] The chemical similarity

of strontium to calcium allows for it to be readily integrated into the bone matrix by one of three mechanisms: apposition, resorption, and surface and diffuse exchange. These processes affect the mineral volume of the bone, the modeling and maintaining of the bone structure, and element exchange between the blood and the skeleton, respectively.[23] Thus, the absence of calcium in a diet would prompt the body to absorb more strontium to compensate, increasing the total activity absorbed after ingestion. The biokinetics for strontium in children differ from those of adults. Absorption by a child's body after ingestion of the radionuclide is higher than in adults, sitting around 73% for infants, tapering through ages one to five years, and matching adult ages beginning at age five years.[22]

Biological removal from the bloodstream via excretion, primarily through urine, has a half-time of only 0.25 days, with removal from the skeleton occurring at a comparable rate to calcium, which is age dependent.[21] A general assumption for the removal of deposited activity is a removal rate of $0.1 d^{-1}$ to bone volume, a conservative estimate applicable to all ages.[22] This removal rate translates to a half-time in exchangeable bone compartments of 80 days.[21] It is important to note that the base model of strontium in the body, based heavily on models developed by Leggett *et al.*, does not explicitly consider the recycling of activity from other tissues, but rather incorporates these values implicitly in a value known as deposition fractions, which quantify what fraction of activity is deposited on various bone surfaces throughout the body.[22, 24] Models further developed in ICRP *Publication 67* assume that activity exchanged with the blood plasma recirculates through the body, redistributing to the tissues and excreta in the same manner as the initial uptake.[21] As mentioned previously, functions such as diffuse surface exchange allow strontium to be integrated into deeper parts of the bone matrix, away from the blood plasma, where activity exchange is then

slowed. These factors are all considered when calculating the time-dependent activity of strontium in the bone matrix.[21]

Retention of inhaled strontium strongly depends upon what compound it exists in, with a higher retention rate in compounds such as strontium titanate, rather than strontium chloride. When inhaled, most strontium is rapidly cleared, with little chance for absorption into the bloodstream. This is, however, dependent on the solubility class, which has the potential to change based upon how the inhaled strontium is bound.[15] In a similar manner to ingested strontium, inhaled strontium circulates through the body, eventually depositing on bone surfaces or being excreted namely through the kidneys.

2.3.2. ^{235}U

As with strontium, the biokinetics of uranium depend upon age, solubility class, and uptake type. However, unlike strontium, the main limits on the uptake of uranium are due to its toxicity as a heavy metal, rather than purely its radioactivity.[17] In order to determine the quantity of uranium uptake by the human body, urinalysis was done to measure the quantity of uranium excreted. With values of excreted uranium around 30-40% of the ingested amount, the fractional absorption of uranium through ingestion of water in adults is determined to average 0.01-0.02. For uranium consumed with food, the average absorption was determined to be negligible.[17] As with strontium, fasting increases the amount of uranium absorbed after ingestion.[17]

For children, the exposure data is even further limited than the data available for adults; however, theses limited data suggests that there is limited impact on absorption based upon age.[17] Animal studies, however, have shown that young animals show a higher retention of uranium than the adults. Based on this information, the conservative approach assumes that infants up to 1 year

of age have an f_1 value twice that of children and adults age 1 year and older, 4×10^{-2} and 2×10^{-2}, respectively.[17]

Most of the limited data on the biokinetics of uranium through the body come from intravenously injected hexavalent uranium, the most commonly encountered form for environmental exposures.[17] Upon injection, only 25% of the administered uranium remains in the blood after only 5 minutes, with the rest either being integrated into the soft tissues or filtered by the kidneys and excreted in urine. Less than 0.5% remained after 100 hours, with major variability between observed subjects.[17] Further studies on humans indicated that up to 90% of the injected uranium is excreted within 24 hours, while the remainder stays in the body for a period of years, retained in the kidneys and skeletal system bone surfaces. Uranium, though not an alkaline earth metal, behaves in a manner similar to the alkalines such as strontium, due to exchanges with Ca^{2+} on the bone surface. However, unlike strontium, it does not incorporate into the crystal formation, nor does it enter existing crystals. It tends to deposit in areas of rapid growth, similar to calcium, and gradually diffuses into the bone matrix. Bone therefore becomes a site of long-term retention, but only accounts for a few per cent of the systemically circulated activity.[17]

Inhalation of uranium tends to be rapidly cleared through urinary excretion due to the Type F solubility of most uranium containing compounds that are inhaled. The absorption into the soft tissues via the lungs happens rather quickly, ranging typically between Type F and Type M solubility classes, where the radionuclide is then rapidly cleared by the kidneys. Inhalation deposition is assumed to be similar to ingestion of the radionuclide, but with limited human data on exposure to uranium, a high level of uncertainty remains.[15]

2.3.3. Tritium

Tritium is found in three main forms when released into the environment: tritium gas, tritiated water, and organically-bound tritium (OBT).[22] When tritiated water is ingested, absorption is considered to be instantaneous and, in adults, is mixed completely with total body water once it enters the bloodstream. A fraction of this tritium can become organically bound, leaving half-time in the body dependent upon the metabolic activity of the soft tissues of the exposed individual. Both the tritiated water and the organically bound tritium are assumed to distribute uniformly through all tissues, leading to the need to break the biokinetics down into components of an exponential equation to accurately account for turnover in the body.[22]

$$R(t) = Ae^{-0.693t/T_1} + Be^{-0.693t/T_2} + Ce^{-0.693t/T_3} \qquad \text{EQ. 6}$$

Where *A* represents the region of body water with a half-time of about 10 days, represented by the turnover T_1, while *B* and *C* represent OBT that incorporates into the soft tissues, contributing to about 10% of the committed dose combined.[22]

In children, the biological half-times of tritiated water vary with age, increasing with each reference age. These values are determined based on the assumption that 1 ml of water is required by the child for each 4.2 kJ of expended energy. The table below outlines the biological half-times for each reference age. However, while the halftimes vary, the generic equation for the retention in adults can be applied to children as well, due to the assumption of components *A* and *B* from Eq. 6 being the same.[22] These half-times are summarized in Table 4 below, taken from ICRP *Publication 56*.

Table 4. Biokinetic data for tritiated water.[18]

	Distribution (%) Total body	Biological half-time (d)

Age	Comps. A	Comp. B	Comp A	Comp. B
3 mo	97	3	3.0	8.0
1 yr	97	3	3.5	15
5 yrs	97	3	4.6	19
10 yrs	97	3	5.7	26
15yrs	97	3	7.9	32
Adult	97	3	10.0	40.0

While tritiated water intake is possible, intake of OBT comprises the larger portion of ingested tritium. However, nearly 50% of this OBT behaves and is incorporated into soft tissues the same as is tritiated water upon entering the bloodstream. The remaining 50% bonds with carbon and therefore behaves in a metabolic pattern similar to carbon. Respectively, these two methods of retention have half-times of 10 days and 40 days.[22] Retention therefore differs from purely tritiated water, and is given by the equation[22]:

$$R(t) = 0.5e^{-0.693t/10} + 0.5e^{-0.693t/40} \quad \text{EQ. 7}$$

Inhalation of tritium usually takes place in the form of inhaling tritiated water vapor, due to the fact that elemental tritium has a low solubility. This means that the lungs are really the only tissue irradiated by elemental tritium. However, similar to ingesting tritiated water, the inhalation of tritiated water vapor results in a uniform dispersal through the body's soft tissues following immediate translocation to the blood after inhalation.[21] Due to the low volatility of the chemical form of tritium, it typically distributes through the body without changing chemical form. For particulate tritium that is inhaled, the most common solubility class has been found to be Type M. However, once absorbed, through the lungs, the biokinetics follow that of tritiated water.[21]

2.3.4. ^{137}Cs

Cesium-137 is similar to tritium insomuch that it is rapidly and near completely absorbed from the GI tract after ingestion, ranking only slightly below how completely tritium is absorbed.[22] In adults, after ingestion and subsequent entry into the blood, it behaves akin to potassium. That is, it accumulates in all body tissues and a uniform distribution of activity is assumed.[22] Retention is similar to tritium, in that it is calculated from two components, a fast component (T_1) and more long term component (T_2), as can be seen in the equation below[22]:

$$R(t) = 0.1e^{-0.693t/T_1} + 0.9e^{-0.693t/T_2} \quad \text{EQ. 8}$$

In children, expulsion of cesium from the body happens at an increased rate as compared to adults for all cases save newborns. That is, the short term clearance term in the previous equation holds a higher weight in children than in adults.[18] The minimal data available for infants places the half-time retention in the range of 12 to 23 days, and supporting animal studies suggest that the rate of cesium loss is affected by the concentration of potassium in the diet.[18] This is supported by a study conducted by Wilson and Spiers (1964) that demonstrated a faster long term cesium loss in bottle-fed infants over breast-fed, due to the fact that the supplied formula had a higher concentration of supplementary potassium.[18, 22] Short-term cesium clearance, however, does not seem to factor in to newborn clearance, according to supporting animal studies, and this is thought to be due to the fact that kidney function development is so slow at newborn ages.[18] The distribution and half-time for cesium deposition after ingestion can be found in Table 5, summarized from ICRP *Publication 67*.[21]

Table 5. Summarized biokinetic data for cesium. [17]

	Distribution (%)	Biological half-time (days)
	Total body	Total body

Age	f_1	Compartment A*	Compartment B^+	Compartment A	Compartment B
3 mo.	1	-	100	-	16
1 yr.	1	-	100	-	13
5 yr.	1	45	55	9.1	30
10 yr.	1	30	70	5.8	50
15 yr.	1	13	87	2.2	93
Adult (20/25 +)	1	10	90	2	110

*From ICRP *Publication 30;* values are appropriate for males. Conservative if applied for calculation dose coefficients for females. [11]

Cesium was first classified by ICRP as having solubility Class D, confirmed by ICRP *Publication 30*.[11] When the classification types for inhalation changed, most chemical forms of cesium were assigned either solubility Type F or Type M. The simple ionic compounds showed rapid and complete absorption while inhaled irradiated fuel fragments and cesium fused into aluminosilicate particles demonstrated absorption qualities consistent with Type M. Given limited available data, solubility Type F should be assumed as the default if information to otherwise determine solubility type is unavailable, due to the fact that is the most common solubility class for both newborns and children through adult age groups.[22]

2.3.5. ^{131}I

Ingestion of iodine, based off of examples such as incorporation in watercress, is assumed to show complete and total absorption when incorporated with food stuffs and aqueous solutions.[22] Iodine is specifically a thyroid-seeking radionuclide, and thus can be defined through the use of a three-compartment model. Upon ingestion, it is absorbed into the blood and distributed to the thyroid and the rest of the body's soft tissues, with a biological half-life of 80 days. The average fraction uptake to the thyroid specifically is determined to be 0.3; however, this can vary based on the diet of the individual. The higher the stable iodine level in an individual's diet, the less radioiodine the exposed individual will absorb.[22] A small portion of the thyroid absorbed iodine is released back into the blood where it is then metabolized by the soft tissues before returning to

the plasma pool as inorganic iodide. This allows for recycling of the iodide by the thyroid. Roughly 20% of the ingested iodine is excreted via feces. The recycling of iodine by the thyroid results in a slightly more complicated retention equation as there is not a single clearance of the organ. Instead, the clearance can by approximated by[22] :

$$\boldsymbol{R(t) = Ae^{-0.693t/T_1} + (1 - A)e^{-0.693t/T_2}} \quad \text{EQ. 9}$$

Where T_1 is the short-term and T_2 is the long-term half-life of iodine in the system. This model is effective; however, most retention data is gathered through the observation of ^{131}I in the system due to the short half-life of only 8 days. This short half-life allows for an exposure follow-up time of only two weeks, but, unfortunately, does not enable a resolution of the two exponentials in the retention equation. Due to this fact, an "apparent" half-time has been derived, which is a single exponential clearance from the thyroid. This value was determined to be 85 days in adults.[22]

In children, specifically newborns, uptake into the thyroid after ingestion is enhanced compared to adults, with an uptake sitting around 70%.[22] For individuals between ages 4 and 49, the range of uptake of radioiodine did not appear to differ from the uptake values of adults, suggesting that there is little dependence on age in regards to uptake after the first year or so of life.[22] However, the turnover rate of iodine does appear to decrease with increasing age, due to the change in rate of utilization of thyroid hormone in the body with respect to age, leading to an increase in biological half-time with respect to age. [22], [21]

Similar to cesium, inhaled iodine was originally labeled as being in inhalation Class D. With the further development of modeling, and the studies conducted on human volunteers to study the deposition and biokinetics of iodine in the human system, it was re-labeled as Type F clearance. Nearly all inhaled radioiodine activity is retained, with deposition mainly in the main

airways and a clearance half-time of 10 minutes. The outlier of inhaled iodine lies with methyl iodide, which shows a Type V clearance, rapid absorption but lower retention. To date, no experimental data have been found indicating Type M or S behavior of any iodine form.[15] Table 6 below, summarized from ICRP *Publication 56*, summarizes the biokinetics for iodine.

Table 6. Summarized biokinetic data for iodine.[18]

		Uptake by thyroid	Fecal excretion	Biological half-time (d)			"Apparent half-time" (d)
				Blood	Thyroid	Rest of body	Thyroid
Age	f_1	%	%	T_a	T_b	T_c	
3 mo	1	30	20	0.25	11.2	1.12	15
1 yr	1	30	20	0.25	15	1.5	20
5 yr	1	30	20	0.25	23	2.3	30
10 yr	1	30	20	0.25	58	5.8	70
15 yr	1	30	20	0.25	67	6.7	80
Adult	1	30	20	0.25	80	12	91

2.4. Uncertainties and Limitations of Biokinetic and Dosimetric Models

Uncertainty of biokinetic models for individual elements or compounds depends upon the uncertainties of the parameter values of the models, as well as the uncertainties of the model structure itself.[10] One of the main sources of these uncertainties is the lack of information in regards to processes within the human system, leading to over-simplifications in model structure. This is a limitation shared by all biokinetic models.[10] Many biokinetic models are informed by human data based on observation of behavior and quantitative measurements of variables, such as excreta. However, the variability between study groups and members within each group can limit the viability of collected data.[10] It was previously mentioned that models can be extrapolated between elements and even between species. However, the qualitative differences between elements and between species lead to an ever widening uncertainty interval, limiting the predictive capability of the models.[10]

Dosimetric models hold their own sources of uncertainty. These models are used to calculate the mean absorbed dose for internal emitters, and as such, the sources of uncertainty are the energy and intensity of the emitted radiations, the interaction coefficient of the emitted radiations in tissues, elemental composition of the human body, organ mass and shape, and the special relationship of the source and target regions.[10] These vary with energy and radiation type; however, the use of voxel phantoms has reduced many of these uncertainty contributors. Finally, improvement of decay data (i.e., half-lives) leads to more accurate dosimetric calculations, reducing uncertainty of the calculated dose coefficients.[10]

2.5. Risk

In FGR 13 risk calculation models, there are two models employed: the absolute risk model and the relative risk model.[2] The absolute risk model is based on the assumption that age-specific excess force of mortality or morbidity due to a radiation dose is independent of cancer mortality or morbidity rates in the population, also known as the baseline cancer risk.[2] Baseline risk is the likelihood of an individual who is free from cancer, developing cancer over a certain time period due only to an exposure. This risk model from FGR 13 is defined as:

$$\epsilon(x, x_e) = \alpha(x_e)\zeta(t) \qquad \text{EQ. 10}$$

where $\alpha(x_e)$ is defined as a non-negative number called a "risk model coefficient" which is dependent on the sex as well as the age at exposure, and $\zeta(t)$ is either 0 or 1 depending on the time since exposure, $t = x - x_e$. This value is also known as the period of time during which the risk is expressed. Here, $\epsilon(x, x_e)$ is the absolute risk at age *x* due to a unit absorbed dose received at an earlier age $x_e (x_e < x)$. [2]

Alternatively, relative risk is defined by the assumption that age-specific effect on mortality

or morbidity due to a radiation dose is the product of an "exposure-age-specific relative risk coefficient", and the baseline cancer mortality and morbidity rate. Relative risk is thus calculated by:

$$\epsilon(x, x_e) = \mu(x)\eta(x, x_e) \quad \text{EQ. 11}$$

Where $\mu(x)$ is the baseline cancer rate at age *x* and $\eta(x, x_e)$ is the relative risk at age *x* due to a unit absorbed dose received at age $x_e (x_e < x)$. This value is calculated as:

$$\eta(x, x_e) = \beta(x_e)\, \zeta(t, x_e) \quad \text{EQ. 12}$$

where $t = x - x_e$, $\beta(x_e)$ is a non-negative risk model coefficient dependent on gender as well as age at exposure, and $\zeta(t, x_e)$ is the relative magnitude of the response at different times after exposure at age x_e. It is important to note that $\zeta(t, x_e)$ is independent of age at exposure, save for leukemia.[2] Each model has its own merits depending on the specific population and cancer of interest, but, for sake of protection calculations, absolute risk is used for bone, skin, and thyroid cancer while the relative risk model is used for other sites, due to the strong age-dependency these cancers portray.[2, 4]

Risk models culminate in the calculation of the lifetime risk, also knowns as the Lifetime Attributable Risk (LAR). LAR is defined by [13]:

$$LAR(D, e) = L_a M(D, e, a) S(a)/S(e) \quad \text{EQ. 13}$$

where *a* is the attained age in years, *L* is the risk-free latent period, $M(D, e, a)$ is the excess absolute risk (EAR), *S*(a) is the probability of surviving to age a, and $S(a)/S(e)$ is the probability of

surviving to age *a* conditional of survival to the age of exposure *e*. This value is specifically for an acute exposure at age *e*. For a chronic exposure, a dose and dose rate response effectiveness factor with a value of 1.5 must be applied. This leads to the LAR in the form of:

$$LAR^{(R)}(D,\beta,stationary) = \frac{\int_0^{110-L} S(e)\cdot LAR^{(R)}(D,e,\beta)\cdot de}{1.5\int_0^{110-L} S(e)de} \qquad \text{EQ. 14}$$

Where the LAR is calculated for a stationary population and $LAR^{(R)}(D,e,\beta)$ is the lifetime attributable risk from an absorbed dose *D* at age *e* with the dose-response parameter β.[25] The age dependence of the LAR for various tissues can be seen in Figure 5.[25]

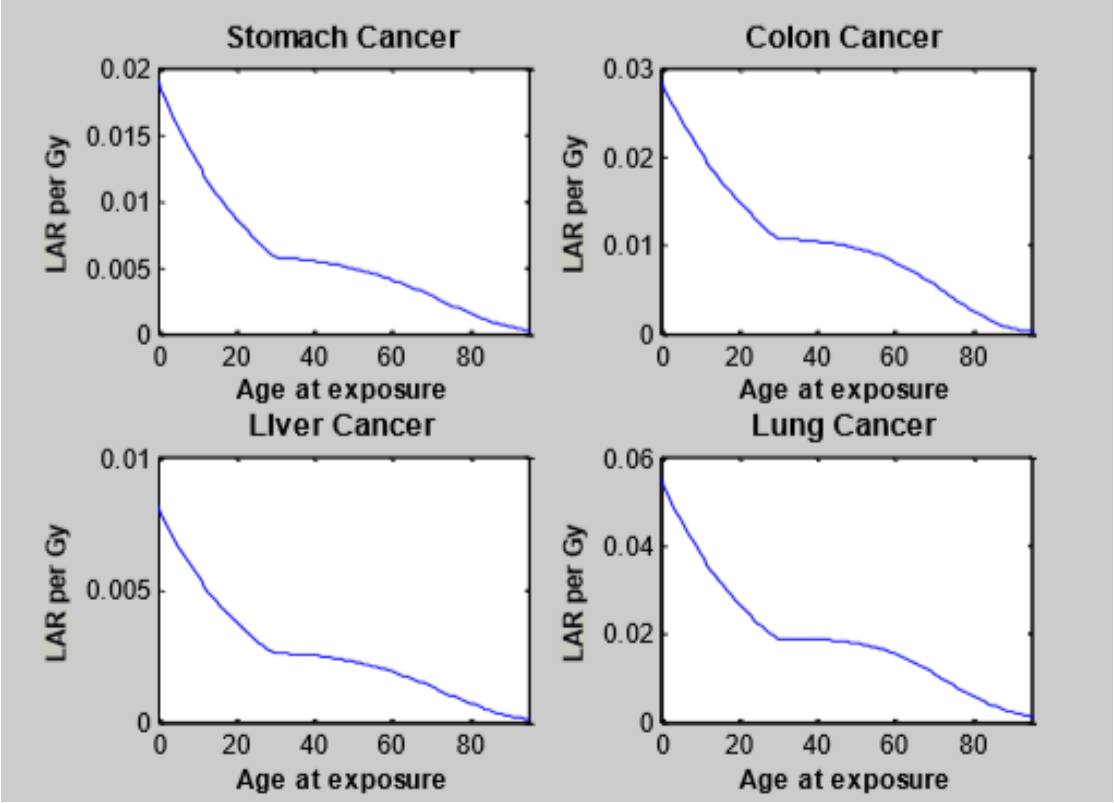

Figure 5. LAR for various cancer sites based on age at exposure. [20]

The LAR value differs between mortality and morbidity, mortality being here defined as the fraction of cancers that are fatal, and morbidity being defined for fatal and non-fatal cancers.

The two values are related to one another through the application of the lethality fraction.[2] A recreation of the lethality fraction table from FGR 13 can be found in Table 7. This factor is used to divide the mortality risk estimate for each tissue in order to produce the morbidity risk estimate for the respective tissues.[2] Skin contributes most heavily to the non-fatal radiation-induced cancers, with at least 83% of all skin cancers being basal cell carcinomas with the remainder being squamous cell carcinomas, 99.99% and 99% of the cancers therein being non-fatal, respectively. For this reason, it is important to note that, while the lethality fraction for skin is incredibly small, risk calculations for skin cancer only consider the fatal cancers in the development of the risk coefficients. [2]

Table 7. Lethality fraction data for site specific cancers in adults. [2]

Cancer site	Lethality fraction *k*
Esophagus	0.95
Stomach	0.90
Colon	0.55
Liver	0.95
Lung	0.95
Bone	0.70
Skin	0.002
Breast	.50
Ovary	0.70
Bladder	0.50
Kidney	0.65
Thyroid	0.10
Leukemia (Acute)	0.99
Residual	0.71

The probability of surviving to age of exposure *e* is also called the survival function. This function is dependent not just upon current age but upon gender as well, with the function being slightly different between males and females. The FGR 13 values for this function are taken from data prepared by the National Center for Health and Statistics for the U.S. Decennial Life Tables for 1989-91, and are tabulated below.[2]

Table 8. Survival function data for males and females tabulated through age 120.[2]

Year After Exposure	Probability of Survival	
	Male	Female
0	1.00	1.00
1	9.90×10^{-01}	9.92×10^{-01}
2	9.89×10^{-01}	9.91×10^{-01}
3	9.88×10^{-01}	9.91×10^{-01}
4	9.88×10^{-01}	9.90×10^{-01}
5	9.88×10^{-01}	9.90×10^{-01}
6	9.87×10^{-01}	9.90×10^{-01}
7	9.87×10^{-01}	9.90×10^{-01}
8	9.87×10^{-01}	9.89×10^{-01}
9	9.86×10^{-01}	9.89×10^{-01}
10	9.86×10^{-01}	9.89×10^{-01}
11	9.86×10^{-01}	9.89×10^{-01}
12	9.86×10^{-01}	9.89×10^{-01}
13	9.86×10^{-01}	9.89×10^{-01}
14	9.85×10^{-01}	9.88×10^{-01}
15	9.85×10^{-01}	9.88×10^{-01}
16	9.84×10^{-01}	9.88×10^{-01}
17	9.83×10^{-01}	9.87×10^{-01}
18	9.81×10^{-01}	9.87×10^{-01}
19	9.80×10^{-01}	9.86×10^{-01}
20	9.79×10^{-01}	9.86×10^{-01}
21	9.77×10^{-01}	9.85×10^{-01}
22	9.75×10^{-01}	9.85×10^{-01}
23	9.74×10^{-01}	9.84×10^{-01}
24	9.72×10^{-01}	9.84×10^{-01}
25	9.71×10^{-01}	9.83×10^{-01}
26	9.69×10^{-01}	9.83×10^{-01}
27	9.67×10^{-01}	9.82×10^{-01}
28	9.65×10^{-01}	9.81×10^{-01}
29	9.64×10^{-01}	9.81×10^{-01}
30	9.62×10^{-01}	9.80×10^{-01}
31	9.60×10^{-01}	9.79×10^{-01}
32	9.58×10^{-01}	9.79×10^{-01}
33	9.55×10^{-01}	$9.78 \times 10^{-0}1$
34	9.53×10^{-01}	9.77×10^{-01}
35	9.51×10^{-01}	9.76×10^{-01}
36	9.48×10^{-01}	9.75×10^{-01}
37	9.46×10^{-01}	9.74×10^{-01}
38	9.43×10^{-01}	9.73×10^{-01}
39	9.40×10^{-01}	9.72×10^{-01}
40	9.38×10^{-01}	9.70×10^{-01}

41	$9.35x10^{-01}$	$9.69x10^{-01}$
42	$9.32x10^{-01}$	$9.67x10^{-01}$
43	$9.28x10^{-01}$	$9.66x10^{-01}$
44	$9.25x10^{-01}$	$9.64x10^{-01}$
45	$9.21x10^{-01}$	$9.62x10^{-01}$
46	$9.18x10^{-01}$	$9.60x10^{-01}$
47	$9.13x10^{-01}$	$9.58x10^{-01}$
48	$9.09x10^{-01}$	$9.55x10^{-01}$
49	$9.04x10^{-01}$	$9.52x10^{-01}$
50	$8.99x10^{-01}$	$9.49x10^{-01}$
51	$8.93x10^{-01}$	$9.46x10^{-01}$
52	$8.87x10^{-01}$	$9.42x10^{-01}$
53	$8.80x10^{-01}$	$9.38x10^{-01}$
54	$8.73x10^{-01}$	$9.34x10^{-01}$
55	$8.65x10^{-01}$	$9.29x10^{-01}$
56	$8.56x10^{-01}$	$9.24x10^{-01}$
57	$8.47x10^{-01}$	$9.18x10^{-01}$
58	$8.37x10^{-01}$	$9.12x10^{-01}$
59	$8.26x10^{-01}$	$9.05x10^{-01}$
60	$8.14x10^{-01}$	$8.97x10^{-01}$
61	$8.01x10^{-01}$	$8.89x10^{-01}$
62	$7.87x10^{-01}$	$8.81x10^{-01}$
63	$7.72x10^{-01}$	$8.71x10^{-01}$
64	$7.56x10^{-01}$	$8.61x10^{-01}$
65	$7.40x10^{-01}$	$8.51x10^{-01}$
66	$7.22x10^{-01}$	$8.39x10^{-01}$
67	$7.03x10^{-01}$	$8.27x10^{-01}$
68	$6.84x10^{-01}$	$8.14x10^{-01}$
69	$6.63x10^{-01}$	$8.00x10^{-01}$
70	$6.41x10^{-01}$	$7.85x10^{-01}$
71	$6.18x10^{-01}$	$7.69x10^{-01}$
72	$5.94x10^{-01}$	$7.52x10^{-01}$
73	$5.68x10^{-01}$	$7.33x10^{-01}$
74	$5.41x10^{-01}$	$7.14x10^{-01}$
75	$5.14x10^{-01}$	$6.93x10^{-01}$
76	$4.86x10^{-01}$	$6.71x10^{-01}$
77	$4.57x10^{-01}$	$6.48x10^{-01}$
78	$4.27x10^{-01}$	$6.23x10^{-01}$
79	$3.98x10^{-01}$	$5.97x10^{-01}$
80	$3.68x10^{-01}$	$5.70x10^{-01}$
81	$3.37x10^{-01}$	$5.41x10^{-01}$
82	$3.06x10^{-01}$	$5.10x10^{-01}$
83	$2.76x10^{-01}$	$4.78x10^{-01}$
84	$2.47x10^{-01}$	$4.45x10^{-01}$

85	$2.18\text{x}10^{-01}$	$4.11\text{x}10^{-01}$
86	$1.91\text{x}10^{-01}$	$3.76\text{x}10^{-01}$
87	$1.66\text{x}10^{-01}$	$3.41\text{x}10^{-01}$
88	$1.41\text{x}10^{-01}$	$3.06\text{x}10^{-01}$
89	$1.19\text{x}10^{-01}$	$2.71\text{x}10^{-01}$
90	$9.88\text{x}10^{-02}$	$2.37\text{x}10^{-01}$
91	$8.05\text{x}10^{-02}$	$2.04\text{x}10^{-01}$
92	$6.44\text{x}10^{-02}$	$1.72\text{x}10^{-01}$
93	$5.05\text{x}10^{-02}$	$1.43\text{x}10^{-01}$
94	$3.88\text{x}10^{-02}$	$1.17\text{x}10^{-01}$
95	$2.93\text{x}10^{-02}$	$9.35\text{x}10^{-02}$
96	$2.17\text{x}10^{-02}$	$7.34\text{x}10^{-02}$
97	$1.57\text{x}10^{-02}$	$5.64\text{x}10^{-02}$
98	$1.12\text{x}10^{-02}$	$4.24\text{x}10^{-02}$
99	$7.76\text{x}10^{-03}$	$3.12\text{x}10^{-02}$
100	$5.29\text{x}10^{-03}$	$2.25\text{x}10^{-02}$
101	$3.51\text{x}10^{-03}$	$1.58\text{x}10^{-02}$
102	$2.28\text{x}10^{-03}$	$1.09\text{x}10^{-02}$
103	$1.44\text{x}10^{-03}$	$7.25\text{x}10^{-03}$
104	$8.79\text{x}10^{-04}$	$4.69\text{x}10^{-03}$
105	$5.21\text{x}10^{-04}$	$2.93\text{x}10^{-03}$
106	$2.98\text{x}10^{-04}$	$1.77\text{x}10^{-03}$
107	$1.64\text{x}10^{-04}$	$1.03\text{x}10^{-03}$
108	$8.69\text{x}10^{-05}$	$5.69\text{x}10^{-04}$
109	$4.39\text{x}10^{-05}$	$3.00\text{x}10^{-04}$
110	$2.11\text{x}10^{-05}$	$1.50\text{x}10^{-04}$
111	$9.57\text{x}10^{-06}$	$7.03\text{x}10^{-05}$
112	$4.09\text{x}10^{-06}$	$3.08\text{x}10^{-05}$
113	$1.63\text{x}10^{-06}$	$1.24\text{x}10^{-05}$
114	$5.99\text{x}10^{-07}$	$4.57\text{x}10^{-06}$
115	$2.02\text{x}10^{-07}$	$1.54\text{x}10^{-06}$
116	$6.12\text{x}10^{-08}$	$4.67\text{x}10^{-07}$
117	$1.64\text{x}10^{-08}$	$1.25\text{x}10^{-07}$
118	$3.82\text{x}10^{-09}$	$2.91\text{x}10^{-08}$
119	$7.39\text{x}10^{-10}$	$5.64\text{x}10^{-09}$
120	$1.13\text{x}10^{-10}$	$8.65\text{x}10^{-10}$

Each of the above variables is a constituent for the calculation of risk. For a unit intake of a radionuclide at age x_i, an absorbed doses rate $\dot{D}(x)$ is assigned to a target tissue. This dose rate

varies continuously with age post-exposure. Thus, to calculate the cancer risk resulting from an exposure at the stated age is as follows:

$$r_a(x_i) = \frac{\int_{x_i}^{\infty} \dot{D}(x) r(x) S(x) dx}{S(x_i)} \qquad \text{EQ. 15}$$

where $r_a(x_i)$ is the cancer risk due to a unit absorbed dose in Gy^{-1} at age x, $r(x)$ is the LAR value at the respective ages, and $S(x)$ is the survival function at the respective ages. For high-LET producing radionuclide, the absorbed dose rate is a combination of the low-LET radiation dose rate plus the RBE modified high-LET radiation dose rate.[2] To calculate the age-averaged risk coefficient for a unit intake of activity at age x_i, $r_a(x_i)$ is a weighted mean that is calculated as follows:

$$r_a(x_i) = \frac{1.05 r_{ma}(x_i) u_m(x_i) S_m(x_i) + r_{fa}(x_i) u_f(x_i) f(x_i)}{1.05 u_m(x_i) S_m(x_i) + u_f(x_i) S_f(x_i)} \qquad \text{EQ. 16}$$

where $r_{ma}(x_i)$ is the male risk per unit activity at age x_i and $r_{fa}(x_i)$ is the female risk per unit activity at age x_i. The usage and survival functions for males and females are represented as $u_m(x_i)$, $S_m(x_i)$, $u_f(x_i)$, and $S_f(x_i)$ respectively. The value 1.05 represents the male-to-female sex ratio at birth. [2]

The sex-averaged risk coefficients can then be integrated and divided by the lifetime intake to yield the average lifetime, sex-averaged risk coefficient for a radionuclide intake, $\overline{r_a}$, as follows:

$$\bar{r_a} = \frac{\int_0^\infty u(x) r_a(x) S(x) dx}{\int_0^\infty u(x) S(x) dx} \quad \text{EQ. 17}$$

For this calculation, it is assumed that the intake results from a constant environmental concentration, and that the population of interest is stationary with fixed gender-specific survival functions and cancer mortality rates. [2]

2.6. Relative Biological Effectiveness

Relative Biological Effectiveness (RBE) is a dimensionless quantity defined as the quantification of the influence of radiation quality on biological systems. It is the ratio of the dose of reference radiation to produce a certain response to the dose of a specific radiation an individual is exposed to in order to produce an equal response, and is important to consider when attempting to quantify risk to an exposed individual.[26] To determine this value, it is important that all other values be held as constant as possible. RBE is a function of radiation quality, which increases with linear energy transfer (LET), also referred to as linear collision stopping power. Radiation quality can be determined by finding the energy imparted to matter divided by the length of the track of the charged particle over which the energy is lost.[26] The maximum RBE is usually reached near an LET of 100 keV μm^{-1}, then declines with increasing LET.[26] While LET is deemed a relatively good indicator of the RBE of radiation, it does not accurately account for energy deposited.

The RBE is essential in radiation protection and is used "to provide a means of determining occupation dose limits for high-LET radiation from accepted limits for low-LET radiation…and to provide a means by which the doses of radiation of different quality might be added."[26] The main difference between high-LET and low-LET is the amount of energy deposited along the track of the particle. This amount of deposited energy can vary based on particle time and energy of the particle. Thus, the RBE for high- and low-LET radiations differ. The effect of LET on RBE in

humans can be visualized through the relationship between average-LET in water and RBE. The following table, summarized from National Council on Radiation Protection and Measurements (NCRP) Report 104, visualizes this relationship.

Table 9. The average LET-RBE relationships in water [21]

Average LET in water (keV μm^{-1})	Relative biological effectiveness (RBE)
3.5 or less	1
3.5 to 7.0	1 to 2
7.0 to 23	2 to 5
23 to 53	5 to 10
53 to 175	10 to 20

High-LET radiations have a significantly higher impact RBE, as they are slower moving, depositing more energy due to causing more ionizations per track.[27] High-LET radiations include alpha particles. Alpha particles are the product of radioactive decay of several different types of radionuclides, including ^{235}U. Thus, in the calculation of risk to an exposed individual, the RBE of the types of radiation emitted by the radionuclide to which one is exposed is essential to consider. Low-LET radiations, such as electrons and photons, are important to consider as well, as there is significant potential to encounter them in both medical exposures and environmental exposure.[28] However, quantifying the effect of low-energy, low-LET particles on mutagenesis and carcinogenesis has proven difficult, and work continues on improving methods to quantify and analyze the effects. While it was originally assumed that the RBE of photons and electors was the same for all energies, further studies have shown this to not be the case.[28] This consideration of low-LET radiation is important, as there are many naturally occurring or medically employed radionuclides that produce such radiations. In the scope of this report, these include tritium and iodine.[28]

Recommendations from ICRP *Publication 60* [13] establish the RBE value for all tissues for alpha particles to be 20, save for leukemia and breast, which are stated to be 1 and 10, respectively.[2] Therefore, EPA has followed this guidance, utilizing these values in the calculation of risk coefficients in FGR 13, and they have thus also been used in the recreation of the FGR 13 values in this report.

2.7. Risk per Unit Dose

The direct comparison of ICRP's effective dose to FGR 13's lifetime risk coefficients is not possible with the values in the units of sieverts (Sv). In order to compare ICRP's effective dose to FGR 13's lifetime risk, a coefficient known as the "risk per unit dose" must be either multiplied across the effective dose values, or divided out from the risk coefficients in order to get the values into the same units for comparison. This coefficient is applied to the dose, in the case of this report, the lifetime committed effective dose, in order to estimate the risk from the exposure. Much like the tissue-weighting coefficients, these risk per unit dose coefficients correlate to each tissue site associated with a specific cancer, and are summed over the entire body. However, differing from w_T, these risk per unit dose coefficients are sex-specific. Risk per unit dose coefficients are also age-averaged, and specific to mortality and morbidity. The FGR 13 risk per unit dose values for mortality and morbidity can be found in Table 10 and Table 11.

Table 10. Age-averaged site-specific cancer mortality risk estimates (cancer deaths per person-Gy^{-1}) from low-dose, low-LET uniform irradiation of the body. [2]

Site	Males	Females	Combined Genders
Esophagus	7.30×10^{-4}	1.59×10^{-3}	1.17×10^{-3}
Stomach	3.25×10^{-3}	4.86×10^{-3}	$4.07\times10^{--3}$
Colon	8.38×10^{-3}	1.24×10^{-2}	1.04×10^{-2}
Liver	1.84×10^{-3}	1.17×10^{-3}	1.5×10^{-3}
Lung	7.71×10^{-3}	1.19×10^{-2}	9.88×10^{-3}
Bone	9.40×10^{-5}	9.60×10^{-5}	9.50×10^{-5}

Skin	9.51×10^{-5}	1.05×10^{-4}	1.00×10^{-4}
Breast	-	9.90×10^{-3}	5.06×10^{-3}
Ovary	-	2.92×10^{-3}	1.49×10^{-3}
Bladder	3.28×10^{-3}	1.52×10^{-3}	2.38×10^{-3}
Kidney	6.43×10^{-4}	3.92×10^{-4}	5.15×10^{-4}
Thyroid	2.05×10^{-4}	4.38×10^{-4}	3.24×10^{-4}
Leukemia	6.48×10^{-3}	4.71×10^{-3}	5.57×10^{-3}
Residual	1.35×10^{-2}	1.63×10^{-2}	1.49×10^{-2}
Total	4.62×10^{-2}	6.83×10^{-2}	5.75×10^{-2}

Table 11. Age-averaged site-specific cancer morbidity risk estimates (cancer deaths per person-Gy) from low-dose, low-LET uniform irradiation of the body. [2]

Site	Males	Females	Combined Genders
Esophagus	7.69×10^{-4}	1.68×10^{-3}	1.23×10^{-3}
Stomach	3.61×10^{-3}	5.40×10^{-3}	4.53×10^{-3}
Colon	1.52×10^{-2}	2.25×10^{-2}	1.89×10^{-2}
Liver	1.94×10^{-3}	1.23×10^{-3}	1.58×10^{-3}
Lung	8.12×10^{-3}	1.26×10^{-2}	1.04×10^{-2}
Bone	1.34×10^{-4}	1.37×10^{-4}	1.36×10^{-4}
Skin[a]	9.51×10^{-5}	1.05×10^{-4}	1.00×10^{-4}
Breast	-	1.98×10^{-2}	1.01×10^{-2}
Ovary	-	4.17×10^{-3}	2.13×10^{-3}
Bladder	6.55×10^{-3}	3.04×10^{-3}	4.76×10^{-3}
Kidney	9.88×10^{-4}	6.03×10^{-4}	7.91×10^{-4}
Thyroid	2.05×10^{-3}	4.38×10^{-3}	3.24×10^{-3}
Leukemia	6.54×10^{-3}	4.75×10^{-3}	5.63×10^{-3}
Residual	1.91×10^{-2}	2.29×10^{-2}	2.11×10^{-2}
Total	6.51×10^{-2}	1.03×10^{-1}	8.46×10^{-2}

[a]Skin cancer morbidity risk only considers fatal cancers. See section on RBE.

3. METHODOLOGY

The main calculations and analyses involved in this work include a detailed analysis of dose rate behavior, a calculation of acute exposure effective doses, chronic effective doses, and risk coefficients, as well as a comparison of the CEDs to the risks. Two data sources are investigated herein, the first informed by ICRP *Publication 60* and *71* methodologies, and the second informed by ICRP *Publication 103* methodologies. Figure 6 depicts the general steps taken in the reproduction of the risk coefficients for FGR 13, as well as the steps taken in calculation of the ICRP 103-based risk coefficients. Beginning from the absorbed dose rates, the data is formatted and manipulated before the FGR 13 risk equations are applied to yield the coefficients from a uniform exposure. Figure 7 depicts the steps taken in the calculation of the corresponding effective dose calculations for both the ICRP *Publication 60* dose rates and the ICRP *Publication 103* dose rates, following the corresponding methodologies to calculate the effective doses.

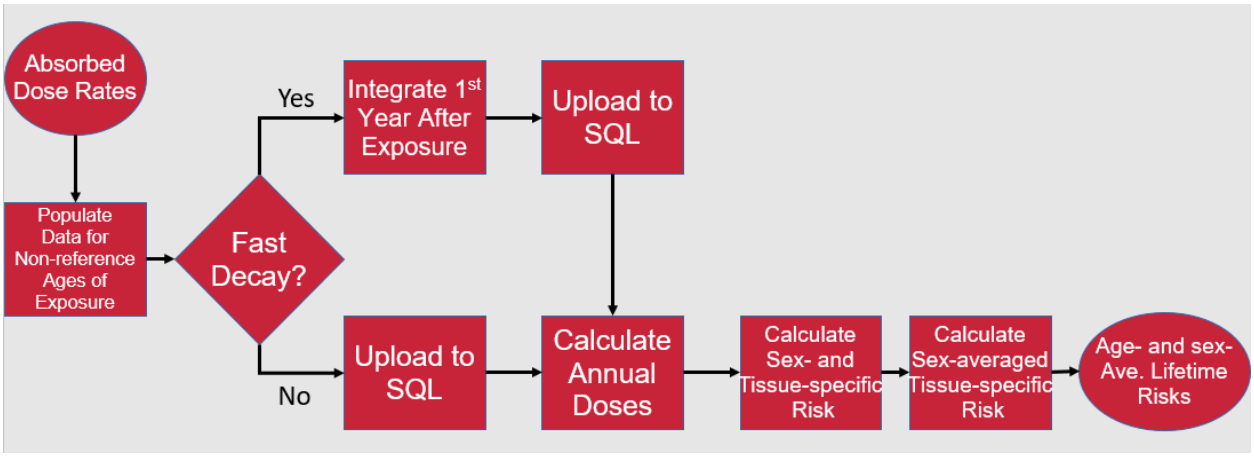

Figure 6. Flow chart of the risk calculations for a uniform exposure beginning from the generation of the absorbed dose rates. SQL here represents the SQL Server software used for data management.

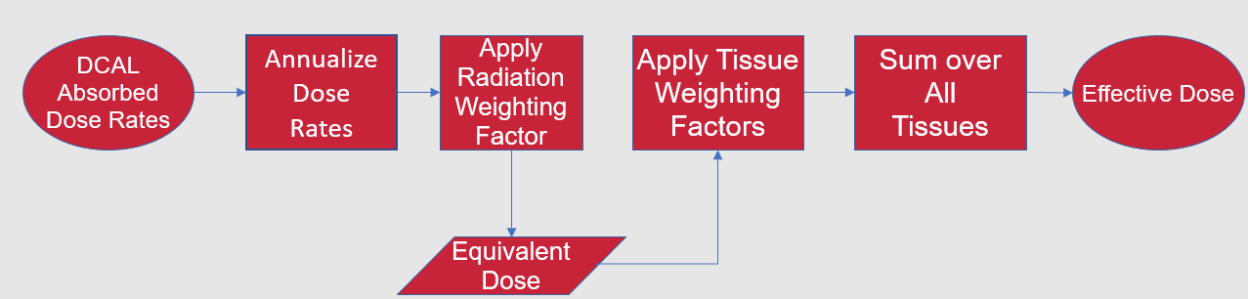

Figure 7. Flow chart of the effective dose calculations for a uniform exposure beginning from the generation of the absorbed dose rates. SQL here represents the SQL Server software used for data management. For chronic exposures, usage is considered in the annualization process.

Several programs were utilized throughout the course of this work at various steps of data manipulation and calculation, including Powershell, Matlab, Visual Studio, DCAL, and SQL Server. Two sets of data were analyzed within this work. The first set included preliminary dose rate data for updated biokinetic models, courtesy of ORNL.[29] In order to benchmark the code utilized to determine risk coefficients from this preliminary data, a corresponding data set generated in DCAL and corresponding to the data informing FGR 13 was leveraged.

Beginning with FGR 13 data, absorbed dose rates through life for all radionuclides of interest at the six reference ages 100 d, 1 yr, 5 yr, 10 yr, 15 yr, and 20 yrs (25 yrs for bone-seeking radionuclides) were generated through the use of the DCAL software. As well, the program was used to generate intermittent age values for each intermediary full-year of age, so as to eliminate any additional variance from interpolation within Matlab later on. This would provide the most accurate and robust set of data possible with which to build the program used to recreate the FGR 13 risk coefficients. DCAL terminates dose rates calculations for a given exposure based on one of two conditions: (1) either end of life has been reached, or (2) the calculated dose rates have all reached a negligible value, defined in the system as 0 dose rate. Typically, this occurred around values at 10^{-31} Gy·d^{-1}·Bq^{-1}. Dose rates are calculated for 31 specified target tissues at time intervals

determined in the default exposure data files stored in the DCAL system. Each year of exposure was stored in its own individual file and, with the original program being written in Fortran, it was necessary to reformat these files into a format that could be implemented in the programs used later in the methodology. To accomplish this, a Powershell script was utilized to pull the time steps, tissue names, and dose rates for each specified organ in each dose rate file. The script looped through each exposure file in a designated folder, compiling them into one singular text file with time step and dose rate concatenated vertically in their own respective columns. From there, this text file was imported into Excel for further manipulation to make it usable in the created Matlab code.

Several modifications to the imported data were necessary before calculations could begin. For calculating risk, values for the colon and residual tissues are needed. DCAL does not calculate the colon independently, so it must be calculated manually external to the code, and the resultant column added to the file. The following formula was used to conduct this calculation[2]:

$$Colon\ Value = 0.568 * ULI\ Wall + 0.432 * LLI\ Wall \qquad \text{EQ. 18}$$

where *ULI Wall* represents the dose rate to the upper large intestine and *LLI Wall* represents the lower large intestine. The residual tissue dose rate was calculated in a similar manner as the colon. The residual is comprised of the muscle tissue, the pancreas, and the adrenals and each tissue is weighted in the following manner[2]:

$$Residual\ Value = 0.3334 * Muscle + 0.3333 * Pancreas + 0.3333 * Adrenals \qquad \text{EQ. 19}$$

The ICRP *Publication 103*-based dose coefficients from ORNL, provided by Dr. Derek Jokisch and herein referred to as the preliminary data, contain absorbed dose rates for significantly

more tissues than the data for FGR 13 does, with the residual being calculated in the same manner as for the FGR 13 data.[30] Therefore, in order to allow for a single Matlab and Visual Studio program to be utilized for both the preliminary dataset and the FGR 13 dataset, keeping formatting consistent between the two data sets was essential. To achieve this, additional columns representing the additional tissues in the preliminary dataset were added to the FGR 13 data, which were then populated with zeroes as place holders before sending it to Matlab. Due to the nature of the shorter-lived radionuclides such at ^{131}I decaying to zero dose at roughly two years post-exposure, additional rows of the last reported non-zero dose rate from DCAL were added for improved accuracy of interpolations within Matlab when populating the remaining years of life. These additional rows were populated with the last non-zero dose rate value, as populating with zeros generated null value and negative value Matlab errors for the dose rates when generating the ages of exposure past the adult reference age. For longer lived radionuclides such as ^{90}Sr and ^{235}U this was unnecessary and no additional rows were added.

For ages past the adult reference age, the biokinetics are age averaged, and thus the assumption is made that the biokinetics do not change all the way through end of life (EOL), as this study does not consider variables associated with the adult subset of a geriatric population, consistent with dose rate coefficients utilized in the risk calculations approach in FGR 13. Thus, it is acceptable to repeat the values for the adult reference age and use these values to populate the ages of exposure beyond the adult reference age. To ensure accuracy when this is done in Matlab, several exposure ages were hand-added to the end of the exposure data files in order to supply datapoints for Matlab's griddata interpolating feature that was used to populate the remaining ages of exposure.

Reformatting of the preliminary data from Oak Ridge National Laboratory (ORNL) differed from reformatting conducted for FGR 13. The data received from ORNL was already in a format that was mostly usable. To improve interpolation for years of exposure beyond the final reference age, values for the last reference age were repeated in five-year increments and appended to the file through the use of a secondary Powershell script. Again, this was done to increase accuracy in Matlab when populating ages of exposure past the adult reference age.

After completion of reformatting of the initial files, Matlab was employed to populate the remaining exposure ages (i.e., 21/26 - EOL) to year 105 for the FGR 13 dataset. For the preliminary dataset informed by the ICRP *Publication 103* methods, griddata was used to interpolated between the reference age groups to generated exposure data for the intermittent ages. This was not necessary for the FGR 13 data, as intermediate ages of exposure can be calculated directly in DCAL. This functionality of DCAL was utilized for the FGR 13 data so as to avoid any potential errors generated in the interpolation. A natural scattered interpolant method was used within the griddata functionality to calculated these extrapolated dose rates for the FGR 13 data. Once this was completed, the data was fed to a secondary Matlab program which ran a Piecewise Cubic Hermite Interpolating Polynomial (PCHIP) spline in order to populate additional intermediate values within each age of exposure out to EOL.[31] The combination of griddata and PCHIP was chosen to replicate the 3-D interpolation that takes place in Matlab. PCHIP is a shape-preserving Hermite spline, ensuring the fewest anomalies in the data during curve fit. This program was also used to apply the high-LET factors to the necessary tissues for ^{235}U, a radionuclide that results in the production of alpha particles during the course of its decay. These values include a factor of 1 for the red bone marrow, a factor of 10 for breast tissue, and a factor of 20 for all other tissues.

This modified and expanded dataset for each radionuclide was then saved under the name "Exposure Data" for upload to a SQL Server database.

Due to the massive amounts of data needed for this work, SQL Server and Visual Studio were chosen to handle the data manipulation and analysis over Matlab, as the programs are superior for handling large amounts of data at any one given time and allow for a shorter processing time than Matlab. Along with the exposure data, the usage function data, survival function data, and LAR data for both males and females were each uploaded to their own respective tables in SQL Server.

For ease of data manipulation, a graphic user interphase (GUI) was developed in Visual Studio to analyze and manipulate the exposure data in order to calculate the risk coefficients. The GUI allows the user to select which dataset they wish to work with, male or female data, the usage type desired, the radionuclide of interest, the ages of exposure to annualize, and the tissues of interest to the calculations. The first tab of the GUI, used to calculate the annual doses throughout lifetime at various ages of exposure, can be seen in Figure 8.

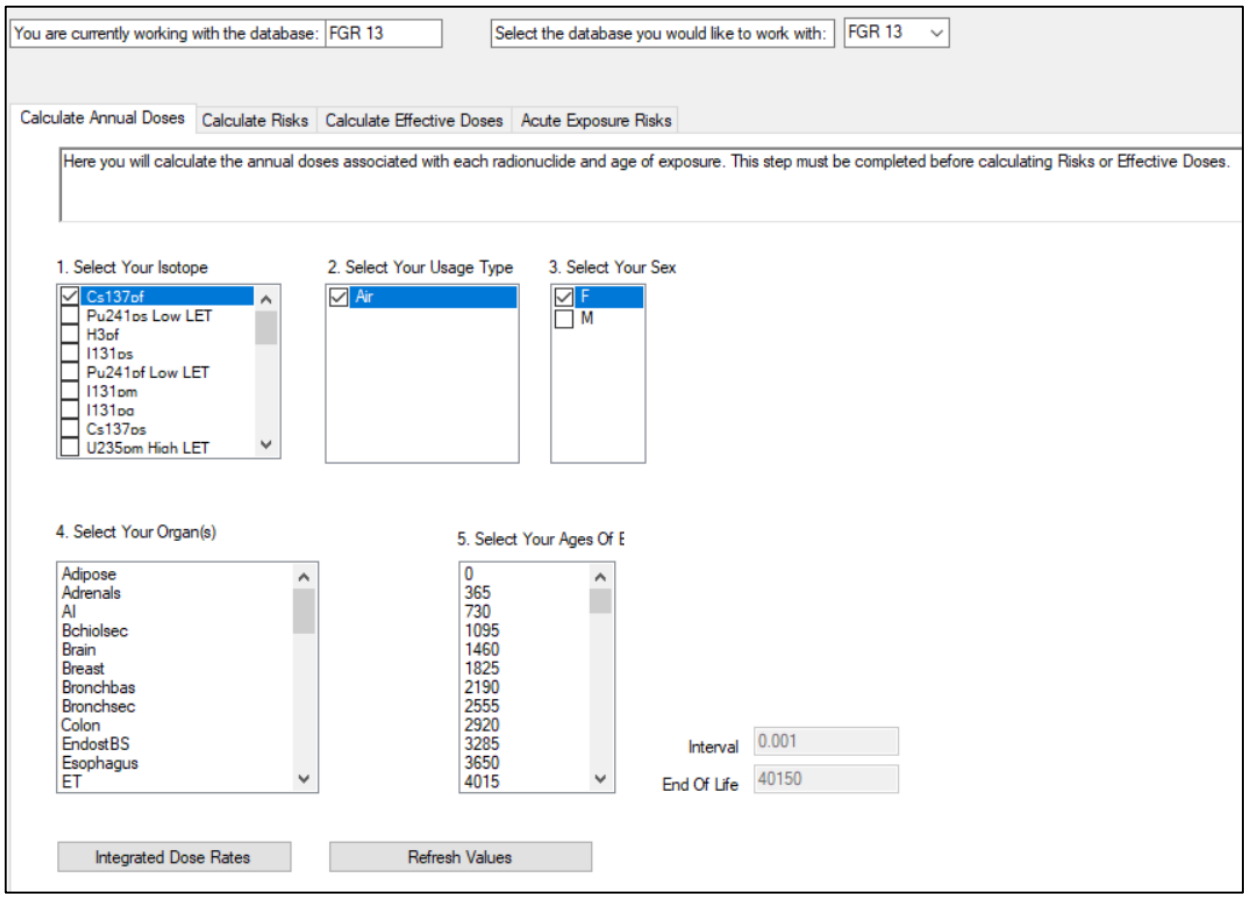

Figure 8. A GUI developed by A. Kalinowski in Visual Studio used to calculate the annual doses for various radionuclides, organs, and ages of exposure.

The first step in recreating the FGR 13 risk coefficients required that the exposure data be annualized, yielding a total absorbed dose per year based on an acute exposure for each age of life. In order to do this, an Akima spline from the Extreme Numerics .Net package was utilized within Visual Studio with a set integration period of 1 year, and a final integration point of 110 years.[32] An Akima spline is a type of cubic spline. Like PCHIP, it is a Hermite interpolating cubic spline that yield specific values for the first derivative at each data point. This spline type was chosen based on its accuracy, lack of anomalies, and similarity to PCHIP.[32] The calculated values were saved to another table within the SQL Server database entitled "NonModifiedAnnualDoses." The modifier "NonModified" is used here to represent that these data have not been modified by the

usage or survival data. The calculated values represent the annual absorbed dose from an acute exposure at each initial age of exposure.

The Akima spline application and further integration revealed an issue, particularly with fast decaying or fast-clearing radionuclides. That is, for the first year after an intake, be it inhalation or ingestion, the drop off in the dose rate was so rapid over such a short period of time for radionuclides such as ^{131}I that the spline over-compensated, dropping negative in an attempt to fit the curve appropriately due to a loss of numerical significance. This resulted in negative doses after the integration. This result is both incorrect and impossible. To address this issue, a third Matlab program was written to integrate the first year of data independently using a trapezoidal integration method, and this value was uploaded to the integrated doses table separately. To ensure no double counting of the first-year data for the necessary radionuclides, the Akima spline and integration was adjusted to exclude the first year after exposure in its calculation of the annual doses. The validity of this alternative method was tested on a long-lived radionuclide, ^{90}Sr, to ensure that replacing the first-year data with the trapezoidal method would not alter the final risk value. The difference between the two resultant risk coefficient values for the whole body was less than half a percent, thus confirming that this trapezoidal approach is viable. The radionuclides this method applied to include all intake classes of ^{131}I, ^{137}Cs, ^{3}H, and the fast-clearing solubility forms as well as the ingestion pathway for ^{235}U for both high- and low-LET considerations.

Once the annual doses were calculated, SQL Server was used to construct a view that would calculate the annual doses based on a chronic exposure. Here, a chronic exposure is defined as an uptake or exposure at every year of life, and is assumed to be on the first day of that year. To calculate this, SQL Server first applied the appropriate usage and survival functions that corresponded to the appropriate age of exposure and then summed along the total time vector for

each exposure to yield a singular vector of annual values from birth to EOL for each radionuclide, a vector of 109 elements. This vector is dependent on radionuclide, sex, organ/tissue, usage type, and total time. This vector is what was then used to calculate the tissue- and sex-specific risk coefficients from a chronic exposure in a similar manner as is done for the acute exposures.

To manipulate these data used to calculate the risks, a secondary GUI tab was created where specifications for the risk that must be calculated was generated, and can be seen in Figure 9. This tab specifically recreates the FGR 13 risk coefficients based upon a chronic exposure.

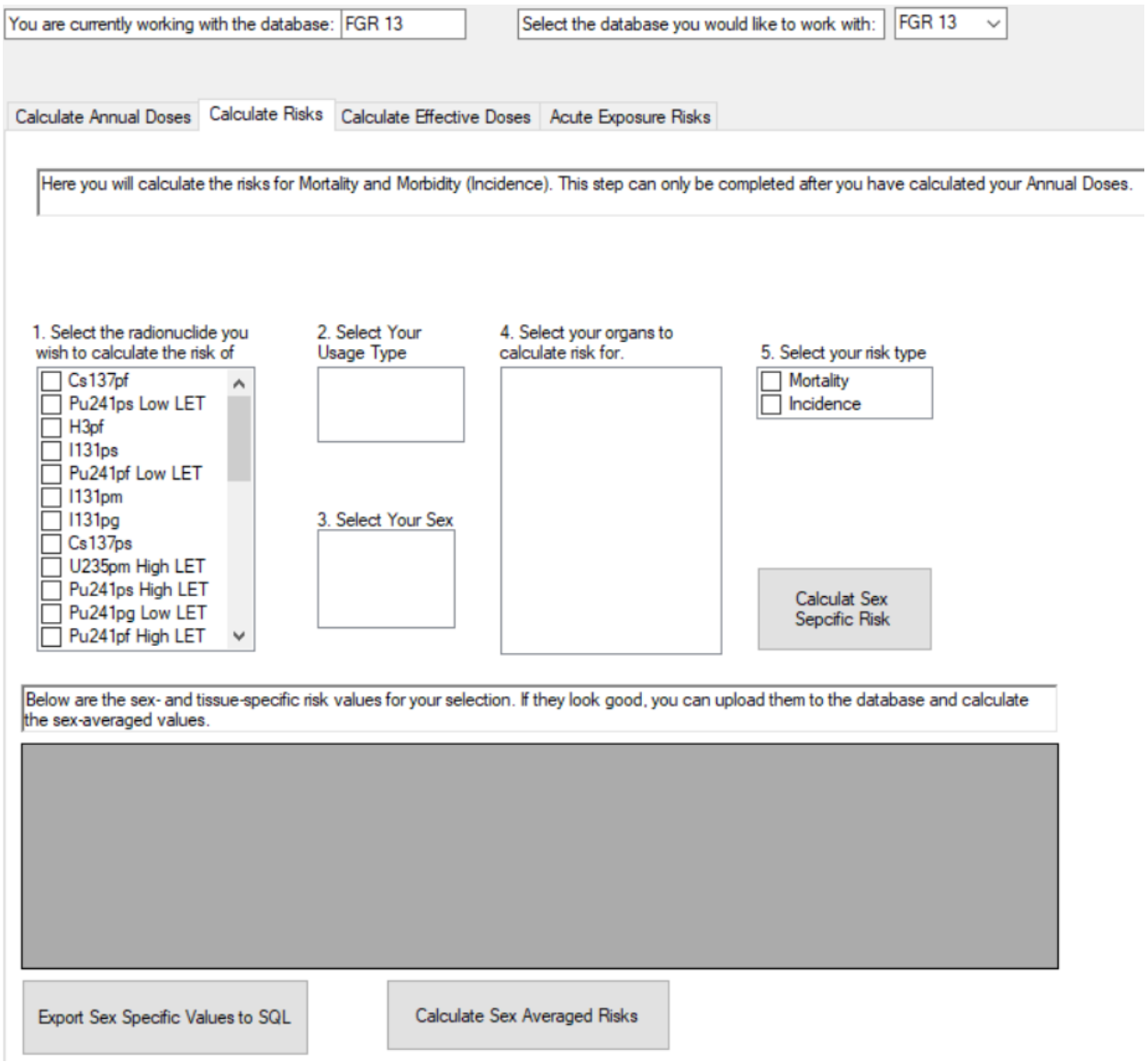

Figure 9. A GUI developed by A. Kalinowski used to calculate the mortality and morbidity risk based on the calculated annual doses.

To calculate the risk coefficients for each sex-specific tissue, the LAR factor must be considered. These factors were applied via another view in SQL server before the final data is referenced by the Visual Studio program. Once referenced, another Akima spline was applied to generate the curve of values to be integrated. This step is identical to the step used to calculate the annual doses, save that the integration period is over the whole lifetime, rather than one-year

increments. This step is taken for both mortality and incidence calculations, as the LAR differs for each risk type.

A secondary calculation takes place here as well. To calculate the lifetime risk coefficient for a chronic intake, the integral described previously must be divided by the lifetime total intake, defined below.

$$Lifetime\ Total\ Intake = \int_0^\infty u(x) * S(x)dx \qquad \text{EQ. 20}$$

where $u(x)$ is the usage function and $S(x)$ is the survival function. This is the last step in calculating the sex- and tissue-specific risk coefficients for a chronic intake, which are then exported to SQL Server.

In SQL server, in order to calculate the sex-averaged risk coefficients, the 1.05 birth ratio of males to females was applied before calculating the average values. The output of this application and calculation is the tissue-specific, sex-averaged, lifetime risk coefficient from a chronic exposure, a total of 14 values for incidence, and 14 values for mortality, each value corresponding to a specific tissue. These values are output to Excel where each set of values for each radionuclide are then summed over all tissues to yield the age- and sex-averaged risk coefficients which can be directly compared to FGR 13 risk coefficients, and a percent difference taken to determine if the calculations are within acceptable limits of one another, as determined by Dr. Keith Eckerman of Oak Ridge National Laboratory (ORNL).

The next computational step necessary is the calculation of the effective doses (*E*). To do this, two sets of views were constructed, one for calculating equivalent and effective for acute exposures, and one for calculating equivalent and effective doses for chronic exposures. Firstly,

the equivalent doses were calculated by applying the ICRP *Publication 60* radiation-weighting factors to the calculated annual doses from the first step in the overall data manipulation. SQL Server was used for calculating the acute exposure committed equivalent doses, as no further integration was needed. The calculated equivalent doses for each age of exposure were simply summed over the dictated commitment period (out to age 70 years for juveniles and a 50 year integration period for adults). Following ICRP *Publication 60* methodologies, the chronic committed equivalent dose was then calculated utilizing another section of Visual Studio code. The difference here is that the commitment period is for the entire lifetime, rather than the predetermined commitment periods. For ages past 60, due to data limitations, the commitment period reduces by one year for each year past 60 of the age at exposure. For example, an exposure at age 80 would only have a 25 year commitment period as age 105 is defined as end of life, and there are no data points beyond that. A third tab was generated in the GUI for manipulation of the equivalent dose data, and can been seen in Figure 10. These calculated committed doses were then exported to SQL Server as well for further manipulation.

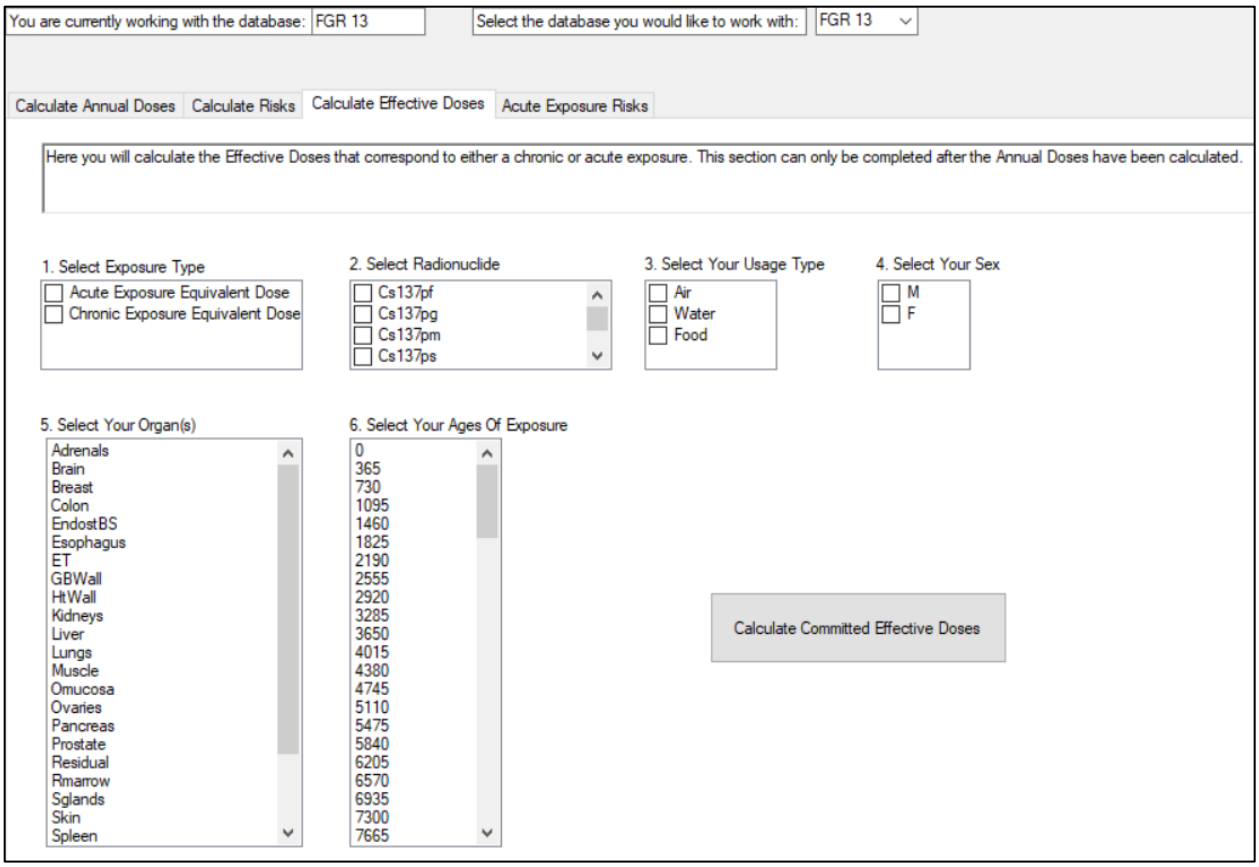

Figure 10. A GUI developed by A. Kalinowski used to calculate acute and chronic exposure equivalent doses.

Once all data driven values are selected, the program runs an Akima spline and integrates over the lifetime to calculate the committed effective dose for either an acute or chronic exposure. These values can be checked against the values generated in ACTCAL for an approximate check of the values. As the committed dose integration period for juveniles is out to age 70 years, and for adults is a 50 year period, having the integration period to EOL (110 years minus the age of exposure), the values are expected to be off marginally. However, they are close enough to point out any glaring errors in the calculations.

Upon calculation of these committed doses for both chronic and acute exposures, the ICRP *Publication 60* tissue-weighting factors were applied to yield the committed effective doses.

Chronic exposures, specifically, were then normalized by dividing by the lifetime intake, as was done in the risk calculation. The final step is then to apply the risk per unit dose conversion factor. For mortality, this value is 0.0575 Gy^{-1} for mortality and for incidence (morbidity) is 0.0846 Gy^{-1}, as defined in FGR 13. Application of this factor allows for a direct comparison to the risk coefficients. A flowchart of the general steps taken to calculate the effective dose, *E*, from the absorbed dose rates can be seen below.

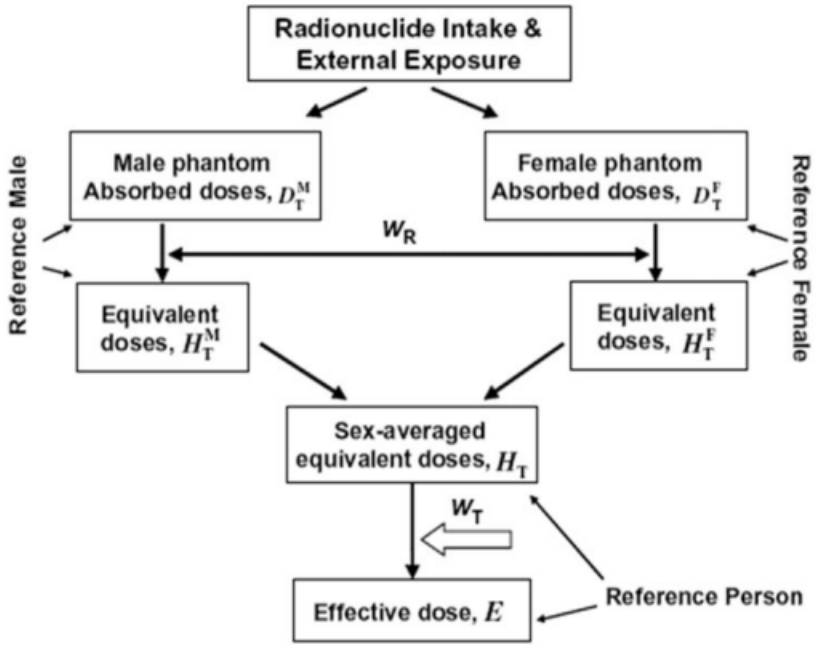

Figure 11. Sex-averaging in the calculation of effective dose, taken from ICRP Publication 147, but applicable to this methodology using ICRP Publication 60.[1, 18]

To compare the risk to the modified committed effective doses, graphical analysis was conducted. The two values were plotted against one another, both for whole body values and for various tissues in order to observe the magnitude of the difference between the two values; risk and committed effective dose. Drastic differences between the CED and the risk points to a lack of reliability on the CEDs to be used as even an approximate indicator of risk. As well, the values

between generations of data were evaluated to determine how the biokinetic changes between generations of data manifest in both the risk and the committed effective doses. For chronic exposures for both generations, percent differences were determined between the risk and the committed CED for a chronic exposure. The larger the percent difference, either positive or negative, the less effective the CEDs are in representing the risk from a chronic exposure.

4. RESULTS AND DISCUSSION

Each subsequent subsection of the results builds upon one another, beginning with the FGR 13 absorbed dose rate coefficients for acute exposure. From there, the resultant acute exposure dose rates are annualized and the doses from a chronic exposure calculated. These acute and chronic exposure doses are then used as the basis for the risk and committed dose calculations. These steps are repeated for the preliminary data, before all of the data is brought together for a final comparison between the FGR 13 and preliminary data. The order of the results presented here reflects this step-by-step building of the resultant data. A summary of data presented is provided in Table 12.

Table 12. Summary of the data presented in the Results.

Data Source	Data Presented
FGR 13	Dose Rates from an Acute Exposure
FGR 13	Annualized Dose Rates from an Acute Exposure
FGR 13	Dose Rates from a Chronic Exposure
FGR 13	Risk Coefficients from a Chronic Exposure
FGR 13	Risk and Committed Effective Dose Comparison from an Acute Exposure
FGR 13	Risk and Committed Effective Dose Comparison from a Chronic Exposure
ICRP *Publication 103* Data	Dose Rates from an Acute Exposure
ICRP *Publication 103* Data	Dose Rates from a Chronic Exposure
ICRP *Publication 103* Data	Comparison of FGR 13 and ICRP *Publication 103* Risk Coefficients from a Chronic Exposure
ICRP *Publication 103* Data	Risk and Committed Effective Dose Comparison from an Acute Exposure
ICRP *Publication 103* Data	Risk and Committed Effective Dose Comparison from a Chronic Exposure

FGR 13 and ICRP *Publication 103* Data	Comparison of Risk Coefficients with Respect to Time between Both Data Generations

In the following section are multiple graphs reflecting the patterns of the data. All plots are plotted along a semilog-y plot. For plots presented in sections 4.1.1. and 4.5.1., the legends represent the ages of exposure plotted. For the risk and committed doses plots, "risk" refers to FGR 13 calculated risk coefficients and "CED" refers to ICRP *Publication* 60 (for DCAL informed data) or ICRP *Publication 103* (for ICRP *Publication 103* dose coefficient informed data) methodology calculated committed effective doses. For plots comparing FGR 13 data to the preliminary data, legends are labeled with "preliminary" and "13" identifiers to distinguish the data generations.

The same naming convention for solubility classes is maintained for all plots where the radionuclide is followed by the usage type and solubility class. A summary of these handles can be seen in Table 13 below. Here 'p' stands for public, defining the type of exposure, and 'f', 'm', 's', and 'g' define the solubility type.

Table 13. Summary of naming conventions for radionuclide plots.

Handle	Usage Type	Uptake Mode	Summary
pf	Air	Inhalation	Fast lung clearance
pm	Air	Inhalation	Moderate lung clearance
ps	Air	Inhalation	Slow lung clearance
pg	Food	Ingestion	Exposure via food
pg	Water	Ingestion	Exposure via tap water

4.1. FGR 13 Dose Rate Coefficient Analysis

Prior to any risk calculation, analysis and characterization of the dose rate coefficients for acute exposures was conducted. In order to visualize the behavior of the absorbed dose rates, the DCAL generated data, once populated through the use of the griddata and PCHIP programs, was then plotted through the use of Matlab. This was done to visualize the biokinetic behavior of the radionuclides in the pertinent tissues used to calculate the risk coefficients at various ages of exposure, as well as to verify the populated dose rate data to ensure they fit with the trend established by the DCAL generated data. Non-reference ages were plotted to ensure consistency in all adult ages after the application of the griddata and PCHIP programs, as the adult dose coefficients should all be the same as the first adult age (20 or 25, depending on whether or not the radionuclide is a bone-seeker). This plotting was also used to visualize the behavior in the specifically sought out tissues for each radionuclide, i.e., the thyroid for ^{131}Iodine and the bone surface for ^{90}Sr, as well as others.

It is important to note that for this work, the dose rates that decayed to 0 dose before the end of life were populated with the last non-zero value as generated by DCAL. Thus, these dose rates will never drop completely to zero. Instead, they drop to a value that is "essentially" zero. This is one of the data limitations based on the programs used to format and manipulate the given data.

4.1.1. Acute Exposures

Further biokinetic compartments for select radionuclides in this section can be found in Appendix B.

4.1.1.a ^{131}I

No difference is seen between males and females for the thyroid for ingestion or inhalation, which is expected, as the reference phantom used to calculated the absorbed doses in DCAL uses

a sex-averaged phantom, where only the gonads differ between males and females. A similar comparison for all radionuclides was conducted to ensure that no anomalies were present in the dose rate data between males and females for all solubility classes and exposure types. Figures Figure 12 (a), (b), and (c) depict the trend in the absorbed dose rates seen in the thyroid for fast-clearing inhalation, slow-clearing inhalation, and tap water ingestion for females. The corresponding plots for males can be found in Appendix A. Anomalous dips are seen for fast-clearing iodine as a result of the limitations on the curve fitting power of griddata and PCHIP in Matlab. Ingested iodine for the adult ages shows a brief equilibrium before dropping off to the "essentially" zero point.

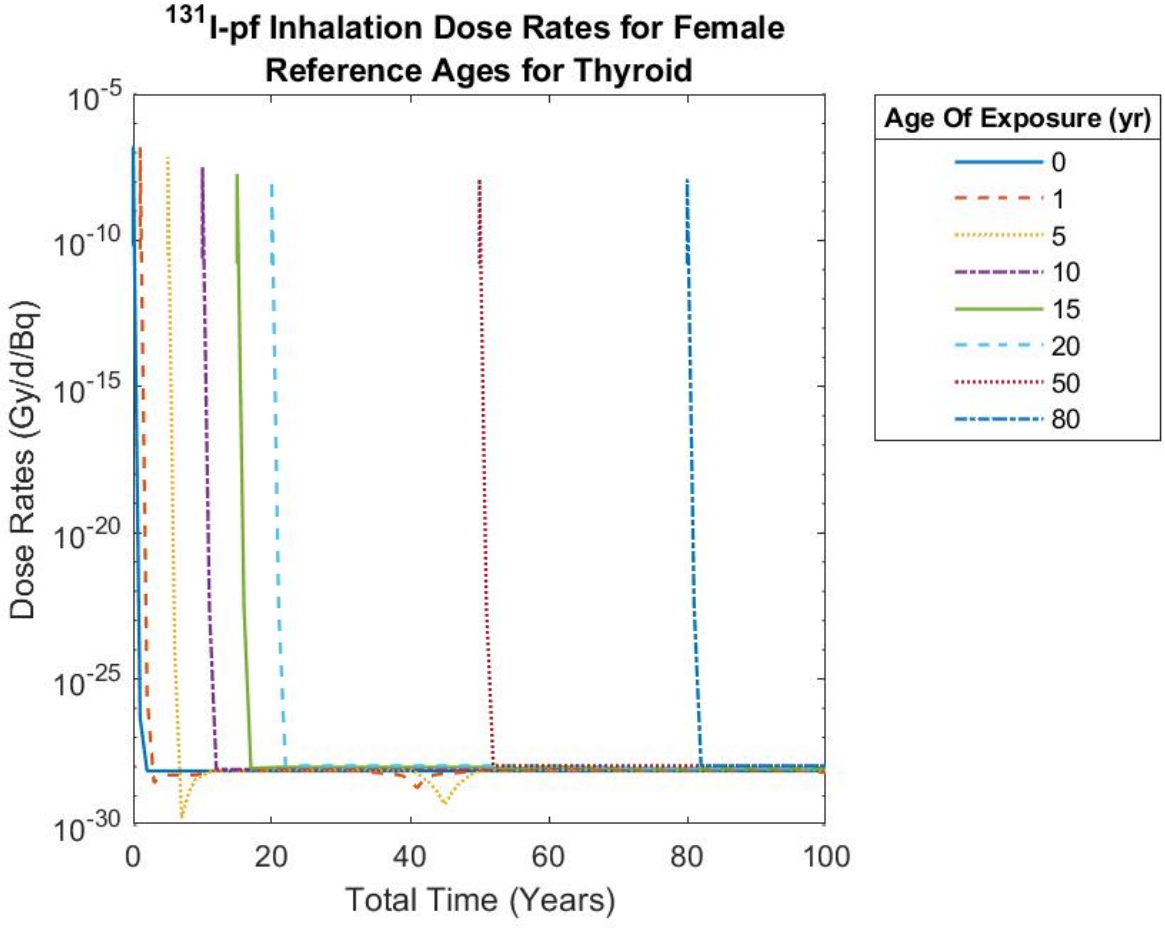

(a)

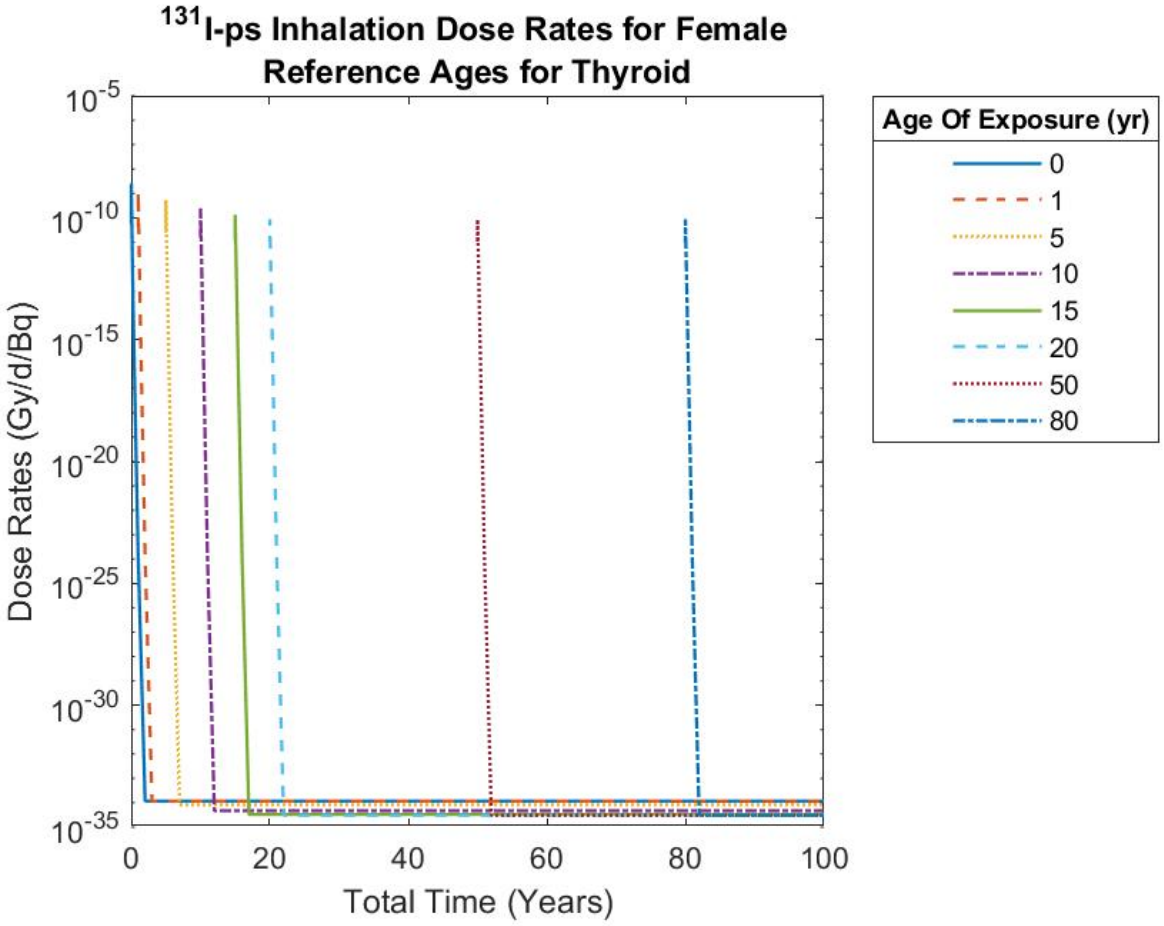
131I-ps Inhalation Dose Rates for Female
Reference Ages for Thyroid
Dose Rates (Gy/d/Bq)
Total Time (Years)
Age Of Exposure (yr)
0
1
5
10
15
20
50
80

(b)

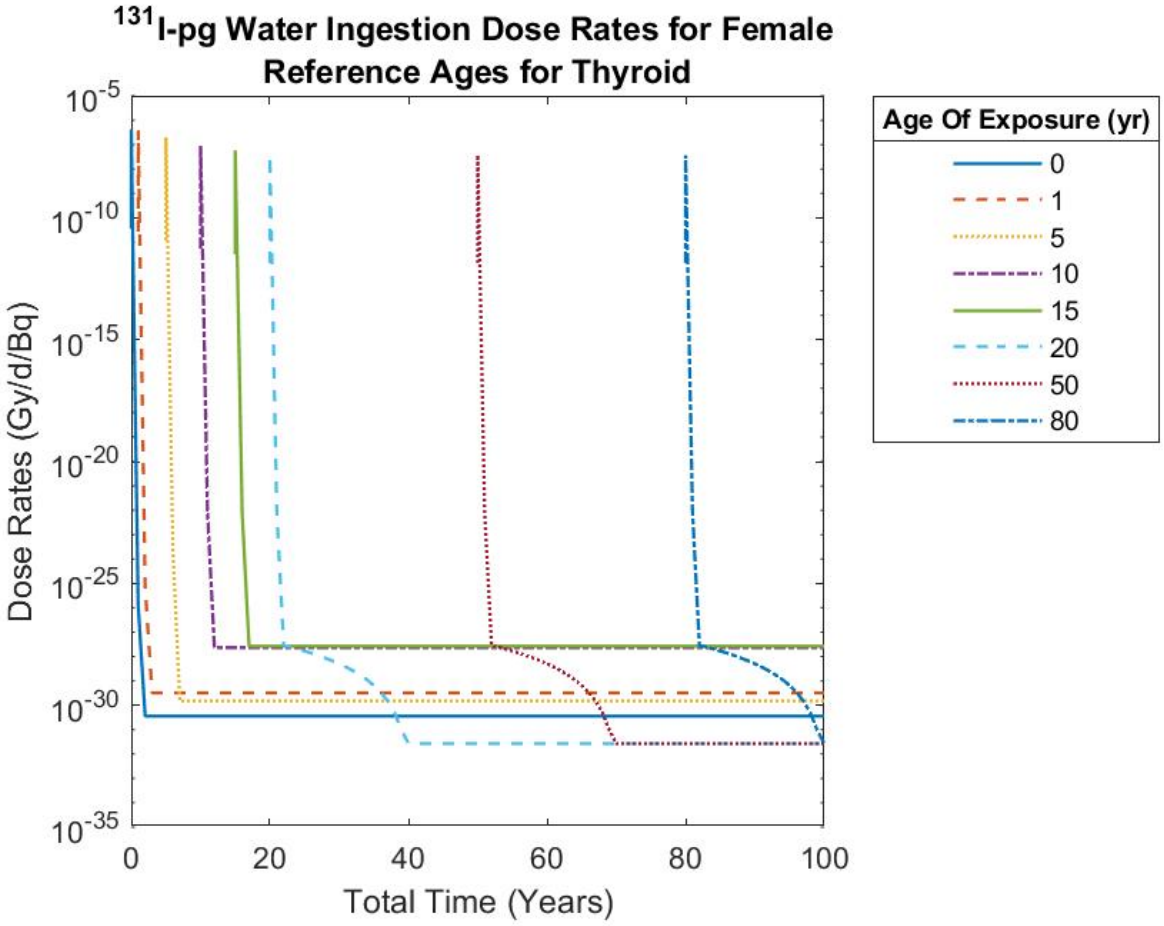

(c)

Figure 12. Absorbed dose rates in the female thyroid for (a) fast and (b) slow-clearing inhaled ^{131}I as well as (c) tap water ingested ^{131}I.

Iodine's behavior post exposure followed similar trends for absorbed dose rates in all soft tissues. For fast-clearing ^{131}I, the lungs show a similarly steep drop off in the dose rates. However, due to iodine being a thyroid seeker, the rate of dose rate drop off in the thyroid is approximately five orders of magnitude lower than in the other soft tissues, such as the lungs, and can be seen in Appendix A. This trend is consistent for all solubility classes and exposure types, save slow-clearing iodine, which has a consistent magnitude drop of approximately five orders across all tissues, including the thyroid, and can be seen in Appendix A. This is anticipated due to the incredibly short physical half-life of ^{131}I of approximately 8 days, and an effective half-life of approximately 5.5 days.

DCAL was used to generate the biokinetic plot of the activity versus time for ^{131}I in the thyroid in order to validate the above stated absorbed dose rate data. There is a sharp peak after inhalation as the radionuclide is delivered to the thyroid, followed by a rapid decrease in activity over the next 23 or so days post the peak in activity. This is a result of the rapid decay of ^{131}I. The trend seen in this activity with respect to time is consistent through all ages. A similar trend is seen in all tissues and ages generated by DCAL; a steep peak followed by a rapid drop off in activity.

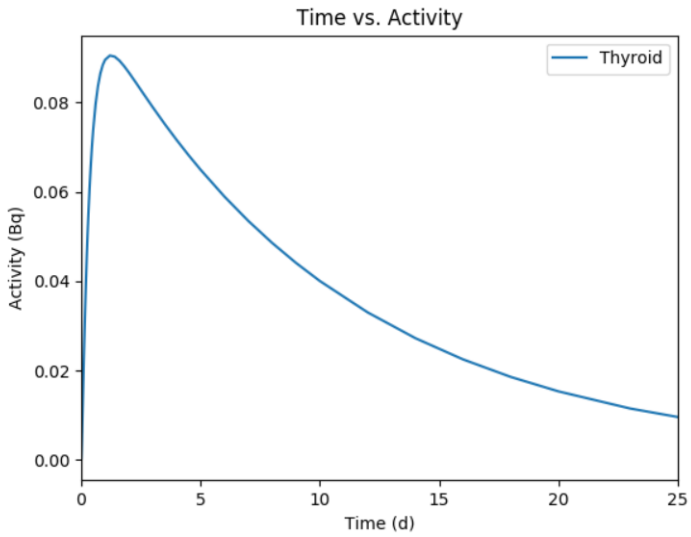

Figure 13. DCAL generated biokinetic activity of inhaled ^{131}I with respect to time in the thyroid at age 5 years.

4.1.1.b. Tritium

With tritium's behavior mimicking that of water in terms of metabolism through the body after an internal exposure, it was expected that within each solubility class and exposure type the absorbed dose rates will be similar. That is, no specific tissue will be targeted, as tritium evenly distributes through the soft tissues through its water adjacent behavior. A depiction of this trend for fast- and moderate-clearing inhaled tritium can be found in Appendix A. For most cases, this proved true, save for slow-clearing inhalation. For this, the magnitude of the stomach's drop in

absorbed dose rate is several orders of magnitude higher than the other soft tissues, as seen in Figure 14. All other soft tissues follow the same trend as seen in the breast, below.

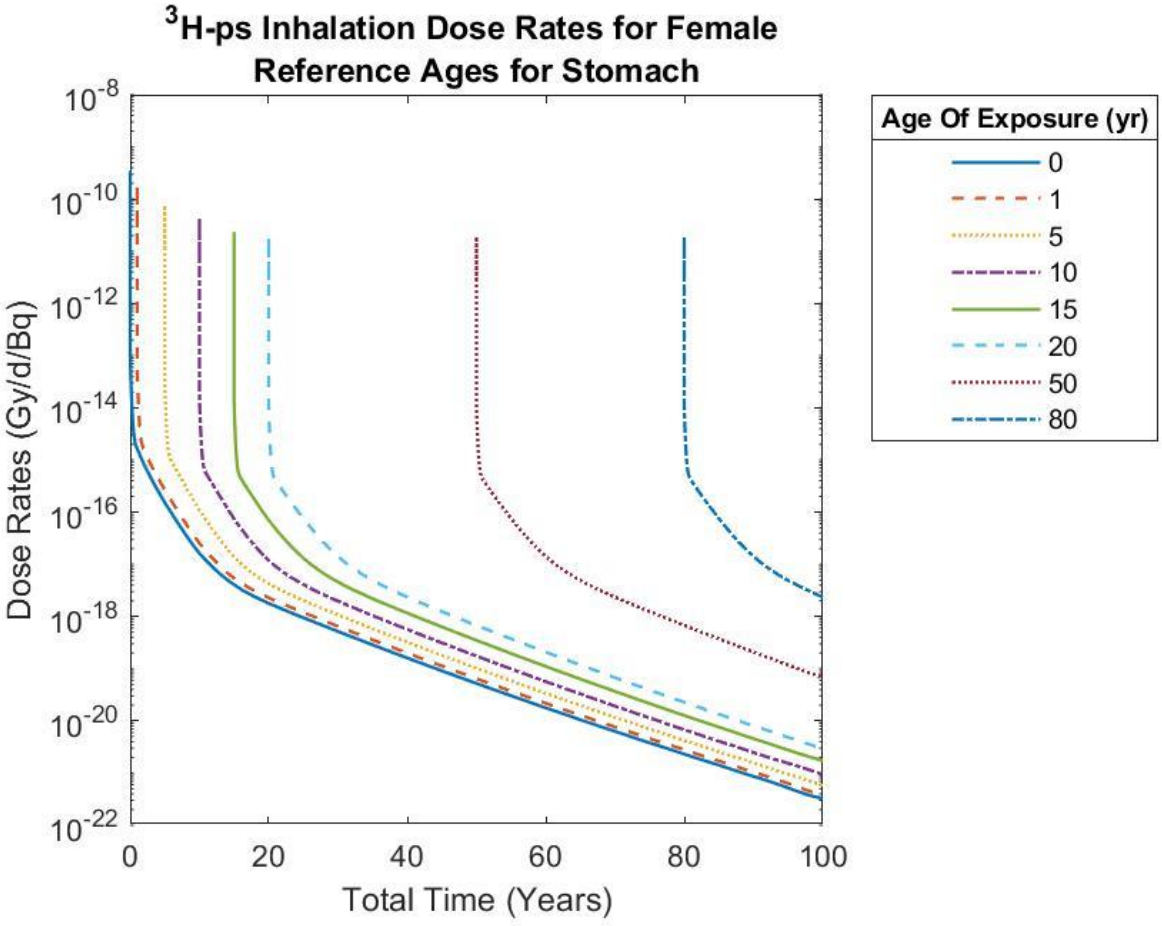

(a)

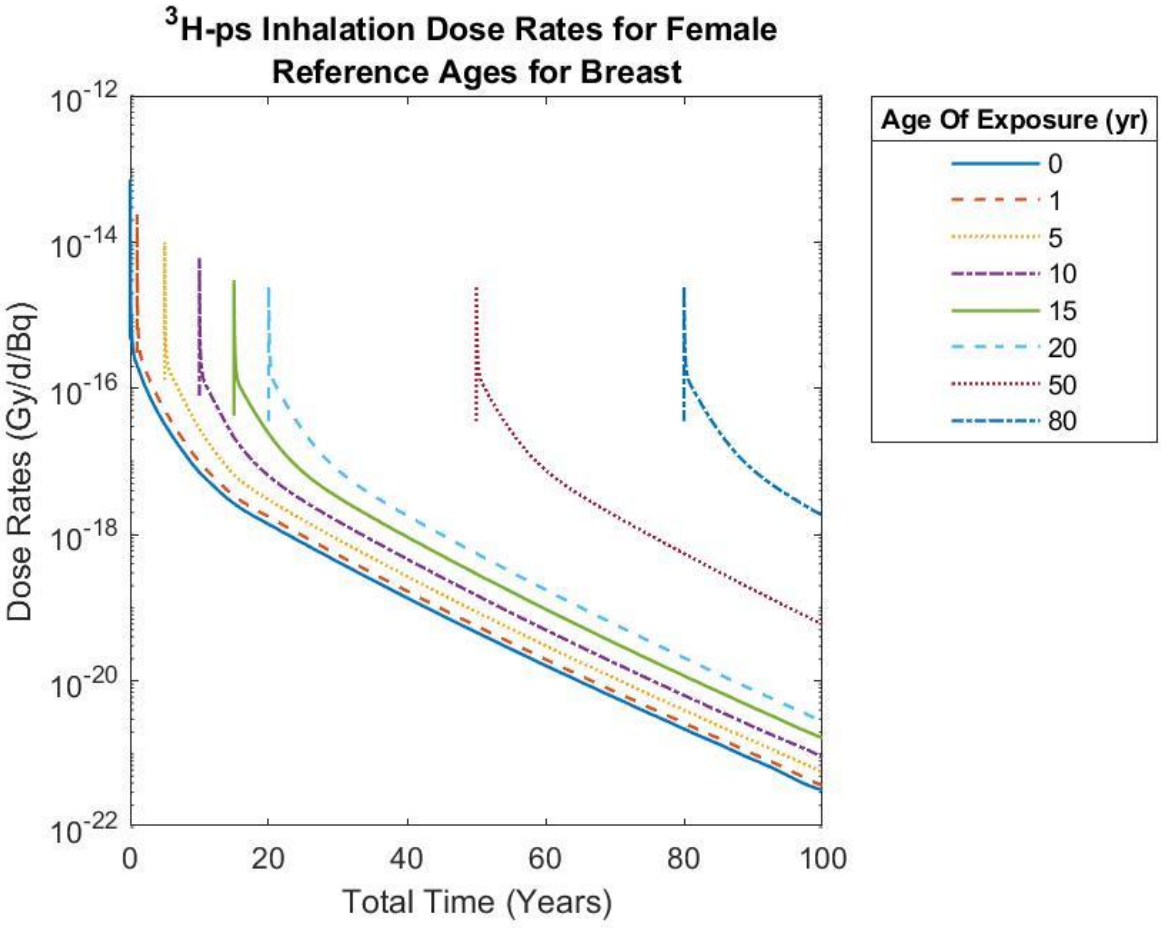

(b)

Figure 14. Absorbed dose rates for the female (a) stomach and (b) breast for slow-clearing tritium at various ages of exposure.

Tritium itself has a physical half-life of 12.4 years; however, it has an effective half-life of only 10 days. Inhaled tritium, specifically, can reach an equilibrium in the body approximately 2 hours after inhalation exposure.[33] It is because of this that a steep drop off can be seen in the dose rates with respect to time post internal exposure. The biokinetic plots for ingested tritium below for various body compartments validate this quick drop off in various tissues of the body, as most of the activity drops off by time stamp 25 days, regardless of compartment, seen in Figure 15 and Figure 16.

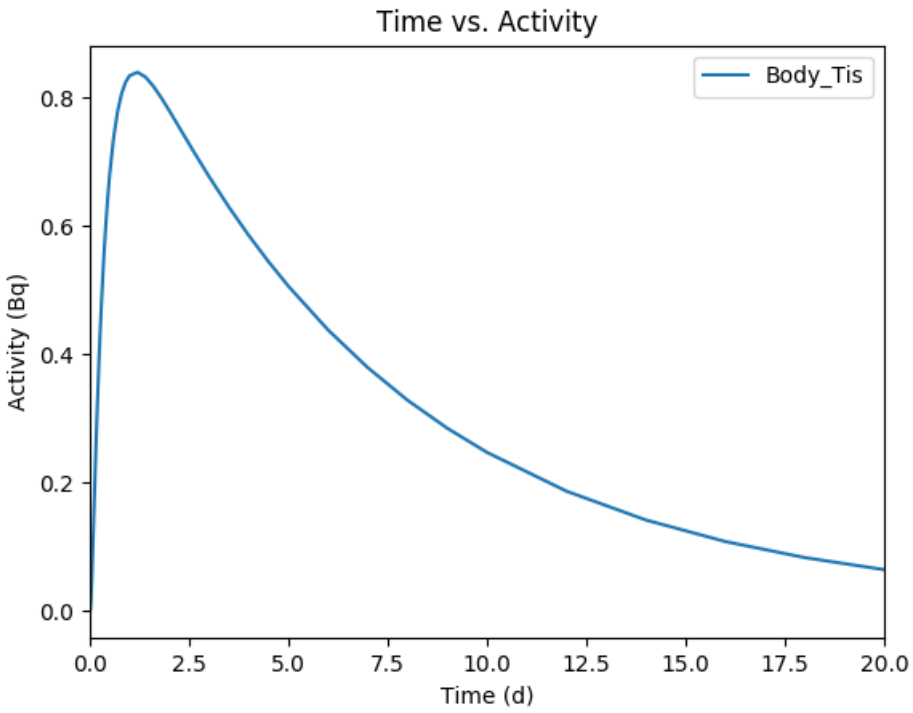

Figure 15. DCAL generated biokinetics of ingested tritiated water in the body tissues at age 5 years.

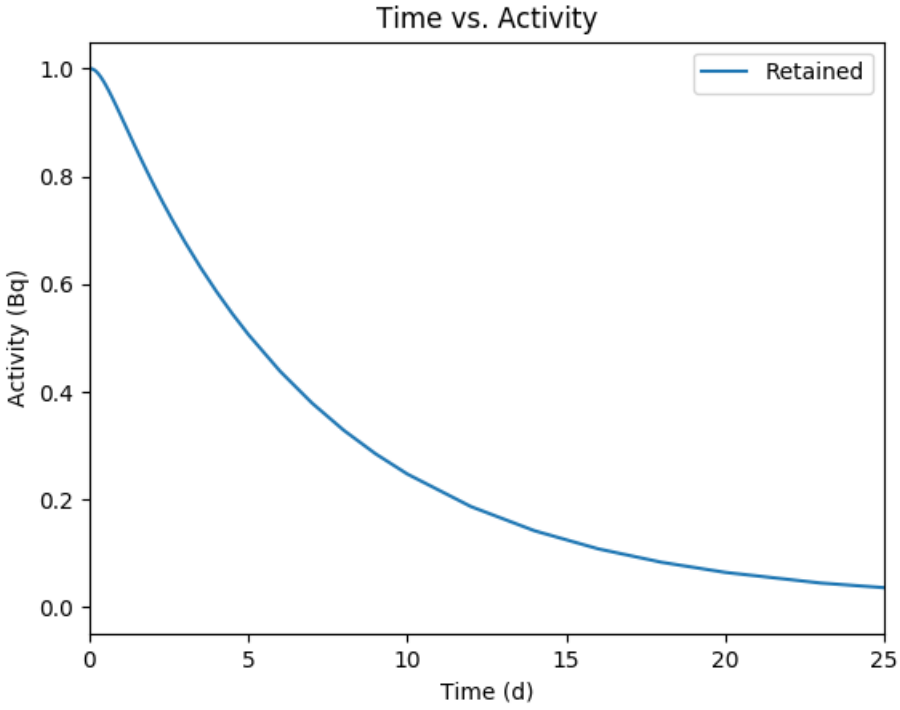

Figure 16. DCAL generated biokinetic activity of retained ingested tritiated water at age 5 years.

Ingested tritiated water behaves in a similar manner as fast-clearing inhaled tritium, evenly distributing through the body. Post internal exposure, the dose rates quickly reach an equilibrium value, slowly decreasing over several years before ultimately dropping to essentially 0, as seen in Figure 17. Ingested tritium differs from fast-clearing tritium, however, in that it resides in the body far longer than fast-clearing inhaled tritium does. This trend is reflected in all tissues for tap water ingested tritium. For this work, only tap water ingested tritium was considered, as the more common usage type for ingested tritium.

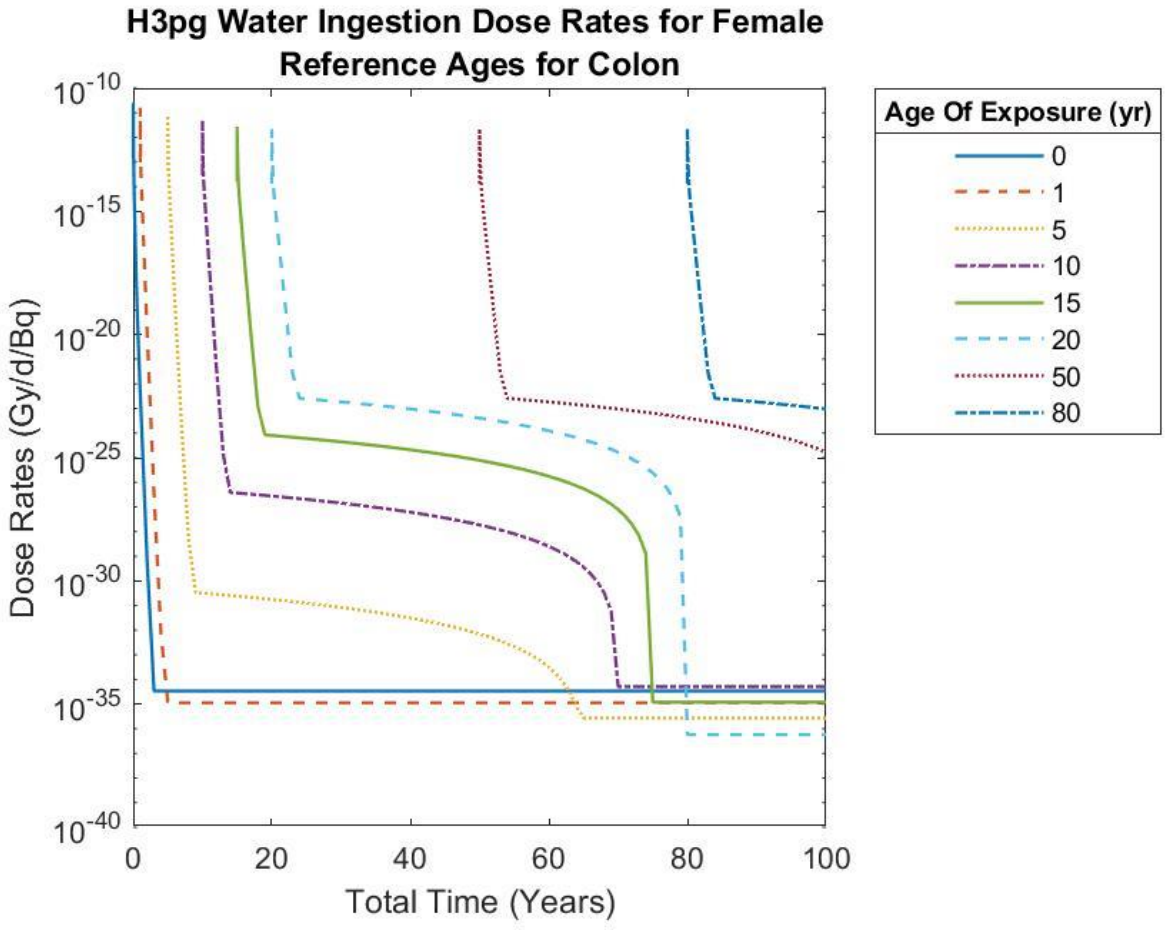

(a)

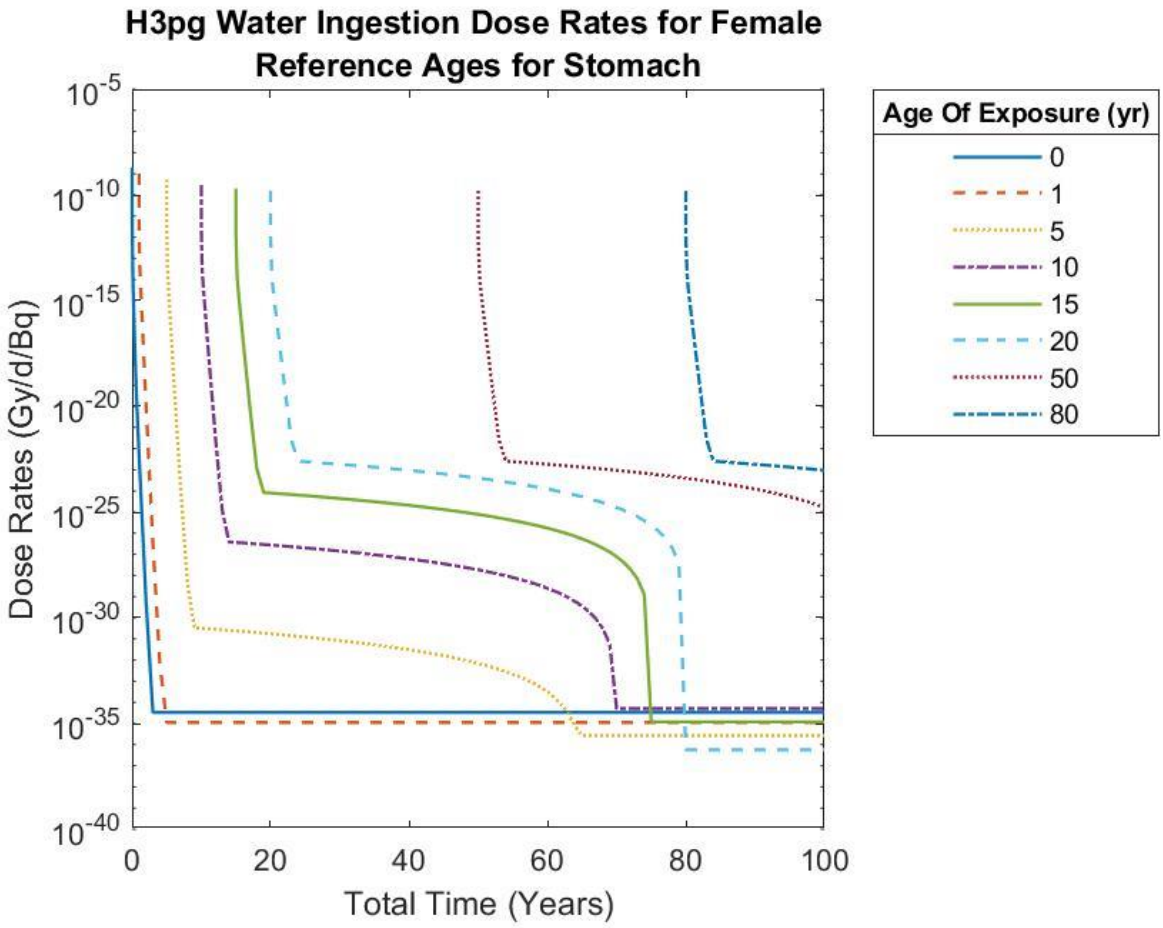

(b)

Figure 17. Absorbed dose rates to the female (a) colon and (b) stomach from ingested tritiated water.

4.1.1.c. ^{137}Cs

Cesium's behavior tends to target the soft tissues, particularly the muscle. Because of this, a concentration was expected to be seen in the residual, as muscle is a component of the residual. This, however, was not the case. Within each solubility classes and exposure type, the magnitude drop in the dose rates was similar for all tissues, the only outlier being for slow-clearing inhalation. For this class, the lungs show a much smaller drop in magnitude as compared to the other soft tissues, as can be seen below in Figure 18. Fast and moderate-clearing cesium plots for select soft tissues can be found in Appendix A.

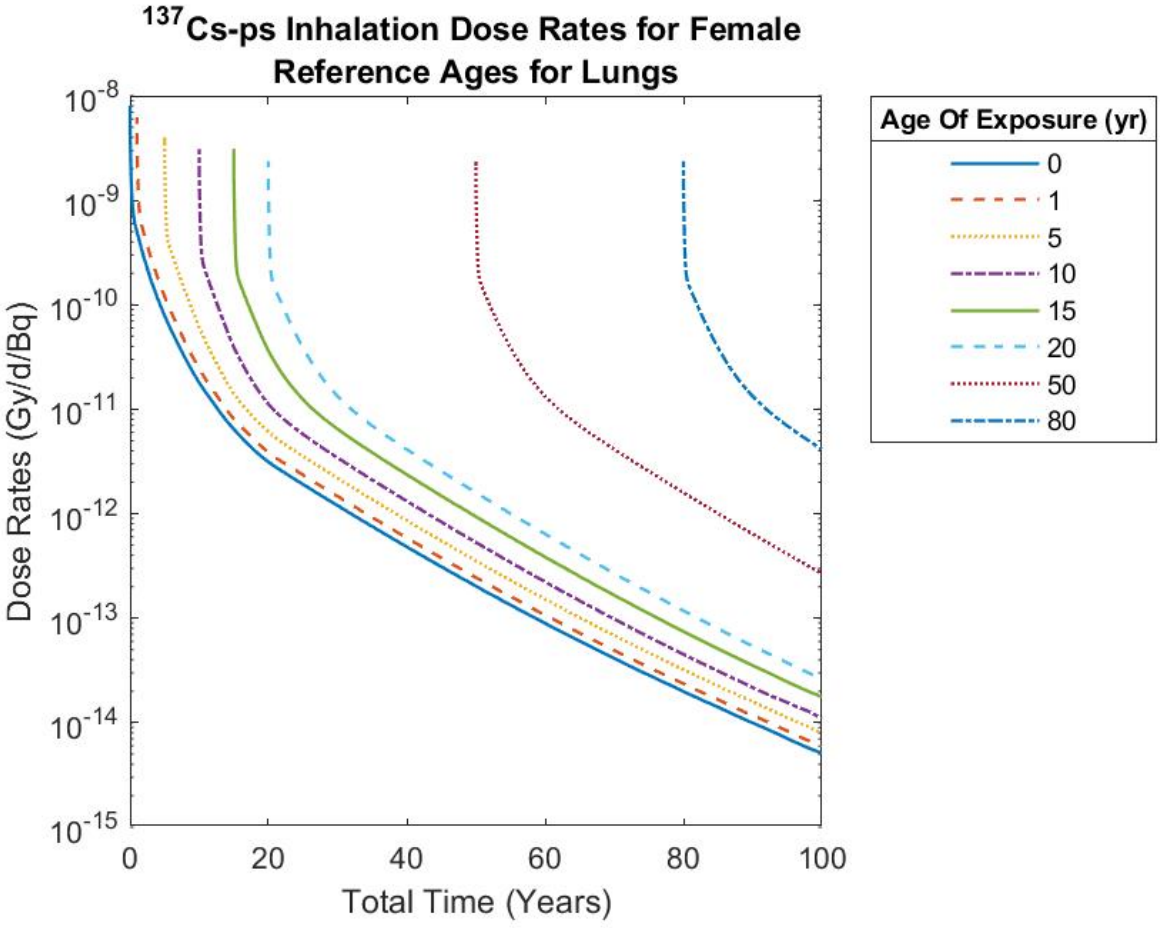
137Cs-ps Inhalation Dose Rates for Female Reference Ages for Lungs
Dose Rates (Gy/d/Bq)
Total Time (Years)
Age Of Exposure (yr)
0
1
5
10
15
20
50
80

(a)

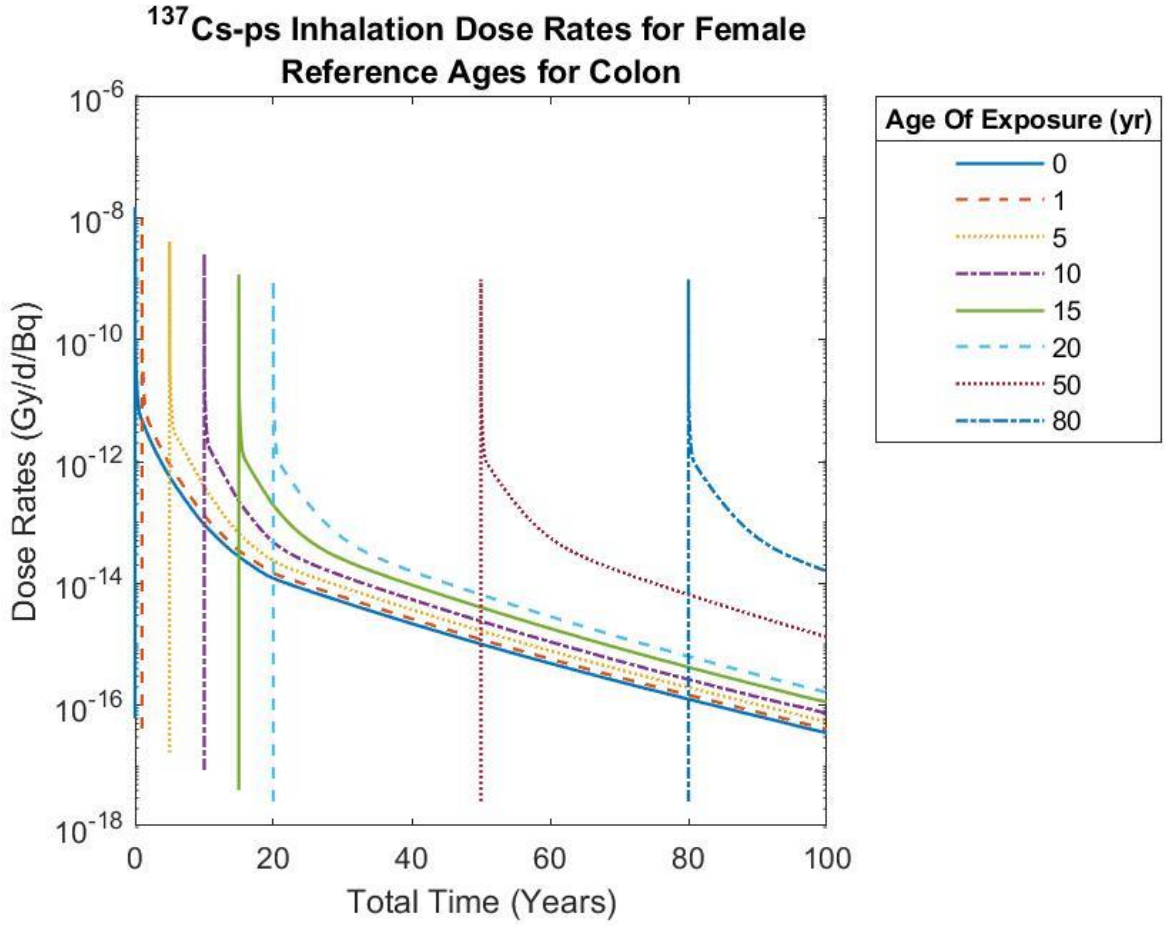

(b)

Figure 18. Absorbed dose rates for the female (a) lungs and (b) colon for slow-clearing ^{137}Cs at various ages of exposure.

Biokinetically, cesium tends to simply pass through the body, not typically readily accumulating in any one single target tissue. With a biological half-life of only 70 days, and a lack of singular target accumulation, it is understandable that most dose rates to the tissues would be incredibly similar as a whole-body soft-tissue seeker. This trend is seen for both inhalation and ingestion exposures. The trend of ingested cesium via tap water for select tissues can be found in Appendix A.

As with iodine, the varying biokinetics in adolescence drive the trend during the first 20 years of life. For cesium, the decay trend is similar to iodine, but takes place over a longer time

period of 70 days, corresponding to the biological half-life of cesium in the body, as compared to 25 days for iodine. This biokinetic behavior is depicted in Figure 19 and Figure 20, below, representing the body tissues and the stomach post inhalation of cesium. For the stomach, cesium simply passes through, the activity dropping off very rapidly.

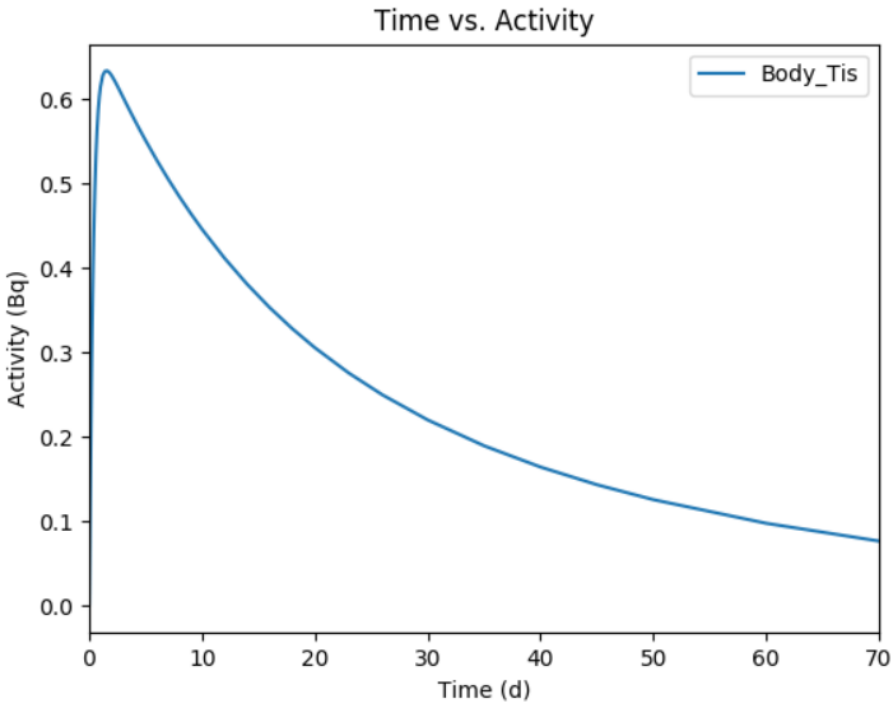

Figure 19. DCAL generated biokinetic activity behavior of fast-clearing ^{137}Cs with respect to time in the body tissues at age 5 years.

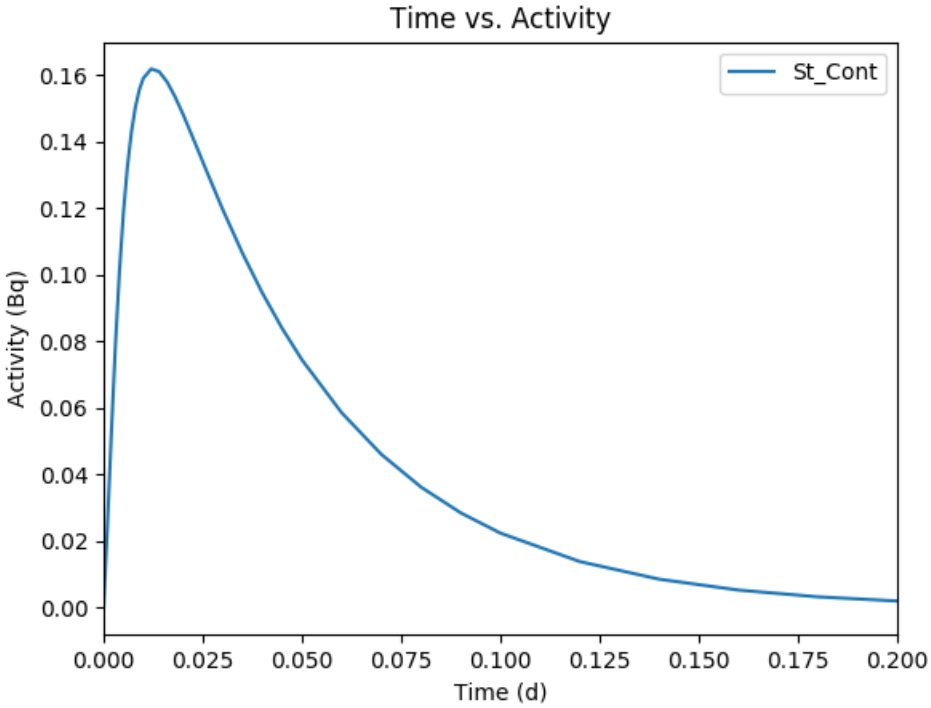

Figure 20. DCAL generated biokinetic activity behavior of fast-clearing ^{137}Cs with respect to time in the stomach at age 5 years.

The biokinetics for the ingestion of cesium show a very rapid drop in activity with respect to time, taking less than a day to clear the system, seen in Figure 21. This is indicative of the fact that ingested cesium simply tends to pass through the GI tract rather quickly. However, the time to clear the body tissues for ingestion is longer than for inhaled cesium, seen in Figure 22.

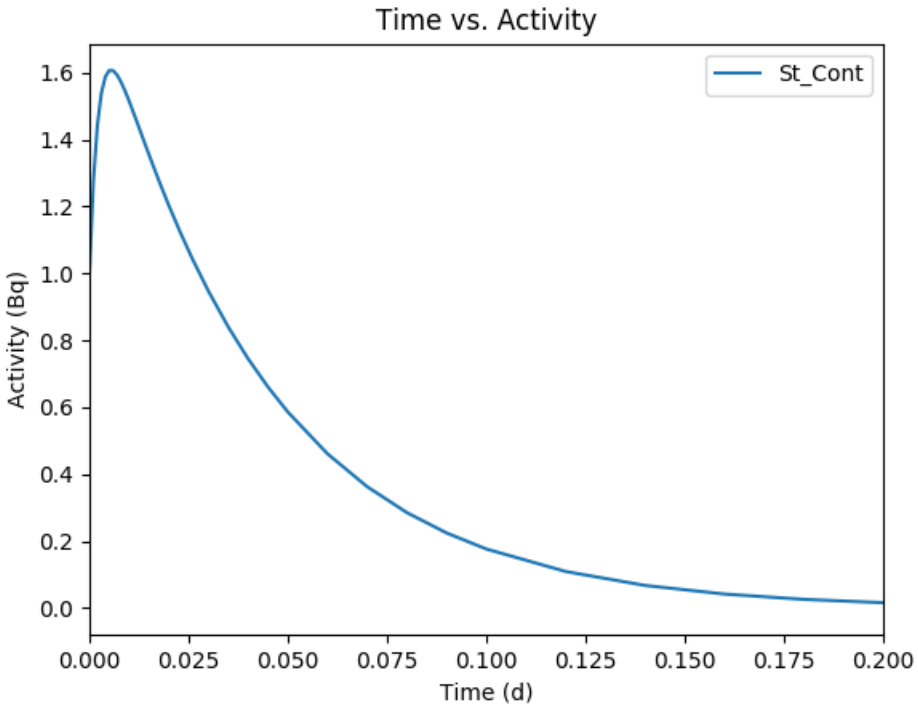

Figure 21. DCAL generated biokinetic activity behavior of ingested ^{137}Cs with respect to time in the stomach at age 5 years.

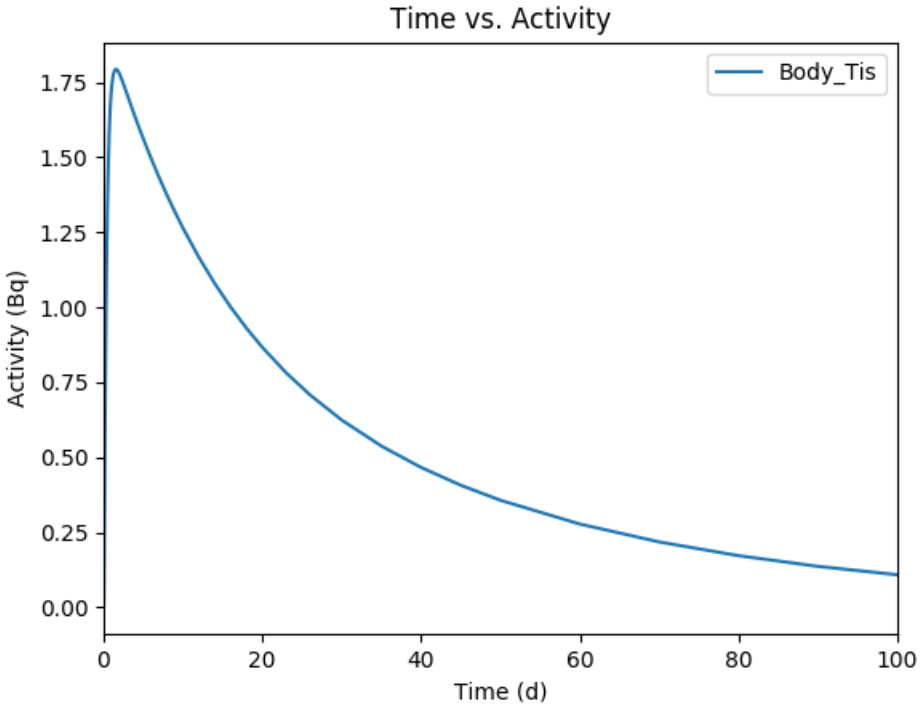

Figure 22. DCAL generated biokinetic activity behavior of ingested ^{137}Cs with respect to time in the body tissues at age 5 years.

4.1.1.d. ^{90}Sr

^{90}Sr is a known bone seeker, behaving in a manner similar to calcium, and has a physical half-life of 28 years and a biological half-life of approximately 49 years.[34] It integrates into the bone matrix after exposure, resulting in higher concentrations of strontium and therefore higher absorbed dose rates in both the bone surface as well as the red bone marrow, and a more constant delivery of dose throughout life.

Figure 23 below shows the difference for fast-clearing ^{90}Sr in the lungs versus in the bone surface for females after an acute exposure at various ages of exposure. While the lung tissue absorbed dose rates drop nearly eight orders of magnitude in the first 40 years of life after an internal exposure at time stamp 0 (here representing age of exposure = 100 days), over the same time frame the absorbed dose rate drops only approximately 5 orders of magnitude. This lower drop in magnitude is similar for red marrow, which is expected, as the strontium integrated into the bone matrix delivers dose to the red marrow, as well as the bone to which it is incorporated. All other tissues for fast-clearing ^{90}Sr exposure follow a similar trend to the lungs, dropping approximately 8 orders of magnitude in the first 40 years after an exposure at time 100 days. Behavior in lungs for all solubility classes of strontium as well as behavior of ^{90}Sr in the bone can be found in Appendix A, while the behaviors of strontium in the bone due to a fast-clearing inhalation and slow-clearing inhalation can be seen below.

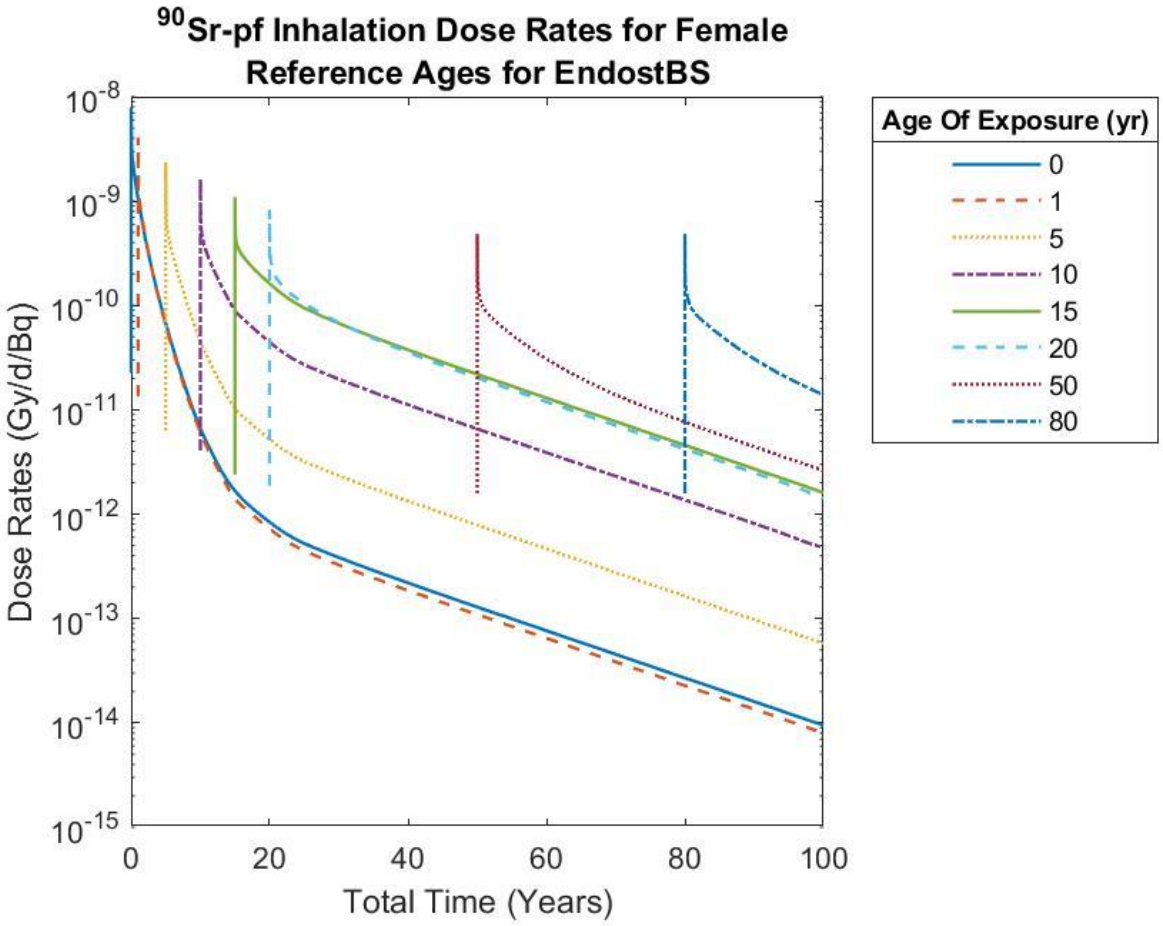

Figure 23. Absorbed dose rates for the female endosteal bone surface (EndostBS) for fast-clearing ^{90}Sr at various ages of exposure.

Slow-clearing strontium shows a much more gradual slope in the trend of the absorbed dose rates throughout life, clearing from the lungs at approximately half the rate of fast-clearing, while decay from the bone occurs at a comparable rate. The difference for the skeletal structure between fast and slow-clearing solubility classes is the dose delivered to the tissue. As it takes more time for the radionuclide to clear from the lungs, it takes more time for the radionuclide to build up in the skeletal system, indicated by the buildup to the peak roughly a year after exposure, followed by the steady rate of decay, seen in Figure 24.

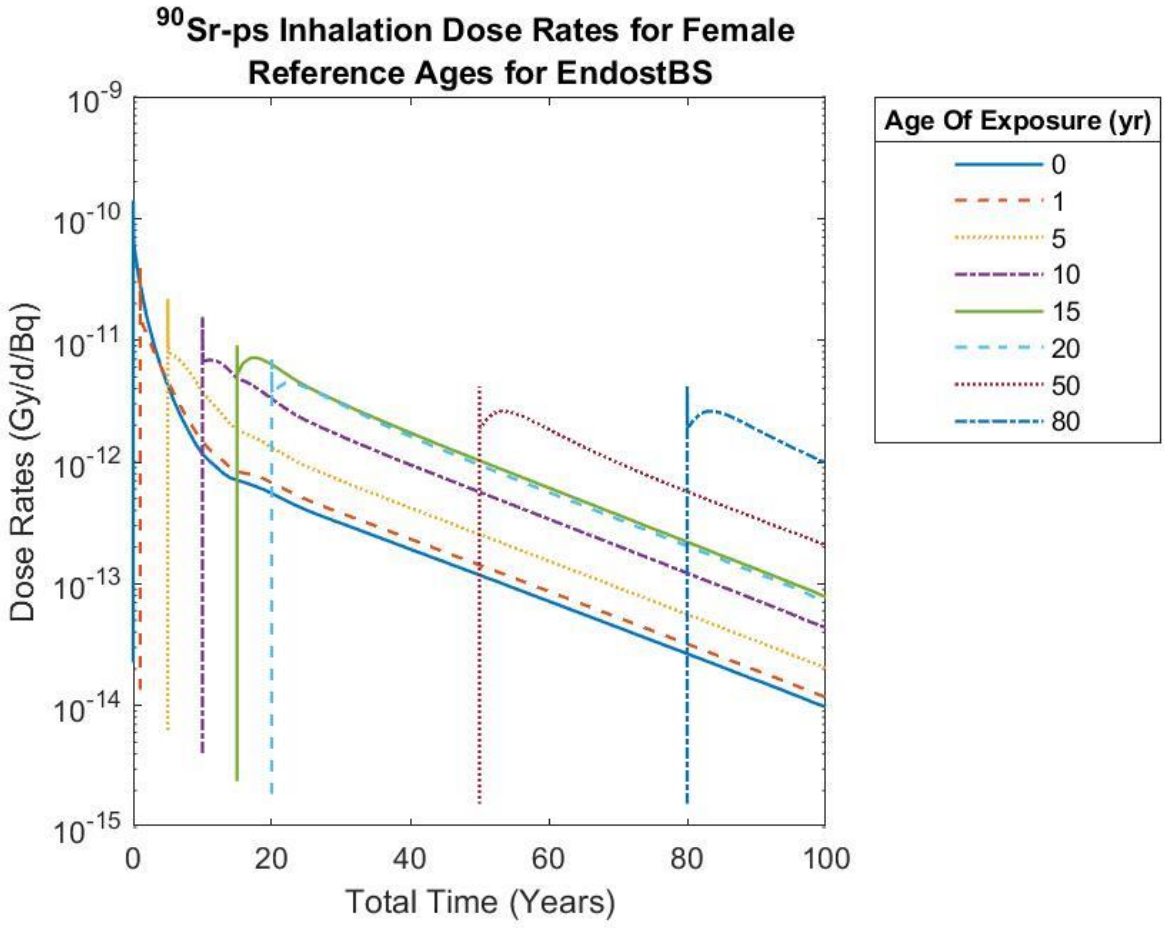

Figure 24. Absorbed dose rates for the female bone surface for slow-clearing ^{90}Sr at various ages of exposure.

Ingestion of strontium, both for food and water, follows a similar trend, with most soft tissues showing drop off of a similar order, while the dose rates for bone drop off at nearly half the rate of the soft tissues, and red marrow drops off at two-thirds the rate, as seen in Figure 25.

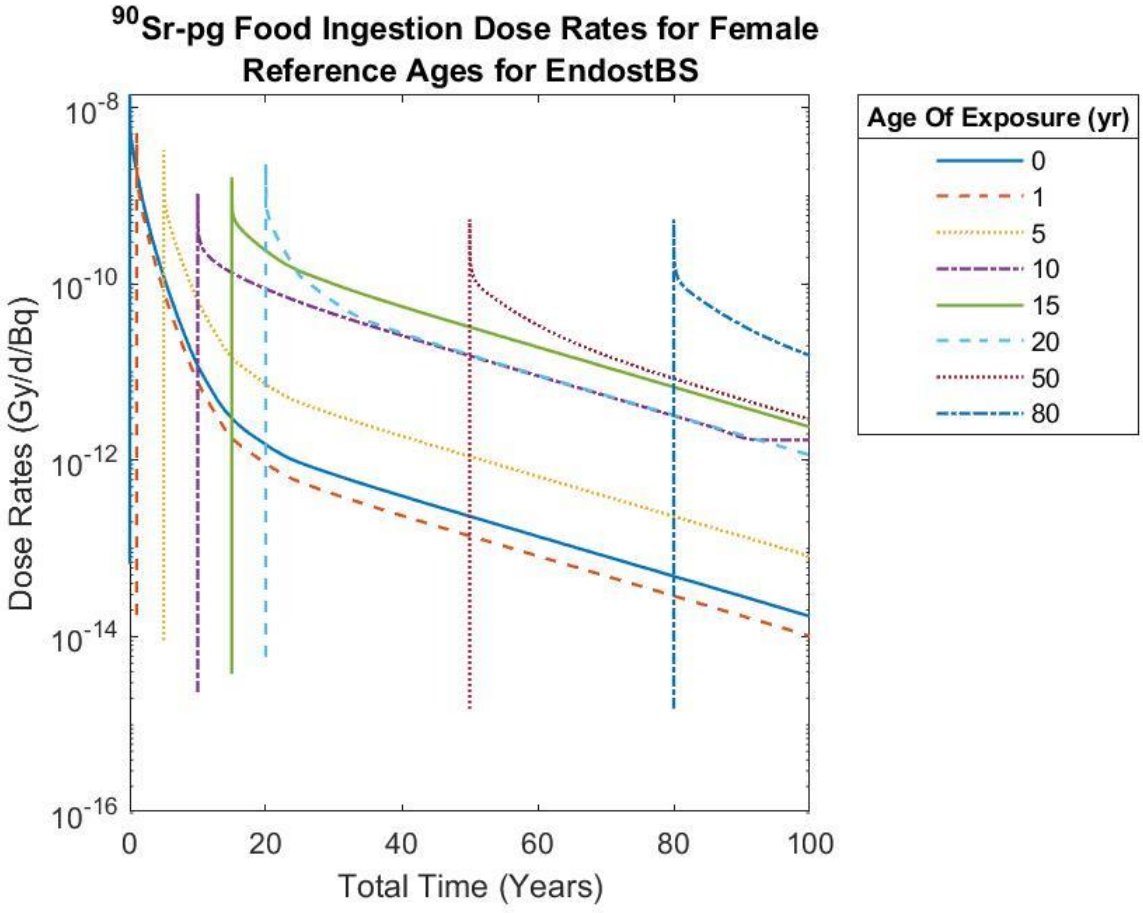
^{90}Sr-pg Food Ingestion Dose Rates for Female Reference Ages for EndostBS
Dose Rates (Gy/d/Bq)
10^{-8}
10^{-10}
10^{-12}
10^{-14}
10^{-16}
0
20
40
60
80
100
Total Time (Years)
Age Of Exposure (yr)
0
1
5
10
15
20
50
80

(a)

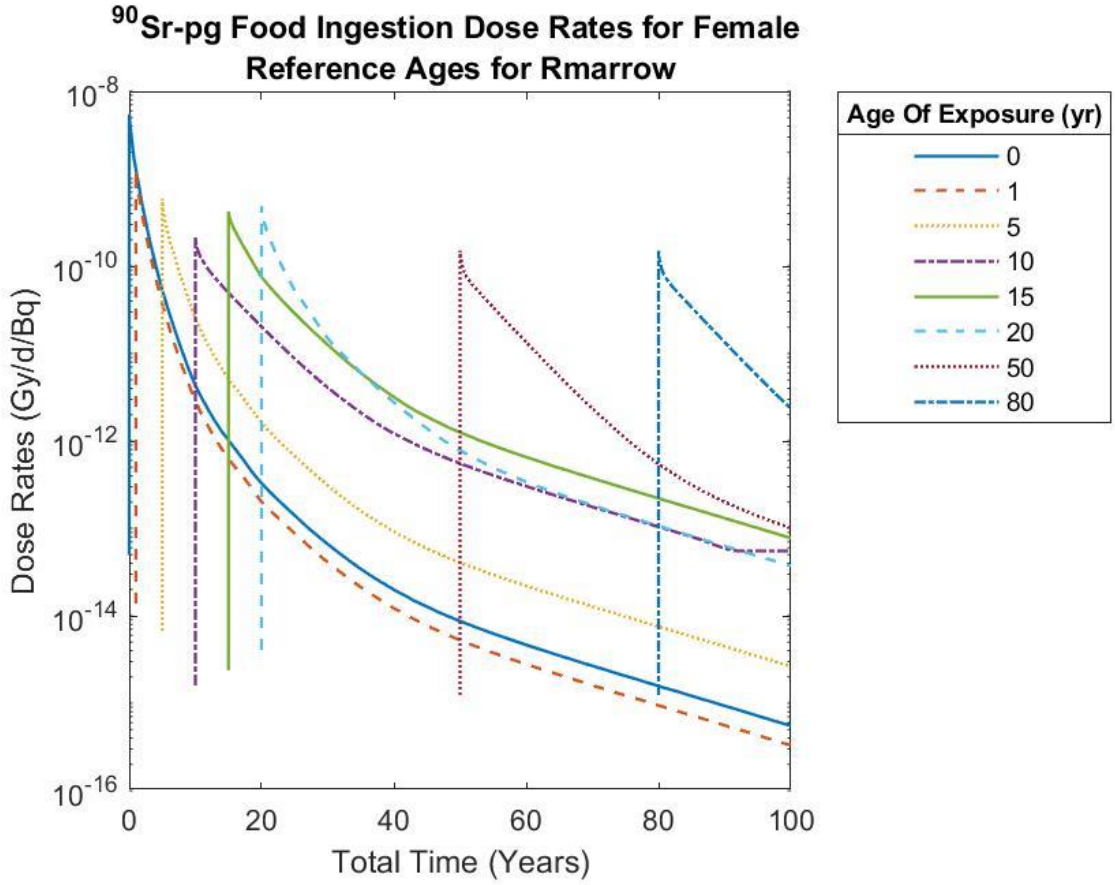

(b)

Figure 25. Absorbed dose rates for the female (a) bone surface and (b) red marrow for ^{90}Sr ingested via food.

4.1.1.e ^{235}U

Graphs for both high- and low-LET components of ^{235}U were plotted separately. Uranium acts as a bone seeker and does not tend to localize in soft tissues. Uranium's biological half-life of 15 days results in tissues such as the colon, stomach, and breast seeing a more rapid drop in the absorbed dose rate than that observed in the bone, red marrow, liver, and kidneys, and can be seen for the colon in Figure 26. This trend is repeatedly seen in the soft tissues that do not partake in filtration or circulation for all solubility classes.

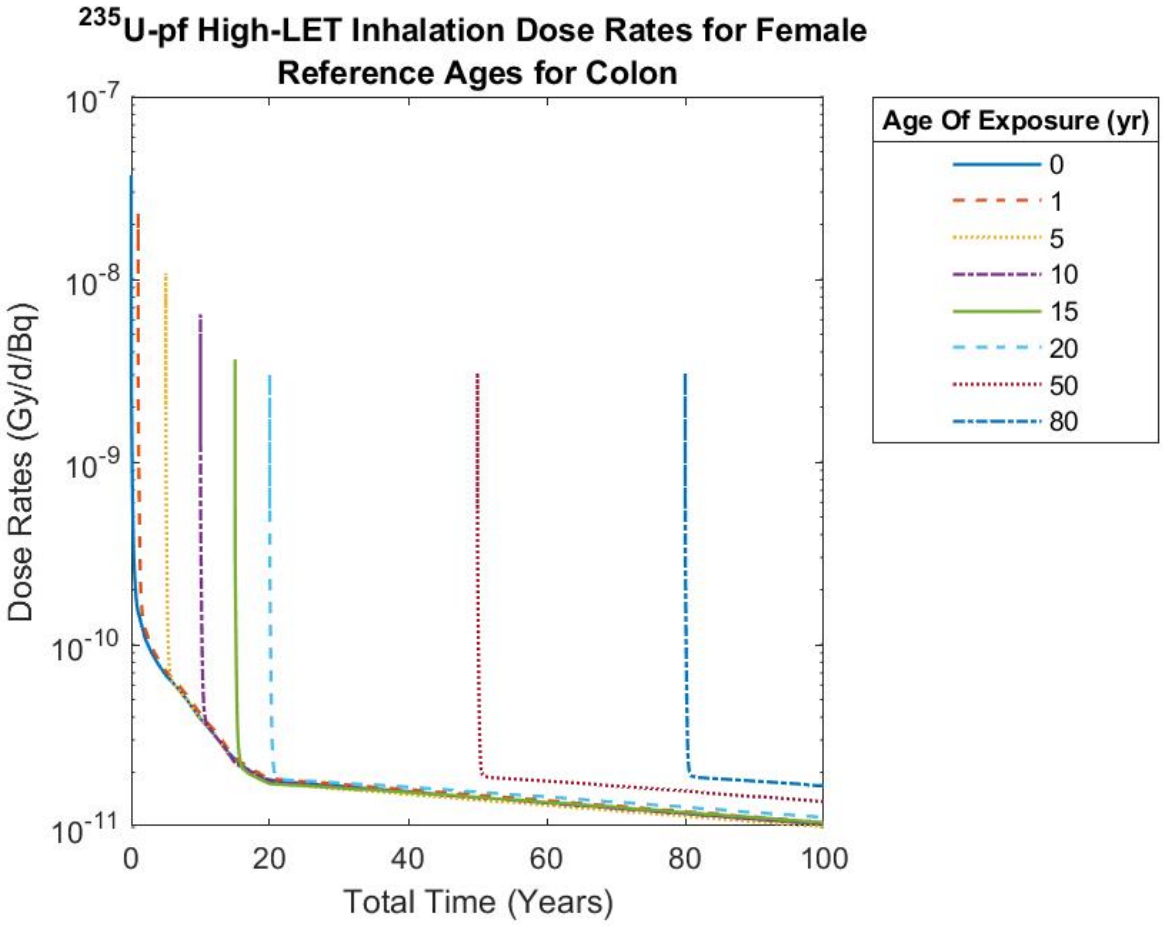
235U-pf High-LET Inhalation Dose Rates for Female
Reference Ages for Colon
Dose Rates (Gy/d/Bq)
Total Time (Years)
Age Of Exposure (yr)
0
1
5
10
15
20
50
80

(a)

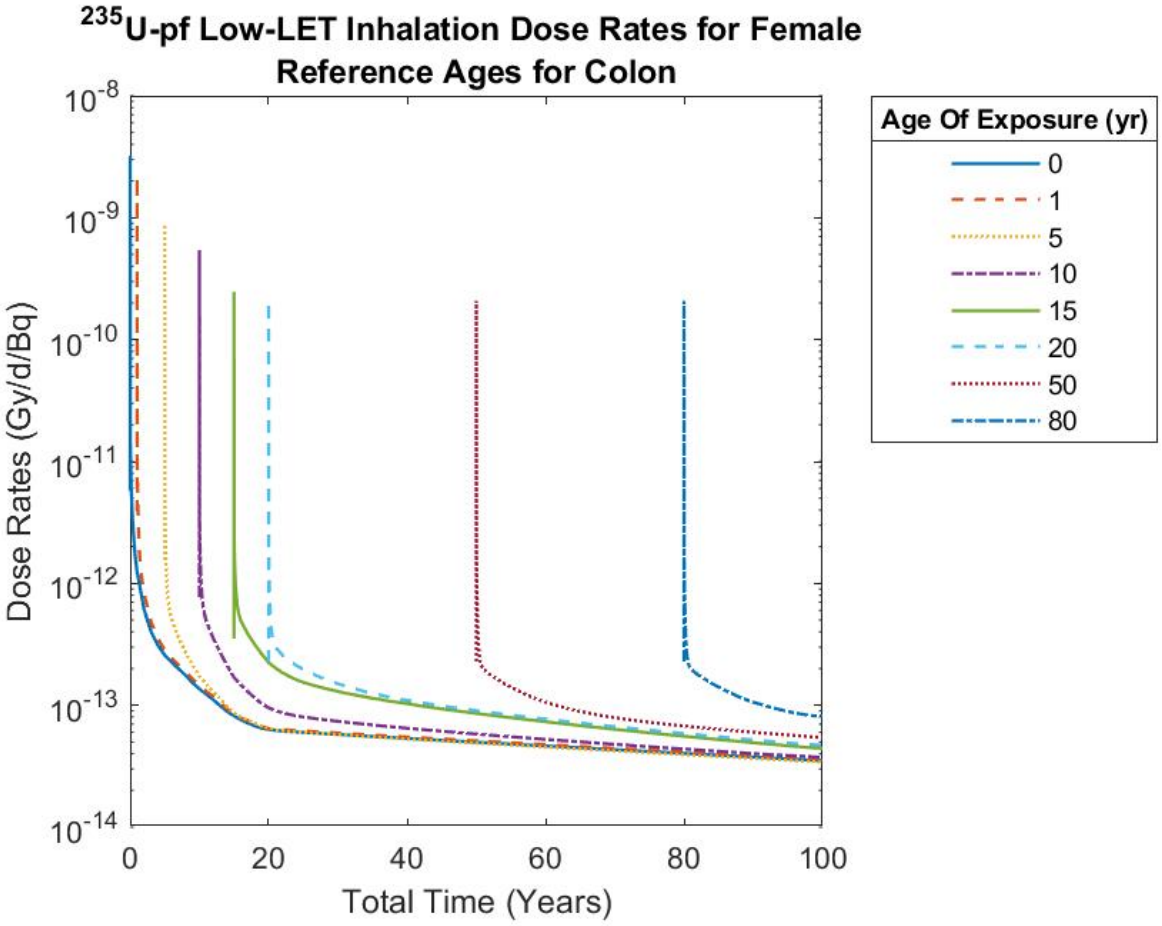

(b)

Figure 26. Absorbed dose rates for the male colon for the (a) high LET component and (b) low LET component of fast-clearing ^{235}U for various ages of exposure.

The liver and kidneys are responsible for excreta filtration and blood circulation and therefore are exposed to any of the radionuclide that passes through them. With bone matrix restructuring, uranium can be removed from the bone matrix and reintroduced into the circulatory system. Thus, as the blood filters through the liver, the liver is exposed again. This trend is consistent for all solubility classes, as well as for both high and low LET radiations, as seen in Figure 27.

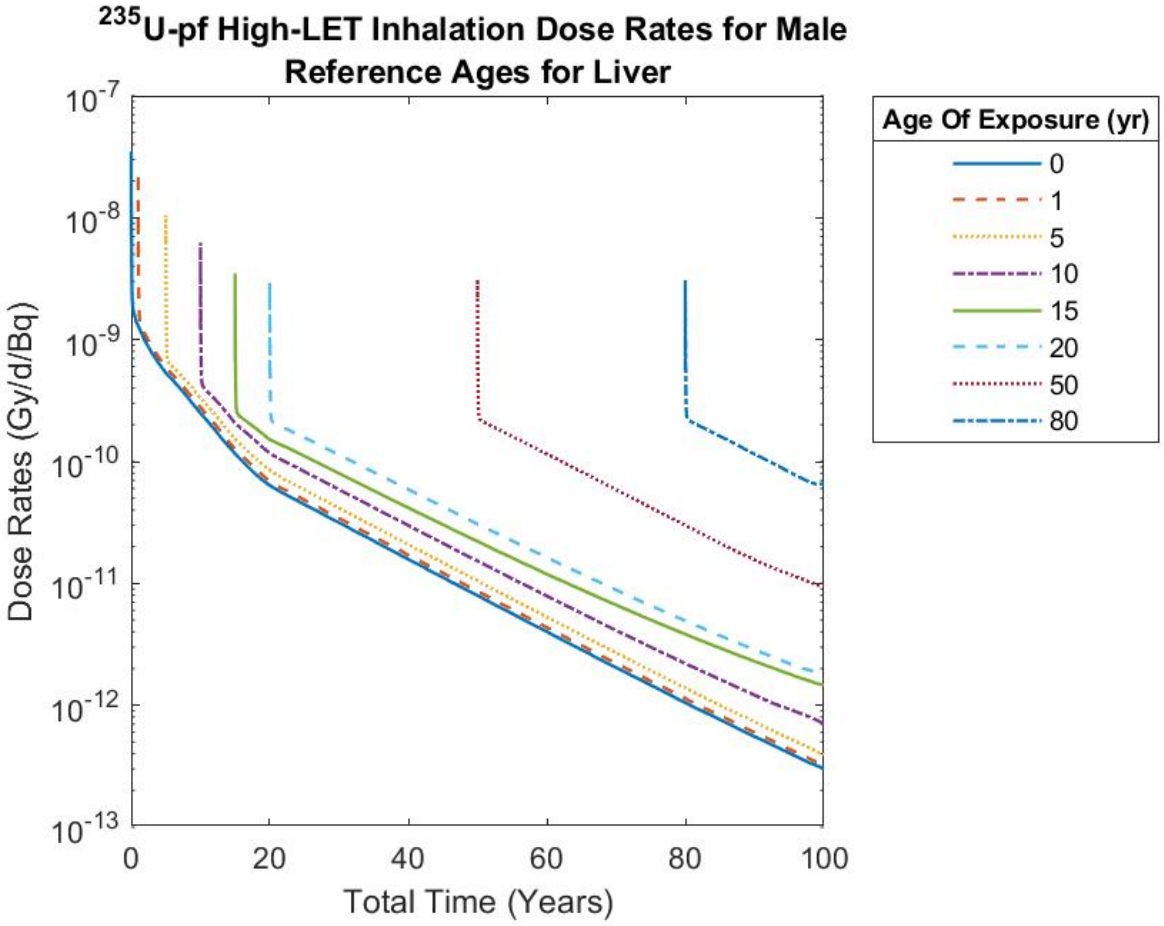
235U-pf High-LET Inhalation Dose Rates for Male
Reference Ages for Liver
Dose Rates (Gy/d/Bq)
Total Time (Years)
Age Of Exposure (yr)
0
1
5
10
15
20
50
80

(a)

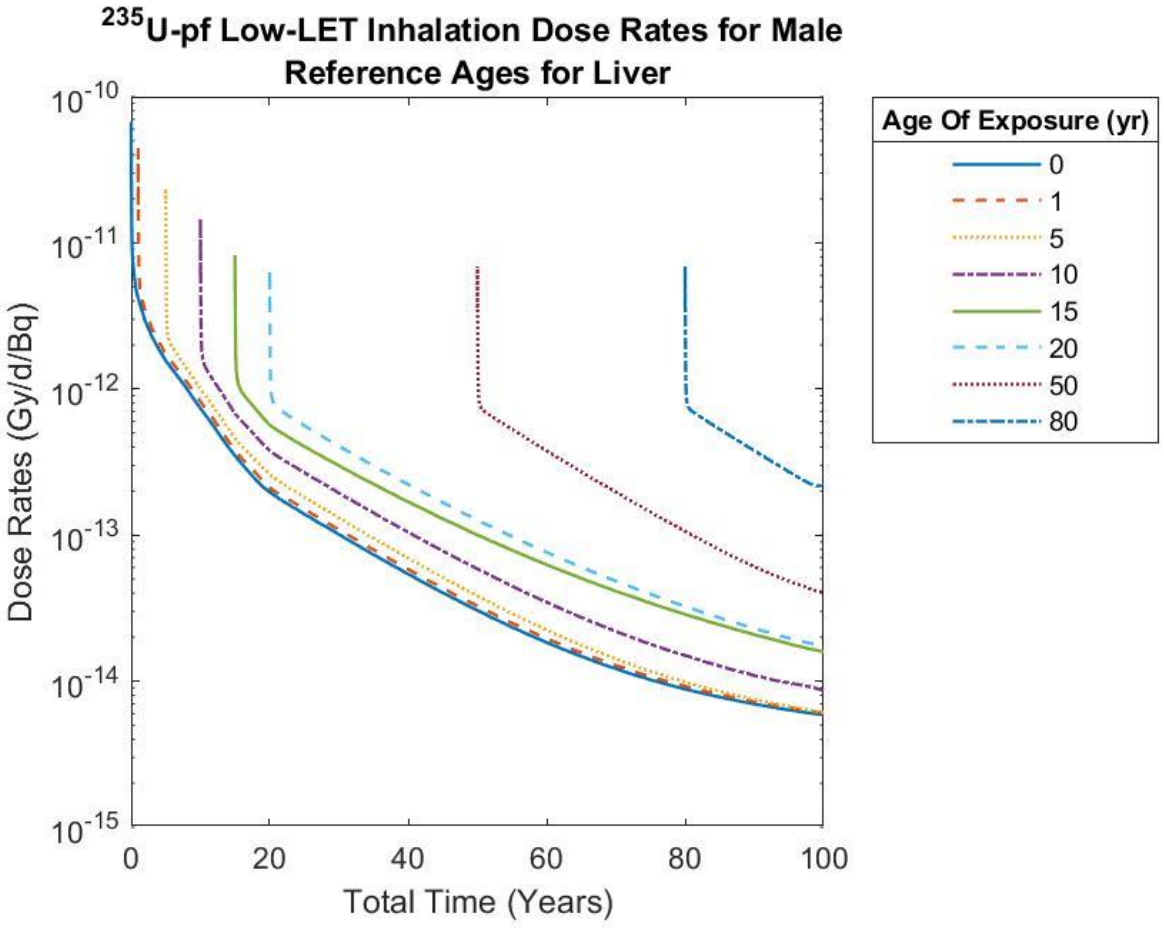

(b)

Figure 27. Absorbed dose rates for the male liver for the (a) high-LET component and (b) low-LET component of fast-clearing ^{235}U for various ages of exposure.

When ingested, similar to inhalation, the radionuclide tends to simply pass right through the colon, with the most gradual rate of decrease being seen in the kidneys, liver, and bone as ^{235}U acts as a bone seeker, and the circulatory system works to remove the heavy metals from the system. Corresponding plots for high-LET components of the values in Figure 28 where this behavior is outlined can be found in Appendix A.

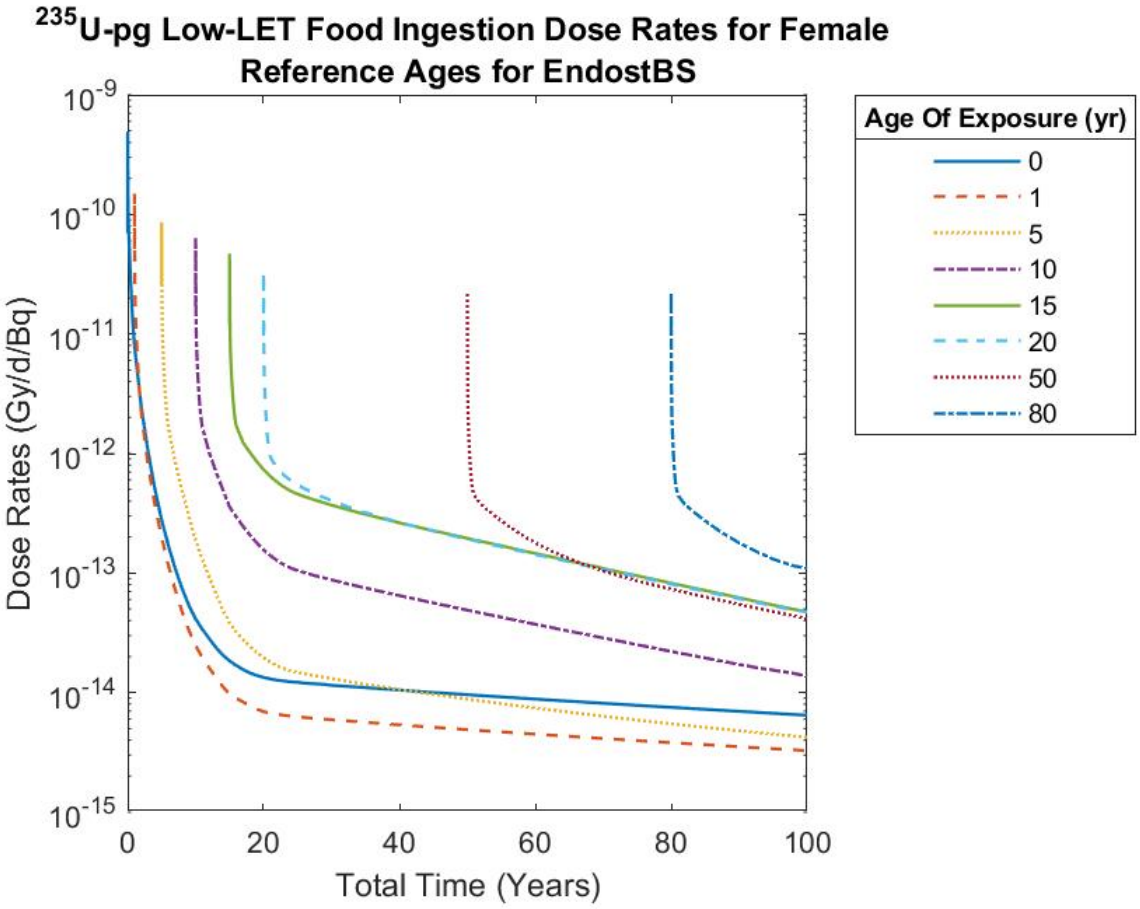
235U-pg Low-LET Food Ingestion Dose Rates for Female Reference Ages for EndostBS
Dose Rates (Gy/d/Bq)
Total Time (Years)
Age Of Exposure (yr)
0
1
5
10
15
20
50
80

(a)

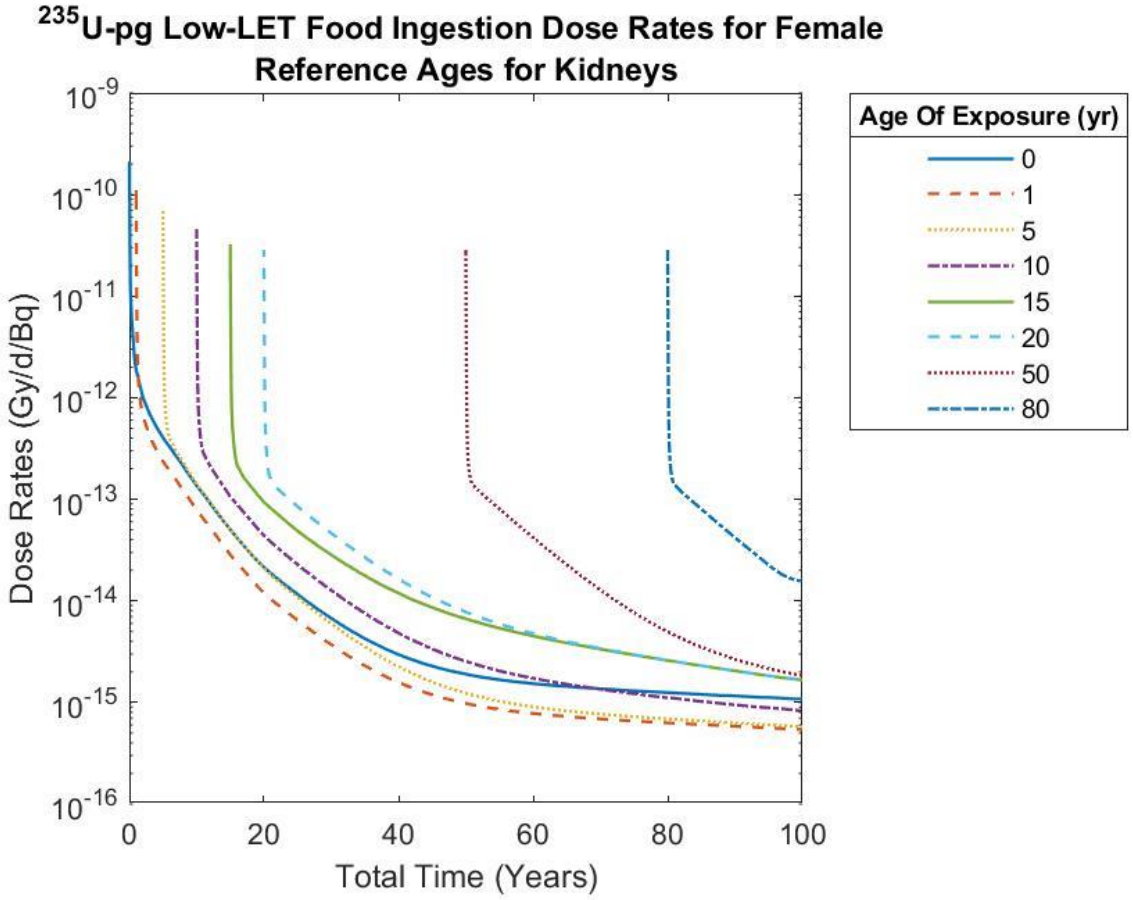

(b)

Figure 28. Absorbed dose rates for the female (a) bone surface and (b) kidneys for the low-LET component of ingested ^{235}U at various ages of exposure.

4.1.2. Annualized Dose Rates

Following the visualization of the acute exposure dose rates, the data was fed through Visual Studio where the applied Akima spline calculated the annual doses for each radionuclide at each age of exposure from age 100 days to age 105 years. These splines were then integrated in one-year increments to yield the annual doses for each year of life post-internal exposure. Similar to the raw exposure data, the annualized data were plotted via Matlab as well to confirm that this spline application did not affect the trend of the doses.

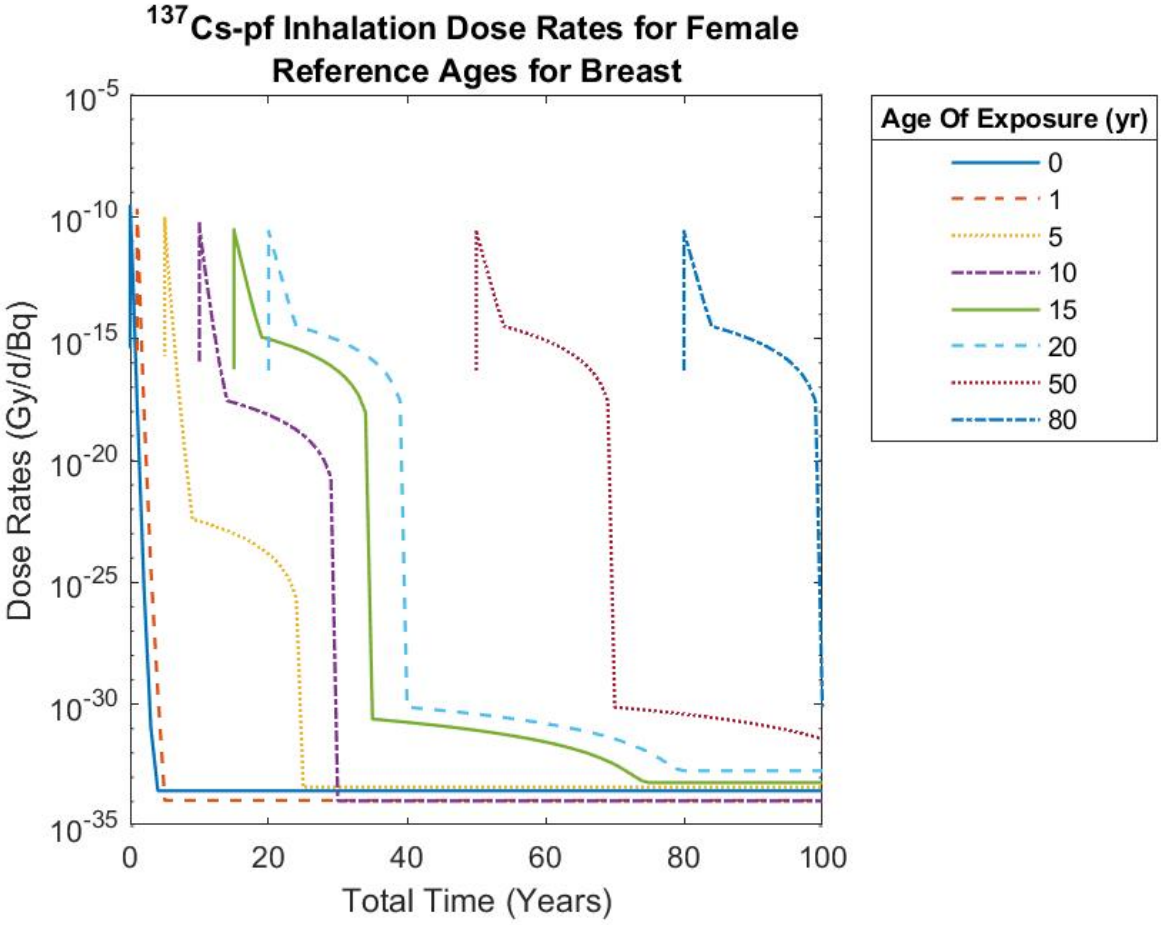
137Cs-pf Inhalation Dose Rates for Female
Reference Ages for Breast
Dose Rates (Gy/d/Bq)
10-5
10-10
10-15
10-20
10-25
10-30
10-35
0
20
40
60
80
100
Total Time (Years)
Age Of Exposure (yr)
0
1
5
10
15
20
50
80

(a)

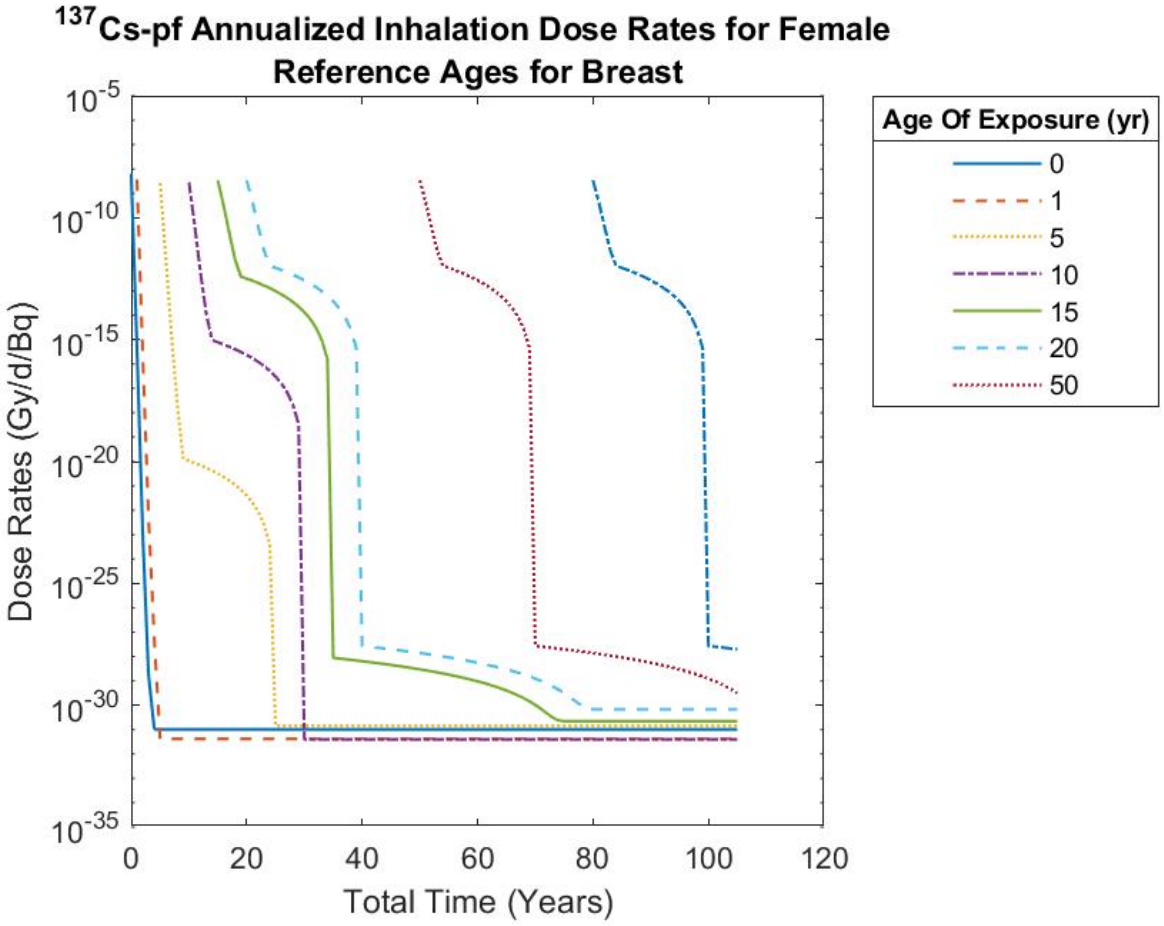

(b)

Figure 29. Absorbed dose rates (a) prior to annualization in Visual Studio and (b) annualized absorbed dose rates post annualization in Visual Studio for fast-clearing ^{137}Cs for the female breast.

Corresponding trends as seen in Figure 29 above are consistent through all radionuclides, solubility classes, and tissues, with the tail in the beginning of life from the initial exposure being dropped after annualization. This is due to the fact that the first year's values are all wrapped into that first year datapoint for the annualized data. Consistency between the raw data and the annualized data validates the spline chosen for preparation for risk calculation.

4.1.3. Chronic Exposure Doses

After annualization, the absorbed dose data were summed along the total time vector for all ages of exposure, resulting in a singular vector of dose rates per age, defined as total time. The vector resultant from this summation was then plotted to depict the biokinetic behavior of the radionuclides as it relates to their effect on a chronic uptake of a given radionuclide throughout life. This therefore defines a chronic exposure as a unit uptake of a radionuclide on the first day of each year of life from newborn to end of life, defined as 110 years in calculations.

4.1.3.a. ^{235}U

Uranium-235's half-life of 700 million years results in a buildup of the radionuclide within the body over time, and therefore a buildup in the absorbed doses, as a result of a chronic exposure. It is therefore expected to see a buildup in all tissues for all usage types and solubility classes.

In all following plots, the chronic doses drop steadily down to a minimum at age 20. This corresponds to the changing biokinetics of juveniles with respect to age. Beginning around age 20, the biokinetics stop changing as drastically, and at age 25 remain constant through the end of life, resulting in the steady buildup that is seen beginning around age 20 for all usage types and solubility classes, seen in Figure 30.

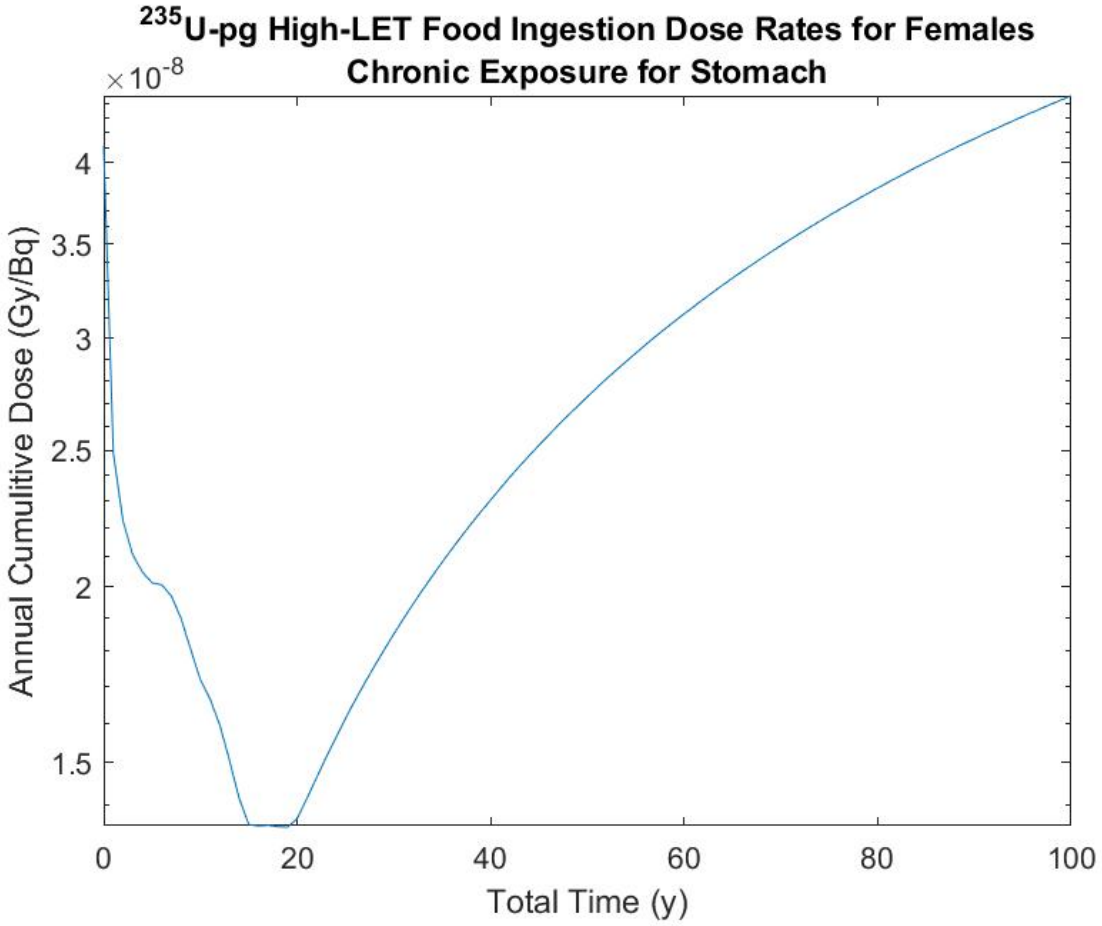
235U-pg High-LET Food Ingestion Dose Rates for Females
Chronic Exposure for Stomach
×10-8
Annual Cumulitive Dose (Gy/Bq)
4
3.5
3
2.5
2
1.5
0
20
40
60
80
100
Total Time (y)

(a)

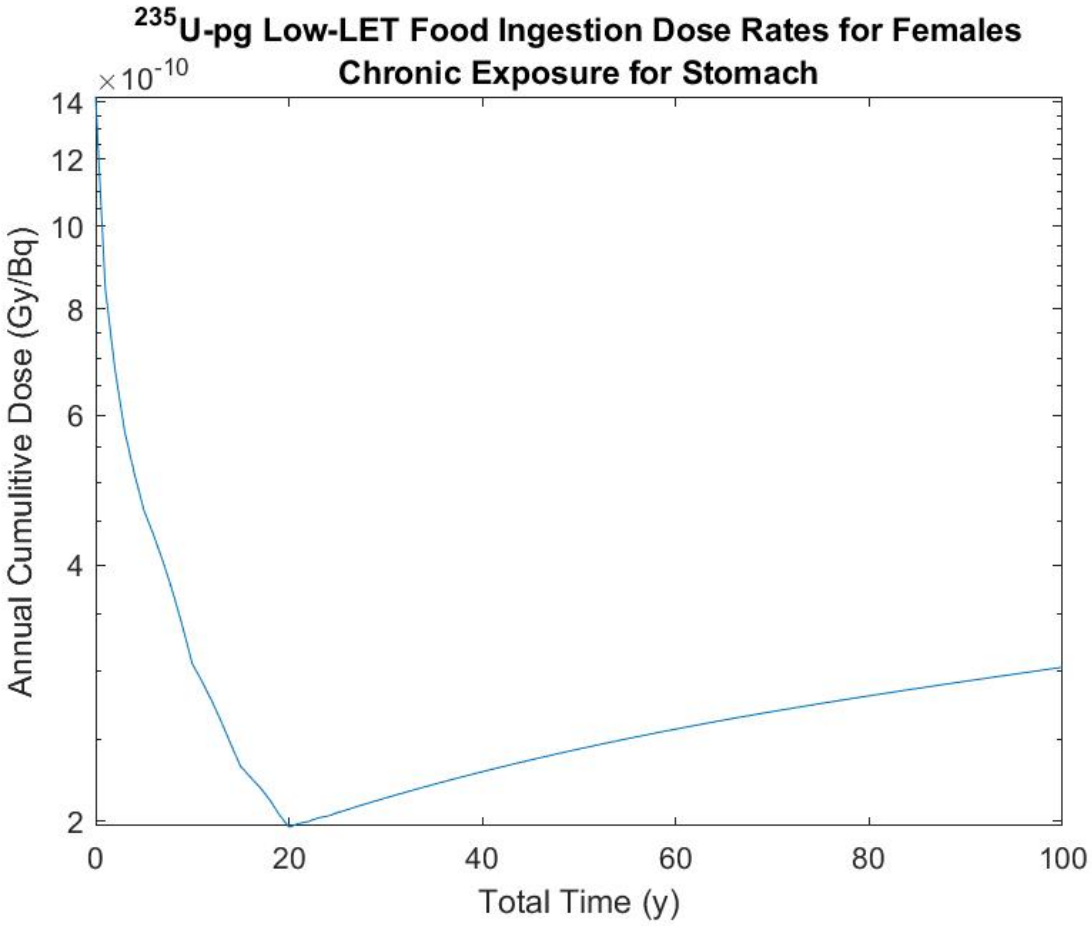

(b)

Figure 30. Comparison of the buildup of the (a) high-LET and (b) low-LET components in the female stomach for ingested ^{235}U. A similar trend is seen in the soft tissues sites for inhalation as well.

As expected, this trend of buildup in the body over time was seen for all solubility classes and usage types for both the high and low-LET components. As well, the low-LET component tends to build up at a slower rate for all solubility classes and usage types. The soft tissues depict this trend best for both inhaled and ingested uranium, as can be seen in Figure 30, where the low-LET buildup in the stomach occurs at a rate nearly three times lower than the high-LET component, and in Figure 31, where the low-LET buildup in the breast occurs at nearly half the rate of the

high-LET component. During juvenile ages, there are fluctuations in the chronic doses, a result of the changing biokinetics at these ages and their impact on the dose rates at each year of life.

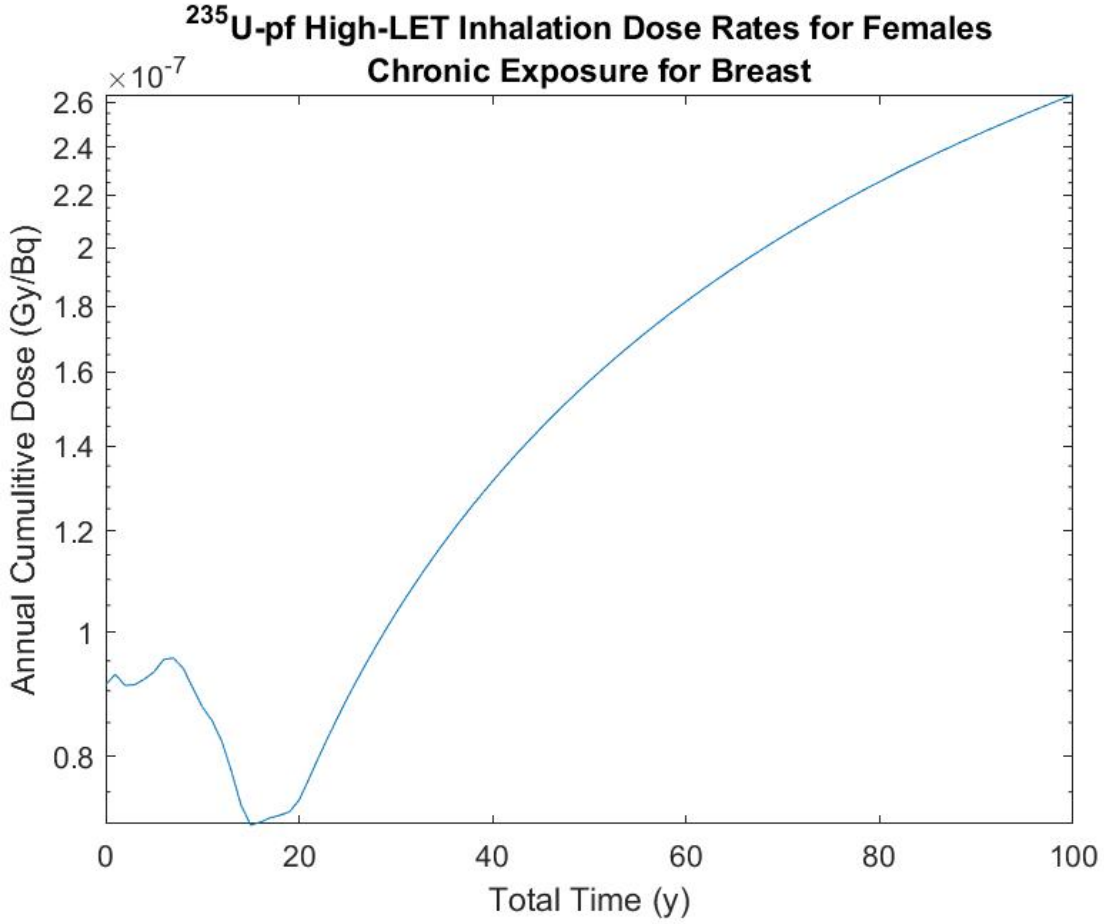

(a)

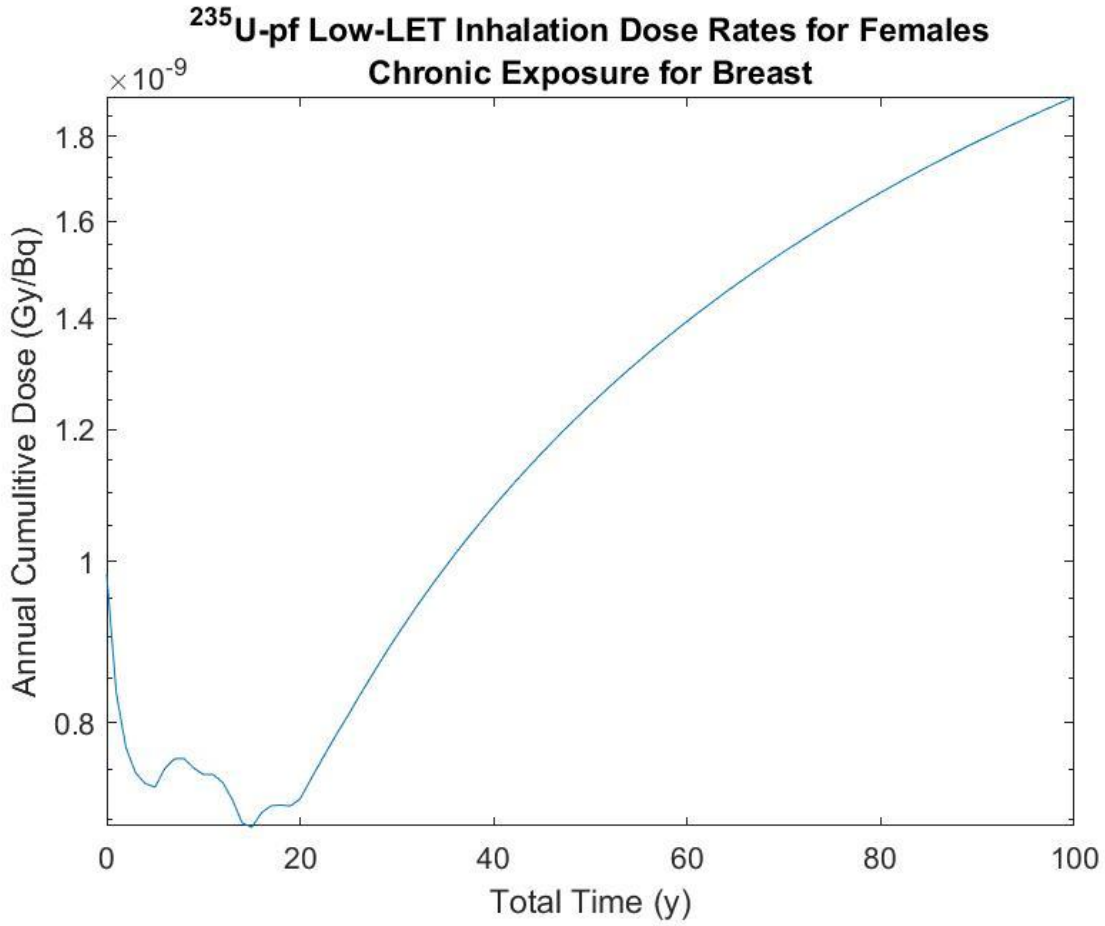

(b)

Figure 31. The (a) high-LET and (b) low-LET components for fast-clearing ^{235}U in the female breast from a chronic exposure.

Note that while all tissues portrayed some level of buildup, for all solubility classes and usage types, the kidneys showed almost no buildup, with the largest amount of buildup seen in slow-clearing inhaled uranium, as seen in Figure 32.

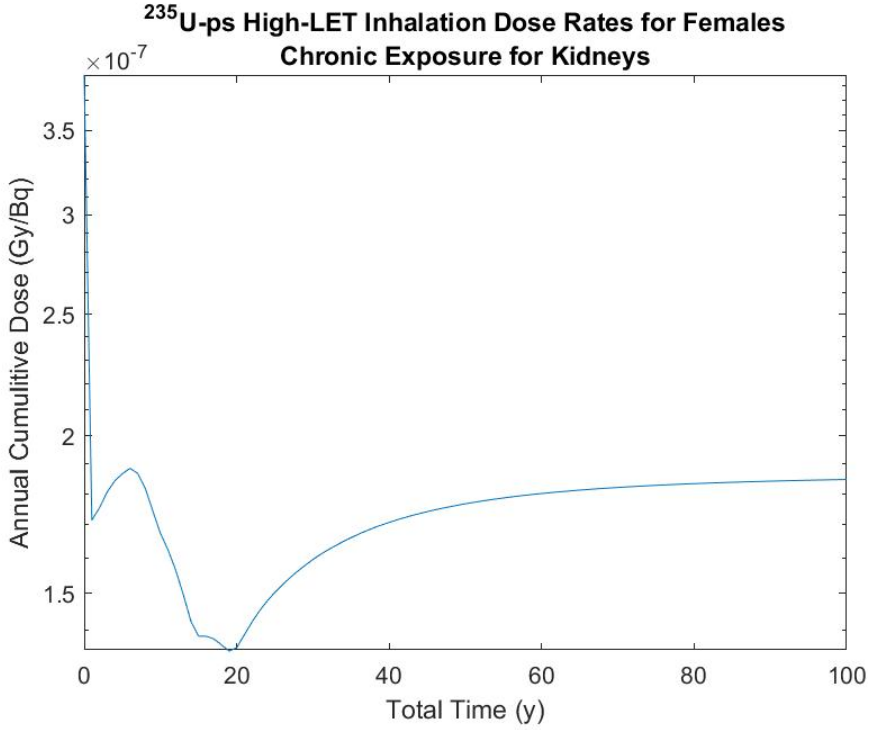

(a)

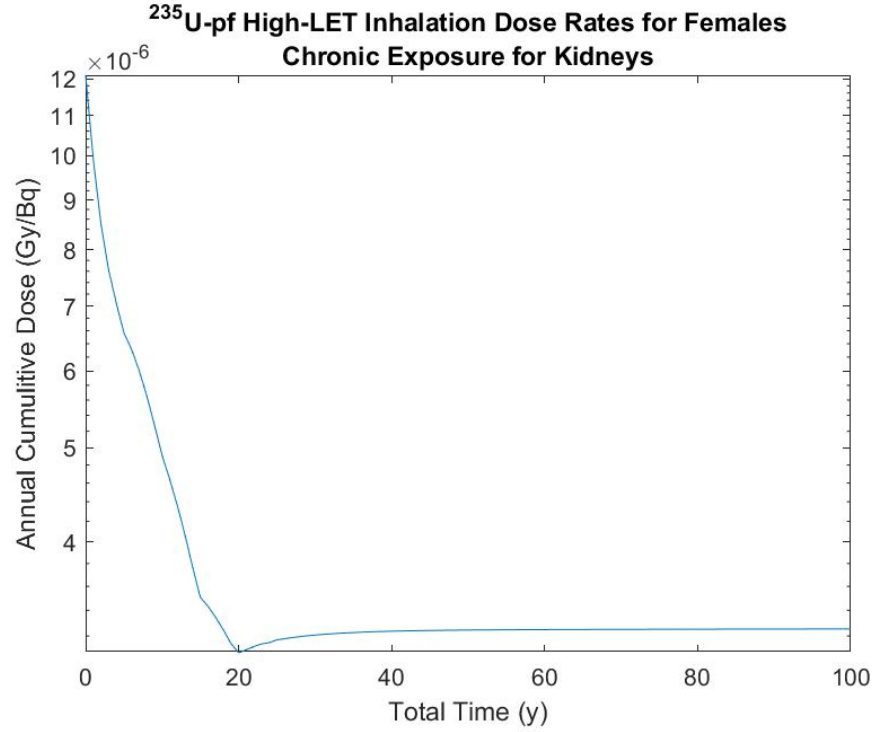

(b)

Figure 32. The high LET component of (a) slow-clearing (ps) and (b) fast-clearing (pf) ^{235}U in the female kidneys as a result of a chronic exposure.

4.1.3.b. ^{131}I

For shorter lived radionuclides, a plateau is seen for the plotting of the annualized chronic exposure with a rapid drop off after exposure stops. This was anticipated, as for a chronic exposure, where the dose is delivered on the first timestep of each year, the radionuclide will have mostly decayed away or been expelled from the body by the time the next exposure is received. This results in a more constant delivery of dose throughout lifetime to the tissues than compared to longer-lived radionuclides

With the first year of life after an acute exposure predominating for short-lived radionuclides, changes in biokinetics with increasing age drive the trend up until the adult ages. This can be seen in all tissues, solubility classes, and exposure types for ^{131}I, and explains why there is a decrease from beginning of life to year 20, followed by a plateau at year 20 to end of life, as seen in Figure 33. All adult ages are treated as biokinetically the same as year 20. Therefore, the dose rates from an adult exposure at year 20 are the same for all following adult ages to end of life.

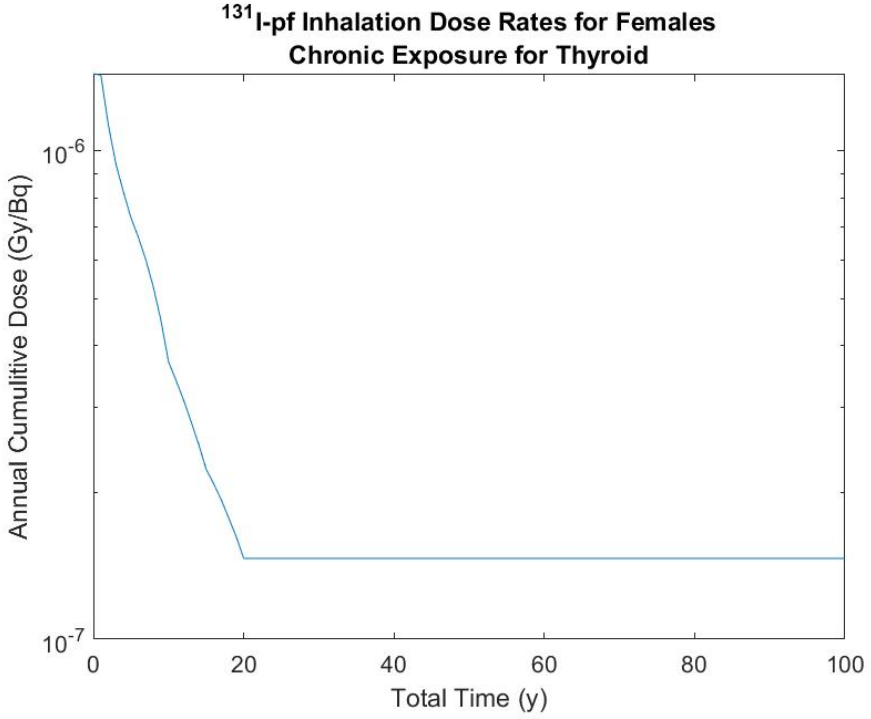

(a)

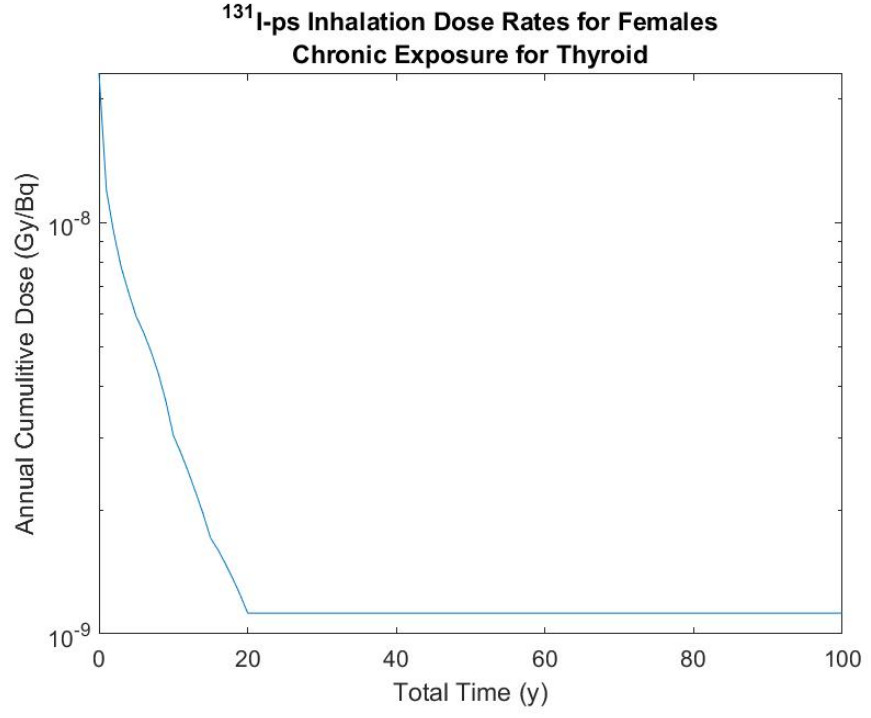

(b)

Figure 33. Absorbed dose rates in the female thyroid from a chronic exposure of (a) fast and (b) slow clearing ^{131}I.

The physical half-life of iodine (8 days) results in the above seen plateau, validated by the DCAL generated biokinetics plotted in Figure 13.

4.1.3.c. ^{137}Cs

Akin to iodine, ^{137}Cs reaches a plateau in the adult age range. However, unlike iodine, which saw little to no variance between fast- and slow-clearing solubility classes, fast- and slow-clearing cesium show differing behaviors in terms of buildup during adulthood.

Cesium tends to target the soft tissues if it does not simply pass through the system, and across all tissues for fast-clearing ^{137}Cs the same plateau can be seen, with the magnitude of the absorbed dose rates being comparable, seen in Figure 34. depicts this trend, showing clearly how the biokinetics stop changing after year 20, with no excess buildup in the adult ages. Akin to iodine, the comparatively short biological half-life of only 70 days results in a plateau in the adult ages, as there is no time for the radionuclide to build up before being excreted form the body. For all plots below, there is variation in the first 20 years of life, indicative of the changing biokinetics with respect to age before the adult age is attained.

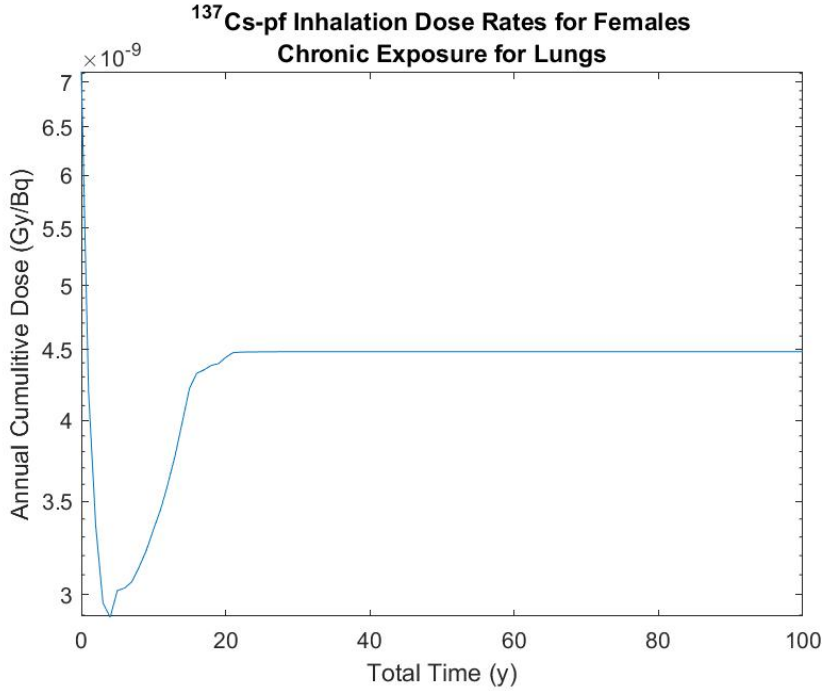
^{137}Cs-pf Inhalation Dose Rates for Females
Chronic Exposure for Lungs
×10^-9
Annual Cumulitive Dose (Gy/Bq)
Total Time (y)
7
6.5
6
5.5
5
4.5
4
3.5
3
0
20
40
60
80
100

(a)

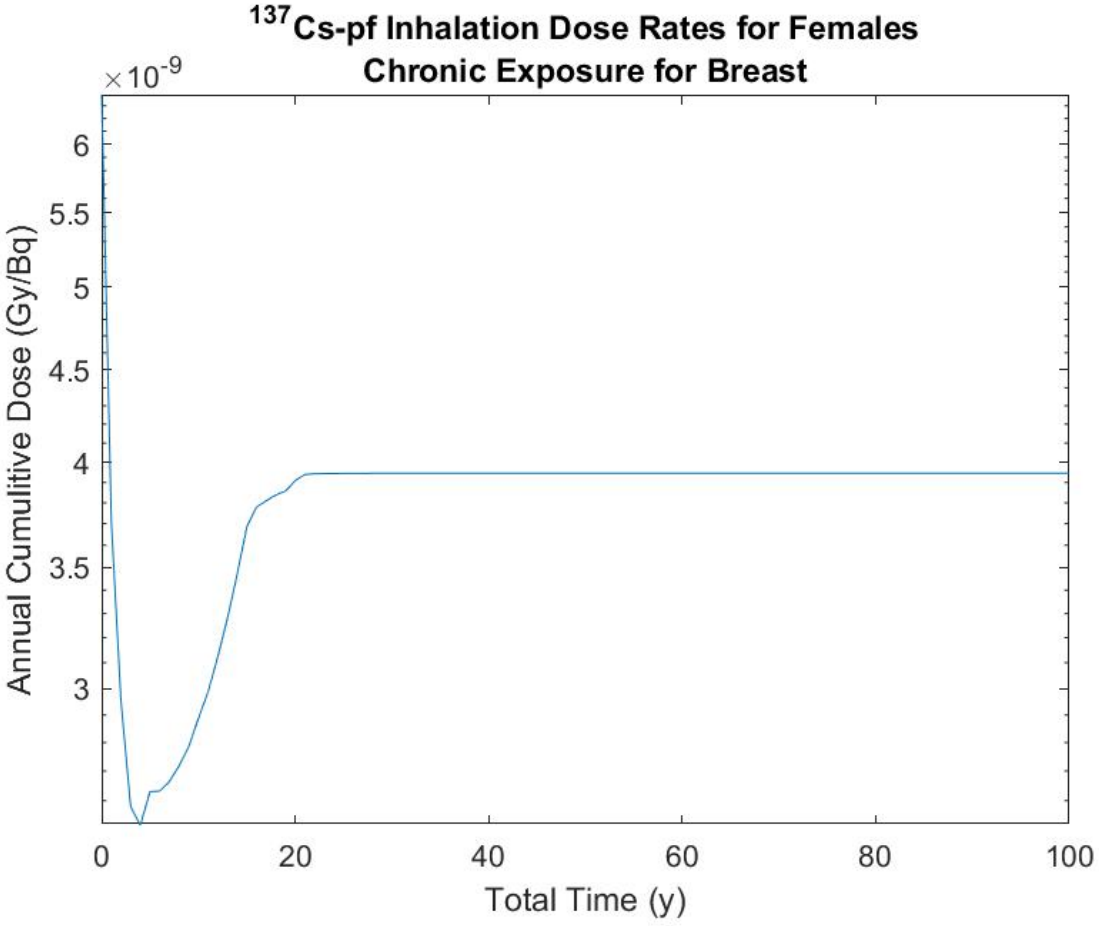
^{137}Cs-pf Inhalation Dose Rates for Females
Chronic Exposure for Breast
×10^-9
Annual Cumulitive Dose (Gy/Bq)
Total Time (y)
6
5.5
5
4.5
4
3.5
3
0
20
40
60
80
100

(b)

Figure 34. Absorbed dose rates due to a chronic exposure of fast-clearing ^{137}Cs in the female (a) lungs and (b) breast.

The slow-clearing behavior from the lungs results in slight buildup of the radionuclide into the adult ages, reaching a plateau around age 40 to 45. Compared to iodine and tritium, the effective half-life of ^{137}Cs is longer (approximately 70 to 100 days as compared to 5.5 days for ^{131}I and 10 days for tritium), resulting in more time for buildup before the radionuclide is expelled from the body or decays away, even if this buildup is only a fraction of an order of magnitude over the course of the time period. The visualization of this comparatively longer half-life can be seen in Figure 35.

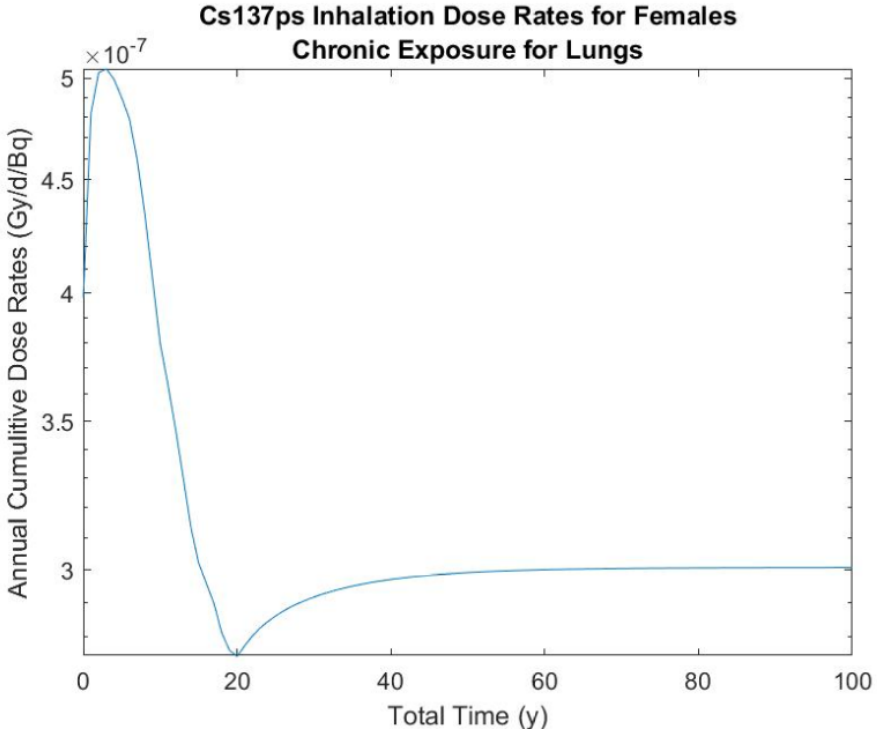

(a)

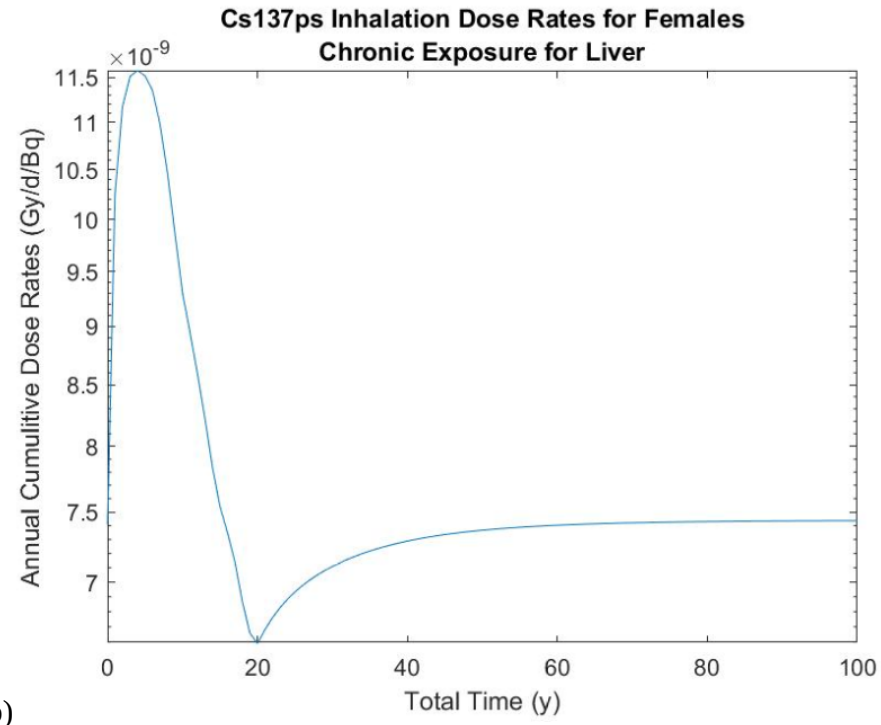

(b)

Figure 35. Absorbed dose rates due to a chronic exposure of slow-clearing ^{137}Cs in the female (a) lungs and (b) liver.

4.1.3.d. Tritium

Tritium portrays a similar biokinetic behavior as iodine, steadily dropping off over adolescence before plateauing at year 20, reflective of the unchanging biokinetics for all adult ages, and can be seen in Figure 36. Tritium's behavior being similar to water, as stated previously, means that it distributes evenly throughout the body, not localizing in any one given tissue. For inhalation, the dose delivered is higher in the lungs, which is to be expected. For ingestion via tap water, the doses delivered is nearly completely consistent for each tissue in the body. This is consistent across solubility classes; however, slow-clearing tritium exhibits a peak around year two that is not seen in the other solubility classes before tapering off in a similar manner. The magnitude of the overall absorbed dose due to a chronic exposure from slow-clearing tritium is higher as well, which is

expected, as the longer the radionuclide remains in the lungs, the more dose it will deliver to the tissue.

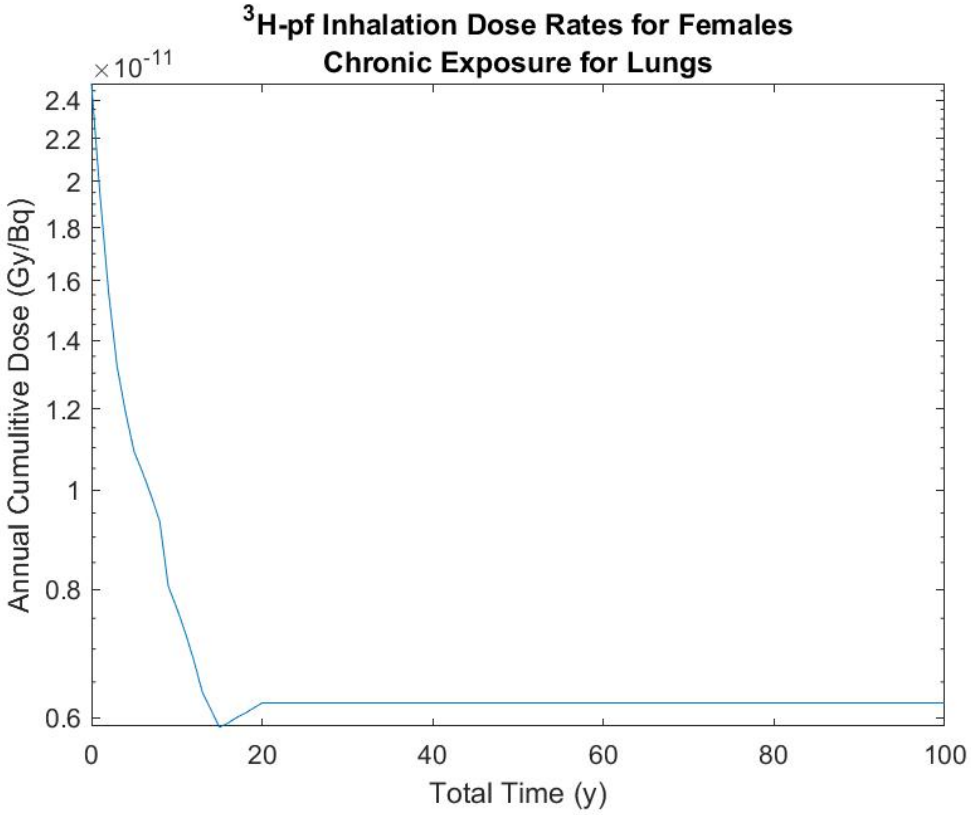

(a)

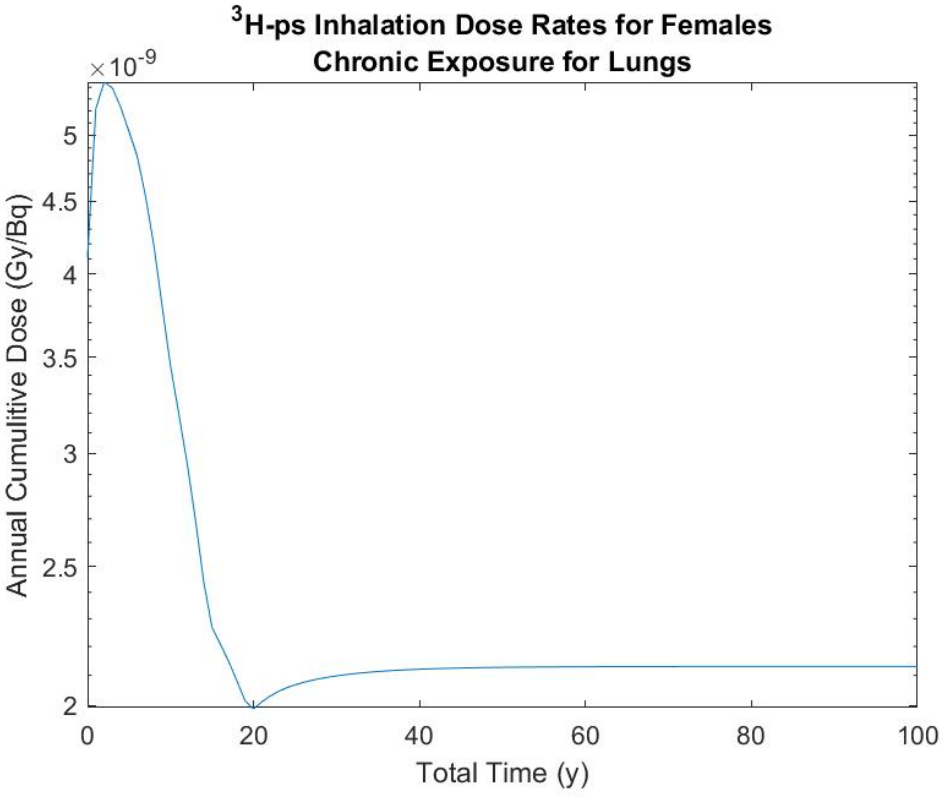

(b)

Figure 36. Absorbed dose rates from a chronic exposure to (a) fast and (b) slow clearing tritium in the female lungs.

4.1.3.e. ^{90}Sr

Strontium behavior for all solubility classes and exposure types for a chronic exposure is quite different from the other radionuclides investigated thus far. Absorbed dose rates for the bone and red marrow show a peak around year 20 for fast-clearing solubility before smoothly declining to an equilibrium rate in the last approximately 25 years of life. This peak followed by a dip is seen in all solubility classes, but is most prominent in the fast-clearing solubility class. As seen with uranium, the fluctuation within the first 20 to 25 years of life results from the changing biokinetics during those ages. Growth of the bone matrix take precedent here as juveniles grow, resulting in an increasing use of calcium-like materials as the bone is built. Strontium, acting biokinetically as calcium, therefore rapidly builds up in the bone as a child grows, that growth

greatly increasing as the child hits puberty, as can be seen in Figure 37 where the chronic exposure doses begin to rapidly increase.

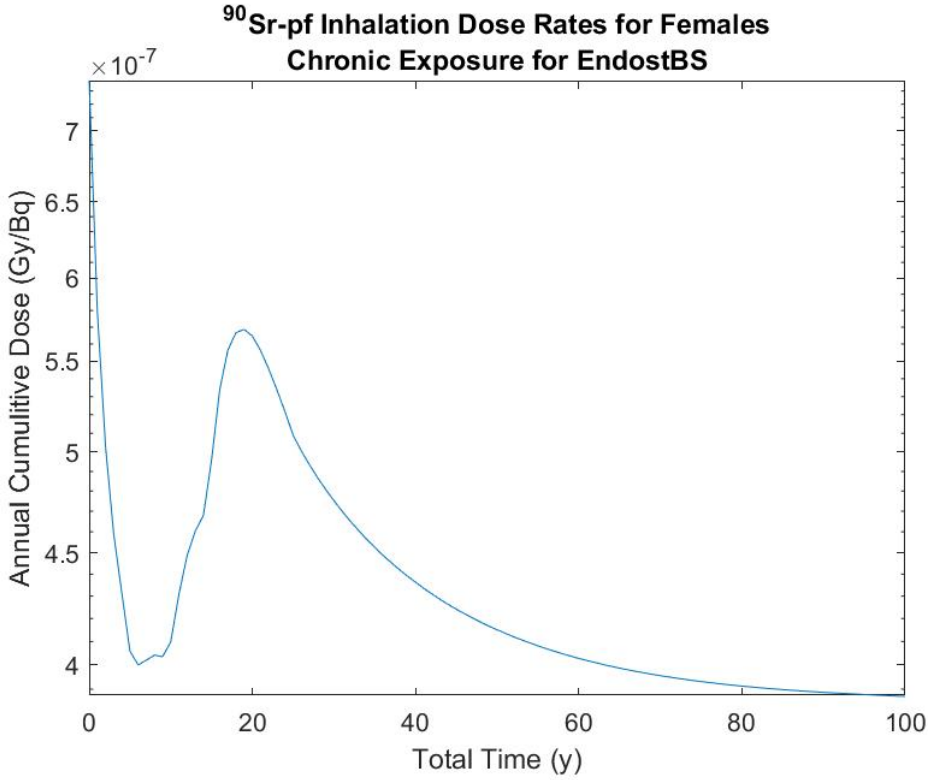

(a)

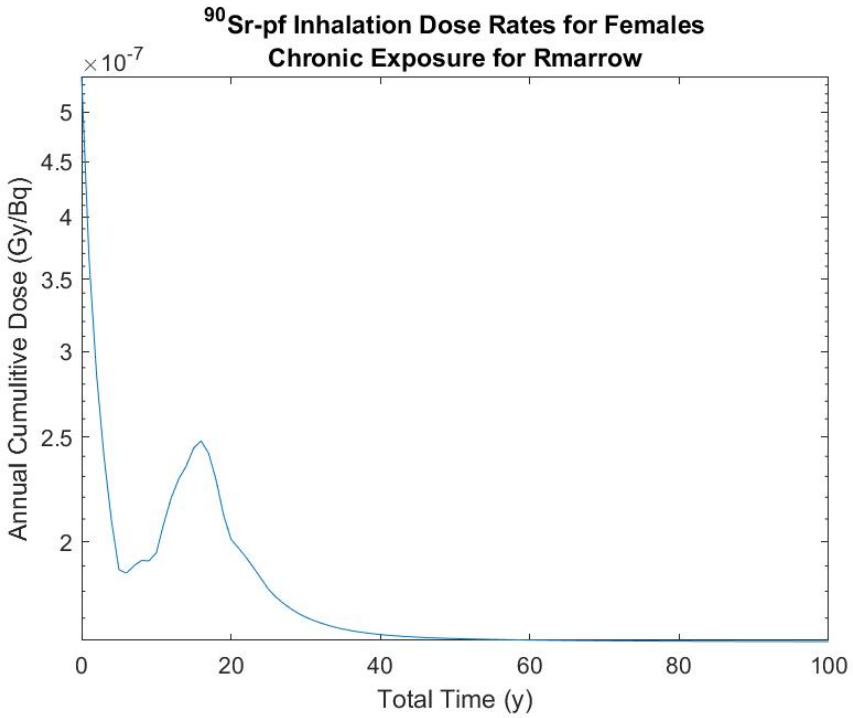

(b)

Figure 37. Absorbed dose rates from a chronic exposure of fast-clearing ^{90}Sr in the (a) female bone surface and (b) red marrow.

Slow-clearing strontium, seen in Figure 38, portrays a similar peak in the chronic dose rates; however, the subsequent decrease in the dose rate is more gradual, reaching a plateau far sooner than fast-clearing.

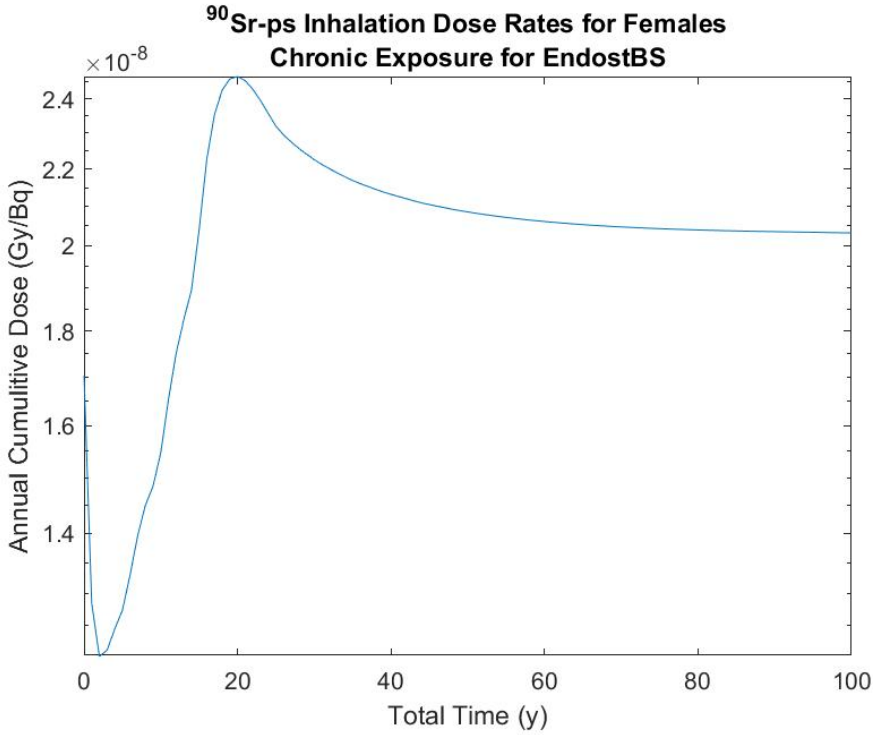

(a)

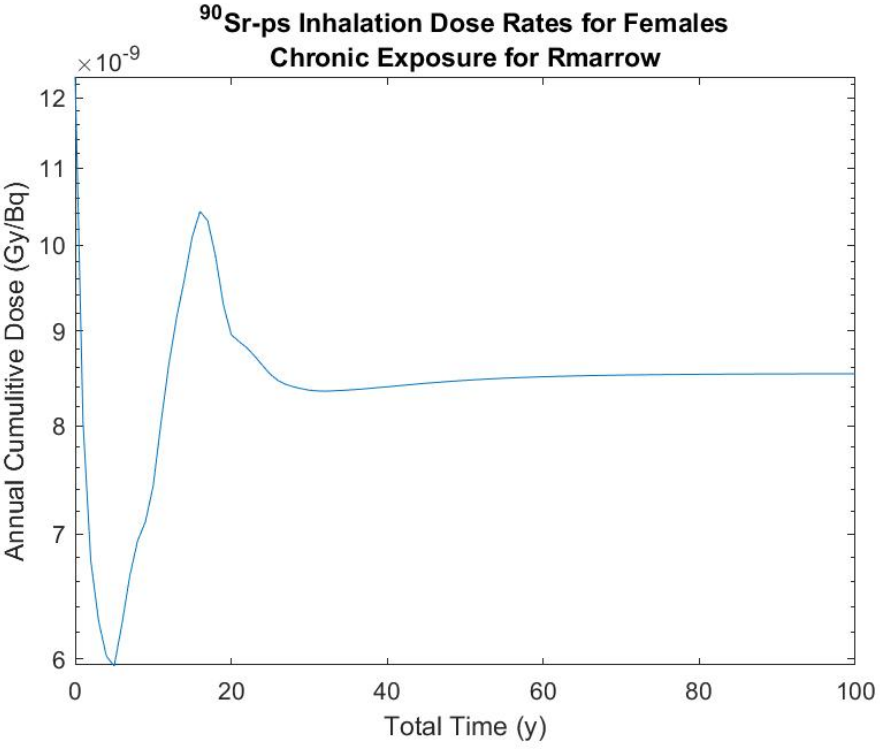

(b)

Figure 38. Absorbed dose rates from a chronic exposure of slow-clearing ^{90}Sr in the female (a) bone surface and (b) red marrow.

Ingestion of ^{90}Sr follows a similar trend as fast-clearing inhaled strontium in the bone surface and red marrow, peaking at year 25 for the bone surface and 15 for the red marrow before tapering off to end of life.

4.2. Risk Calculations for Federal Guidance Report 13 Data

The replication of the FGR 13 risk coefficients from a chronic exposure proved successful, with all radionuclides falling within a 6% difference and most falling within 4% difference of FGR 13 reported values. Sources of discrepancy stem primarily from differences in interpolation methods, as DCAL's original programming utilizes a 3-D interpolation method to populate intermittent data, a functionality unavailable during this work given the programs of choice. Validity of risk coefficient recreation was confirmed by Dr. Keith Eckerman of Oak Ridge National Labs. Table 14 summarizes the results for the sex- and age-averaged risk coefficients for a chronic uptake of the outlined radionuclides for both incidence and mortality. Note that the coefficients in FGR 13 are applicable to either an acute or chronic uptake.

Table 14. Summary of the calculated risks from a chronic exposure as compared to published FGR 13 data.

Radionuclide*	Calculated Incidence	FGR 13 Incidence	% Difference	Calculated Mortality	FGR 13 Mortality	% Difference
^{131}I - pf	5.362×10^{-10}	5.27×10^{-10}	1.74	5.65×10^{-11}	5.55×10^{-11}	1.81
^{131}I - pm	2.251×10^{-10}	2.2×10^{-10}	2.30	1.30×10^{-10}	1.29×10^{-10}	1.12
^{131}I - ps	1.724×10^{-10}	1.69×10^{-10}	2.02	1.42×10^{-10}	1.4×10^{-10}	1.53
^{131}I - pg Food	1.791×10^{-09}	1.75×10^{-09}	2.35	1.89×10^{-10}	1.85×10^{-10}	2.16
^{131}I - pg Water	1.266×10^{-09}	1.23×10^{-09}	2.89	1.34×10^{-10}	1.31×10^{-10}	2.53
^{3}H - pm	5.653×10^{-12}	5.38×10^{-12}	5.08	4.82×10^{-12}	4.58×10^{-12}	5.20
^{3}H - pf	5.316×10^{-13}	5.28×10^{-13}	0.69	3.63×10^{-13}	3.61×10^{-13}	0.63
^{3}H - ps	2.364×10^{-11}	2.3×10^{-11}	2.77	2.18×10^{-11}	2.12×10^{-11}	2.71
^{3}H - pg Water	1.400×10^{-12}	1.37×10^{-12}	2.16	9.66×10^{-13}	9.44×10^{-13}	2.30
^{137}Cs - pf	3.326×10^{-10}	3.21×10^{-10}	3.62	2.27×10^{-10}	2.19×10^{-10}	3.64
^{137}Cs - pm	9.244×10^{-10}	8.91×10^{-10}	3.75	8.09×10^{-10}	7.81×10^{-10}	3.64
^{137}Cs - ps	3.115×10^{-09}	3.03×10^{-09}	2.82	2.85×10^{-09}	2.77×10^{-09}	2.79
^{137}Cs - pg Food	1.047×10^{-09}	1.01×10^{-09}	3.61	7.13×10^{-10}	6.88×10^{-10}	3.61
^{137}Cs - pg Water	8.587×10^{-10}	8.22×10^{-10}	4.47	5.92×10^{-10}	5.66×10^{-10}	4.58
^{90}Sr - pf	1.146×10^{-09}	1.17×10^{-09}	-2.07	1.06×10^{-09}	1.08×10^{-09}	-1.70
^{90}Sr - pm	2.915×10^{-09}	2.84×10^{-09}	2.65	2.71×10^{-09}	2.65×10^{-09}	2.34
^{90}Sr - ps	1.172×10^{-08}	1.15×10^{-08}	1.94	1.11×10^{-08}	1.08×10^{-08}	2.39
^{90}Sr - pg Food	1.816×10^{-09}	1.86×10^{-09}	-2.36	1.57×10^{-09}	1.62×10^{-09}	-3.17
^{90}Sr - pg Water	1.496×10^{-09}	1.51×10^{-09}	-0.96	1.32×10^{-09}	1.34×10^{-09}	-1.48
^{235}U - pf	1.627×10^{-08}	1.59×10^{-08}	2.34	1.15×10^{-08}	1.12×10^{-08}	2.33
^{235}U - pm	2.780×10^{-08}	1.59×10^{-08}	1.84	2.60×10^{-07}	2.57×10^{-07}	1.02
^{235}U - ps	6.892×10^{-07}	6.77×10^{-07}	1.80	6.54×10^{-07}	6.42×10^{-07}	1.92
^{235}U - pg Food	2.640×10^{-09}	2.55×10^{-09}	3.54	1.68×10^{-09}	1.62×10^{-09}	3.92
^{235}U - pg Water	1.951×10^{-09}	1.88×10^{-09}	3.77	1.26×10^{-09}	1.321×10^{-09}	4.03

*pf, ps, pm, and pg are to indicate fast clearing inhalation, slow clearing inhalation, moderate clearing inhalation, and ingestion, respectively.

Reproduction of FGR 13 dose rates utilizing the annualized absorbed doses from the absorbed dose rates from the DCAL software validates the annualization process used to inform the risk calculations. This provides a basis for the calculation of the equivalent, effective,

committed equivalent, and committed effective doses through the use of these annualized dose rates for both the acute and chronic exposures.

In order to prepare for the comparison of the CED's to the calculated risks, the lifetime risks from an acute exposure were calculated for each radionuclide. The calculation of these acute exposure risks is an intermittent step on the way to calculating the lifetime risk from a chronic exposure, and as such, the calculations are also validated by the accurate replication of the FGR 13 risk coefficients.

Lifetime risk as it varies with age of exposure for acute exposures depends on several factors including the lifetime attributable risk (LAR) over the lifetime post internal exposure, the probability of surviving to the age at which the exposure is received, the probability of surviving to an attained age post internal exposure, and the dose rates resultant from the exposure. All of these elements are time dependent, so there is expected to be a fluctuation in all radionuclides and tissue, but ultimately a decreasing trend as survival, LAR, and the dose rates all decrease with time. These trends of the acute risks respective to age of intake are included in plots generated in section 4.4.

4.3. Committed Effective Dose Calculations and Risk Per Unit Dose Modification

The CED was calculated after the completion and validation of the risk coefficients. For the FGR 13 data, ICRP *Publication 60* methodologies were followed in regards to applied radiation and tissue-weighting factors and commitment periods. Updated values have been produced in ICRP *Publication 103* for tissue and radiation weights, but in order to keep consistency within the dataset, ICRP *Publication 60* was determined the best choice for manipulation of FGR 13 informing data. CEDs were calculated for both acute exposures and chronic exposures, with acute

exposures integration period being to age 70 years for juveniles and a 50 year period for adults. For chronic exposures, the survival and usage modified values were integrated over a commitment period of the total lifetime in a similar manner as was used to calculate the risks from a chronic exposure, and then this resultant value was divided by the lifetime intake in order to normalize the ingested lifetime intake of the radionuclide.

In order to utilize CED as an approximate indicator of possible risk, the value must be converted to the same units as risk for the most accurate comparison. This is done through the application of the risk per unit dose factor. A comparison of the results for both chronic and acute risks can be found in the following section. For this step, in order to avoid "double counting" of the tissue weights, the risk per unit dose factor for mortality and incidence for the whole body were applied to the calculated CEDs, rather than the tissue specific component of this factor.

4.4. FGR 13 Risk and Committed Effective Dose Comparisons

4.4.1. Acute Exposure

To show the trend of this risk per unit dose modified CED, the results were plotted with respect to age of exposure alongside the risk from acute exposure with respect to time in order to point out any large divergences between the two values. In this analysis, the proportional difference between the FGR 13 calculated risks, and the ICRP *Publication 60* methodology to calculate the committed doses followed by the risk per unit dose factors from FGR 13 was analyzed as well. This section is broken up by radionuclide to discuss the differences seen within each radionuclide solubility classes and ingestion type.

The plots in the following section are all plotted on a semilog-y scale, with risk corresponding to the primary (left) axis and the risk per unit dose modified CEDs corresponding

to the secondary (right) axis. Consistent across most tissues, solubility classes, and usage types, CED values maintain a straight line through all adult ages of exposure. This is due to the fact that there is nothing strictly age dependent that informs the CED calculations, save the informing dose rates. These dose rates, as previously mentioned, are treated as biokinetically the same for each age of exposure in adulthood, as this study does not consider separate models from geriatrics, who are integrated as part of the adult models. Thus, with no variables changing through adulthood, CED would remain constant through all adult ages, as seen. The outliers are for radionuclides that are not fast decaying. For these radionuclides, post age 60, the number of datapoints in the commitment period decrease with increasing age. For slow decaying radionuclides, and radionuclides that are retained in the body for extended periods of time, every datapoint out to EOL is non-negligible. Therefore, with the reduction of non-negligible datapoints in the commitment period, a dip in the CED can be seen, which is purely a data limitation. To remove this limitation, one could extrapolate the data past the end of life time step (105 years) when calculating the CED, which would result in the solid 50-year commitment period for every year of exposure through end of life.

4.4.1.a. ^{131}I

For all solubility classes, usage types, and tissues, the trend between the FGR 13 calculated mortality and incidence risk and the ICRP *Publication 60* methodology utilized to calculate what is being referred to in this report as tissue-specific detriment-weighted committed equivalent doses showed reasonable correspondence. This value is not a defined ICRP quantity, but is rather the tissue specific components of effective dose. Where effective dose is the summation over all tissues, this tissue-specific detriment-weighted committed equivalent dose will look at the individual tissue components used to calculate effective dose to see how the components of the

ICRP quantity compare with the tissue specific risks. Risk per unit dose modified CEDs for the whole body fall well within an order of magnitude. For most soft tissues, the tissue-specific detriment-weighted committed equivalent doses follow this trend as well when compared to the tissue specific components of risk, and divergence in the trend increases with increasing age. It is important to note that using tissue weights to calculate the tissue-specific components of CED without aggregating across all tissues is not the intended use of effective dose, nor is it an ICRP quantity. However, it was determined that there is utility in comparing tissue to tissue to ensure proper trending between the calculated modified doses and the FGR 13 calculated risks.

Iodine, as previously established, is a thyroid-seeking radionuclide, localizing in the thyroid post internal exposure. Thus, a comparison of the detriment-weighted committed equivalent dose as compared to the tissue-specific risk is of interest. Figure 39 depicts the trends for both incidence and mortality in the thyroid, comparing across FGR 13 calculated risk and ICRP *Publication 60* calculated dose. ICRP *Publication 60*'s committed focus is on incidence of cancer, so it is expected that for cancers that are not highly fatal, the mortality risk would be overestimated by the committed dose. This was supported for the thyroid. While the incidence risk of thyroid cancers was under estimated by the committed dose, the mortality swings the other way, over estimating the true mortality risk. For the other soft tissues when exposed to fast-clearing iodine, the committed doses track along with the calculated risks, all falling within an order of magnitude difference. The trend also holds for both the lungs and the other soft tissues for moderate and slow-clearing iodine.

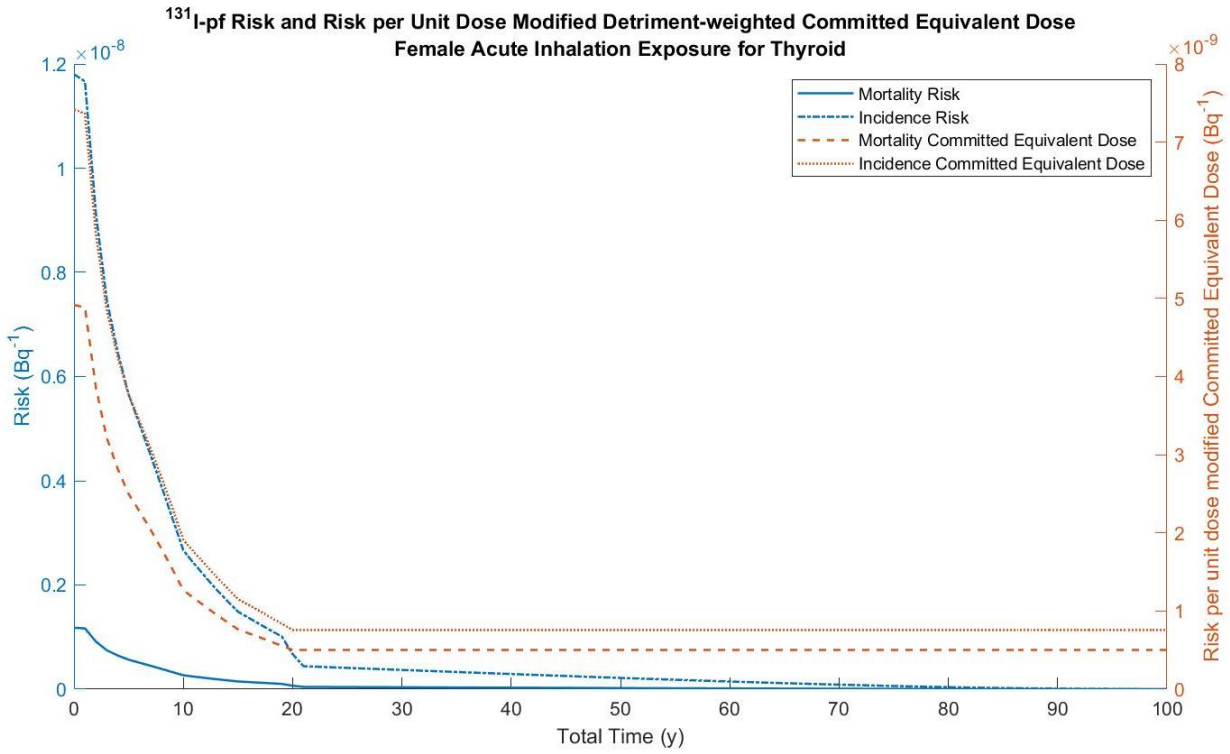

Figure 39. FGR 13 calculated risk as compared to ICRP *Publication 60* calculated detriment-weighted committed equivalent dose from an acute inhalation of fast-clearing ^{131}I in the female thyroid.

For inhalation of radionuclides, the lungs are of particular interest. For fast, moderate, and slow-clearing iodine, the detriment-weighted committed equivalent doses consistently under represent the true risk to the tissues for both mortality and incidence. However, the values do trend with one another through life, until the reduction of the survival function and LAR towards the second half of life begin to see a divergence in the trend, as anticipated. The behavior in the lungs due to moderate- and slow-clearing ^{131}I can be found in Appendix C.

Ingested iodine, through both water and food ingestion, shows a closer relation for the thyroid between FGR 13 risk and the detriment-weighted CED. However, as with inhalation of the radionuclide, the detriment-weighted CED overestimates the tissue-specific risk for the thyroid for

mortality. For incidence, the detriment-weighted CED underestimates the tissue-specific risk until approximately year ten, at which point the CED over estimates the true risk to the tissue.

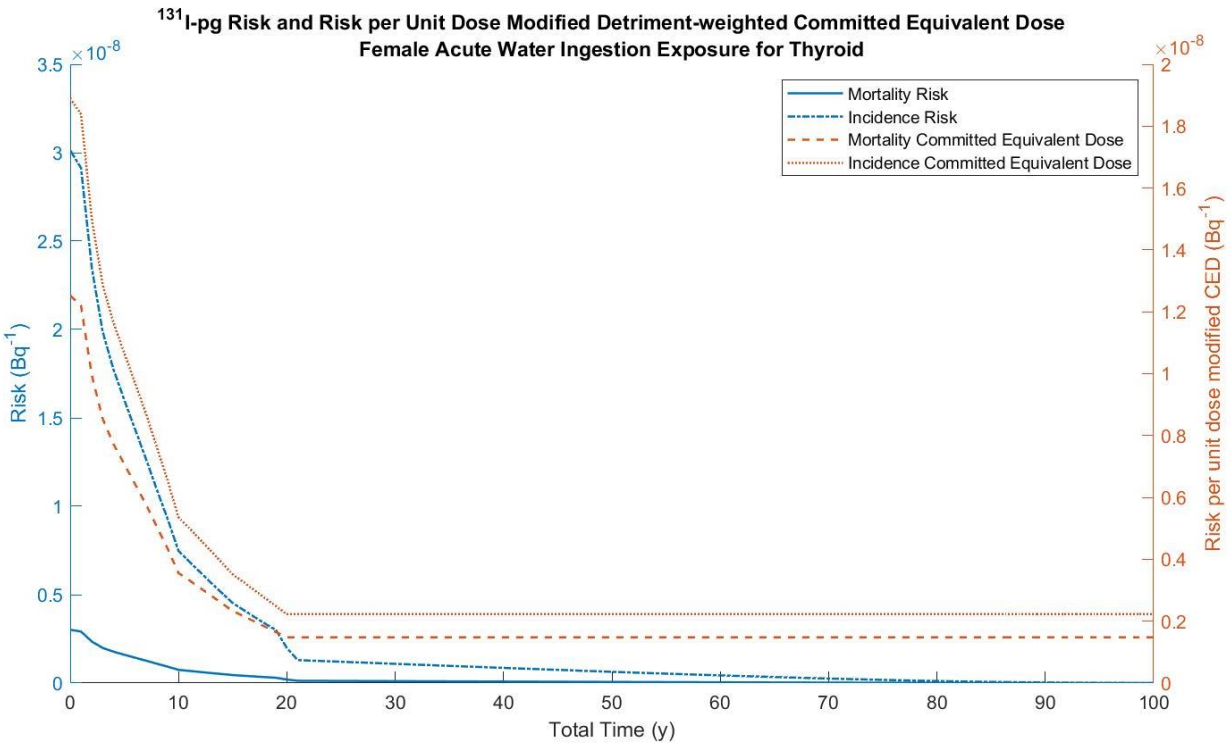

Figure 40. Risk and detriment-weighted committed equivalent dose to females from tap water ingestion of ^{131}I.

While information regarding the general tissue-specific behavior of the radionuclide in regards to the risk and the committed equivalent doses can be gleaned from the tissue-specific comparisons, CED is meant to be applied as a uniform whole-body irradiation; a summation over all tissues. Thus, for each solubility class and usage type, the risk from an acute uniform exposure throughout life was compared to the whole body committed effective dose from an acute exposure throughout life. For all stated solubility classes and usage types, a corresponding trend was seen. However, the committed effective dose consistently underestimated the true risk by an order of

magnitude for both sexes for both mortality and incidence. The corresponding male values for Figure 41 can be found in Appendix D.

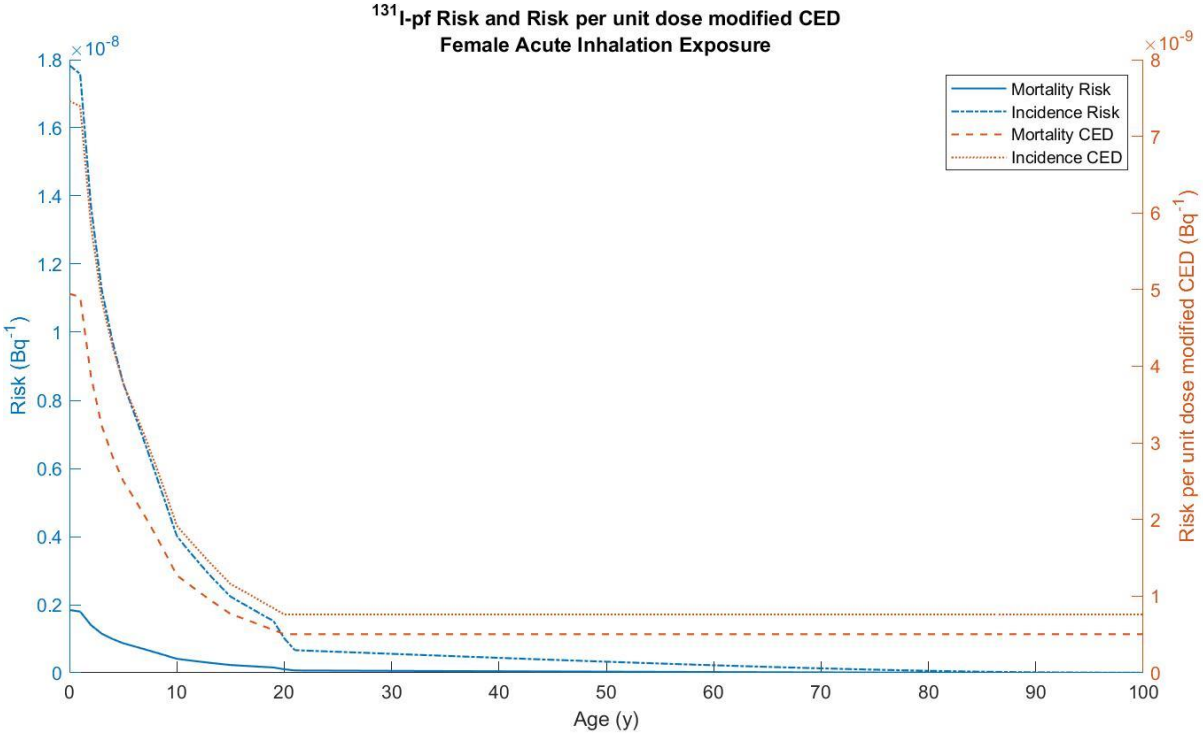

(a)

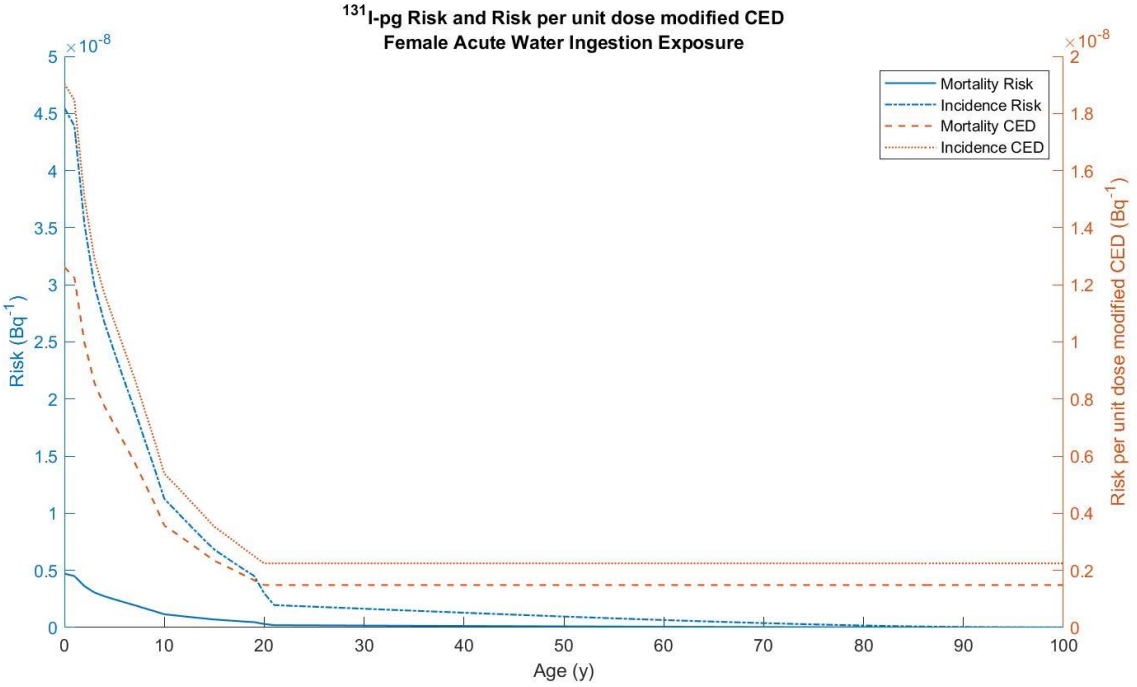

(b)

Figure 41. FGR 13 risk compared to ICRP *Publication 60* committed effective dose from an acute exposure through life for (a) fast-clearing and (b) water ingested ^{131}I for females.

4.4.1.b. ^{137}Cs

^{137}Cs tends to pass through the body after update, however, whatever does not simply pass through tends to favor the soft tissues and the muscle as a uniform whole-body emitter. For all solubility classes and usage types, the detriment-weighted CED was found to typically underestimate the true tissue-specific risk. This holds true between the sexes as well. The outliers to this general rule include the skin, which typically overestimates the true risk by approximately an order of magnitude; the colon, bone surface, and red marrow, which tend to rather accurately represent the true risk; and the liver, which beginning at approximately year 15, begins to overestimate the incidence risk while the mortality CED tends to reflect the mortality risk with a degree of accuracy. Plots of these tissues can be found in Appendix C. Decent correspondence between the risk and detriment-weighted CED is expected for the bone surface and red marrow, as cesium tends to locate in the muscle around the bone, rather than in the bone matrix itself. This

reduces the dose to the bone from within the bone, ultimately leading to a lower CED that better corresponds with the FGR 13 calculated risk.

For inhaled cesium of all solubility classes, the lungs are of key interest as the primary irradiated tissue. It was seen that the detriment-weighted CED consistently underestimated the FGR 13 calculated risk, regardless of solubility class, by approximately an order of magnitude. Figure 42 depicts this trend for both fast- and moderate-clearing cesium. Corresponding plots to the ones listed in the following figures for this section can be found in Appendix C, showing the values for the other sex, as well as the values for slow-clearing cesium.

All plots in this section show a step function pattern between ages 20 and 40. This is due to variations in the LAR value between these ages, as the dose rates are not changing with increased age of exposure. LAR does not steadily decrease for all tissues. For the lungs, specifically, the LAR stagnates between ages 20 and 29, then increases at age 30, stagnates again with only a slight increase to age 40 before finally dropping off all the way through end of life. For cesium, the dose rates drop off at the perfect rate that the effect of the slight increase in the LAR at these values can be seen in the tissue-specific plots. This behavior was not seen in iodine, as the rate of decay of the dose rates is too rapid to see an effect on the risk curve for this age range.

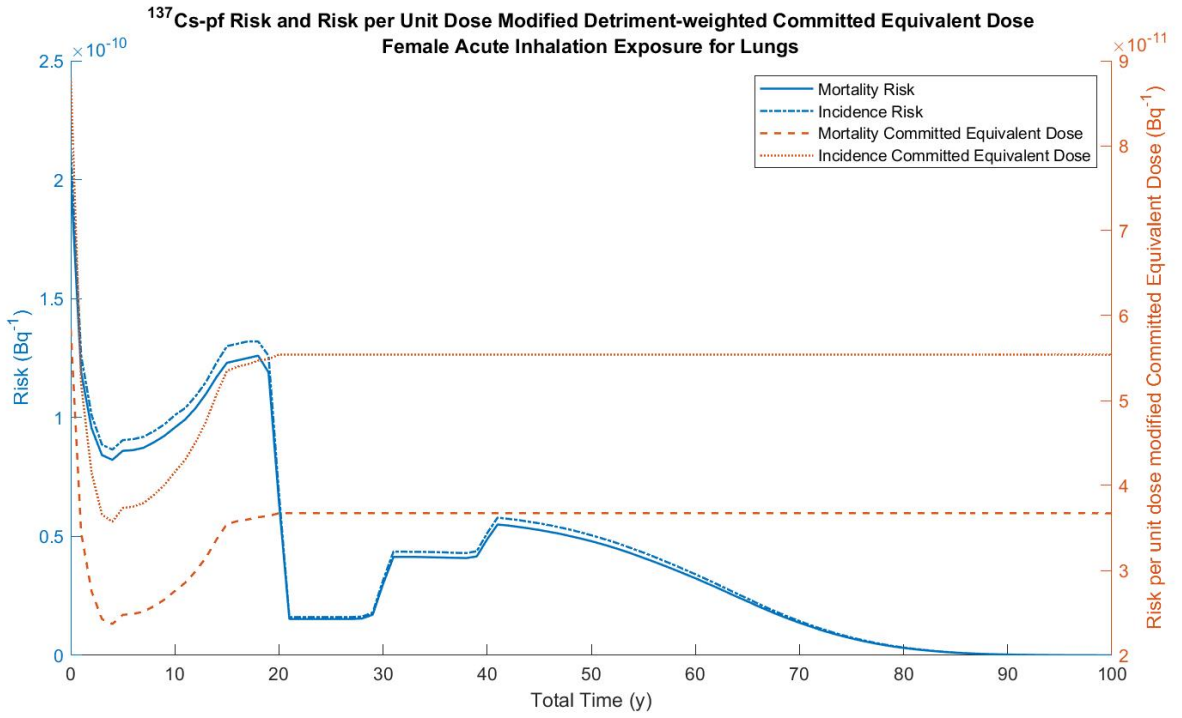

(a)

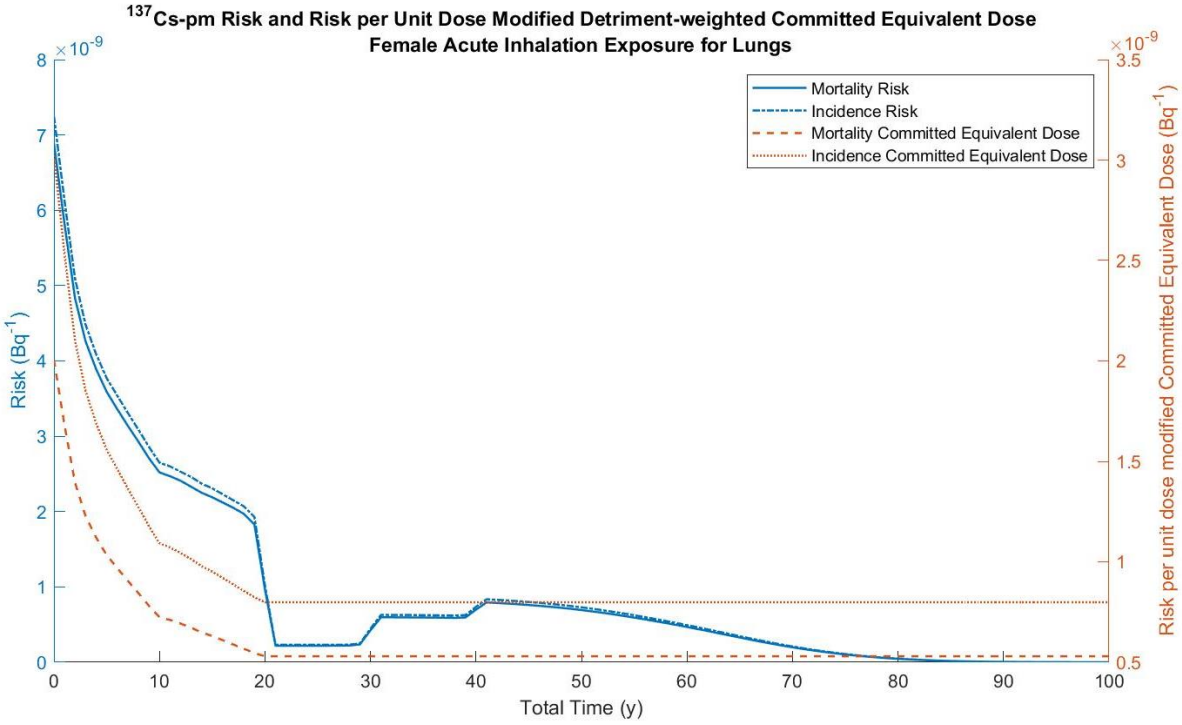

(b)

Figure 42. FGR 13 calculated risk compared to ICRP *Publication 60* calculated committed effective dose for the lungs for (a) fast and (b) moderate-clearing ^{137}Cs.

As the tissue-specific detriment-weighted committed equivalent doses tends to underestimate the true risk to the tissues, it was expected that the comparison of the CED due to a uniform exposure to the FGR 13 calculated risk would also show an underrepresentation for both males and females. This trend is in fact seen for all solubility classes and usage types, with the CED underestimating the true risk by approximately an order of magnitude at its largest difference, with the difference narrowing with decreasing rate of clearance from the lungs, seen in Figure 43. Again, the effect of the behavior of the LAR values between ages 20 and 40 are clearly visible. Corresponding male values can be found in Appendix D.

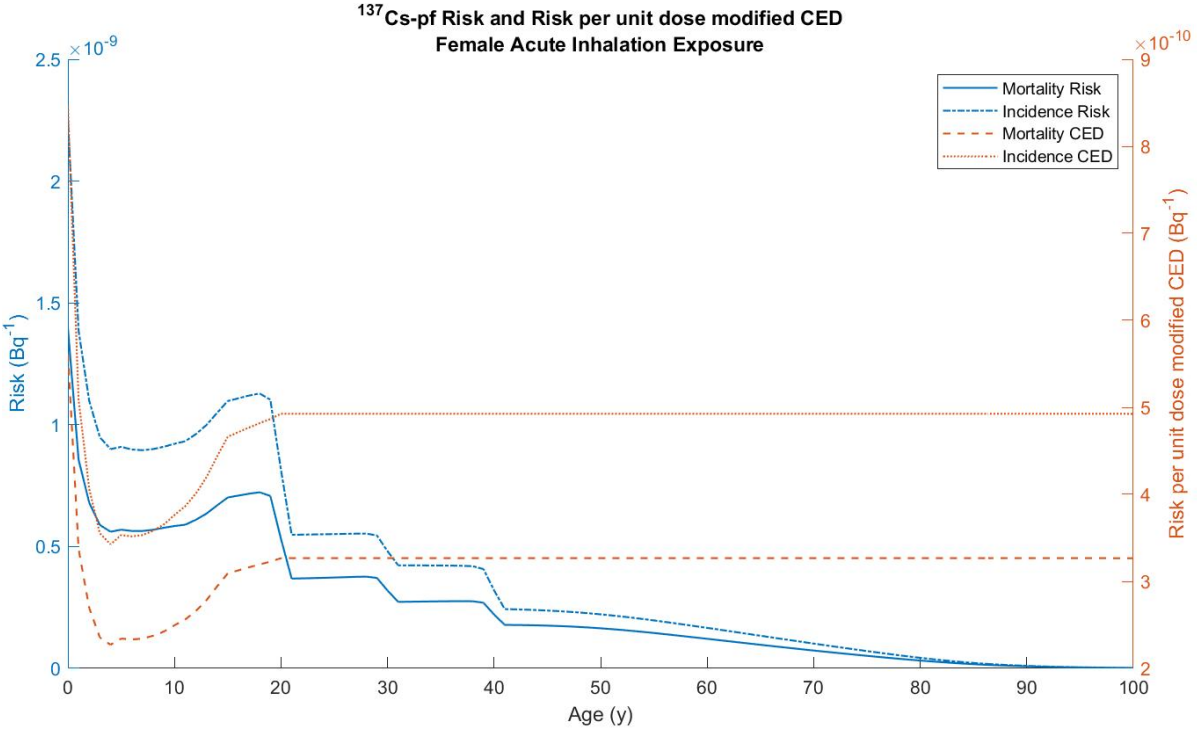

(a)

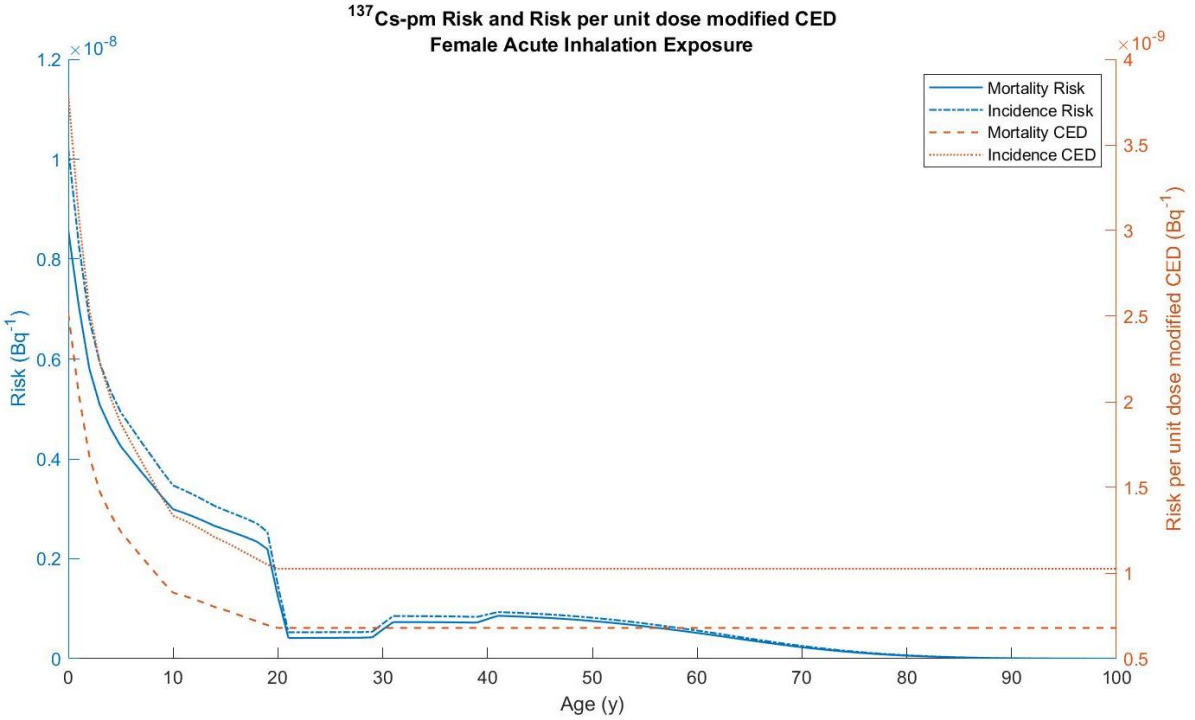

(b)

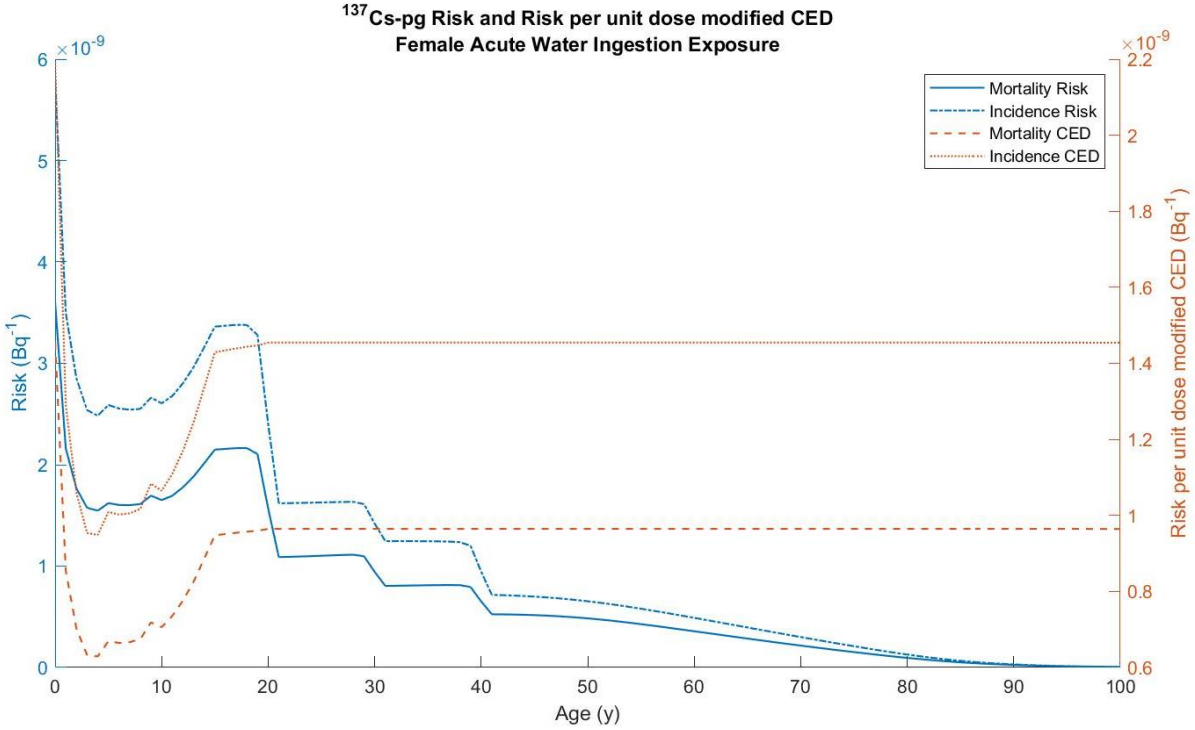

(c)

Figure 43. FGR 13 calculated risk compared to ICRP *Publication 60* calculated committed effective dose for the whole body for (a) fast-clearing, (b) moderate-clearing, and (c) tap water ingested ^{137}Cs for females.

The trend in the decrease of the risk and CED for ingestion for both food and water follows the trend of fast-clearing inhaled cesium, the only difference being the risk and CED both being slightly higher than the values calculated for fast-clearing inhaled cesium.

4.4.1.c. Tritium

Tritium's behavior being akin to water ensures a very even distribution through the body's soft tissues, without radioactive material locating in any one tissue. Thus, similar trends of risk and detriment-weighted committed equivalent dose were expected to be seen.

Between all solubility classes, usage types, and most tissues, the detriment-weighted committed equivalent dose tends to underestimate the true risk, typically within an order of magnitude. The only tissue where the opposite is true is for the skin, where the detriment-weighted committed equivalent dose overestimates both the incidence and mortality risks, and can be seen in Figure 44. This holds true for all solubility classes and both sexes, with the over estimation ranging between one and two orders of magnitude. However, a similar trend in the decrease in the risk as compared to the detriment-weighted committed equivalent dose can be seen. For certain tissues, such as the breast and the liver, the detriment-weighted committed equivalent dose is fairly accurate in its representation of the true tissue-specific risk, and is consistent across all solubility classes and usage types, as well as between male and female tissues. The corresponding plots for males for the detriment-weighted committed equivalent dose plots listed in this section, as well as the plots for slow-clearing tritium, can be found in Appendix C.

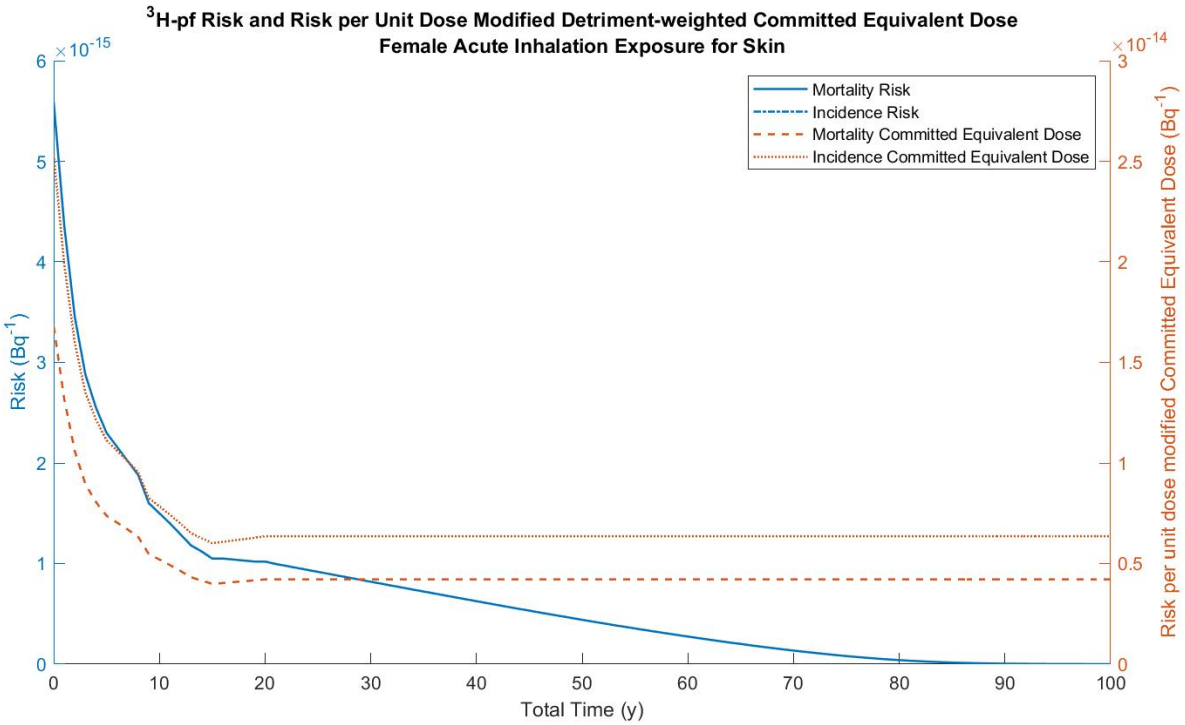

(a)

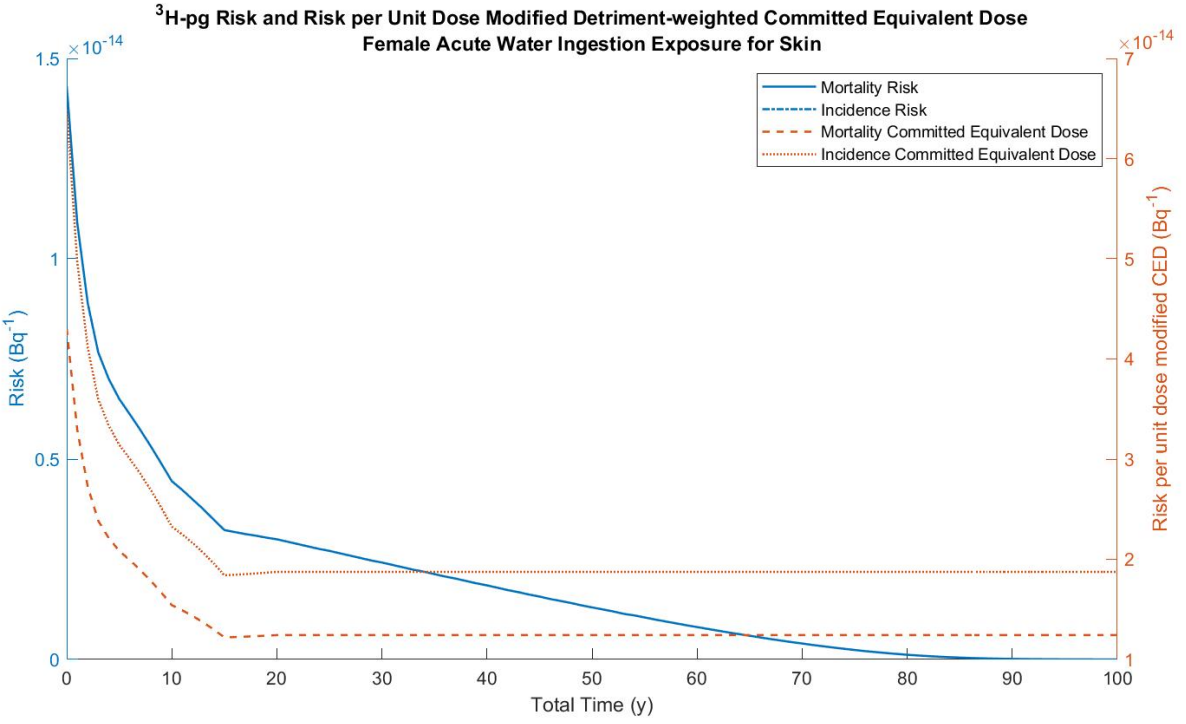

(b)

Figure 44. Risk and detriment-weighted committed equivalent dose to the female skin due to fast-clearing (a) and tap water ingested (b) tritium.

As with inhaled iodine and cesium, the lungs are of interest as the primarily irradiated organ from an inhalation uptake. For the detriment-weighted committed equivalent dose for the lungs, the FGR 13 calculated risk is underestimated by an order of magnitude for all three solubility classes, with an increasing divergence as the LAR and survival functions decrease as well, as was seen with iodine. The trend is consistent between males and females. Moderate clearing tritium is selected in Figure 45 to represent this trend.

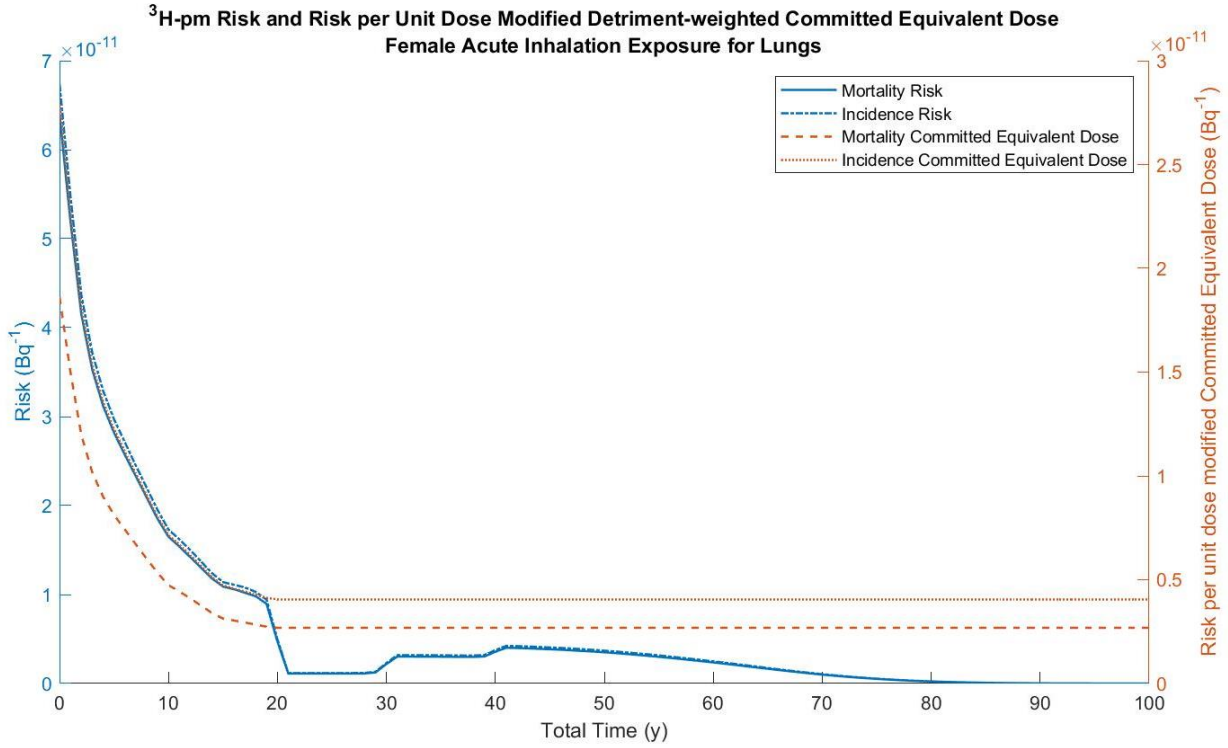

Figure 45. Risk and detriment-weighted committed equivalent dose to the female lungs due to moderate-clearing tritium.

For uniform exposures, the CED closely represents the risk, with the closest correspondence being with ingested tritiated water, where the difference is only 4.8×10^{-11} at its largest gap and very nearly 0 at its smallest, for females. It is noteworthy that for uniform exposures, the CED more accurately represents the female risk as compared to the male risk, where the CED

under represents the risk from a uniform exposure. CED for inhaled tritium can be found in Appendix E.

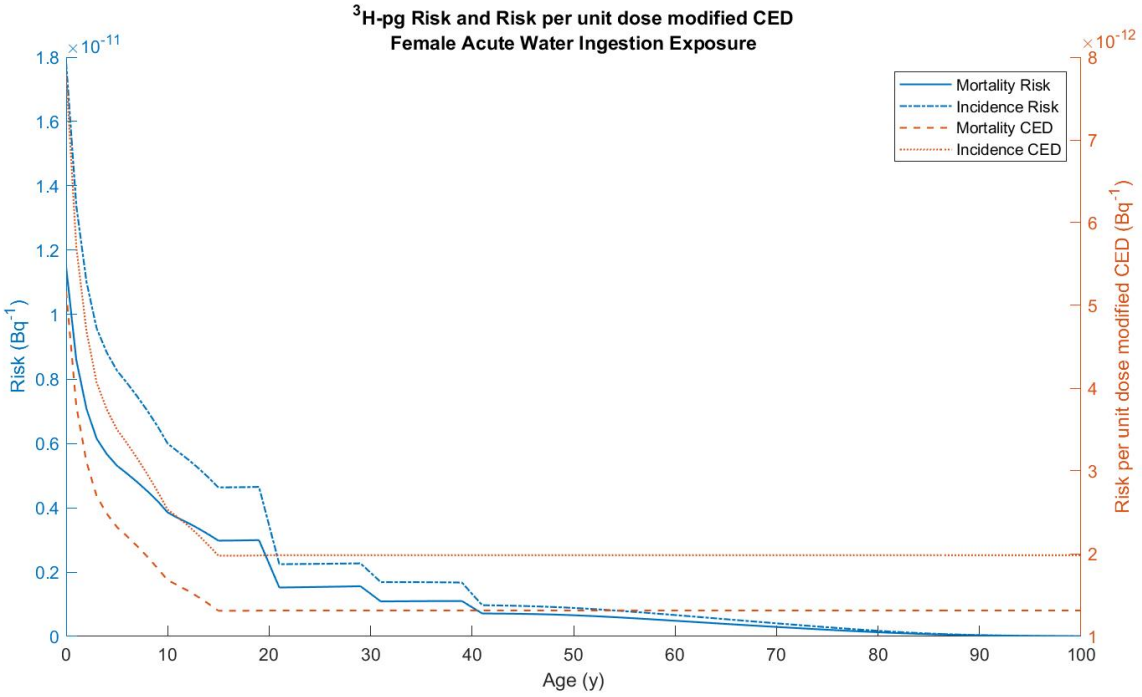

(a)

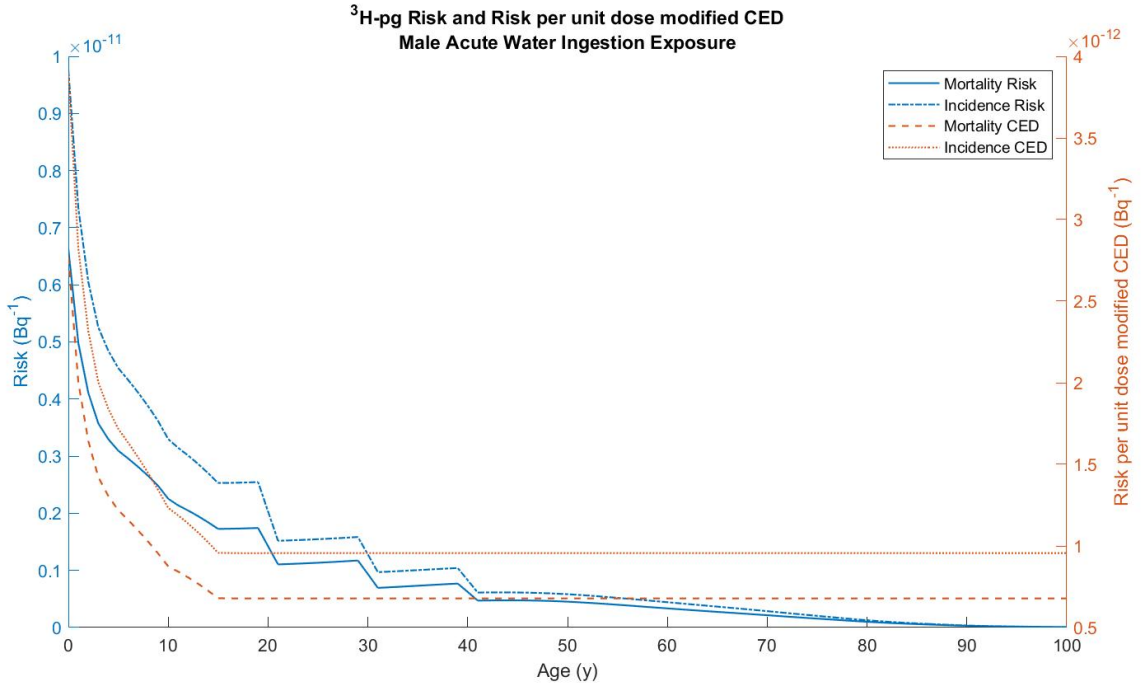

(b)

Figure 46. The FGR 13 risk and ICRP *Publication 60* CED for a uniform acute exposure for the ingestion of tritiated water for (a) females and (b) males.

4.4.1.d. ^{90}Sr

For strontium, the plateau in the committed doses begins tapering off post age 60. This is due to the data limitation mentioned in the preface of this section. Post age 60, the commitment period shrinks as end of life is approached. For long lived radionuclides, the data towards the end of life is non-negligible, unlike with fast decaying radionuclides. Thus, as the data steadily approaches end of life and non-negligible datapoints are removed, the committed dose summation will decrease.

^{90}Sr acts as a bone seeker, integrating itself into the bone matrix in a similar manner to calcium. Therefore, for all solubility classes and usage types, the bone surface and red marrow are of particular interest. For all solubility classes and usage types, the detriment-weighted committed equivalent dose to the bone surface from an acute exposure overestimates the tissue-specific risk by an order of magnitude, the trend following closely with the risks otherwise, as seen in Figure 47. This trend holds for both sexes as well. Corresponding plots for males can be found in Appendix C.

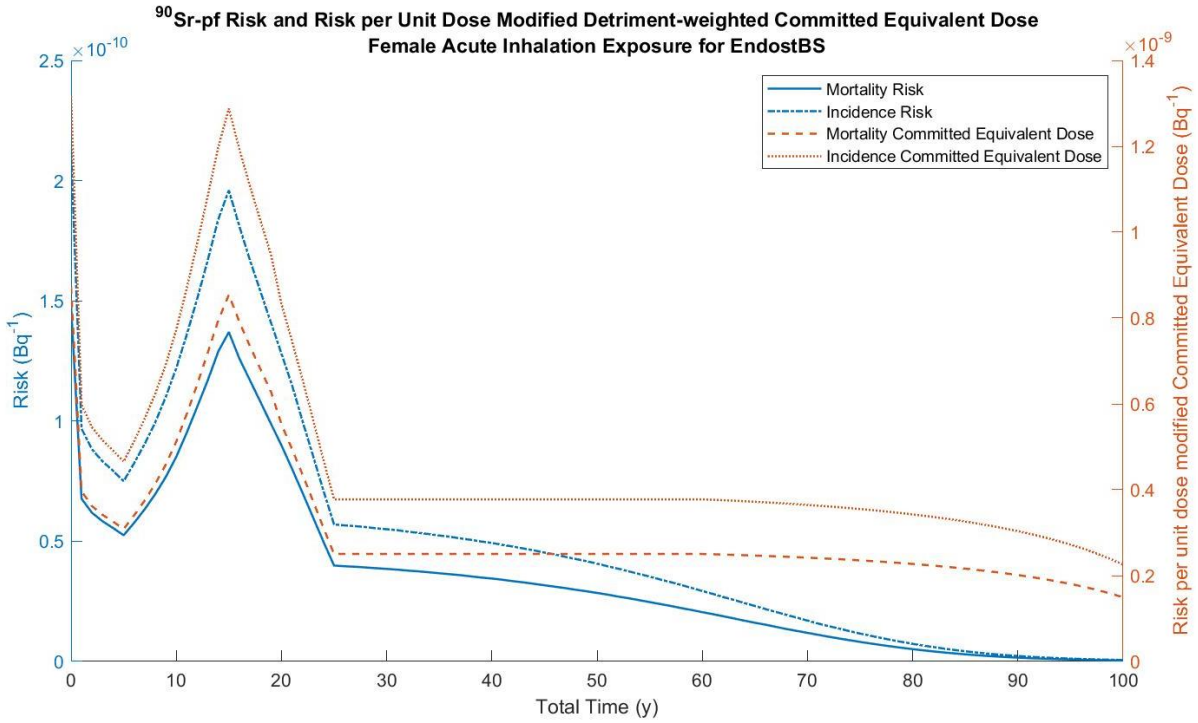

(a)

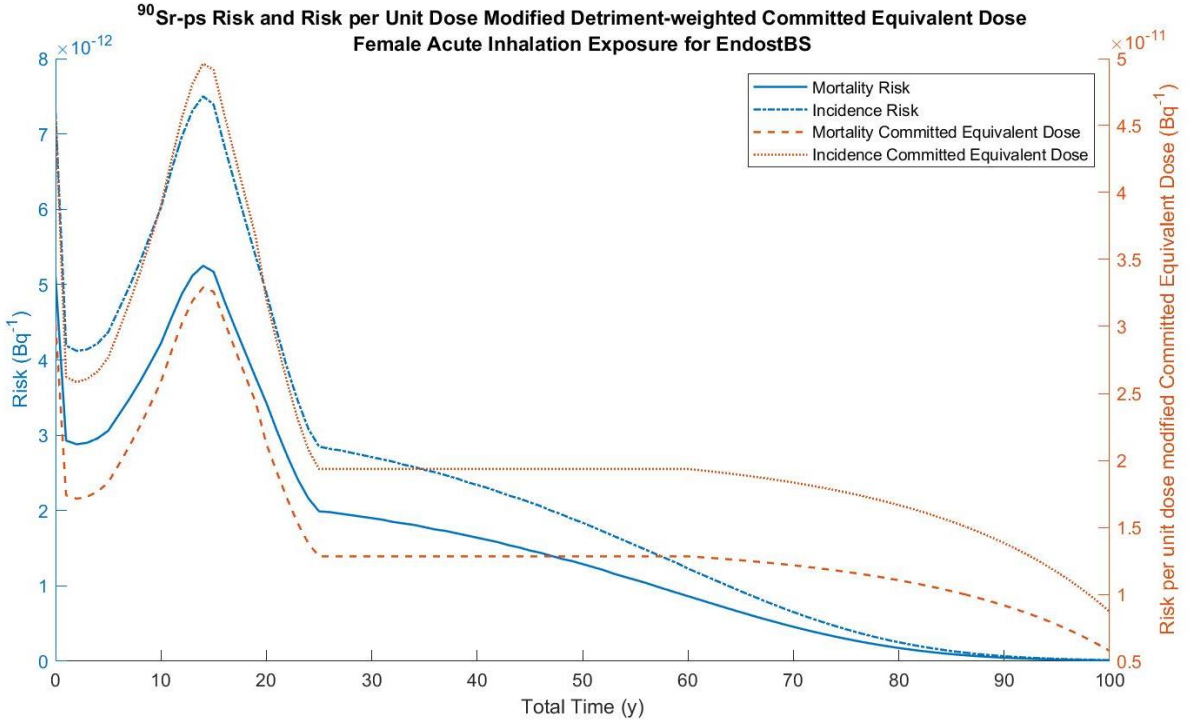

(b)

Figure 47. Risk and detriment-weighted committed equivalent dose to the female bone surface due to (a) fast and (b) slow-clearing ^{90}Sr.

Plots for the lungs for inhalation of strontium can be found in Appendix C. For inhaled strontium, the lungs are of interest. For all solubility classes, beginning of life is where the largest difference between the FGR 13 calculated tissue-specific risks and the ICRP *Publication 60* calculated detriment-weighted committed equivalent dose occur. With increasing age, that gap narrows.

Comparing the FGR 13 calculated risk coefficients from an acute exposure to the CEDs sees a comparatively accurate representation of the risks via the CEDs. The largest divergence from the true risk can be seen in slow-clearing strontium for females, specifically. However, as was seen in the tissue-specific plots above, with increasing age, the gap between the CED and true risk narrows, depicted in Figure 48. Plots for males can be found in Appendix D.

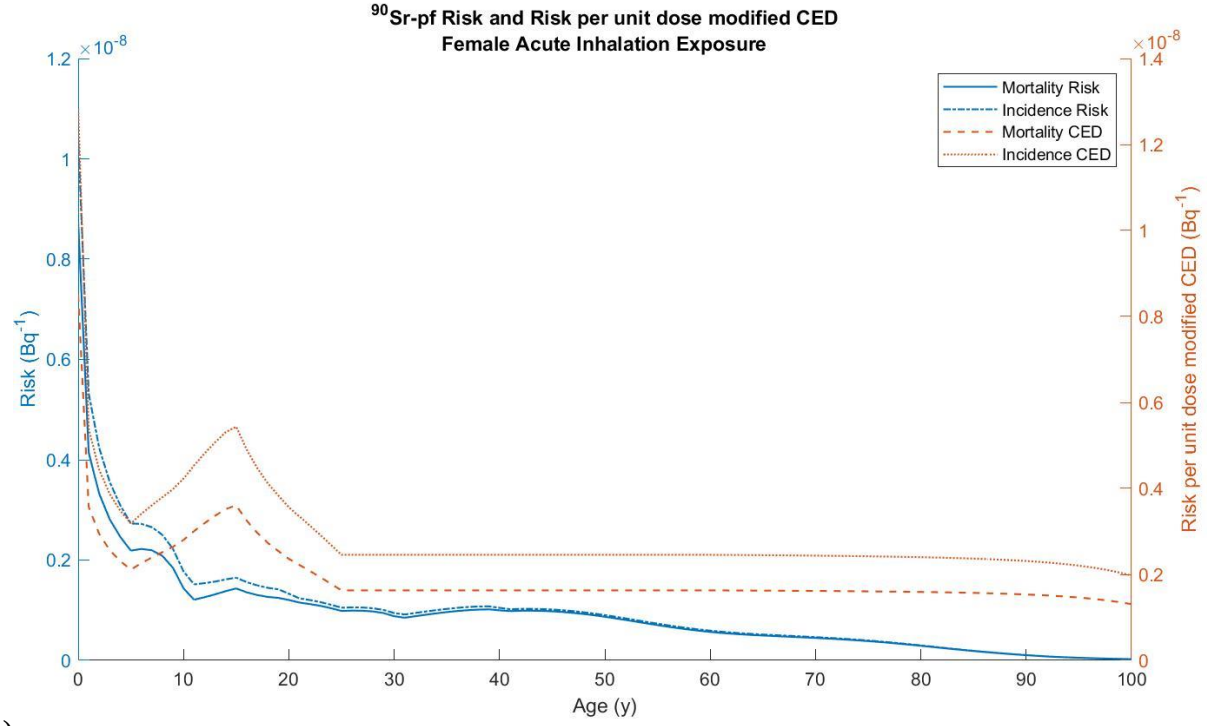

(a)

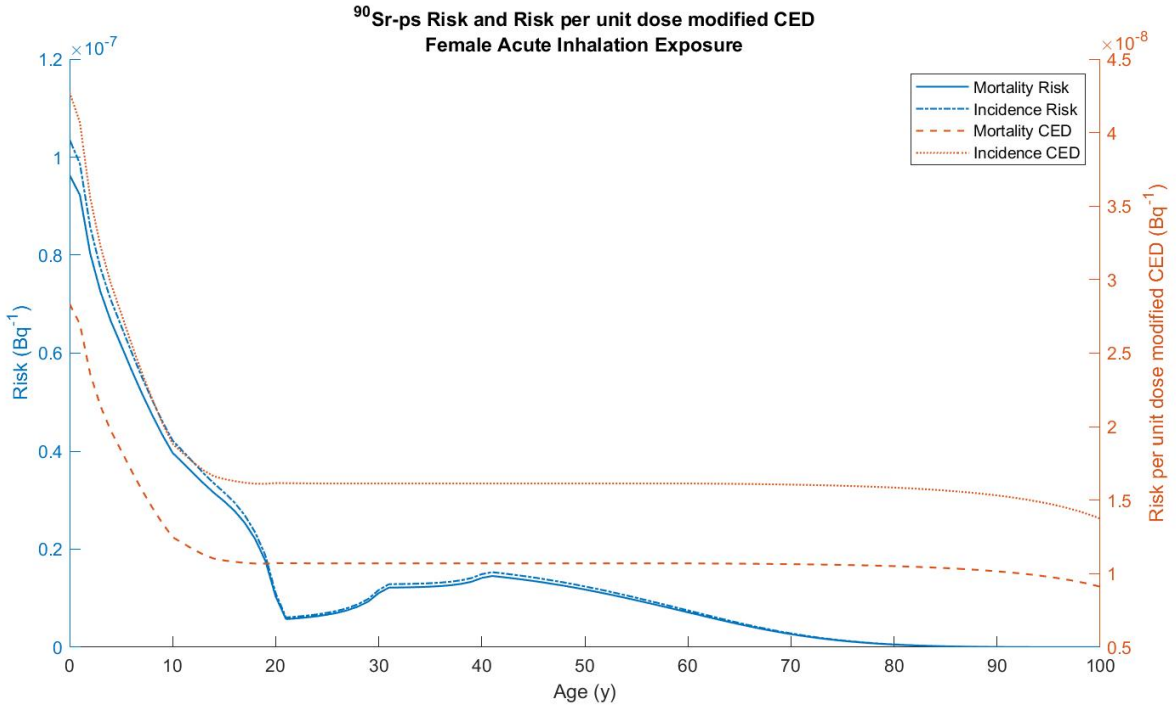

(b)

Figure 48. Risk and CED to females due to (a) fast and (b) slow-clearing ^{90}Sr.

4.4.1.e. ^{235}U

As with strontium, the CED values plotted in this section drop off beginning at age 60 for both high- and low-LET components, for the same reason as explained for ^{90}Sr. The high- and low-LET components of this radionuclide are therefore plotted separately.

^{235}U, while not a strong bone seeker, does integrate itself into the bone matrix as well, affecting the bone surface, red marrow, and surrounding muscle to a higher degree than the other target tissues. For both the high- and low-LET components of ^{235}U, the detriment-weighted committed equivalent dose for the bone surface overestimates the tissue-specific risk to the bone surface. This is seen in all solubility classes and usage types, as well as between sexes. Plots for both the high- and low-LET components for fast-clearing uranium can be seen in Figure 49, and the corresponding plots for males can be found in Appendix C.

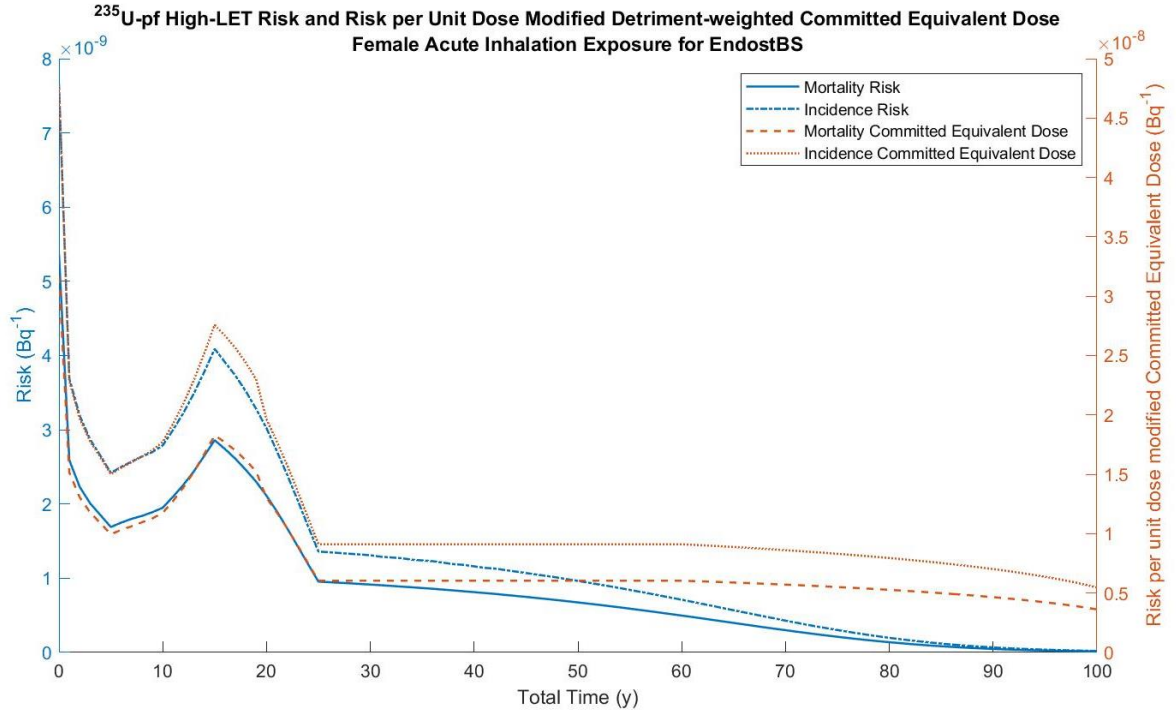

(a)

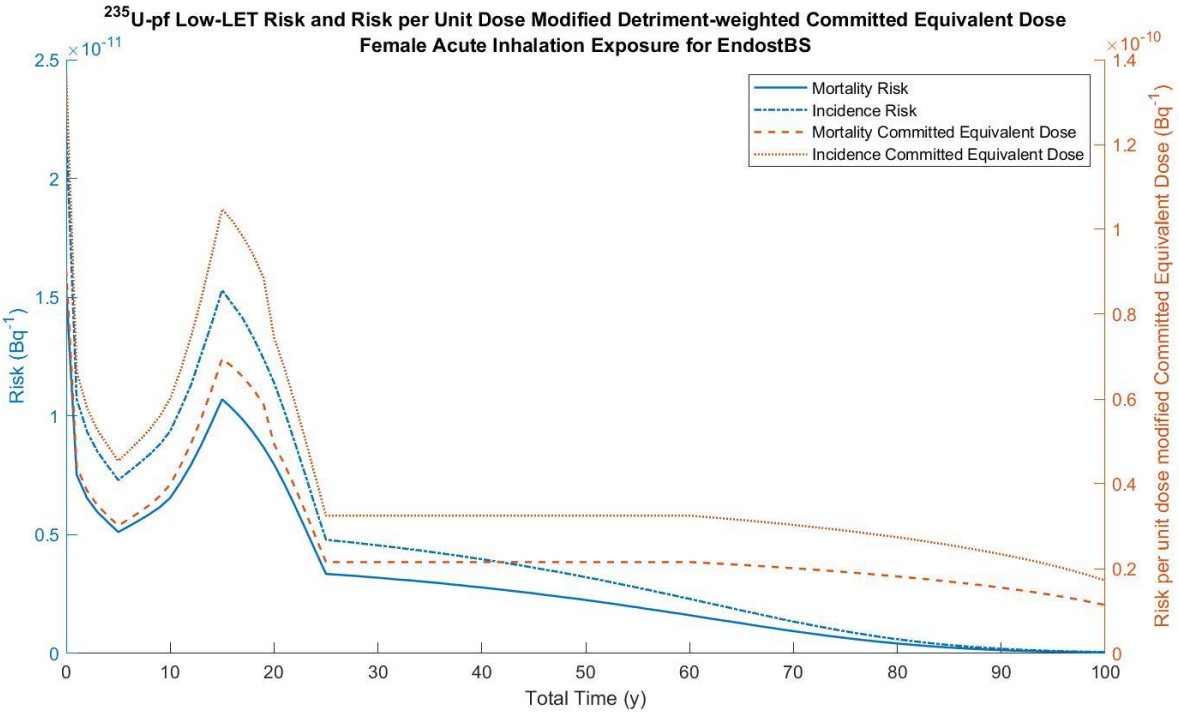

(b)

Figure 49. Risk and detriment-weighted committed equivalent dose to the female bone surface due to fast-clearing ^{235}U, (a) high-LET and (b) low-LET.

For inhaled uranium, primary dose is delivered to the lungs. Following the trend seen with other radionuclides, the dose delivered to the lungs is higher overall for slow-clearing uranium, as

compared to fast-clearing. However, for both fast- and slow-clearing inhaled uranium, the detriment-weighted committed equivalent doses for the lungs display a fairly accurate representation of the tissue-specific risk to the lungs for both mortality and incidence, with the accuracy of the representation increasing with increasing age, as was seen for the other observed radionuclides. The plots of this trend can be found in Appendix C. A similar trend is seen in the low-LET components for uranium as well, the ICRP *Publication 60* detriment-weighted committed equivalent doses reasonably representing the FGR 13 risks to the lungs.

Overall, the detriment-weighted committed equivalent doses show a reasonable following of the trend seen in the tissue-specific risks across all solubility classes, usage types, and sexes. The values for the detriment-weighted committed equivalent doses tend to fall within 20% of one another. Due to this, a similar correspondence between the CEDs due to a uniform exposure and the FGR 13 calculated risk coefficient was anticipated.

For the high-LET component of inhaled uranium, closest correspondence between the risks and CEDs was seen in fast-clearing uranium. Between the two sexes, the correspondence for males is slightly closer than that of females, with the modified CEDs slightly overestimating the FGR 13 calculated risks by approximately 50% at the widest point. Through the lifetime, the CED shifts from underestimating the risk to overestimating beginning at year 10.

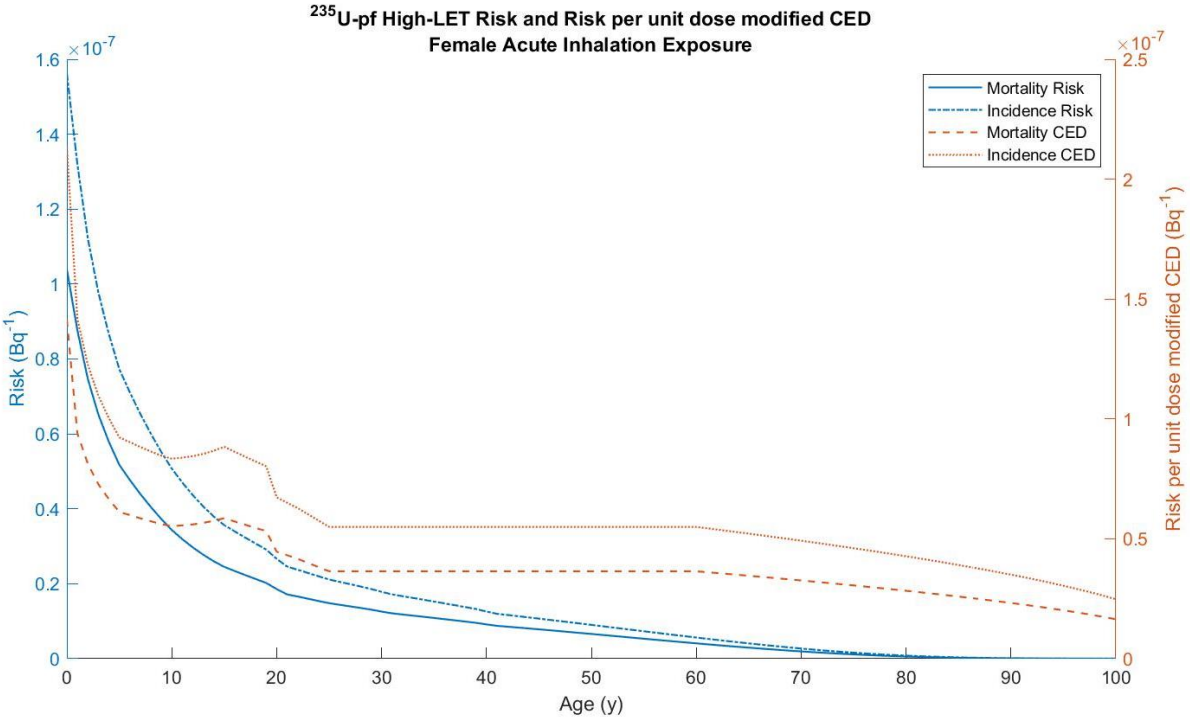

(a)

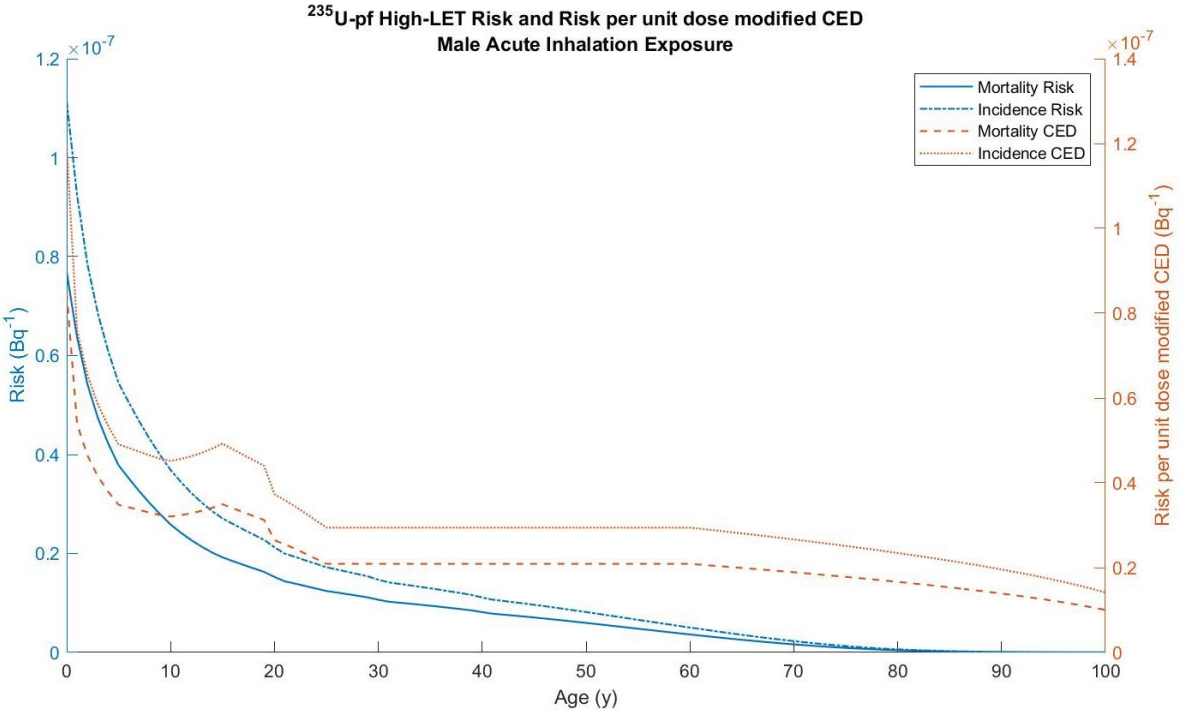

(b)

Figure 50. Comparison of the risk and CED for the fast-clearing, high-LET component of ^{235}U in (a) females and (b) males.

The trend seen in Figure 50 for the high-LET component for inhaled uranium holds true for the low-LET component as well, with the closest correspondence being for males for the fast-clearing solubility class seen in Figure 51. With decreasing solubility rate, the difference between the risk and CED increases, with the CED underestimating the risk.

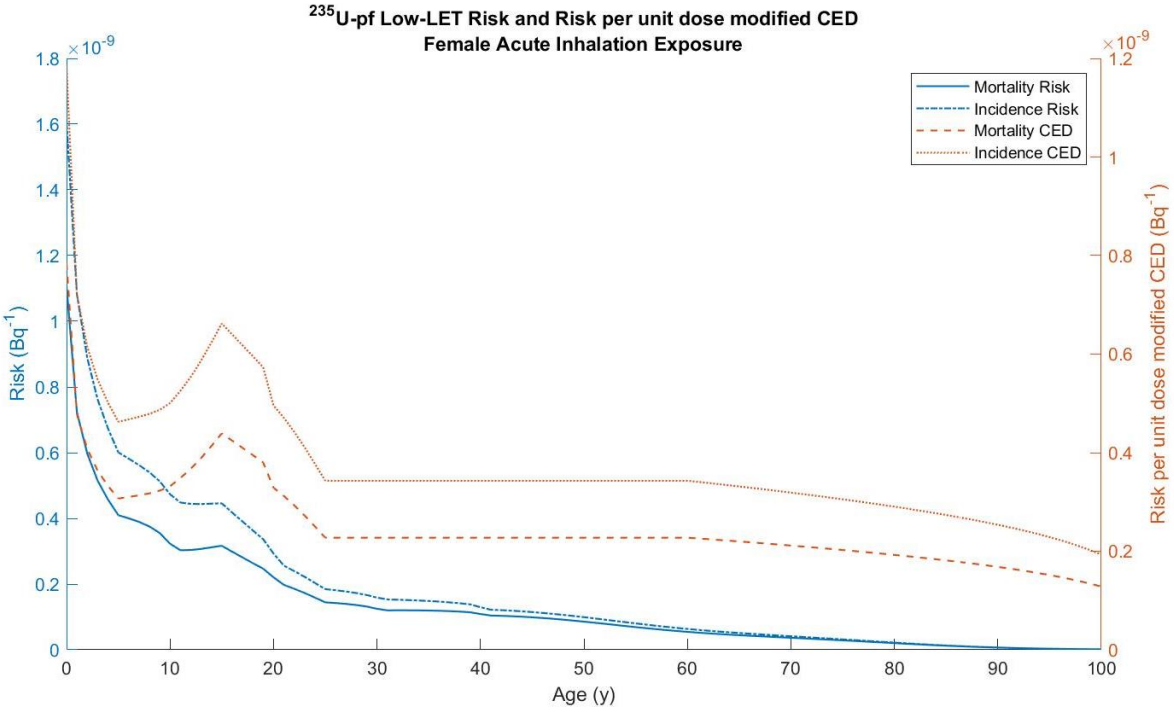

(a)

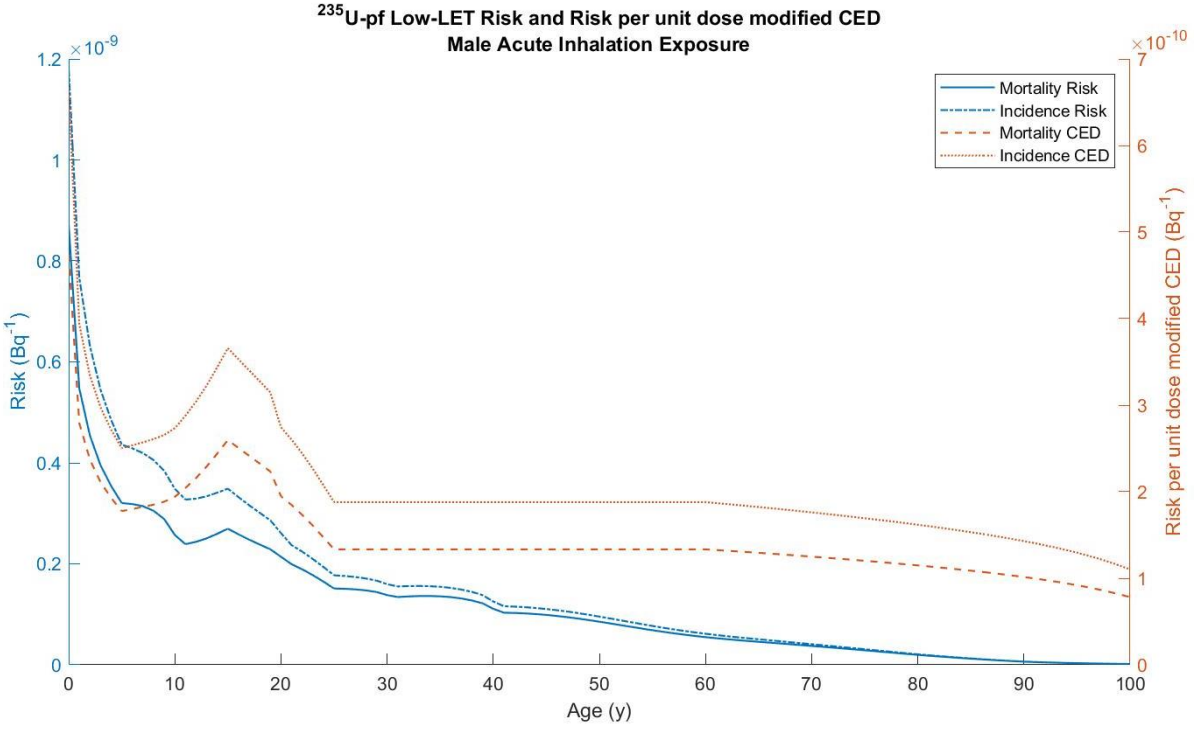

(b)

Figure 51. Risk and CED for the low-LET component of fast-clearing ^{235}U in (a) females and (b) males.

For ingested uranium, the correspondence between the CED and risk is closest for the high-LET components for females, the CED tracking almost perfectly along the risk, while the low-LET component underestimates the risk, seen in Figure 52.

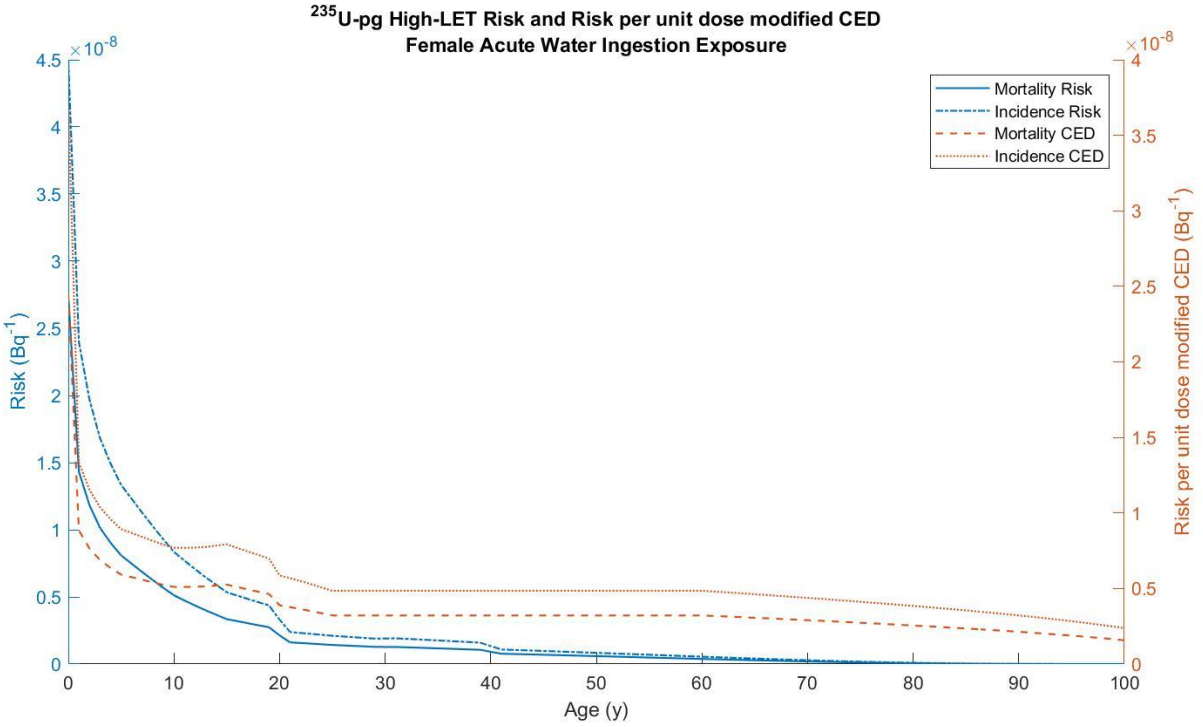

(a)

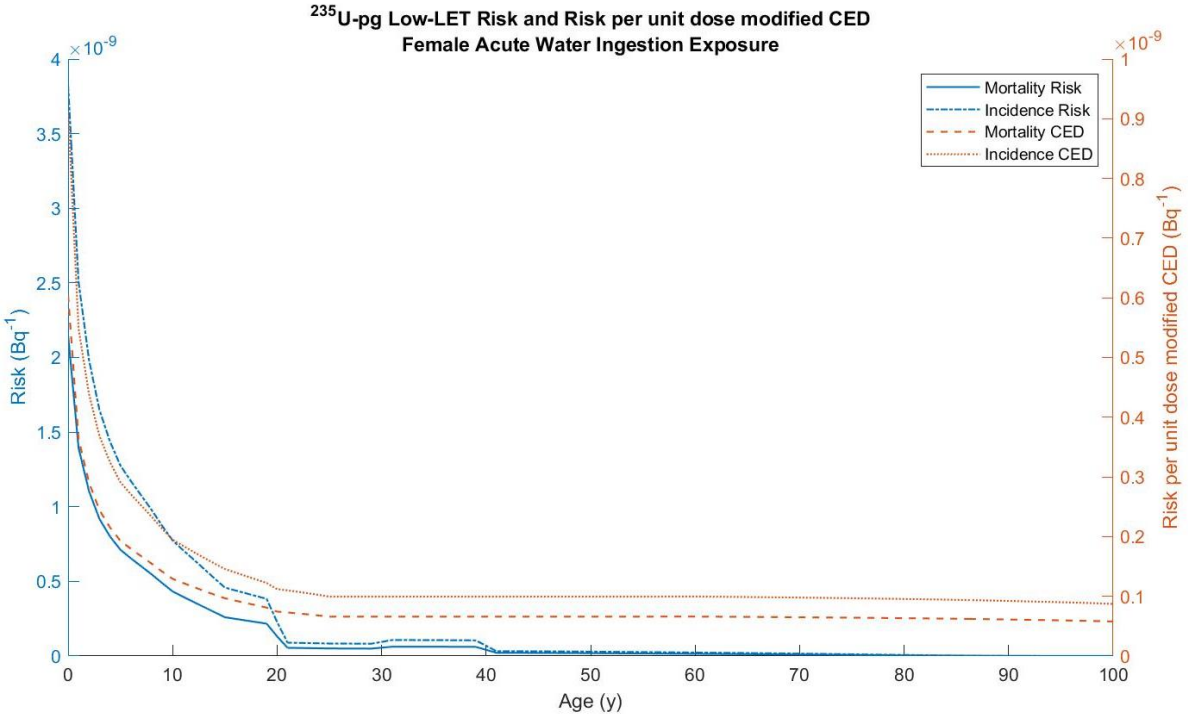

(b)

Figure 52. Risk and CED for the (a) high-LET and (b) low-LET component of tap water ingested ^{235}U in females.

4.4.2. Chronic Exposures

For chronic exposures, the calculated values for the whole body were tabulated alongside the calculated risks from a chronic exposure and a percent difference between the two values was taken. Recall, the modified CED employed in this study is only an approximate indicator of the true risk, making a high difference for some tissues to be expected, but nothing more than an order of magnitude should be seen so as for the approximation to be useful. A summary of the risks from a chronic exposure for both mortality and incidence as compared to the associated adjusted CED's can be found in Table 15.

Table 15. Summary of the mortality and incidence risks compared to their associated risk per unit dose adjusted committed effective doses for chronic exposures.

Isotope	Usage Type	FGR 13 Mortality Risk	Mortality Adjusted CED	% Difference	FGR 13 Incidence Risk	Incidence Adjusted CED	% Difference
Cs137pf	Air	2.27×10^{-10}	3.49×10^{-10}	53.95	4.92×10^{-10}	5.13×10^{-10}	4.35
Cs137pm	Air	8.09×10^{-10}	8.61×10^{-10}	6.38	9.94×10^{-10}	1.26×10^{-09}	26.81
Cs137ps	Air	2.85×10^{-09}	3.17×10^{-09}	11.26	3.20×10^{-09}	4.63×10^{-09}	44.62
Cs137pg	Food	7.13×10^{-10}	8.96×10^{-10}	25.67	1.55×10^{-09}	1.31×10^{-09}	-15.01
Cs137pg	Water	5.92×10^{-10}	1.01×10^{-09}	70.04	1.28×10^{-09}	1.48×10^{-09}	15.01
H3pf	Air	3.63×10^{-13}	4.88×10^{-13}	34.39	8.45×10^{-13}	7.17×10^{-13}	-15.13
H3pm	Air	4.82×10^{-12}	4.34×10^{-12}	-9.94	5.76×10^{-12}	6.35×10^{-12}	10.17
H3ps	Air	2.18×10^{-11}	2.18×10^{-11}	0.25	2.36×10^{-11}	3.19×10^{-11}	34.98
H3pg	Water	9.66×10^{-13}	1.45×10^{-12}	50.56	2.22×10^{-12}	2.13×10^{-12}	-3.98
I131pf	Air	8.31×10^{-11}	7.67×10^{-10}	823.06	8.03×10^{-10}	1.12×10^{-09}	39.60
I131pm	Air	1.34×10^{-10}	2.35×10^{-10}	74.54	2.66×10^{-10}	3.43×10^{-10}	28.91
I131ps	Air	1.42×10^{-10}	1.45×10^{-10}	1.99	1.76×10^{-10}	2.12×10^{-10}	20.77
I131pg	Food	2.78×10^{-10}	2.12×10^{-09}	663.76	2.68×10^{-09}	3.10×10^{-09}	15.43
I131pg	Water	1.97×10^{-10}	2.11×10^{-09}	970.05	1.89×10^{-09}	3.08×10^{-09}	62.46
Sr90pf	Air	1.06×10^{-09}	1.57×10^{-09}	47.97	1.18×10^{-09}	2.30×10^{-09}	94.39
Sr90pm	Air	2.71×10^{-09}	2.25×10^{-09}	-16.94	2.93×10^{-09}	3.30×10^{-09}	12.53
Sr90ps	Air	1.11×10^{-08}	9.27×10^{-09}	-16.22	1.17×10^{-08}	1.36×10^{-08}	15.74
Sr90pg	Food	1.57×10^{-09}	2.00×10^{-09}	27.72	1.87×10^{-09}	2.93×10^{-09}	56.22
Sr90pg	Water	1.32×10^{-09}	1.85×10^{-09}	40.40	1.54×10^{-09}	2.71×10^{-09}	76.16
U235pf High LET	Air	1.13×10^{-08}	3.12×10^{-08}	175.16	2.39×10^{-08}	4.58×10^{-08}	91.18
U235pf Low LET	Air	1.32×10^{-10}	2.00×10^{-10}	51.05	2.06×10^{-10}	2.94×10^{-10}	42.40
U235pm High LET	Air	2.59×10^{-07}	1.90×10^{-07}	-26.67	2.77×10^{-07}	2.78×10^{-07}	0.32

U235pm Low LET	Air	6.76×10^{-10}	5.12×10^{-10}	-24.30	7.61×10^{-10}	7.50×10^{-10}	-1.44
U235ps High LET	Air	6.52×10^{-07}	5.11×10^{-07}	-21.58	6.87×10^{-07}	7.49×10^{-07}	9.00
U235ps Low LET	Air	2.03×10^{-09}	1.67×10^{-09}	-17.79	2.21×10^{-09}	2.44×10^{-09}	10.31
U235pg High LET	Food	1.58×10^{-09}	2.85×10^{-09}	80.39	3.20×10^{-09}	4.17×10^{-09}	30.27
U235pg High LET	Water	1.19×10^{-09}	2.67×10^{-09}	125.40	2.39×10^{-09}	3.91×10^{-09}	63.69
U235pg Low LET	Food	1.05×10^{-10}	6.39×10^{-11}	-39.37	1.88×10^{-10}	9.36×10^{-11}	-50.21
U235pg Low LET	Water	7.36×10^{-11}	5.90×10^{-11}	-19.84	1.30×10^{-10}	8.65×10^{-11}	-33.71

A large portion of the difference seen between the risks and CEDs for both acute and chronic exposures stems from the tissue-weighting factors. Where risk calculation has an age-dependent LAR value, CED only utilized tissue weights, which are age-nonspecific. As well, ICRP tissue weights take into account more than simply the risk of contracting a fatal or non-fatal cancer. For ICRP *Publication 60*, tissue weights consider the probability of all stochastic effects, not just the specific stochastic effect of cancer. That is, the tissues weights indicate the total detriment due to the stochastic effects resulting from a uniform irradiation to the whole body. These stochastic effects include the probability of attributable fatal cancer, the weighted probability of attributable non-fatal cancer, the weighted probability of severe hereditary effects, and the relative length of life lost.[13]

The largest difference between the ICRP *Publication 60* calculated CED and the FGR 13 calculated risk can be seen in the mortality calculation for ^{131}I. The incidence calculations fall decently in line with expected differences between the risk and chronic CED, while the morality calculations near a 1000% difference. Such a drastic difference can be explained through the fact that ^{131}I is a thyroid seeker, with a majority of the dose concentrating in the thyroid. However, thyroid cancer has a decently low mortality rate, especially when compared to the corresponding incidence rate. The Commission's consideration of total detriment in the ICRP *Publication 60* tissue-weighting factors therefore intrinsically guarantees an overestimation for the mortality risk

of high incidence, low mortality cancers that would still have a high detriment to quality of life post carcinogenesis.

Basis for the validation of the large percent differences based on a chronic exposure comes from the 2011 paper by Kaye et el. titled "Method of Estimating Lifetime Cancer Risk Due to Chronic Radionuclide Intake."[35] In this paper, the radionuclides of interest are ^{137}Cs ingested through cow's milk and ^{235}U uptake via tap water, utilizing UNSCEAR risk calculation methods. Kaye et el.'s methods show an overestimation in the dose of nearly 70% during the first 20 years of life when using CED as a risk representation and, when compared to risk, CED results in a nearly 50% higher risk than the UNSCEAR models for risk depicted for a 50-year integration period.[35] Using this 50% overestimation as a comparison checkpoint, the calculated CEDs for a chronic exposure using ICRP *Publication 60* methods and comparing to FGR 13 risk coefficients are appropriate. As a final check on the generated values, they were sent to Dr. Eckerman at Oak Ridge National labs for verification, who believes these values to be reasonable.[36]

4.5. Preliminary Data Dose Rate Analysis

Development of dose rates utilizing ICRP *Publication 103* biokinetics is underway. Through Dr. Derek Jokisch at Francis Marrion, this preliminary dose rate data was obtained.[30] While there will be alterations in how things such as the RBE will be handled in future publications and risk calculations, the main point of interest in regards to the preliminary data was to see how changes in biokinetics are reflected in the dose rates, as there have been substantial changes to the biokinetics for radionuclides since the publication of FGR 13 and the corresponding DCAL system. Therefore, for the analysis and comparison of FGR 13 and preliminary data, only radionuclides without a high-LET component were utilized. ICRP *Publication 103* values for tissue weights and radiation-weighting factors were used in place of ICRP *Publication 60* to better reflect the

preliminary dataset, and the LAR values, survival function, and usage function were all converted to updated values provided by David Pawel of EPA.[37] All calculations outlined henceforth are preliminary in order to depict the change biokinetics has on the resultant risks in order to determine if patterns are maintained across generations of datasets and are not to be considered final as compared to up and coming Federal guidance.

4.5.1. ^{131}I

As with the FGR 13 DCAL generated data, no difference was seen between the male and female dose rates to the thyroid, which was expected. Generally, ^{131}I follows the same trend for all solubility classes and usage types between males and females. This section will outline the plots for females, and corresponding male data can be found in Appendix E. Plots in this section appear to stop before end of life. The end of these lines indicates a drop to zero dose, as the ICRP *Publication 103* data was not populated with the last non-zero value as the FGR 13 data was, seen in Figure 53.

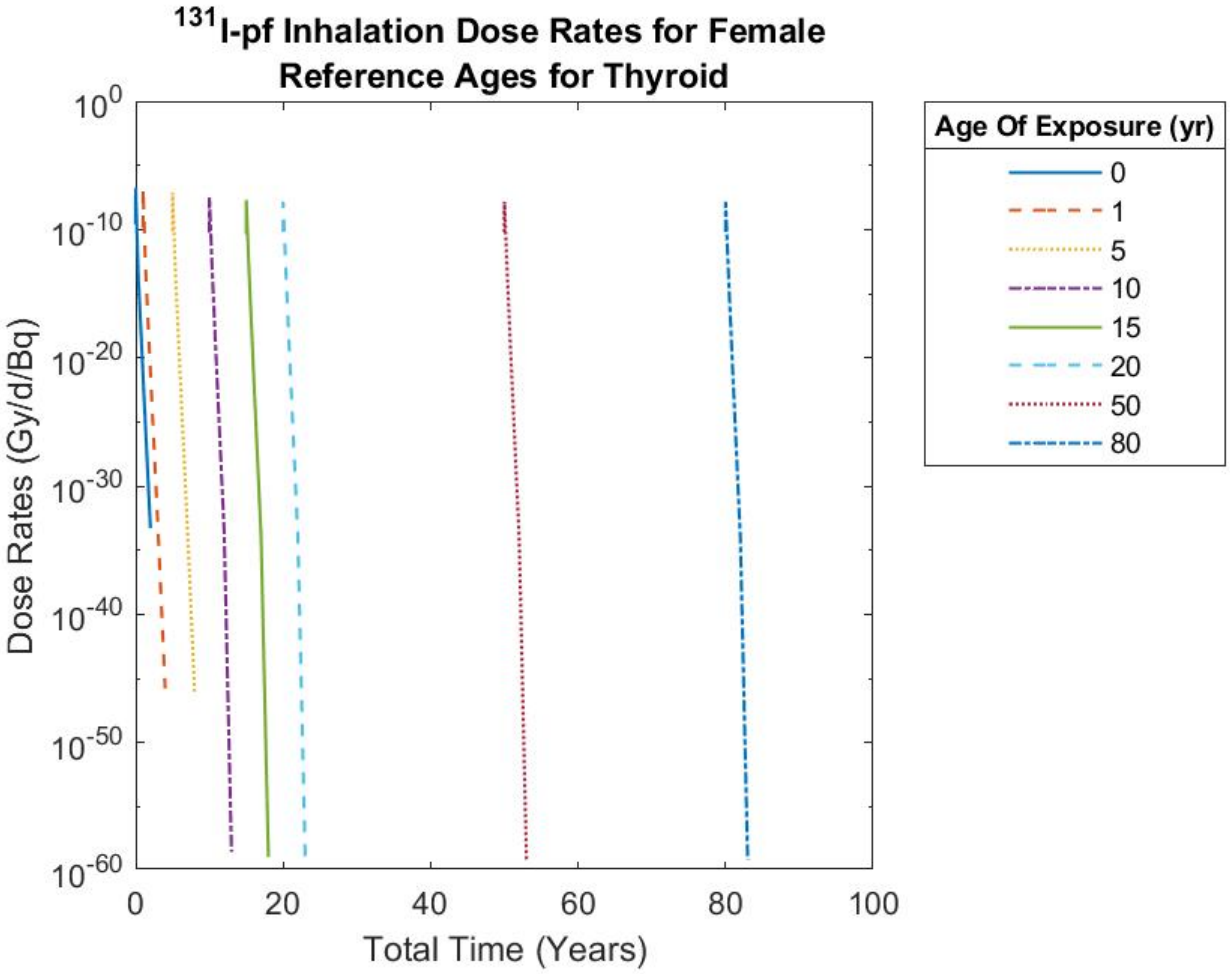

Figure 53. Dose rates to the thyroid for females from an acute exposure of fast-clearing ^{131}I.

Due to the fact that iodine is a thyroid seeker, in general, the dose rate to the thyroid is higher than the other tissues of the body by nearly five orders of magnitude, save for slow-clearing inhaled iodine. For this solubility class, dose rates to the thyroid are on par with the other soft tissues. This is consistent with what was seen in the FGR 13 DCAL generated dose rates, as can be seen in Figure 54.

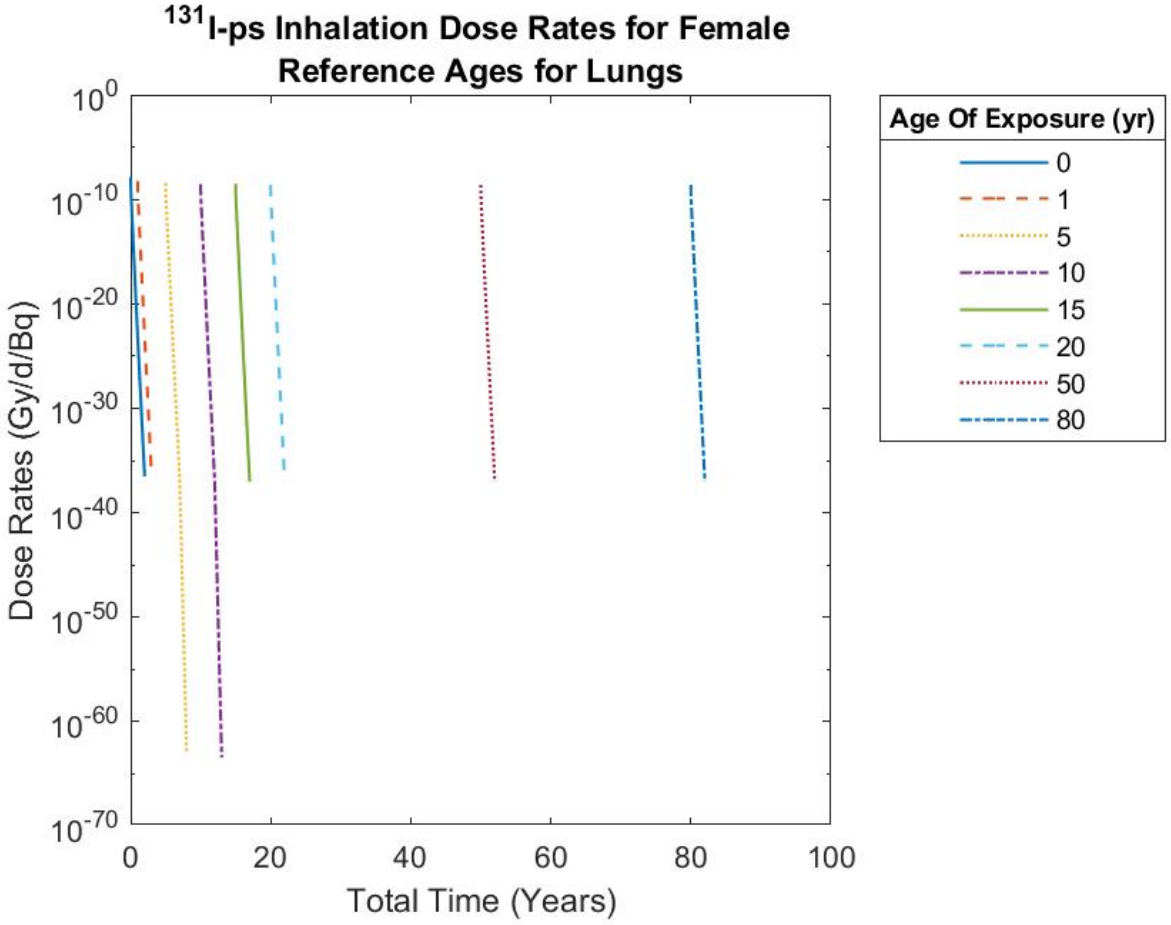
131I-ps Inhalation Dose Rates for Female
Reference Ages for Lungs
Dose Rates (Gy/d/Bq)
Total Time (Years)
Age Of Exposure (yr)
0
1
5
10
15
20
50
80

(a)

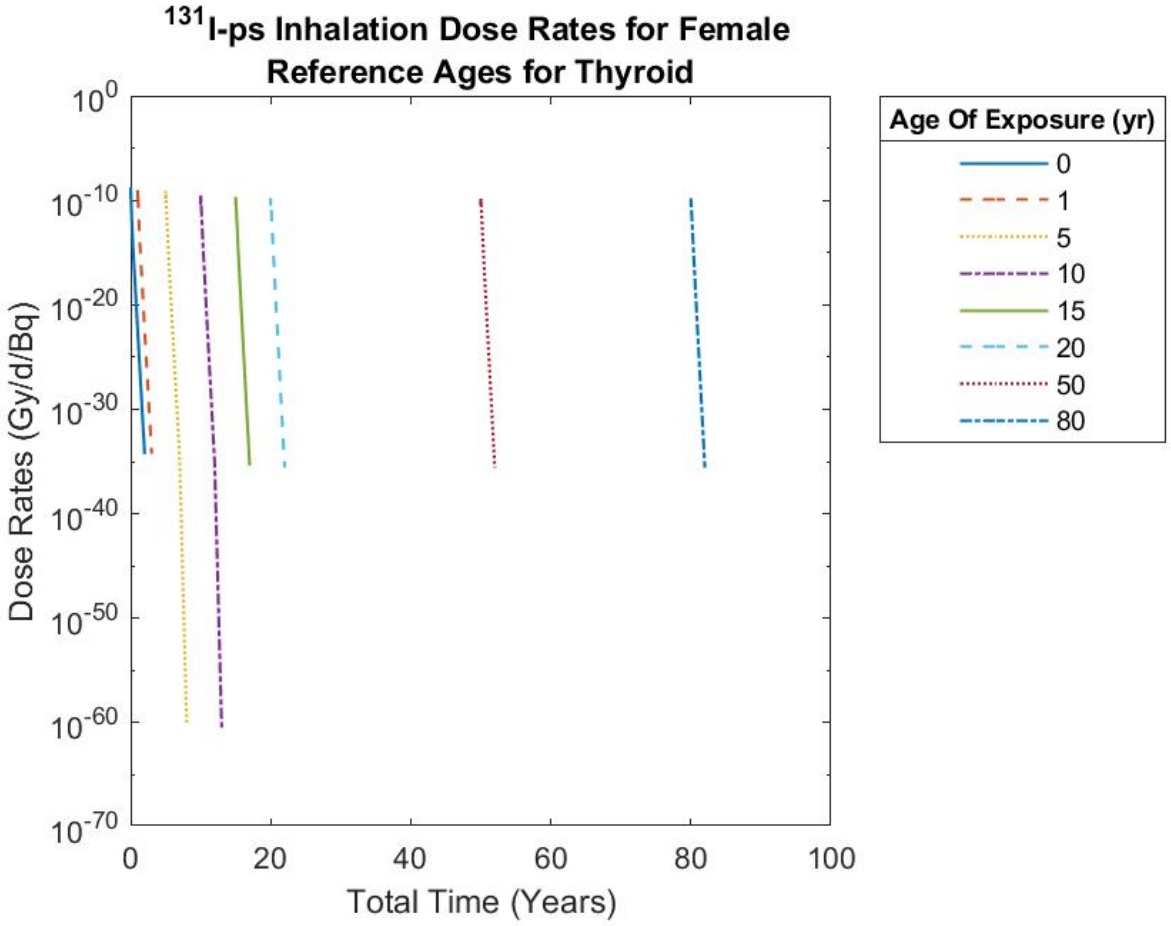

(b)

Figure 54. Dose rates to the (a) lungs and (b) thyroid for an acute exposure of slow-clearing ^{131}I in females.

For ingestion of iodine, the similar trend is seen between the thyroid and the other soft tissues as is seen with fast- and moderate-clearing inhaled iodine. The difference between the thyroid and colon, specifically, at the highest dose rate to the tissue, is approximately five orders of magnitude higher in the thyroid than in the colon, seen in Figure 55.

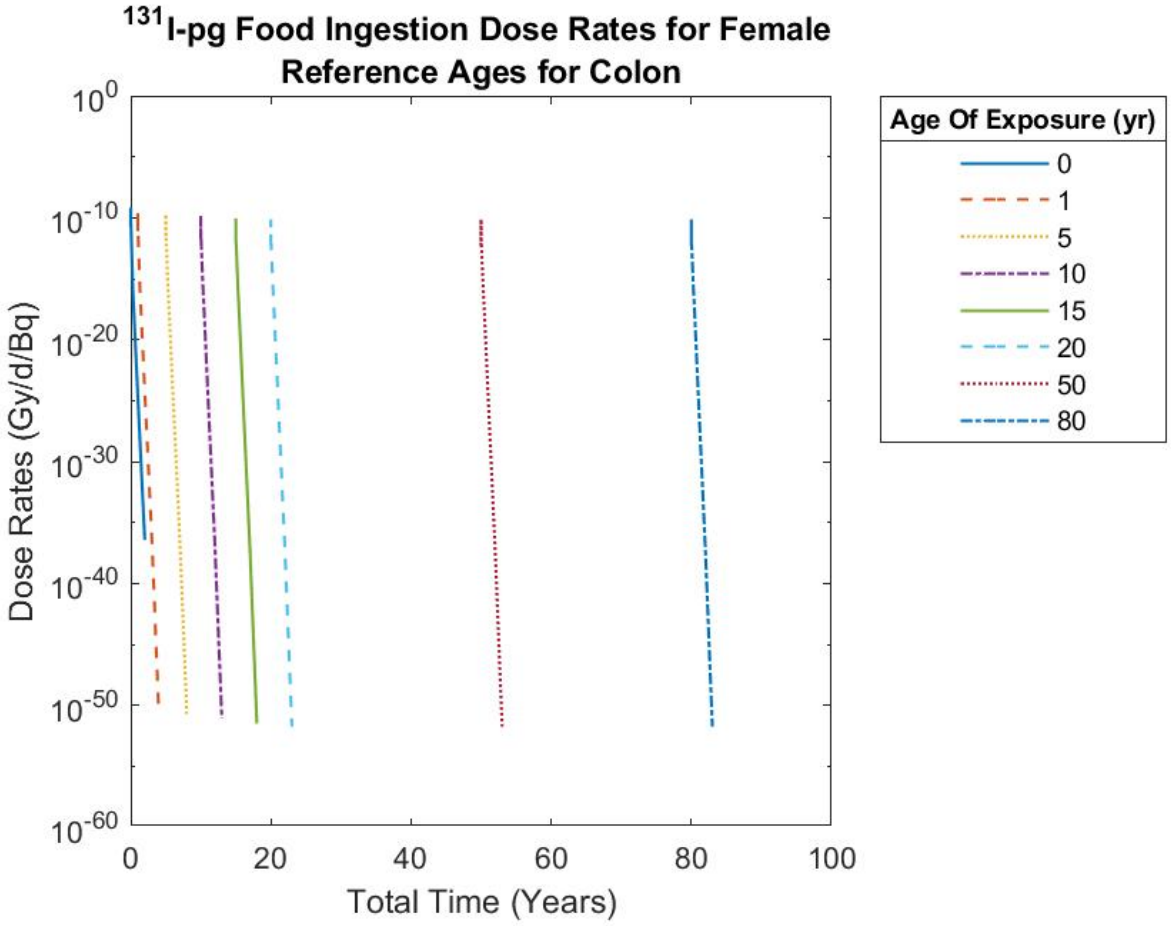
131I-pg Food Ingestion Dose Rates for Female
Reference Ages for Colon
Dose Rates (Gy/d/Bq)
Total Time (Years)
Age Of Exposure (yr)
0
1
5
10
15
20
50
80

(a)

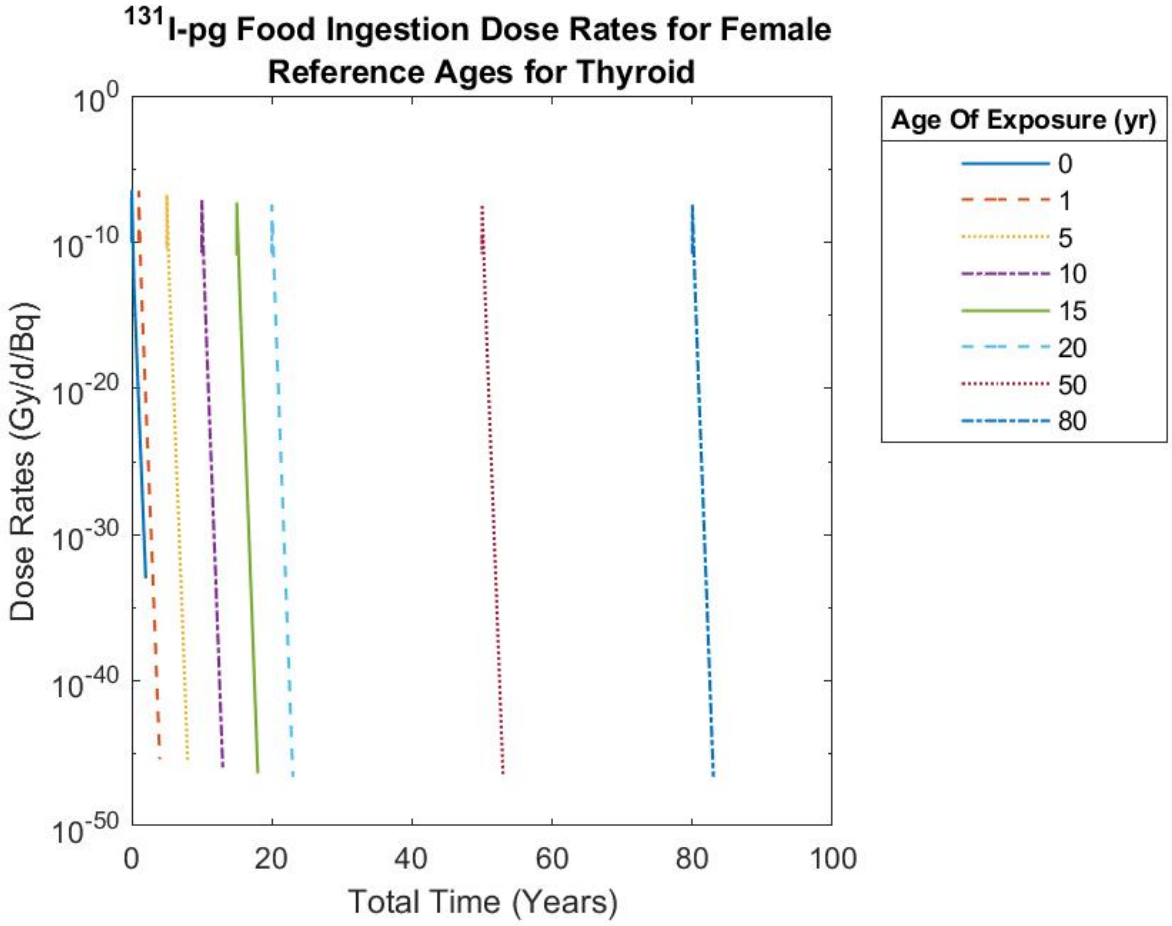

(b)

Figure 55. Dose rate data from an acute exposure of ingested ^{131}I in food for the (a) colon and (b) thyroid for females.

4.5.2. ^{137}Cs

The absorbed dose rate behavior of ^{137}Cs for the preliminary data follow a similar trend as for the FGR 13 data, save for a smoother curve for ingested cesium and fast-clearing cesium. The trend of the preliminary data for fast-clearing now more closely resembles the trend seen in the moderate- and slow-clearing cesium. The largest drop in magnitude for the dose rates occurs in slow-clearing inhaled cesium, seen in Figure 56.

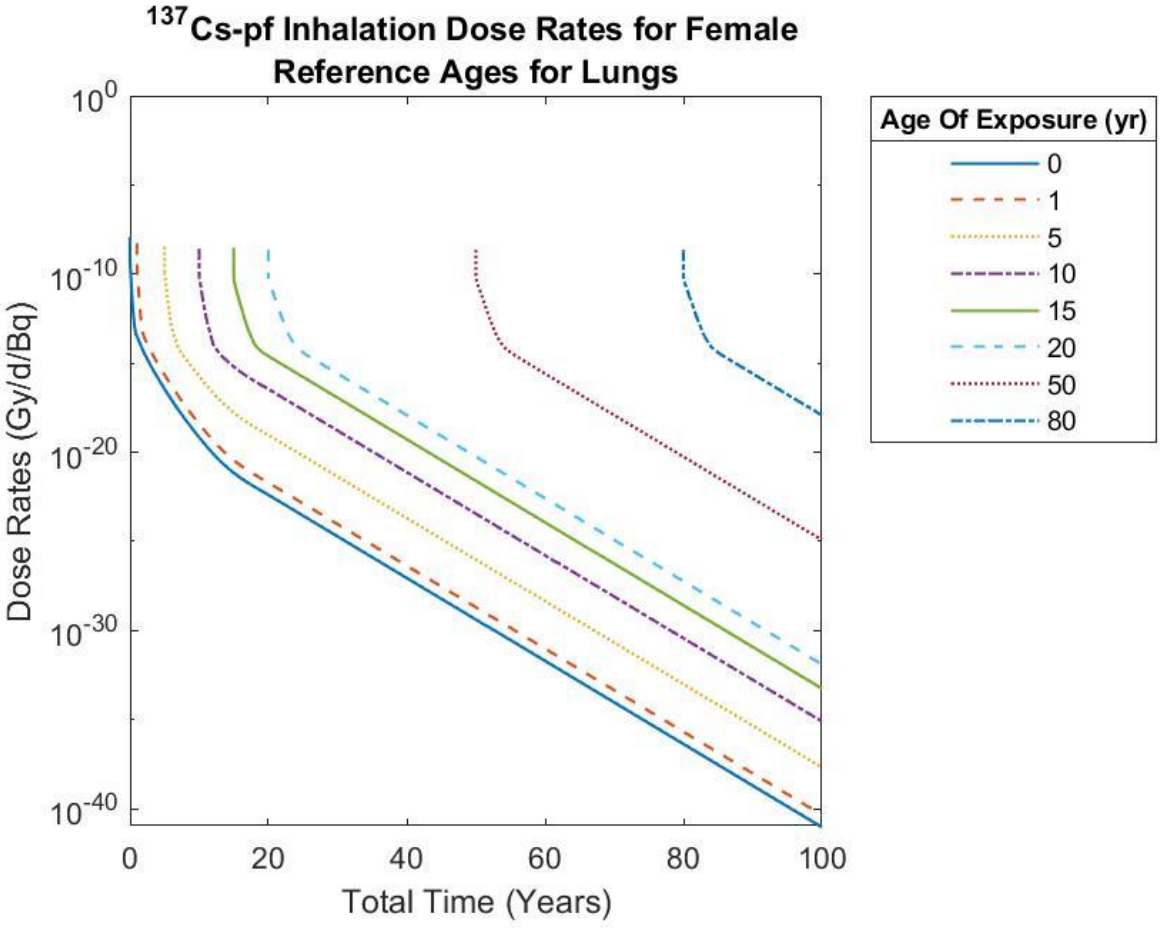
137Cs-pf Inhalation Dose Rates for Female
Reference Ages for Lungs
Dose Rates (Gy/d/Bq)
Total Time (Years)
Age Of Exposure (yr)
0
1
5
10
15
20
50
80

(a)

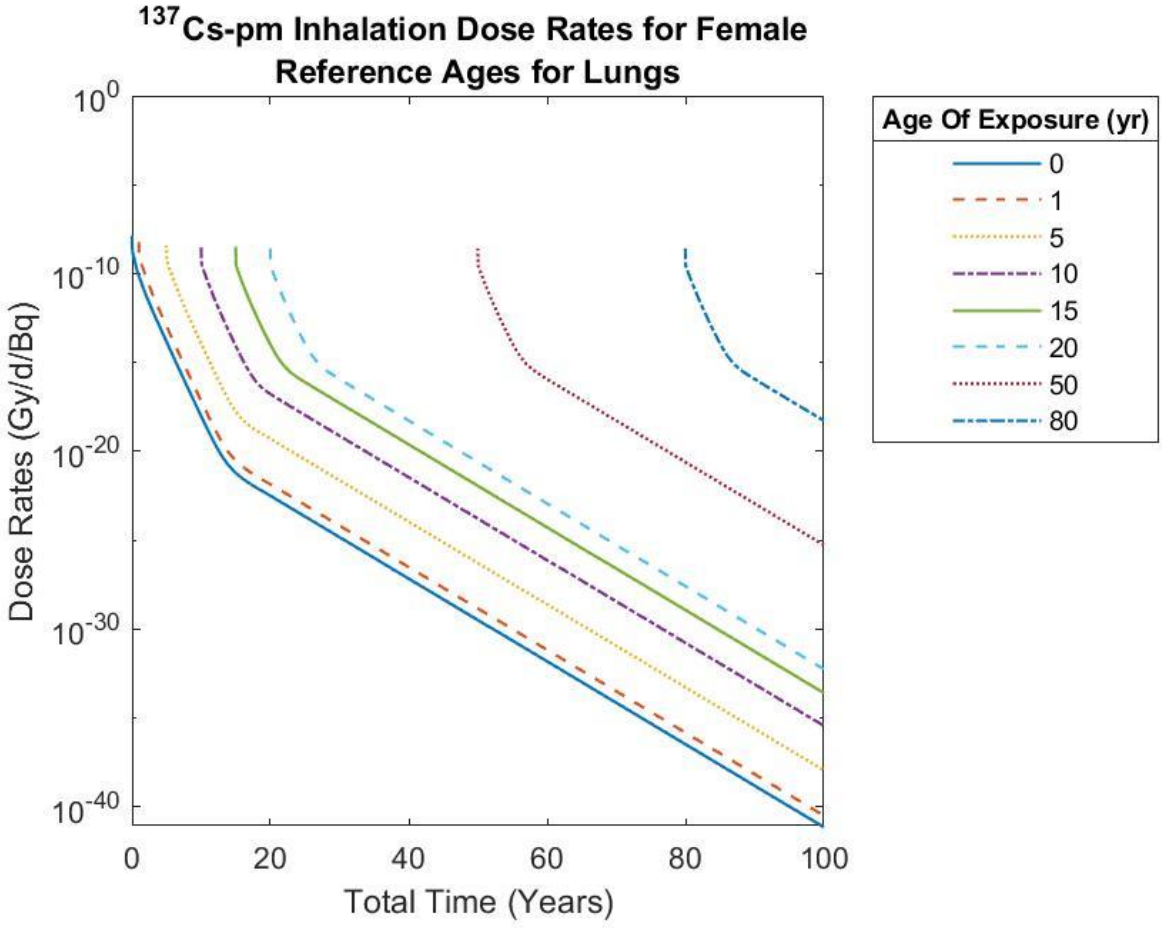
137Cs-pm Inhalation Dose Rates for Female Reference Ages for Lungs
Dose Rates (Gy/d/Bq)
Total Time (Years)
Age Of Exposure (yr)
0
1
5
10
15
20
50
80

(b)

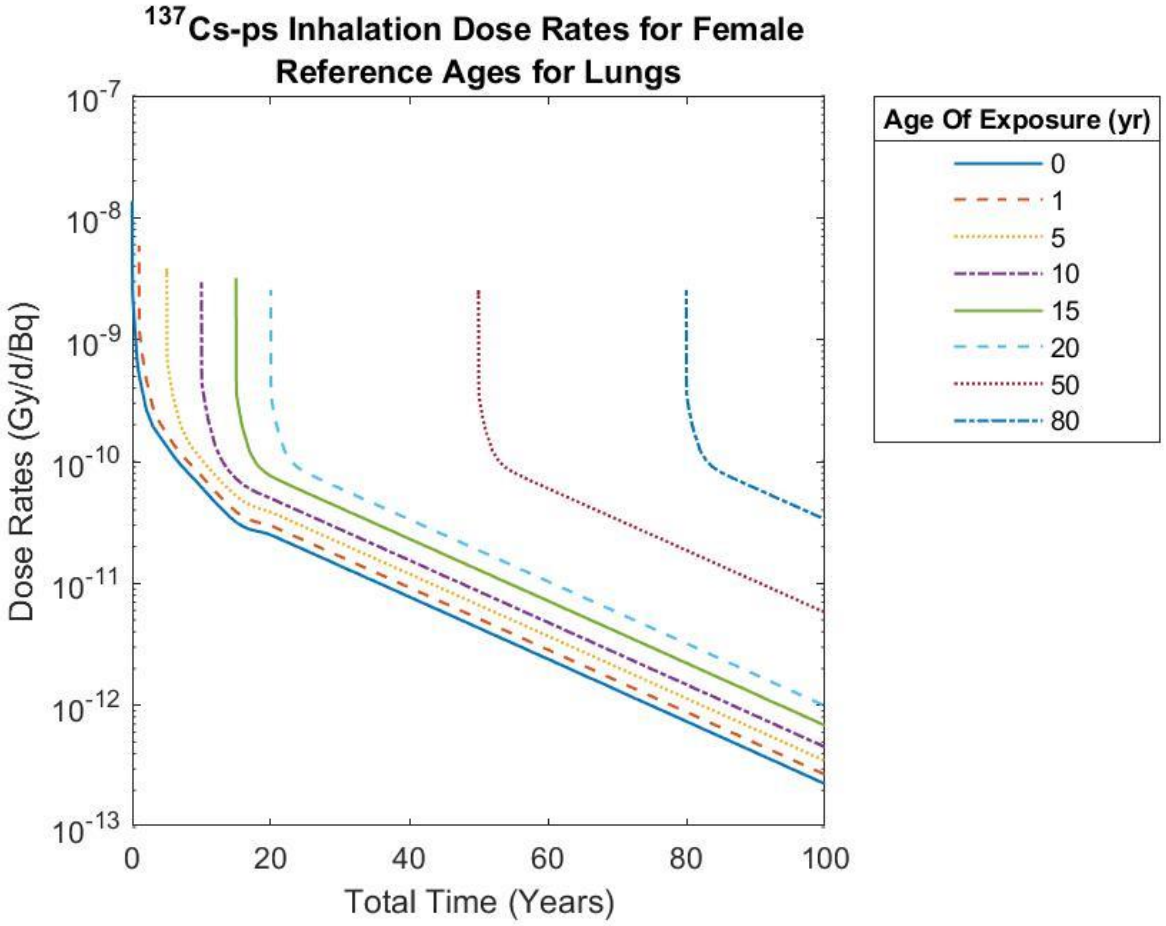

(c)

Figure 56. Dose rates to the female lungs for (a) fast-clearing, (b) moderate-clearing, and (c) slow-clearing ^{137}Cs.

Slow-clearing cesium results in the highest dose rates to the lungs due to the fact that the inhaled radionuclide resides in the lungs longer than for the other two solubility classes. Within each solubility class, the trend in the rate of drop off of the dose rates is consistent across tissue and sex. The male colon is depicted in Appendix E for fast- and slow-clearing cesium to depict this trend.

Ingested cesium, be it via food or water, shows a comparable trend in the dose rates to fast-clearing inhaled cesium soft tissues other than the lungs. A brief peak is reached before a steady

tapering can be seen, reflecting the time it takes for the radionuclide to distribute to the body tissues after ingestion, depicted in Figure 57.

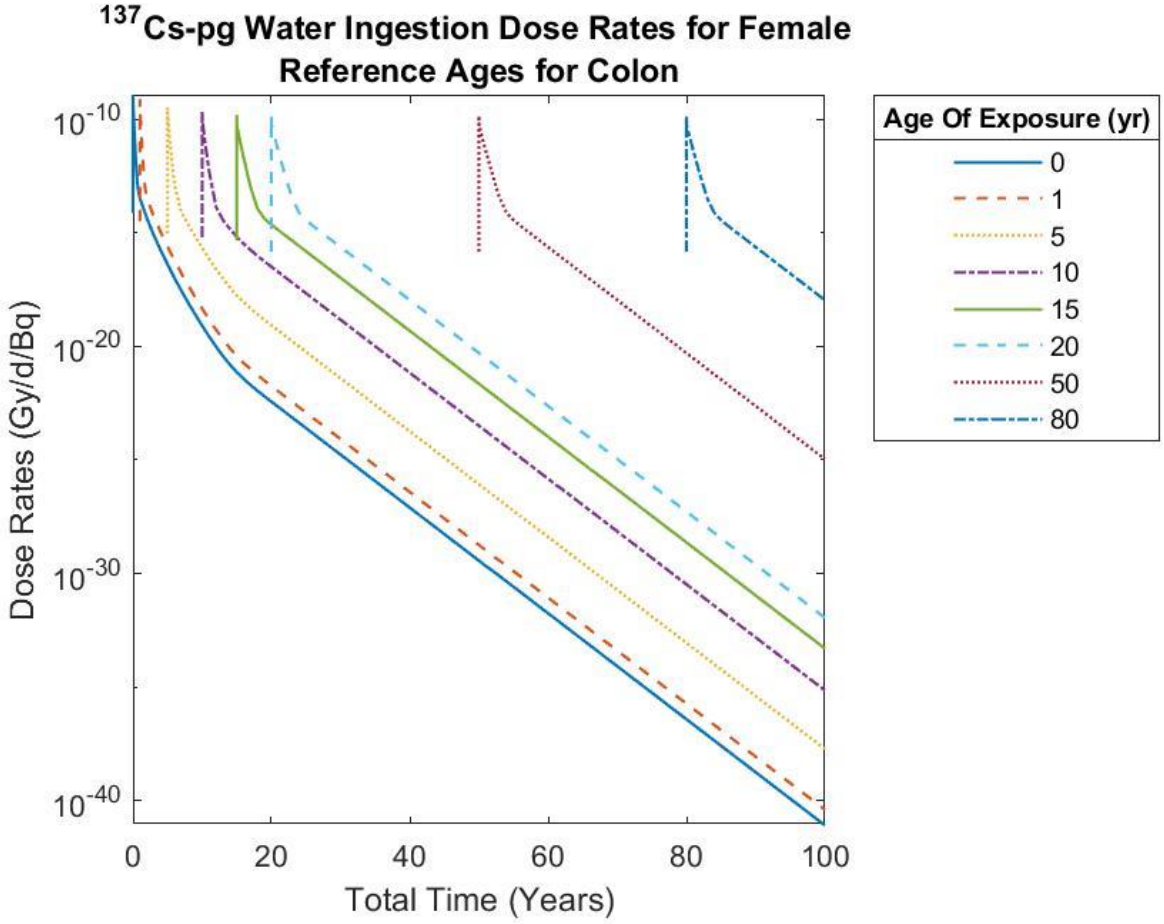

Figure 57. Dose rates to the female colon for tap water ingested ^{137}Cs.

4.5.3. Tritium

Tritium, like cesium, is a whole-body emitter. Due to this fact, the patterns seen with decreasing clearance rate from the lung for tritium resembles the same pattern as for cesium, with the sharpest drop in the dose rates occurring in fast-clearing inhaled tritium. This is a similar behavior as was seen in the FGR 13 data. In Figure 58, dose rates for ages 0 and 1 appear to drop off before reaching end of life. This is due to the fact that the dose rates dropped to 0, and the

limitations of Maltab could not handle the discontinuity. Corresponding male values can be found in Appendix E.

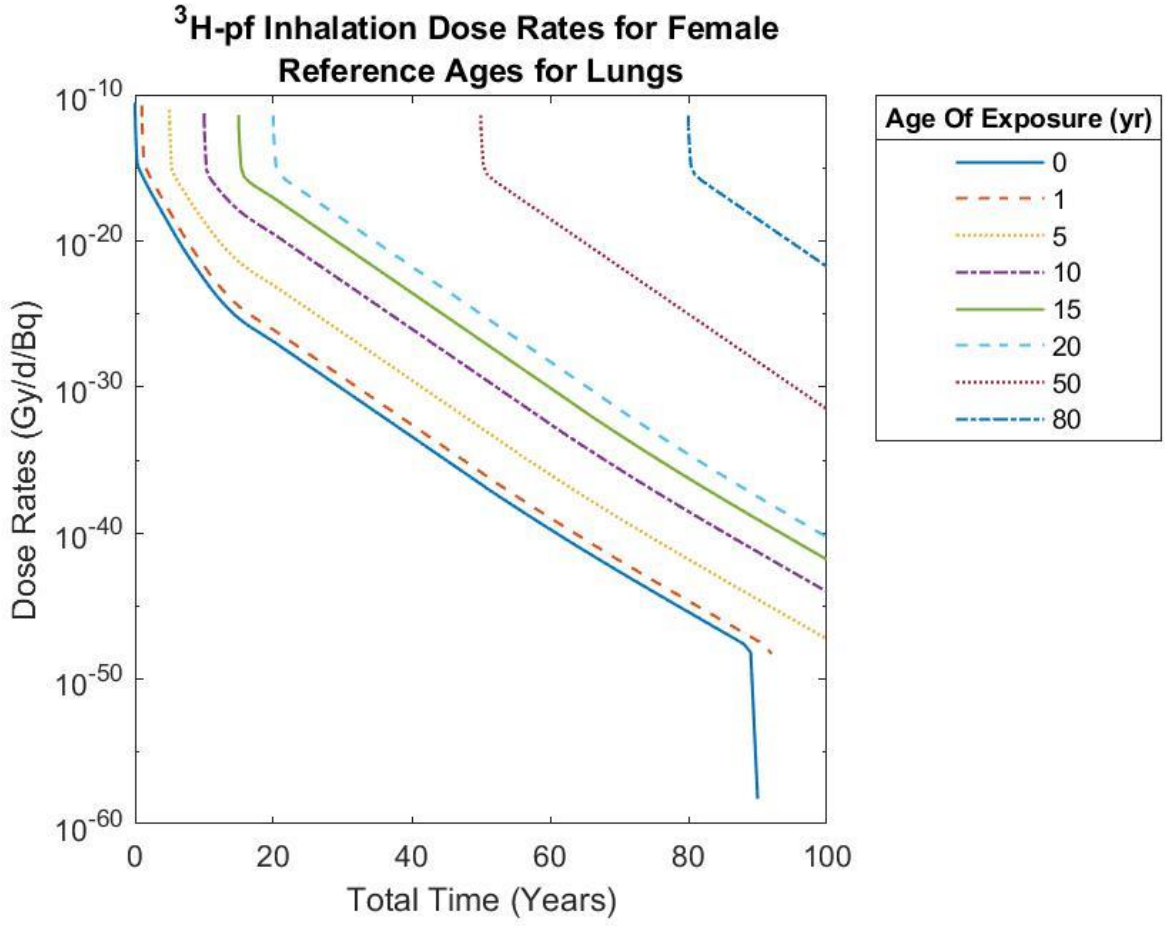

(a)

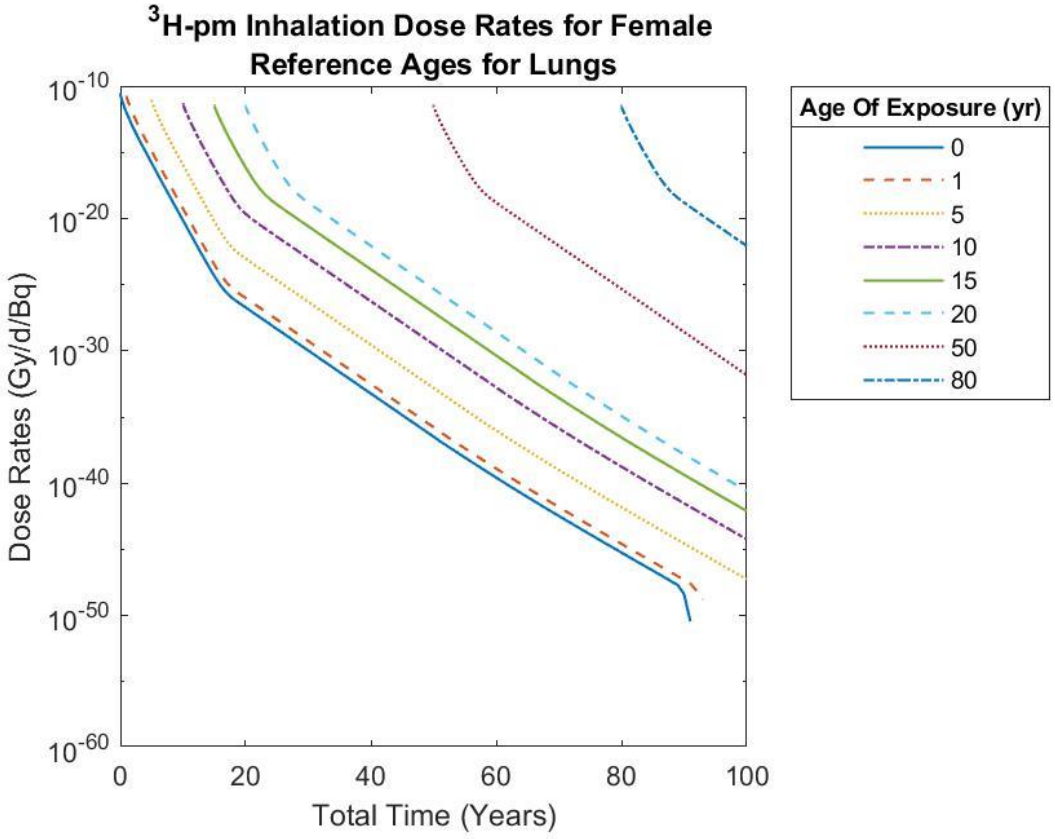
^{3}H-pm Inhalation Dose Rates for Female
Reference Ages for Lungs
Dose Rates (Gy/d/Bq)
10^{-10}
10^{-20}
10^{-30}
10^{-40}
10^{-50}
10^{-60}
0
20
40
60
80
100
Total Time (Years)
Age Of Exposure (yr)
0
1
5
10
15
20
50
80

(b)

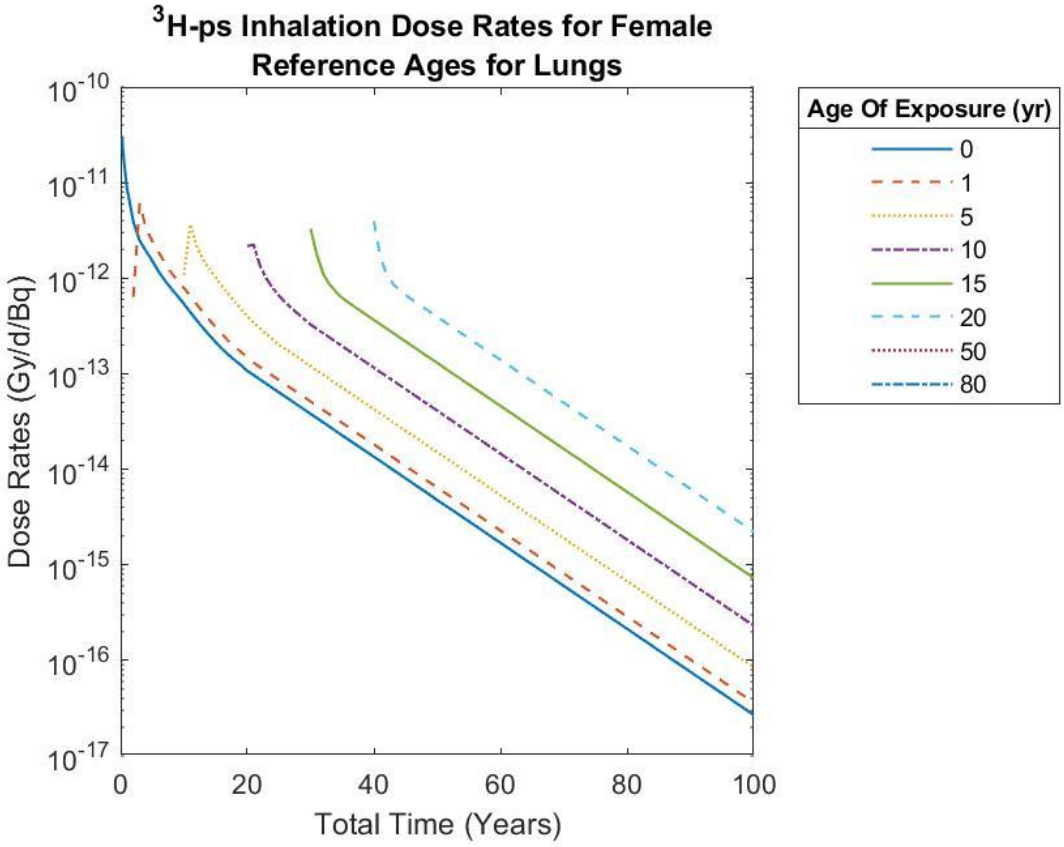

(c)

Figure 58. Dose rates to the female colon for (a) fast-clearing, (b) moderate-clearing, and (c) slow-clearing tritium.

Ingested tritium behaves in a similar manner as fast-clearing inhaled tritium, distributing through the entire body rather evenly without focusing in any one tissue, seen in Figure 59.

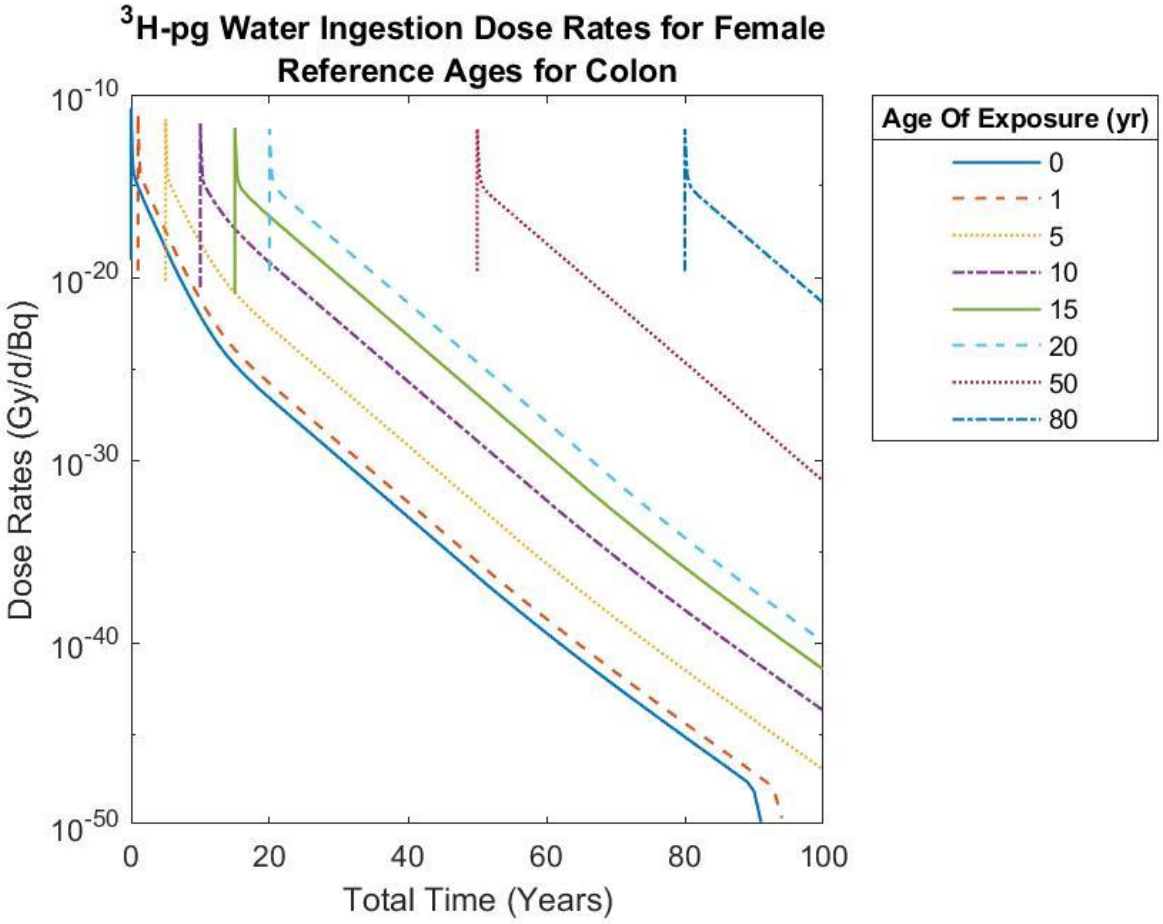

Figure 59. Dose rates to the female colon due to tap water ingested tritium.

4.5.4. ^{90}Sr

Strontium's behavior being akin to calcium results in the integration into the bone matrix, as was seen with the FGR 13 dose rate data. Thus, the rate of removal of ^{90}Sr from the body is slower in the bone than in other soft tissues. This pronounced difference can be seen clearly with fast-clearing inhaled strontium, in Figure 60. Corresponding male values can be found in Appendix E.

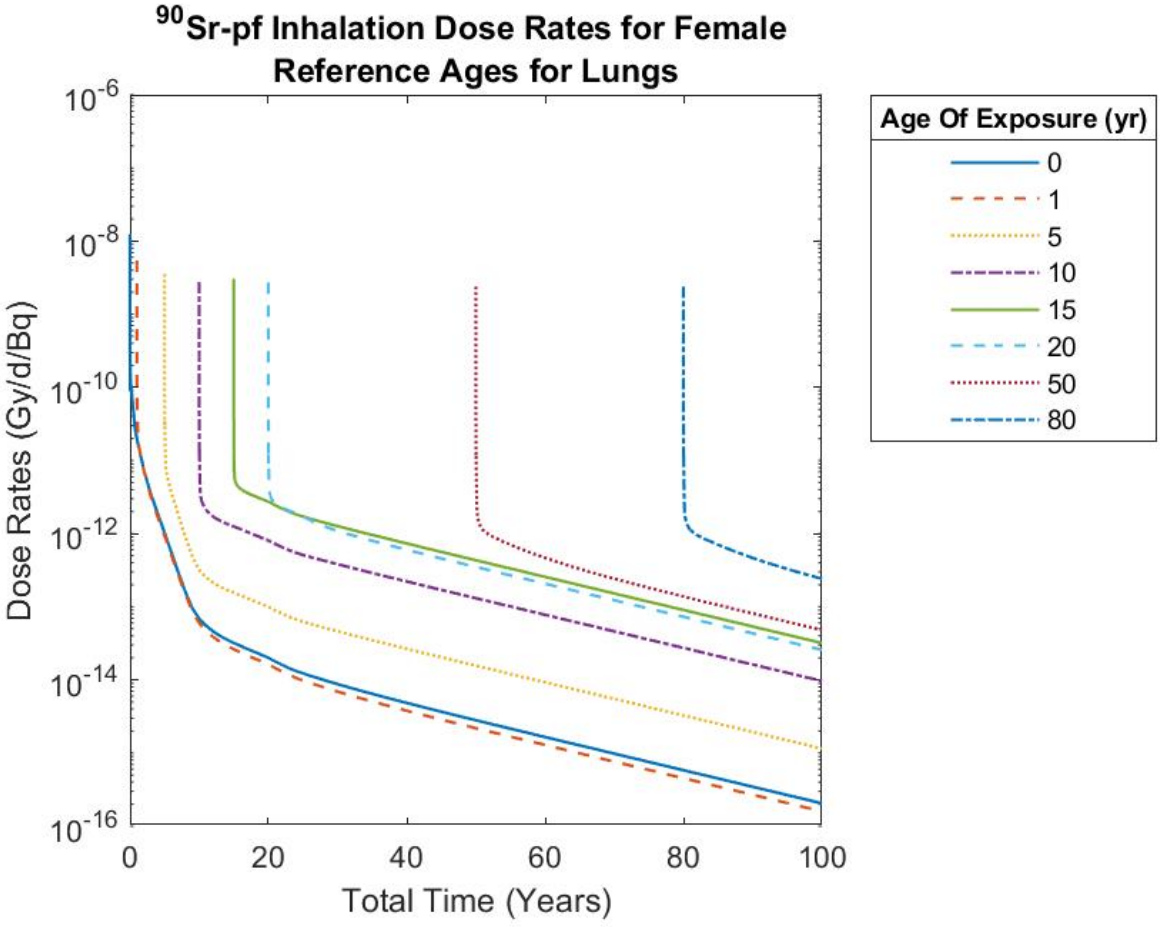
^{90}Sr-pf Inhalation Dose Rates for Female Reference Ages for Lungs
Dose Rates (Gy/d/Bq)
10^{-6}
10^{-8}
10^{-10}
10^{-12}
10^{-14}
10^{-16}
0
20
40
60
80
100
Total Time (Years)
Age Of Exposure (yr)
0
1
5
10
15
20
50
80

(a)

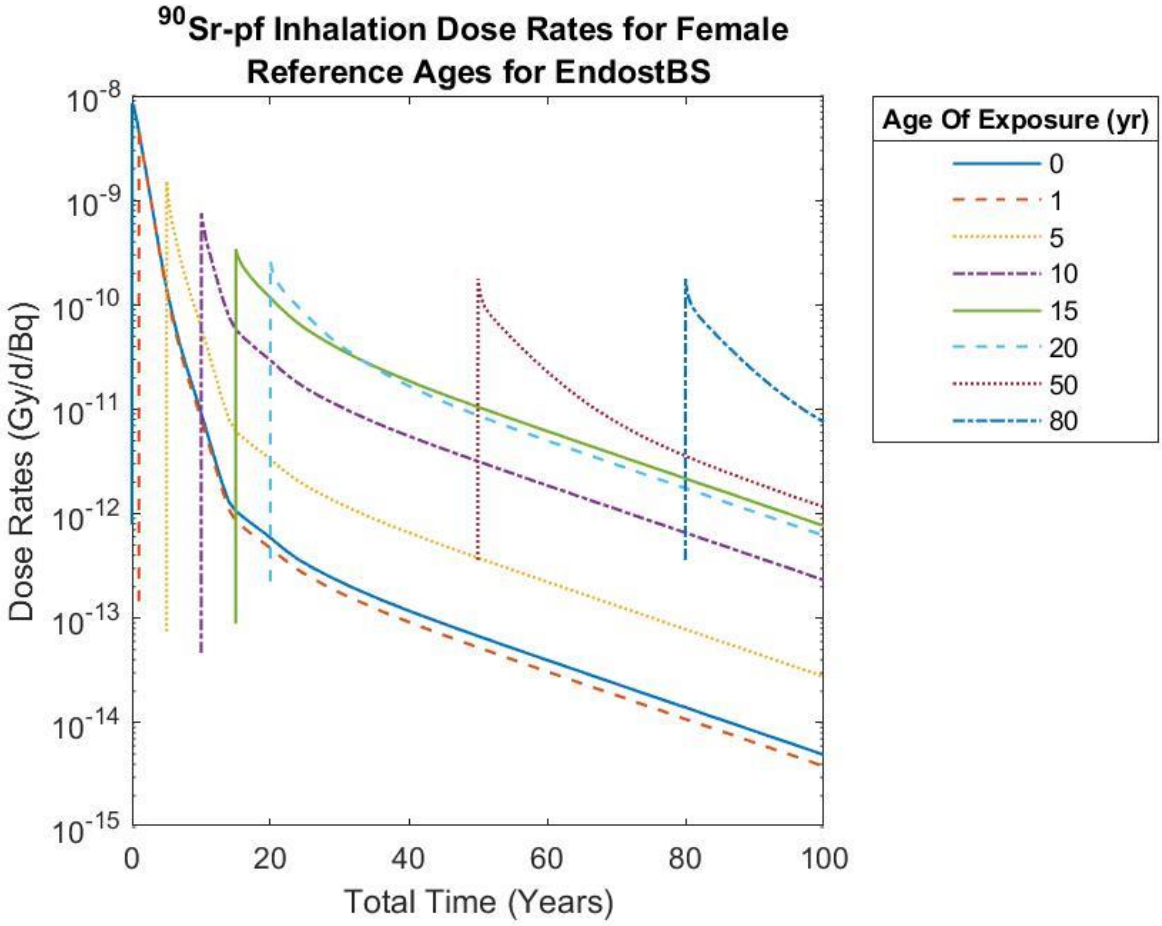

(b)

Figure 60. Dose rates to the female (a) lung and (b) endosteal bone surface for fast-clearing ^{90}Sr.

Slow-clearing strontium for the preliminary data shows the same trend as the FGR 13 data does, the strontium taking time to build up in the bone surface as it takes longer to clear from the lungs, seen in Figure 61. Moderate-clearing strontium trends can be found in Appendix E.

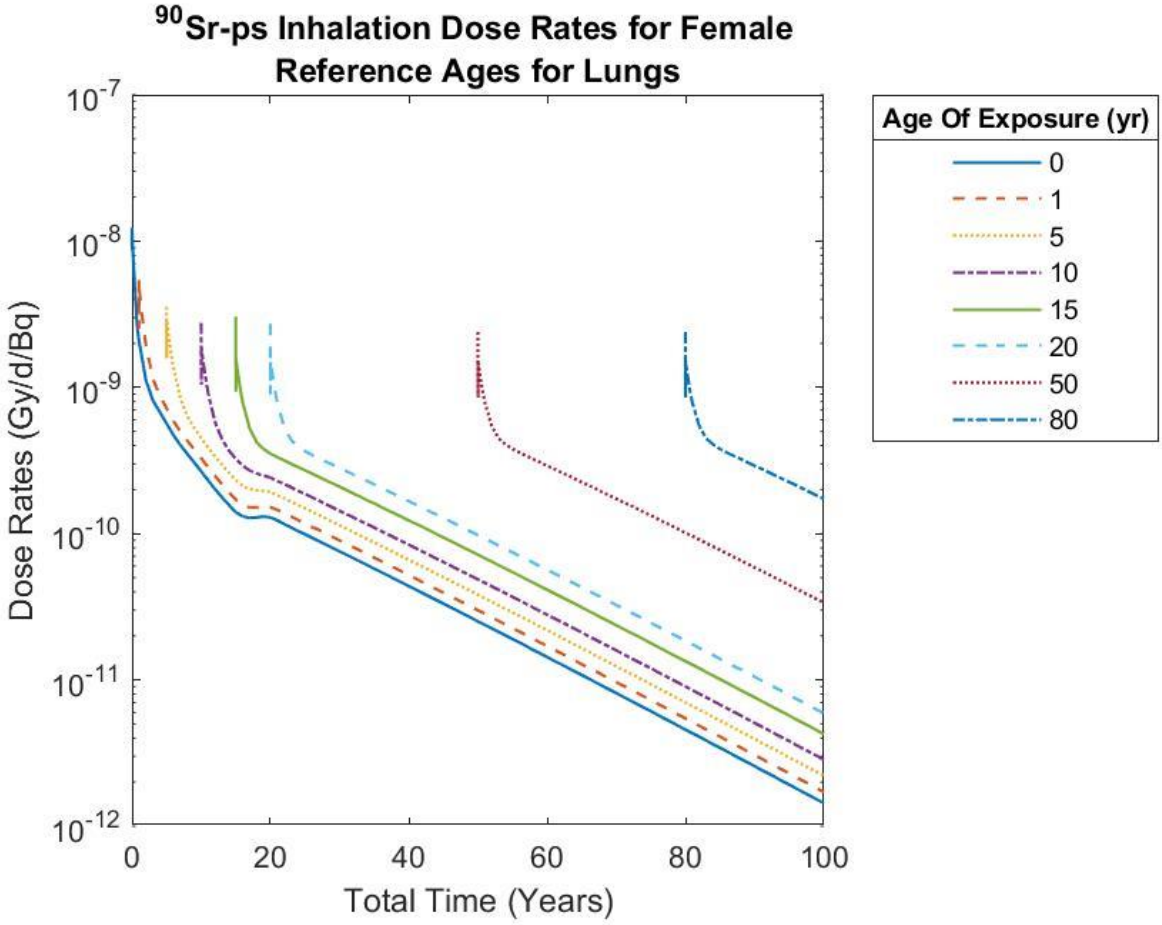
^{90}Sr-ps Inhalation Dose Rates for Female Reference Ages for Lungs
Dose Rates (Gy/d/Bq)
Total Time (Years)
Age Of Exposure (yr)
0
1
5
10
15
20
50
80

(a)

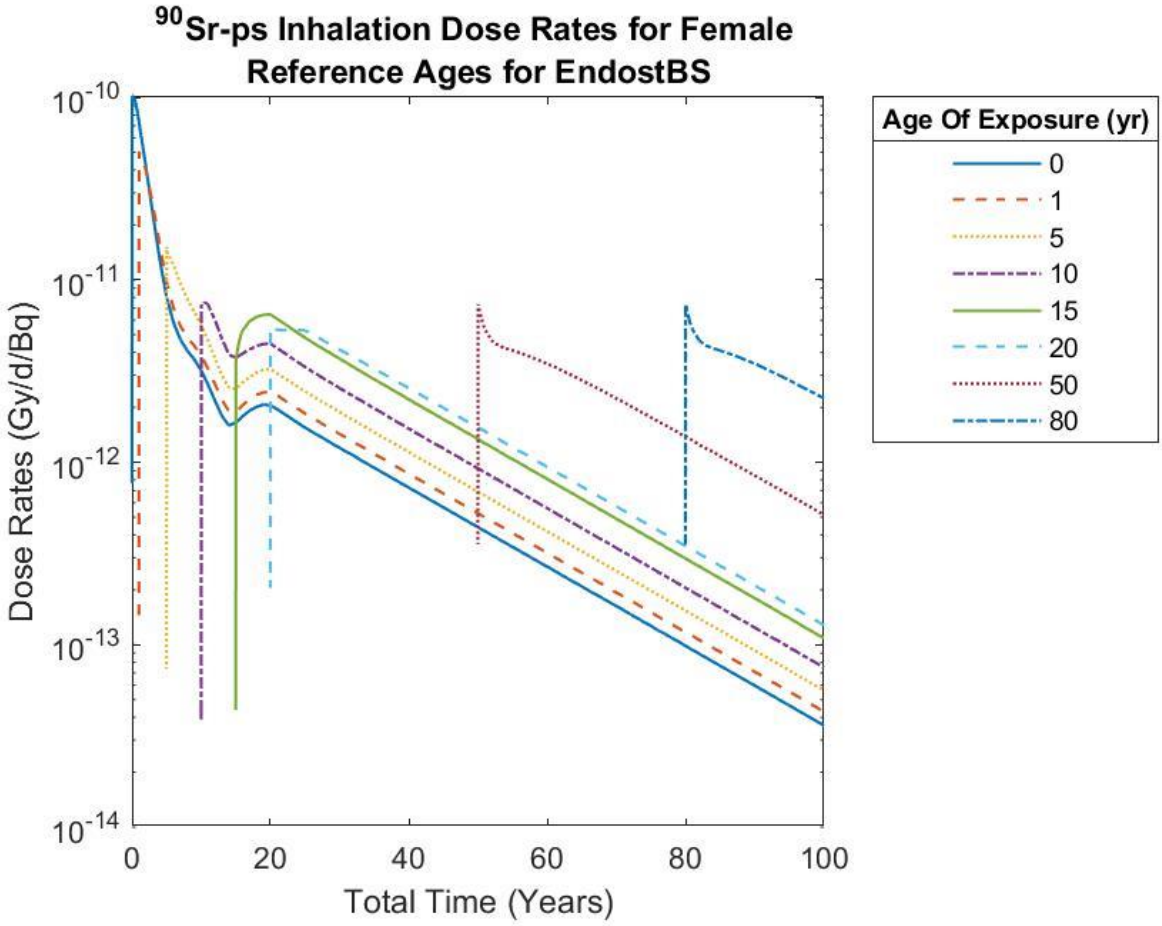

(b)

Figure 61. Dose rates to the female (a) lungs and (b) endosteal bone surface for slow-clearing ^{90}Sr.

Ingested strontium shows noteworthy but not inexplicable behavior. There is very little time required for buildup for the radionuclide to reach the bone after ingestion, however, all tissue show a slight peak before dipping off in a similar decreasing trend, depicted in Figure 62.

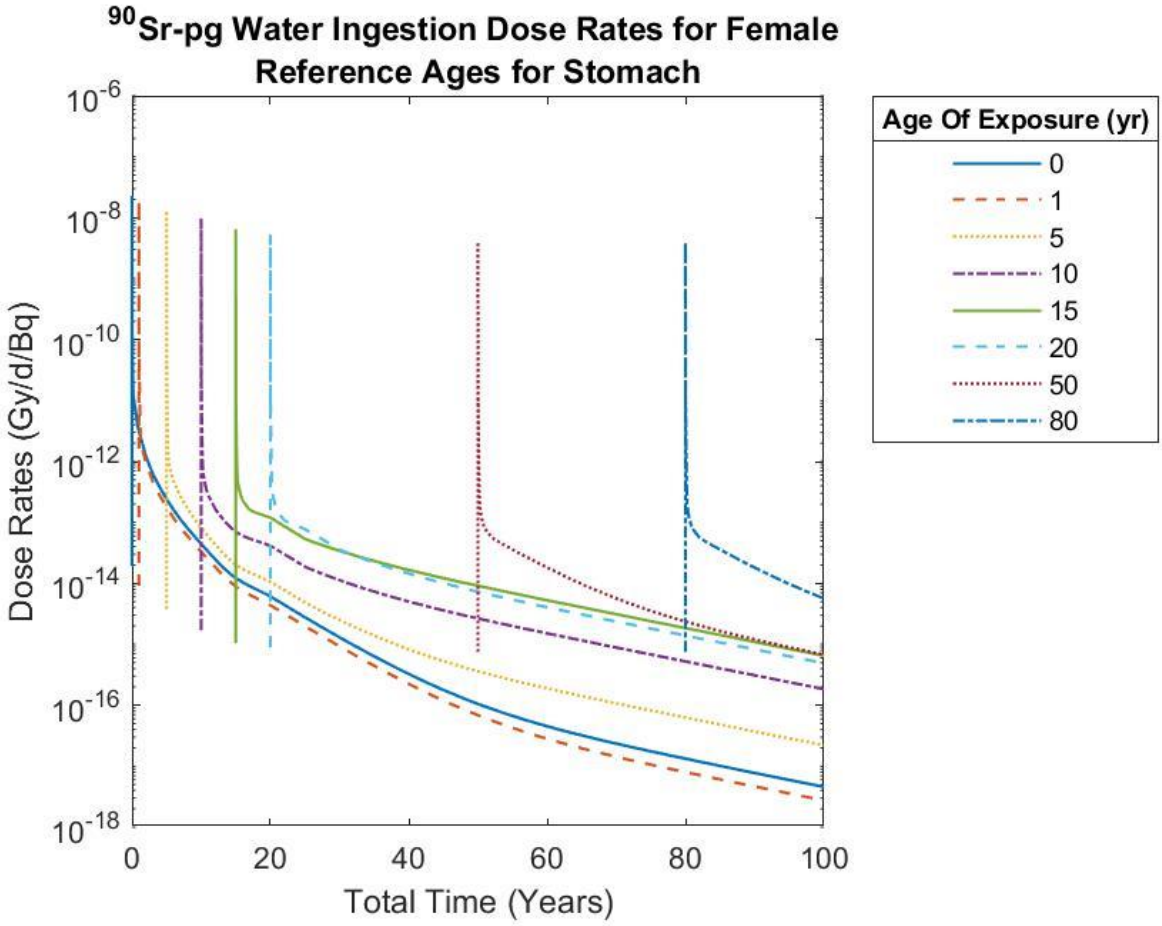
^{90}Sr-pg Water Ingestion Dose Rates for Female
Reference Ages for Stomach
Dose Rates (Gy/d/Bq)
10^{-6}
10^{-8}
10^{-10}
10^{-12}
10^{-14}
10^{-16}
10^{-18}
0
20
40
60
80
100
Total Time (Years)
Age Of Exposure (yr)
0
1
5
10
15
20
50
80

(a)

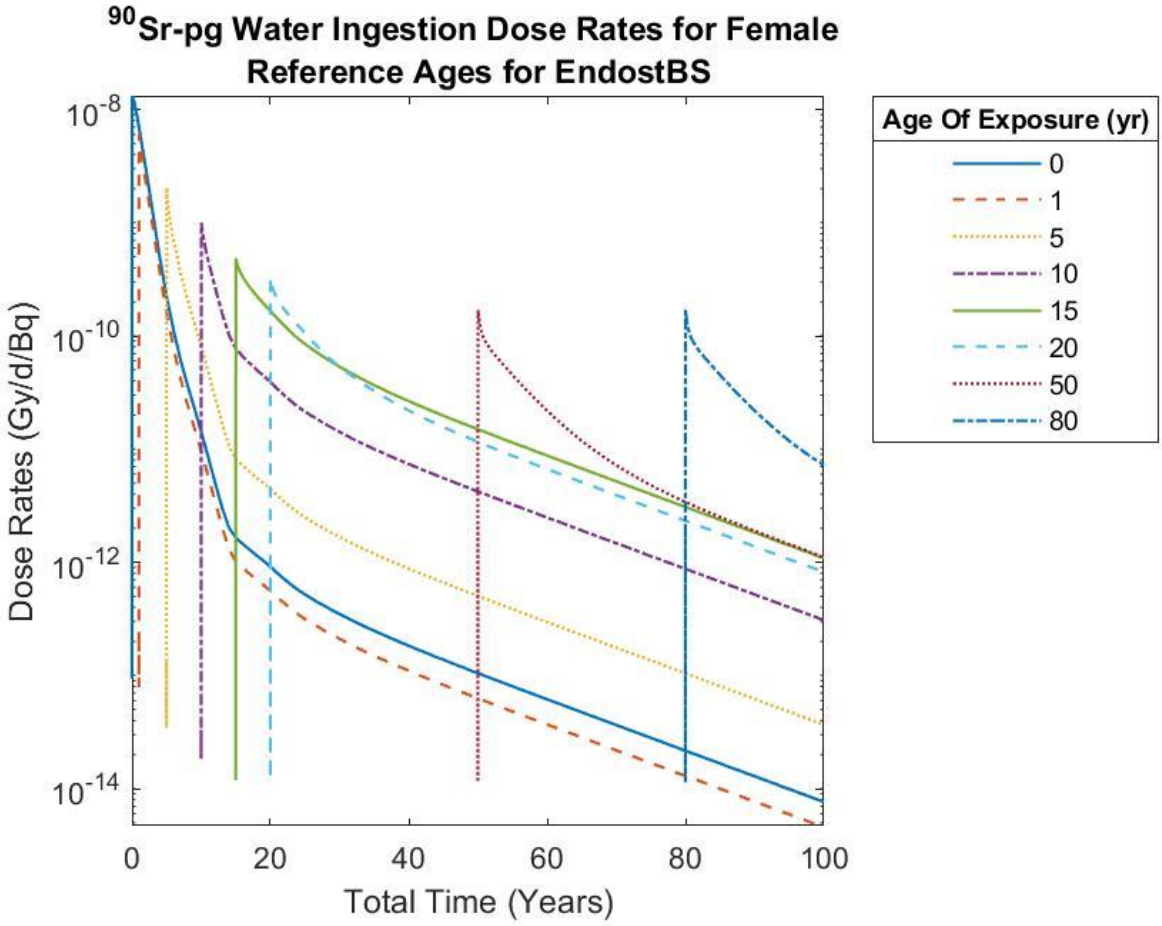

(b)

Figure 62. Dose rates to the female (a) stomach and (b) endosteal bone surface from tap water ingested ^{90}Sr.

Overall, the trends and patterns of the dose rates for the preliminary data track well with established FGR 13 DCAL generated dose rate data, with only slightly visible changes in the behavior. As with the FGR 13 data, the preliminary data was annualized in an identical manner. This resulted in the leading tail of the dose rates for all radionuclides, solubility classes, and usage types disappearing as the leading data was incorporated in with the rest of the year one post exposure dose rate values, exactly like with the FGR 13 annualized data seen Figure 29.

4.6. Preliminary Data Doses from a Chronic Exposure

Following the same methods utilized to calculate the chronic exposures for the FGR 13 data, the chronic exposure dose rates for the preliminary data were calculated, and compared to FGR 13's plots to determine any variation and the sources of such variation – whether biokinetic, dosimetric, or detriment-weighting.

4.6.1. ^{131}I

As with the FGR 13 data, the preliminary data for ^{131}I shows a steady drop off in the dose rates before reaching a plateau at age 20, where the biokinetics cease variation. The difference, however, between chronic exposure dose rates given by FGR 13 informed data and the preliminary data is that the dose rates for a chronic exposure for all solubility classes for inhaled iodine are orders of magnitude lower for the preliminary data than those in FGR 13, and can be seen in Figure 63.

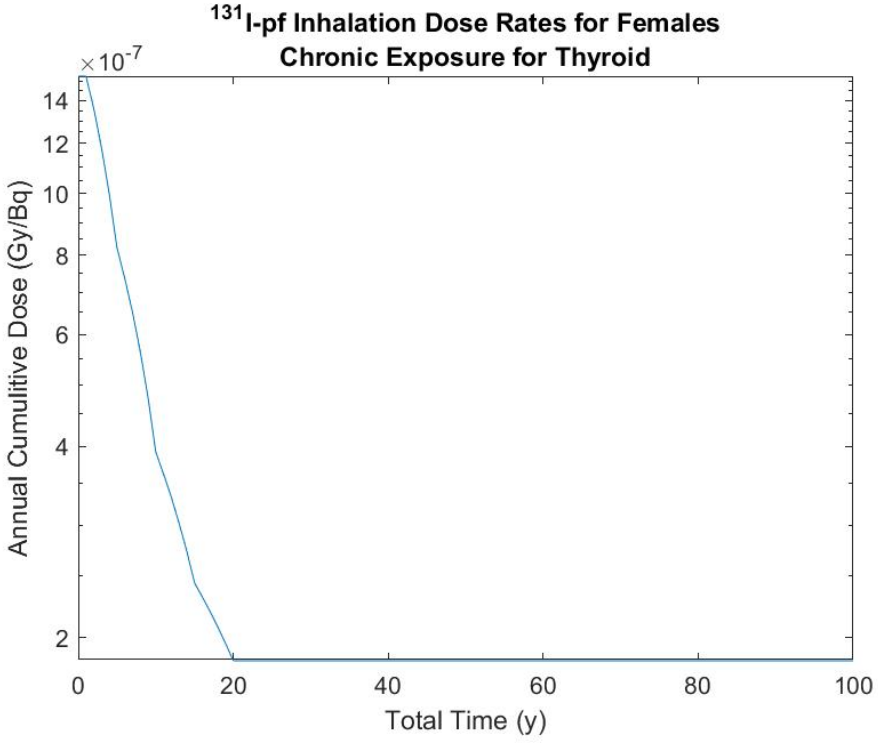

(a)

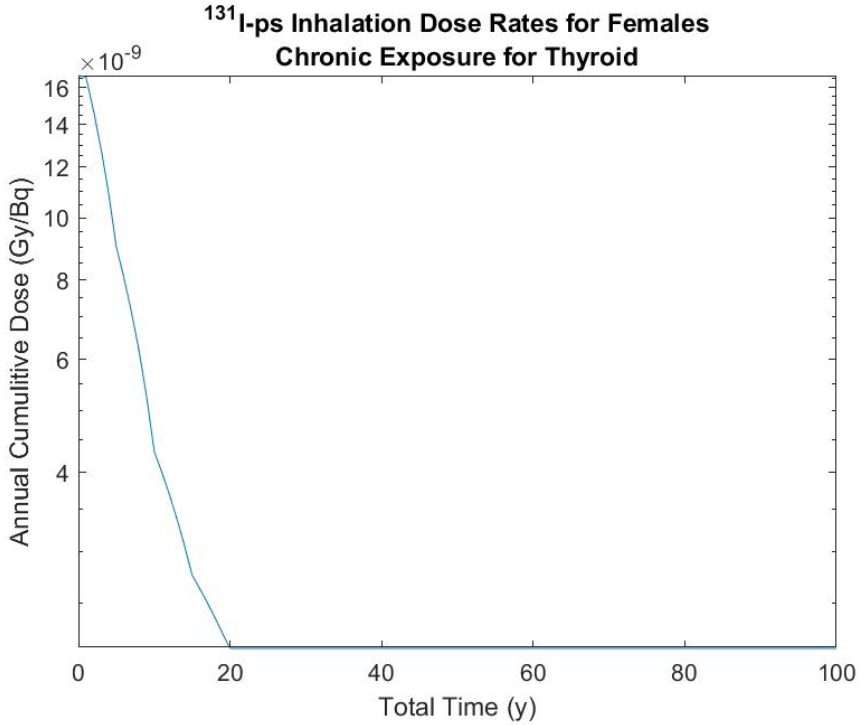

(b)

Figure 63. Dose rates from a chronic exposure for (a) fast-clearing and (b) slow-clearing ^{131}I in the female thyroid.

For ingested iodine, seen in Figure 64, the dose rates from a chronic exposure for the preliminary data align much more closely with chronic exposure dose rates given in FGR 13, indicating a biokinetic change in the handling of the lungs between data generations. These changes in biokinetic behavior are a contributing factor to the risk calculation for the preliminary data, as will be explained in the following section.

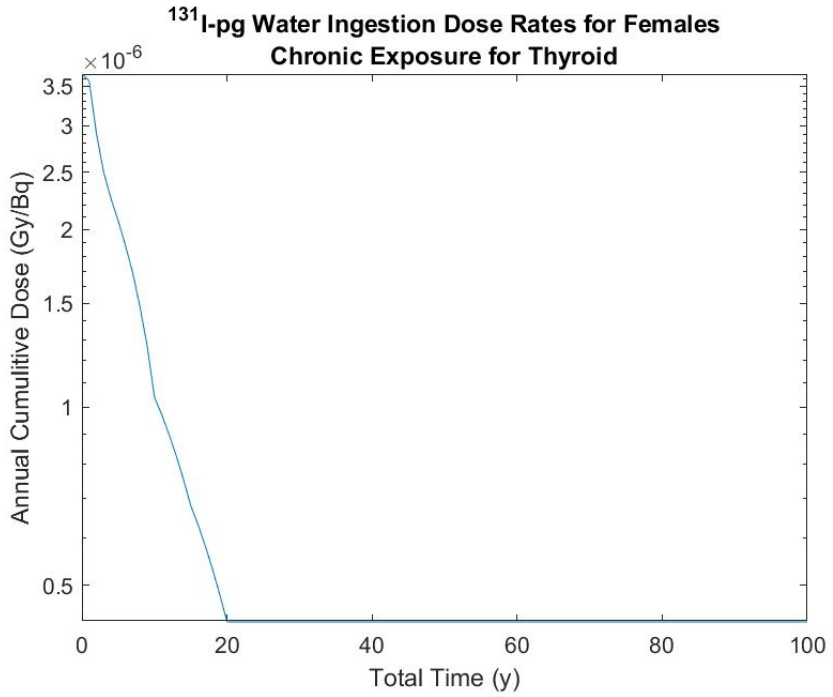

(a)

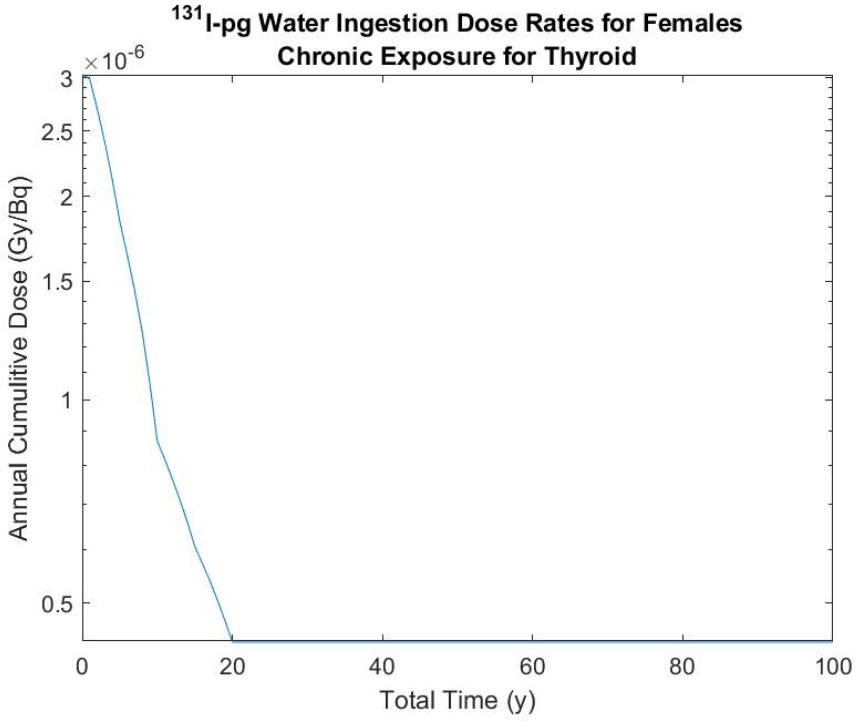

(b)

Figure 64. Comparison of the (a) FGR 13 and (b) preliminary data dose rates to the female thyroid from a chronic exposure of tap water ingested ^{131}I.

4.6.2. ^{137}Cs

Trends for cesium between the preliminary data and FGR 13 again are similar, with a few key differences. For fast-clearing inhaled cesium, the overall dose rates to the lungs from a chronic exposure is higher for the preliminary data as compared to FGR 13, while for other soft tissues, such as the breast, it is lower. A similar plateau at age 20 can be seen, as was seen in the data provided by FGR 13. As with the FGR 13 data, variation leading up to age 20 for all plots in this section are attributed to varying biokinetics up until age 20, and can be seen in Figure 65.

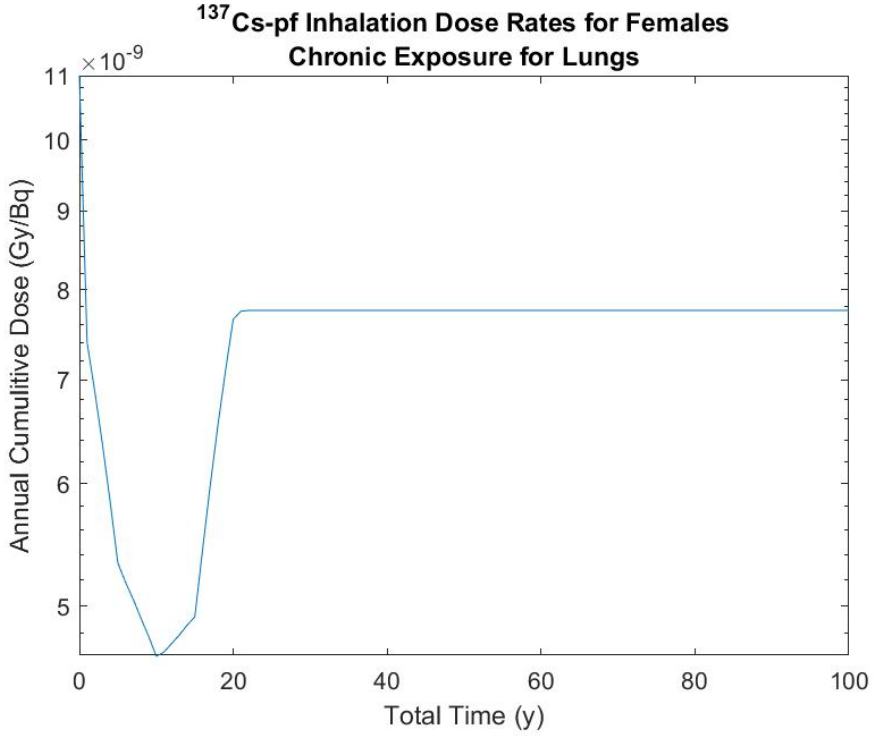

(a)

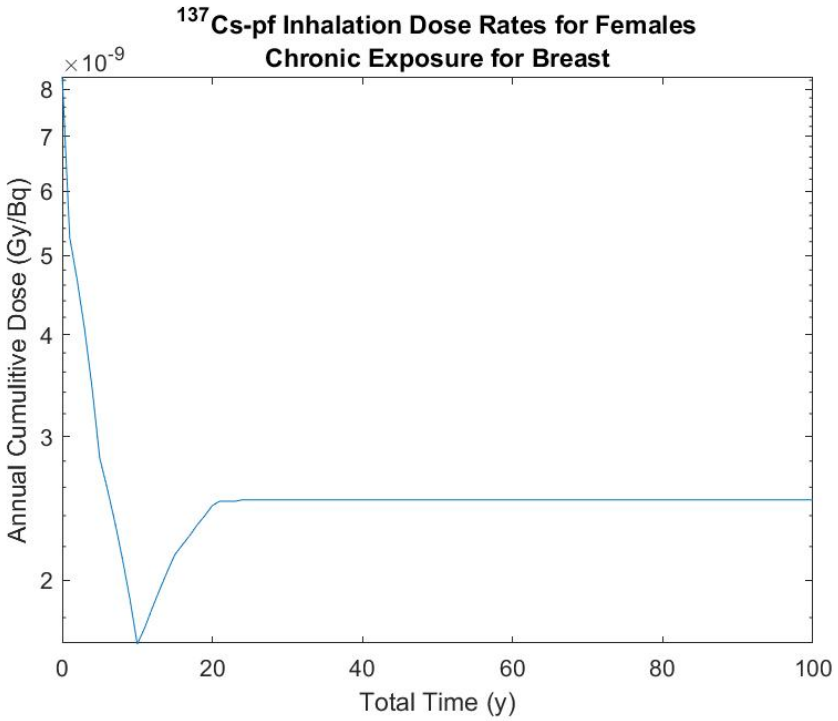

(b)

Figure 65. Absorbed dose rates to the female lungs (a) and breast (b) from a chronic exposure to slow-clearing ^{137}Cs.

For slow-clearing cesium in the FGR 13 data, a slight buildup was seen in the soft tissues. Buildup was also seen in the preliminary data, however, the buildup in the lungs for the preliminary data is significantly more substantial across both sexes, and can be seen in Figure 66. For the other soft tissues, the buildup was less prominent, however, was still slightly greater than that of the FGR 13 data. Figure 66 corresponds to Figure 35, previously.

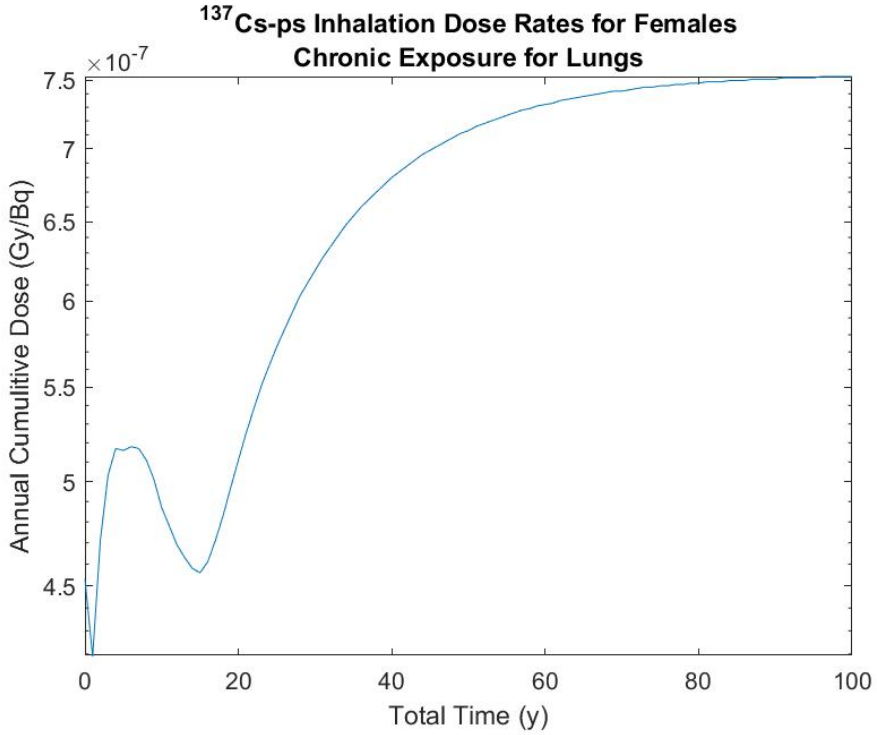

(a)

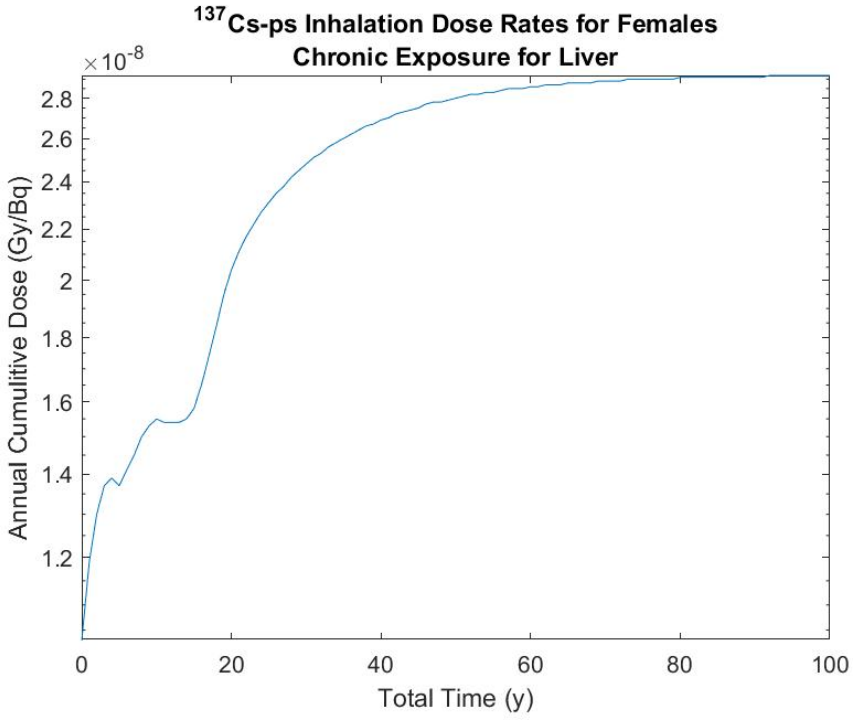

(b)

Figure 66. Dose rates to the (a) female lungs and (b) liver from a chronic exposure to slow-clearing ^{137}Cs.

Ingestion of ^{137}Cs through tap water and food saw behavior akin to fast-clearing inhaled cesium, with a plateau occurring beginning at year 20 for all tissues, with no buildup seen through end of life. However, as has been the case for most tissues, the overall dose rates from a chronic exposure to ^{137}Cs ingested through either food or tap water for the preliminary data are lower than the dose rates from FGR 13's data, seen in Figure 67.

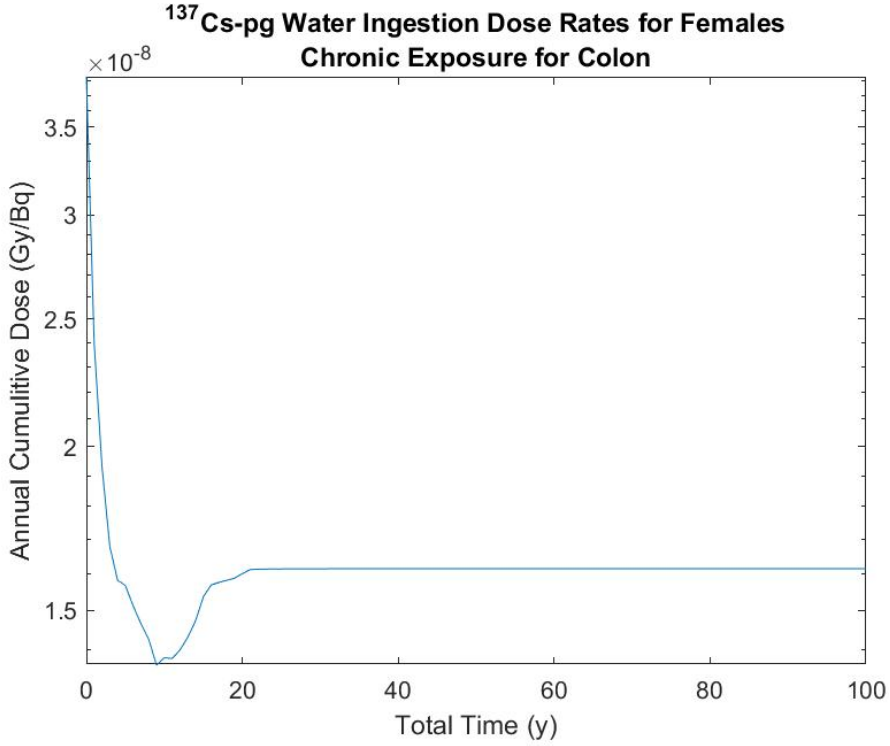

(a)

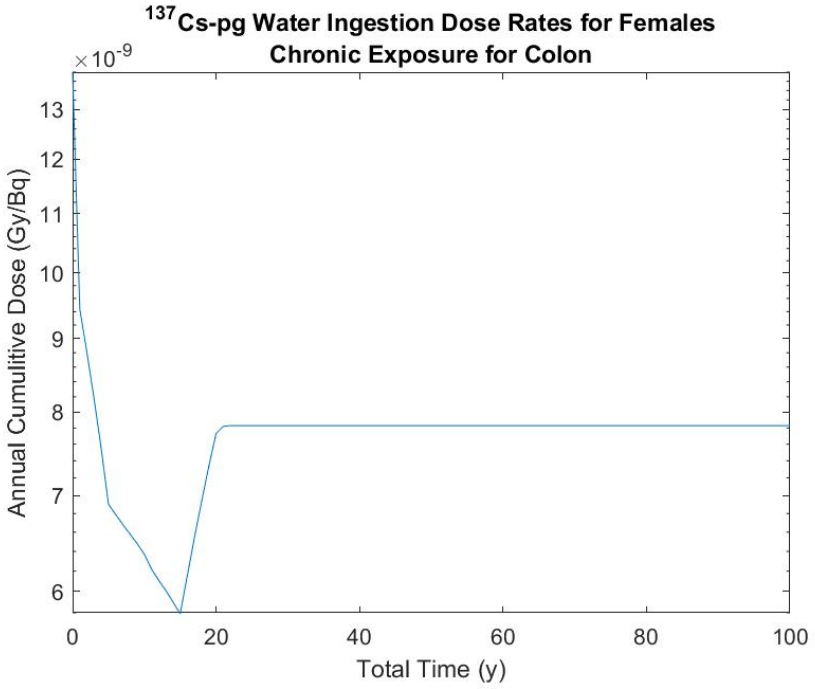

(b)

Figure 67. Absorbed dose rates to the female colon from a chronic tap water ingestion of ^{137}Cs for (a) FGR 13 and the (b) preliminary data.

4.6.3. Tritium

The behavior of tritium for a chronic exposure for the preliminary data tracks rather consistently with the data from FGR 13, with magnitudes being similar across the board for all solubility classes, indicating that the change in biokinetics between generations of data for the different solubility classes and usage types were not overly substantial, comparted to the changes seen in iodine and cesium depicted by Figure 68. For ingested tritium, the preliminary data happens to be only marginally higher at the beginning of life, but quickly tapers off to a rate akin to what was seen in FGR 13, seen in Figure 69.

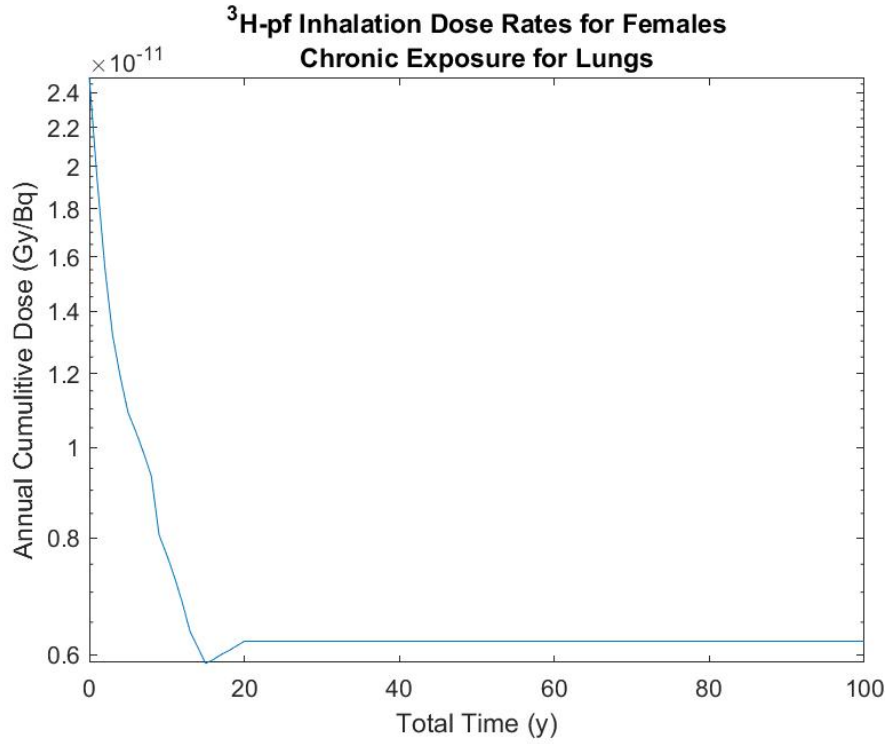

(a)

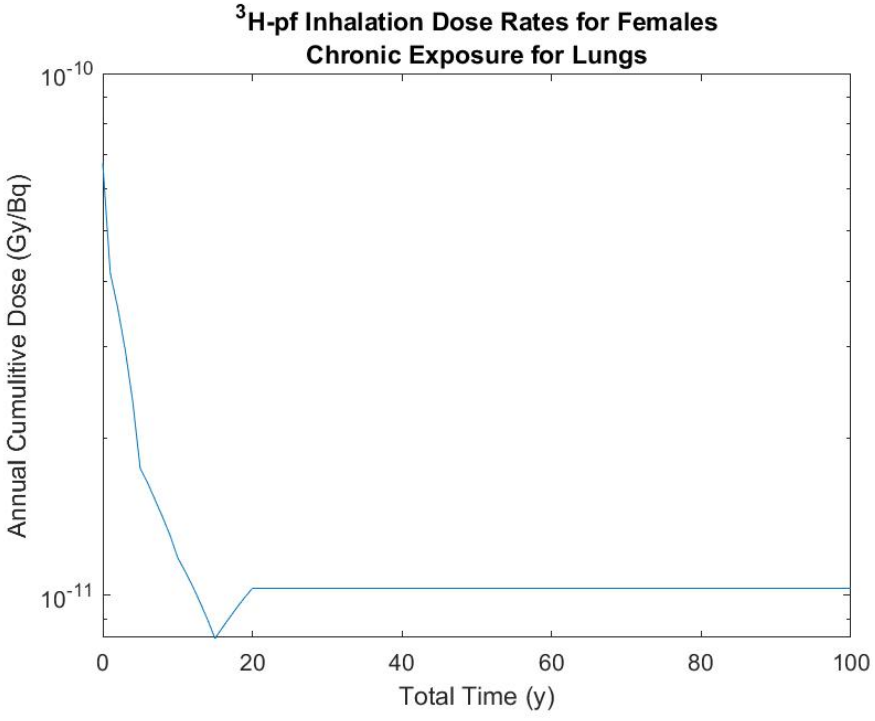

(b)

Figure 68. Absorbed dose rates from a chronic exposure of fast-clearing tritium in the female lungs for the (a) FGR 13 and (b) preliminary data.

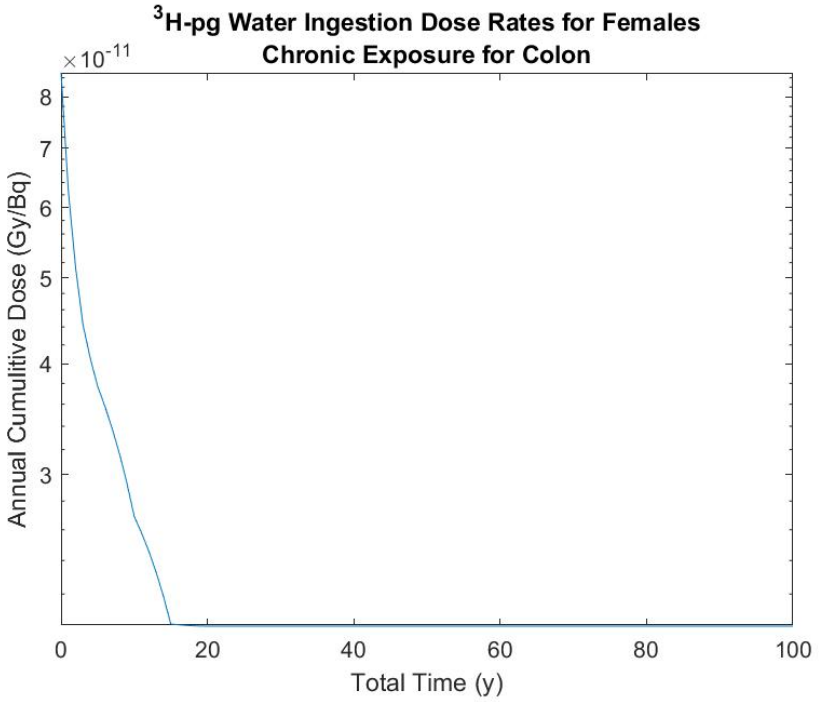

(a)

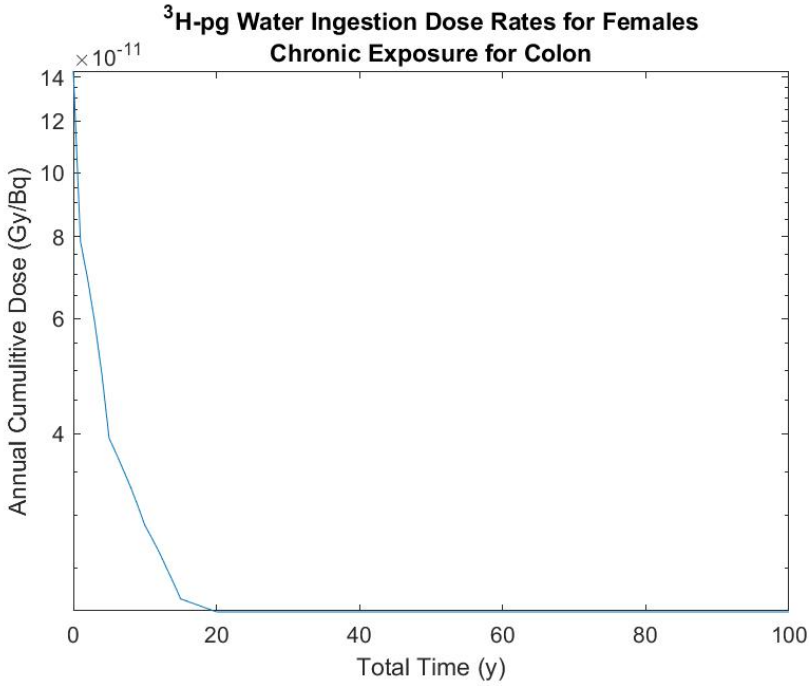

(b)

Figure 69. Absorbed dose rates from a chronic exposure of tap water ingested tritium in the female colon for the (a) FGR 13 and (b) preliminary data.

4.6.4. ^{90}Sr

The preliminary data for strontium follows similar trends to the data presented in FGR 13 for fast-clearing inhaled strontium, as seen in Figure 70. The only difference here being that the initial dose rates from a chronic exposure are an order of magnitude higher than for FGR 13. However, this quickly drops back down to a comparable dose rate by age 20, trending along with the FGR 13 data.

Tritium's long biological and comparatively long physical half-life results in a plateau not being seen in the chronic exposure data for strontium. As well, as with the FGR 13 data, variations are seen leading up to age 20 that are indicative of the changing biokinetics of strontium through juvenile ages.

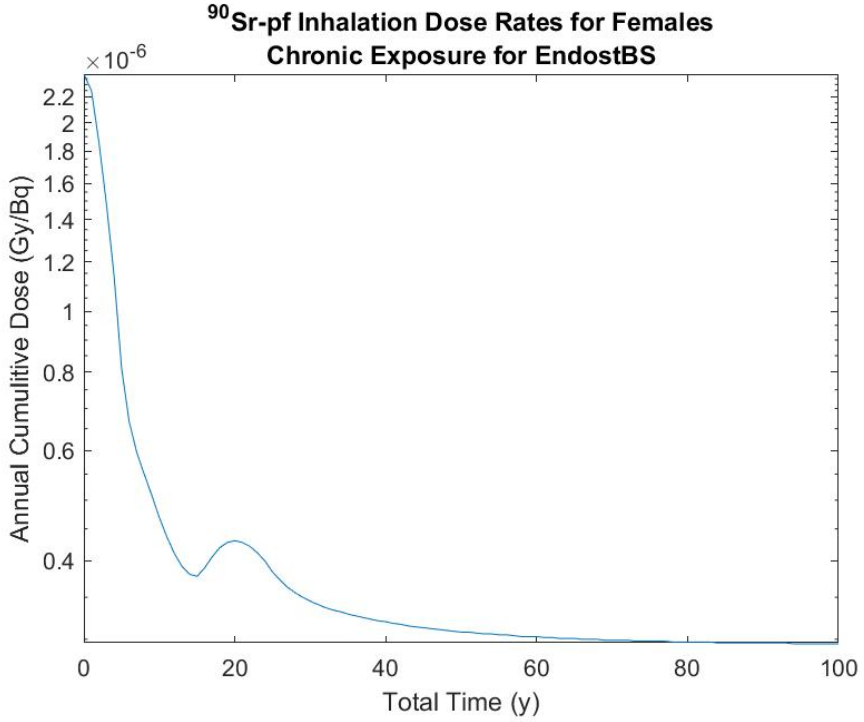

Figure 70. Dose rates from a chronic exposure to the female bone surface from fast-clearing ^{90}Sr.

Slow-clearing strontium shows quite a different behavior for the preliminary data as compared to the FGR 13 data. Rather than plateauing after a brief decrease just before year 25, as in the FGR 13 data, the preliminary data trend results in a continuous buildup through end of life within the bone matrix beginning at age 20, indicating a potential biokinetic change between data generations in the handling of integration of strontium into the bone matrix and suggesting the radionuclide in fact spends longer in the bone matrix. This behavior is depicted in Figure 71.

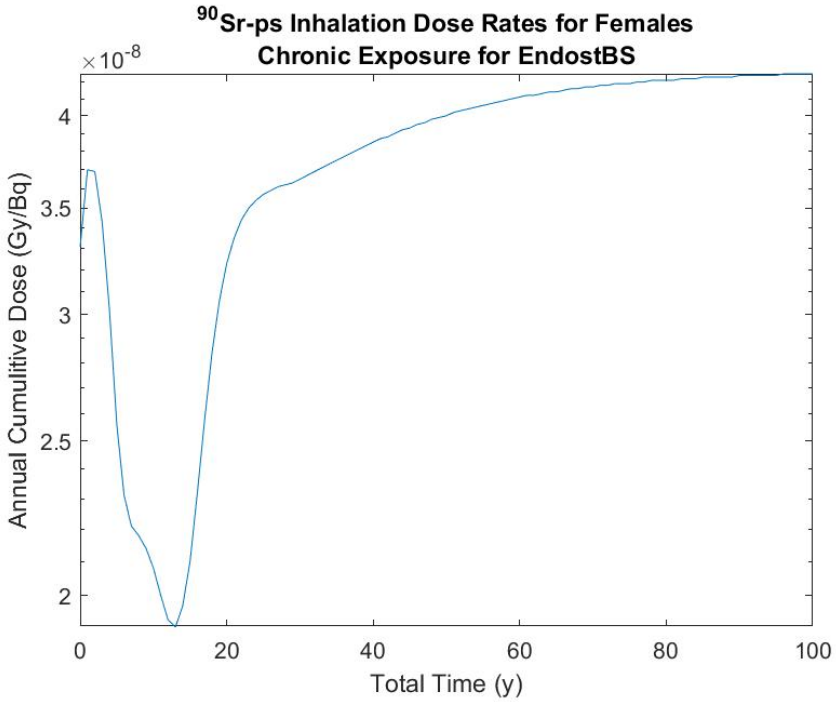

Figure 71. Dose rates from a chronic exposure to the female bone surface from slow-clearing ^{90}Sr.

For ingested strontium, both through tap water and food ingestion, the dose rates from a chronic exposure followed a similar trend as fast-clearing inhaled strontium, peaking at year 20 before steadily decreasing, seen in Figure 72. This trend parallels what was seen in the FGR 13 data, however, the overall absorbed dose rates to the bone surface are higher for the preliminary data by approximately an order of magnitude.

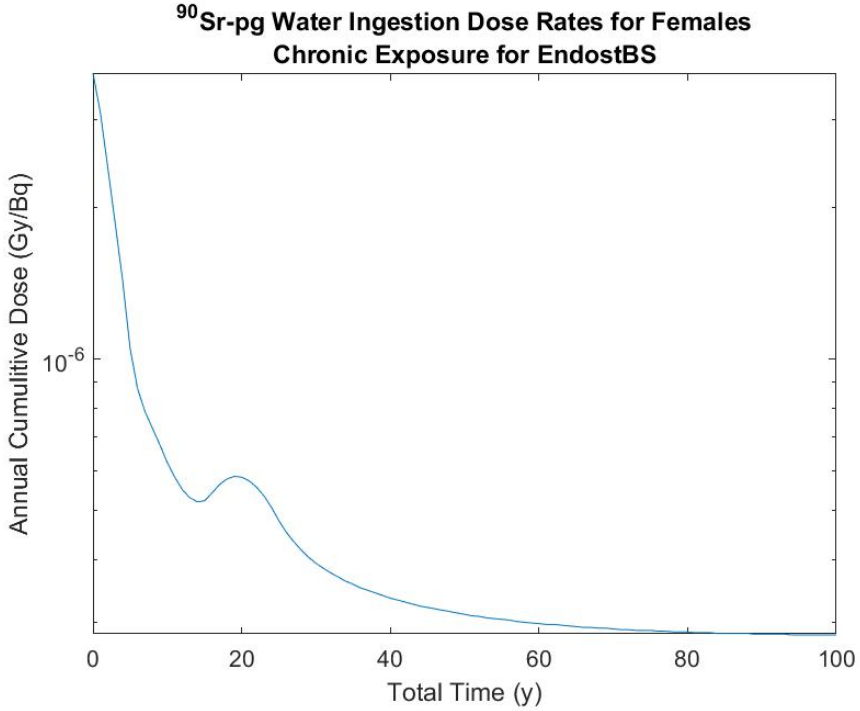

Figure 72. Dose rates from a chronic exposure to the female bone surface due to a tap water ingestion of ^{90}Sr.

4.7. Comparison of FGR 13 and ICRP *Publication 103* Informed Risk Coefficients

Differences between FGR 13 risks and the preliminary data risks stem from several sources. Firstly, the dose rates differ between the two data sets due to the non-negligible change in biokinetics used to calculate the dose rates, as cautioned by Dr. Derek Jockisch.[30] This difference is substantially more drastic in some radionuclides as compared to others, as seen in the comparison of the absorbed dose rates from acute and chronic exposures, in the previous section. The specific biokinetics used to inform this data have not yet been published, so from henceforth, conclusions drawn about the changes in biokinetic behavior are purely speculation based upon the data made available for this study. Other factors such as updates to phantom models, also currently unpublished, and decay data play parts in the variation of the dose rates between generations of

data as well. The LAR values used to inform risk calculations have changed between generational data sets, as have the survival function and usage function data sets.

Outlined in Table 16Table 16. Incidence and mortality risk coefficients for preliminary ICRP *Publication 103* informed data as compared to the calculated FGR 13 mortality and risk coefficients. below is a comparison of the risk coefficients calculated for the preliminary dataset as compared to the FGR 13 risk coefficients.

Table 16. Incidence and mortality risk coefficients for preliminary ICRP *Publication 103* informed data as compared to the calculated FGR 13 mortality and risk coefficients.

Radionuclide	Calculated Preliminary Incidence	FGR 13 Incidence	% Difference	Calculated Preliminary Mortality	FGR 13 Mortality	% Difference
I131pf	$2.86x10^{-09}$	$1.75x10^{-09}$	63.69	$1.63x10^{-10}$	$1.85x10^{-10}$	-11.72
I131pm	$2.40x10^{-10}$	$2.2x10^{-10}$	8.89	$8.93x10^{-11}$	$1.29x10^{-10}$	-30.75
I131ps	$1.30x10^{-10}$	$1.69x10^{-10}$	-23.32	$9.77x10^{-11}$	$1.4x10^{-10}$	-30.18
I131pg Food	$2.86x10^{-09}$	$1.75x10^{-09}$	63.69	$1.63x10^{-10}$	$1.85x10^{-10}$	-11.72
I131pg Water	$1.87x10^{-09}$	$1.23x10^{-09}$	52.26	$1.09x10^{-10}$	$1.31x10^{-10}$	-16.63
H3pf	$1.05x10^{-12}$	$5.28x10^{-13}$	99.52	$5.51x10^{-13}$	$3.61x10^{-13}$	52.76
H3pm	$9.70x10^{-12}$	$5.38x10^{-12}$	80.37	$8.15x10^{-12}$	$4.58x10^{-12}$	78.03
H3ps	$4.38x10^{-11}$	$2.3x10^{-11}$	90.25	$3.75x10^{-11}$	$2.12x10^{-11}$	76.70
H3pg Water	$2.14x10^{-12}$	$1.37x10^{-12}$	56.46	$1.15x10^{-12}$	$9.44x10^{-13}$	21.52
Cs137pf	$6.05x10^{-10}$	$3.21x10^{-10}$	88.48	$3.42x10^{-10}$	$2.19x10^{-10}$	56.36
Cs137pm	$1.29x10^{-09}$	$8.91x10^{-10}$	44.26	$1.00x10^{-09}$	$7.81x10^{-10}$	28.33
Cs137ps	$1.07x10^{-08}$	$3.03x10^{-09}$	254.78	$8.93x10^{-09}$	$2.77x10^{-09}$	222.51
Cs137pg Food	$6.48x10^{-10}$	$1.01x10^{-09}$	-35.87	$3.57x10^{-10}$	$6.88x10^{-10}$	-48.09
Cs137pg Water	$5.57x10^{-10}$	$8.22x10^{-10}$	-32.21	$3.22x10^{-10}$	$5.66x10^{-10}$	-43.11
Sr90pf	$2.13x10^{-09}$	$1.17x10^{-09}$	81.85	$1.44x10^{-09}$	$1.08x10^{-09}$	33.31
Sr90pm	$4.86x10^{-09}$	$2.84x10^{-09}$	71.01	$4.00x10^{-09}$	$2.65x10^{-09}$	51.03
Sr90ps	$4.63x10^{-08}$	$1.15x10^{-08}$	302.33	$3.95x10^{-08}$	$1.08x10^{-08}$	266.02
Sr90pg Food	$2.91x10^{-09}$	$1.86x10^{-09}$	56.47	$1.85x10^{-09}$	$1.62x10^{-09}$	14.36
Sr90pg Water	$2.02x10^{-09}$	$1.51x10^{-09}$	33.76	$1.38x10^{-09}$	$1.34x10^{-09}$	3.12

The absolute value of the percent difference between the preliminary data calculated risk coefficients and the FGR 13 published risk coefficients, while still following the FGR 13 risk calculation methodology, paired with the visible changes in the absorbed dose rates from a chronic exposure, potentially depicts effect of the changed biokinetic between data generations on the final risk coefficient. The largest differences are seen in slow-clearing cesium and strontium, and this is reflected in the absorbed dose rates from a chronic exposure. With buildup in the tissues being far more substantial in the preliminary data as compared to the FGR 13 data, a far larger difference between the preliminary data risk coefficients and FGR 13 risk coefficients is justifiable.

The overall smallest difference between the FGR 13 and preliminary data risk coefficients occurs with ^{131}I, potentially indicating that the biokinetics changed the least for this radionuclide between data generations. The following section will outline the comparison of the acute, tissue-specific risks and detriment-weighted doses, as well as the risks and CED between data generation, helping to explain the change in the biokinetics that are reflected in Table 16.

4.8. Preliminary Data Risk and CED Analysis

CED calculated for the preliminary data differ from those of FGR 13 as well. The tissue weights have been updated between generations of data, with FGR 13 data utilizing ICRP *Publication 60* tissue weights and the preliminary data utilizing ICRP *Publication 103* values. Between these two generations of the tissue weights, there has been an expansion of the tissues considered, as well as a shift in how the detriment to certain tissues is calculated. Whereas *Publication 60* considered an estimate based on cancer mortality weighted for non-fatal cancer, relative life lost for fatal cancers, and life impairment for non-fatal cancers, *Publication 103* bases calculations on cancer incidence weighted for mortality and life impairment. [6] It also brings into consideration the risk of heritable diseases in order to more appropriately base the assessment of

radiation detriment, greatly reducing the weight of heritable effects on detriment calculation, particularly for the gonads. [6] As with ICRP *Publication 60* weighting factors, the years of life lost are wrapped into the new factors as well. Beyond the change in values, the methods used to calculate the chronic and acute exposure committed effective doses remain the same for the preliminary data.

4.8.1. Acute Exposures

4.8.1.a. ^{131}I

Iodine biokinetics for the preliminary data follow the same trend as in the DCAL FGR 13 generated data. However, the potential shift in biokinetics for the preliminary data results in a noticeable change in the calculated risks from acute exposures and the detriment-weighted committed equivalent doses from an acute exposure. Comparing the trends of the preliminary data in Figure 73 to the FGR 13 data in Figure 39, while the risks and detriment-weighted committed equivalent doses are on the same order of magnitude for the thyroid, the calculated risks have increased for both incidence and mortality while the detriment-weighted committed equivalent doses for incidence have slightly decreased and for mortality have slightly increased. The rate of decrease for the calculated risks has increased as well, the risks falling off more steeply up to age 10 rather than age 20 as seen in the FGR 13 data.

The potential effect of the change inhalation kinetics is noticeable as well, with both the calculated risks and the detriment-weighted committed equivalent doses decreasing by approximately an order of magnitude between generations when comparing Figure 73 to the FGR 13 DCAL informed data.

For the preliminary data, mortality risk to the thyroid is overestimated by the detriment-weighted committed equivalent dose, while incidence risk is underestimated until approximately year 20, a similarly observed trend in the FGR 13 data. For the skin, however, both mortality and incidence risk are consistently underestimated. Corresponding male data for detriment-weighted tissue-specific committed equivalent dose plots as well as plots for slow clearing iodine can be found in Appendix F.

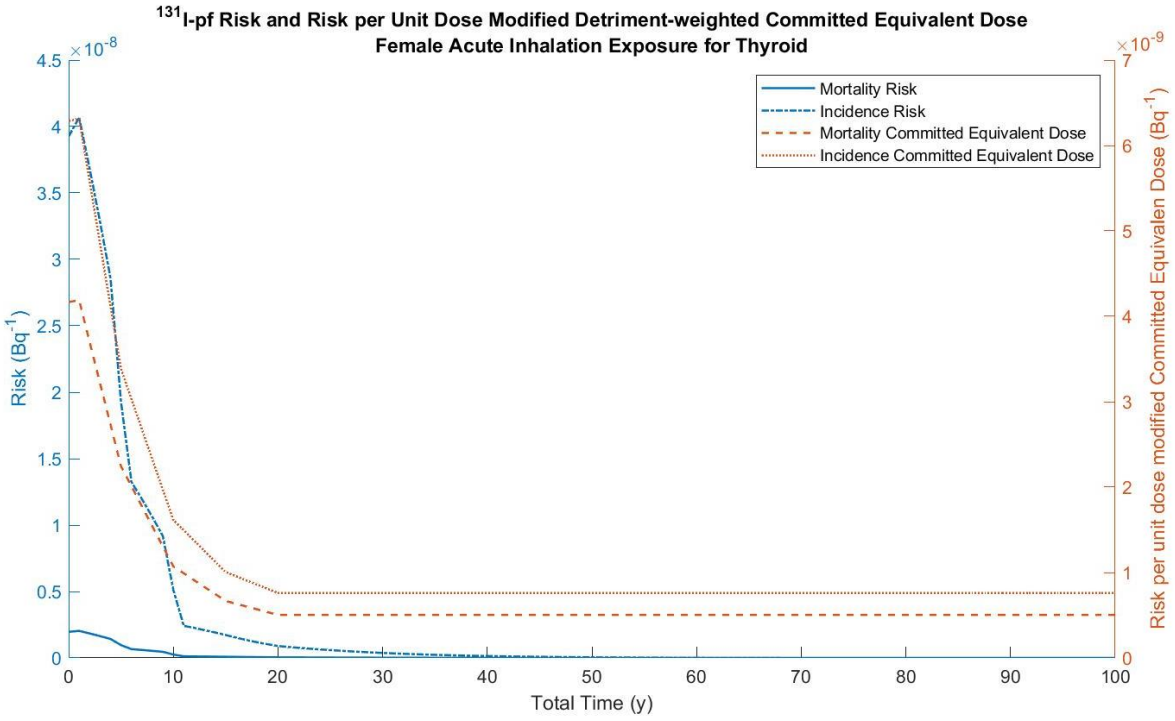

(a)

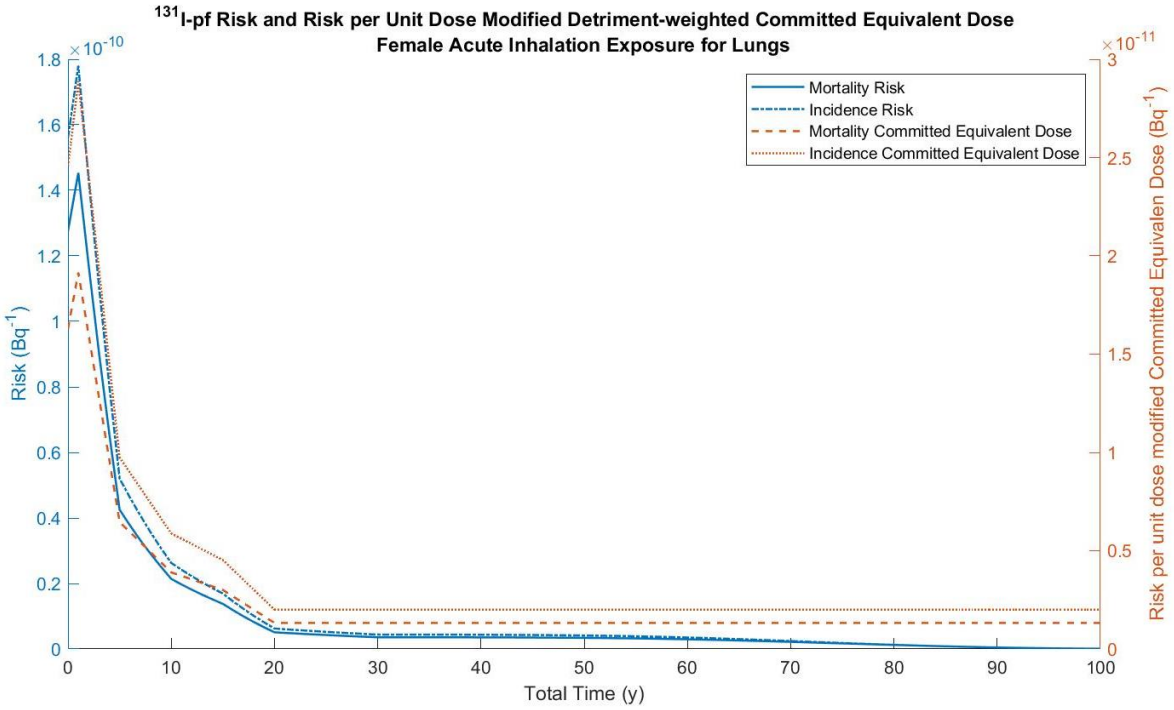

(b)

Figure 73. Comparison of the risk calculations for the preliminary data to the ICRP *Publication 103* detriment-weighted committed equivalent doses for the (a) female thyroid and (b) female lungs for fast-clearing ^{131}I.

Ingested iodine behaves in a similar manner to fast-clearing iodine for the preliminary data as it did for the FGR 13 data. As with inhaled iodine, female mortality risk to the thyroid is overestimated by a large margin, only slightly less than an order of magnitude to begin with, while incidence risk is underestimated up until year ten, approximately. However, for male risks, the representation of the detriment-weighted committed equivalent dose is significantly closer to the true risk to the tissue for incidence, seen in Figure 74, while mortality is still vastly overestimated.

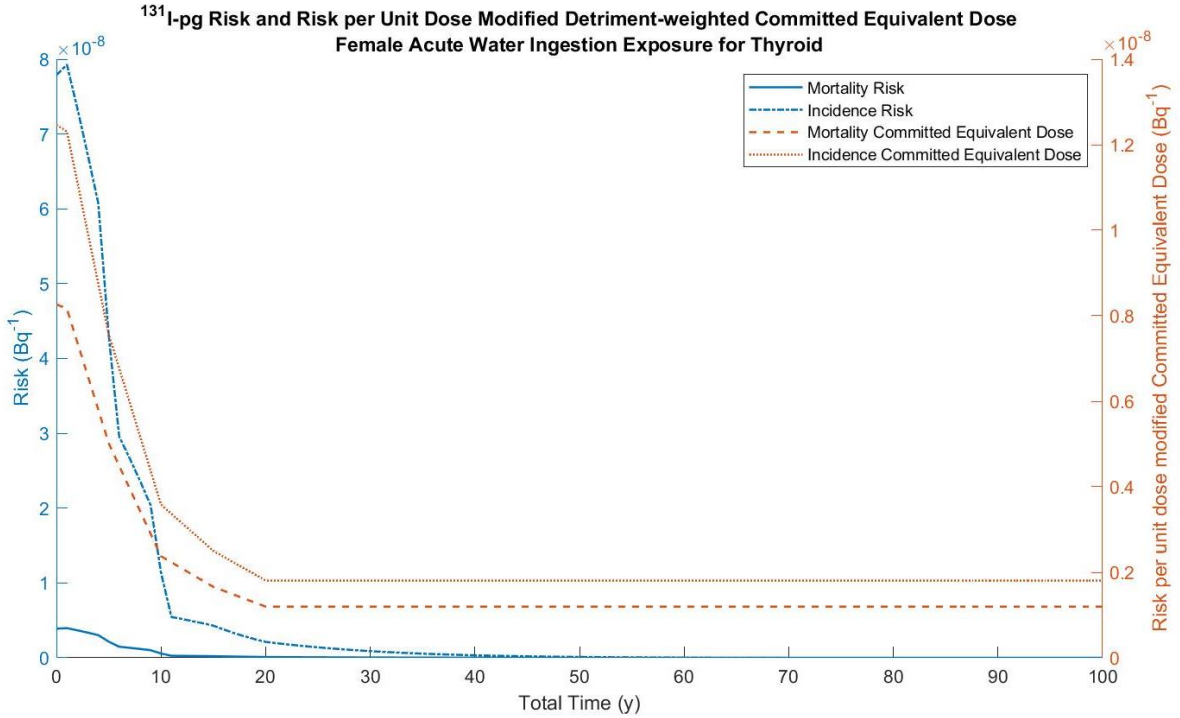

(a)

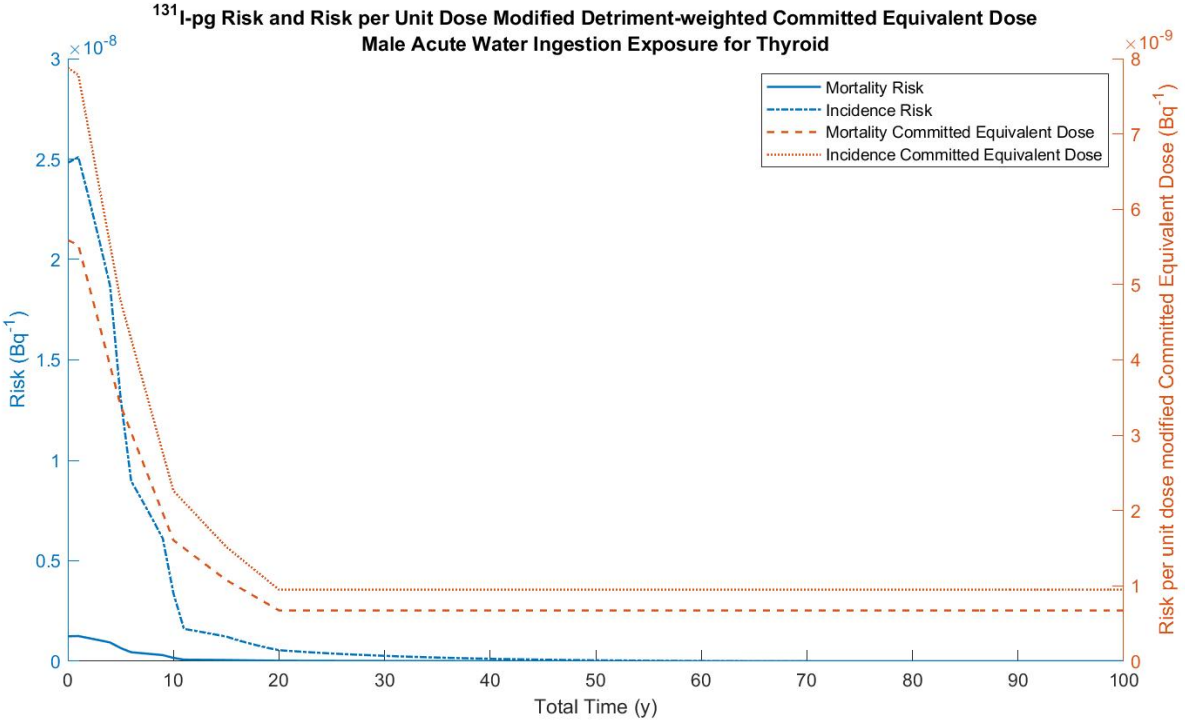

(b)

Figure 74. Risk and detriment-weighted committed equivalent dose to the (a) female thyroid and the (b) male thyroid from tap water ingestion of ^{131}I.

For a uniform, whole-body exposure via inhalation of ^{131}I, the behavior is similar to the behavior in the thyroid, specifically. Mortality modified CED only slightly overestimates the mortality risk from an acute exposure at all ages of life, while the incidence modified CED underestimates by a whole order of magnitude for females. This gap in the incidence comparison seen in Figure 75

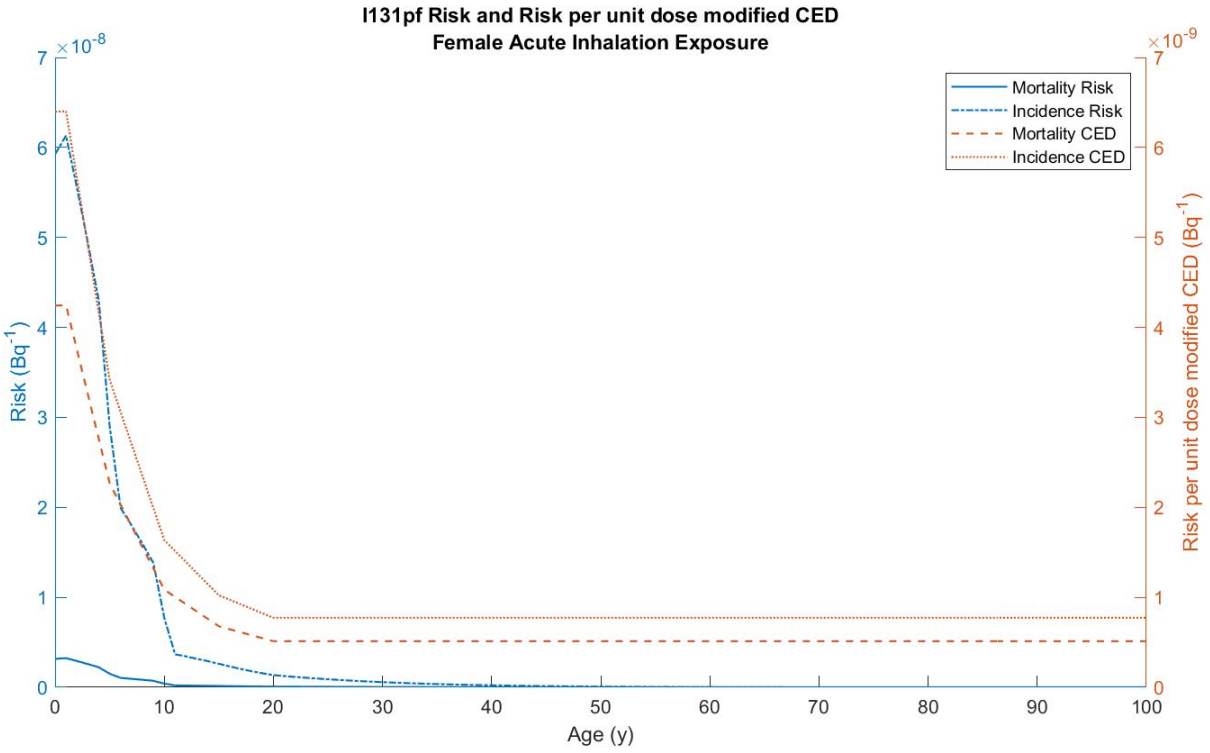

Figure 75 is significantly wider for the preliminary data than for the FGR 13 data, seen in Figure 41. Corresponding male values can be found in Appendix G.

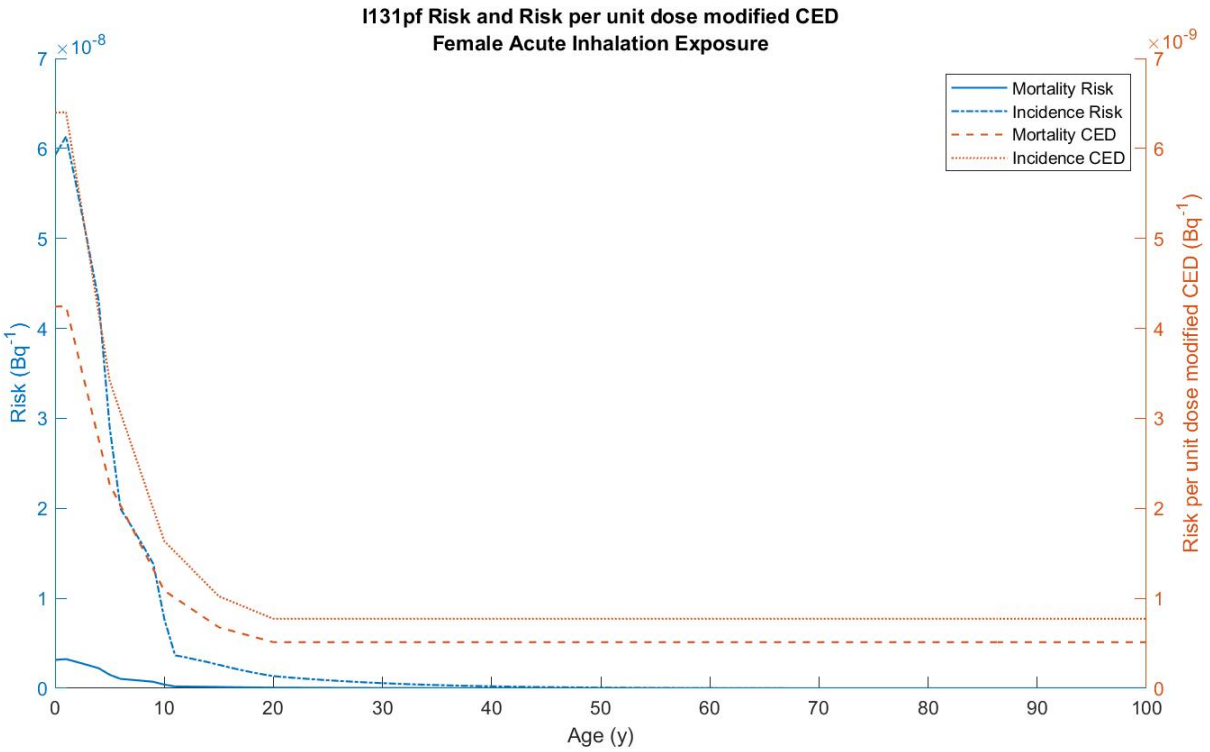

Figure 75. Uniform exposure risk and CED to females from fast-clearing ^{131}I.

A uniform, whole-body exposure to ingested ^{131}I shows a similar pattern as fast-clearing iodine, with the mortality risk being overestimated and the incidence risk being underestimated by nearly an order of magnitude. As well, comparing the risk to that of the FGR 13 data, risks are higher to start for both mortality and incidence before dropping back down to a level comparable to the FGR 13 data, a trend seen in Figure 76. Corresponding values for males can be found in Appendix G.

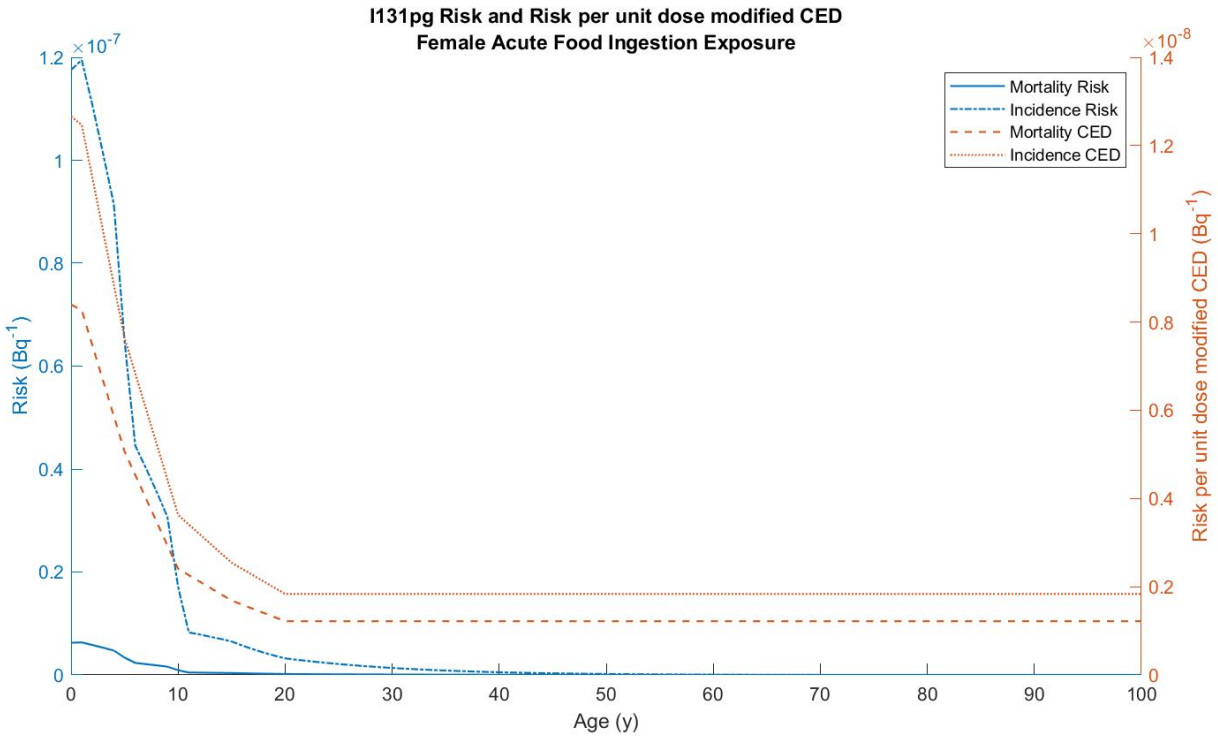

Figure 76. Uniform exposure risk and CED for females from acute food ingestion of ^{131}I.

For fast-clearing inhaled iodine, it is relevant to compare the FGR 13 data to the preliminary data for the whole body. A comparison of the risks with respect to age between the two generations shows a substantial increase in the incidence risk when moving from the FGR 13 to the preliminary data. The increase between the FGR 13 and preliminary data in reference to incidence is significantly higher than the increase in the mortality risk between the generations. A similar trend is seen in the data for males as well, the incidence risk increasing by a far greater degree between generations of data than the morality risk, seen in Figure 77.

The above stated trend does not hold true for slow-clearing iodine. For the slow-clearing solubility class, the preliminary data risks for both mortality and incidence are both lower than the FGR 13 informed data by nearly and order of magnitude for mortality, and half and order of magnitude for incidence. However, this difference between the data generations is significantly

less pronounced than for fast-clearing iodine. Corresponding male values can be found in Appendix H.

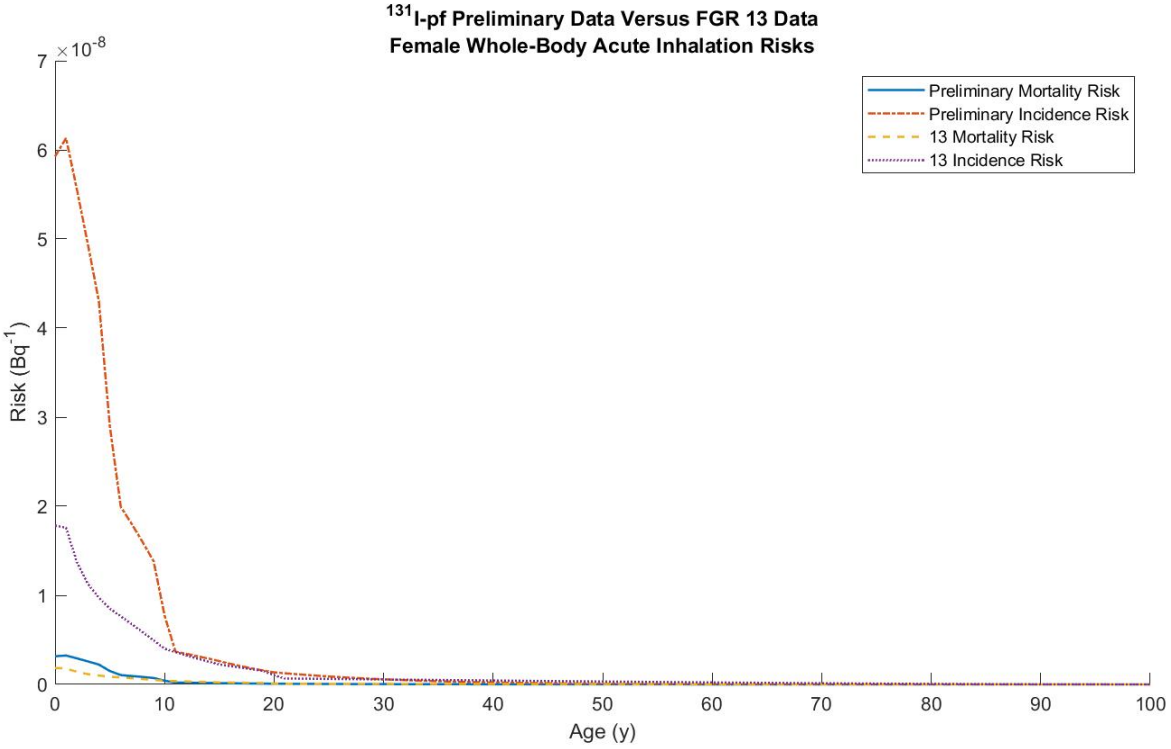

(a)

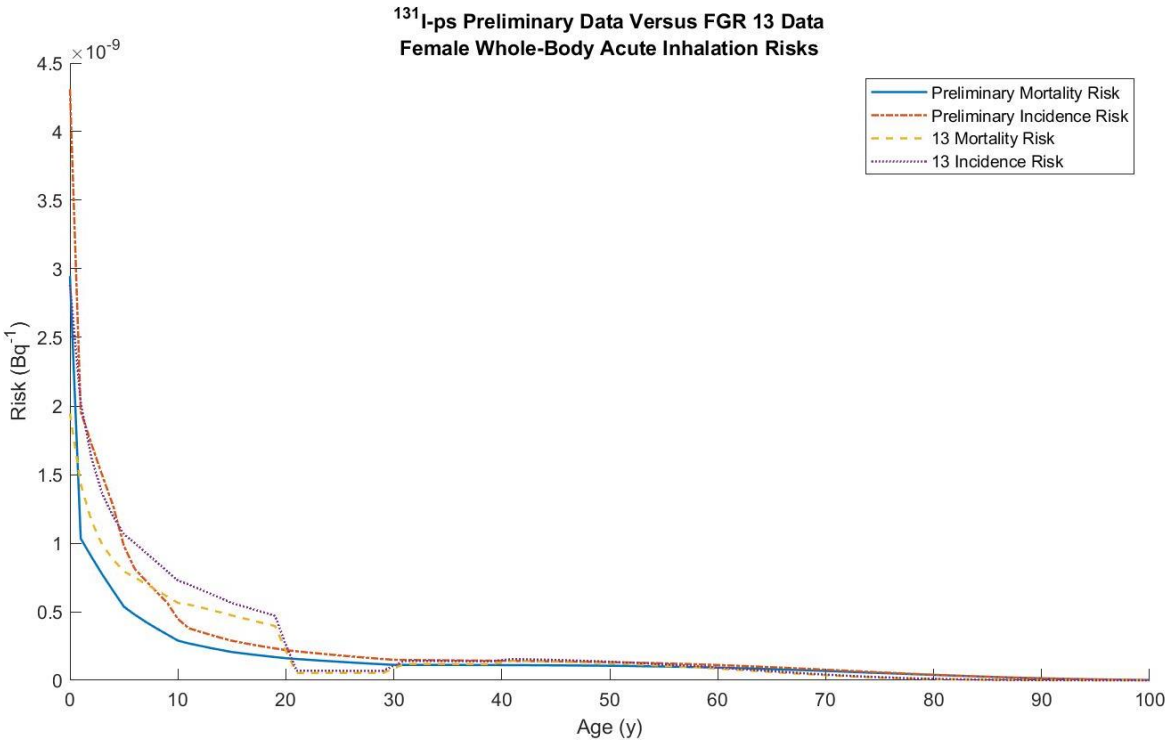

(b)

Figure 77. Comparison of the preliminary and FGR 13 data for acute risks from (a) fast-clearing and (b) slow-clearing ^{131}I in females.

For the CEDs for each generation, the opposite effect was seen as compared to the acute risks. For the CEDs, the preliminary data values decreased in comparison to the FGR 13 values for both incidence and mortality for both males and females. As well, the difference between the preliminary data and the FGR 13 data for the CEDs is significantly smaller in reference to incidence, specifically. This trend holds up between all solubility class; FGR 13 data yields slightly higher CEDs than the preliminary data. However, with decreasing rate of clearance from the lungs, the gap between the FGR 13 data and the preliminary data widens, seen in Figure 78. Male values can be found in Appendix I.

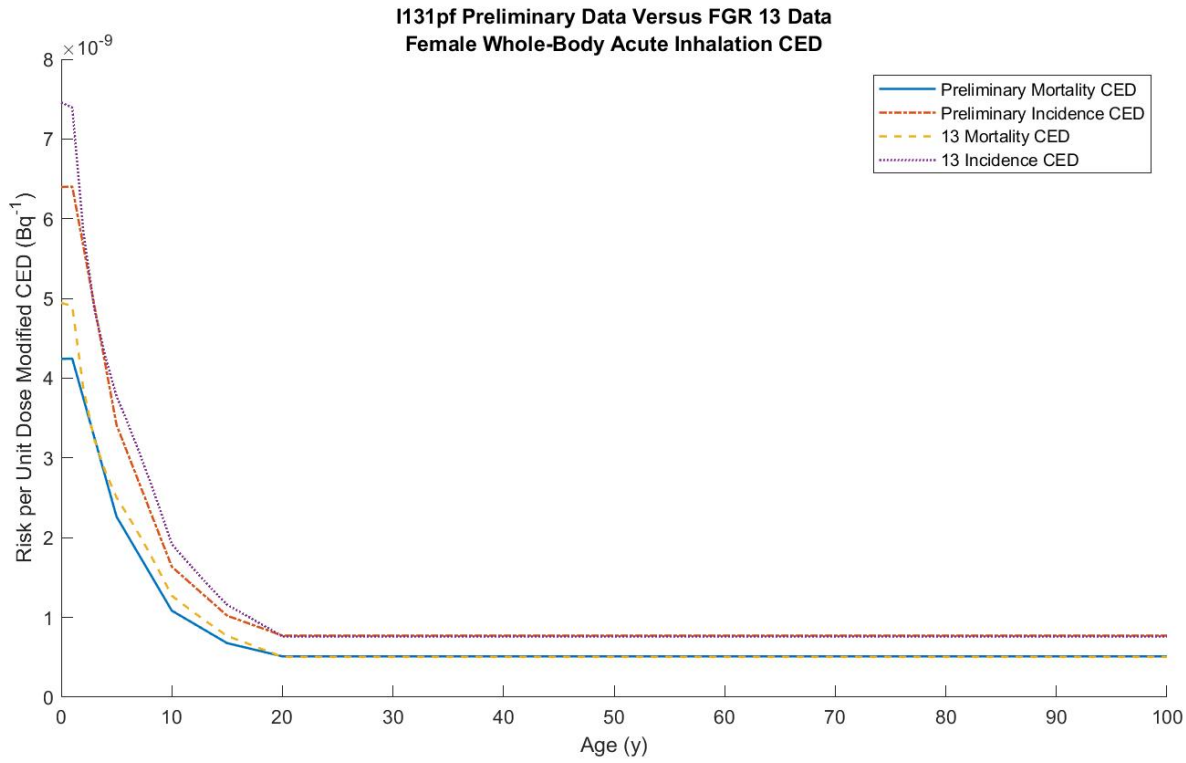

(a)

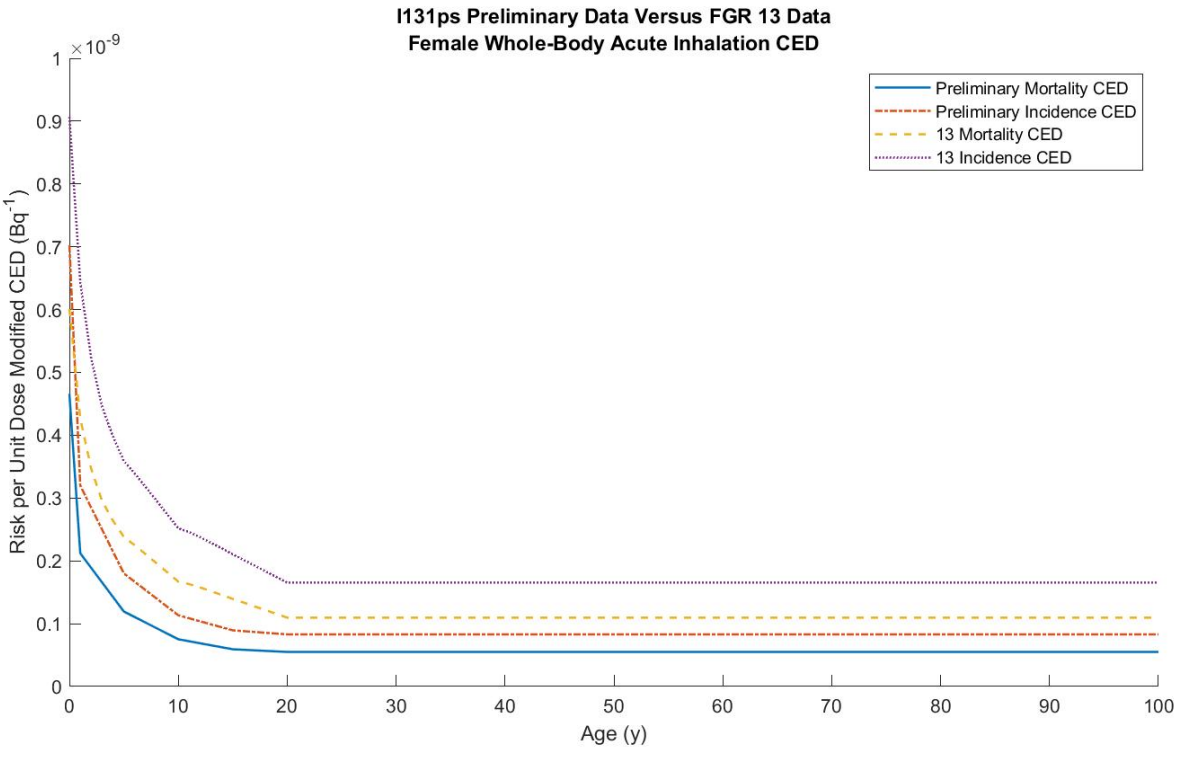

(b)

Figure 78. Comparison of the preliminary and FGR 13 data for risk modified CED from (a) fast-clearing and (b) slow-clearing ^{131}I.

Ingested iodine follows closely with fast-clearing inhaled iodine when comparing between data generations. The preliminary data risk for incidence is substantially higher than the FGR 13 calculated incidence risk while the preliminary data mortality risk, while being slightly higher, tracks fairly closely. For the CEDs, a similar trend is followed as well when compared to fast-clearing iodine. The preliminary data actually yields lower CEDs than the FGR 13 data. These trends for risk and CED can be found for both males and females in Appendix H and I, respectively.

4.8.1.b. Tritium

As a whole-body emitter, the preliminary data also showed no one tissue where the radionuclide concentrated, as anticipated. For all solubility classes and usage types, as well as for most tissues, the detriment-weighted committed equivalent doses either tracked very closely to or slightly underestimated the tissue-specific risk from an acute exposure. The main outlier for this generic rule is for the skin, which in both males and females showed an overestimation for both the mortality and the incidence risks, as seen in Figure 79. With a decreasing rate of clearance from the lungs, this overestimation on the part of the detriment-weighted committed equivalent dose to the skin increases. Corresponding male values for the detriment-weighted committed equivalent doses can be found in Appendix F.

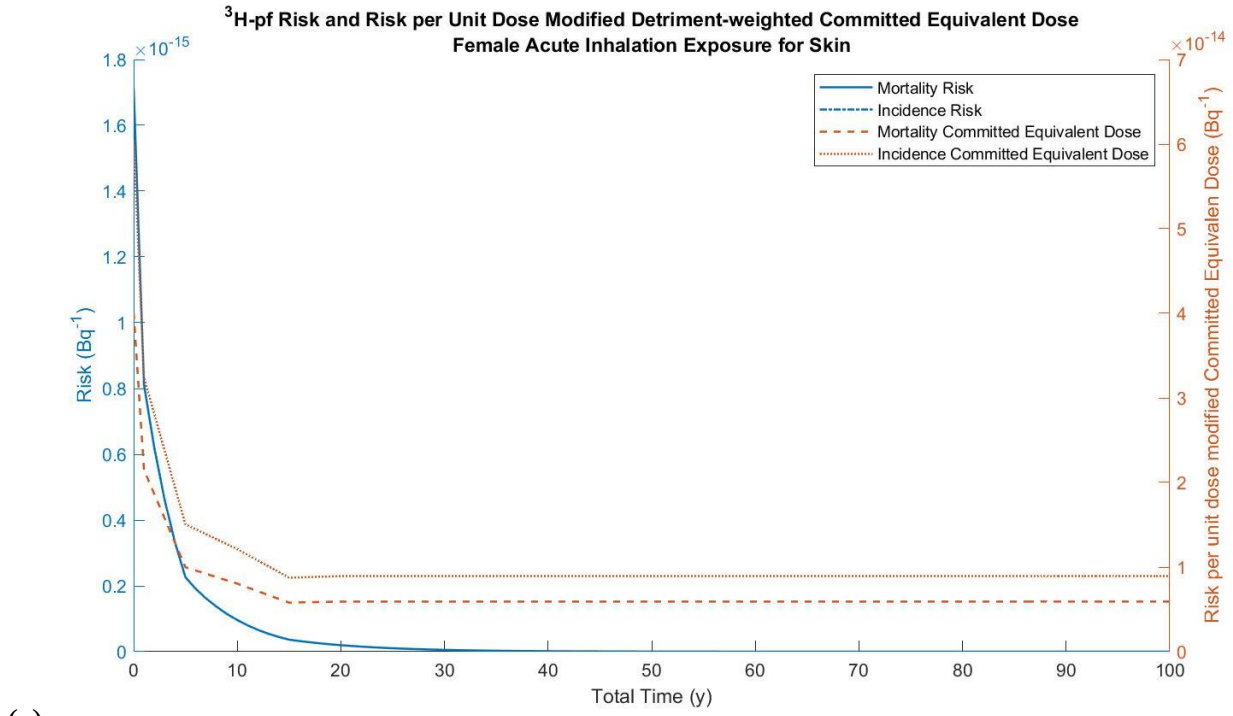

(a)

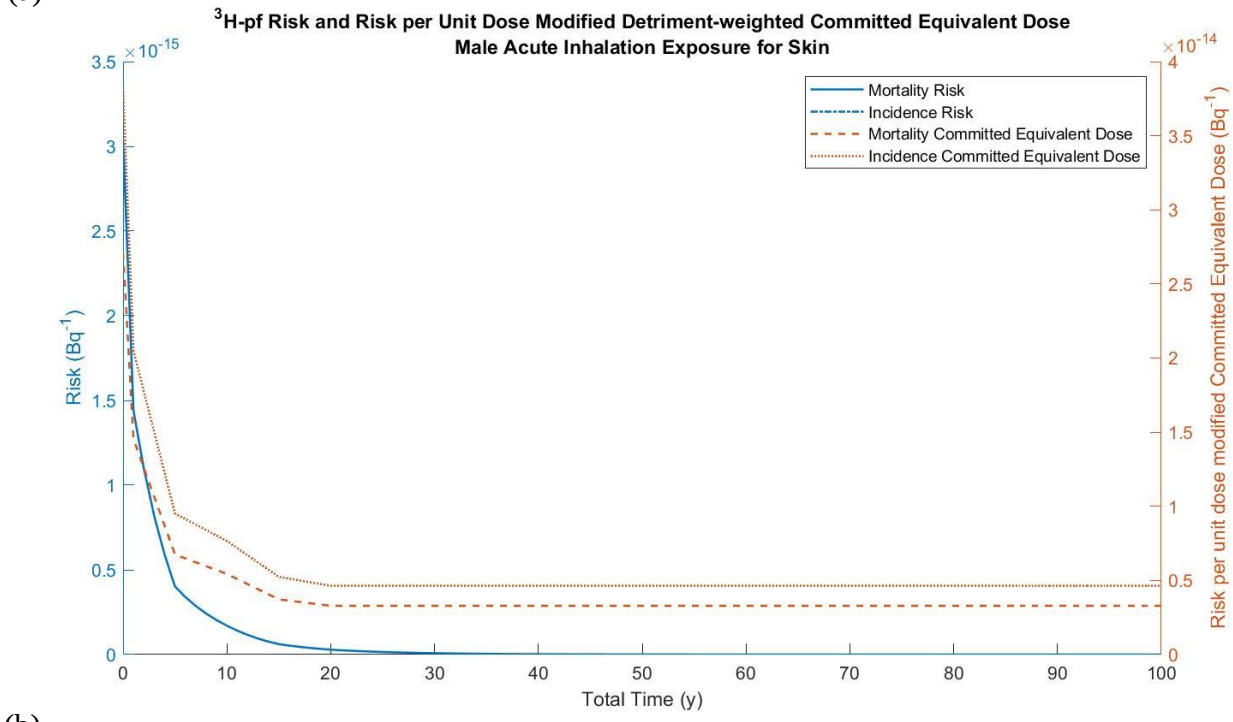

(b)

Figure 79. Risk and detriment-weighted committed equivalent doses to the (a) female and (b) male skin due to fast-clearing tritium.

Looking more closely at the lungs for the inhaled solubility classes, seen in Figure 80, for both males and females within all solubility classes, the detriment-weighted committed equivalent doses consistently underestimated the tissue-specific risk to the lungs by a significant margin, typically within an order of magnitude. As well, when compared to plots for the FGR 13 data, the risks overall to the lungs for inhaled tritium are higher for the preliminary data than for the FGR 13 data. Corresponding male data can be found in Appendix F.

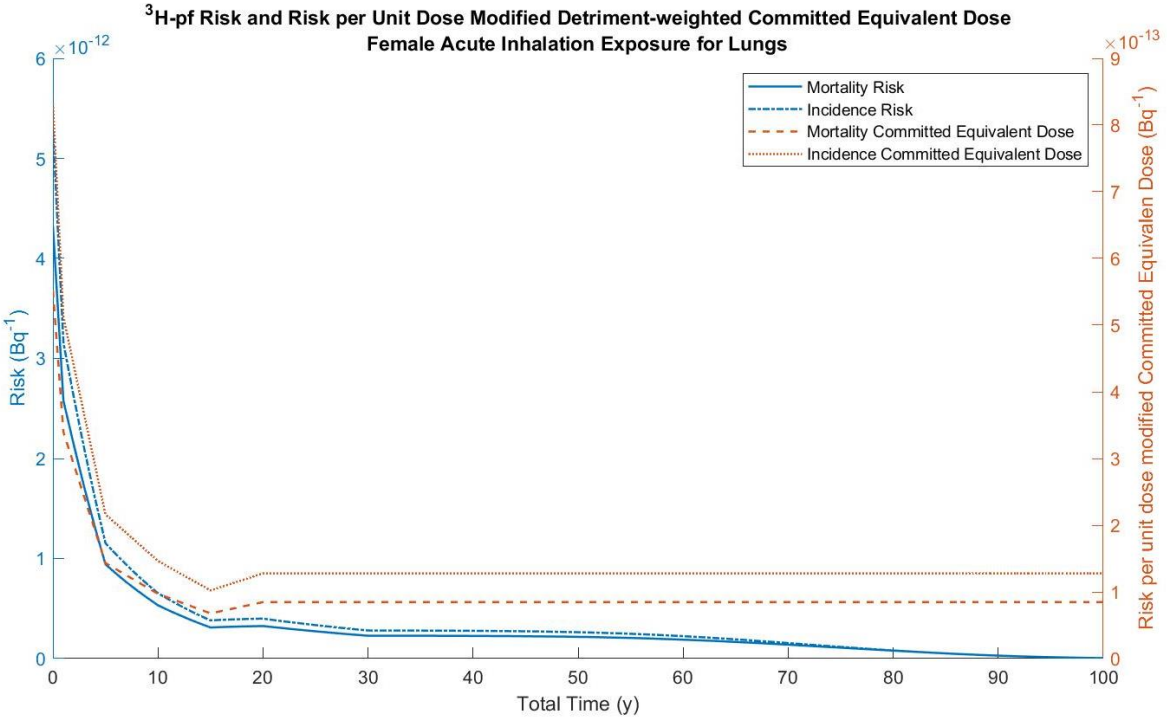

(a)

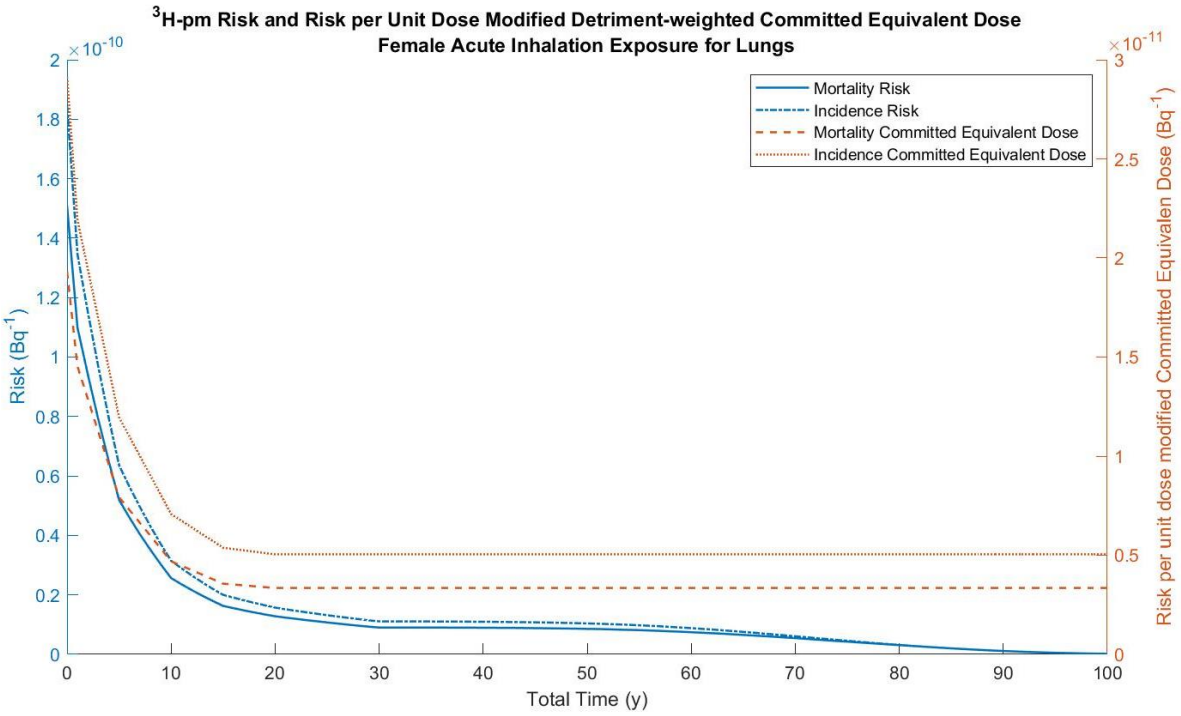

(b)

Figure 80. Risk and detriment-weighted committed equivalent doses to the female lungs for (a) fast and (b) moderate clearing tritium.

Ingested tritium shows a similar trend as inhaled tritium in regards to the skin. For both males and females, the detriment-weighted committed equivalent doses overestimate the tissue-specific risk by nearly the same margin as for inhaled tritium. However, for the colon, which is of particular interest for ingested tritium, the committed doses slightly underestimate the true risk to the tissue. For the colon, seen in Figure 81, it is important to note that the underestimation is slight, the values being on the same order of magnitude and within a close range within that order. Corresponding male values can be found in Appendix F.

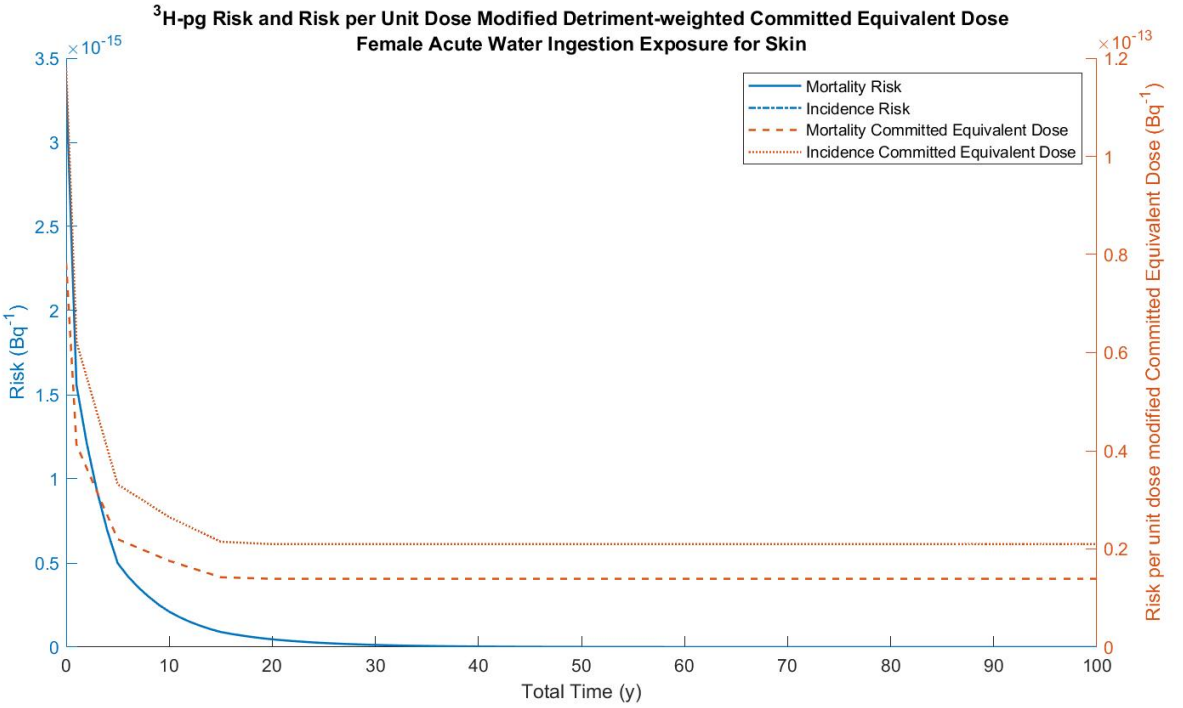

(a)

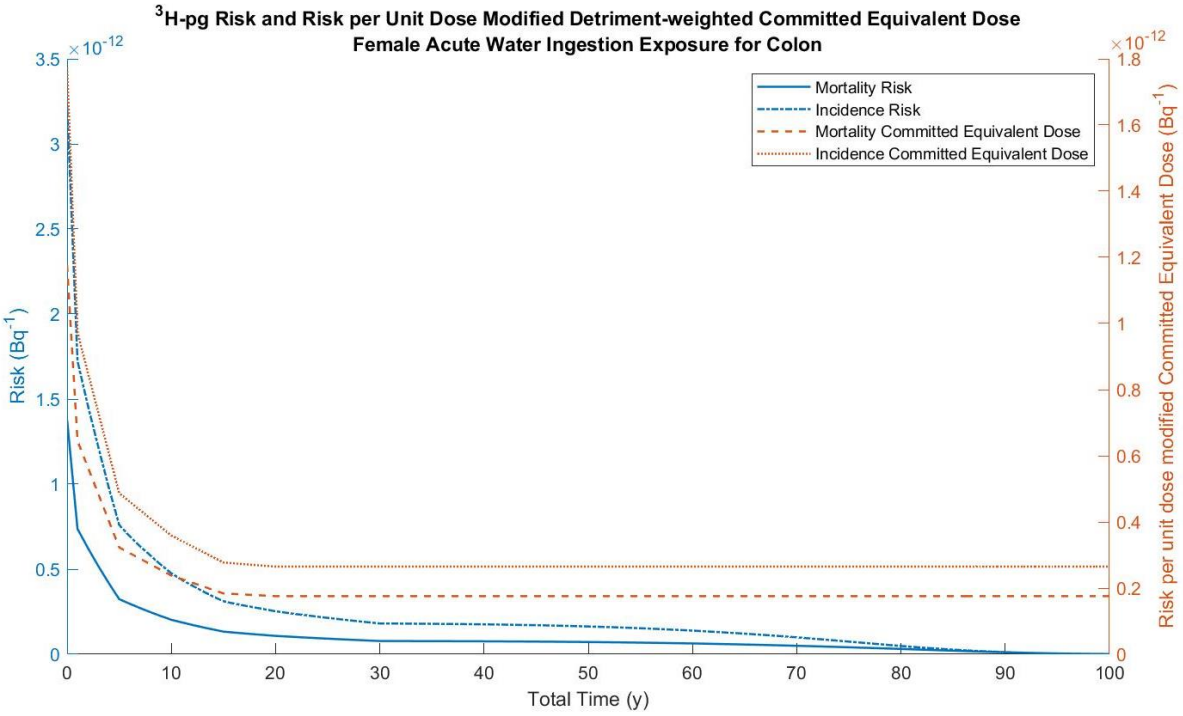

(b)

Figure 81. Risk and detriment-weighted committed equivalent dose to the female (a) skin and (b) colon due to ingestion of tritium in tap water.

For a uniform, whole-body exposure to fast-clearing tritium, based on the tissue-specific detriment-weighted committed equivalent dose values namely underestimating the true FGR

calculated risk, it was anticipated that the plots would follow the same trend. This held true for both males and females for fast-clearing tritium, the CEDs underestimating the risk with the gap in the estimation narrowing with increasing age; just over an order of magnitude at the beginning of life, and approximately 20% at end of life, seen in Figure 82.

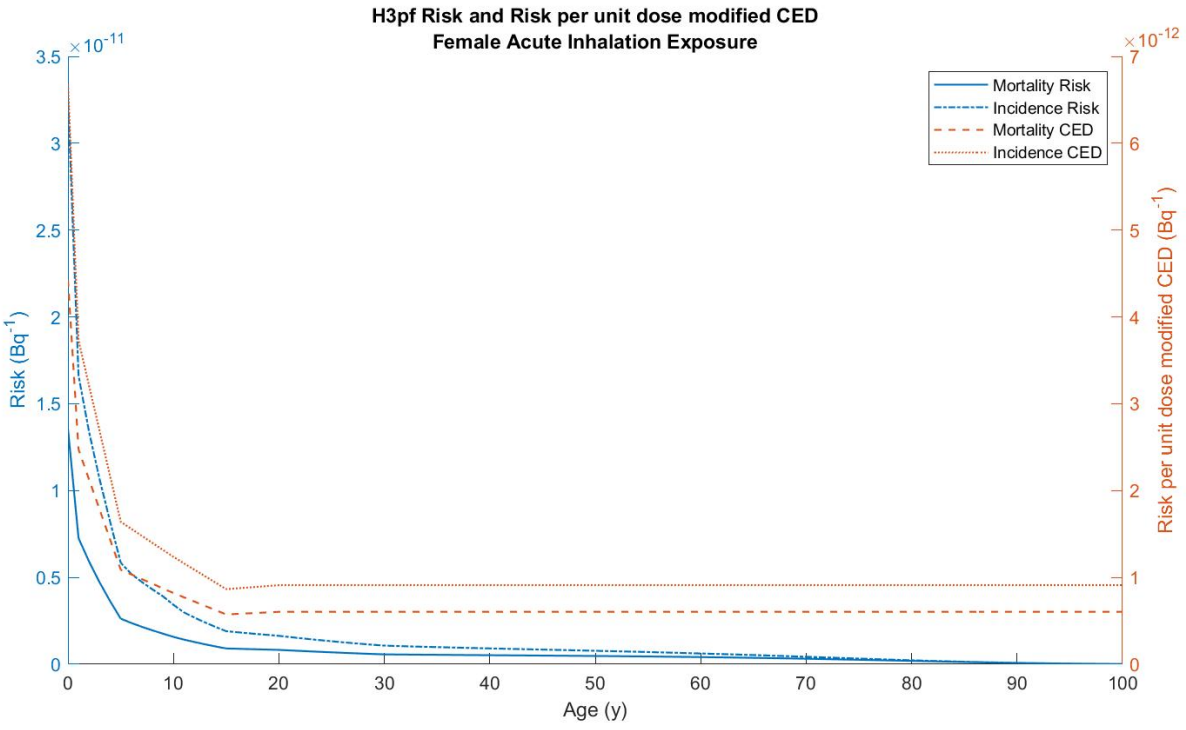

(a)

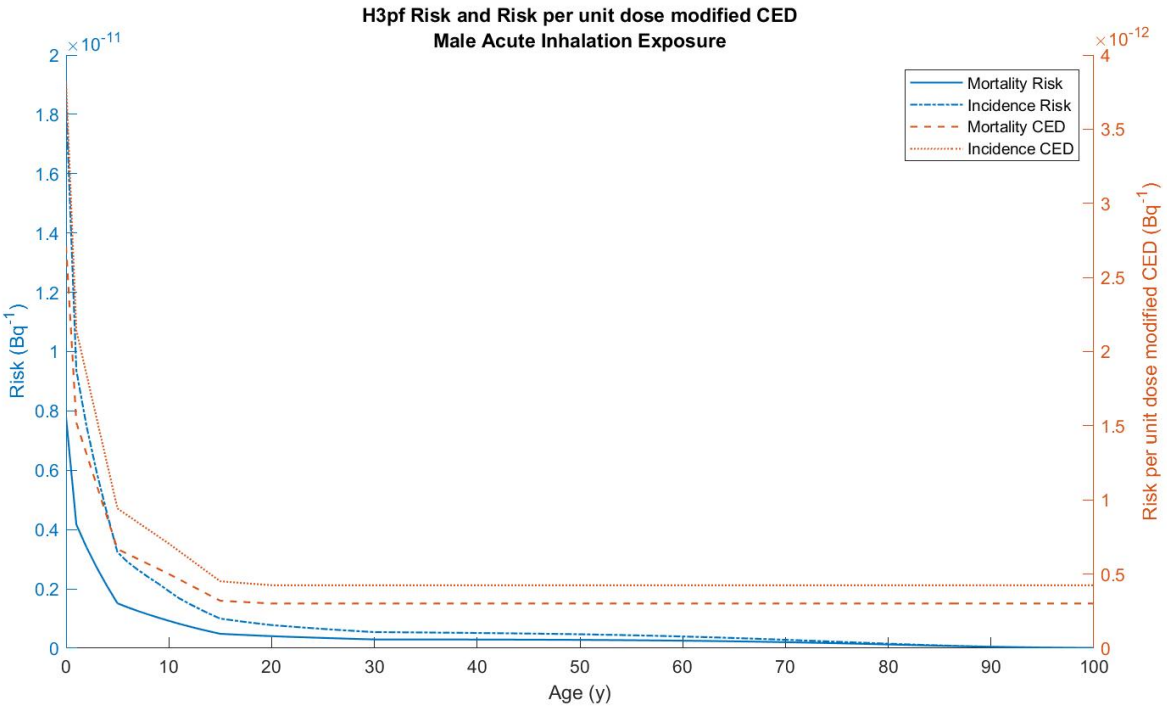

(b)

Figure 82. Risk and committed effective dose from fast-clearing tritium for (a) females and (b) males.

Tap water ingested tritium shows a similar trend of underestimation for both males and females, with the correspondence being closer for males than for females, and the gap between the risk and CED for both sexes narrowing with increasing age, as seen in Figure 83.

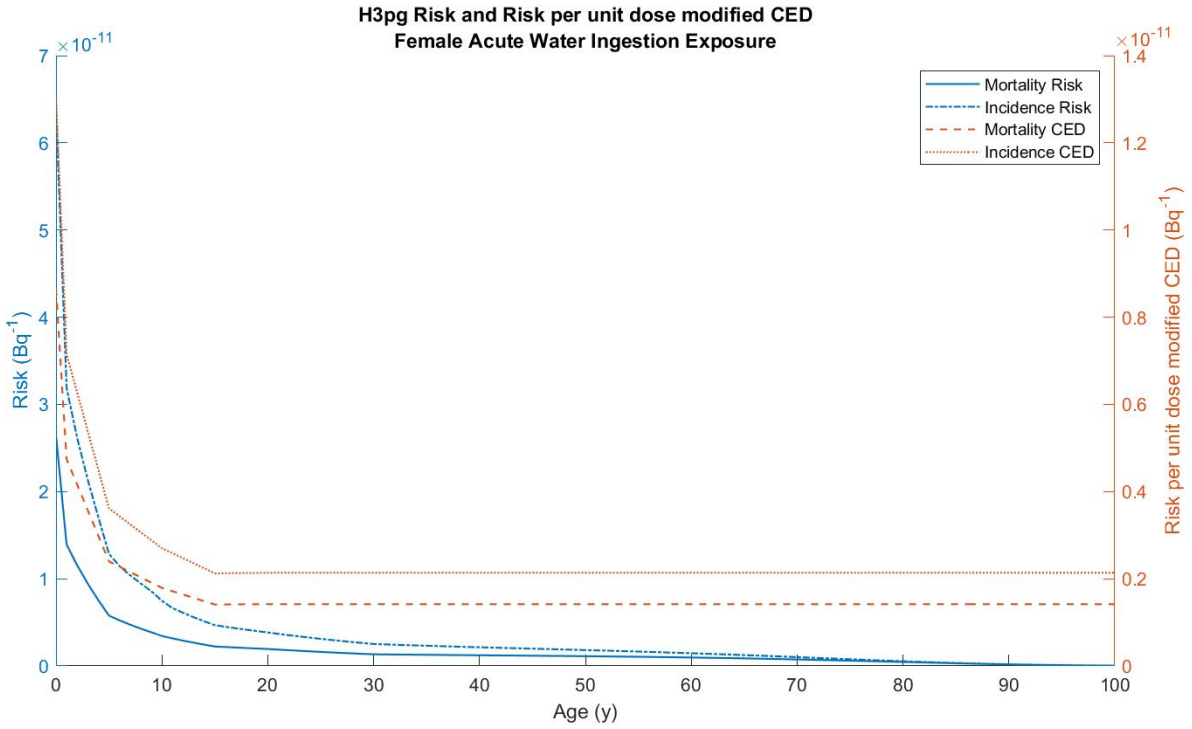

(a)

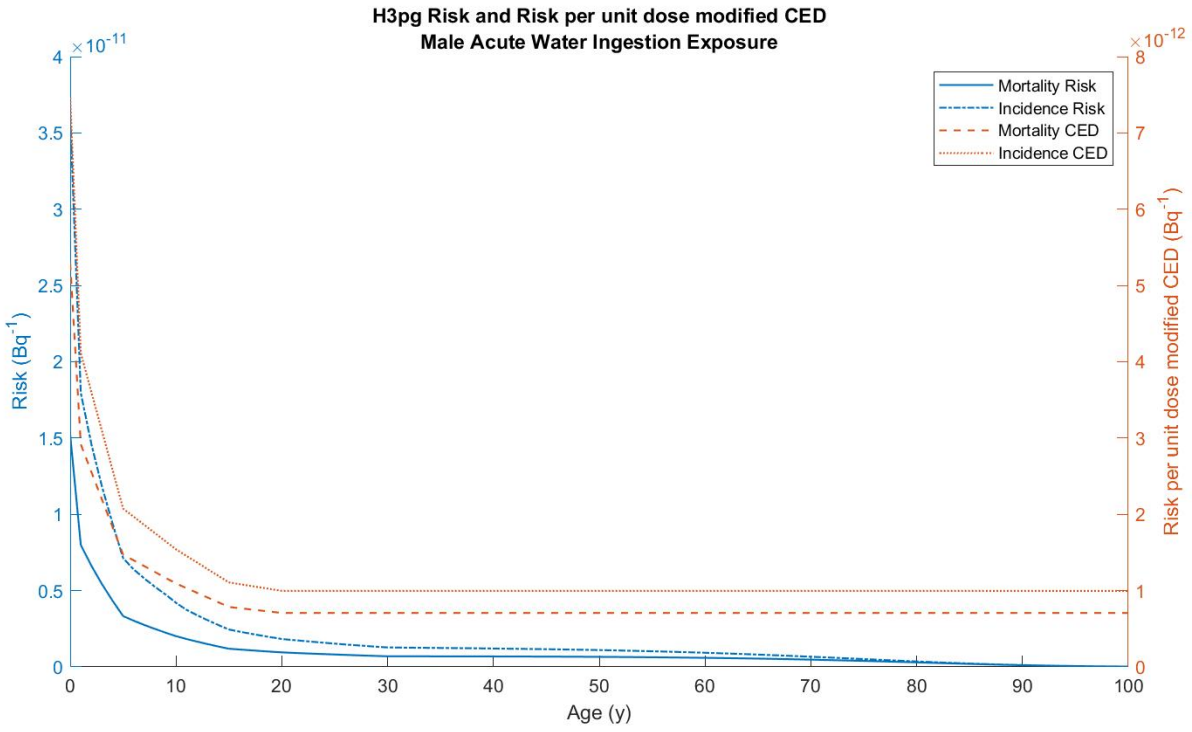

(b)

Figure 83. Risk and committed effective dose from tap water ingested tritium for (a) females and (b) males.

A comparison of the trends between data generations for the risks and CEDs for tritium shows reasonably close correspondence between the two generations for both sexes, as well as all solubility classes and usage types, typically within 80%. Fast-clearing inhaled tritium shows the larges difference between generation, specifically in reference to the incidence risk, however, that difference is still drastically smaller than what was seen for iodine. This close correspondence indicates a limited change in the biokinetics between the generations of data. These trends can be seen in Figure 84. Risks for males for fast-clearing tritium, as well as risks for ingested tritium can be found in Appendix H, while CED for males for fast-clearing tritium and the CEDs for ingested tritium can be found in Appendix I.

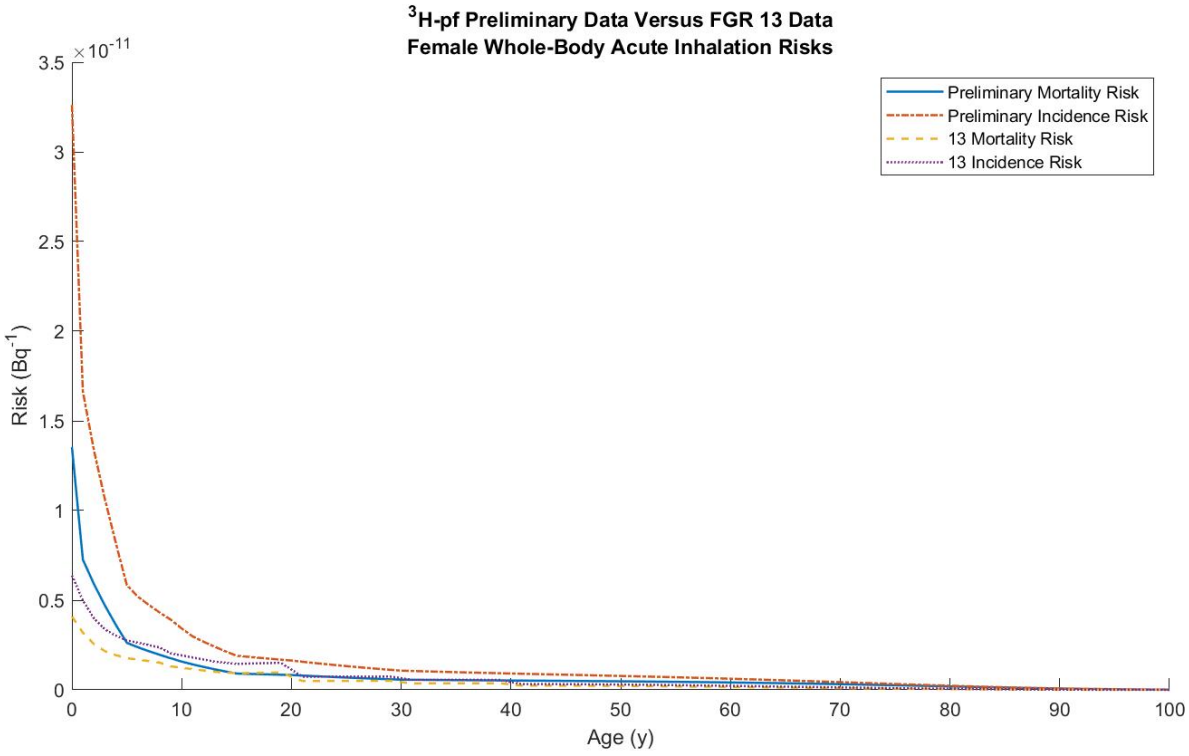

(a)

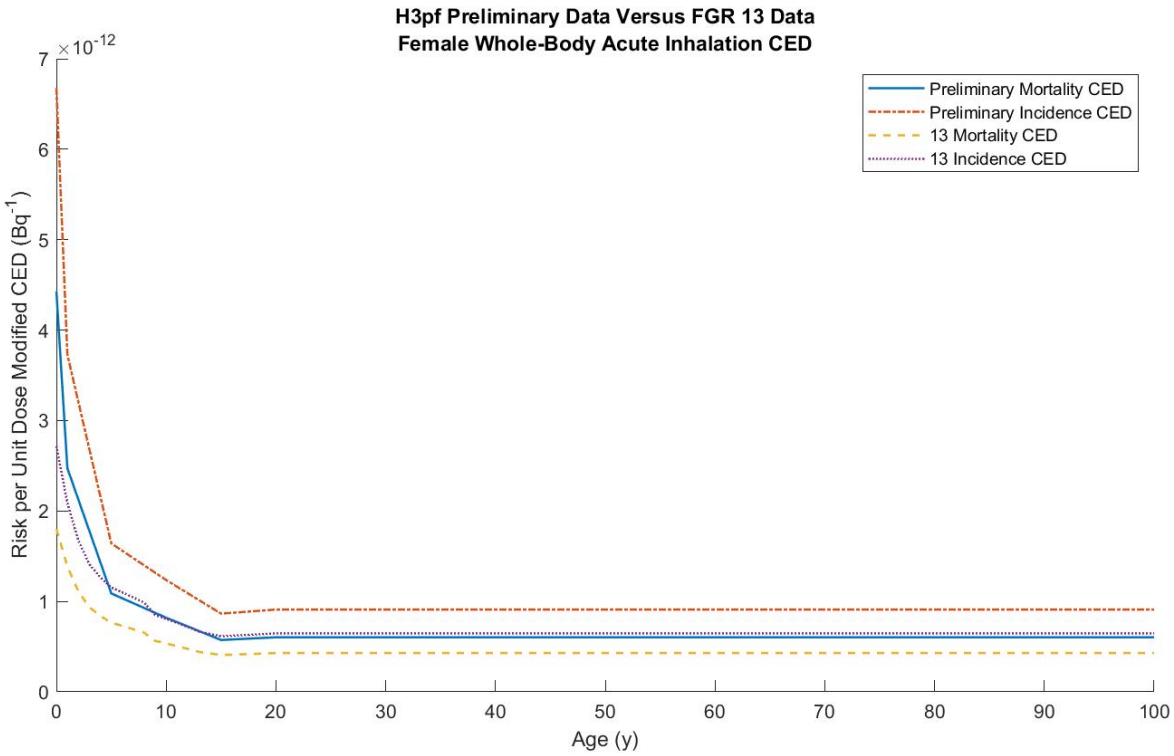

(b)

Figure 84. Preliminary and FGR 13 data comparison of (a) Risk and (b) CED for fast-clearing tritium in females.

4.8.1.c. ^{137}Cs

Akin to tritium, ^{137}Cs is a whole-body emitter. However, unlike tritium, cesium tends to mostly pass through the body, resulting in overall lower doses to the whole body. For what does not get immediately excreted from the body post exposure, typically distributes to the soft tissues, as previously stated. This behavior does not change between generations of data.

For inhaled cesium, including all solubility classes and both sexes, the preliminary exposure is to the lungs. For all cases, the detriment-weighted committed equivalent doses underestimate both the mortality and incidence risks by an order of magnitude at its largest difference, the gap narrowing with increasing age, which can be seen in Figure 85. Specifically, for slow-clearing cesium, a divergence from the expected plateau in the detriment-weighted committed equivalent doses is seen. This is due to the same fact that was outlined in previous

sections for uranium and strontium, a data limitation. With increasing age past age 60, fewer and fewer non-negligible datapoints are a part of the summation of the committed dose, leading to a drop off in the committed dose. Corresponding male values for the following plots for detriment-weighted committed equivalent doses can be found in Appendix F.

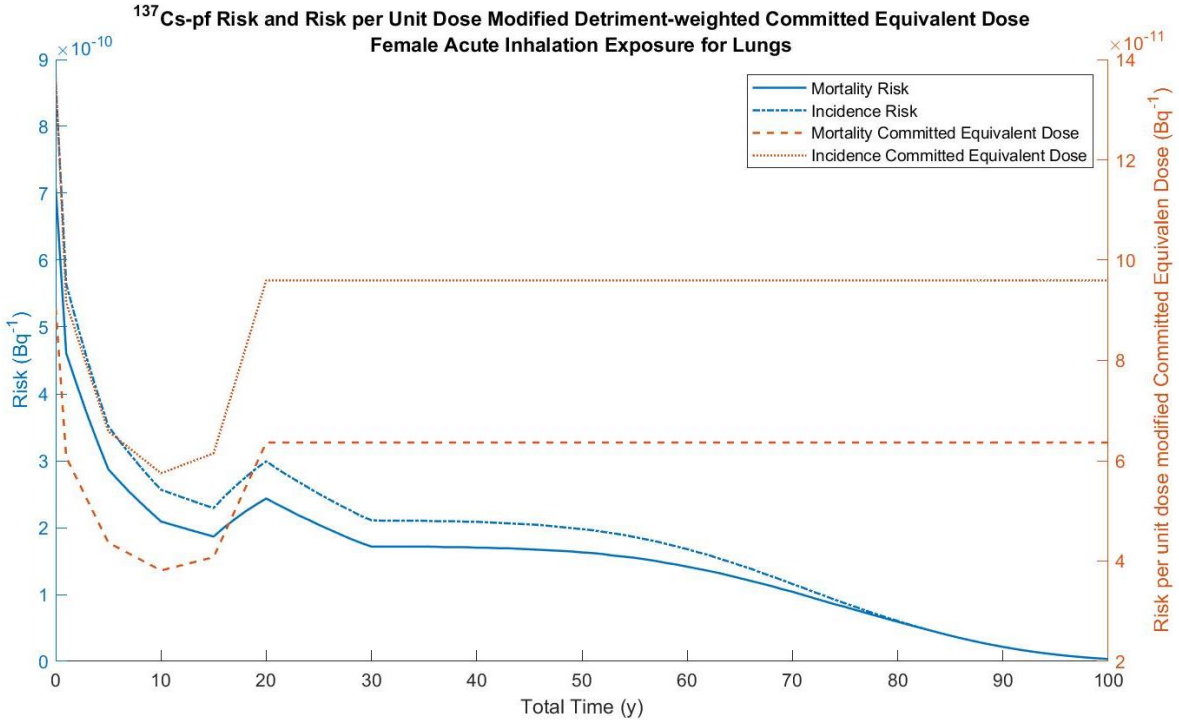

(a)

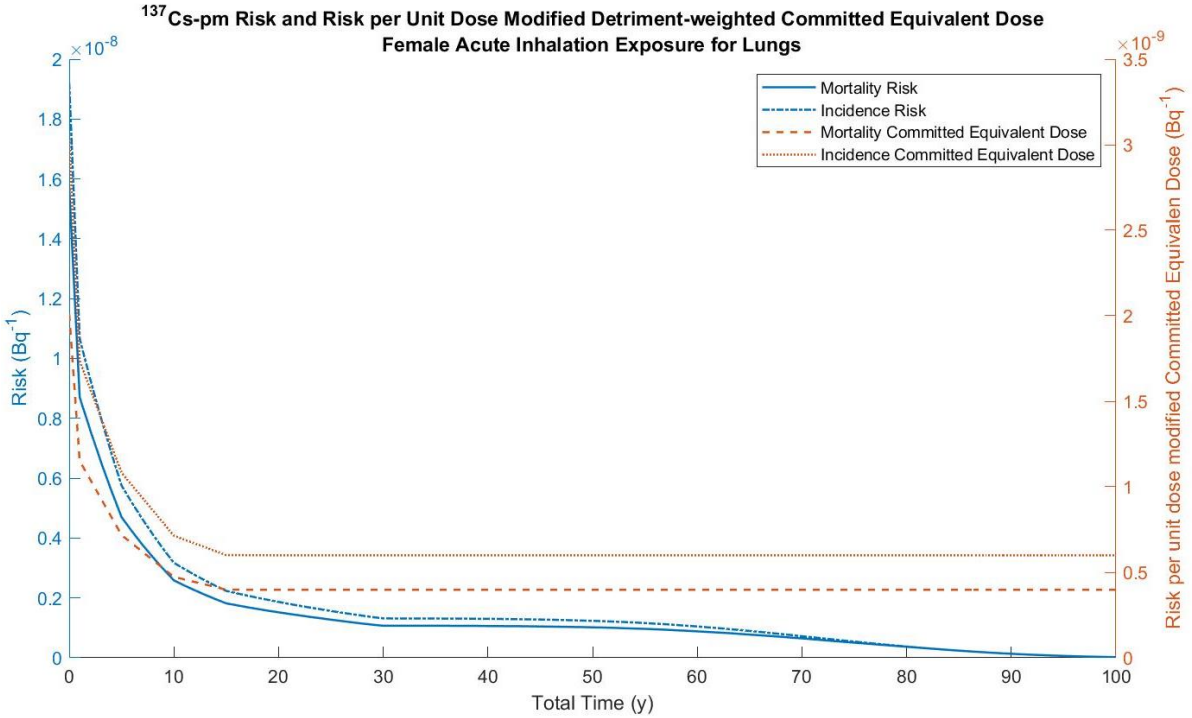

(b)

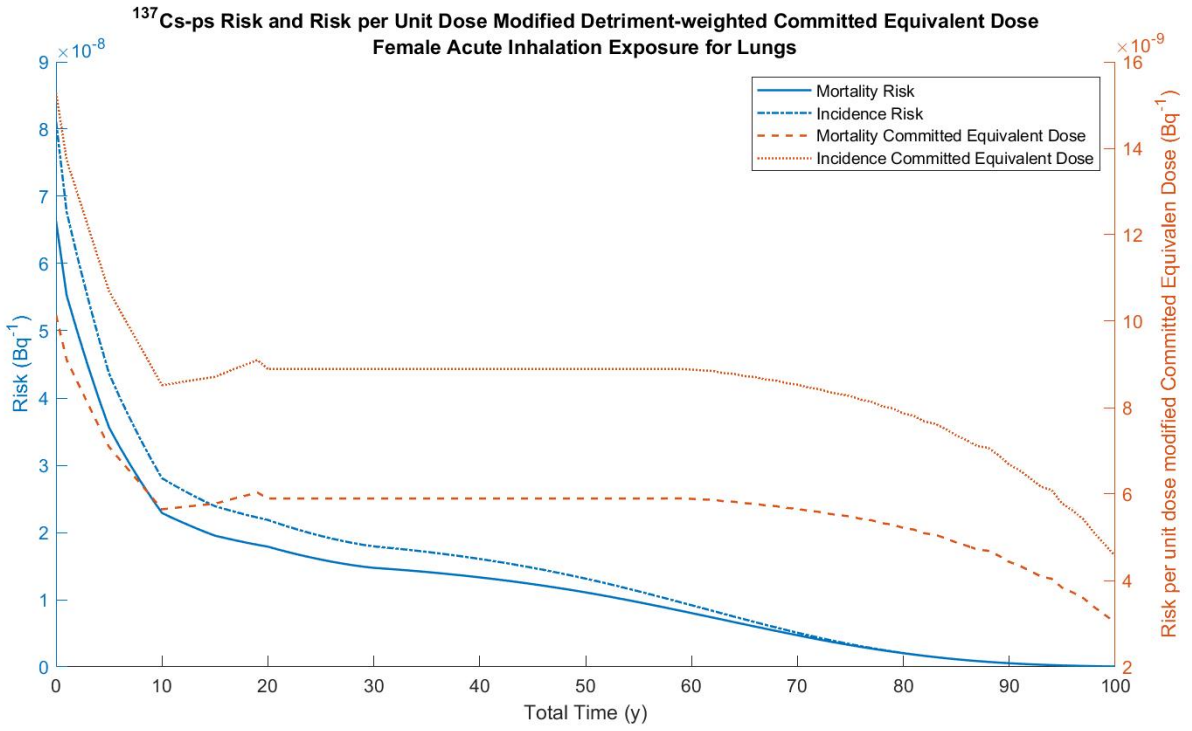

(c)

Figure 85. Risk and detriment-weighted committed equivalent doses to the female lungs from (a) fast-clearing, (b) moderate-clearing, (c) and slow-clearing ^{137}Cs.

The underestimating trend of the detriment-weighted committed equivalent doses for inhaled cesium holds true for most of the tissues of interest for both males and females. As with tritium, the outlier in this trend is for the skin, which is overestimated by approximately an order of magnitude for both incidence and mortality for all solubility types and both sexes, represented in Figure 86.

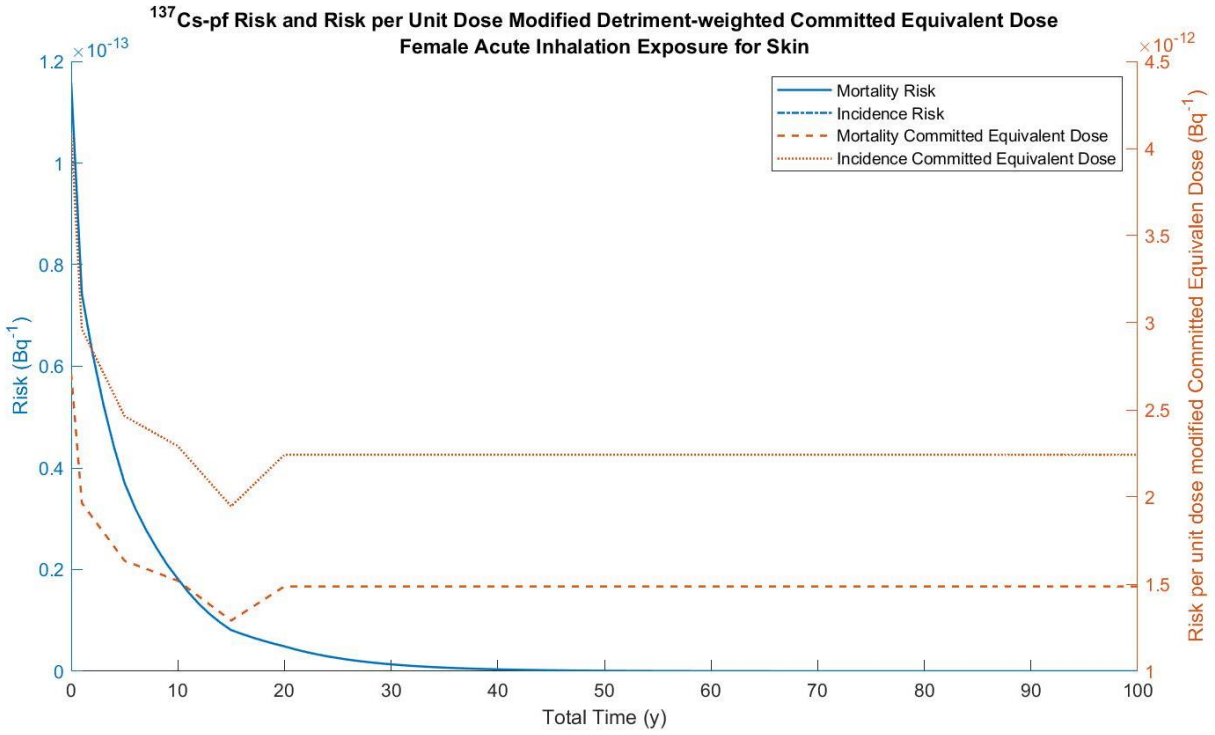

Figure 86. Risk and detriment-weighted committed equivalent doses to the female skin due to fast-clearing ^{137}Cs.

Deviation from the underestimating trend can also be seen in the colon, seen in Figure 87, which for all solubility classes and both sexes, depicts a reasonable agreement between the risk and detriment-weighted doses. At very early ages, the risk is slightly underestimated by the detriment-weighted committed equivalent doses, but they quickly falling within 20% of one another with increasing age.

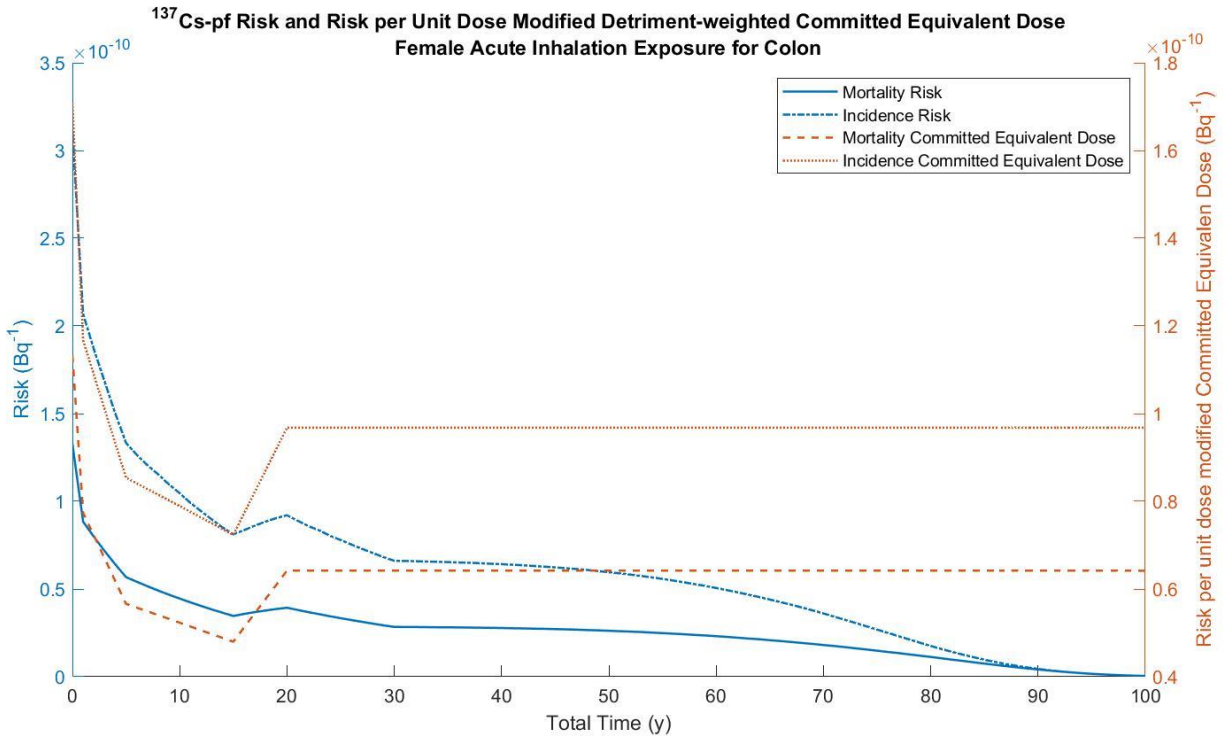

Figure 87. Risk and detriment-weighted committed equivalent doses to the female colon due to fast-clearing ^{137}Cs.

Based on the consistent underestimating of the tissue-specific risk via the detriment-weighted committed equivalent doses, it was anticipated that the risk would also be underestimated by the CEDs from a uniform exposure for both incidence and mortality, with that underestimation decreasing with increasing age. In fact, this is what was seen across all solubility classes and both sexes, the difference between the risk and CEDs sitting around 40% by age 20, seen in Figure 88. A similar trend is seen for ingested cesium as well, seen in Figure 89, with the difference between the calculated risk and the CEDs sitting at approximately 50%. Corresponding male values for plots of the risk and CED comparison can be found in Appendix G.

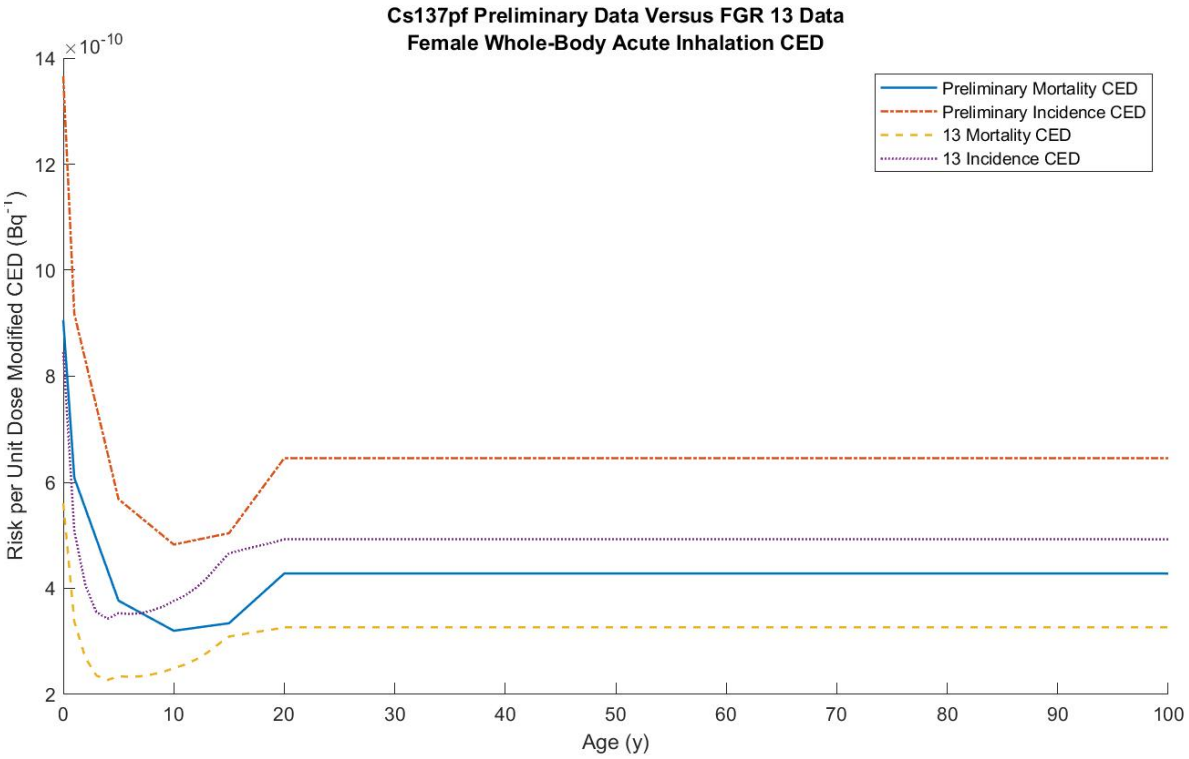
Cs137pf Preliminary Data Versus FGR 13 Data
Female Whole-Body Acute Inhalation CED
Preliminary Mortality CED
Preliminary Incidence CED
13 Mortality CED
13 Incidence CED
Risk per Unit Dose Modified CED (Bq-1)
Age (y)

(a)

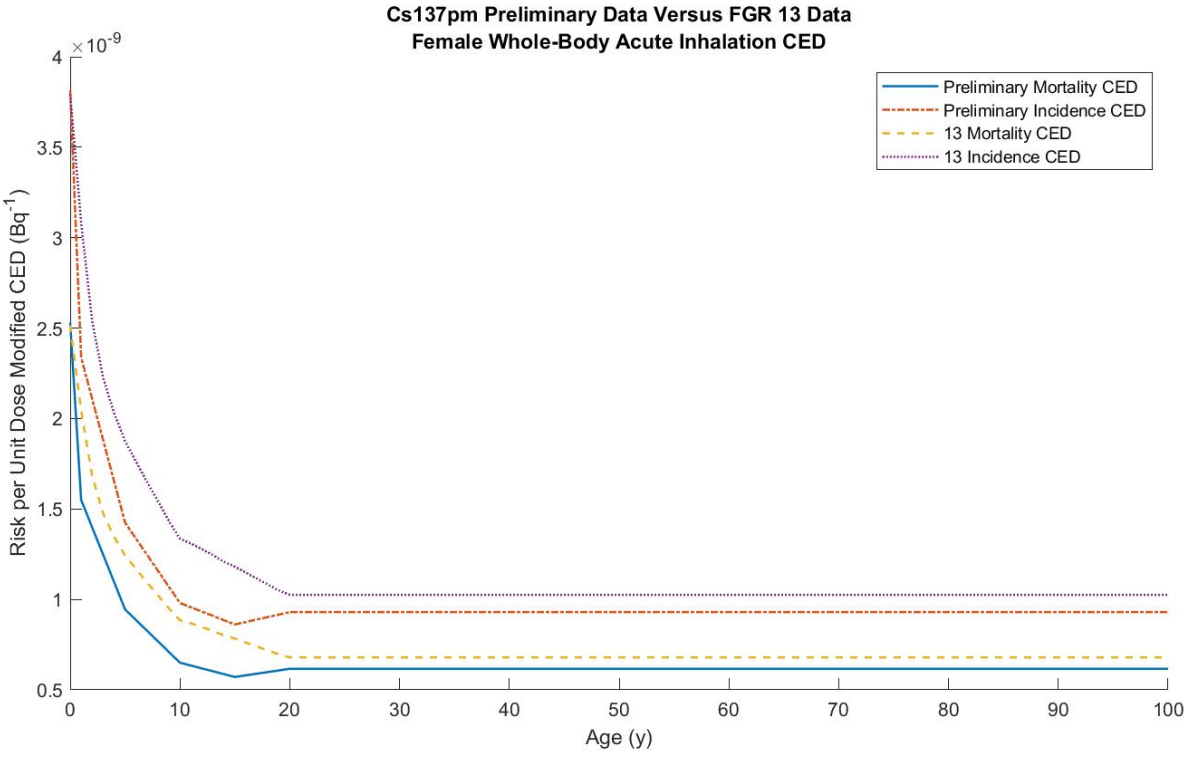
Cs137pm Preliminary Data Versus FGR 13 Data
Female Whole-Body Acute Inhalation CED
Preliminary Mortality CED
Preliminary Incidence CED
13 Mortality CED
13 Incidence CED
Risk per Unit Dose Modified CED (Bq-1)
Age (y)

(b)

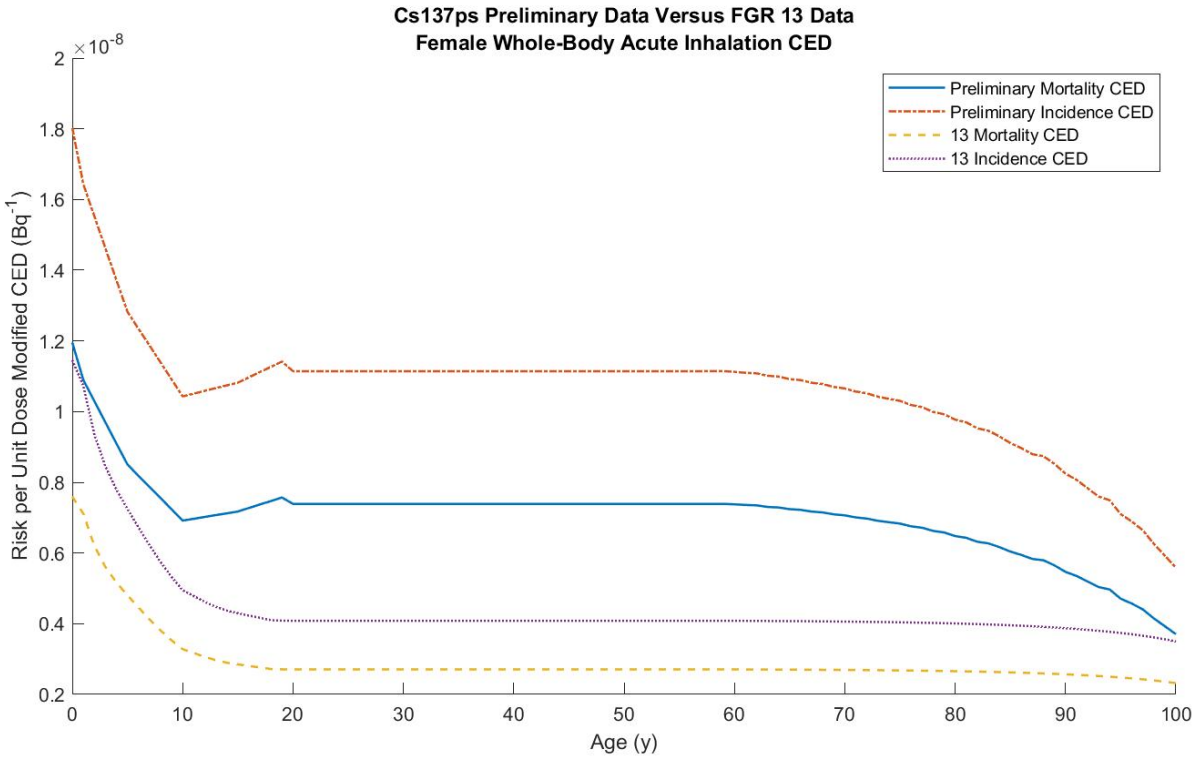

(c)

Figure 88. Uniform exposure risk versus committed effective dose for (a) fast, (b) moderate, and (c) slow clearing ^{137}Cs for females.

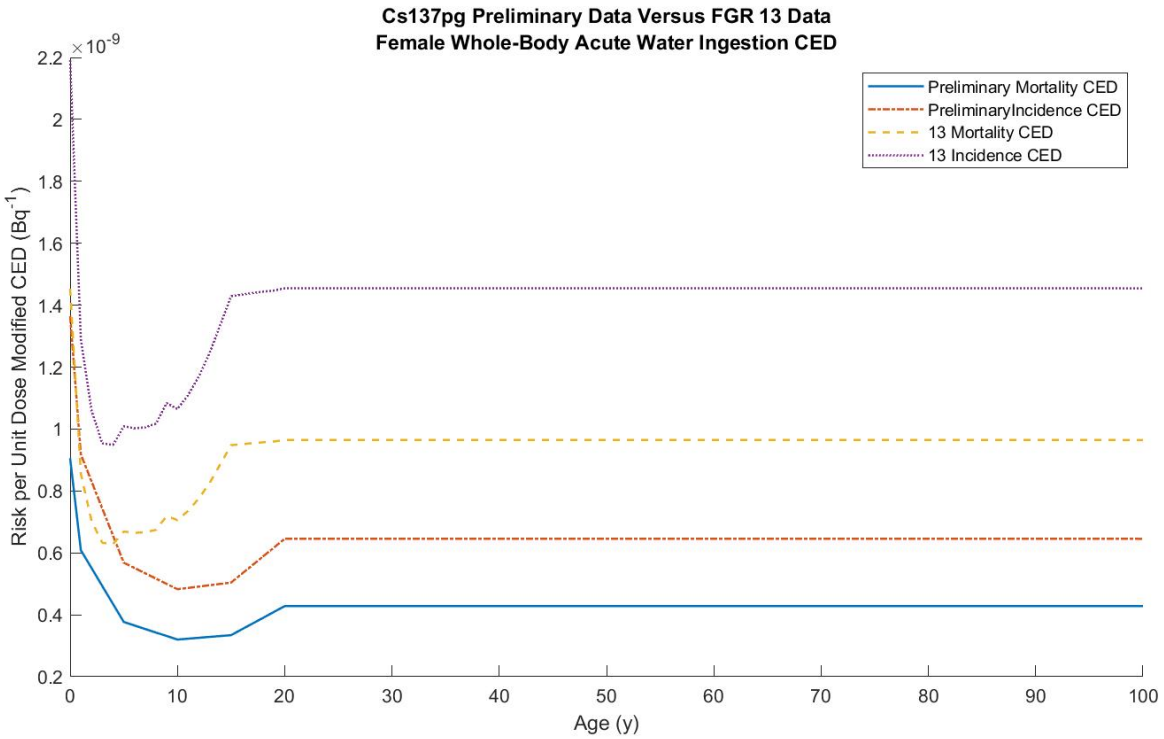

Figure 89. Uniform exposure risk versus committed effective dose for tap water ingested ^{137}Cs for females.

Comparison between generations of data for the risks show reasonable correspondence between the two generations of data for fast-clearing cesium in both males and females. Preliminary data for incidence begins nearly 65% higher than the FGR 13 data, however, it quickly drops to on par with the FGR 13 data. The mortality risk for the preliminary data is also higher than FGR 13, but by a considerably smaller margin, seen in Figure 90. With decreasing rate of clearance from the lungs, the difference between the FGR 13 data and the preliminary data widens, with the preliminary data yielding higher risks than the FGR 13 data, which indicates a potentially noteworthy change in the underlying biokinetics for cesium throughout the body, particularly in the lungs. This trend holds true between both males and females. Plots for the comparisons of risk for males can be found in Appendix H.

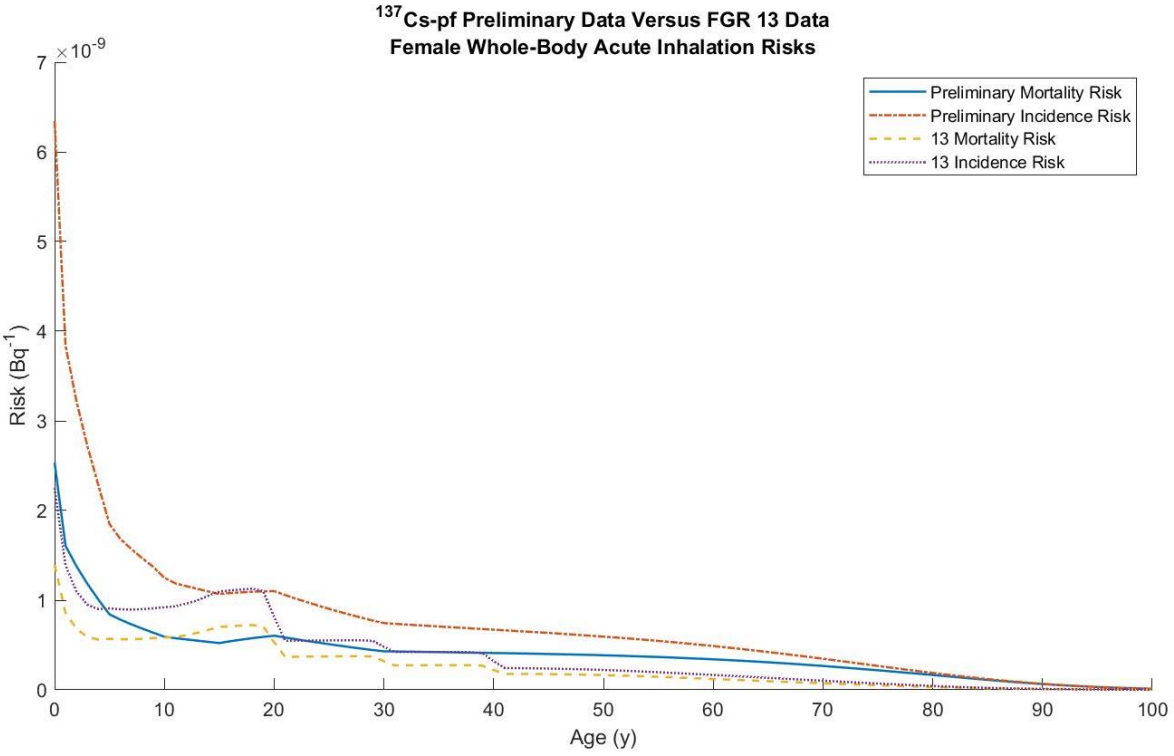

(a)

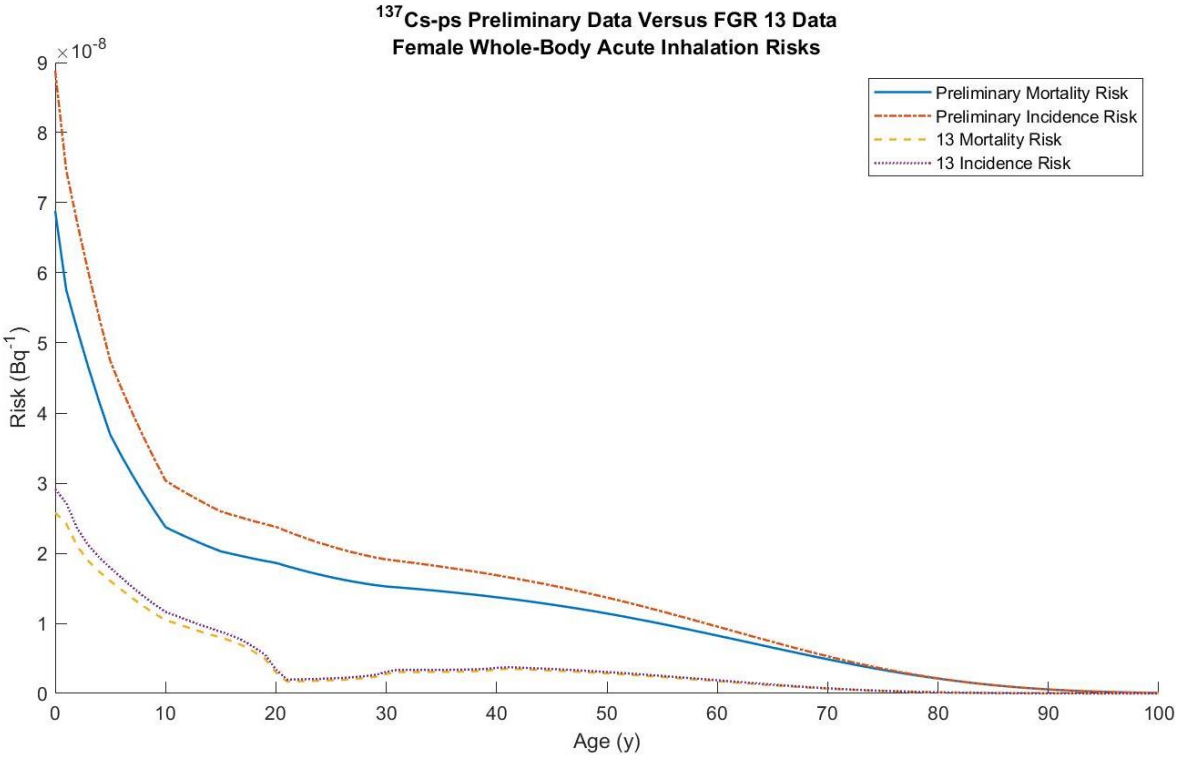

(b)

Figure 90. Comparison of preliminary data and FGR 13 risk coefficients from (a) fast-clearing and (b) slow-clearing ^{137}Cs.

For the corresponding CEDs, all solubility classes show a non-negligible difference between the FGR 13 data and the preliminary data. For both males and females for all solubility classes, the preliminary data yields higher CEDs than the FGR 13 data, said gap widening with decreased rate of clearance from the lungs, as expected. Fast-clearing cesium is represented in Figure 91, and plots for moderate and slow clearing can be found in Appendix I.

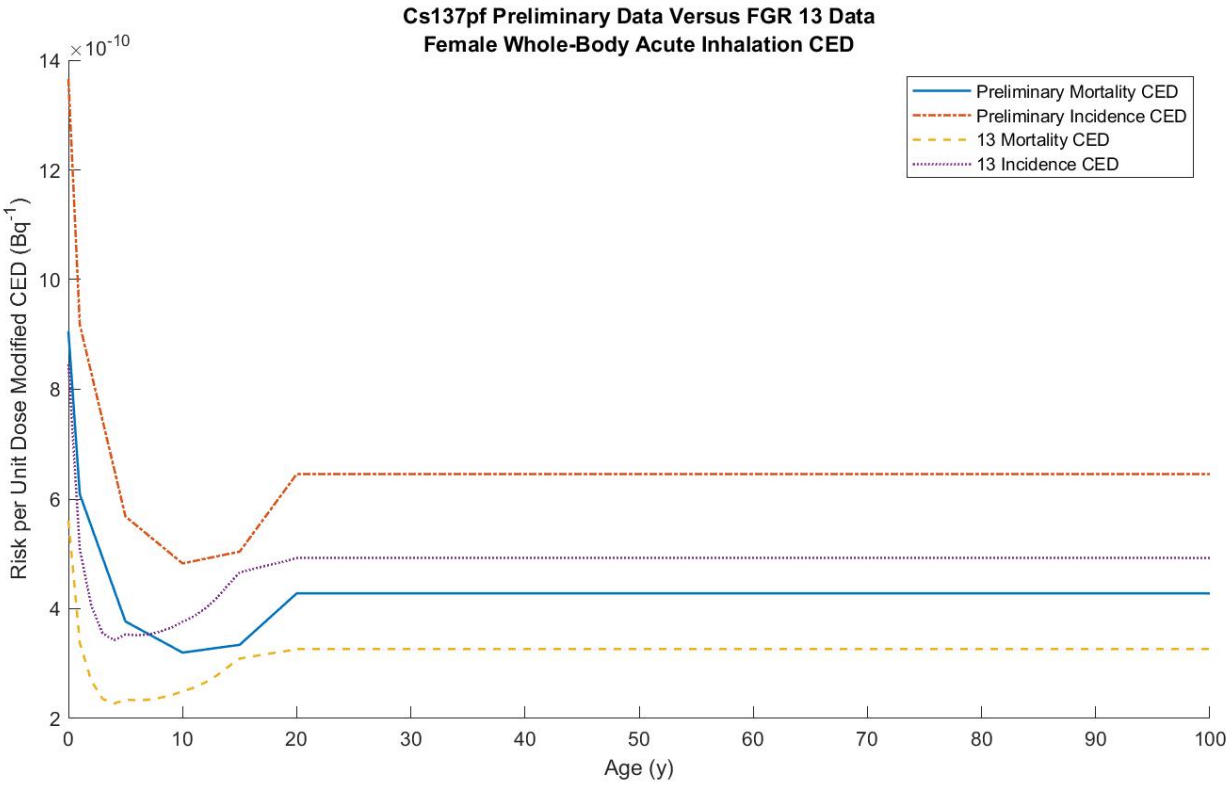

Figure 91. Comparison of the preliminary data and FGR 13 data CED for fast-clearing ^{137}Cs in females.

Notably, ingestion of cesium shows the opposite trend as compared to inhaled cesium. For both the risk and the CEDs, the FGR 13 data yields higher values than the preliminary data, indicating substantial change in the biokinetic behavior of ingested cesium between generations of data. This trend holds for both males and females, and is depicted in Figure 92. Risks for males can be found in Appendix H, and CEDs for males in Appendix I.

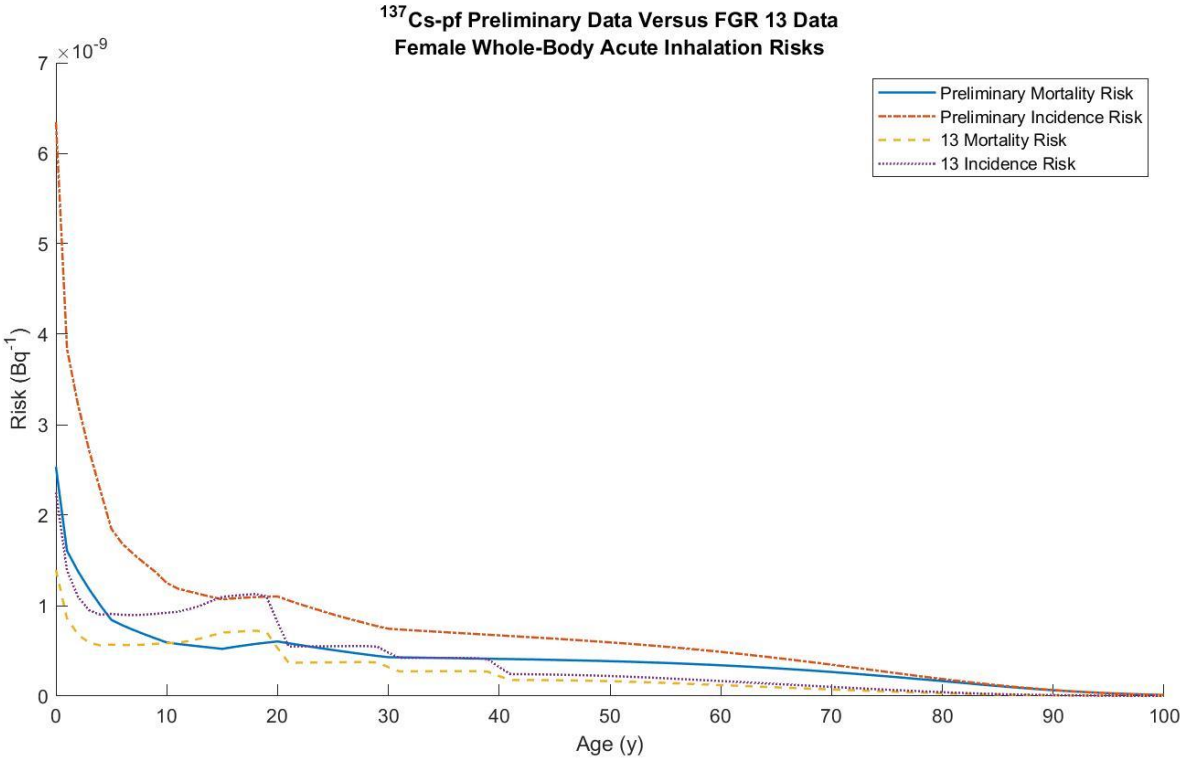

(a)

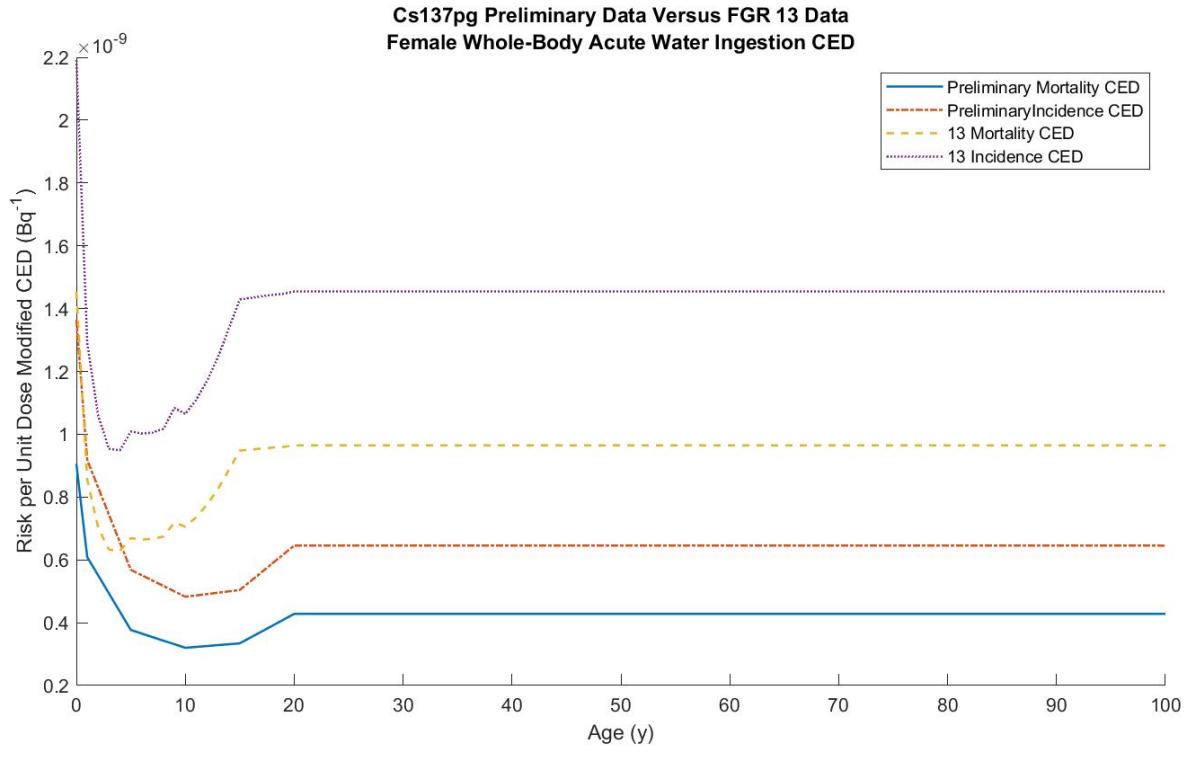

(b)

Figure 92. Comparison of the preliminary data and the FGR 13 data for (a) risks and (b) CED from the ingestion of ^{137}Cs in tap water for females.

4.8.1.d. ^{90}Sr

For inhaled strontium, the bones and lungs are of predominant interest. For both males and females in regards to fast-clearing strontium, the detriment-weighted committed equivalent doses actually track extremely closely with the true risk to the tissue. For females, there is a very slight overestimation and for males, a very slight underestimation, and can be seen in Figure 93. However, as committed dose is only an approximate indicator of possible risk, the committed dose values so accurately reflecting the risk to the primary cancer site for strontium is very encouraging.

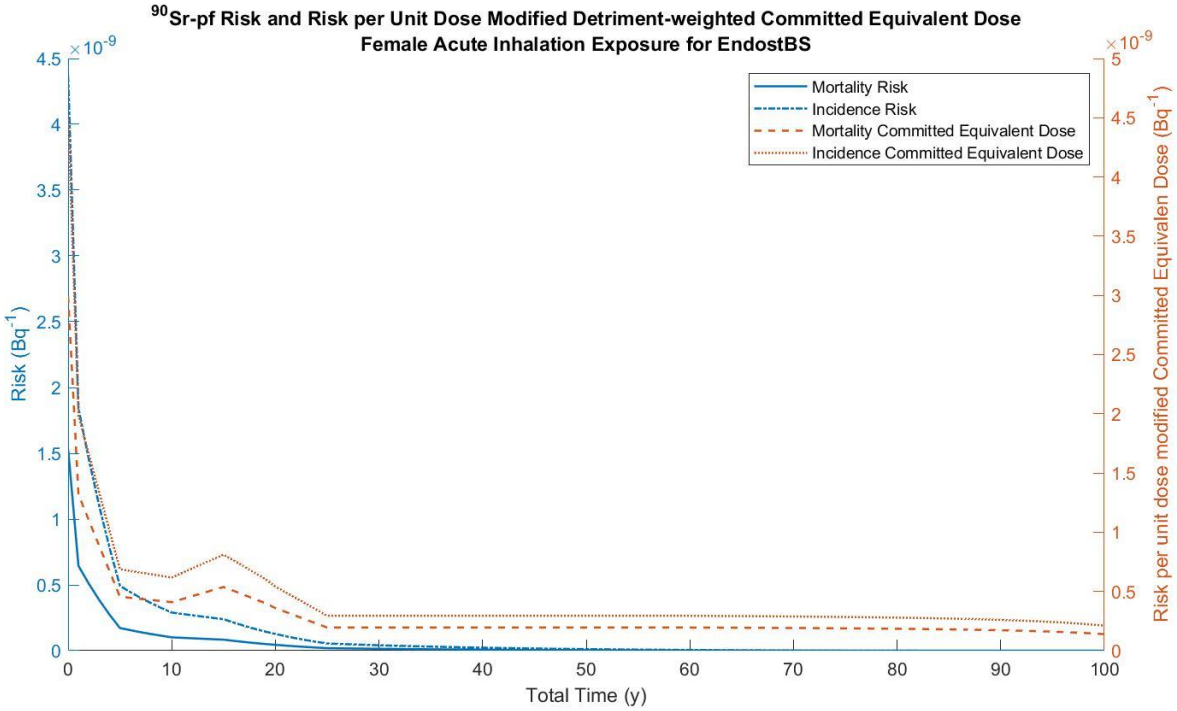

(a)

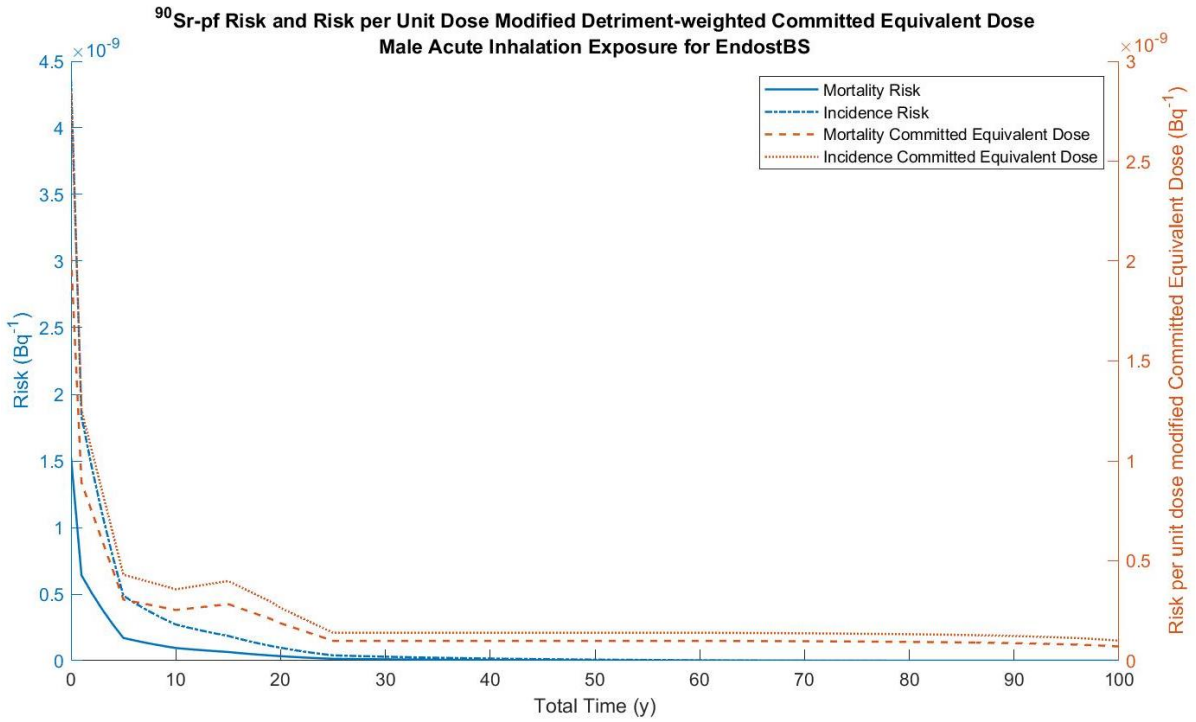

(b)

Figure 93. Risk and detriment-weighted committed equivalent dose to the (a) female and (b) male bone surface from fast-clearing ^{90}Sr.

For the lungs, however, the trend does not follow as closely as with the bone surface. For all solubility classes and both sexes, inhaled strontium risk to the lungs is underestimated by the detriment-weighted committed equivalent doses. This underestimation gap widens with decreasing rate of clearance from the lungs, seen in Figure 94. With decreasing rate of clearance from the lungs, the detriment-weighted committed equivalent doses continue to overestimate the true risk, the gap between the risk and the detriment-weighted doses widening with decreasing rate of clearance for both males and females. However, the gap between the two measures of risk is still perceptively small for the inhaled version of this radionuclide for the bone surface. Corresponding male values can be found in Appendix F.

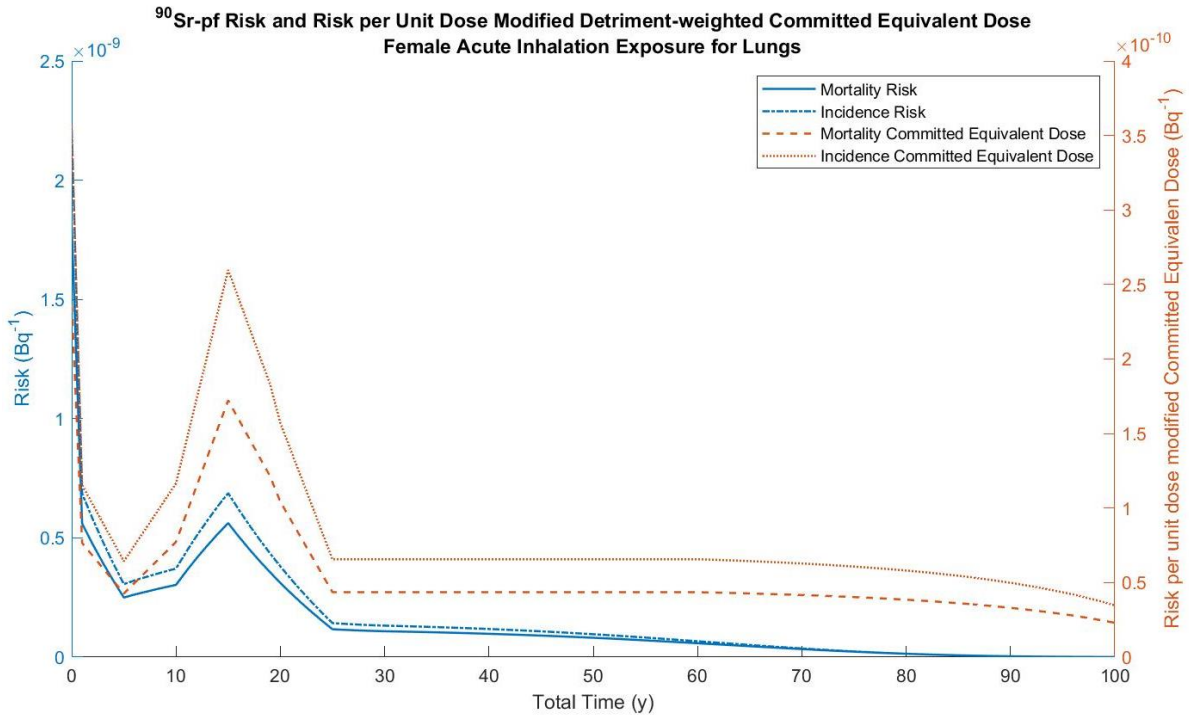

(a)

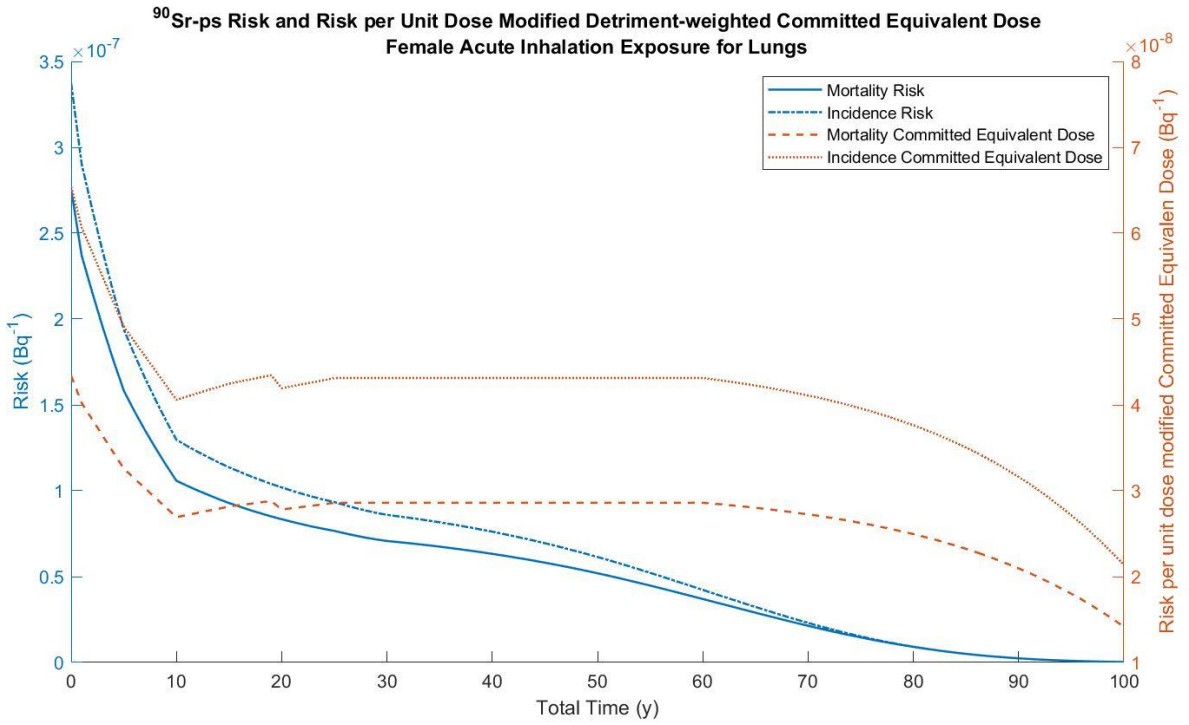

(b)

Figure 94. Risk and detriment-weighted committed equivalent dose to the female lungs due to fast-clearing ^{90}Sr.

The behavior of ingested strontium in the bone surface is very similar to the behavior of fast-clearing strontium on the bone surface. The detriment-weighted committed equivalent dose for

both males and females tracks very closely with the tissue-specific risk, with the female doses very slightly overestimating and the male doses slightly underestimating. However, as with fast-clearing strontium, the difference is incredibly slight, seen in Figure 95.

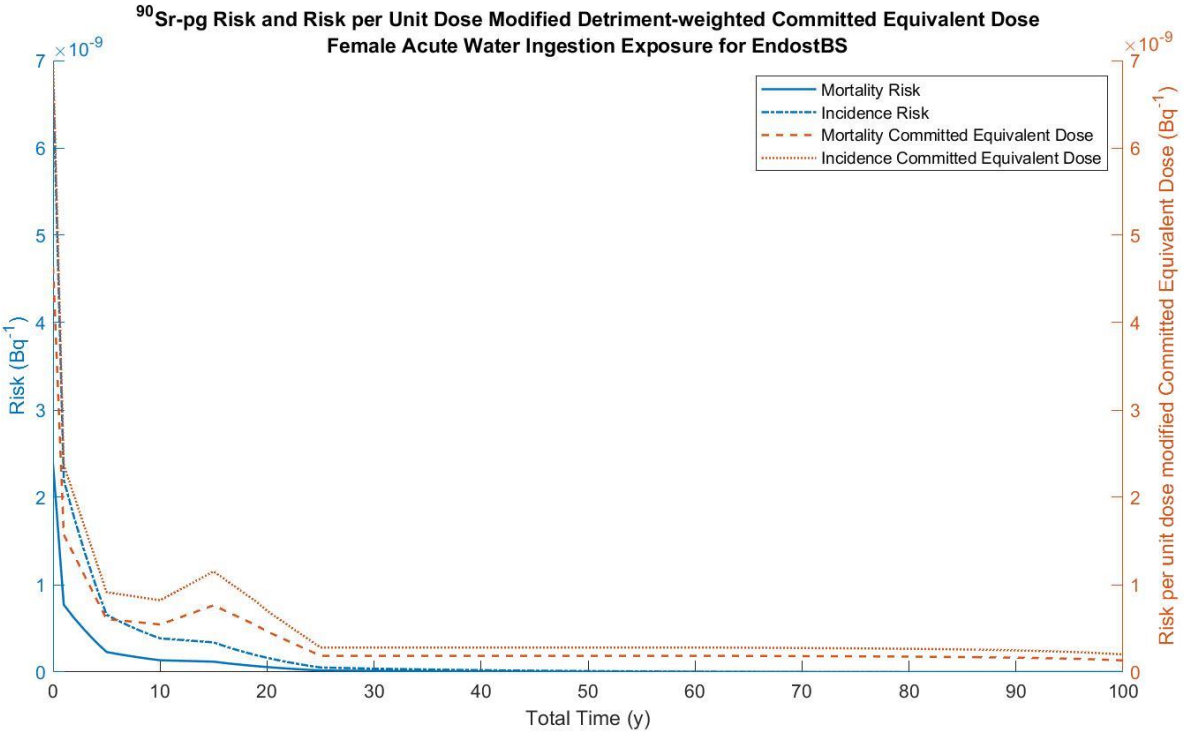

(a)

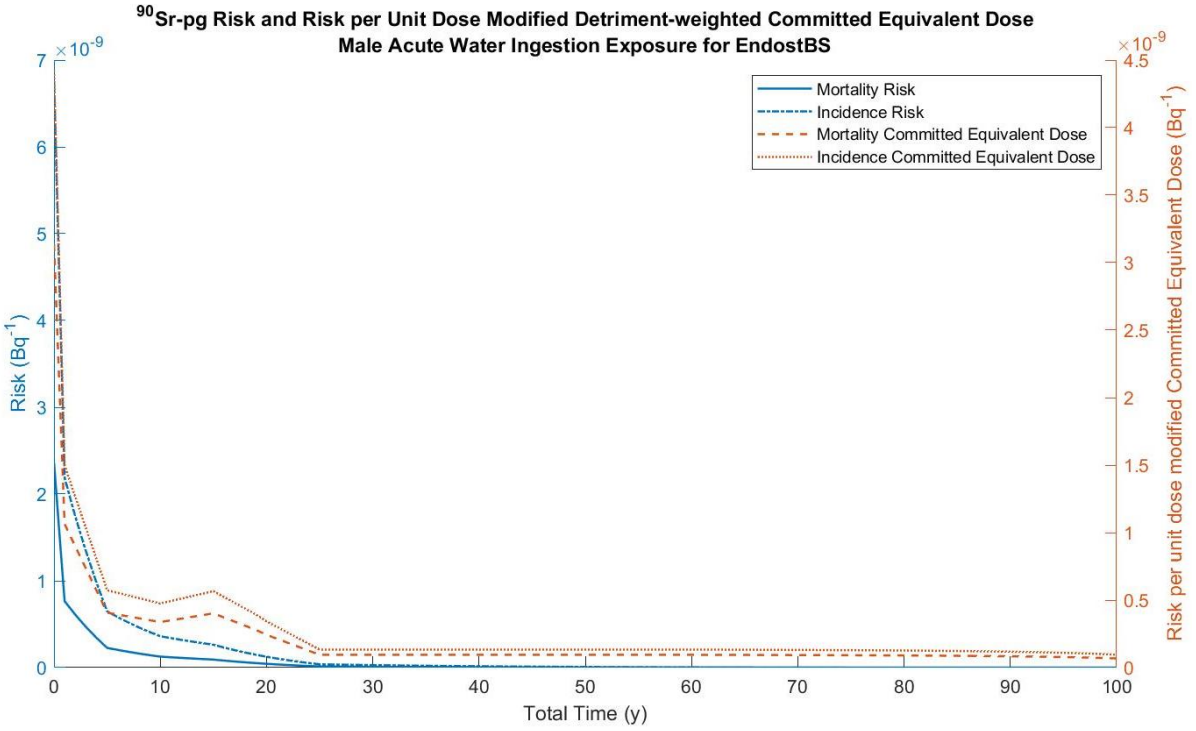

(b)

Figure 95. Risk and detriment-weighted committed equivalent dose to the (a) female and (b) male bone surface from tap water ingested ^{90}Sr.

Due to the very close representation of the tissue-specific risk from the detriment-weighted committed equivalent doses for both males and females, it was anticipated that the CED would closely represent the risk as well, with an underestimation for males being slightly larger than that for females. This was, in fact, what was seen in Figure 96, with the underestimation of the risk via the CED increasing with decreasing rate of clearance from the lungs for both sexes, seen in Figure 97.

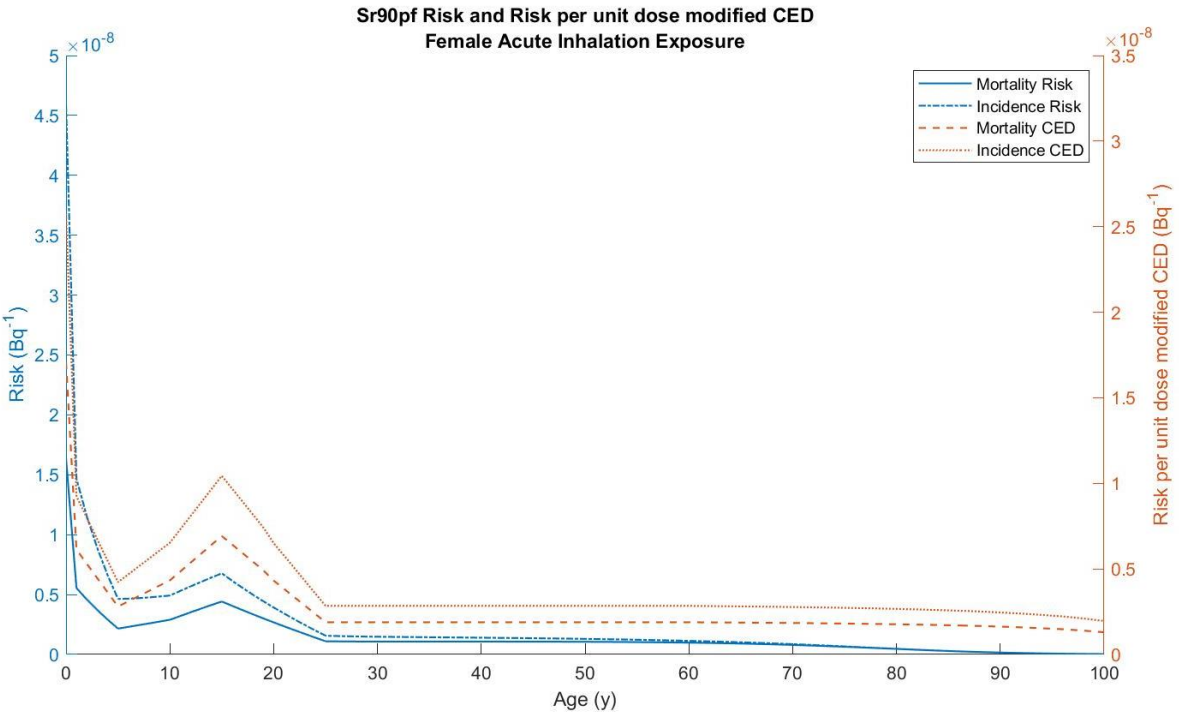

(a)

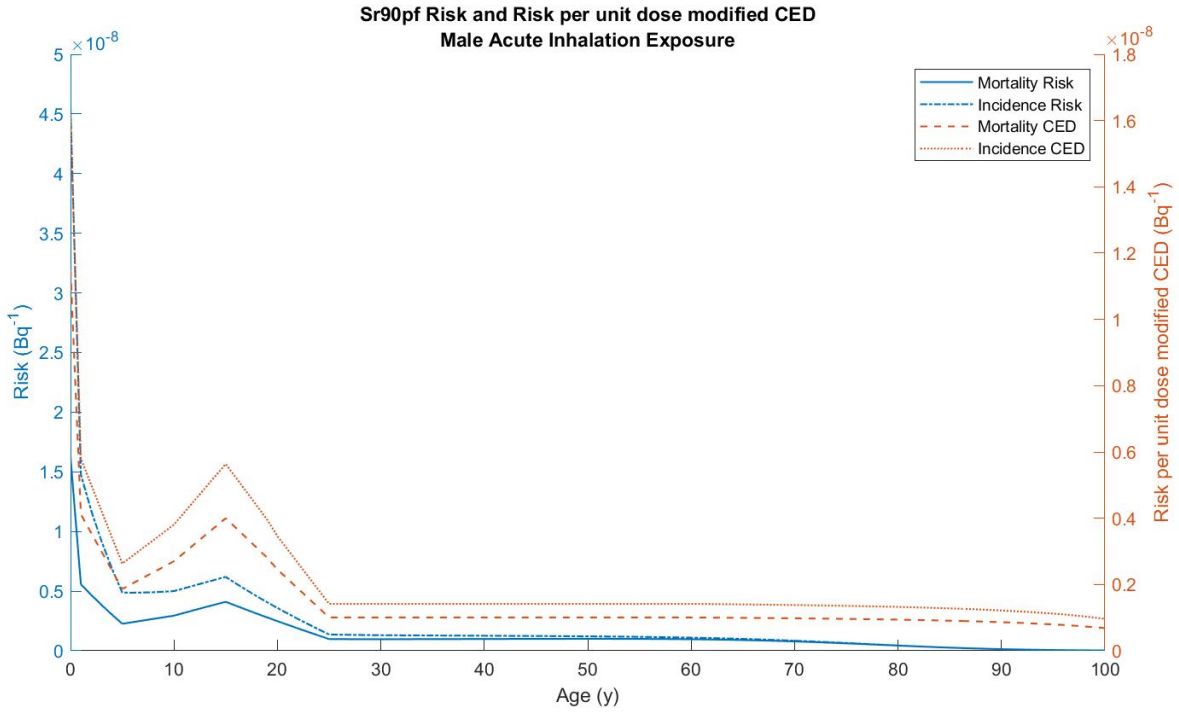

(b)

Figure 96. Risk and CED to females (a) and males (b) due to fast-clearing ^{90}Sr.

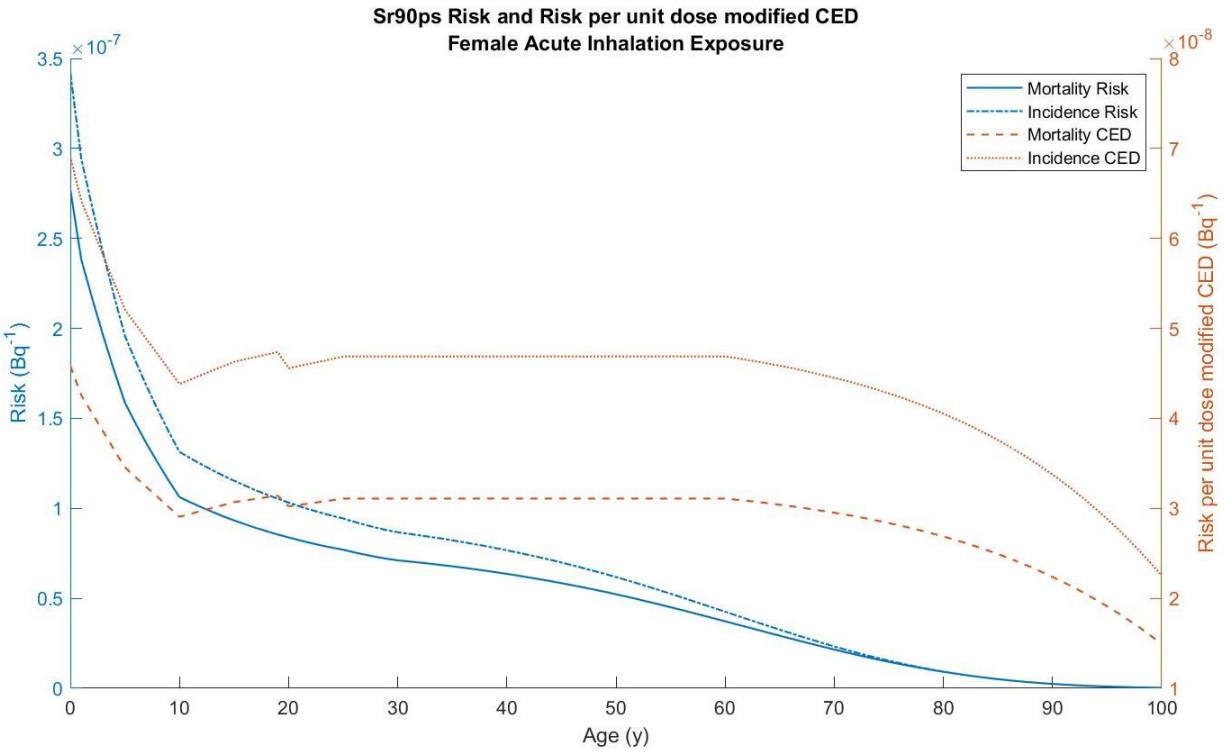

Figure 97. Risk and CED to females due to slow-clearing ^{90}Sr.

Following the trend for the other radionuclides, as well as the tissue-specific patterns between fast-clearing inhaled strontium as compared to tap water ingested strontium, it was anticipated that for the whole body, that ingested strontium would follow a similar trend as the trends for fast-clearing inhaled strontium. This was, in fact, what was seen, with females and males both slightly underestimating the risk with respect to the CED, seen in Figure 98.

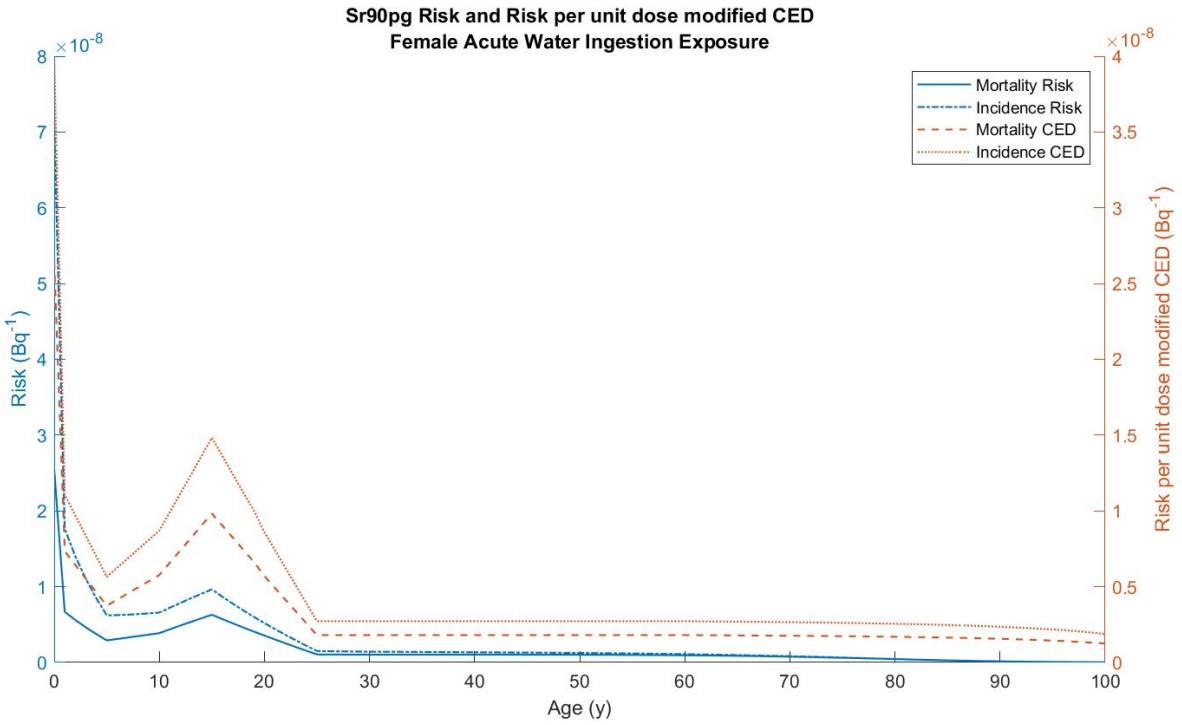

(a)

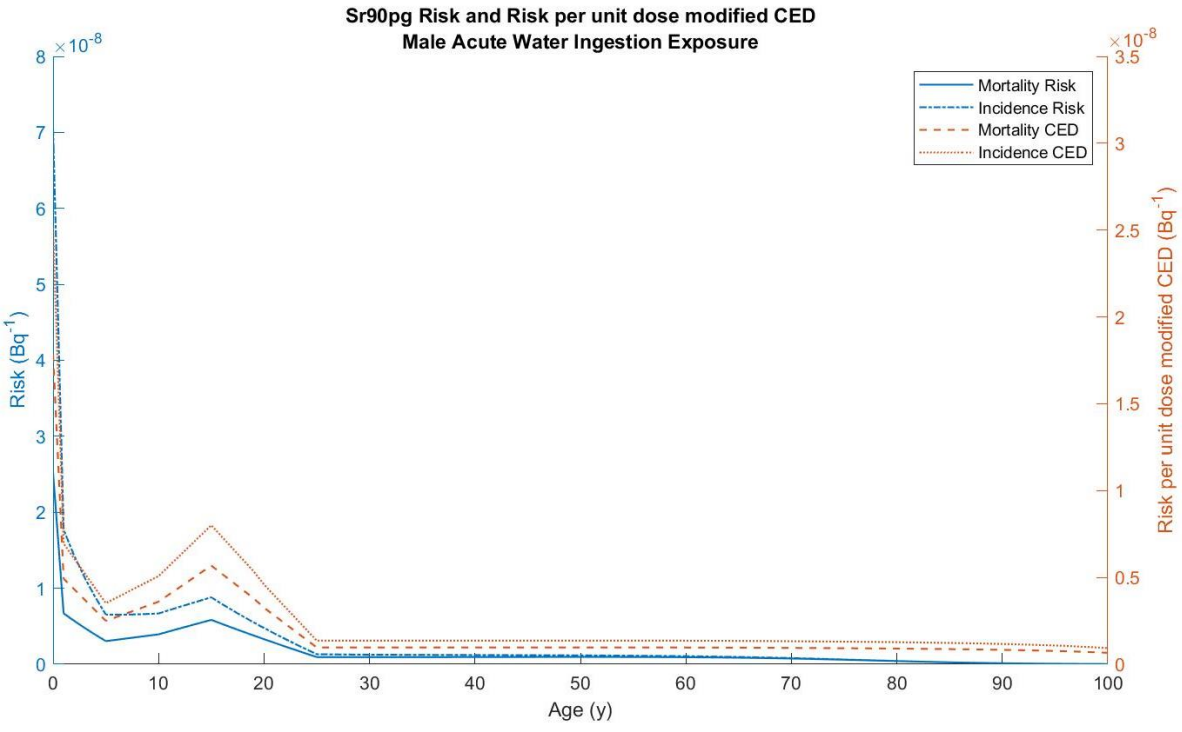

(b)

Figure 98. Uniform exposure risk and CED for (a) females and (b) males due to tap water ingestion of ^{90}Sr.

Comparisons between generations of data for inhaled strontium risks revealed that for all solubility classes, the preliminary data results in a higher risk overall than the FGR 13 data does. As well, with decreasing rate of clearance from the lungs, the difference between the preliminary data and the FGR 13 data increases, with fast-clearing strontium showing extremely close correspondence between the preliminary and FGR 13 data, as seen in Figure 99. Corresponding male values can be found in Appendix H.

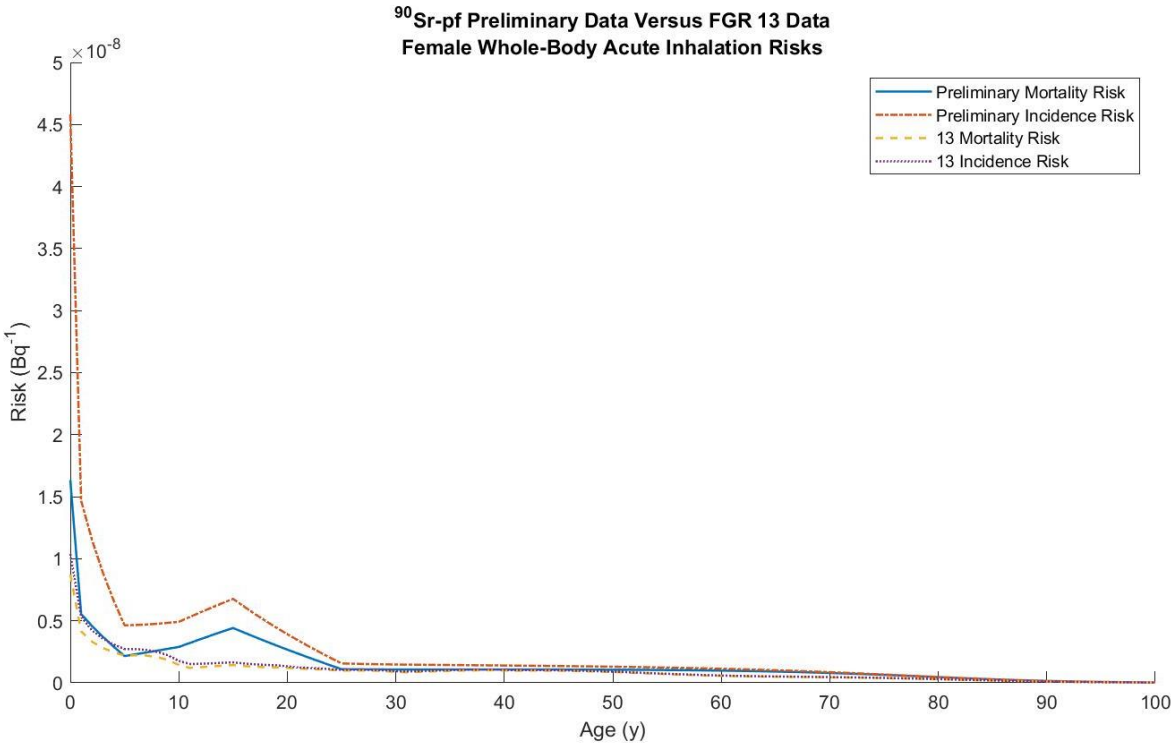

(a)

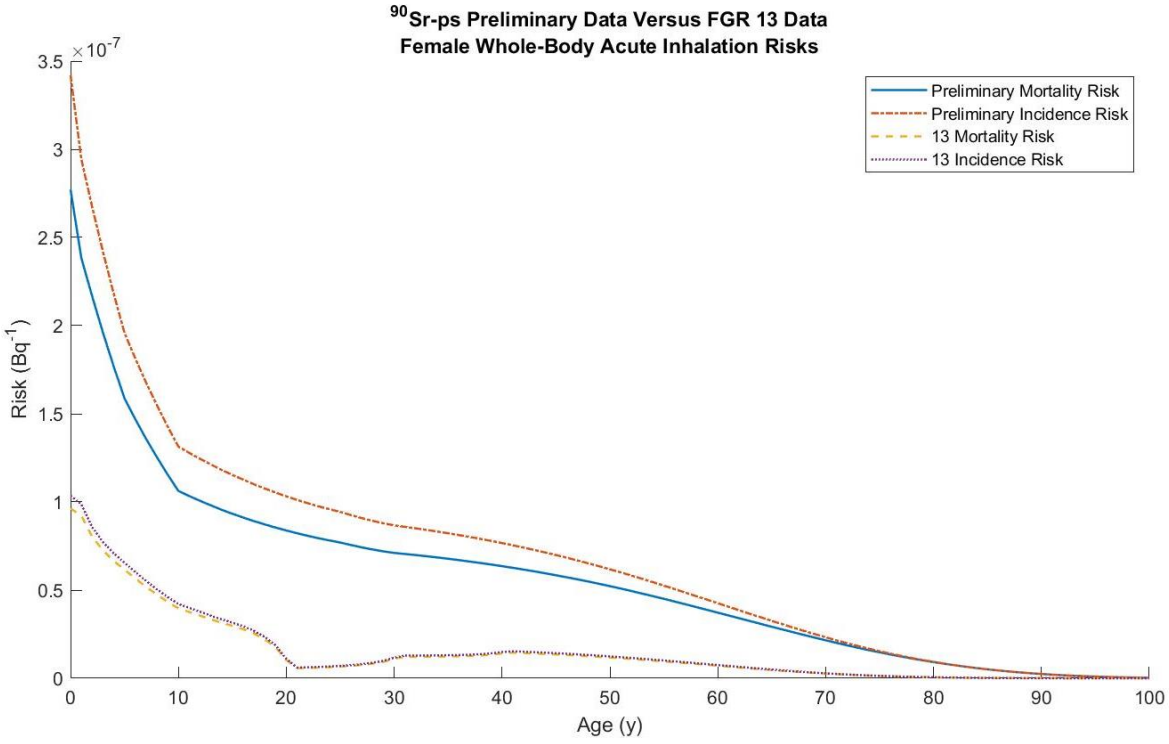

(b)

Figure 99. Uniform exposure risks for the preliminary data and FGR 13 data for (a) fast and (b) slow clearing ^{90}Sr in females.

For the CEDs for both males and females for all solubility classes, a similar trend is seen as was seen for the risks. With decreasing rate of clearance from the lungs, the gap between the preliminary data and the FGR 13 data widens. These widening gaps between generations of data indicate a potential perceptible change in the biokinetics between data generations, reflected in Figure 100. Corresponding male values can be found in Appendix I.

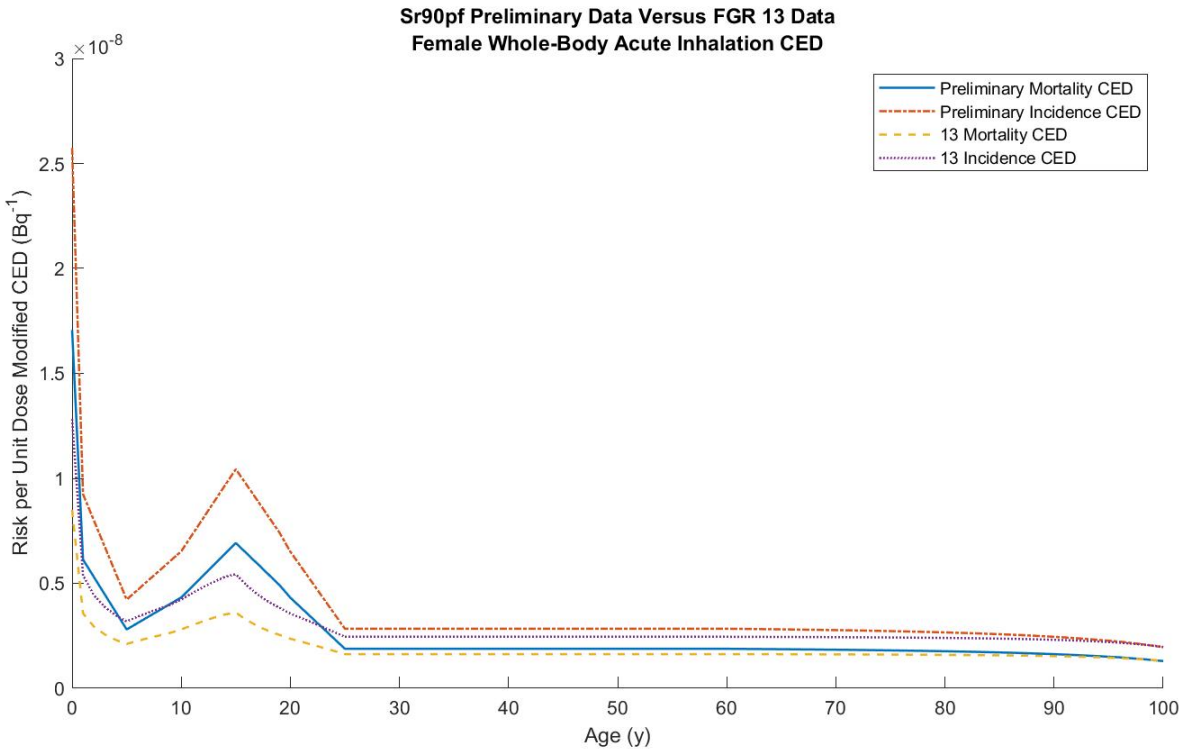

(a)

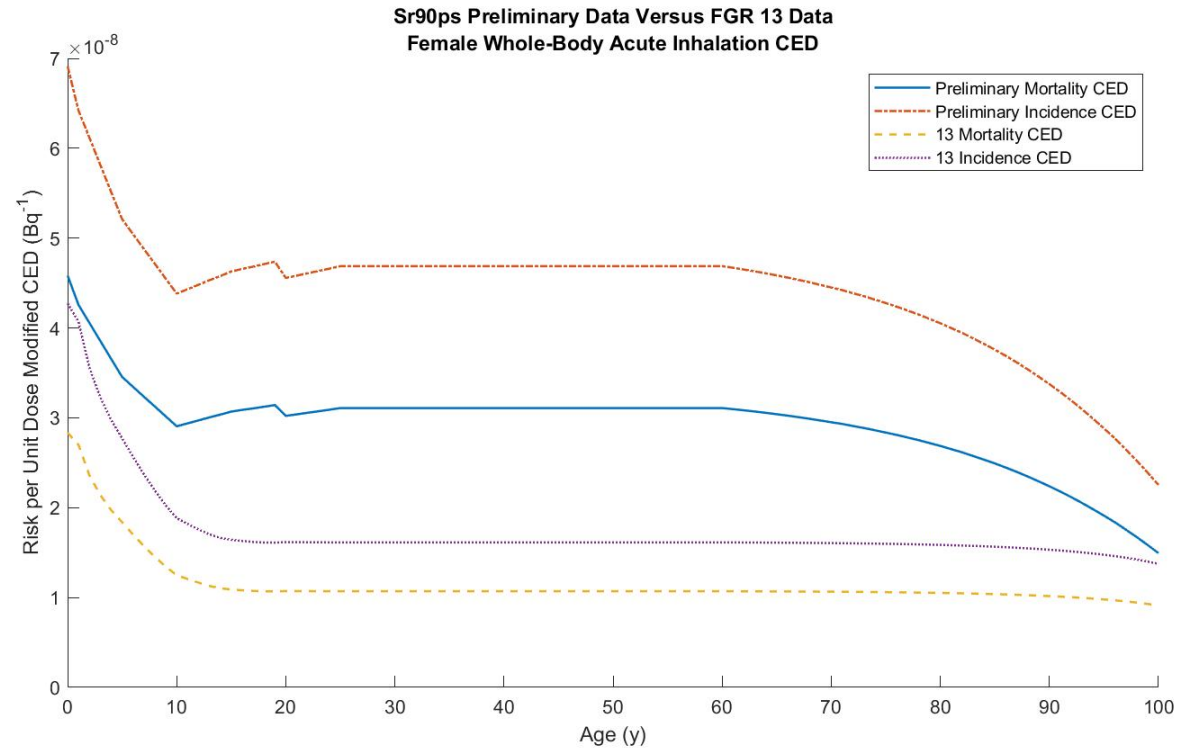

(b)

Figure 100. CED for the preliminary data and the FGR 13 data in females for (a) fast- and (b) slow-clearing ^{90}Sr.

4.8.2. Chronic Exposures

Following the procedure established for the FGR 13 data, the chronic exposure risk coefficients and CEDs for the whole body were calculated and a percent difference taken between the two values, depicted in Table 17. All values for both mortality and risk fall within a 60% difference, save for the mortality coefficient for iodine. This is a similar behavior as was seen with the FGR 13, with the mortality adjusted CED drastically overestimating the risk from a chronic exposure to the radionuclide. It is noteworthy that this comparisons between the risks and CEDs using the ICRP *Publication 103* informed data and the comparisons between the risks and CEDs using the ICRP *Publication 60* informed data show a comparable difference, with overall variation in values being slightly less for the ICRP *Publication 103* informed data.

Table 17. Preliminary data mortality and incidence risk as compared to the mortality and incidence risk per unit dose adjusted committed effective doses.

Isotope	Usage Type	Mortality Risk	Mortality Adjusted CED	% Difference	Incidence Risk	Incidence Adjusted CED	% Difference
Cs137pf	Air	$1.08x10^{-09}$	$1.44x10^{-09}$	33.32	$1.89x10^{-09}$	$2.12x10^{-09}$	11.81
Cs137pm	Air	$9.66x10^{-10}$	$6.89x10^{-10}$	-28.66	$1.22x10^{-09}$	$1.01x10^{-09}$	-17.17
Cs137ps	Air	$8.84x10^{-09}$	$7.20x10^{-09}$	-18.60	$1.06x10^{-08}$	$1.06x10^{-08}$	-0.22
Cs137pg	Food	$2.79x10^{-10}$	$3.71x10^{-10}$	32.98	$5.06x10^{-10}$	$5.44x10^{-10}$	7.54
Cs137pg	Water	$2.54x10^{-10}$	$3.21x10^{-10}$	26.25	$4.35x10^{-10}$	$4.71x10^{-10}$	8.20
H3pf	Air	$4.46x10^{-13}$	$6.20x10^{-13}$	39.03	$9.41x10^{-13}$	$9.11x10^{-13}$	-3.20
H3pm	Air	$8.12x10^{-12}$	$4.37x10^{-12}$	-46.20	$9.66x10^{-12}$	$6.40x10^{-12}$	-33.70
H3ps	Air	$3.75x10^{-11}$	$1.96x10^{-11}$	-47.70	$4.38x10^{-11}$	$2.87x10^{-11}$	-34.30
H3pg	Water	$9.29x10^{-13}$	$1.08x10^{-12}$	16.74	$1.90x10^{-12}$	$1.59x10^{-12}$	-16.48
I131pf	Air	$8.22x10^{-11}$	$7.11x10^{-10}$	764.93	$1.50x10^{-09}$	$1.04x10^{-09}$	-30.51
I131pm	Air	$9.38x10^{-11}$	$2.02x10^{-10}$	115.27	$4.17x10^{-10}$	$2.96x10^{-10}$	-28.98
I131ps	Air	$9.71x10^{-11}$	$6.68x10^{-11}$	-31.20	$1.33x10^{-10}$	$9.79x10^{-11}$	-26.68
I131pg	Food	$2.32x10^{-10}$	$1.58x10^{-09}$	579.69	$4.28x10^{-09}$	$2.31x10^{-09}$	-45.97
I131pg	Water	$1.54x10^{-10}$	$1.23x10^{-09}$	695.88	$2.79x10^{-09}$	$1.79x10^{-09}$	-35.78

Sr90pf	Air	$2.18x10^{-08}$	$3.51x10^{-08}$	60.93	$3.18x10^{-08}$	$5.15x10^{-08}$	61.85
Sr90pm	Air	$1.59x10^{-08}$	$8.62x10^{-09}$	-45.70	$1.92x10^{-08}$	$1.27x10^{-08}$	-34.05
Sr90ps	Air	$3.95x10^{-08}$	$2.32x10^{-08}$	-41.37	$4.62x10^{-08}$	$3.41x10^{-08}$	-26.25
Sr90pg	Food	$6.95x10^{-09}$	$9.67x10^{-09}$	39.18	$1.08x10^{-08}$	$1.42x10^{-08}$	31.10
Sr90pg	Water	$5.53x10^{-09}$	$6.52x10^{-09}$	18.02	$8.23x10^{-09}$	$9.55x10^{-09}$	16.14

In comparison to FGR 13 data, overall, the preliminary data produces mortality-adjusted CEDs that are more representative of the true risk, when FGR 13 risk calculation methodologies are used. As with FGR 13, as well, the values for the mortality for ^{131}I are extremely different from the true risk. Again, this is due to what is factored into the tissue weights. Consideration of other factors such as loss of life and loss of quality of life that contribute to the overall detriment will show a tendency of drastic overestimation of the mortality for radionuclides that tend to cause less fatal cancers, such as iodine in the thyroid. However, the overall closer representation of the chronic committed doses to the chronic risk coefficients for the preliminary data indicates overall improvements in the biokinetics that are used to generate the absorbed doses, as well as improvements in the calculation of the tissue-weighting factors and how they represent the tissue response to radiation.

4.9 General Limitations of the Study

The data presented in this study is subject to several limitations. Firstly, the limitations of the computational programs utilized in the analysis of the ICRP *Publication 60* informed data result in computational variations with respect to the FGR 13 risk coefficients. Predominantly, this data limitation on the dose rates can be seen in the CED plots for slower clearing and slower decaying radionuclides, where the CED drops off beginning at age 60 years. This data limitation

artificially indicates a conversion of the risk and CED values that does not actually exist as the age of exposure approaches end of life.

Assumptions were made in the handling of the data, particularly imposed by insufficient computing resources. In this work, it was assumed that a chronic exposure is defined as an exposure occurring on the first day of each year of life, and the results then summed. This is not a true depiction of a chronic exposure and holds potential to severely reduce the clarity of fast clearing radionuclides during the annualization process. An attempt to increase granularity was made, however, due to lack of computing resources, was determined to be inviable to the study at its current level. In attempt to preserve this granularity at the first year for fast-decaying radionuclides, the afore mentioned interpolation and integration of the first year was done independently. In future iterations of this study, increased fidelity and granularity for these chronic exposures is desirable.

The ICRP *Publication 103* informed data is subjected to a wider array of limitations in terms of data analysis. All analysis and conclusions drawn from this data are resultant of the data made available, as ICRP *Publication 103* dose rate and biokinetic data have not yet been published. As well, risk coefficients have not yet been published based on this dataset, therefore lending to a level of uncertainty in the risk coefficients calculated herein. Finally, the methodology used in the calculation of the ICRP *Publication 103* informed risk coefficients is limited by the RBE used in calculation. Future work will include an energy dependent RBE in updated models, but for the sake of this study, was limited to the RBE values assigned in FGR 13.

5. CONCLUSION

The purpose of this study was to examine the effectiveness of the use of CED as a possible indicator of possible risk for chronic exposures to determine the validity of the use of an age-nonspecific term for an age-dependent representation in order to justify the potential pursuit of something more age-specific when considering radiation protection. To determine this, the absorbed dose rates from both ICRP *Publication 60* and *Publication 103* informed datasets, as well as their corresponding CEDs and risks were investigated through the use of their respective methodologies as established in published literature. The CEDs for both sets were compared both to their respective risk coefficients from an acute and a chronic exposure, and the tissue-specific, detriment-weighted committed equivalent doses were compared to the tissue specific risks to establish trends between usage types and radionuclides to determine pattern outliers. An analysis of these trends revealed whether CED is valid as a reasonable approximator of the risk for both acute and chronic exposures, and it is concluded that for both datasets, CED is a reasonable approximator of possible risk for acute exposures, while it is potentially not as reasonable to use for most radionuclide chronic exposures.

Based on the data presented herein, it can be seen that for most radionuclides and usage types, the CED from an acute exposure trends closely with the risk due to the same exposure. The age-dependency of the risk is clearly seen when compared to the CED graphically, as risk continues to decrease through life, while CED plateaus in the adult ages. For chronic exposures, large differences can be seen for certain radionuclides and solubility classes, particularly ^{131}I mortality. Uranium also sees large differences, particularly for ingestion and fast-clearing inhalation for the ICRP *Publication 60* data. However, barring these particular outliers, most radionuclides show between a 35 and 65% difference when comparing the risk per unit dose

modified CED to the risk due to a uniform exposure. CED for a chronic exposure shows a large overestimation of the risk for more radionuclides in the ICRP *Publication 60* dataset, and a decent underestimation for the ICRP *Publication 103* informed dataset, leading to the conclusion that for chronic exposures, an age-dependent value in place of the ICRP tissue-weights is desirable.

5.1. Relation to Ongoing Work

For both generations of data, a consistent, non-negligible difference between the FGR 13 methodology calculated risk and the ICRP *Publication 60* and ICRP *Publication 103* methodologies calculated CEDs can be seen. This difference is exacerbated for chronic exposures for both generations of data. A key factor in this difference is the use of age-non-specific tissue weights used in the calculation of the committed effective doses. If effective dose is to be used as an "approximate indicator of possible risk" then, to limit confusion and potentially reduce inaccuracy with respect to age of exposure, it is best to fold in some consideration of age of exposure into the calculation, which is reinforced by the large difference between the risk coefficient and the chronic exposure CED.

Such age-specific consideration has been mentioned in work by Brenner, where he has suggested the development of an intermediate term, coined "effective risk", specifically for use in medical procedures where effective dose is often misused. Such a value would be calculated in a similar manner to the current methodologies used to calculate effective dose, but would utilize a "lifetime radiation-attributable tissue-specific cancer risk (per unit equivalent dose to [the] tissue)" derived from the BEIR-VII report data for age-at-exposure dependencies for certain cancers in a Western population.[3] Incorporating this value, one that is akin to the LAR value used in calculating risk, and which is age dependent, would yield an indicator of risk that is also age dependent.

Investigations have been done utilizing this “effective risk” term, specifically for medical exposures as was conducted by Andrade et el. in the investigation of computed tomography examinations.[38] Comparing the efficacy of this term versus established ICRP quantities are necessary in order to validate their use and potential improve guidance and protection of workers, patients, and members of the general population. While “effective risk” is suggested by Brenner in a medical setting use, there is potential for a similar path to be taken when considering effective dose in radiological protection.

Currently, as outlined in ICRP *Publication 147*, work is being done to improve protection methods and the calculations done to inform protective guidance.[1] As it stands, effective dose maintains its status as the ICRP quantity used as “an approximate indicator of possible risk” and is used alongside equivalent dose in order to inform protective guidance. However, studies are being done to explore the use of organ and tissue absorbed doses instead to inform protective guidance as phantoms for males and females at various ages steadily improve.[1]

Reference to the plots outlined in this work depict non-negligible differences between the risks for males and females, even for the FGR 13 data, which utilized a common phantom between males and females, simply filling in the tissues for females (breast and ovaries) that differed. Thus, the potential detriment to the tissues between males and females for the FGR 13 data as a result of being sex-averaged is that the risk disparity between male and female is not specifically delineated. This is not the practice of ICRP, in the utilization of sex-averaged data, and carried into the calculations of FGR 13. Subsequent studies for risk estimation using the models and approach here in populations may consider focusing on sex-specific risk, as is suggested in ICRP *Publication 147*.[1] However, this still does not solve the issue of the lack of age-specificity when calculating detriment and effective dose, as by their very nature the tissue weights blur the age dependency.

The Commission states its hesitancy in the use of a term such as “effective risk”, fearing that it could imply a spurious degree of accuracy than it actually represents, unless all sources of uncertainty are accounted for.[1] However, such measures are already accounted for when using effective dose, and the caveats of “possible” and “approximate” when referring to effective dose as an indicator of risk indicate a high degree of uncertainty, specifically with the tissue weights currently used. It is not out of the realm of possibility to use similar language when utilizing a term such as “effective risk”, ensuring that the degree of uncertainty is considered. The use of this age-specific term, at very least, holds the potential to remove a degree of uncertainty that is rolled in through age-averaged tissue weights, particularly for chronic exposures.

As well as potentially improving accuracy, specifically for chronic exposures, by looping in age dependency for the calculation of an “effective risk”, such a term also allows for a more direct comparison to the true risk.[3] While the application of a risk per unit dose factor as outlined in FGR 13 allows for a more direct comparison between the effective dose and the true risk, it still borders on an indirect comparison due to the fact that tissue weights take into consideration committee determined factors other than strictly the risk of cancer incidence and mortality, hence the term “detriment” being used in reference to this quantity. This is one of the reasons that effective dose is only an approximate indicator, as extra subjective considerations drive the calculations further from the risk calculations. A term that does not take into consideration more subjective considerations such as quality of life would allow for a more direct type comparison with an easier interpretation.

This is not to say that the use of effective dose should be completely removed. There is substantial value in the consideration of loss of life and potential decrease in quality of life due to treatments. However, the development of a term such as “effective risk” has the potential to

improve protective guidance for both workers and members of the public from both acute and chronic exposures, as well as to decrease misuse and misinterpretation, and should be used, since adequate protection is a must in the field of radiation protection. Furthermore, the fact that it is calculated in a similar manner as effective dose, simply altering the tissue weights to reflect age dependency, the resultant value is still a single, concise numerical value that could easily be interpreted, not adding an increased level of complexity to the term.

5.2. Future Work

As mentioned, the data herein referred to as "preliminary" data references dose rate data generated using improved biokinetics, dosimetric models, and ICRP *Publication* 103 recommendations as compared to DCAL generated data. These data will be used in the informing of risk calculations for the pending Federal Guidance Report 16. In expanding this work, it would be beneficial to redo the work within this text while applying the appropriate modified RBE to the preliminary data, which will take into account the energy dependence of the radiation spectrum. This is particularly true for any radionuclide with a high-LET component, which was not explored in the preliminary data for this thesis.

In regards to the development of a term such as "effective risk", it is of interest to repeat the stated calculations and comparisons utilizing BEIR-VII models for the age-specific tissue weights in a manner as suggested by Brenner, and observe the difference between this calculated "effective risk" and the true risk to the tissues following FGR 13 methodologies. This is a logical next step as the work within this thesis has shown the substantial difference for both generations of data between the risk per unit dose modified effective dose and true risk.

REFERENCES

1. ICRP, *Use of Dose Quantities in Radiological Protection.* ICRP Publication 147. Ann. ICRP 50(1).
2. K. F. Eckerman, R.W.L., *Federal Guidance Report No. 13: Cancer Risk Coefficients for Environmental Exposure to Radionuclides*. 1999, United States Environmental Protection Agency: Oak Ridge National Laboratory.
3. Brenner, D.J., *Effective dose: a flawed concept that could and should be replaced.* Br J Radiol, 2008. **81**(967): p. 521-3.
4. 2006, N.R.C., *Health Risks from Exposure to Low Levels of Ionizing Radiation: BEIR VII Phase 2.* . 2006, Washington, DC: The National Academies Press.
5. ICRP, *Conversion Coefficients for Radiological Protection Quantities for External Radiation Exposures.* ICRP Publication 116, Ann. ICRP 40(2-5) 2010.
6. ICRP, *The 2007 Recommendations of the International Commission on Radiological Protection.* ICRP Publication 103. Ann. ICRP 37 (2-4), 2007.
7. Dewji, S.A., et al., *Advanced Radiation Protection Dosimetry*. 2019, Boca Raton: CRC Press.
8. ICRP, *Radionuclide Transformations - Energy and Intensity of Emissions.* ICRP Publication 38. Ann. ICRP 11-13., 1983.
9. ICRP, *Nuclear Decay Data for Dosimetric Calculations.* . ICRP Publication 107. Ann. ICRP 38 (3). 2008.
10. ICRP, *Occupational Intakes of Radionuclides: Part 1.* . ICRP Publication 130. Ann ICRP 44(2), 2015.
11. ICRP, *Limits for Intakes of Radionuclides by Workers. ICRP Publication 30 (Part 1). Ann. ICRP 2 (3-4).* 1979.
12. ICRP, *Age-dependent Doses to the Members of the Public from Intake of Radionuclides - Part 5 Compilation of Ingestion and Inhalation Coefficients. ICRP Publication 72. Ann.* 1995.
13. ICRP, *1990 Recommendations of the International Commission on Radiological Protection.* ICRP Publication 60. Ann. ICRP 21 (1-3), 1991.
14. ICRP, *Human Respiratory Tract Model for Radiological Protection.* ICRP Publication 66. Ann. ICRP 24 (1-3), 1994.
15. ICRP, *Age-dependent Doses to Members of the Public from Intake of Radionuclides - Part 4 Inhalation Dose Coefficients. ICRP Publication 71. Ann. ICRP 25 (3-4).* 1995.
16. ICRP, *Human Alimentary Tract Model for Radiological Protection.* . ICRP Publication 100. Ann. ICRP 36 (1-2), 2006.
17. ICRP, *Age-dependent Doses to Members of the Public from Intake of Radionuclides - Part 3 Ingestion Dose Coefficients.* ICRP Publication 69. Ann. IcRP 25 (1), 1995.
18. ICRP, *Adult Reference Computational Phantoms.* ICRP Publication 110. Ann. ICRP 39 (2), 2009.
19. McDowell, M.A.B., R.D ; Alaimo, K. ; Bischof, A.M. ; Caughman, C.R. ; Carroll, M.D. ; Loria, C.M. ; Johnson, C.L., *Energy and Marcronutrient Intakes of Persons Ages 2 Months and Over in the United States: Third National Health and Nutrition Examination Survey, Phase 1, 1989-91.* Advance Data 225, 1994.
20. Ershow, A.G.C., K.P. , *Total Water and Tabp water Intake in the United States: Population-Based Estimates of Quantities and Sources.* Order No. 263-MD-810264 (National Cancer Institues, Bethesda, MD) 1989.

21. ICRP, *Age-dependent Doses to Members of the Public from Intake of Radionuclides - Part 2 Ingestion Dose Coefficients.* ICRP Publication 67. Ann ICRP 23 (3-4), 1993.
22. ICRP, *Age-dependent Doses to Members of the Public from Intake of Radionuclides - Part 1.* ICRP Publication 56. Ann. ICRP 20 (2), 1990.
23. Dahl, S.G., et al., *Incorporation and distribution of strontium in bone.* Bone, 2001. **28**(4): p. 446-453.
24. R. W. Leggett, K.F.E., *A model for the age-dependent skeletal retention of plutonium. .* Radiation Risk Protection, 1984. **1**: p. 454-457.
25. Pawel, D.J.P., Jerome S., *EPA Radiogenic Cancer Risk Models and Projections for the U.S. Population*. 2011, U.S. Environmental Protection Agency: Office of Radiation and Indoor Air. 1200 Pennsylvania Ave., NW, Washington, DC 20460.
26. NCRP, *The relative biological effectiveness of radiations of different quality. .* Recommendations of the National Council on Radiation Protection and Measurements. Report 104, 1990.
27. Jeff Buchsbaumn, E.J.B., Jacek Capala, Richard Pelroy, *Defining High-LET Radiaition Molecular and Cellular Damage and Responses Relevent to Oncology*. National Cancer Institute
28. NCRP, *Evaluation of the Relative Effectiveness of Low-Energy Photons and Electrons in Inducing Cancer in Humans.* Recomendation of the National Council of Radiation Protection and Measurements. NCRP Report 181, 2018.
29. Eckerman, K.F., *Dose and Risk Calculation*. 2010, Oak Ridge, Tennessee: Oak Ridge Nathional Laboratory.
30. Jokisch, D., A.E. Kalinowski, Editor. 2020: Oak Ridge National Laboratory
31. *Piecewise Cubic Hermite Interpolating Polynomial (PCHIP)* 2021, The MathWorks, Inc.
32. Inc., E., *Extreme.Numerics*. 2021, Microsoft: NuGet Gallery.
33. Hee Geun Kim, T.Y.K., Goung Jin Lee, Woo Tae Jeong, Seok Tae Kim, *Analysis of Metabolism and Effective Half-life for Radiation Workers' Tritium Intake at Pressuraized Heavy Water Reactors.* Progress in Nuclear Science and Technology, 2011. **1**: p. 545-548.
34. *Half Lives Explained*. 2021; Available from: https://dec.alaska.gov/eh/radiation/half-lives-explained/.
35. Kaye, W.R., Z.S. Beauvais, and K.J. Kearfott, *Method of Estimating Lifetime Cancer Risk Due to Chronic Radionuclide Intake.* Health Physics, 2011. **100**(2): p. 167-175.
36. Eckerman, K.F., A.E. Kalinowski, Editor. 2021.
37. Pawel, D.J., A.E. Kalinowski, Editor. 2019: EPA.
38. M.E. Andrade, C.B., H.J. Khoury, et al., *Organ Doses and Risks of Computed Tomography Examination in Recife, Brazil. .* J. Radiol. Prot. , 2012. **32**: p. 251-260.

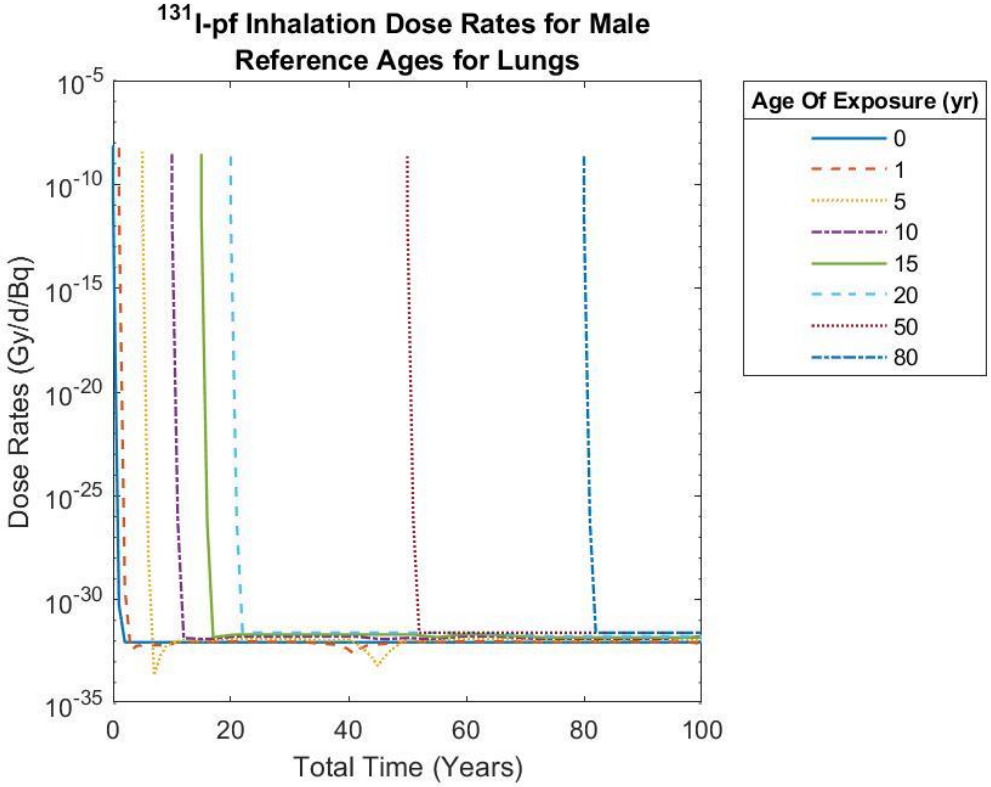
131I-pf Inhalation Dose Rates for Male
Reference Ages for Lungs
Dose Rates (Gy/d/Bq)
Total Time (Years)
Age Of Exposure (yr)
0
1
5
10
15
20
50
80

(a)

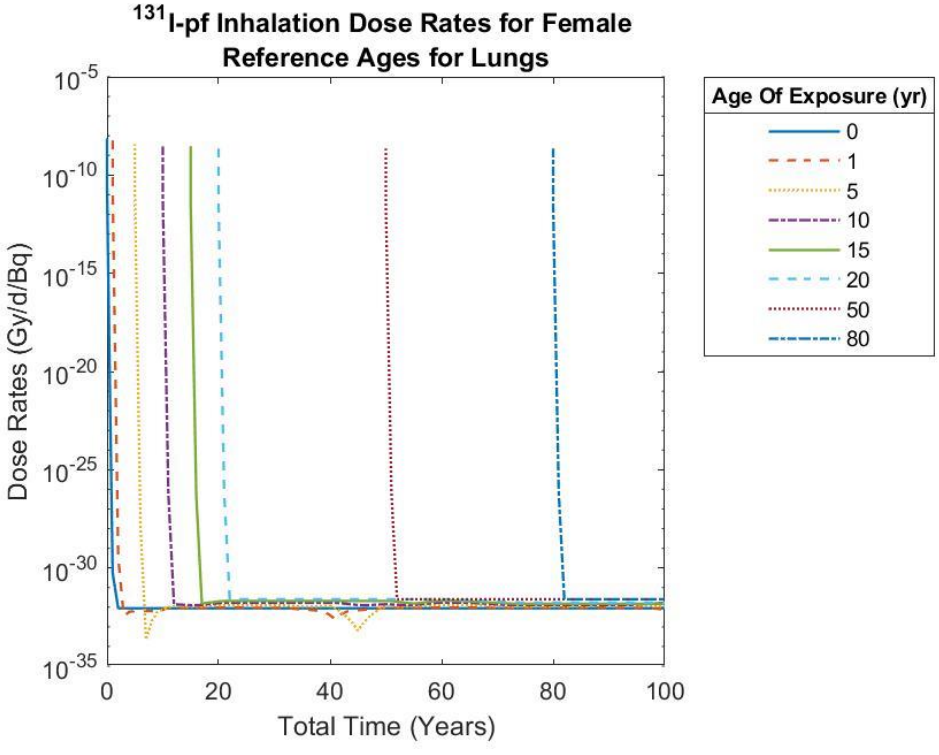
131I-pf Inhalation Dose Rates for Female
Reference Ages for Lungs
Dose Rates (Gy/d/Bq)
Total Time (Years)
Age Of Exposure (yr)
0
1
5
10
15
20
50
80

(b)

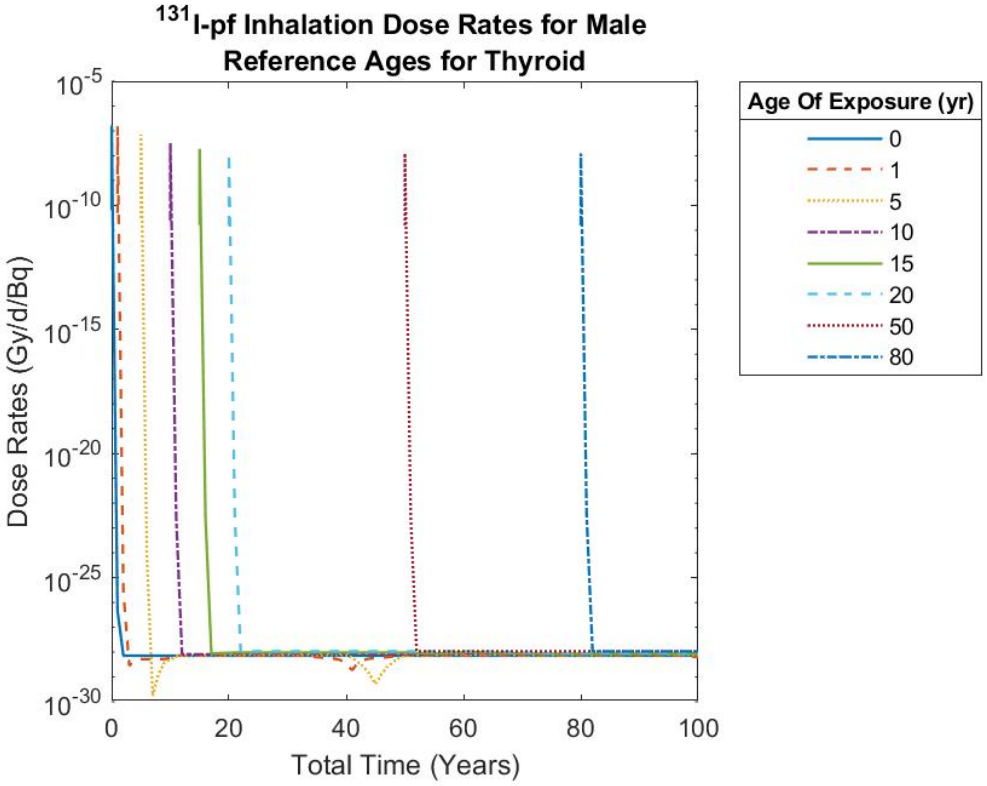

(c)

Figure 101. Dose rates for fast clearing ^{131}I in the (a) male lungs, (b) female lungs, and (c) male thyroid.

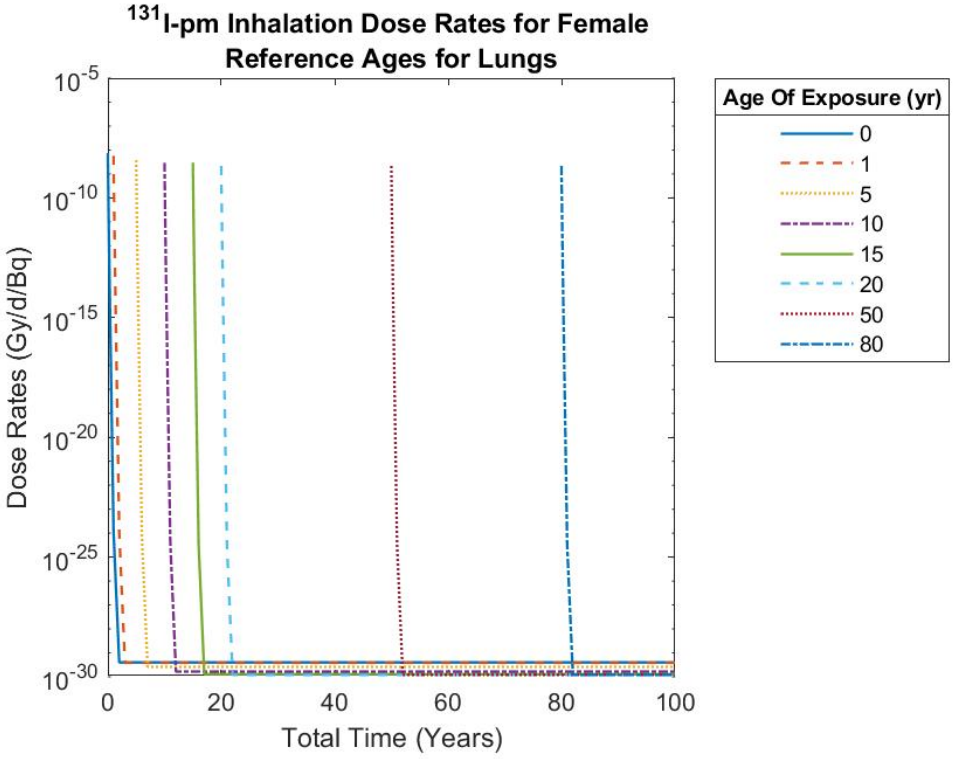

(a)

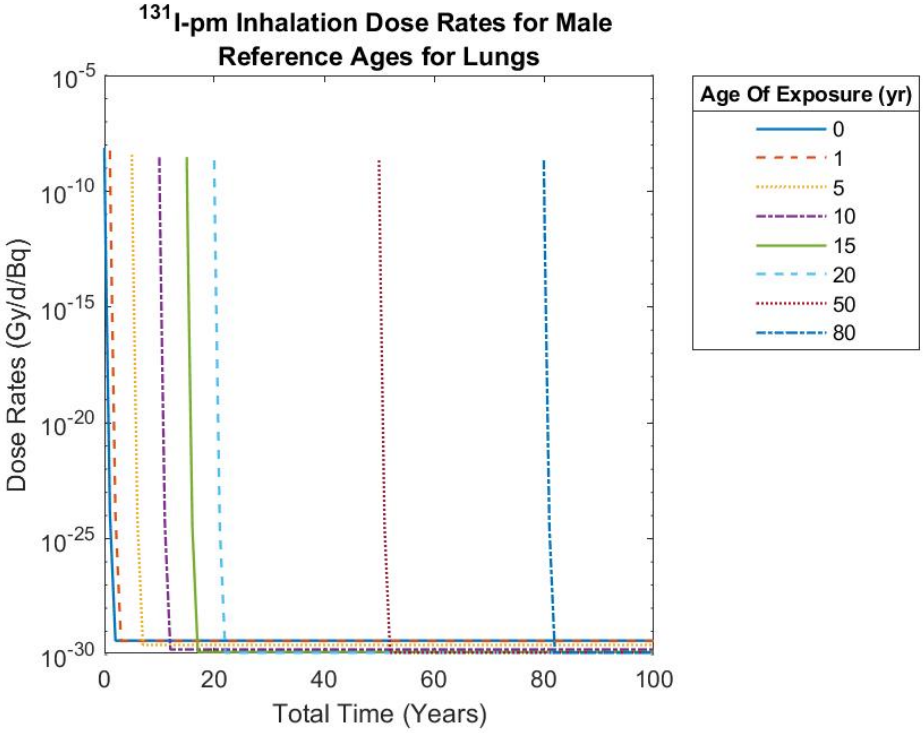

(b)

Figure 102. Dose rates for moderate clearing ^{131}I in the (a) female lungs and (b) male lungs.

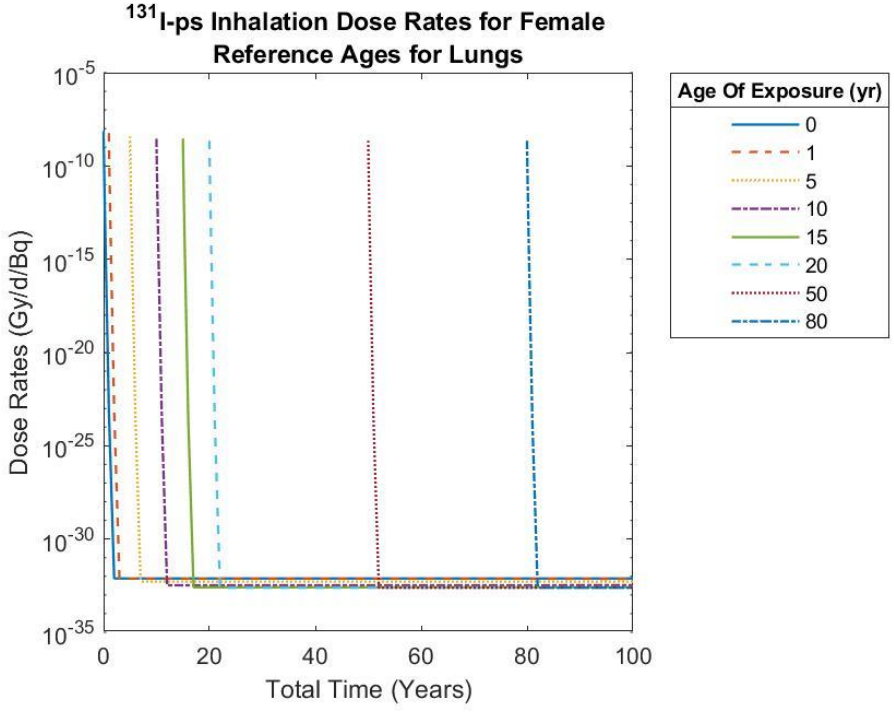

(a)

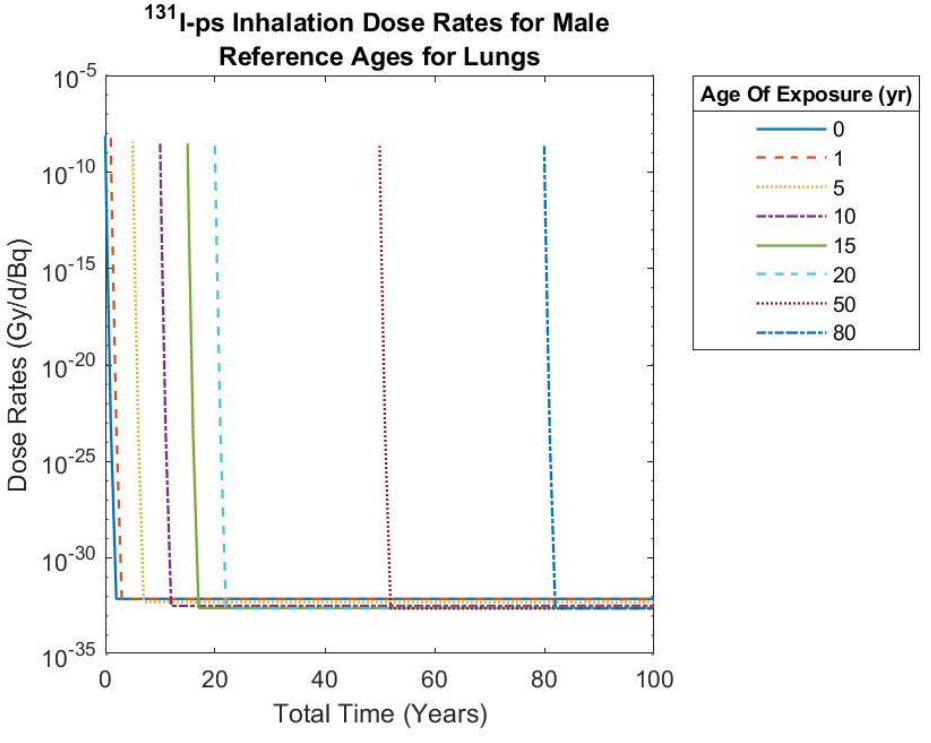

(b)

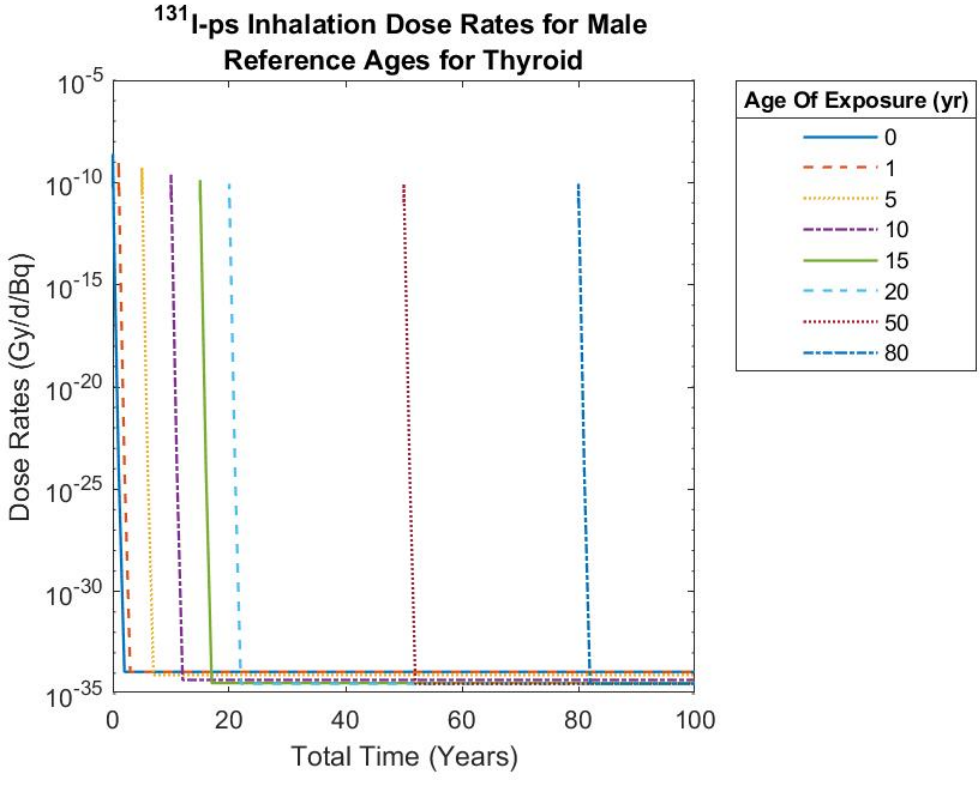

(c)

Figure 103. Dose rates for fast clearing ^{131}I in the (a) female lungs, (b) male lungs, and (c) male thyroid.

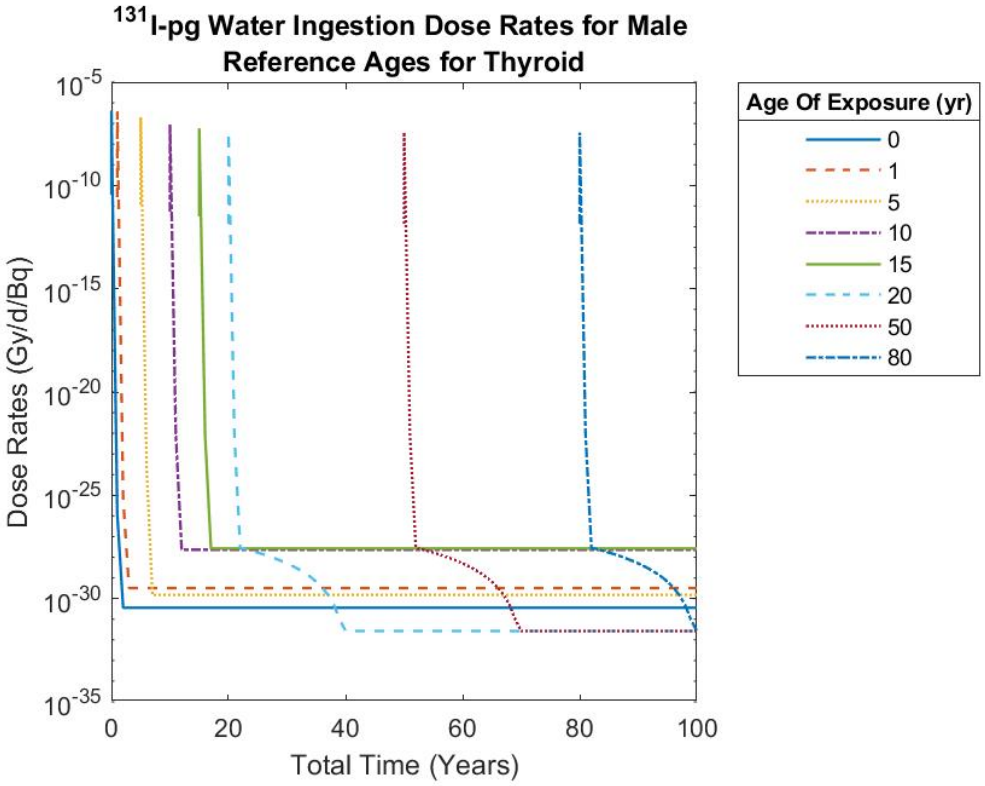

Figure 104. Dose rates due to tap water ingest ^{131}I to the male thyroid.

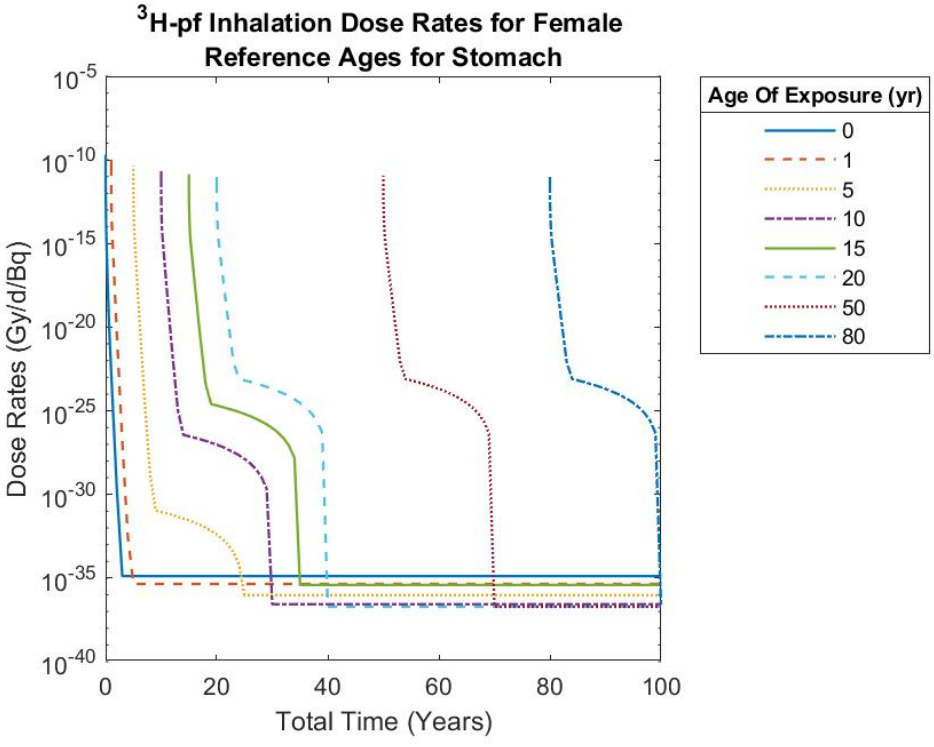

(a)

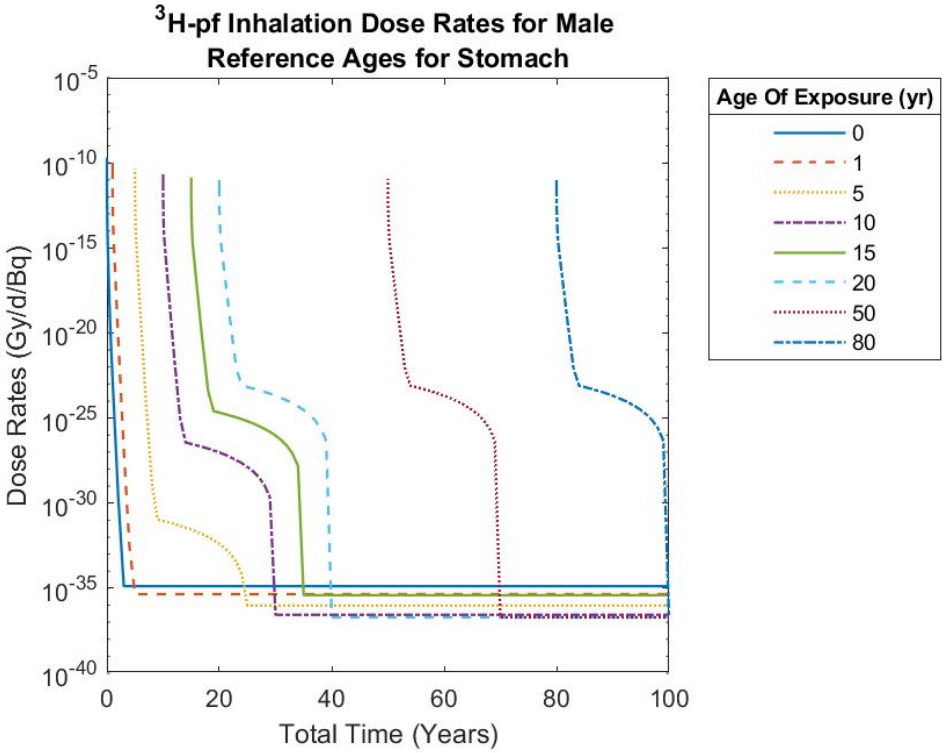

(b)

Figure 105. Dose rates due to fast clearing tritium in the (a) female stomach and (b) male stomach.

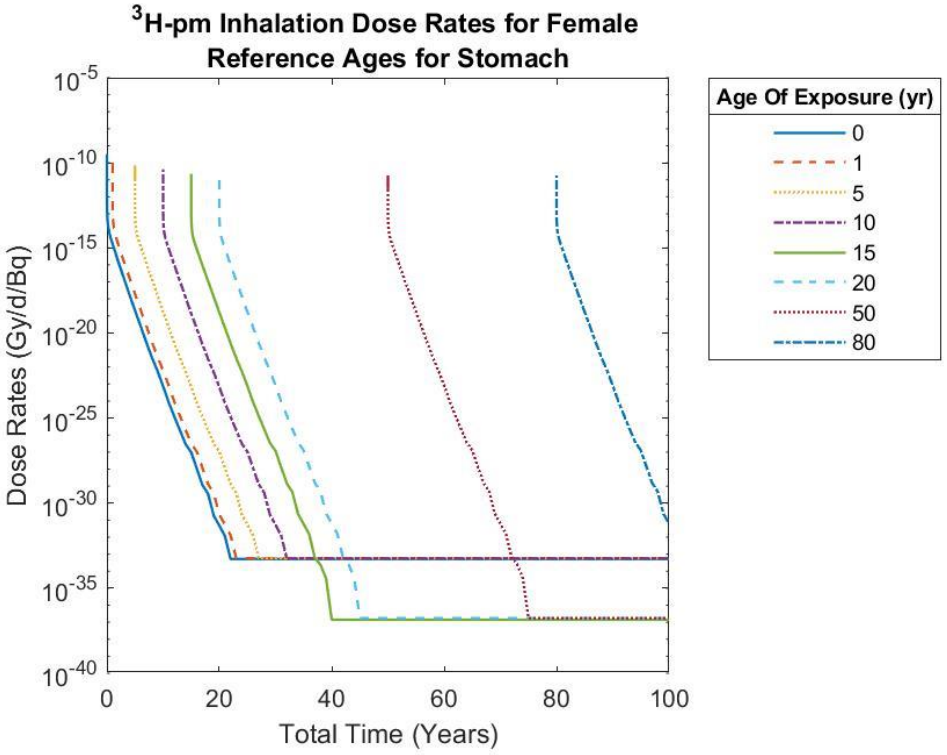

(a)

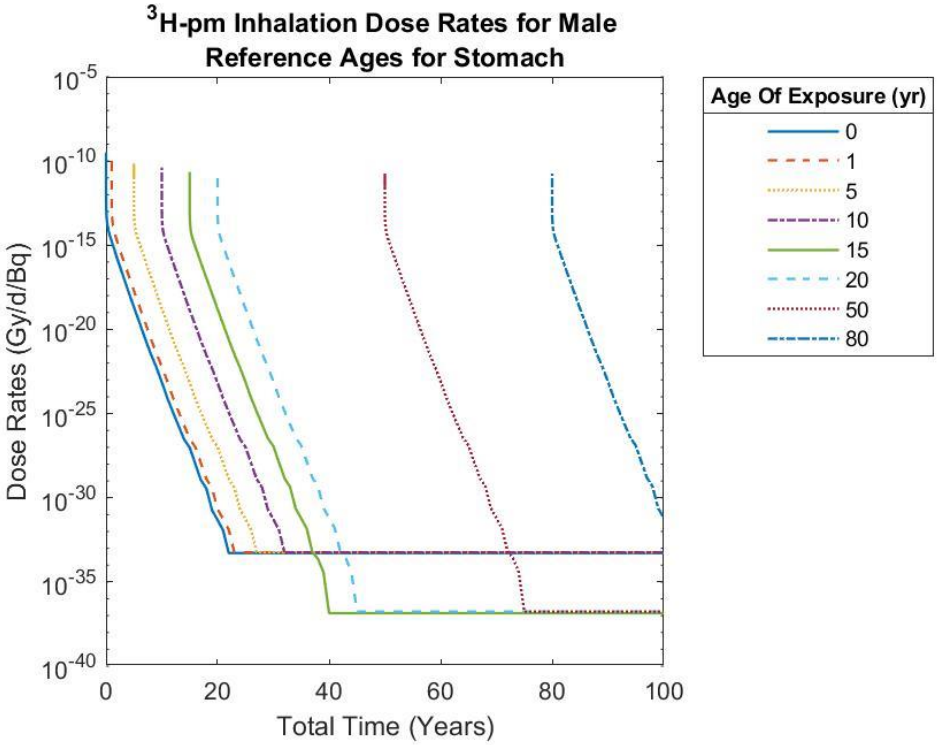

(b)

Figure 106. Dose rates due to moderate clearing tritium in the (a) female stomach and (b) male stomach.

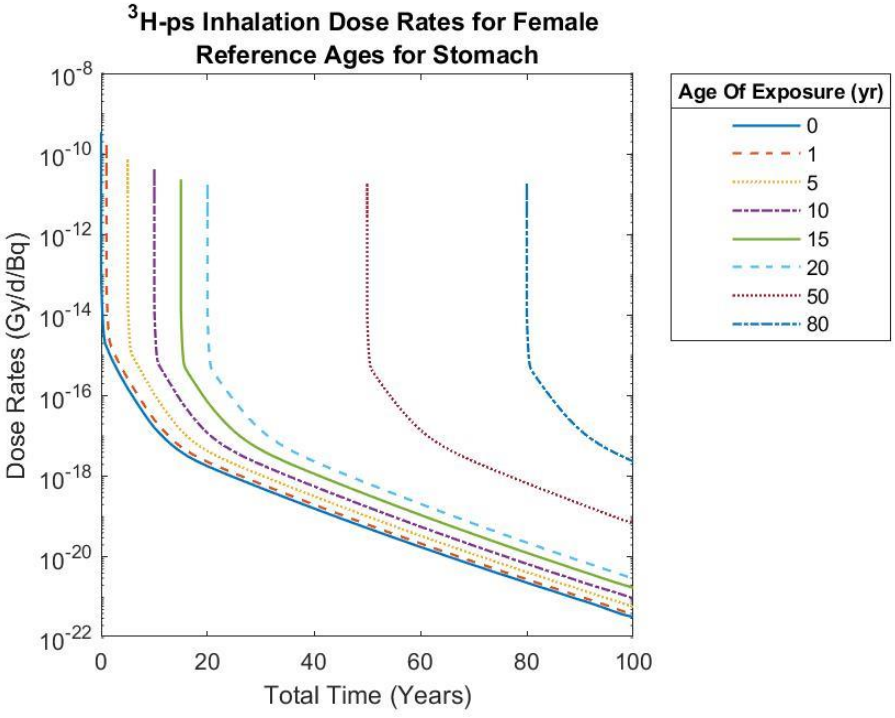

(a)

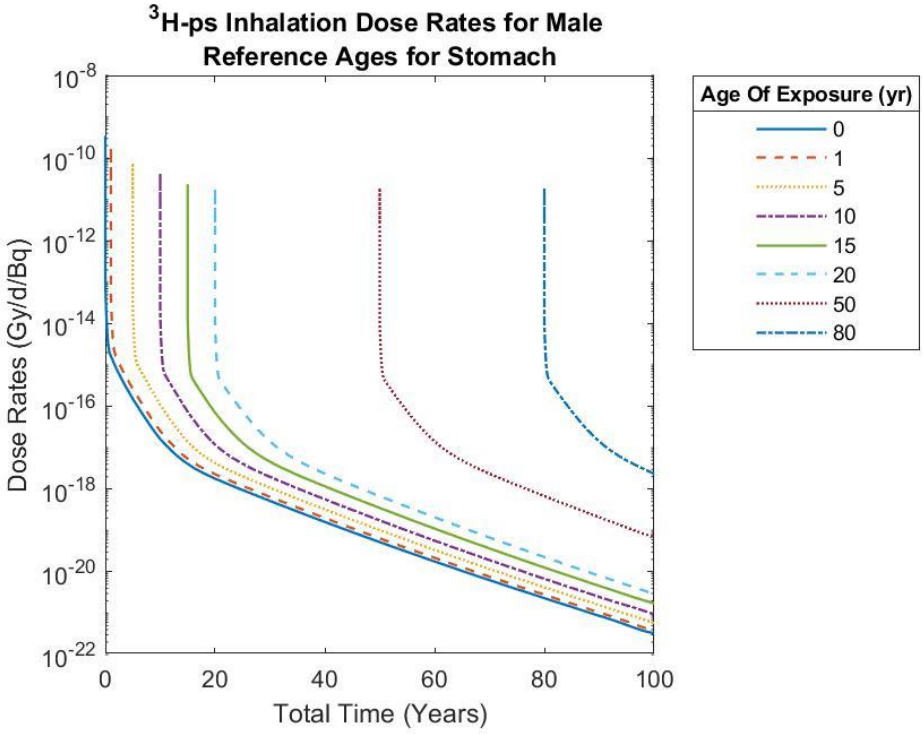

(b)

Figure 107. Dose rates due to slow clearing tritium in the (a) female stomach and (b) male stomach.

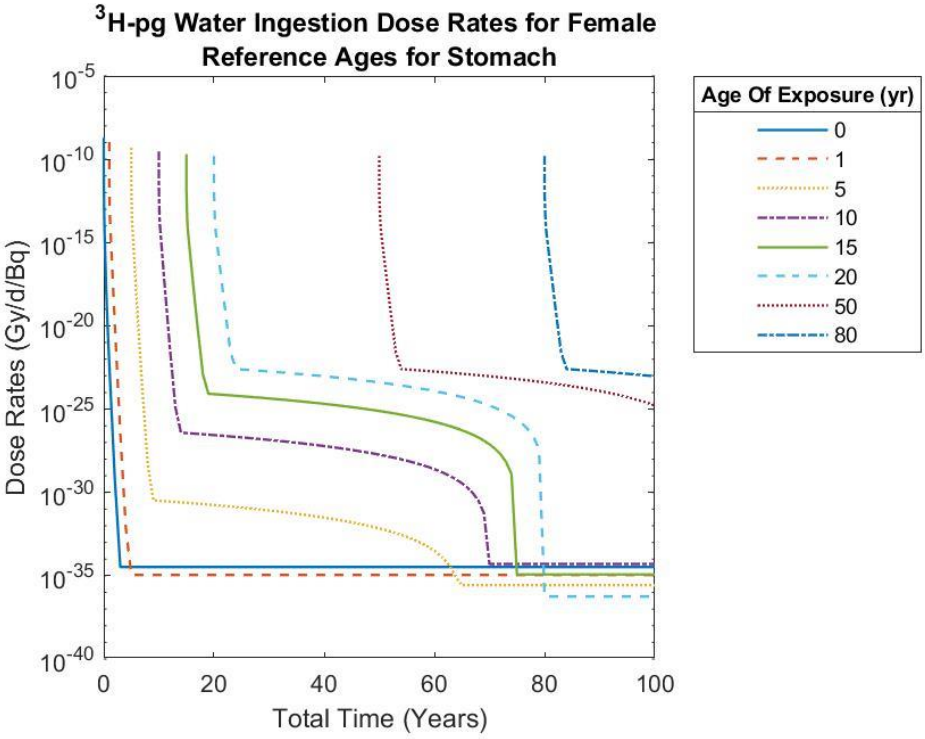

(a)

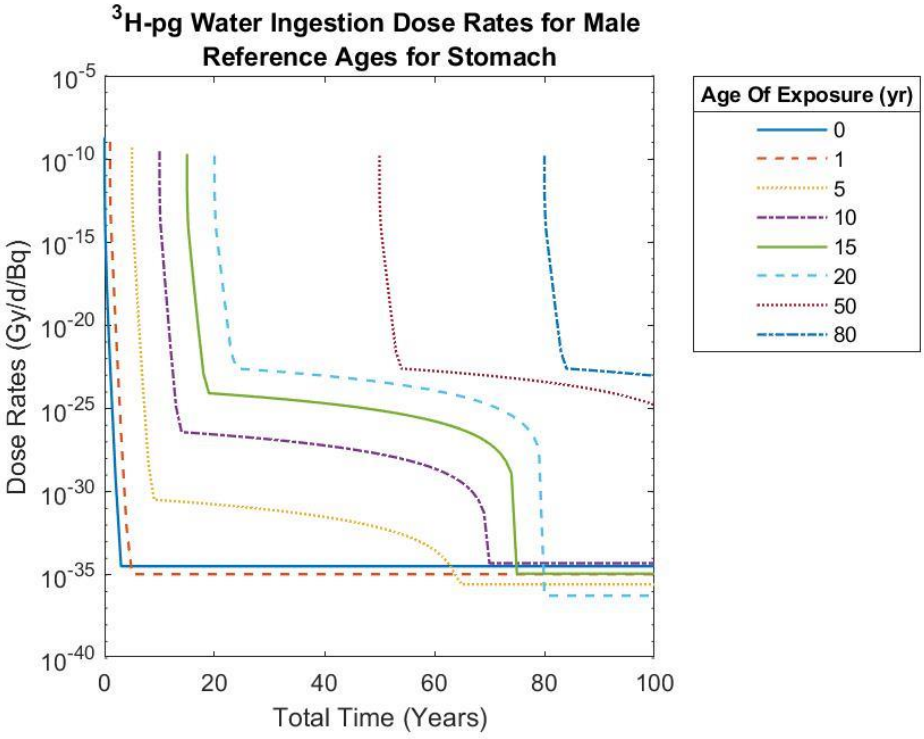

(b)

Figure 108. Dose rates due to tap water ingested tritium in the (a) female stomach and (b) male stomach.

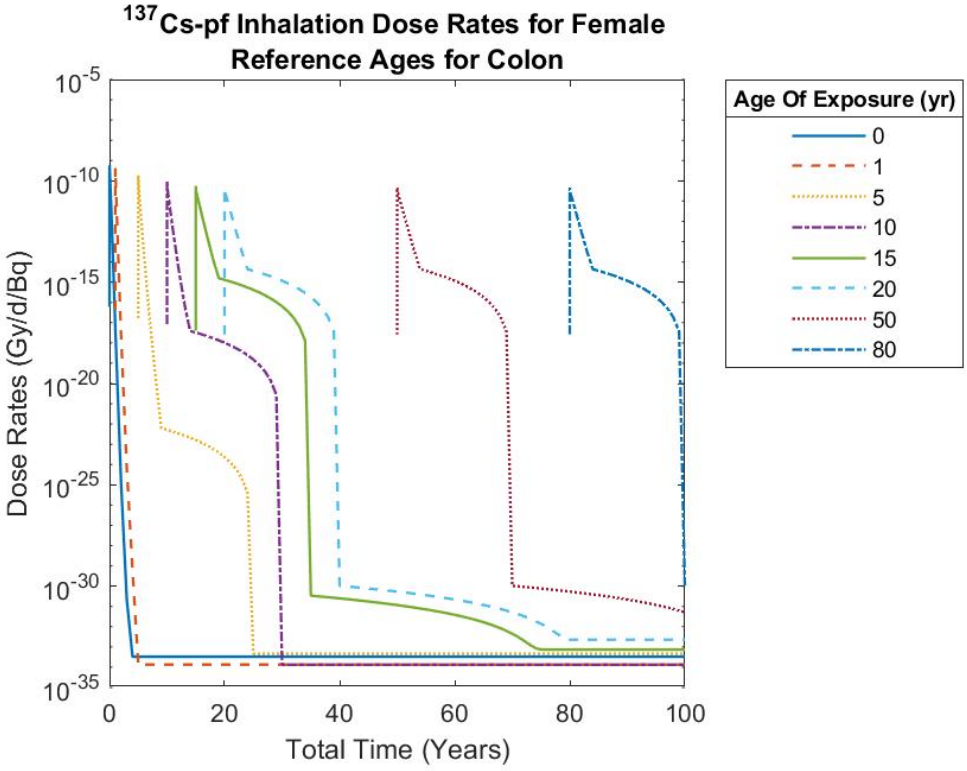

(a)

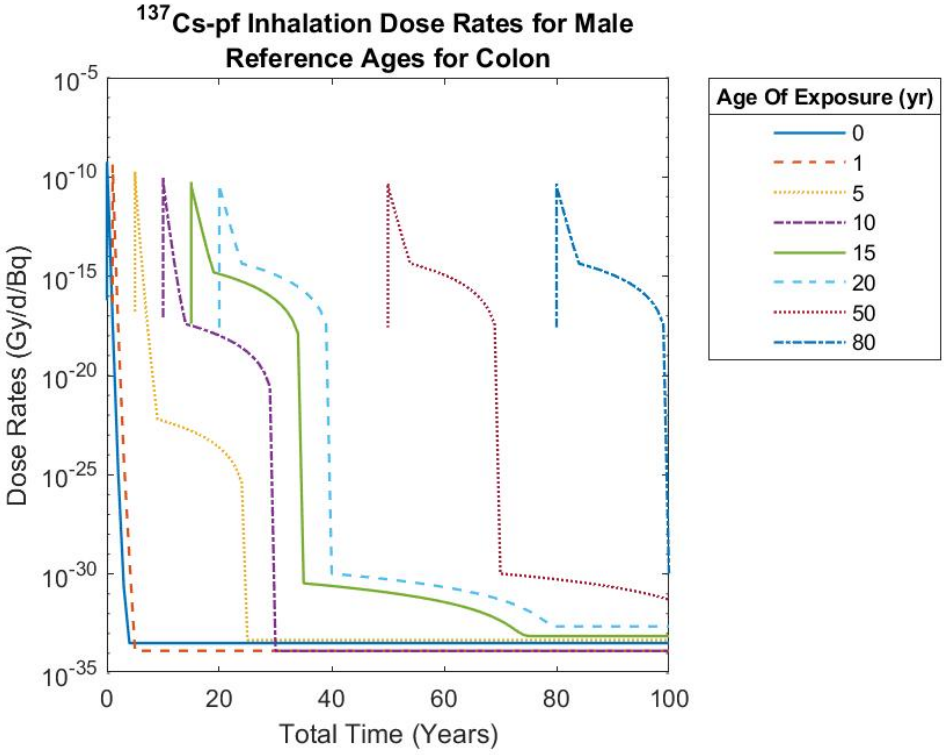
^{137}Cs-pf Inhalation Dose Rates for Male
Reference Ages for Colon
Dose Rates (Gy/d/Bq)
Total Time (Years)
Age Of Exposure (yr)
0
1
5
10
15
20
50
80

(b)

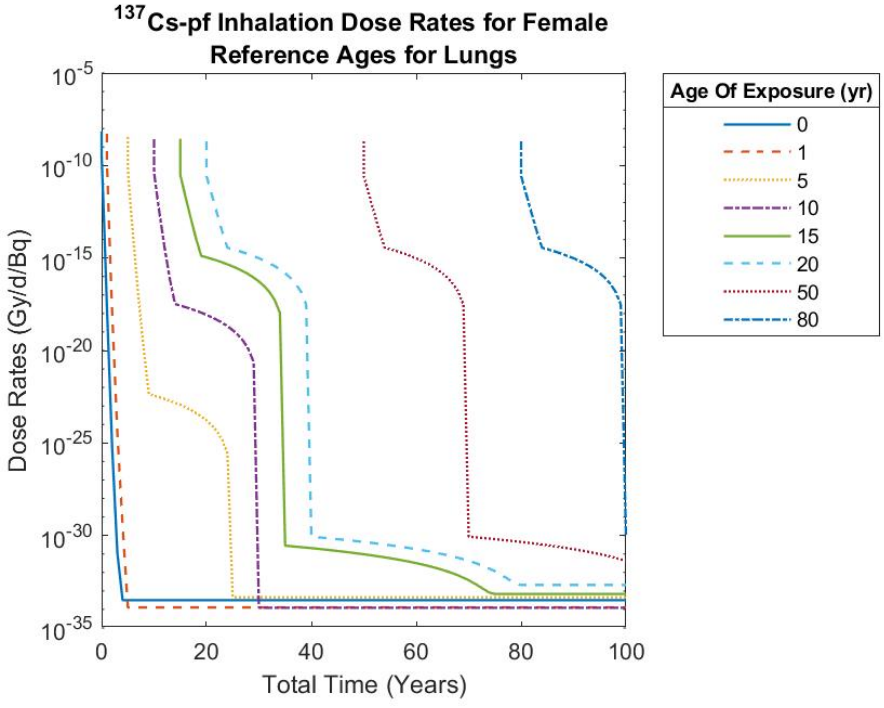
^{137}Cs-pf Inhalation Dose Rates for Female
Reference Ages for Lungs
Dose Rates (Gy/d/Bq)
Total Time (Years)
Age Of Exposure (yr)
0
1
5
10
15
20
50
80

(c)

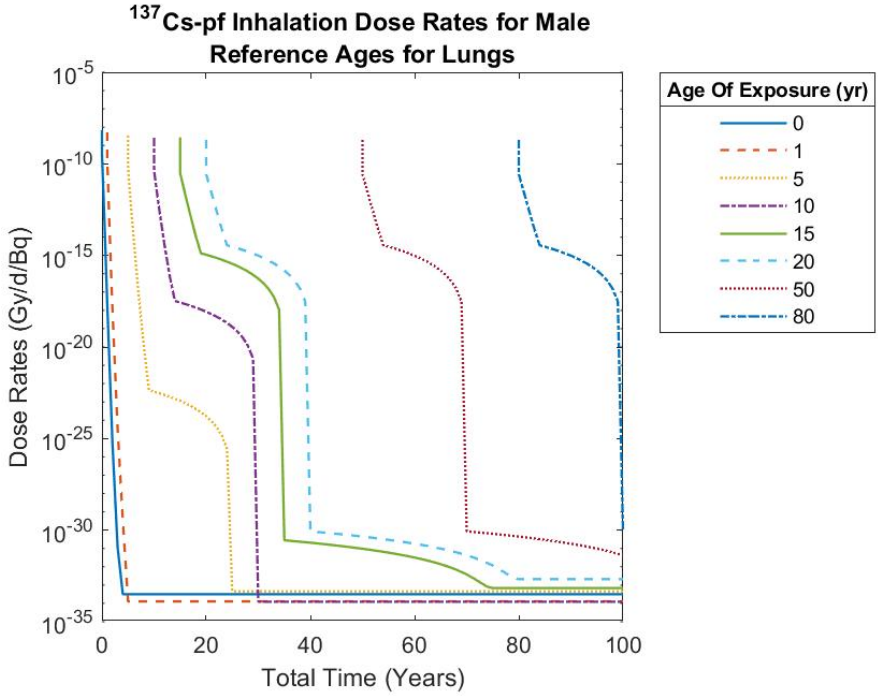

(d)

Figure 109. Dose rates due to fast clearing ^{137}Cs in the (a) female colon, (b) male colon, (c) female lungs, (d) male lungs.

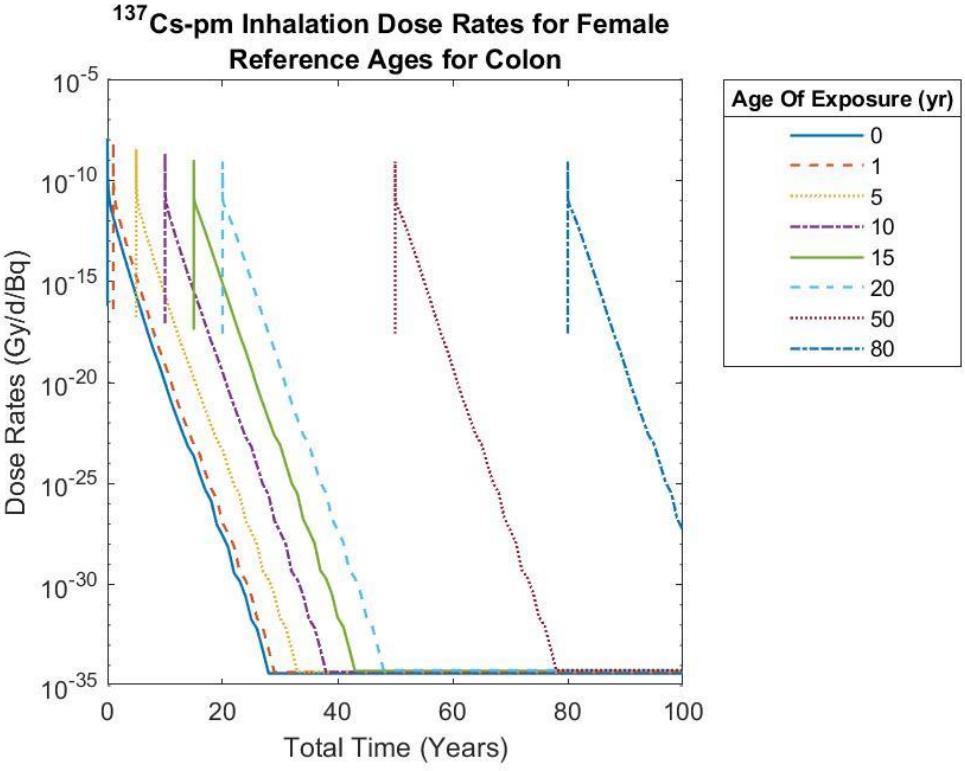

(a)

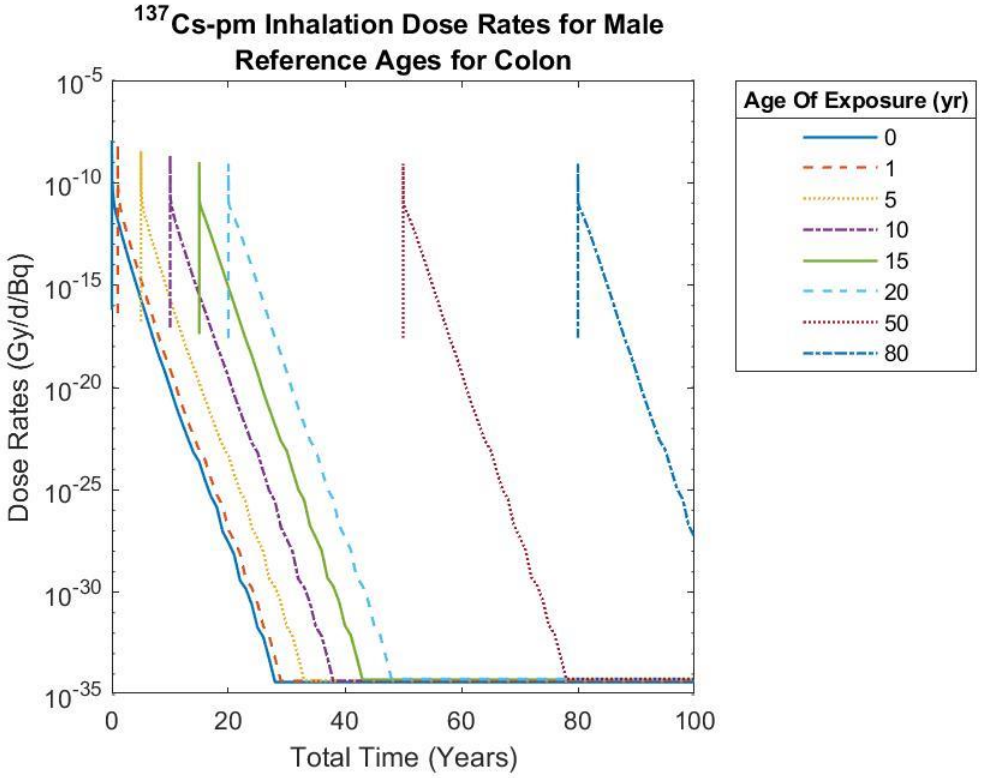
137Cs-pm Inhalation Dose Rates for Male
Reference Ages for Colon
Dose Rates (Gy/d/Bq)
Total Time (Years)
Age Of Exposure (yr)
0
1
5
10
15
20
50
80

(b)

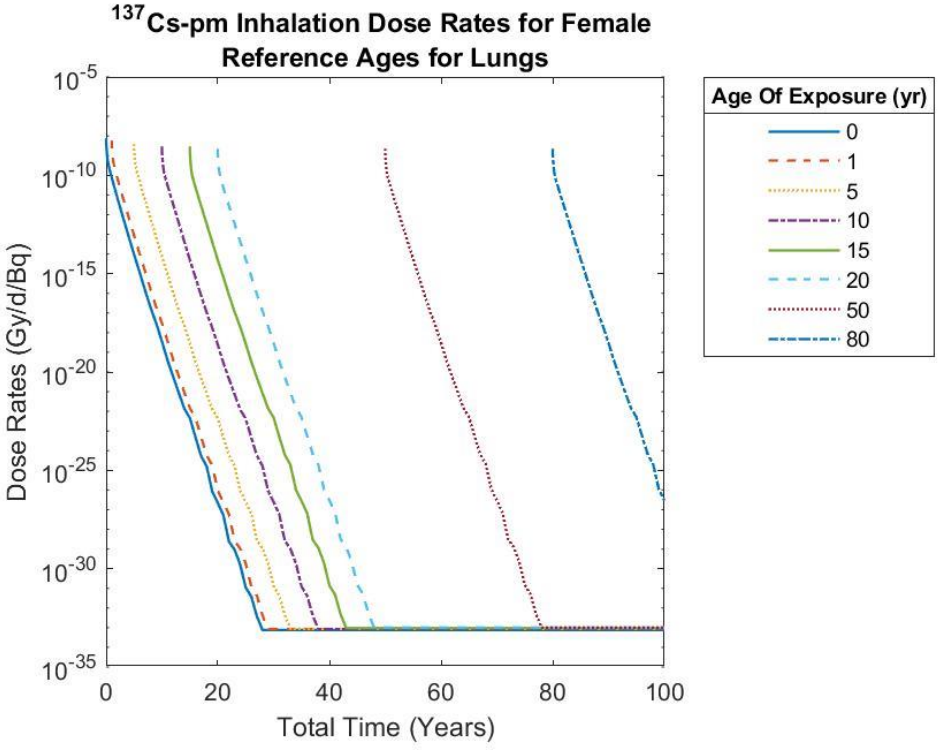
137Cs-pm Inhalation Dose Rates for Female
Reference Ages for Lungs
Dose Rates (Gy/d/Bq)
Total Time (Years)
Age Of Exposure (yr)
0
1
5
10
15
20
50
80

(c)

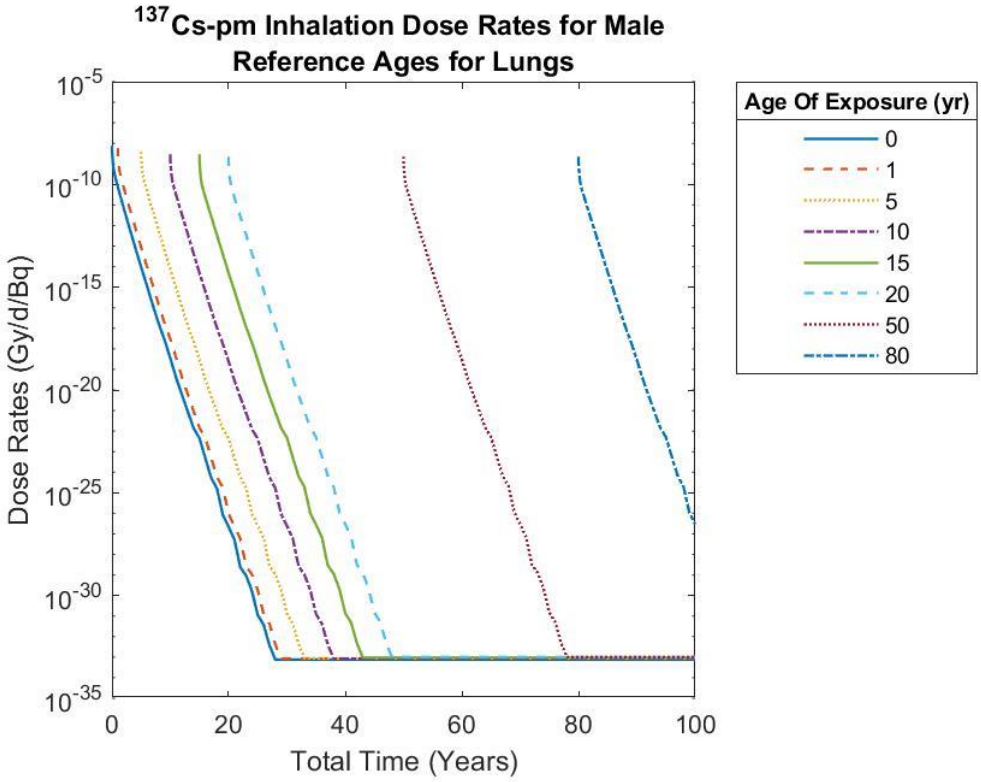

(d)

Figure 110. Dose rates due to moderate clearing ^{137}Cs in the (a) female colon, (b) male colon, (c) female lungs, (d) male lungs.

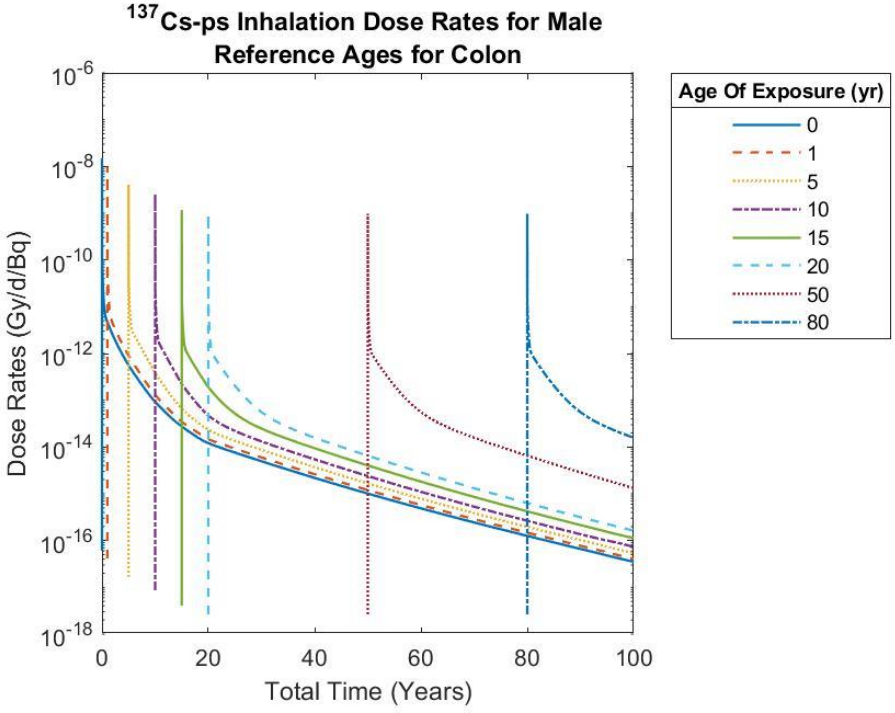

(a)

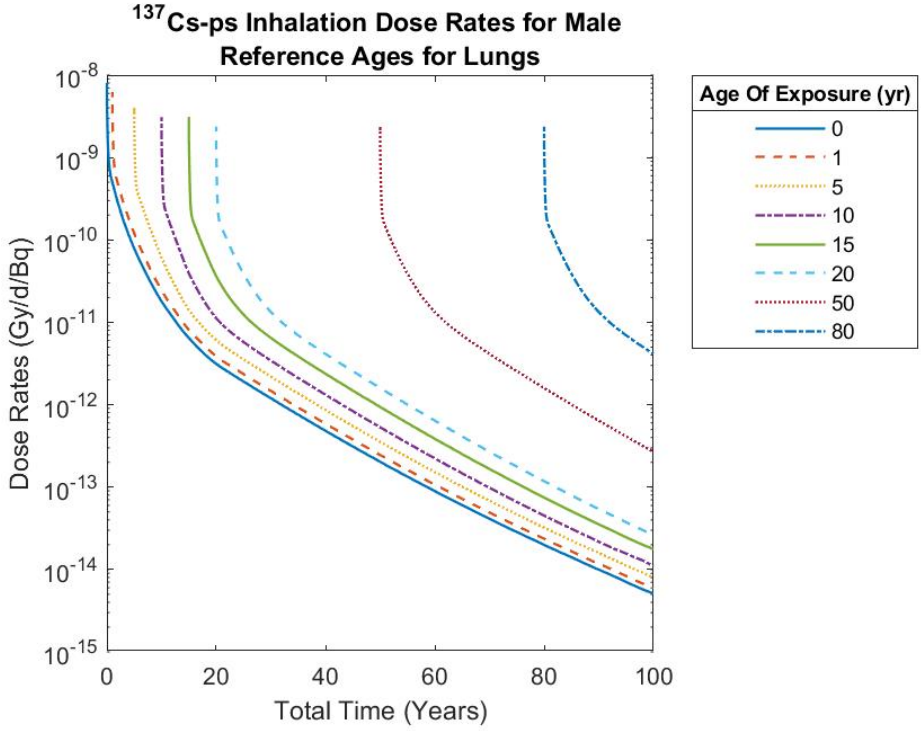

(b)

Figure 111. Dose rates due to slow clearing ^{137}Cs to the (a) male colon and (b) male lungs.

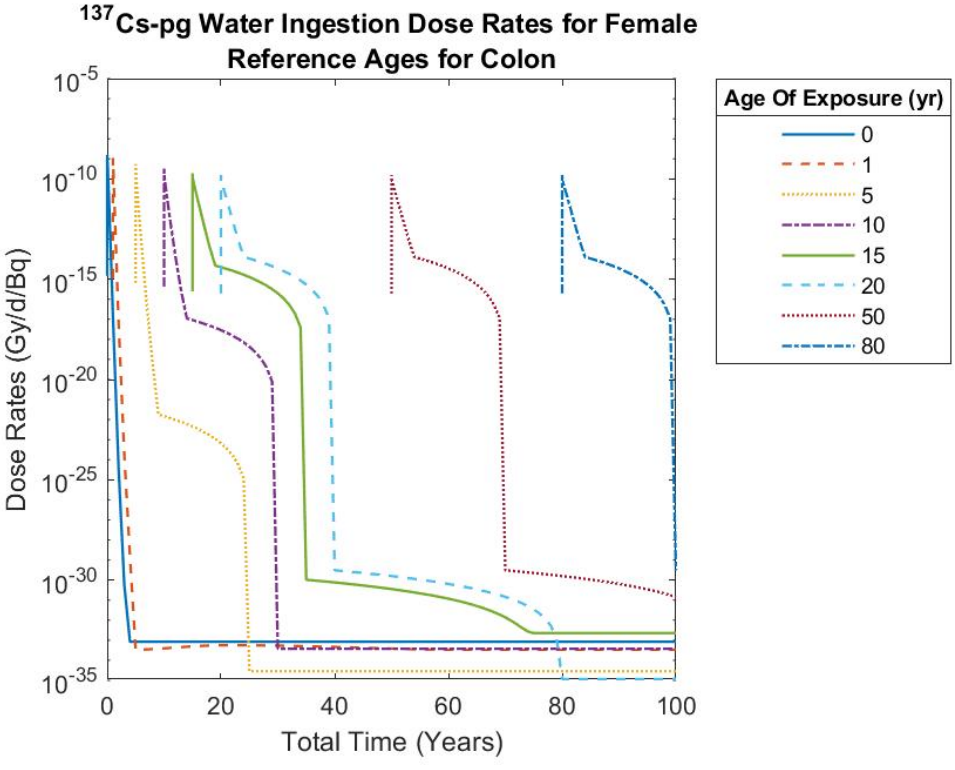

(a)

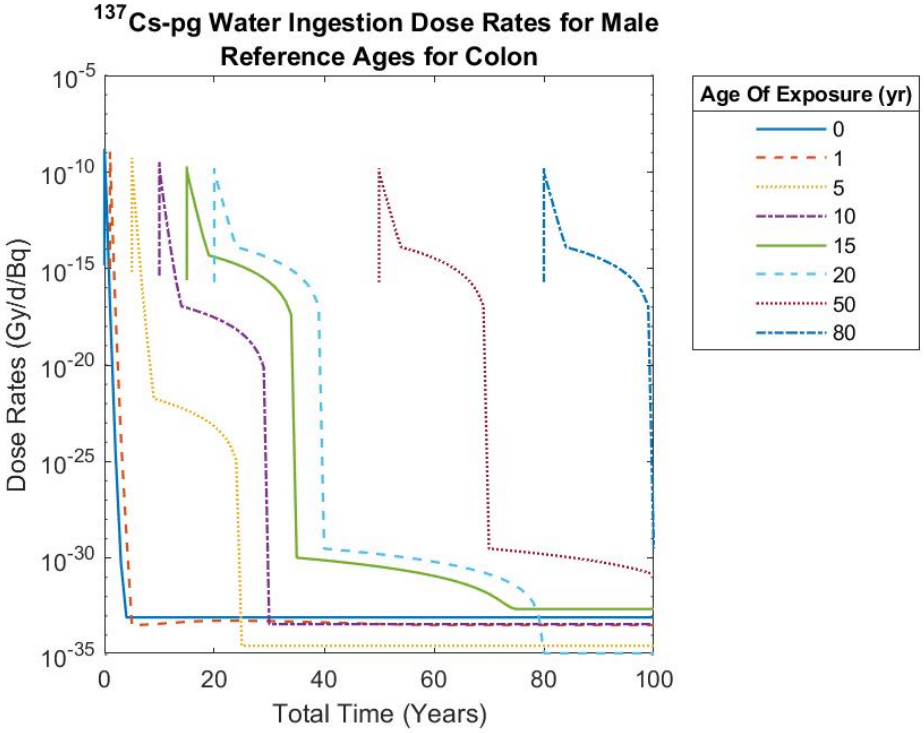
^{137}Cs-pg Water Ingestion Dose Rates for Male
Reference Ages for Colon
Dose Rates (Gy/d/Bq)
Total Time (Years)
Age Of Exposure (yr)
0
1
5
10
15
20
50
80

(b)

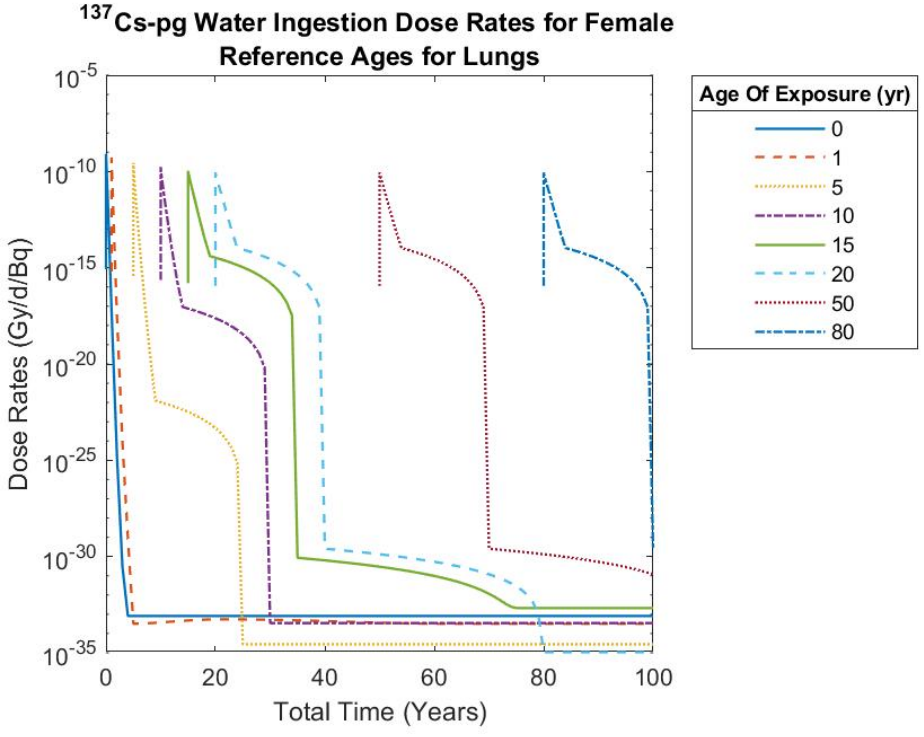
^{137}Cs-pg Water Ingestion Dose Rates for Female
Reference Ages for Lungs
Dose Rates (Gy/d/Bq)
Total Time (Years)
Age Of Exposure (yr)
0
1
5
10
15
20
50
80

(c)

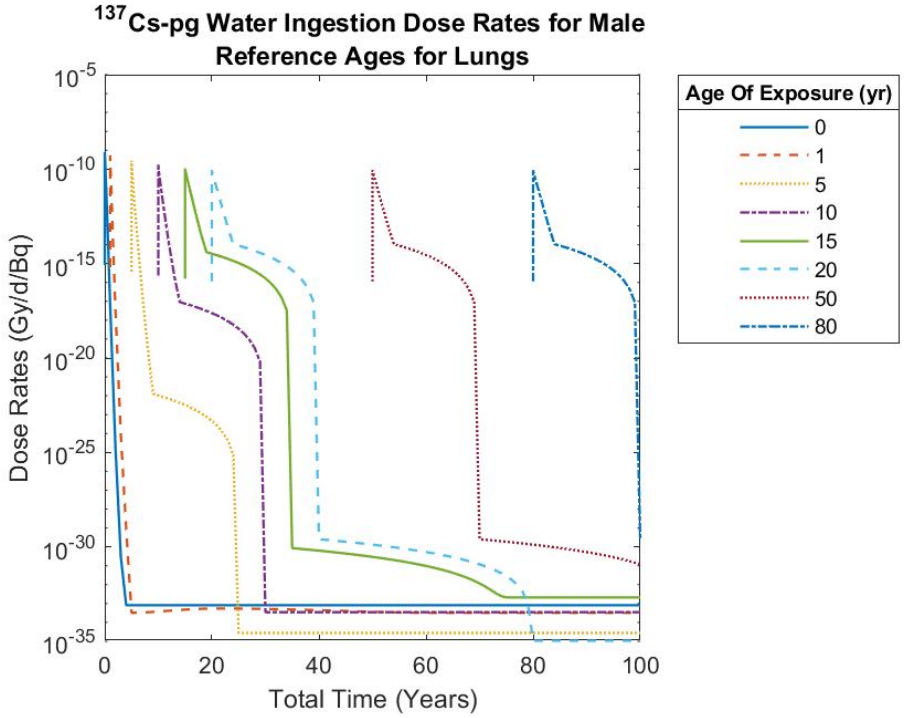

(d)

Figure 112. Dose rates due to tap water ingested ^{137}Cs in the (a) female colon, (b) male colon, (c) female lungs, (d) male lungs.

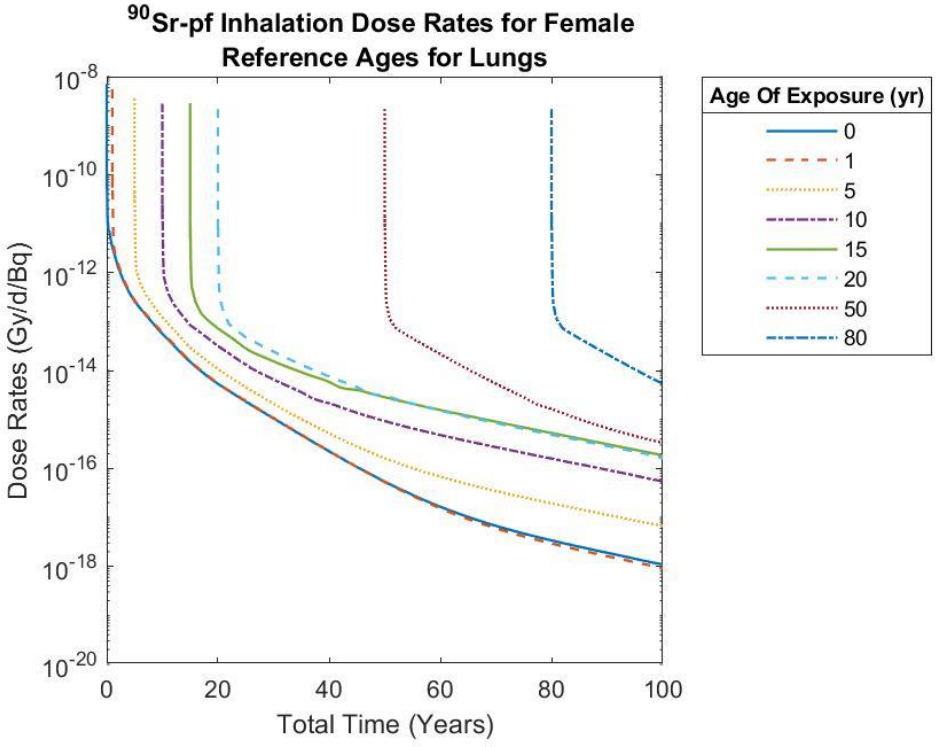

(a)

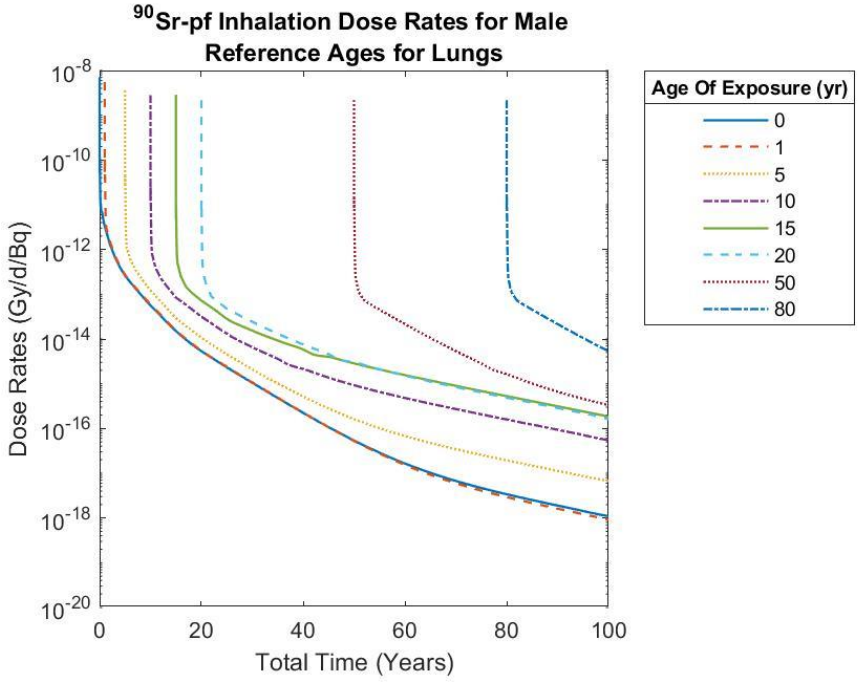

(b)

Figure 113. Dose rates due to fast clearing ^{90}Sr in the (a) female lungs and (b) male lungs

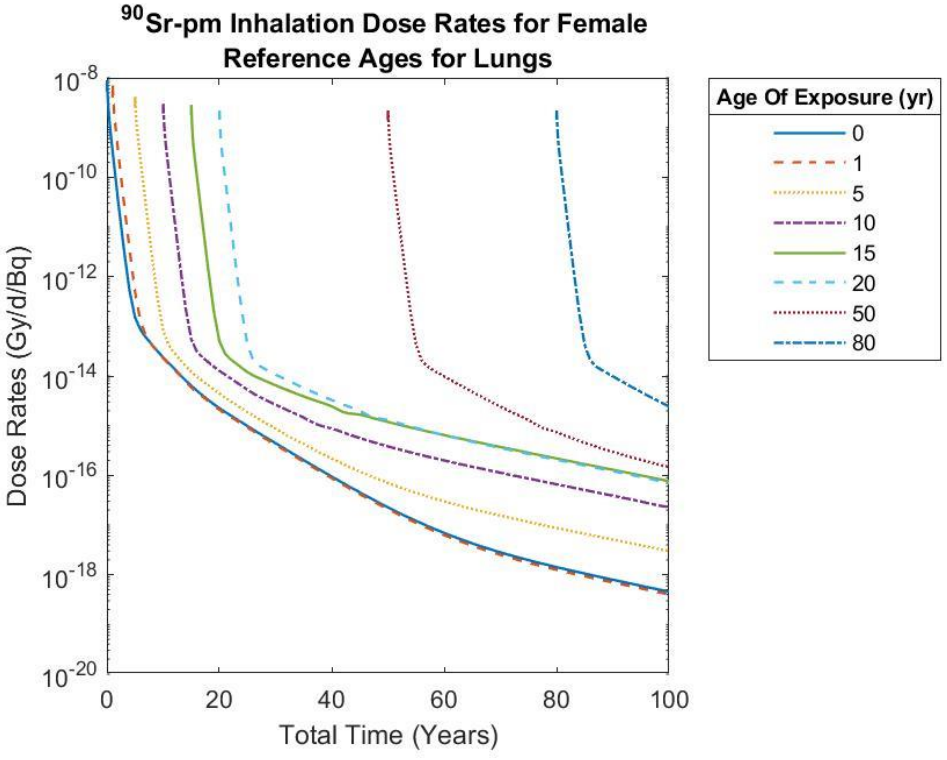

(a)

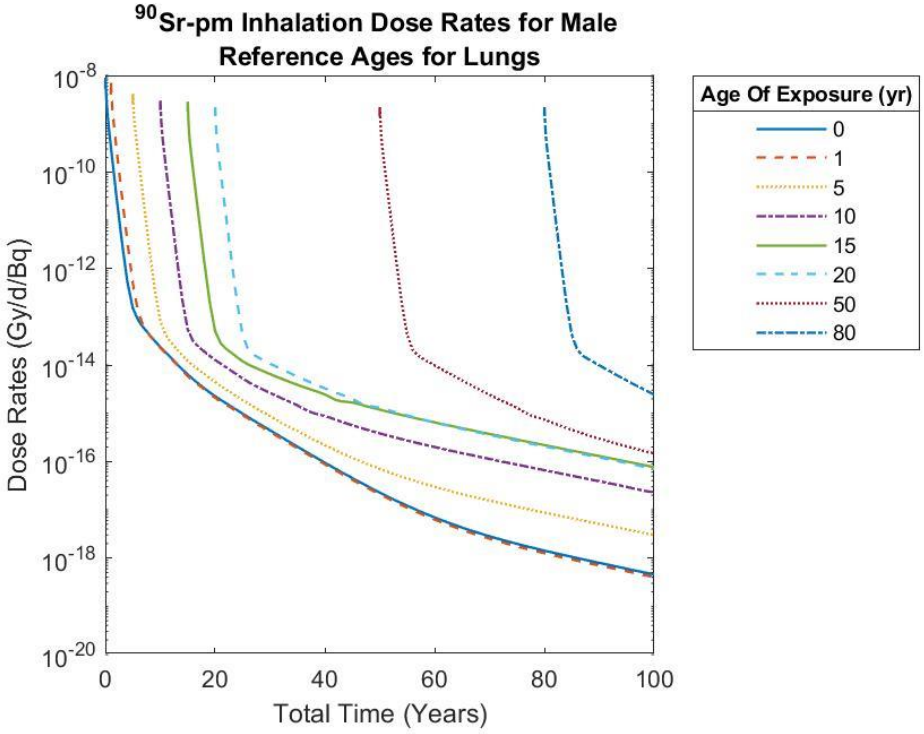
^{90}Sr-pm Inhalation Dose Rates for Male
Reference Ages for Lungs
Dose Rates (Gy/d/Bq)
Total Time (Years)
Age Of Exposure (yr)
0
1
5
10
15
20
50
80

(b)

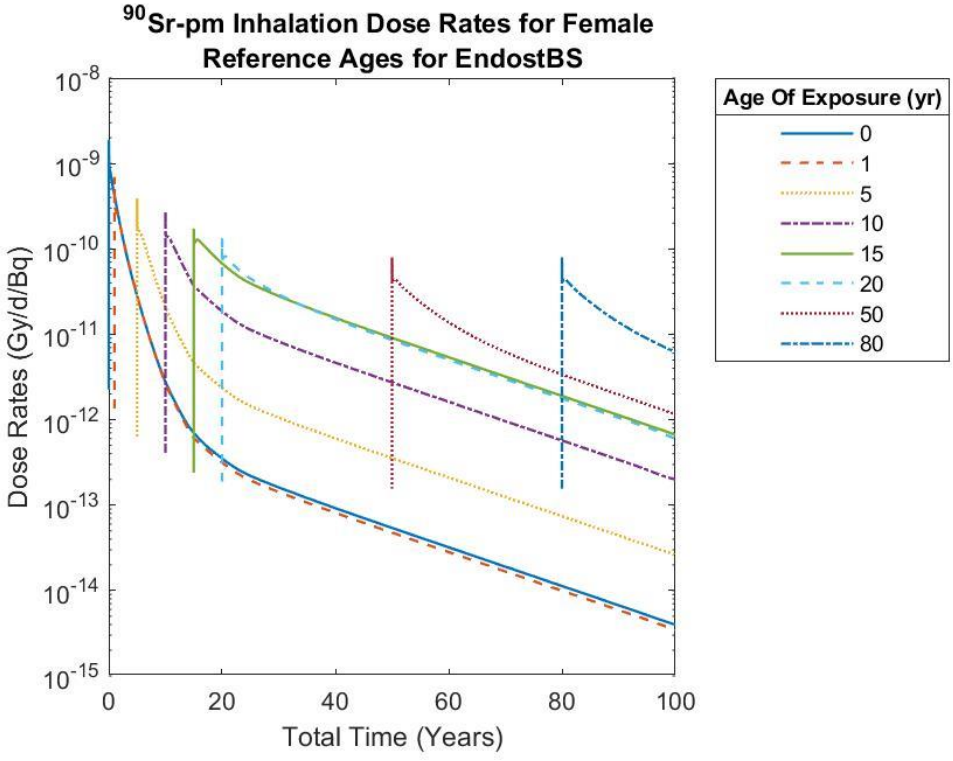
^{90}Sr-pm Inhalation Dose Rates for Female
Reference Ages for EndostBS
Dose Rates (Gy/d/Bq)
Total Time (Years)
Age Of Exposure (yr)
0
1
5
10
15
20
50
80

(c)

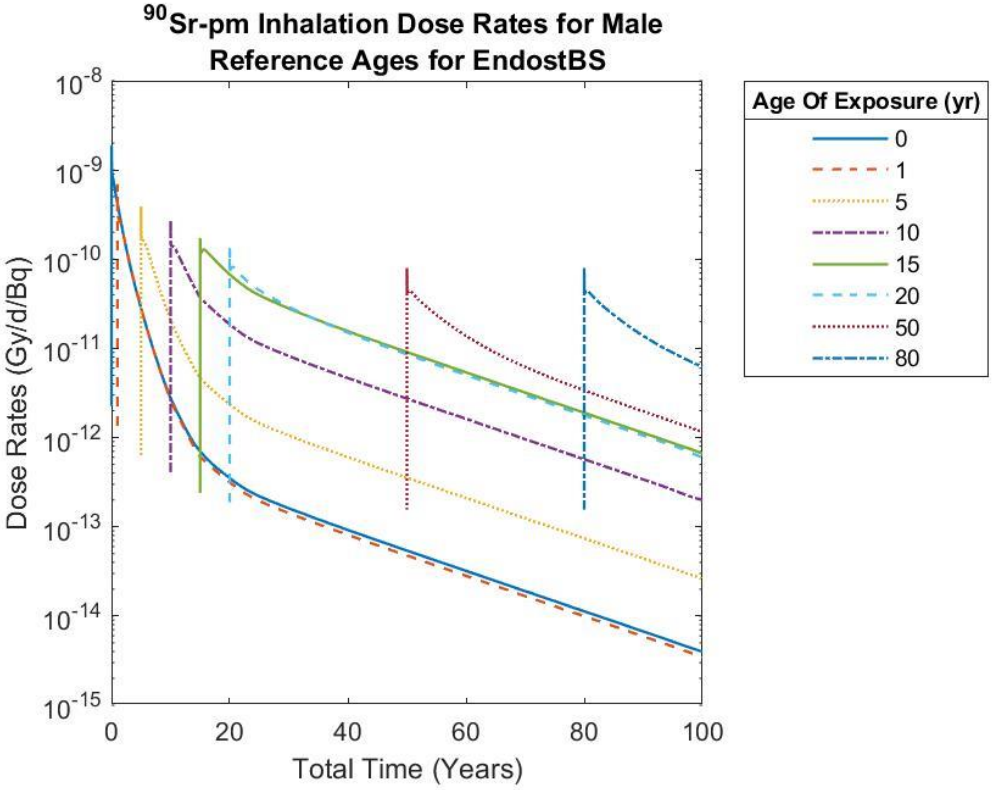

(d)

Figure 114. Dose rates due to fast clearing ^{90}Sr in the (a) female lungs, (b) male lungs, (c) female bone surface, and (d) male bone surface.

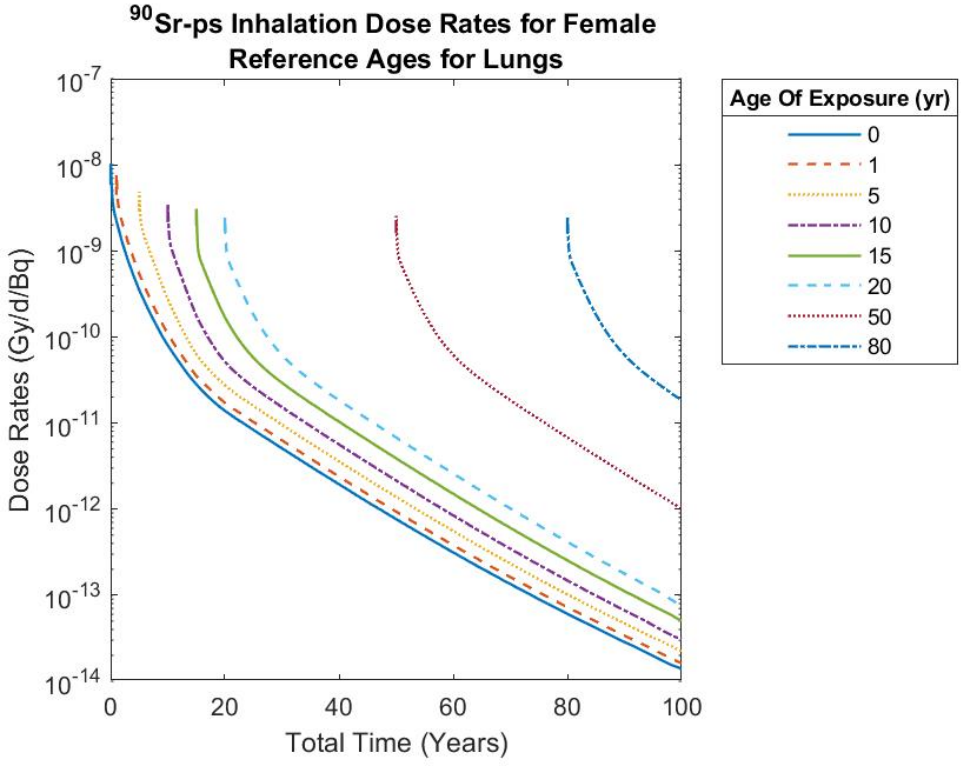

(a)

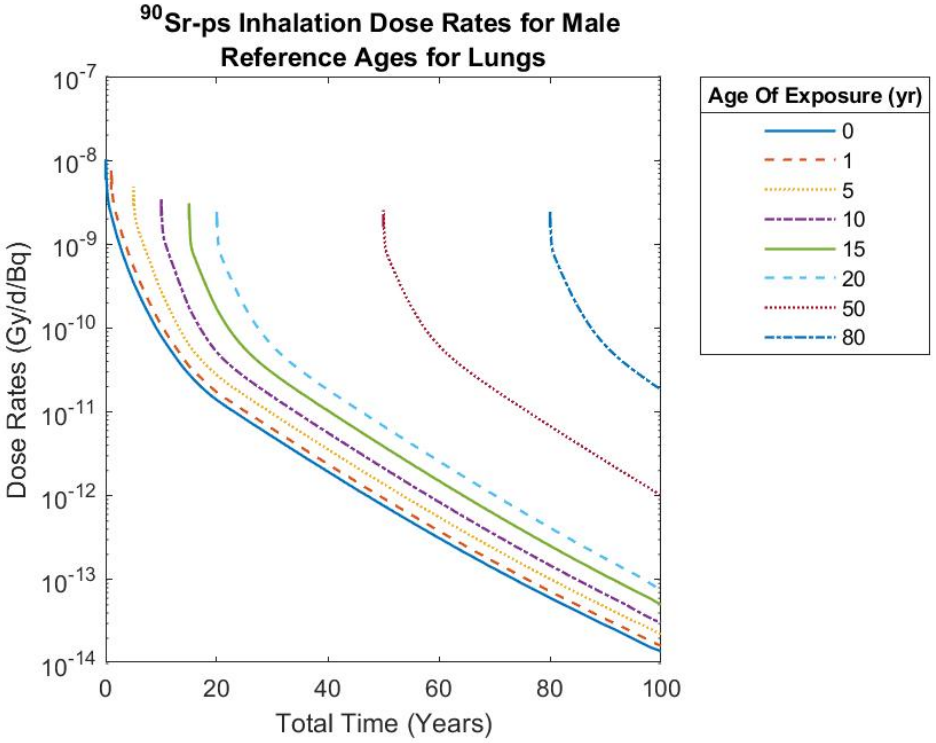

(b)

Figure 115. Dose rates due to slow clearing ^{90}Sr in the (a) female lungs and (b) male lungs.

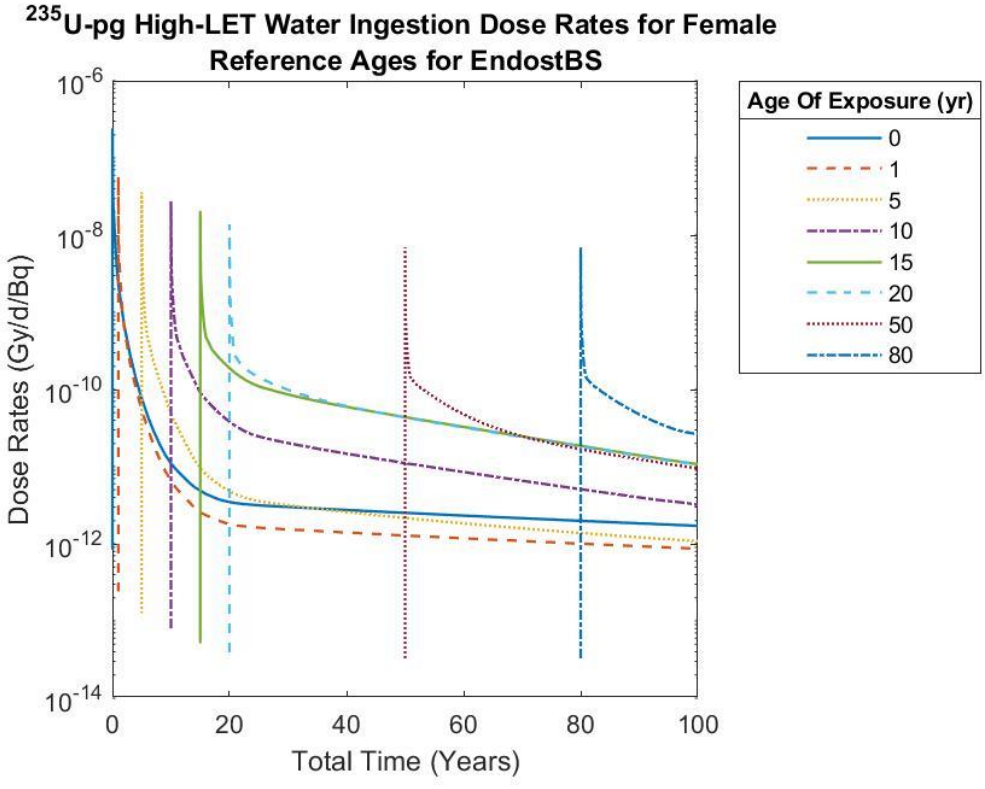

(a)

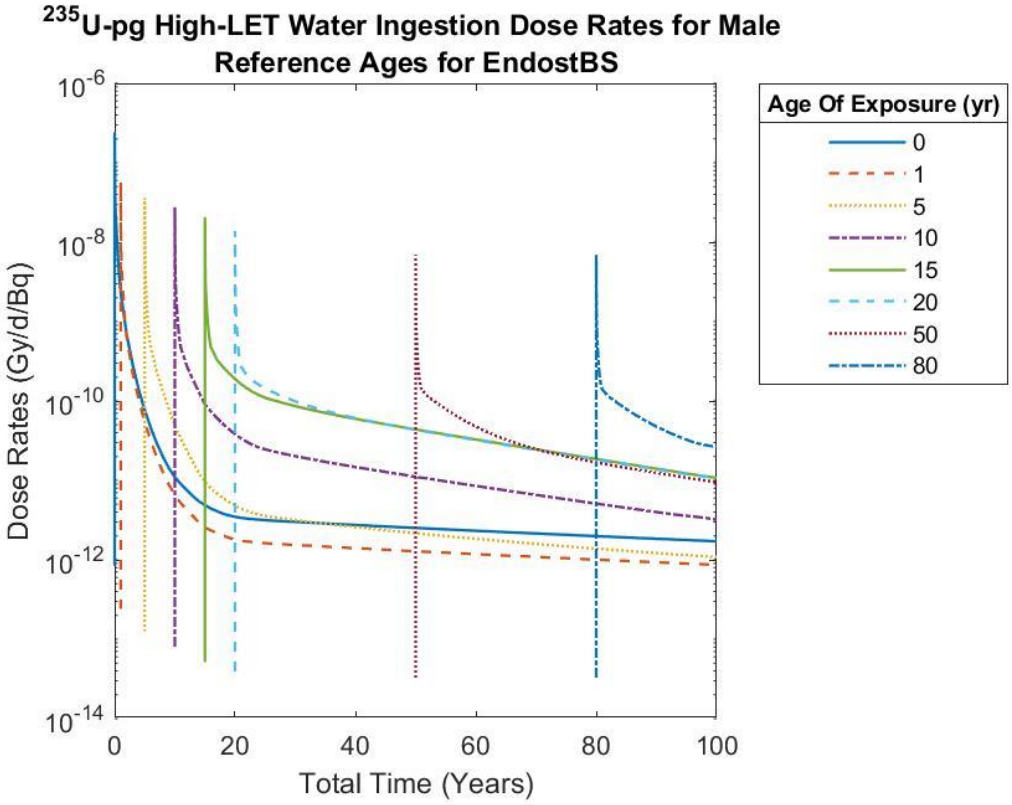
235U-pg High-LET Water Ingestion Dose Rates for Male
Reference Ages for EndostBS
Dose Rates (Gy/d/Bq)
Total Time (Years)
Age Of Exposure (yr)
0
1
5
10
15
20
50
80

(b)

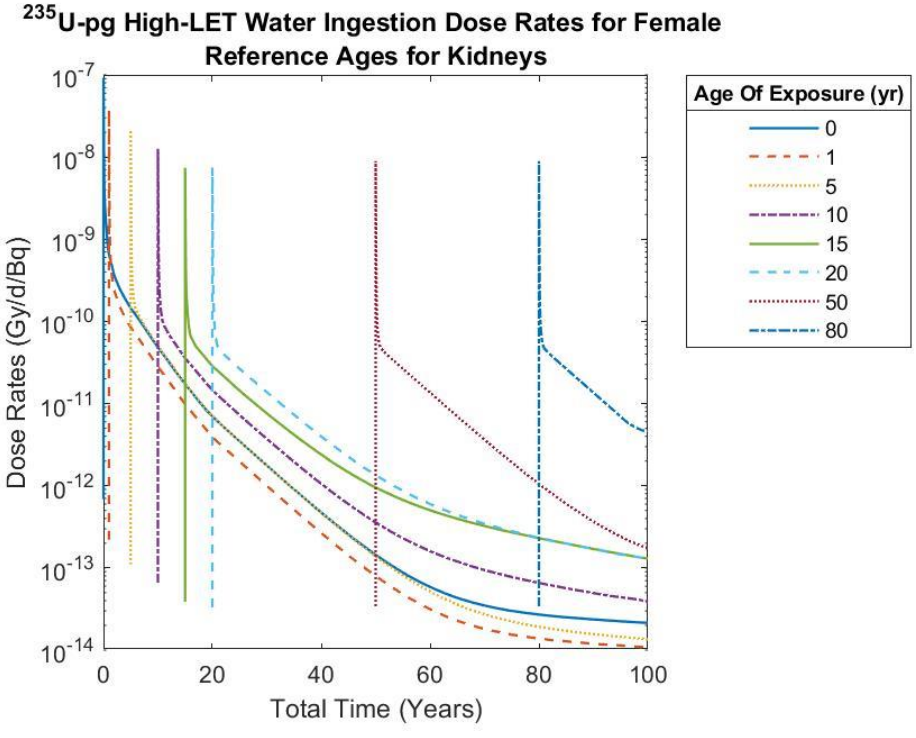
235U-pg High-LET Water Ingestion Dose Rates for Female
Reference Ages for Kidneys
Dose Rates (Gy/d/Bq)
Total Time (Years)
Age Of Exposure (yr)
0
1
5
10
15
20
50
80

(c)

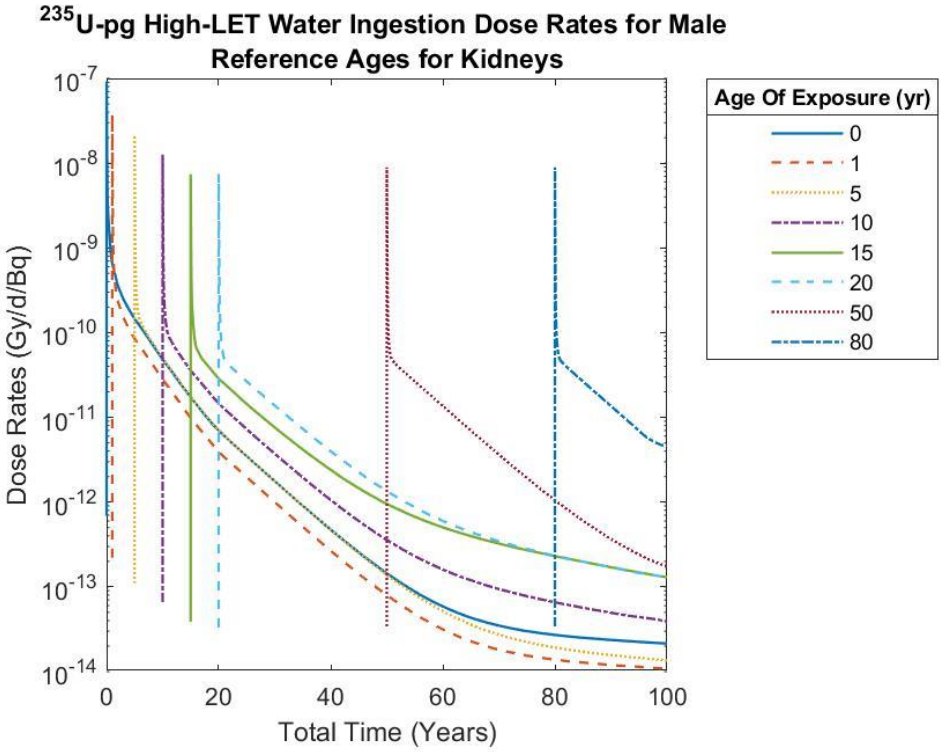

(d)

Figure 116. Dose rates due the high-LET component of tap water ingested ^{235}U in the (a) female bone surface, (b) male bone surface, (c) female kidneys, and (d) male kidneys.

APPENDIX B: ICRP 60 BIOKINETICS

Abbreviations for the diagrams here in are stomach (St_Cont), small intestine (SI_Cont), body tissue (Body_tis), and urinary bladder (UB_Cont).

(a) Biokinetic compartments for ^{131}I – Ingestion. The age of exposure is 10 years. The organs outlined herein are the stomach, small intestine, blood, and urinary bladder.

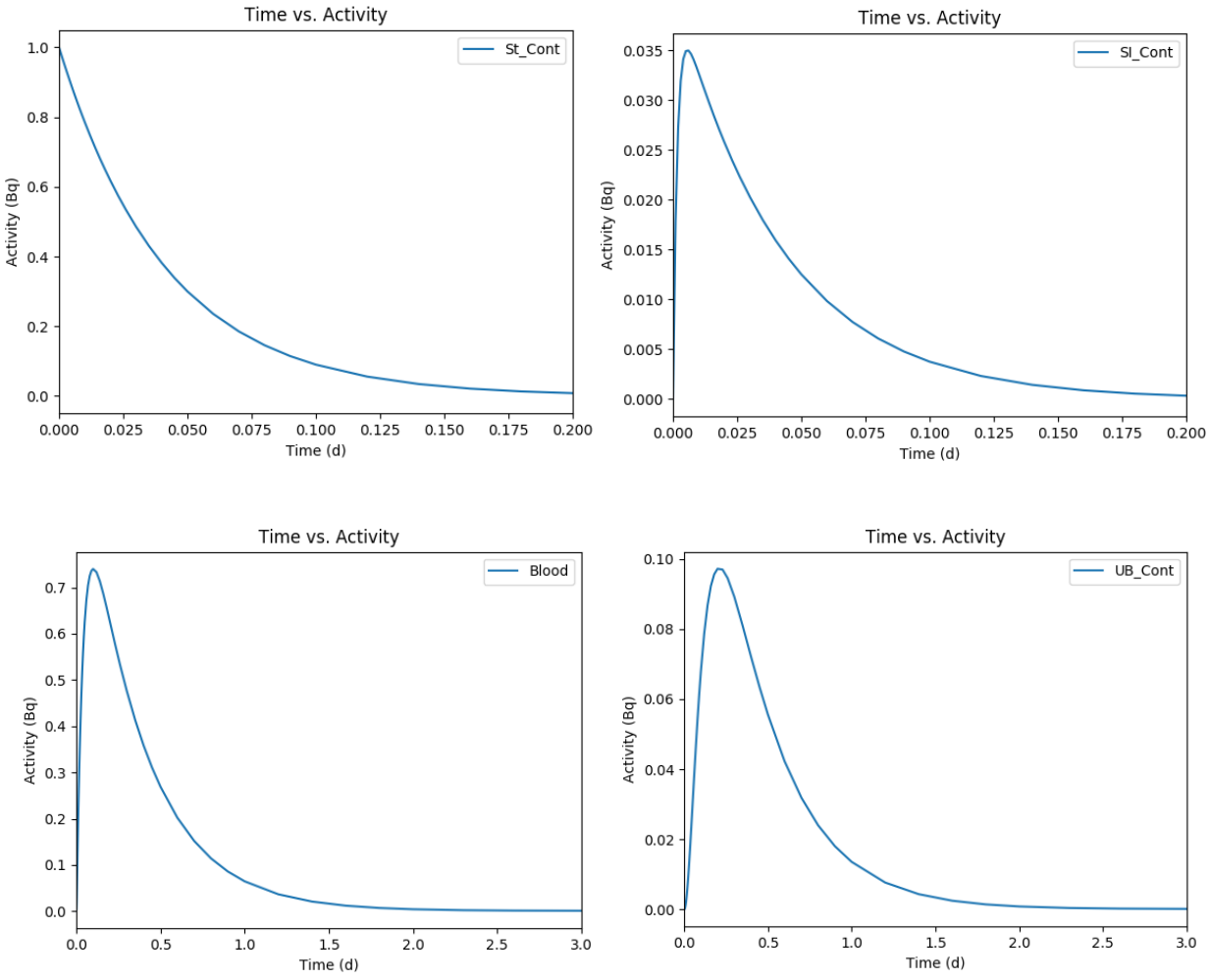

(b) Biokinetic compartments for ^{131}I – Ingestion. The age of exposure is 10 years. The organs outlined herein are the stomach, small intestine, blood, and urinary thyroid.

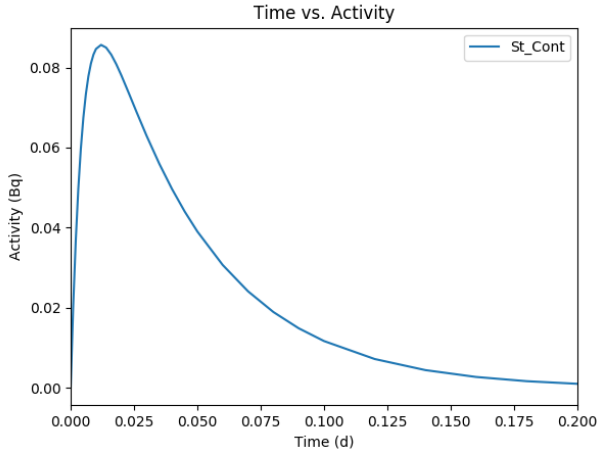

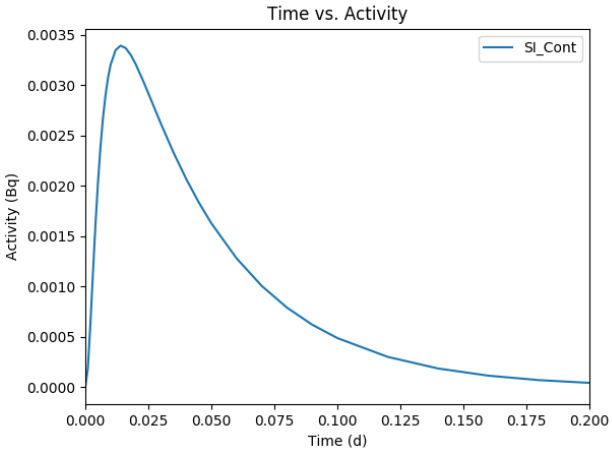

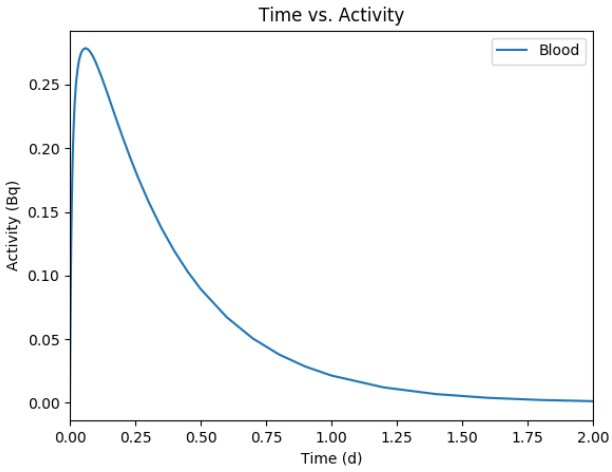

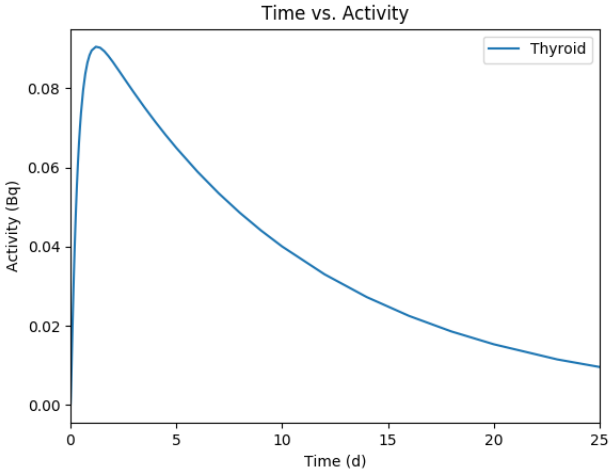

(c) Biokinetic compartments for ^{3}H – Ingestion. The age of exposure is 10 years. The organs outlined herein are the stomach, small intestine, blood, and body tissue.

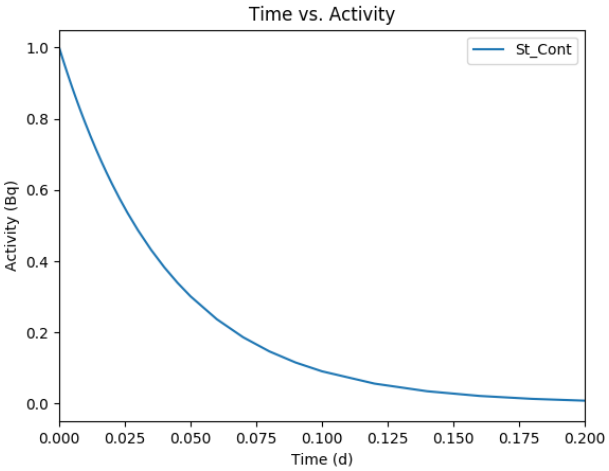

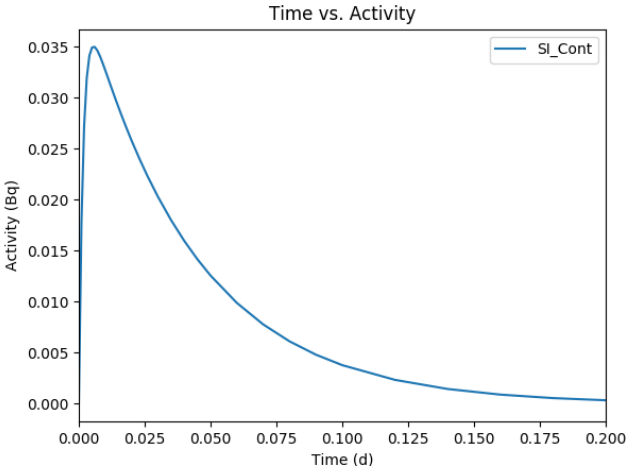

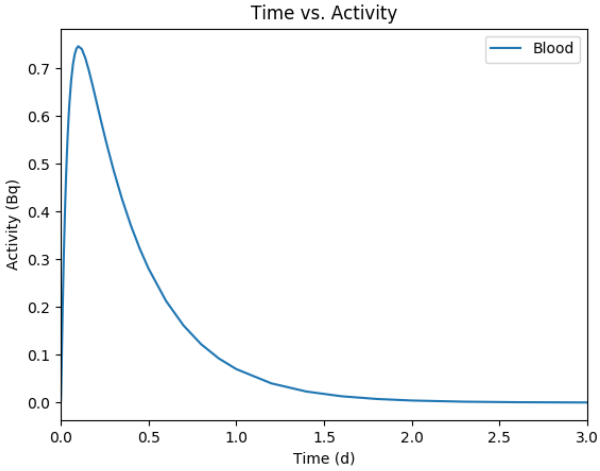

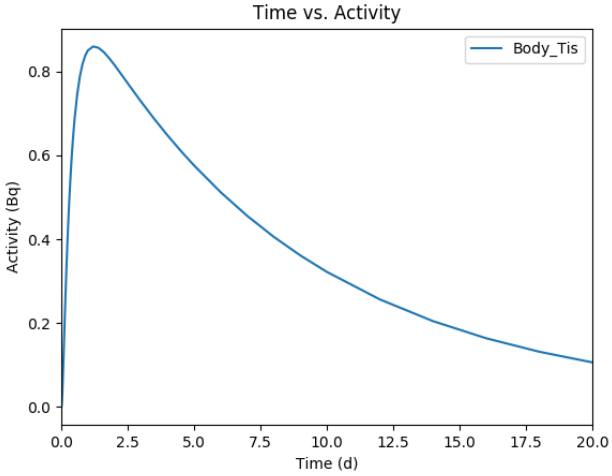

(d) Biokinetic compartments for ^{137}Cs – Ingestion. The age of exposure is 10 years. The organs outlined herein are the stomach, small intestine, blood, and body tissue.

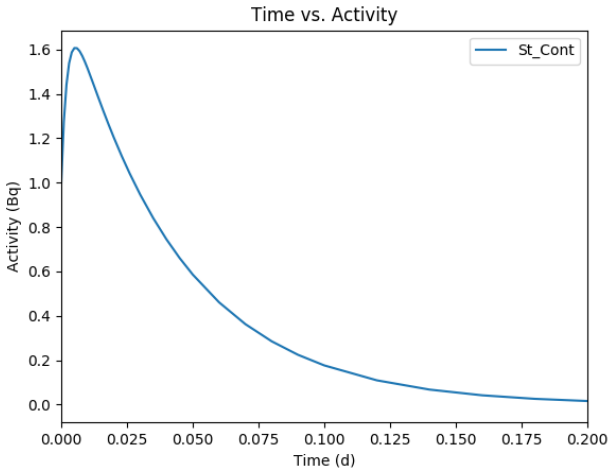

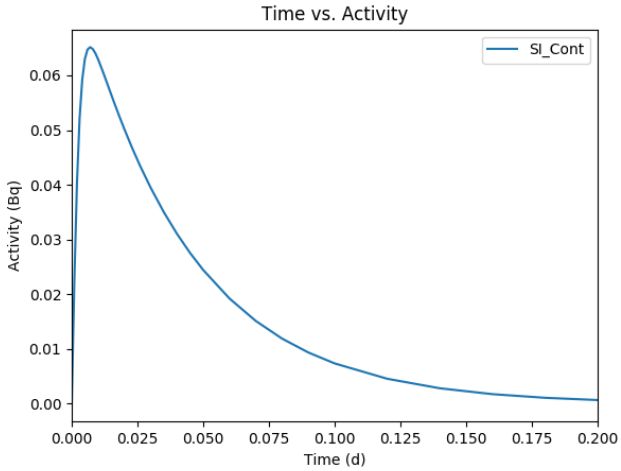

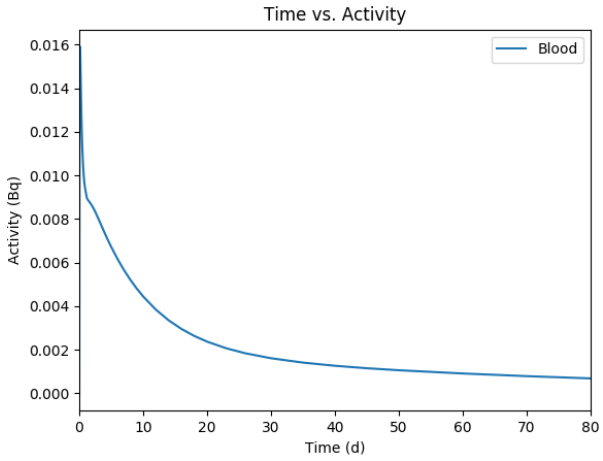

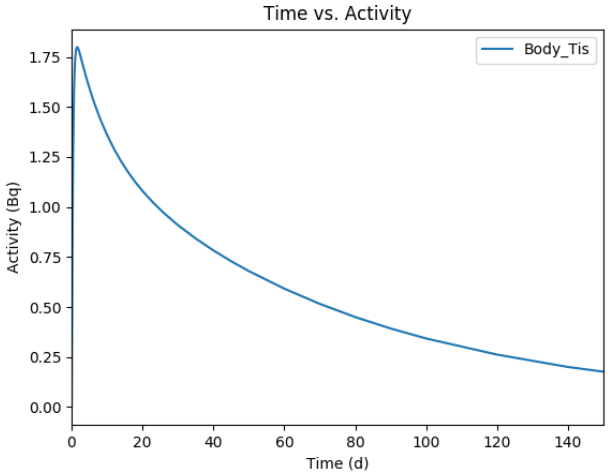

(e) Biokinetic compartments for ^{137}Cs – Inhalation. The age of exposure is 10 years. The organs outlined herein are the stomach, small intestine, blood, and body tissue.

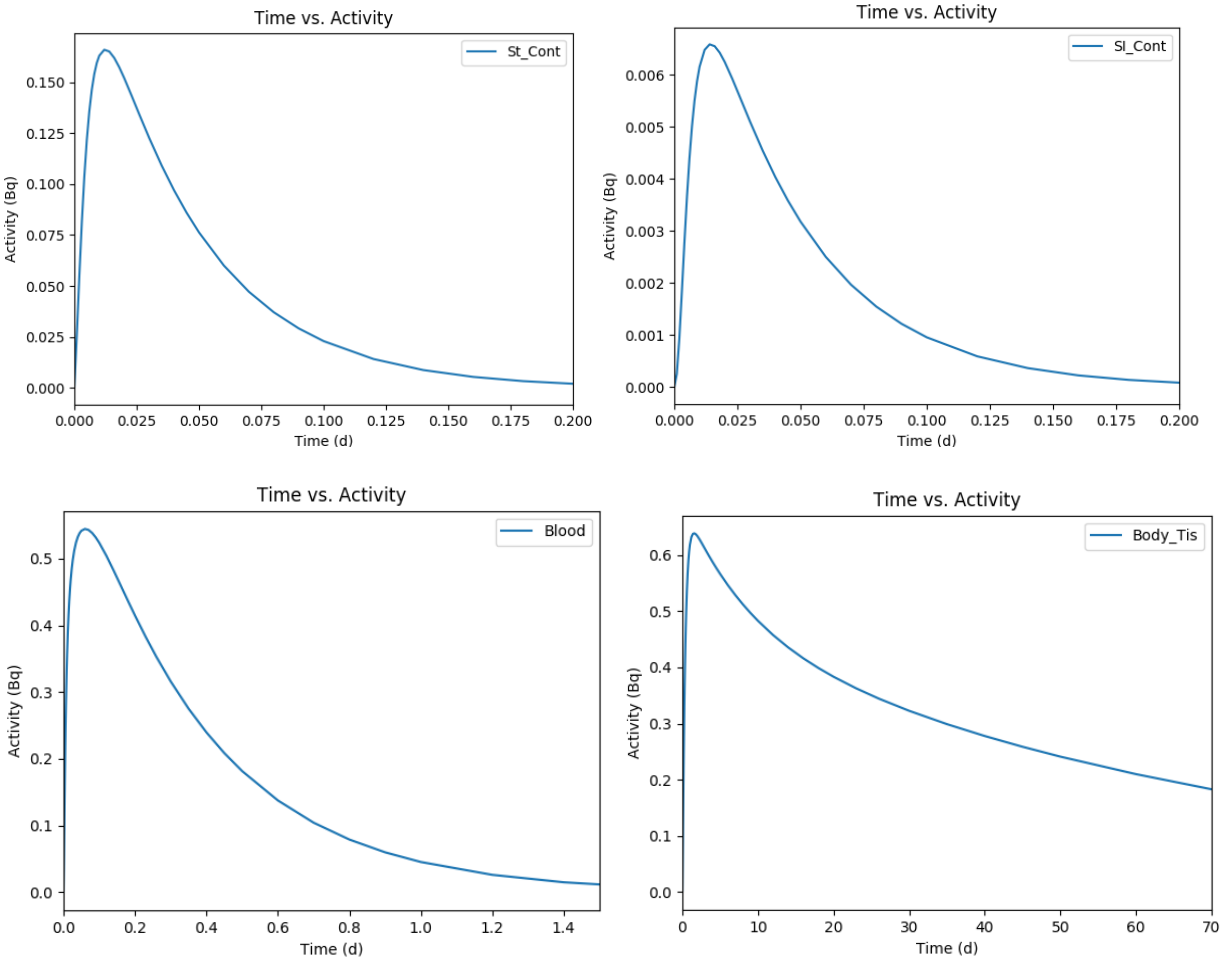

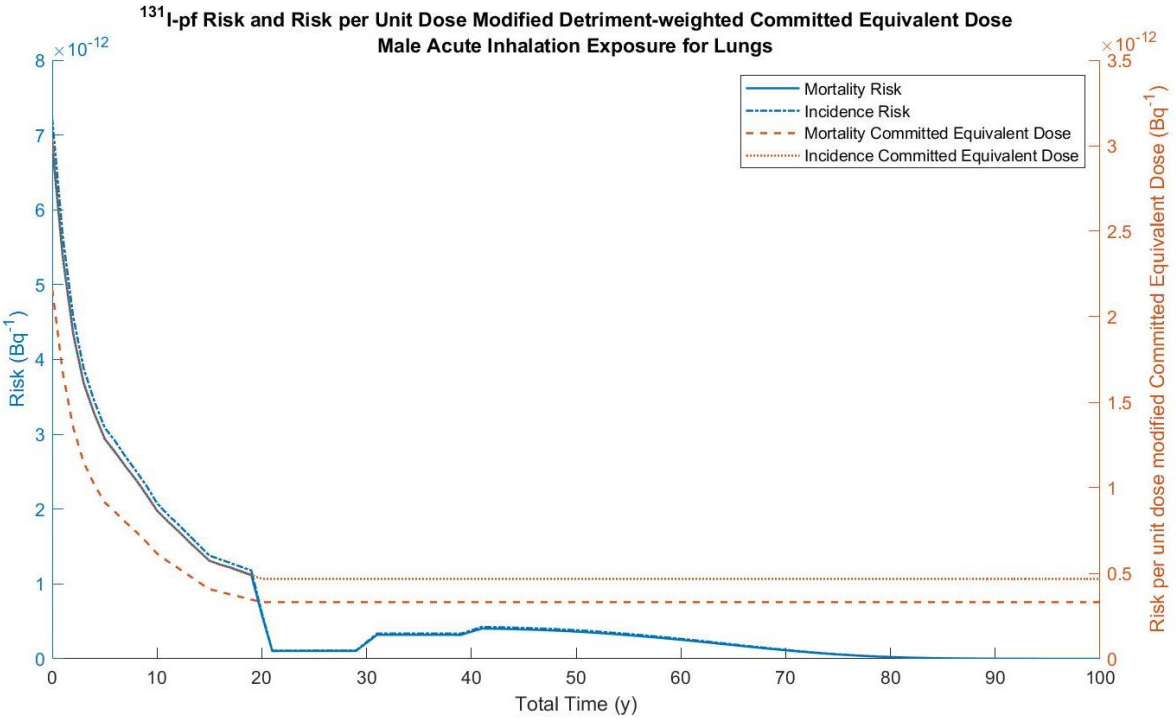

Figure 117. Risk and detriment-weighted committed equivalent dose to the male lungs due to fast clearing ^{131}I.

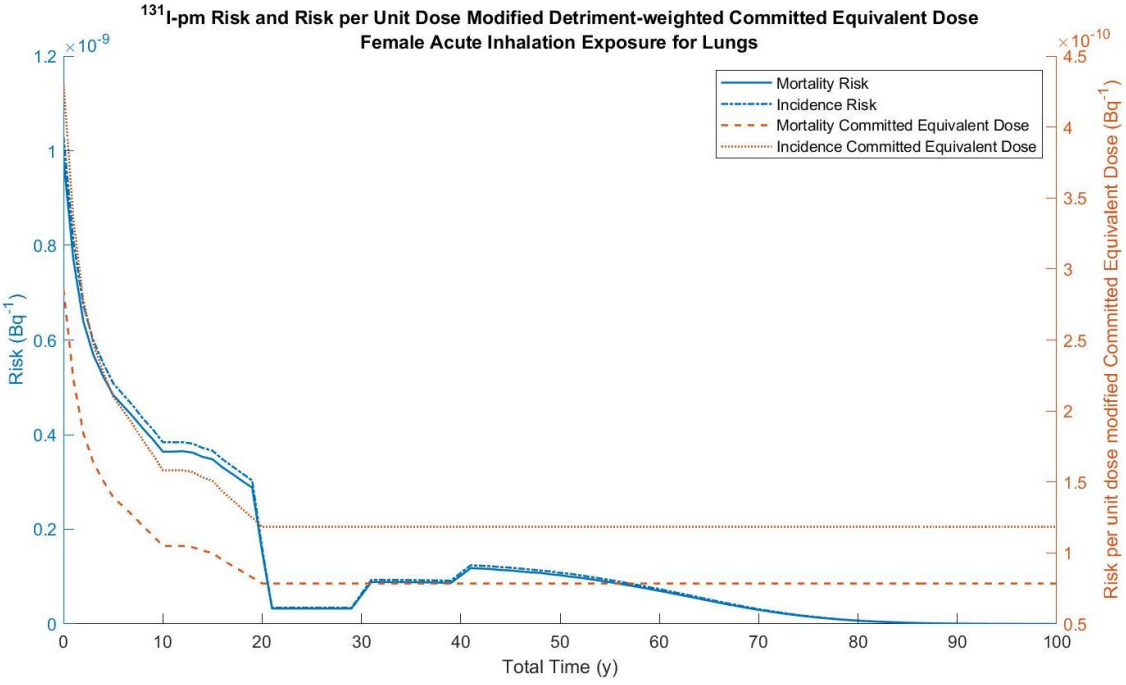

(a)

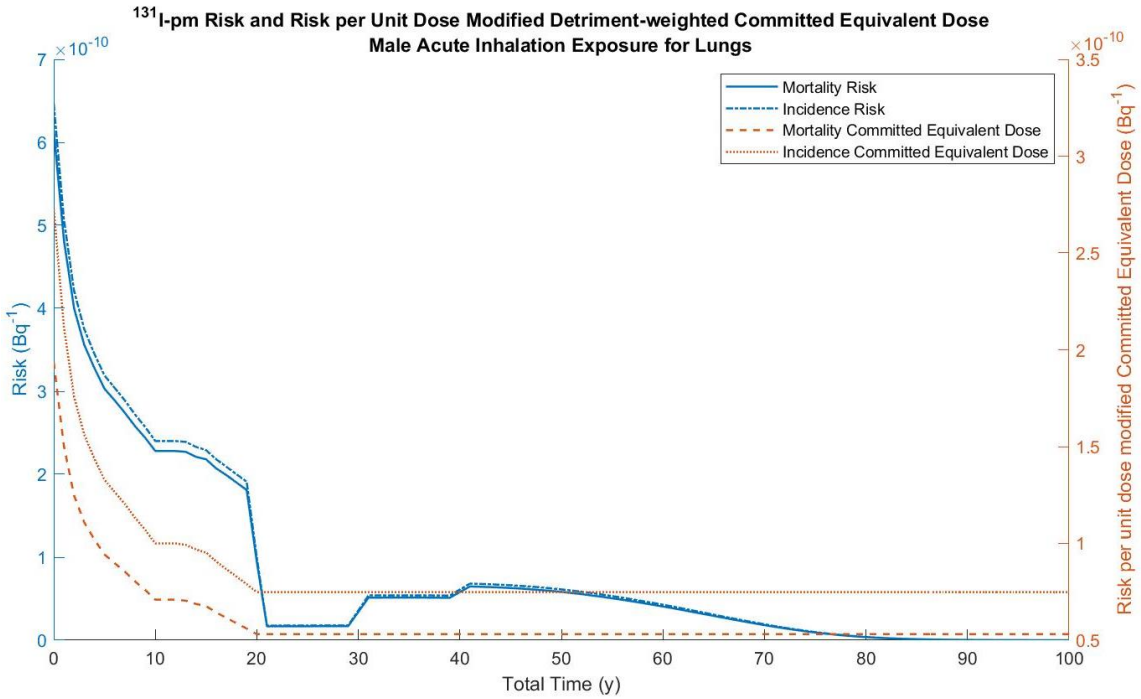

(b)

Figure 118. Risk and detriment-weighted committed equivalent dose to the (a) female lungs and (b) male lungs due to moderate clearing ^{131}I.

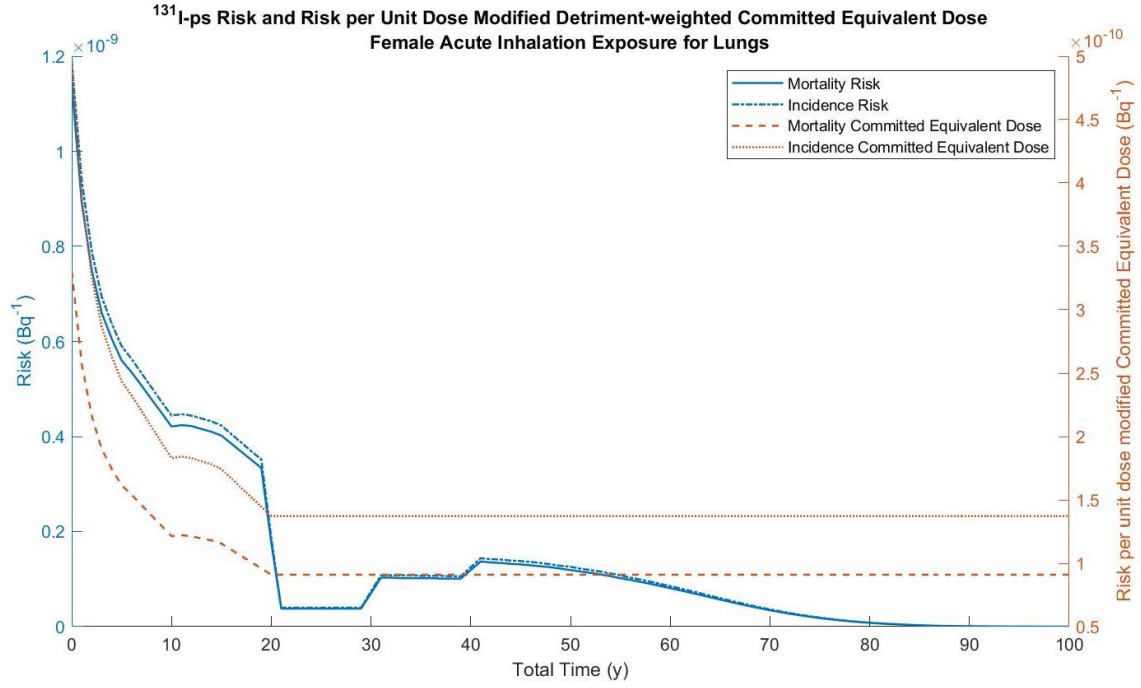

(a)

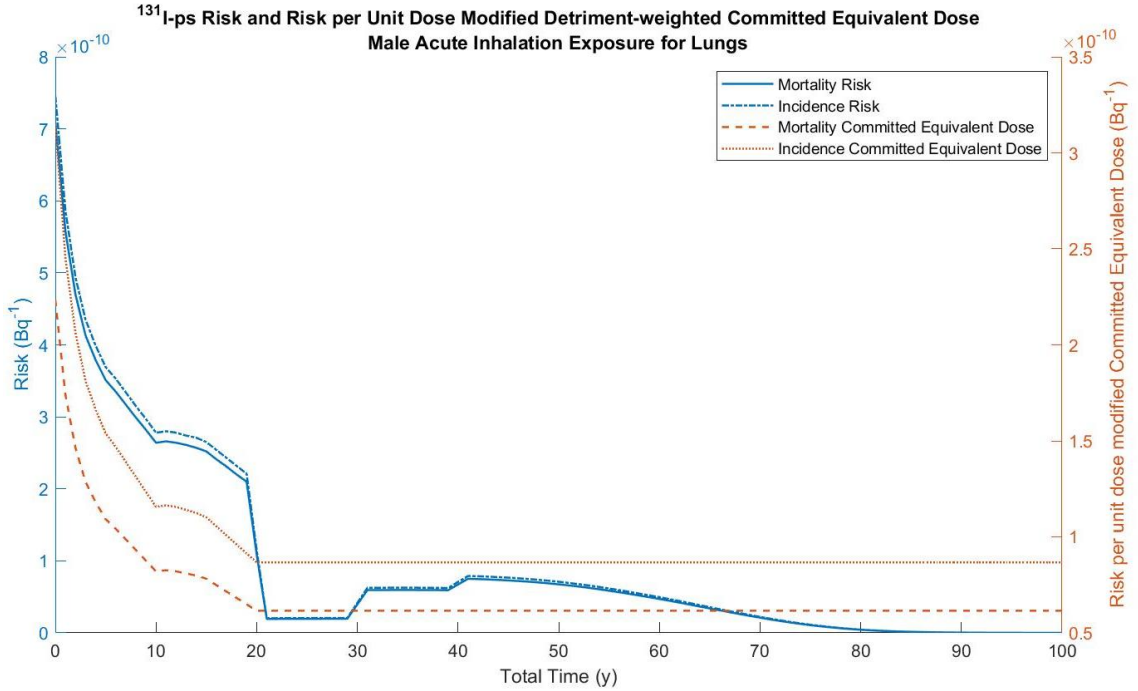

(b)

Figure 119. Risk and detriment-weighted committed equivalent dose to the (a) female lungs and (b) male lungs due to slow clearing ^{131}I.

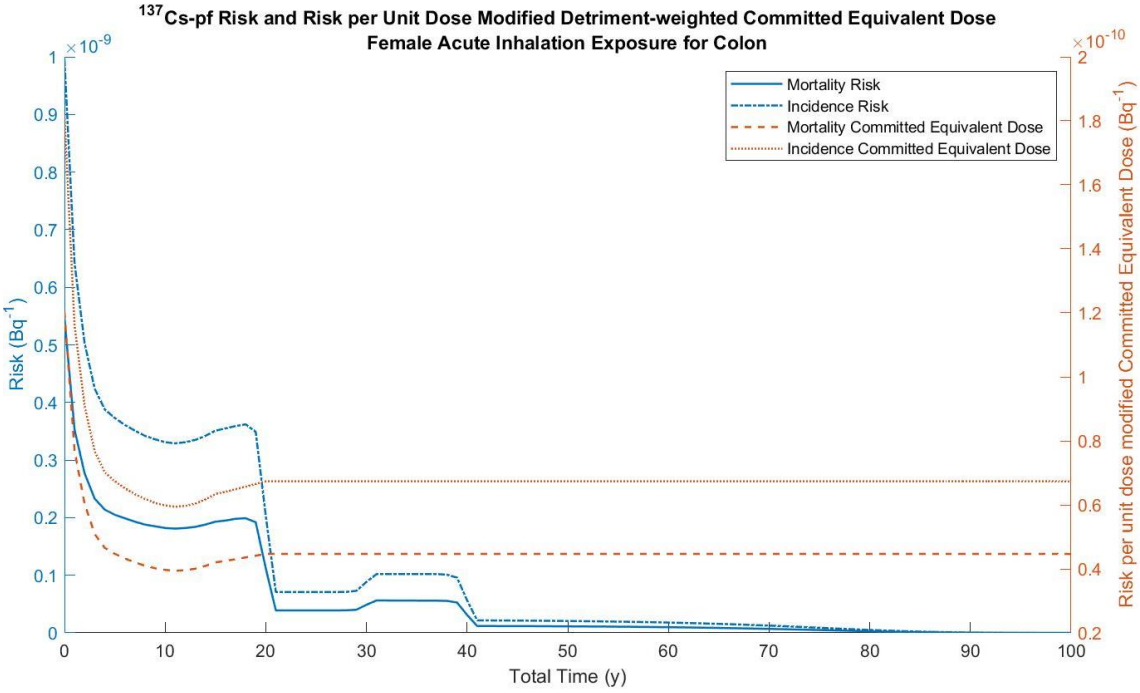

(a)

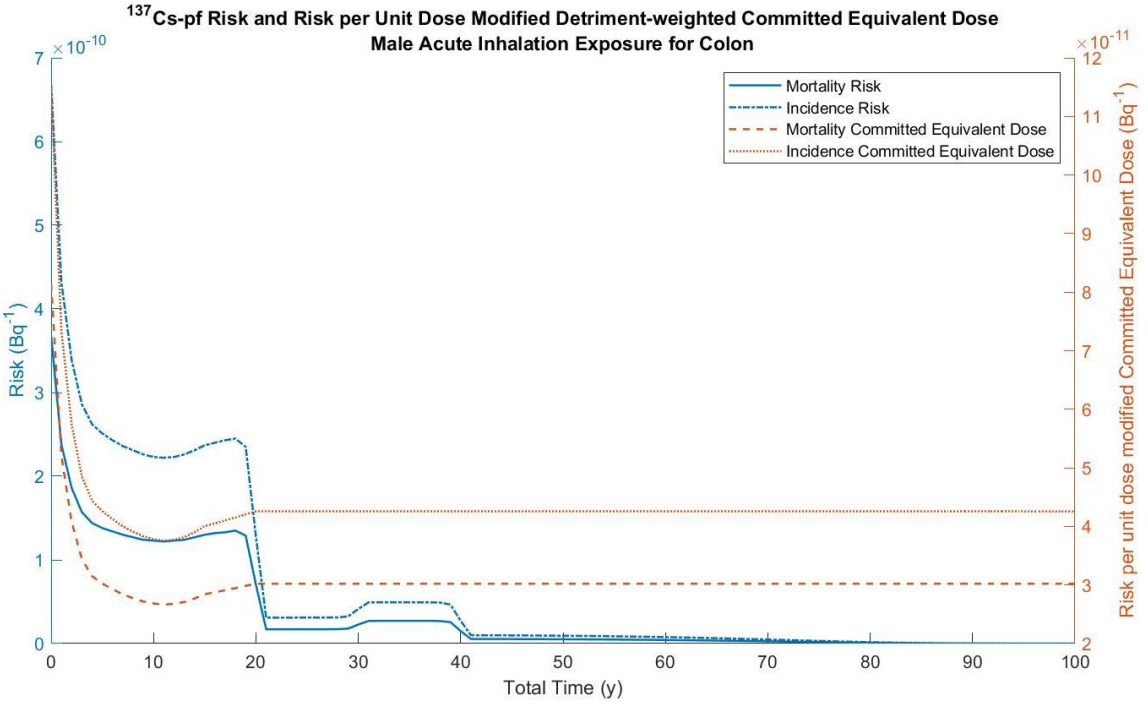
137Cs-pf Risk and Risk per Unit Dose Modified Detriment-weighted Committed Equivalent Dose
Male Acute Inhalation Exposure for Colon
Mortality Risk
Incidence Risk
Mortality Committed Equivalent Dose
Incidence Committed Equivalent Dose
Risk (Bq-1)
Risk per unit dose modified Committed Equivalent Dose (Bq-1)
Total Time (y)

(b)

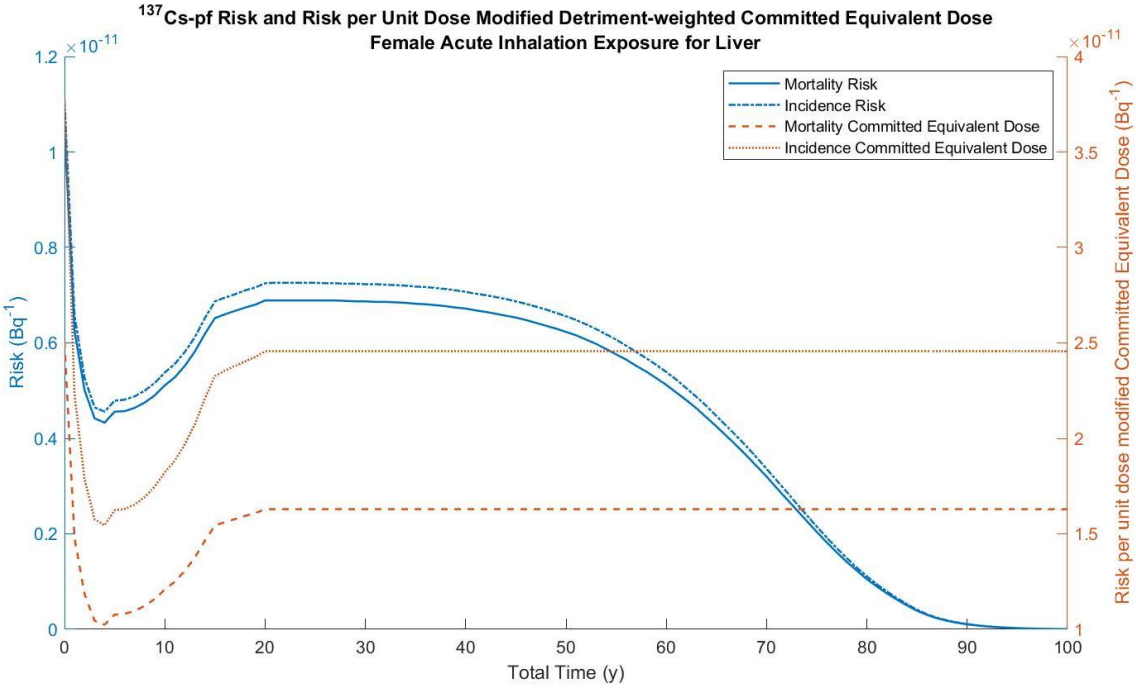
137Cs-pf Risk and Risk per Unit Dose Modified Detriment-weighted Committed Equivalent Dose
Female Acute Inhalation Exposure for Liver
Mortality Risk
Incidence Risk
Mortality Committed Equivalent Dose
Incidence Committed Equivalent Dose
Risk (Bq-1)
Risk per unit dose modified Committed Equivalent Dose (Bq-1)
Total Time (y)

(c)

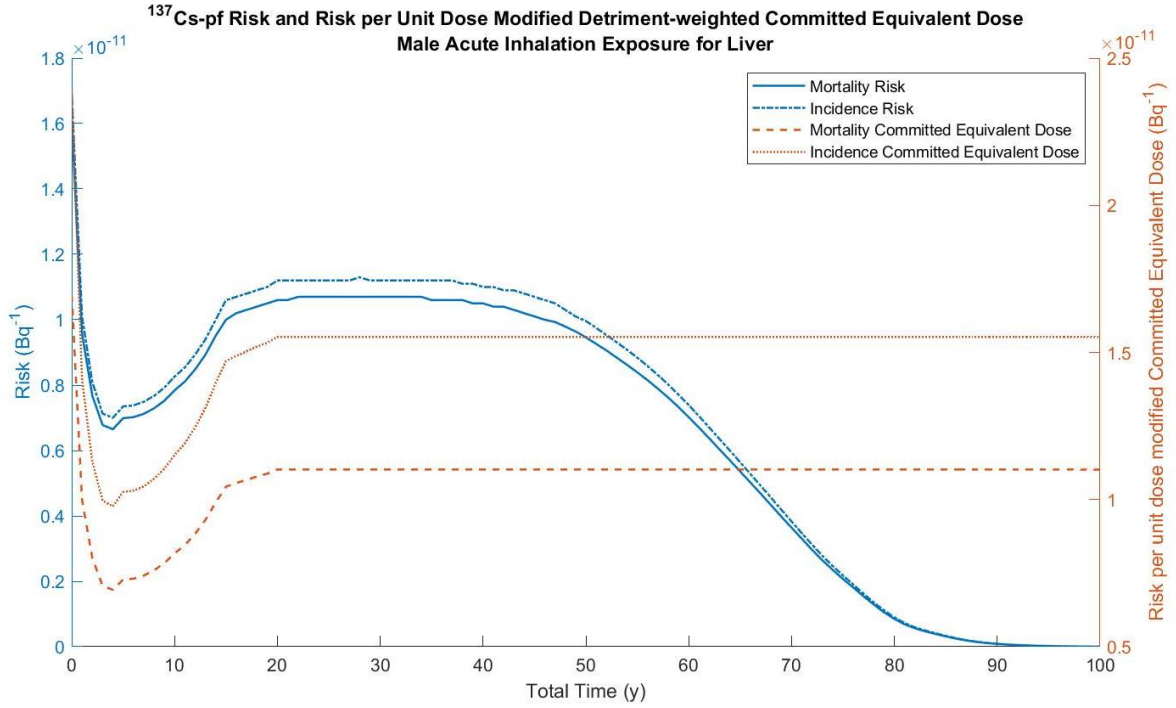

(d)

Figure 120. Risk and detriment-weighted committed equivalent dose to the (a) female lungs, (b) male lungs, (c) female liver, and (d) male liver due to fast clearing ^{137}Cs.

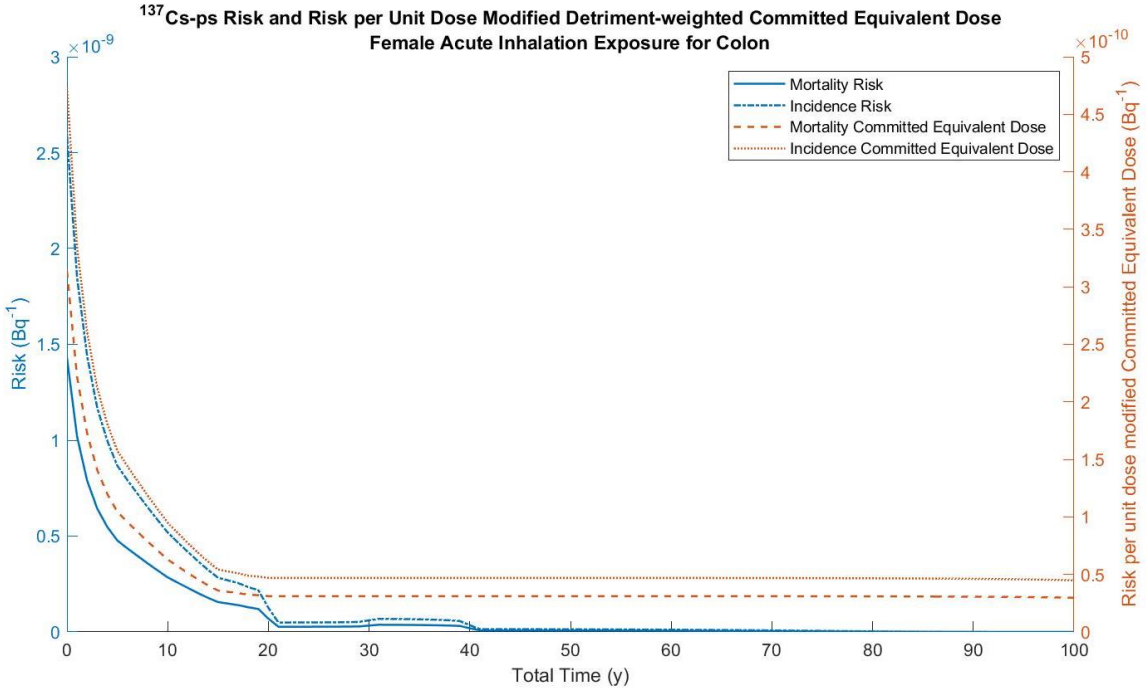

(a)

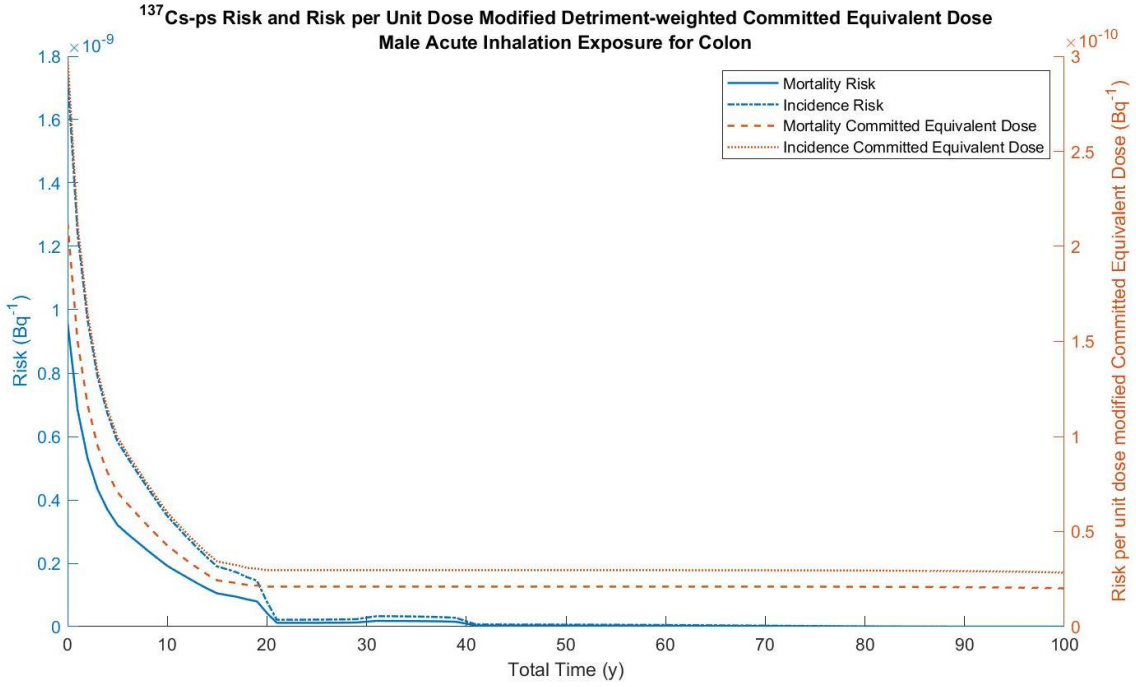
137Cs-ps Risk and Risk per Unit Dose Modified Detriment-weighted Committed Equivalent Dose
Male Acute Inhalation Exposure for Colon
Mortality Risk
Incidence Risk
Mortality Committed Equivalent Dose
Incidence Committed Equivalent Dose
Risk (Bq-1)
Risk per unit dose modified Committed Equivalent Dose (Bq-1)
Total Time (y)

(b)

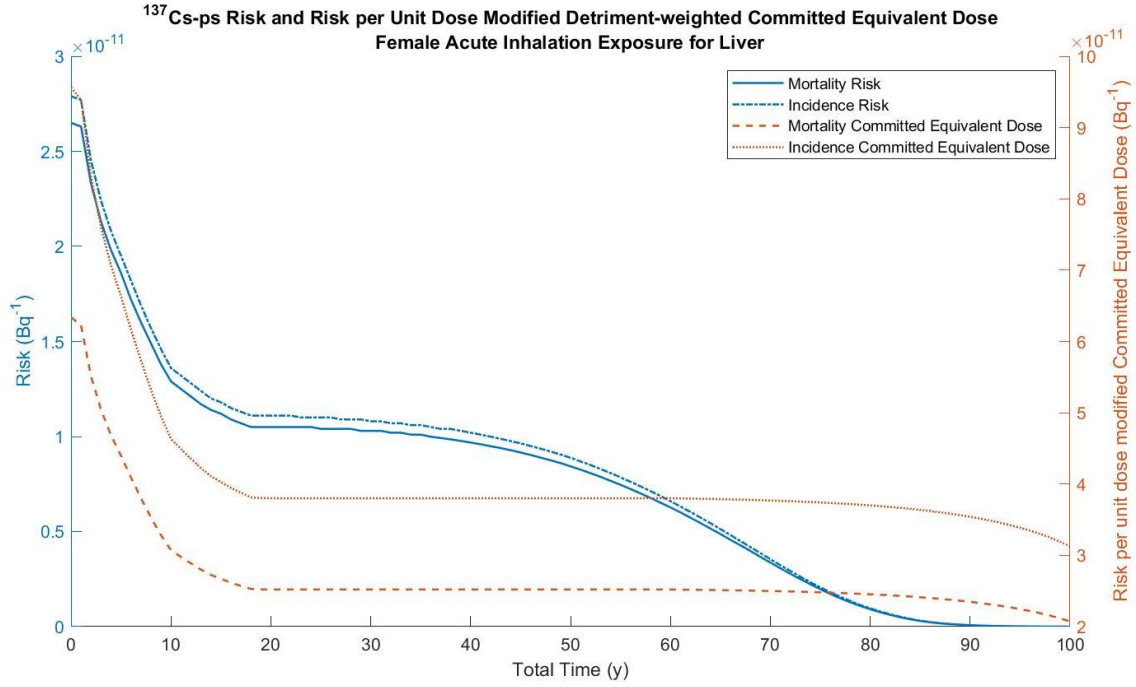
137Cs-ps Risk and Risk per Unit Dose Modified Detriment-weighted Committed Equivalent Dose
Female Acute Inhalation Exposure for Liver
Mortality Risk
Incidence Risk
Mortality Committed Equivalent Dose
Incidence Committed Equivalent Dose
Risk (Bq-1)
Risk per unit dose modified Committed Equivalent Dose (Bq-1)
Total Time (y)

(c)

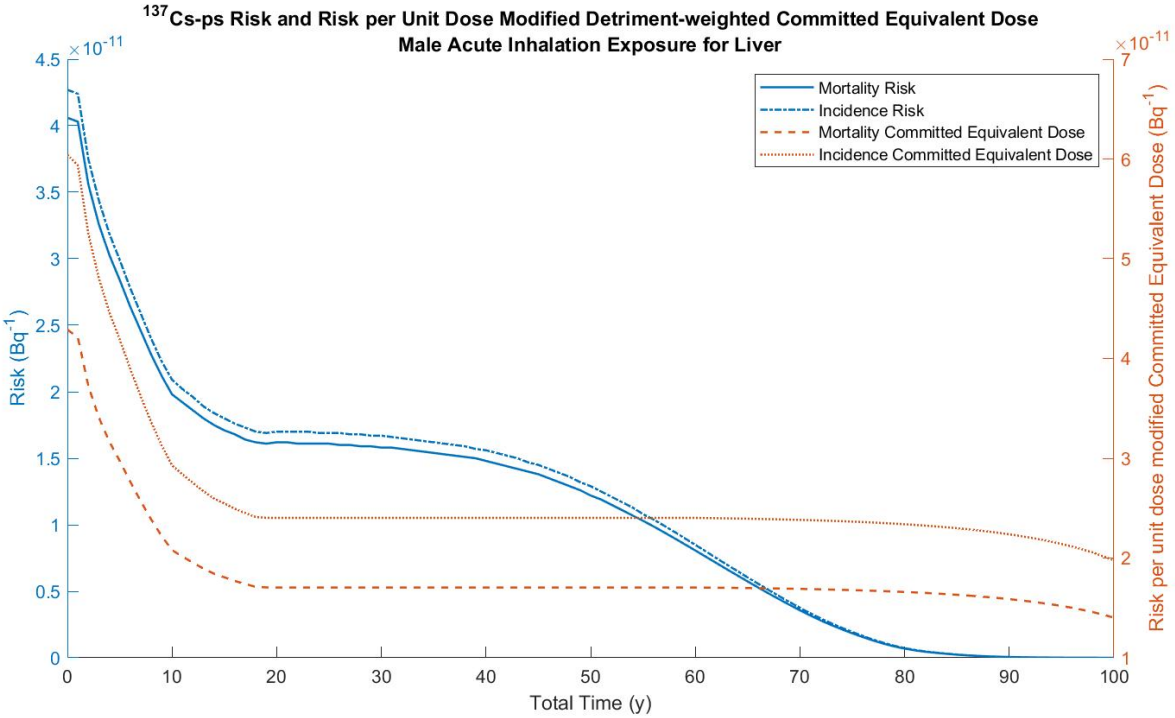

(d)

Figure 121. Risk and detriment-weighted committed equivalent dose to the (a) female lungs, (b) male lungs, (c) female liver, and (d) male liver due to slow clearing ^{137}Cs.

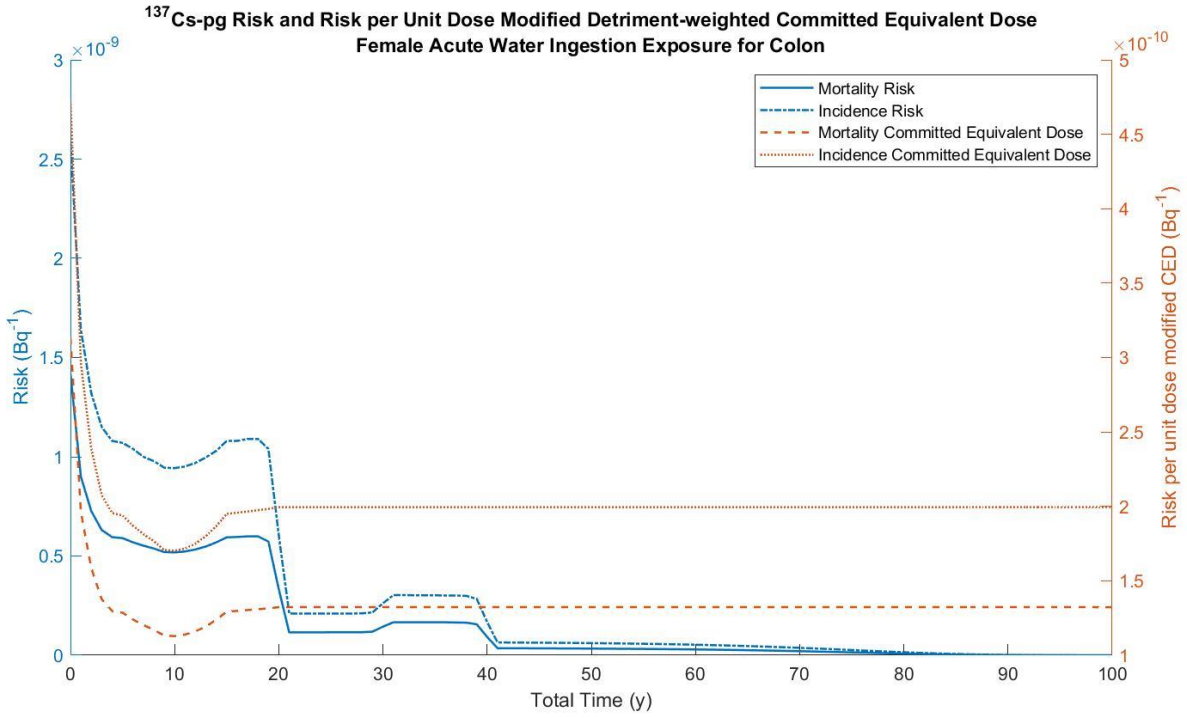

(a)

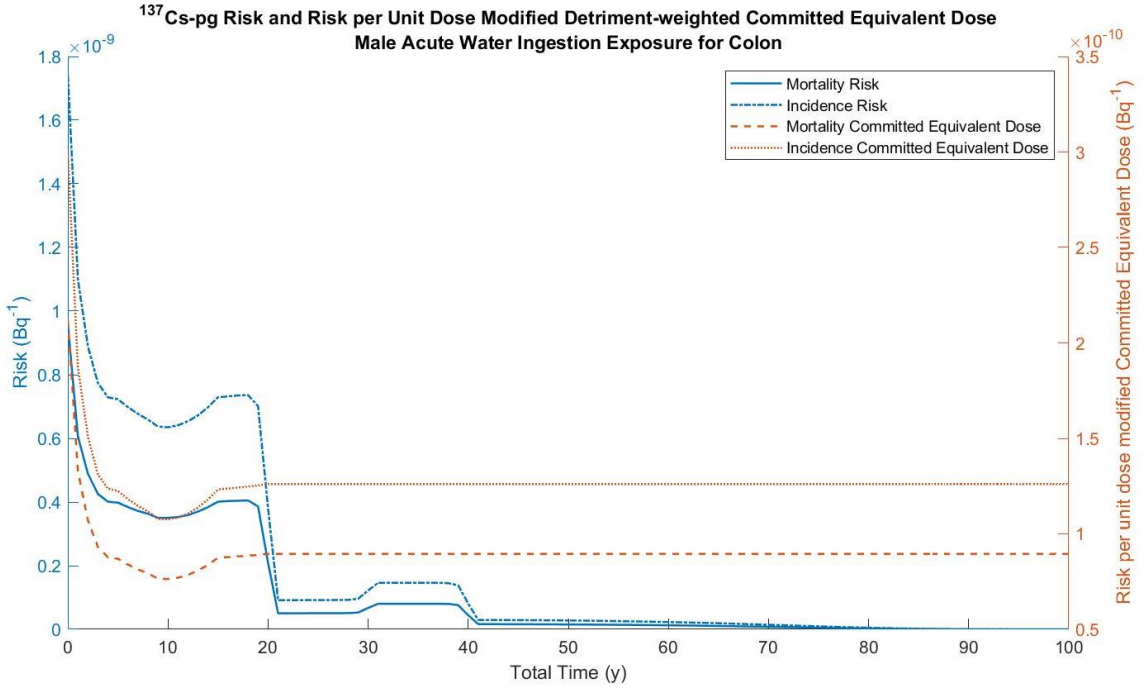
137Cs-pg Risk and Risk per Unit Dose Modified Detriment-weighted Committed Equivalent Dose
Male Acute Water Ingestion Exposure for Colon
Mortality Risk
Incidence Risk
Mortality Committed Equivalent Dose
Incidence Committed Equivalent Dose
Risk (Bq-1)
Risk per unit dose modified Committed Equivalent Dose (Bq-1)
Total Time (y)

(b)

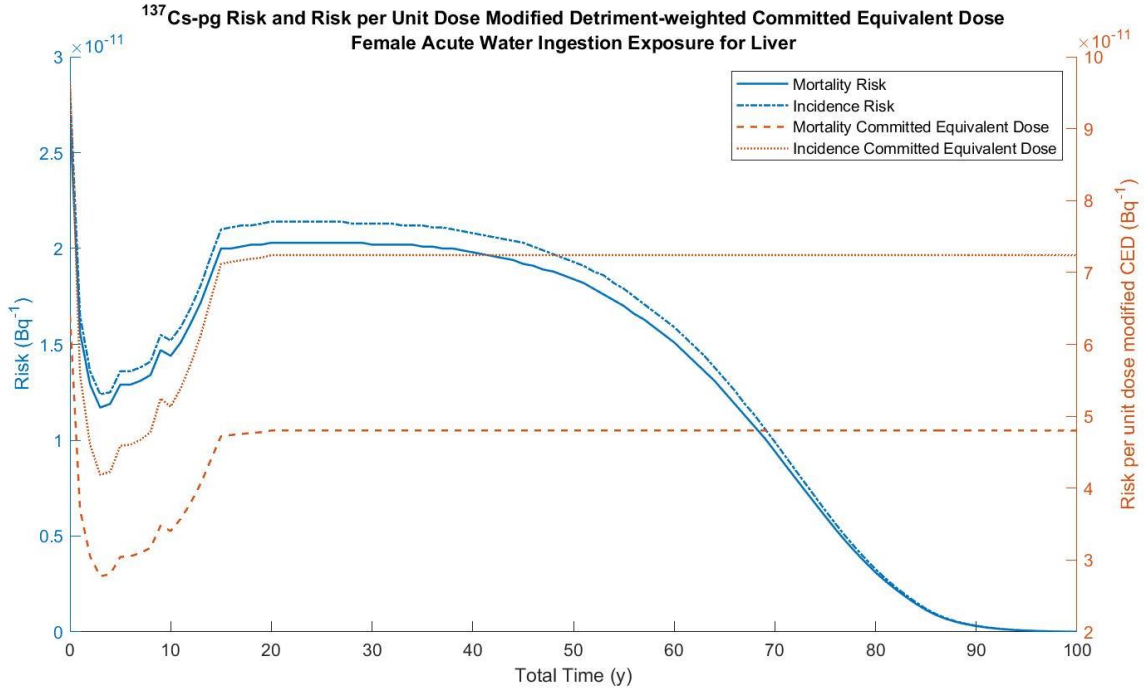
137Cs-pg Risk and Risk per Unit Dose Modified Detriment-weighted Committed Equivalent Dose
Female Acute Water Ingestion Exposure for Liver
Mortality Risk
Incidence Risk
Mortality Committed Equivalent Dose
Incidence Committed Equivalent Dose
Risk (Bq-1)
Risk per unit dose modified CED (Bq-1)
Total Time (y)

(c)

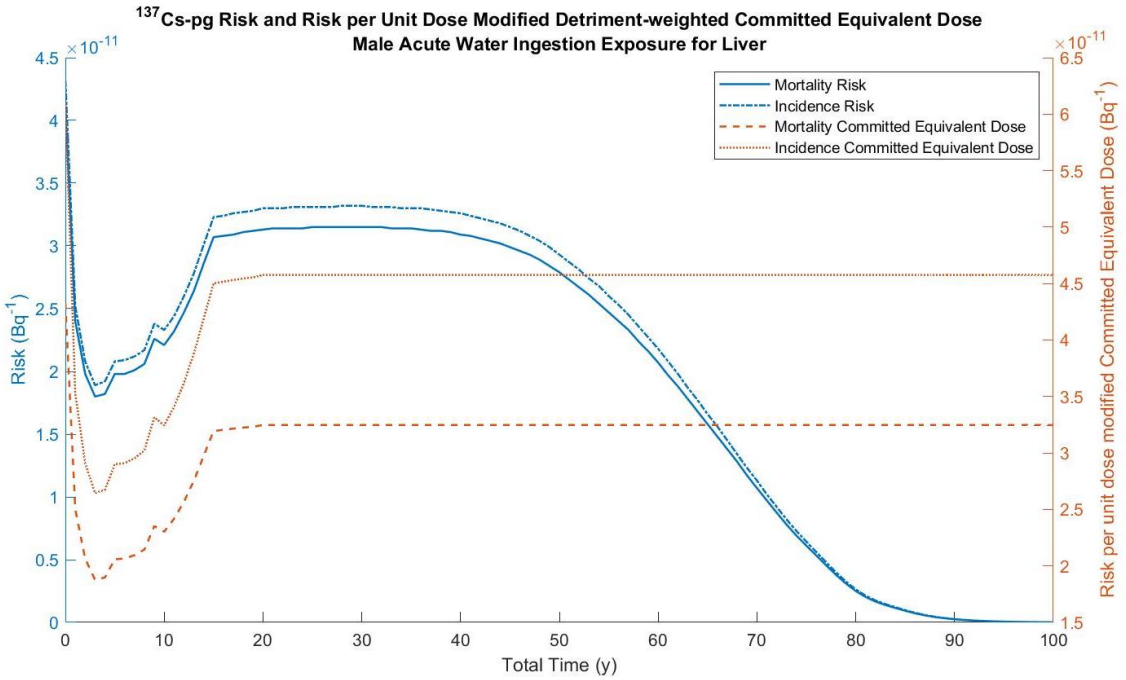

(d)

Figure 122. Risk and detriment-weighted committed equivalent dose to the (a) female lungs, (b) male lungs, (c) female liver, and (d) male liver due to tap water ingested ^{137}Cs.

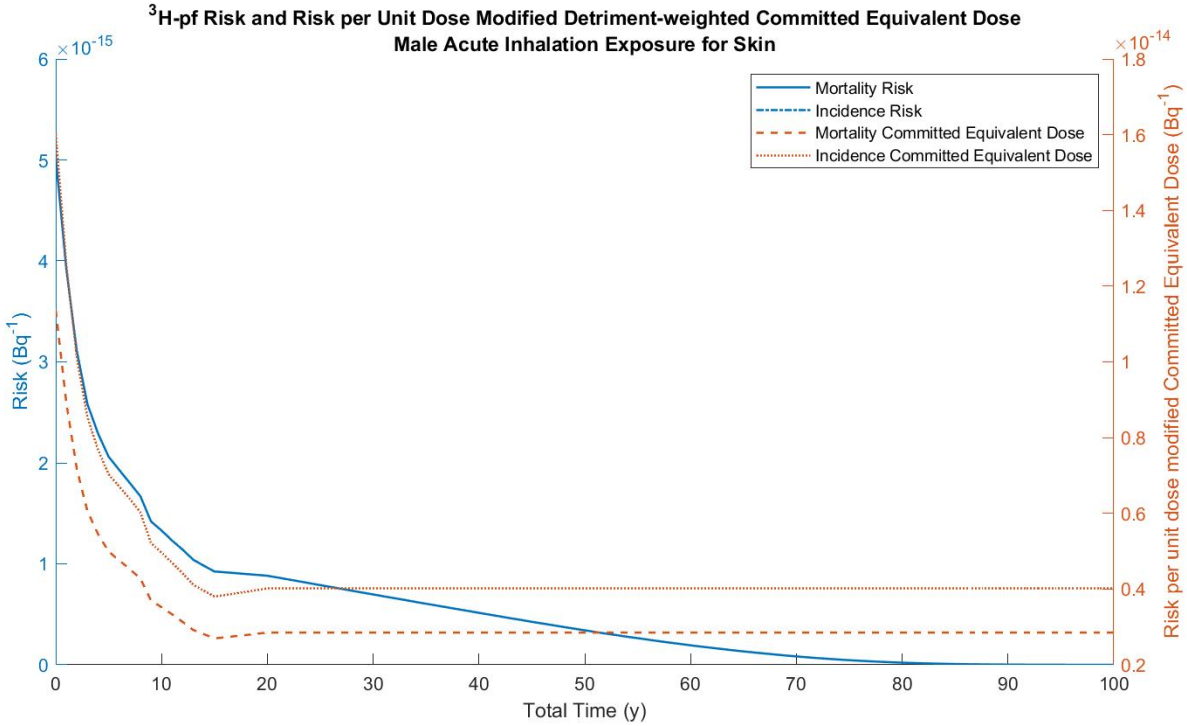

Figure 123. Risk and detriment-weighted committed equivalent dose to the male skin due to fast clearing tritium.

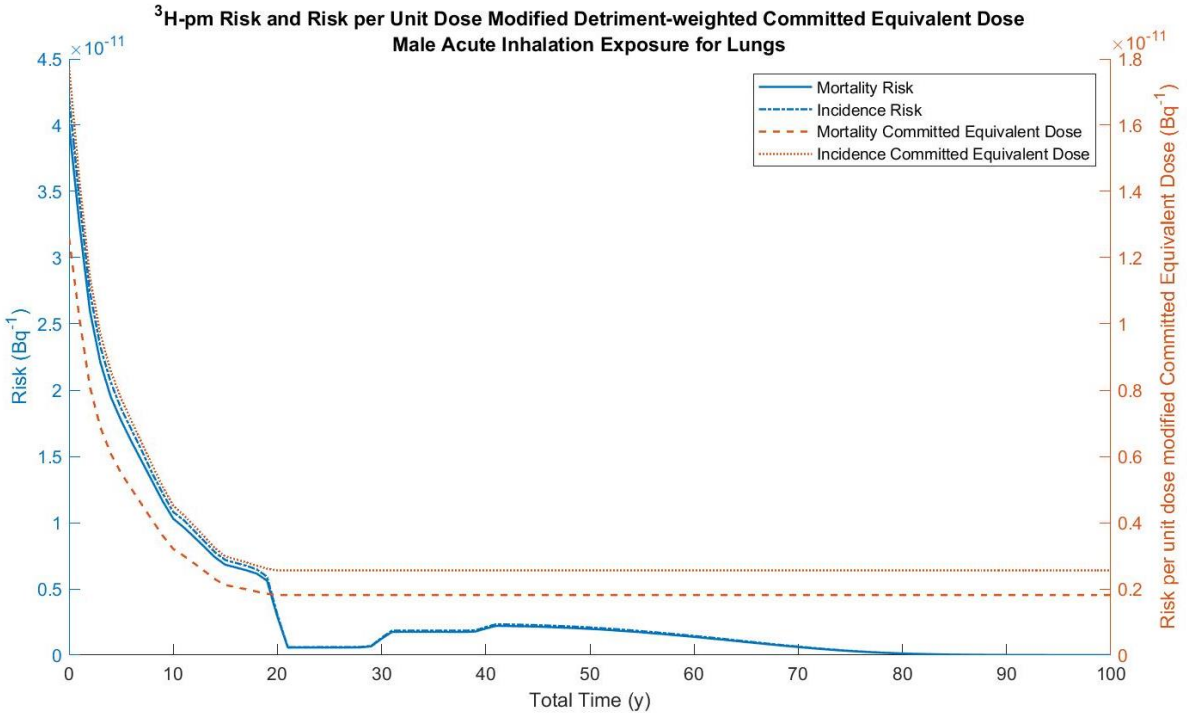

Figure 124. Risk and detriment-weighted committed equivalent dose to the male lungs due to moderate clearing tritium.

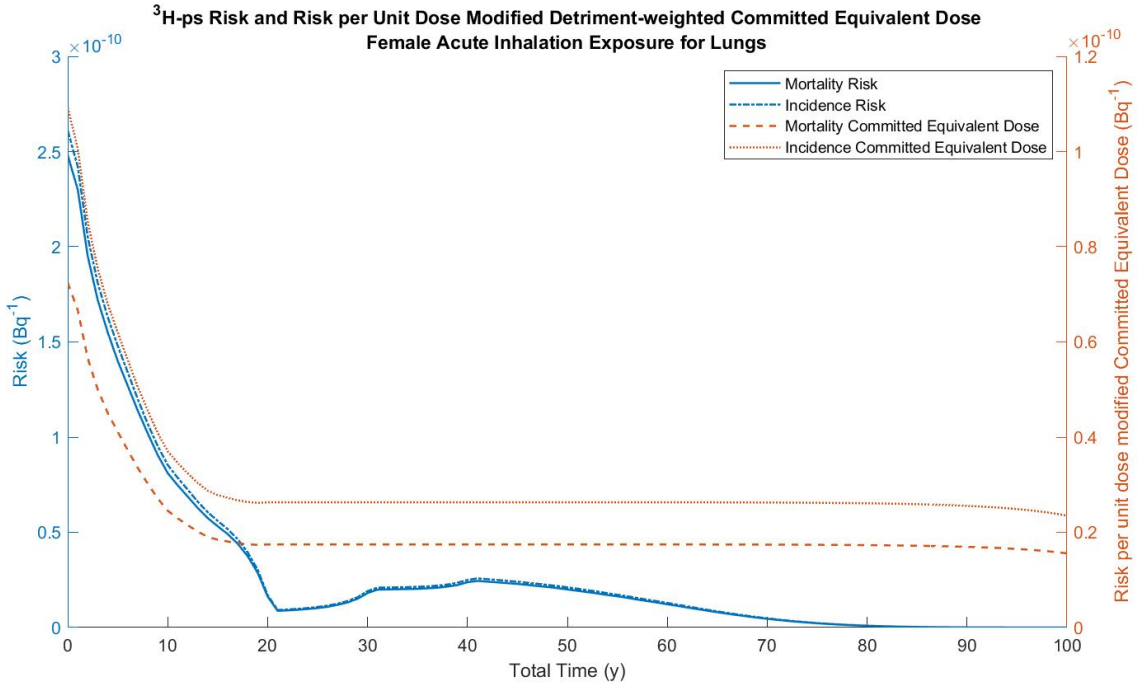

(a)

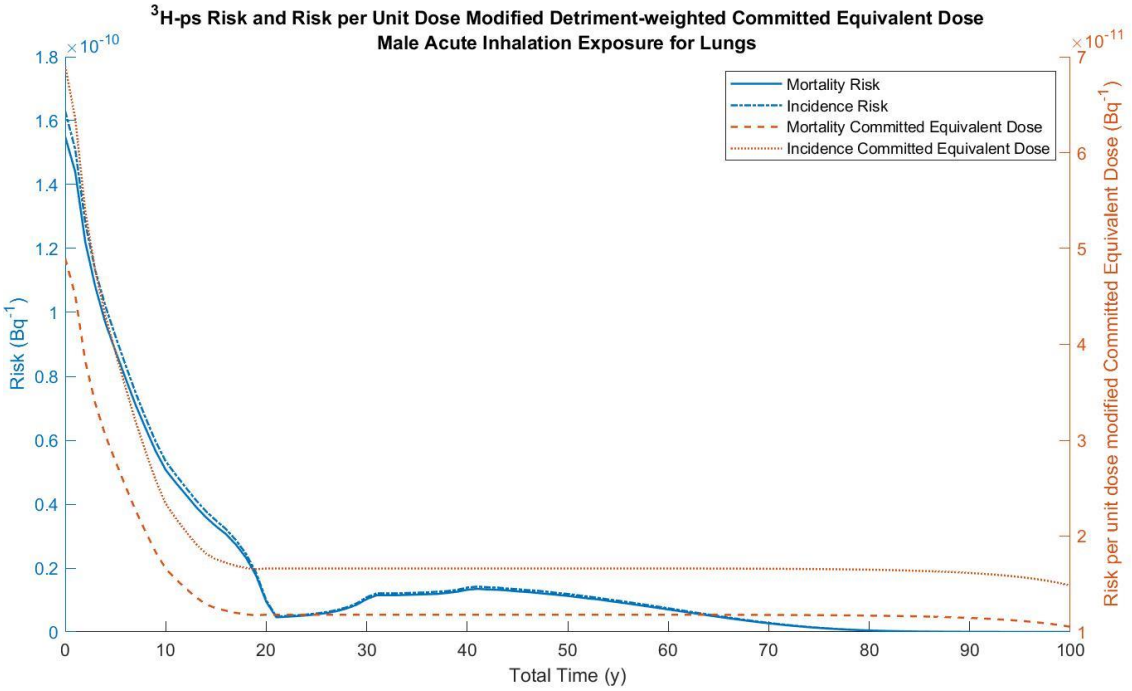
^{3}H-ps Risk and Risk per Unit Dose Modified Detriment-weighted Committed Equivalent Dose
Male Acute Inhalation Exposure for Lungs
Mortality Risk
Incidence Risk
Mortality Committed Equivalent Dose
Incidence Committed Equivalent Dose
Risk (Bq^{-1})
Risk per unit dose modified Committed Equivalent Dose (Bq^{-1})
Total Time (y)

(b)

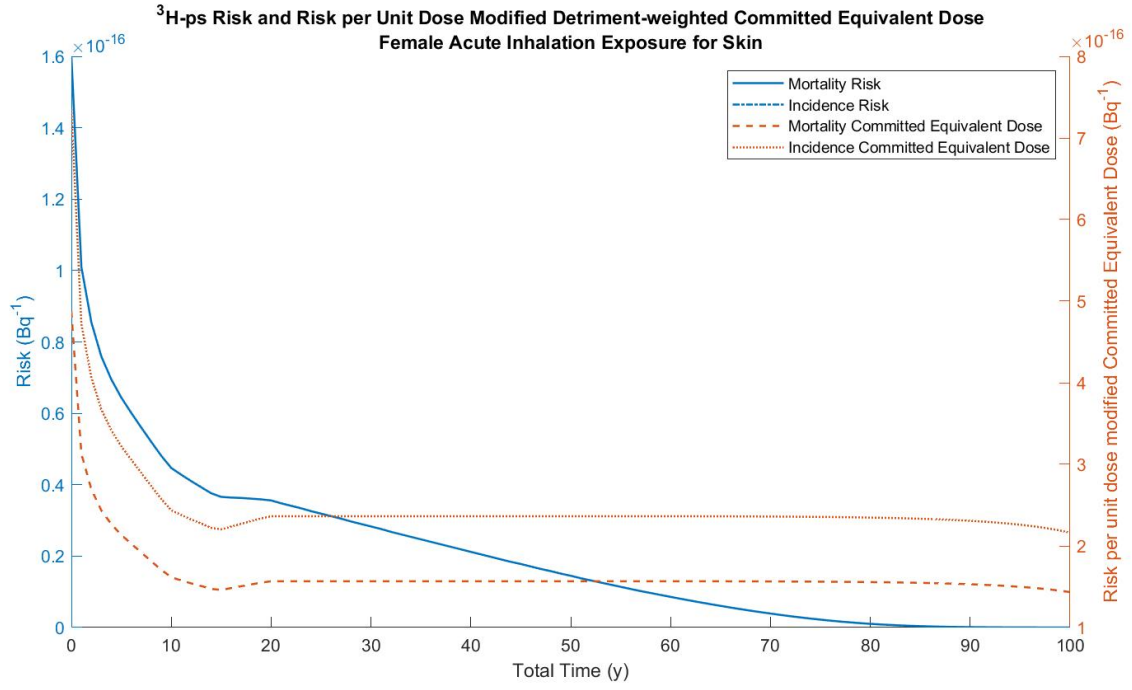
^{3}H-ps Risk and Risk per Unit Dose Modified Detriment-weighted Committed Equivalent Dose
Female Acute Inhalation Exposure for Skin
Mortality Risk
Incidence Risk
Mortality Committed Equivalent Dose
Incidence Committed Equivalent Dose
Risk (Bq^{-1})
Risk per unit dose modified Committed Equivalent Dose (Bq^{-1})
Total Time (y)

(c)

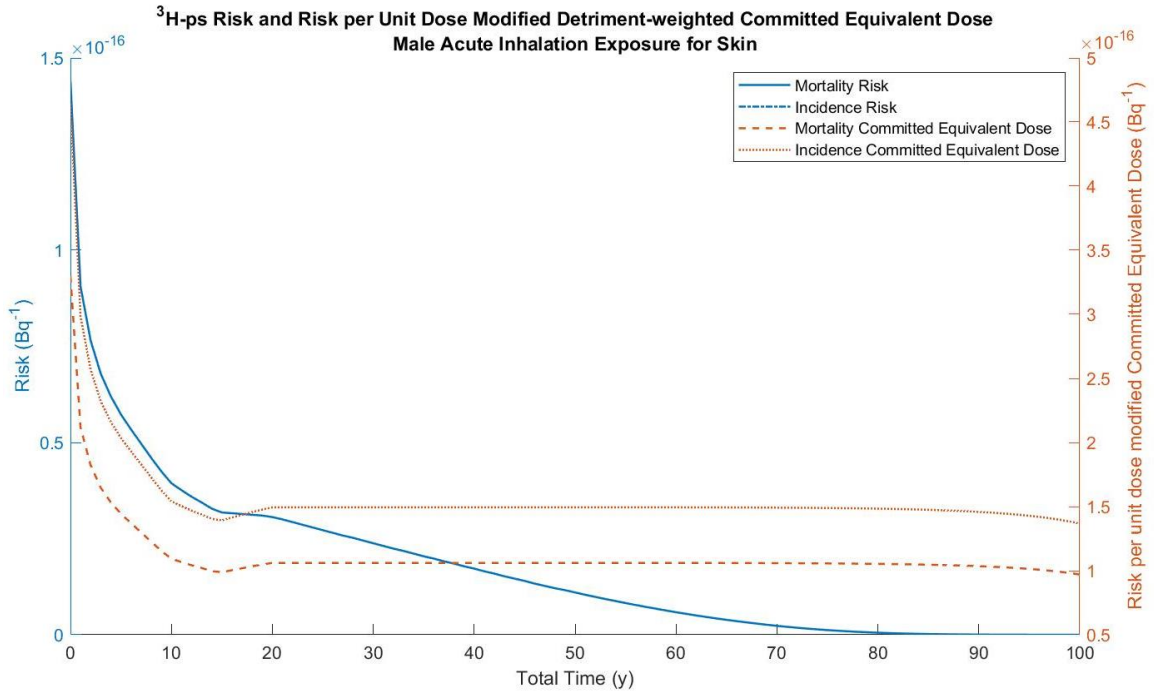

(d)

Figure 125. Risk and detriment-weighted committed equivalent dose to the (a) female lungs, (b) male lungs, (c) female skin, (d) male skin due to slow clearing tritium.

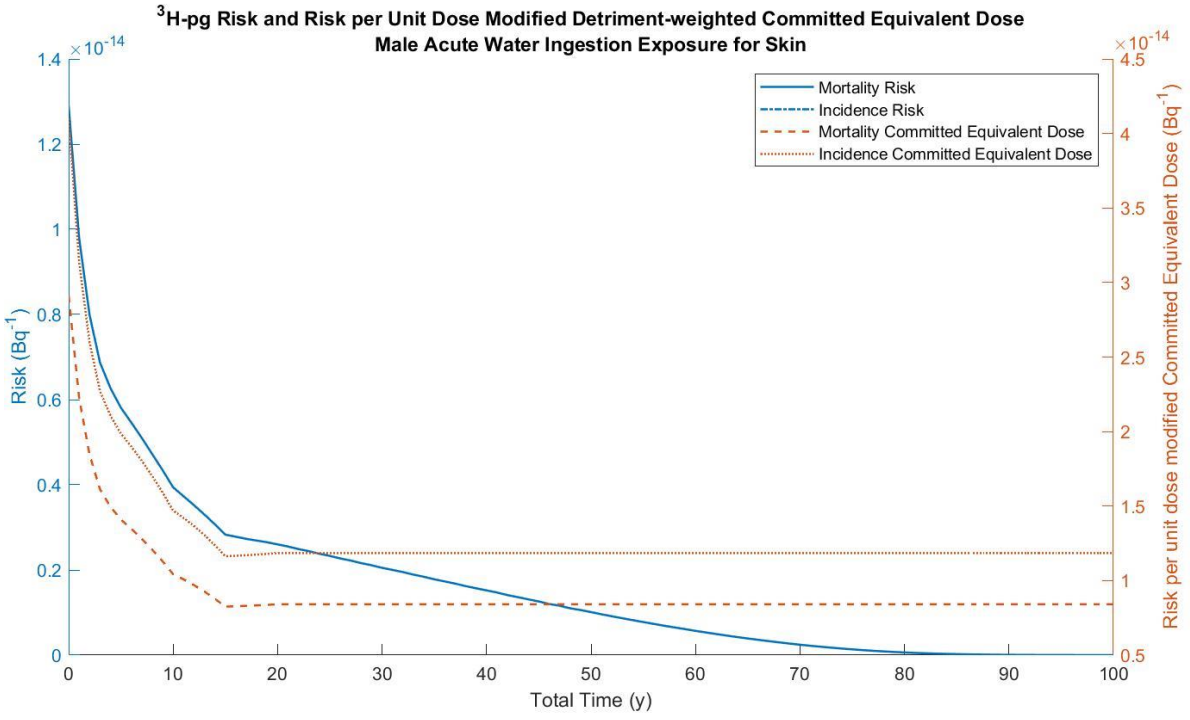

Figure 126. Risk and detriment-weighted committed equivalent dose to male skin for tap water ingested tritium.

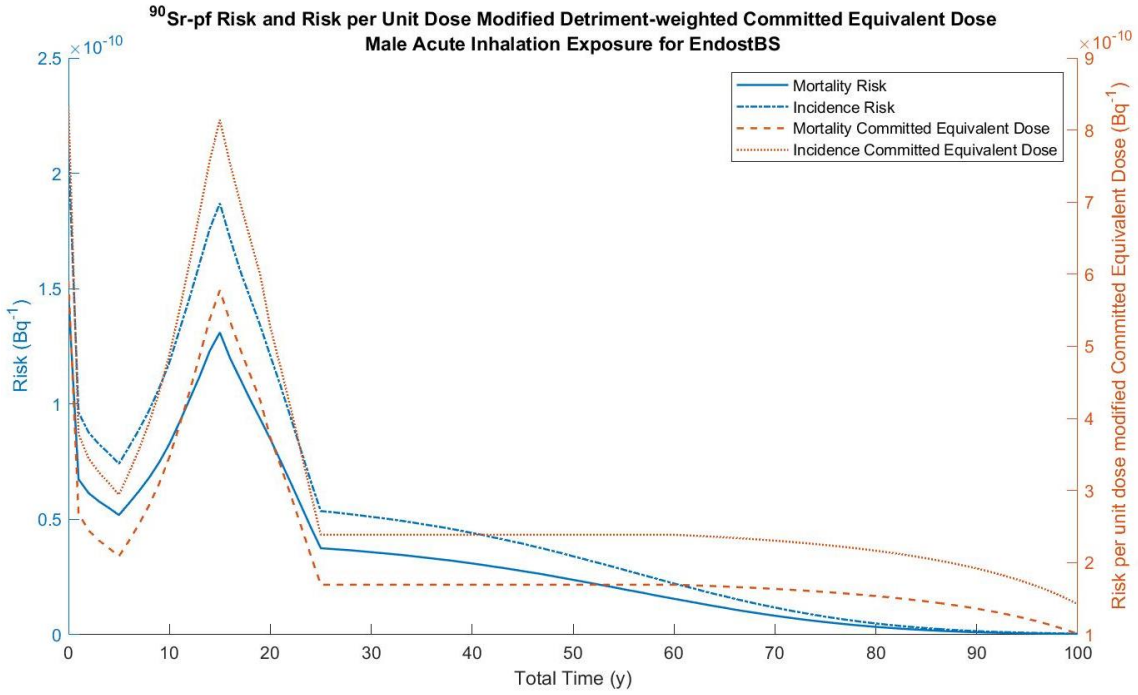
^{90}Sr-pf Risk and Risk per Unit Dose Modified Detriment-weighted Committed Equivalent Dose
Male Acute Inhalation Exposure for EndostBS
Mortality Risk
Incidence Risk
Mortality Committed Equivalent Dose
Incidence Committed Equivalent Dose
Risk (Bq^{-1})
Risk per unit dose modified Committed Equivalent Dose (Bq^{-1})
Total Time (y)

(a)

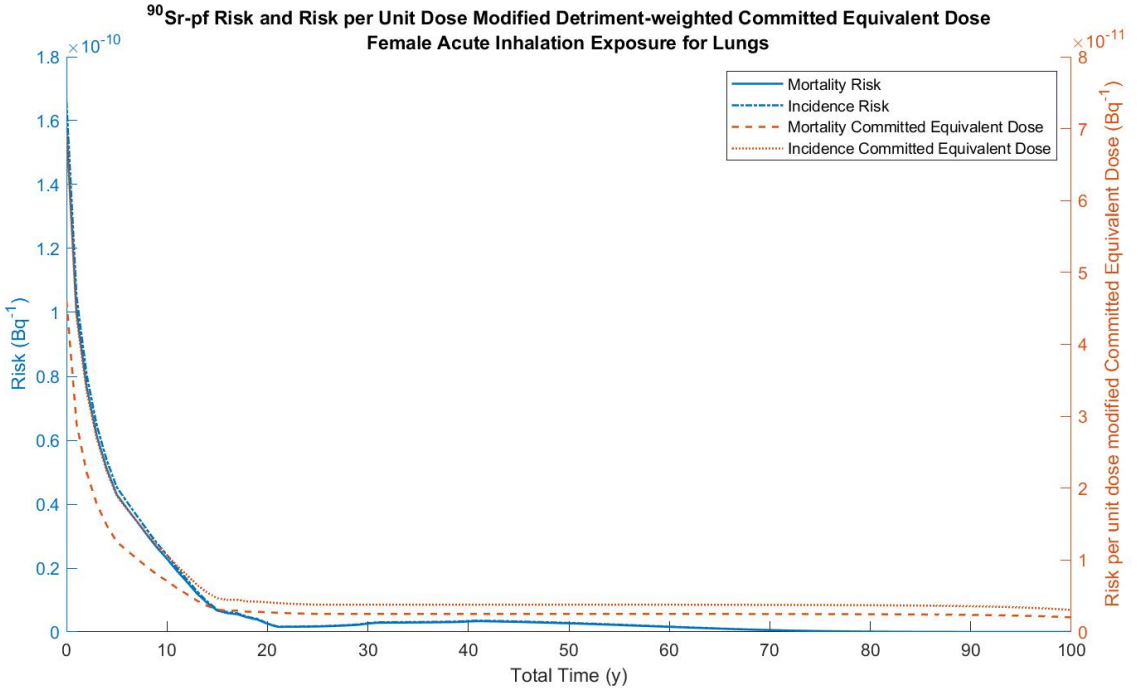
^{90}Sr-pf Risk and Risk per Unit Dose Modified Detriment-weighted Committed Equivalent Dose
Female Acute Inhalation Exposure for Lungs
Mortality Risk
Incidence Risk
Mortality Committed Equivalent Dose
Incidence Committed Equivalent Dose
Risk (Bq^{-1})
Risk per unit dose modified Committed Equivalent Dose (Bq^{-1})
Total Time (y)

(b)

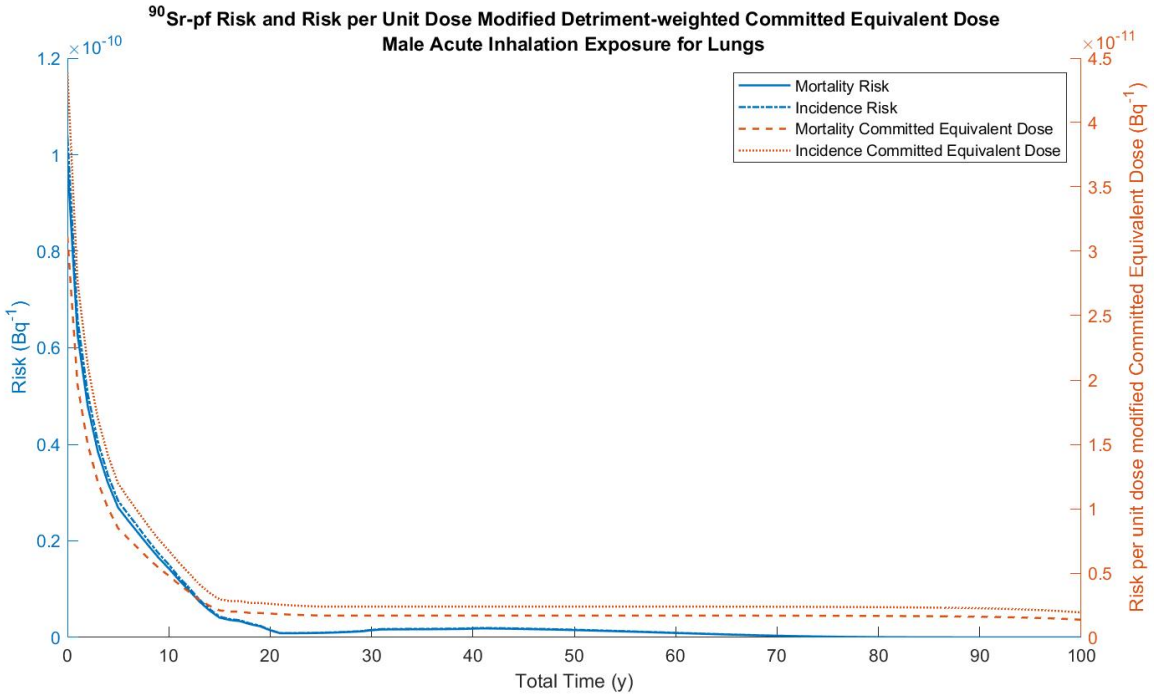

(c)

Figure 127. Risk and detriment-weighted committed equivalent dose to the (a) male bone surface, (b) female lungs, and (c) male lungs due to fast clearing ^{90}Sr.

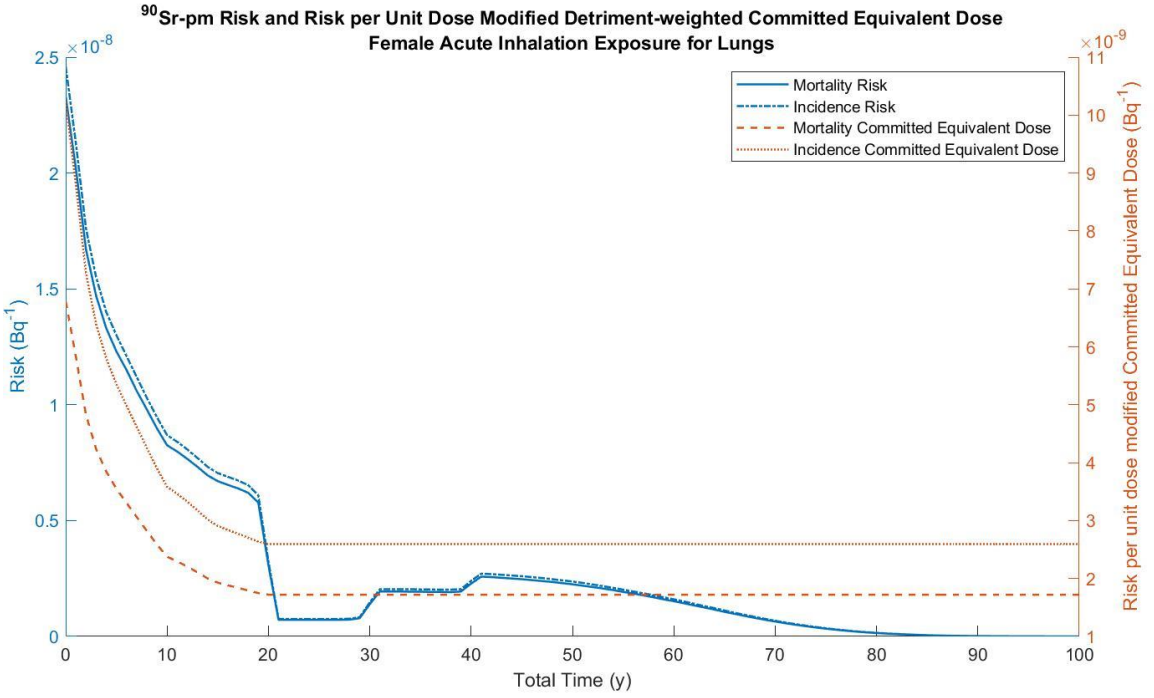

(a)

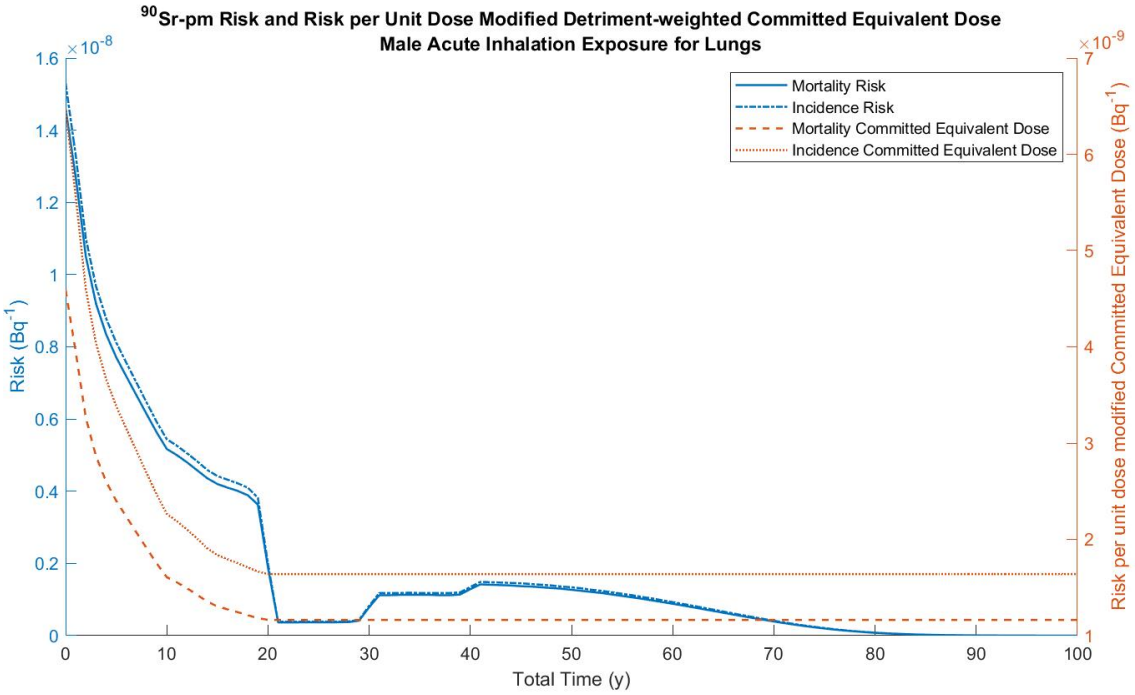

(b)

Figure 128. Risk and detriment-weighted committed equivalent dose to the (a) female lungs, and (b) male lungs due to moderate clearing ^{90}Sr.

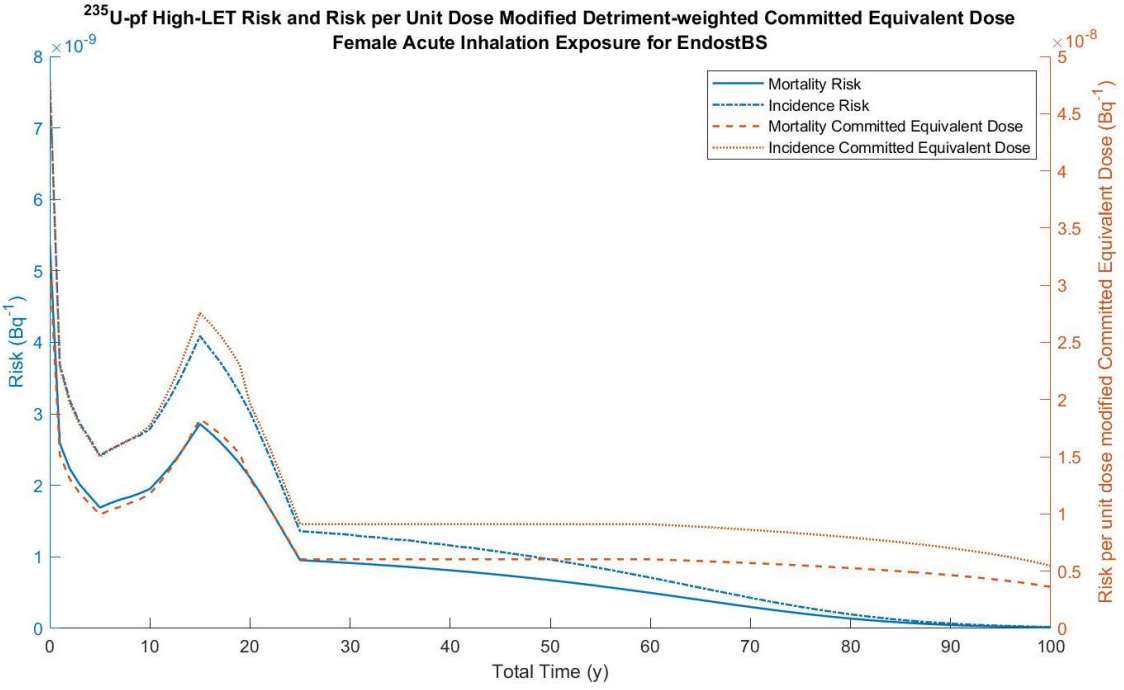

(a)

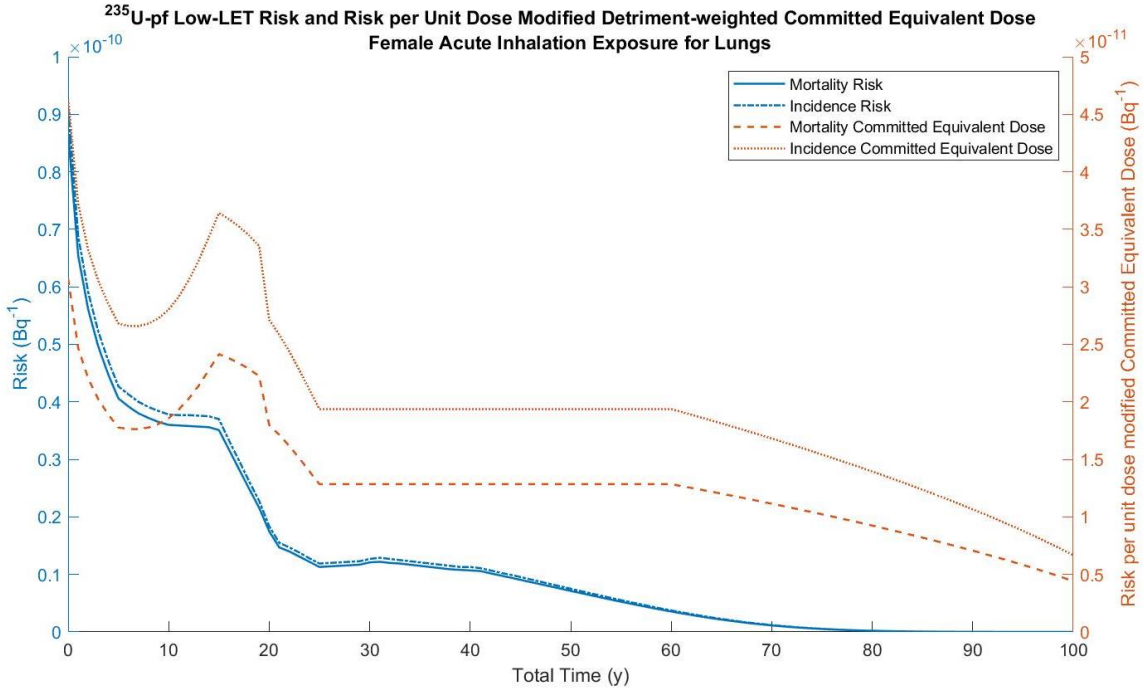
235U-pf Low-LET Risk and Risk per Unit Dose Modified Detriment-weighted Committed Equivalent Dose
Female Acute Inhalation Exposure for Lungs
Mortality Risk
Incidence Risk
Mortality Committed Equivalent Dose
Incidence Committed Equivalent Dose
Risk (Bq-1)
Risk per unit dose modified Committed Equivalent Dose (Bq-1)
Total Time (y)

(b)

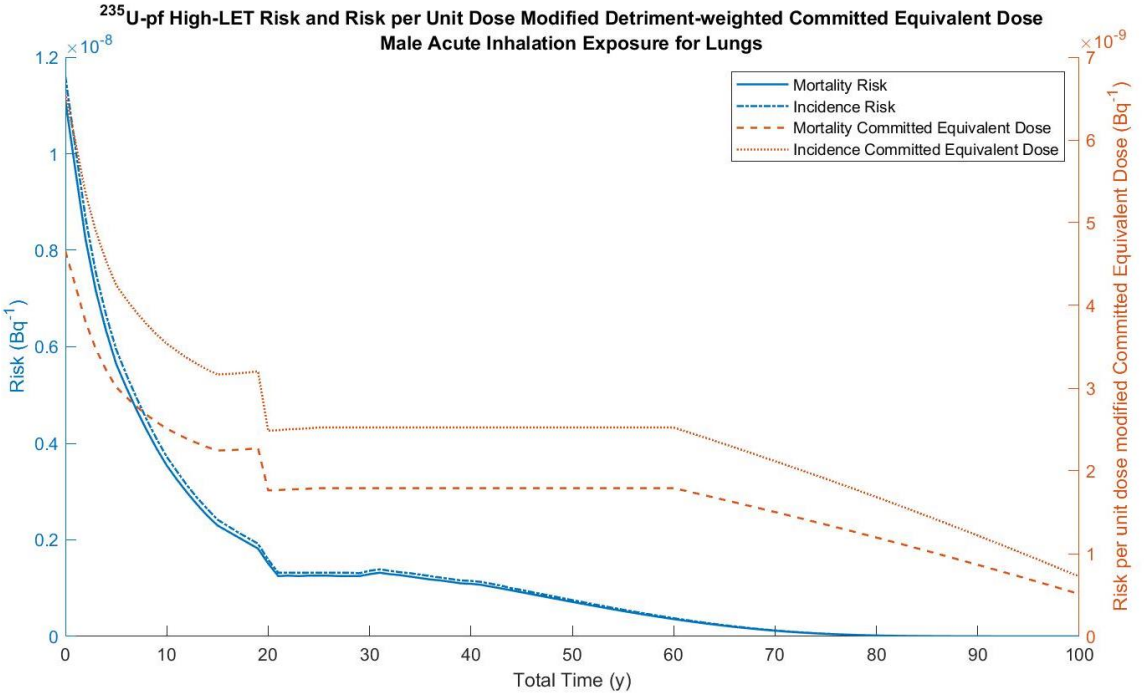
235U-pf High-LET Risk and Risk per Unit Dose Modified Detriment-weighted Committed Equivalent Dose
Male Acute Inhalation Exposure for Lungs
Mortality Risk
Incidence Risk
Mortality Committed Equivalent Dose
Incidence Committed Equivalent Dose
Risk (Bq-1)
Risk per unit dose modified Committed Equivalent Dose (Bq-1)
Total Time (y)

(c)

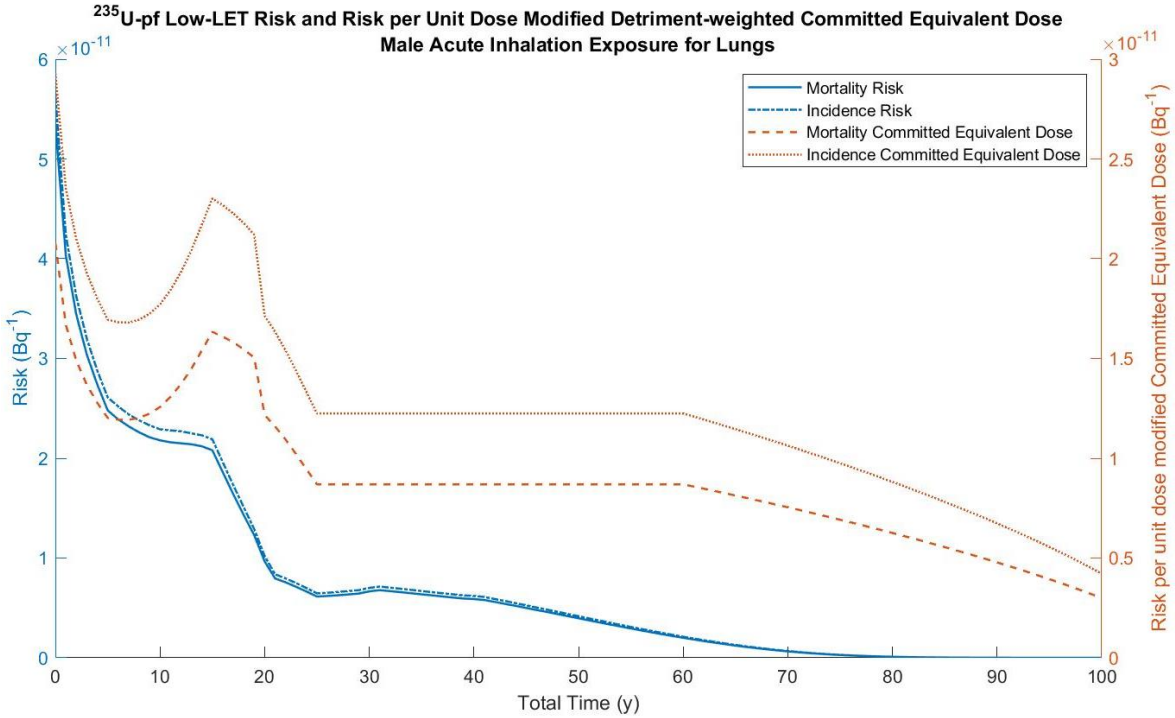

(d)

Figure 129. Risk and detriment-weighted committed equivalent dose to the male bone surface due to the (a) high-LET component and (b) low-LET component and to the male lungs due to the (c) high-LET component and (d) low-LET component of fast clearing ^{235}U.

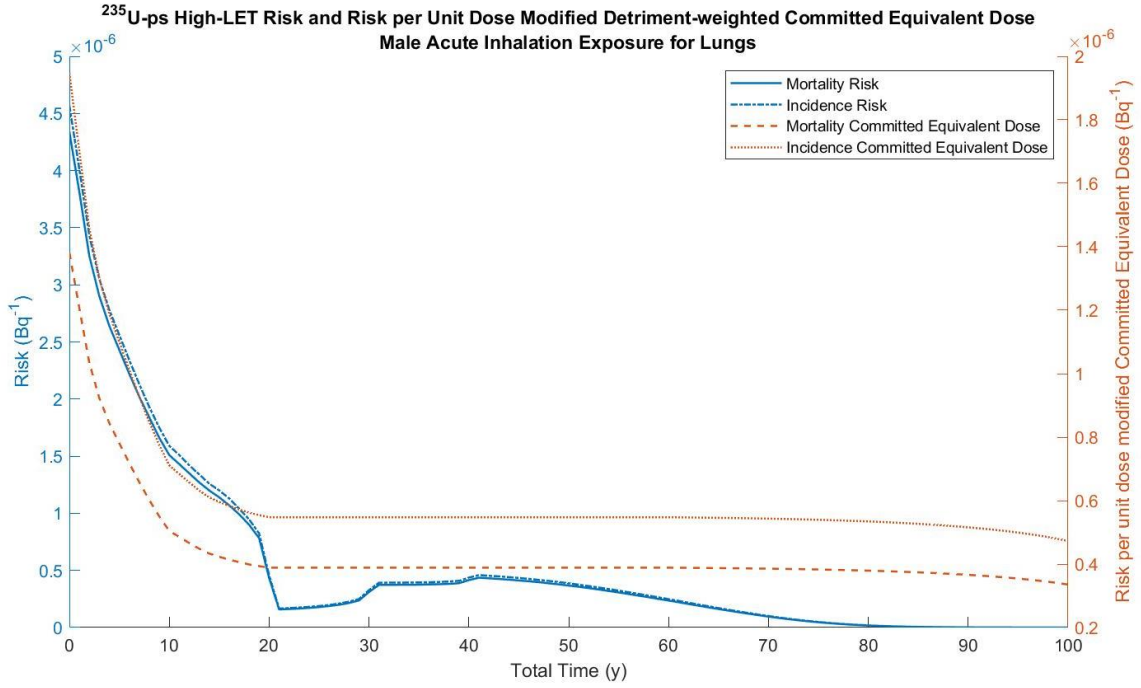

(a)

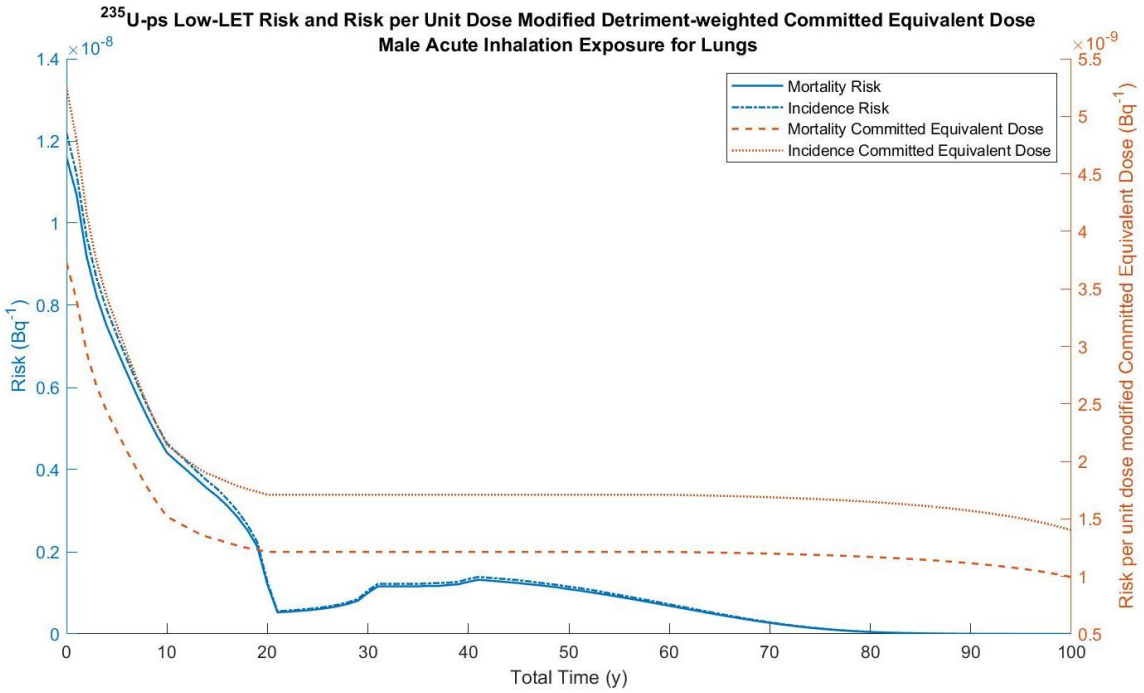

(b)

Figure 130. Risk and detriment-weighted committed equivalent dose to the male lungs due to (a) the high-LET component and (b) low-LET component of slow clearing ^{235}U.

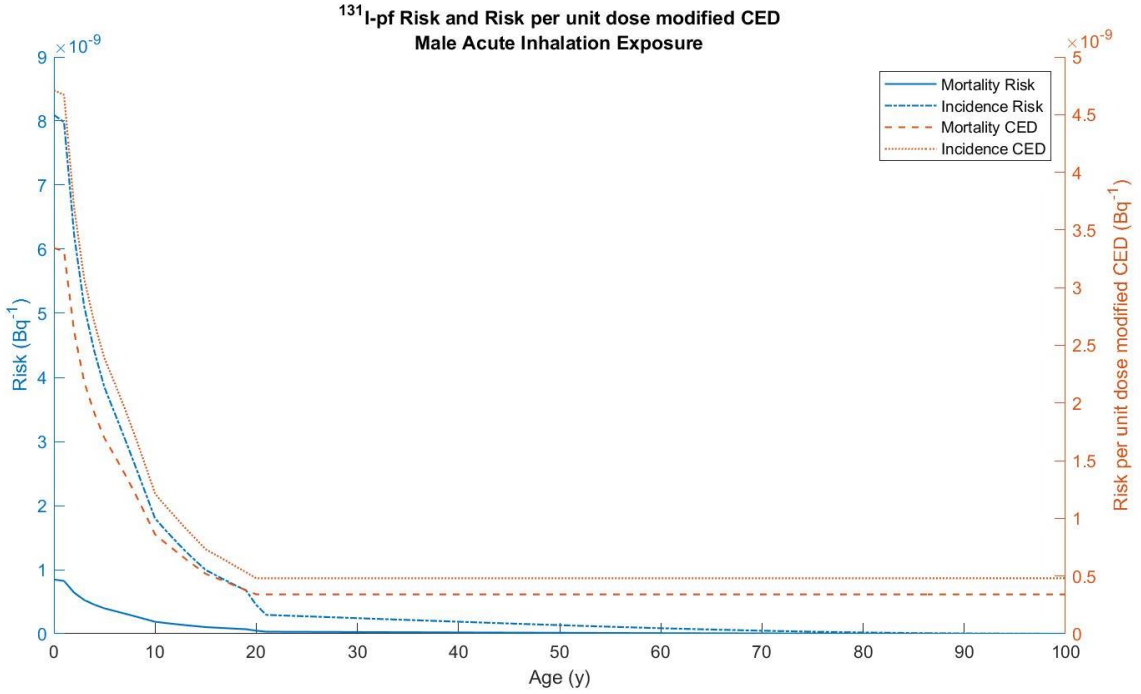

(c)

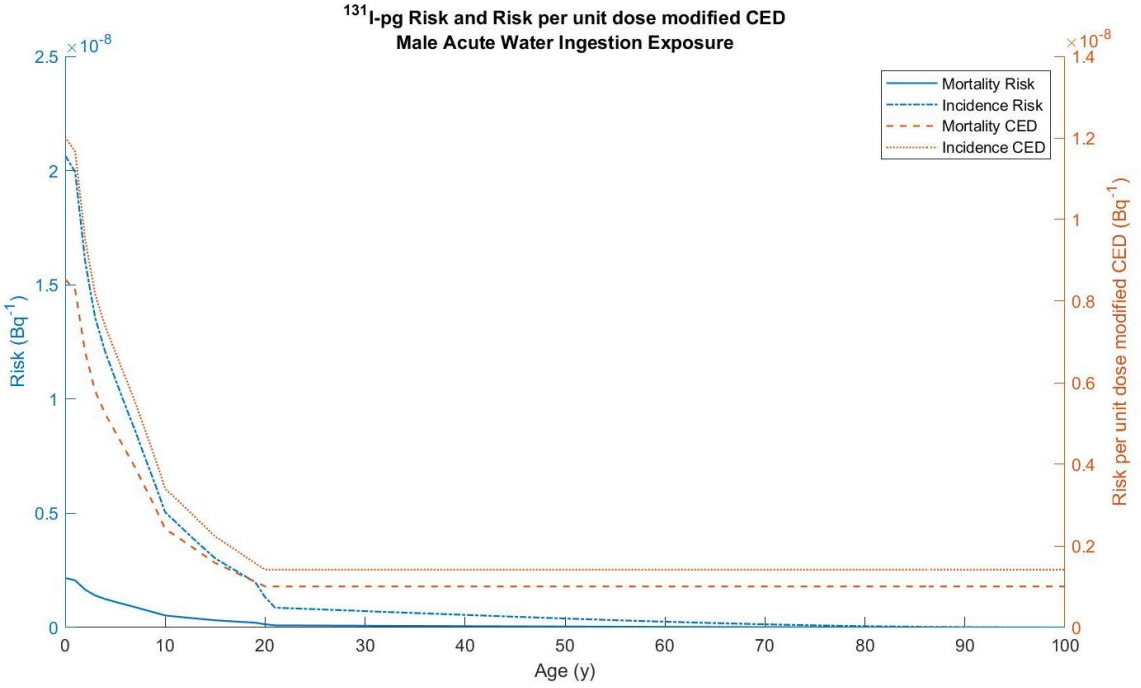

(d)

Figure 131. Risk and risk per unit dose modified CED for the whole body in males due to (a) fast-clearing and (b) tap water ingested ^{131}I.

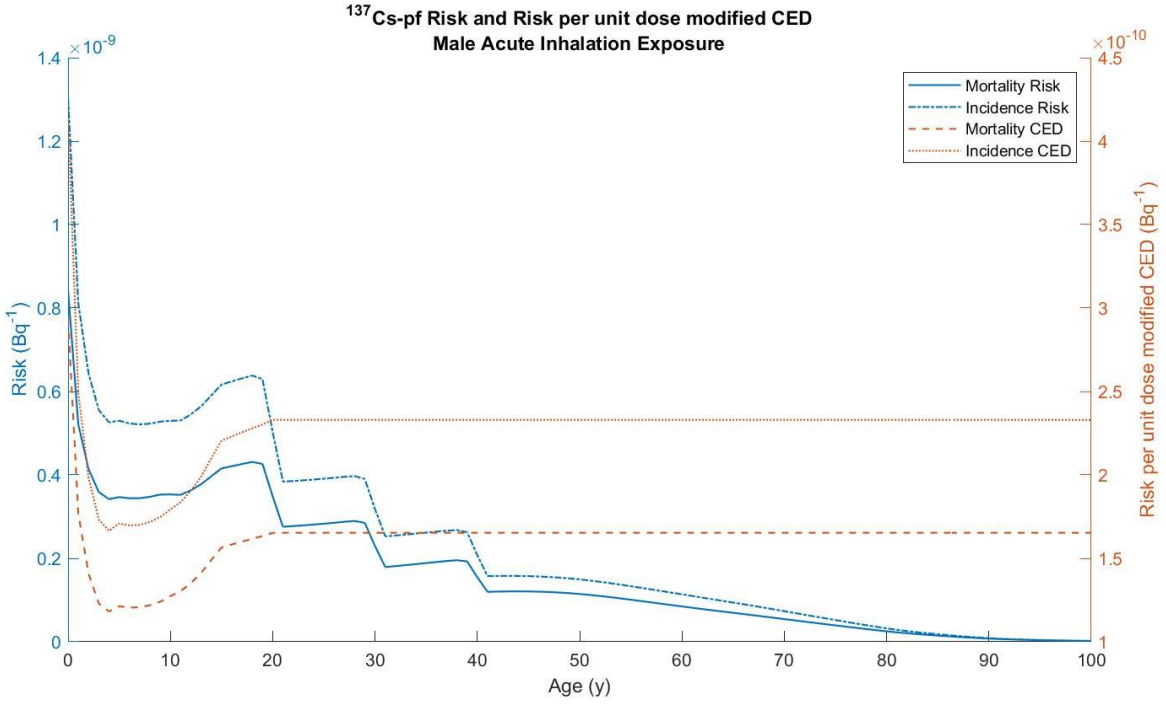
137Cs-pf Risk and Risk per unit dose modified CED
Male Acute Inhalation Exposure
Mortality Risk
Incidence Risk
Mortality CED
Incidence CED
Risk (Bq-1)
Risk per unit dose modified CED (Bq-1)
Age (y)

(a)

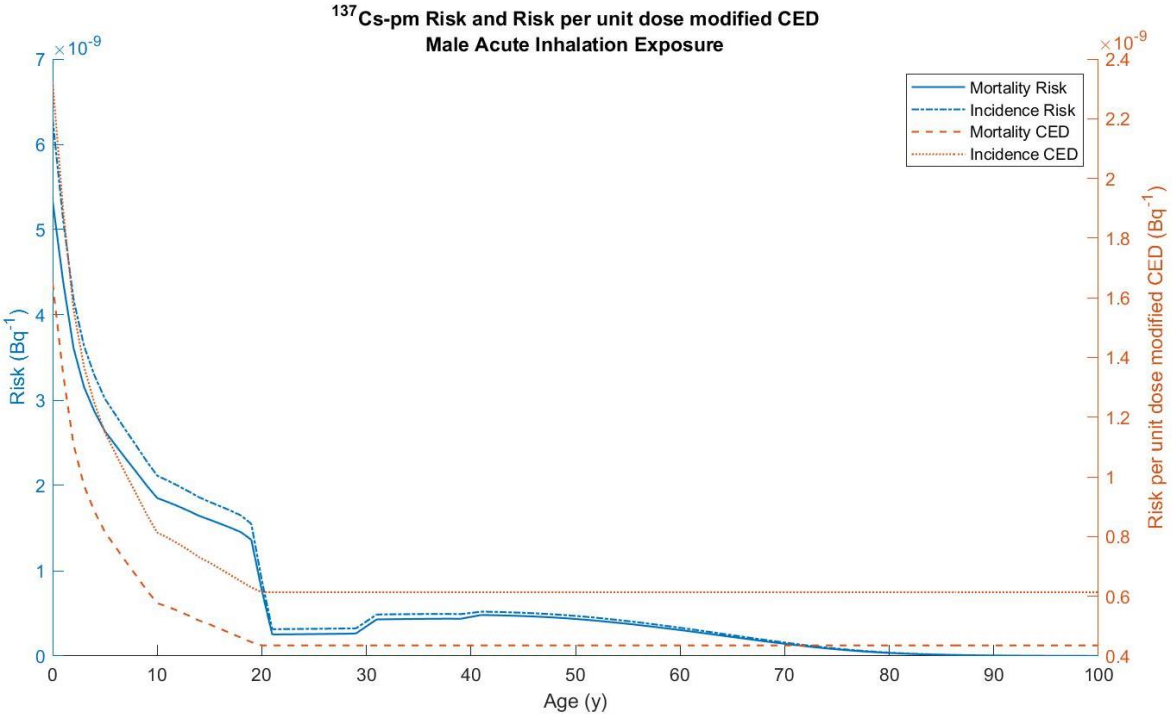
137Cs-pm Risk and Risk per unit dose modified CED
Male Acute Inhalation Exposure
Mortality Risk
Incidence Risk
Mortality CED
Incidence CED
Risk (Bq-1)
Risk per unit dose modified CED (Bq-1)
Age (y)

(b)

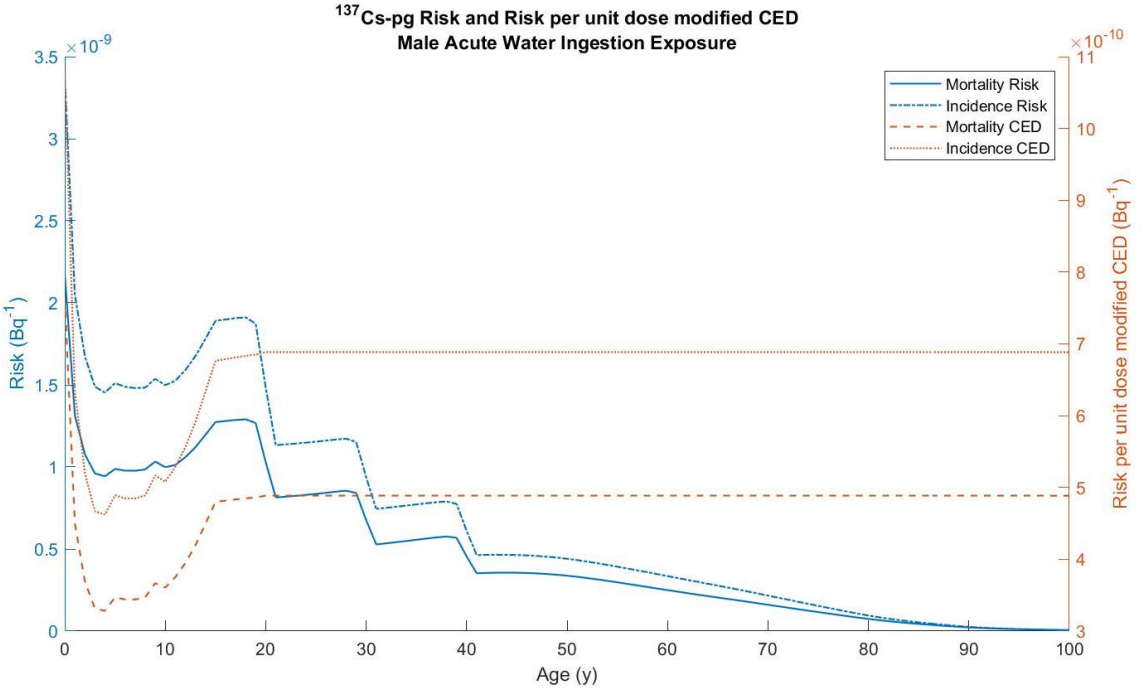

(c)

Figure 132. Risk and risk per unit dose modified CED for the whole body in males due to (a) fast-clearing, (b) moderate-clearing, and (c) tap water ingested ^{137}Cs.

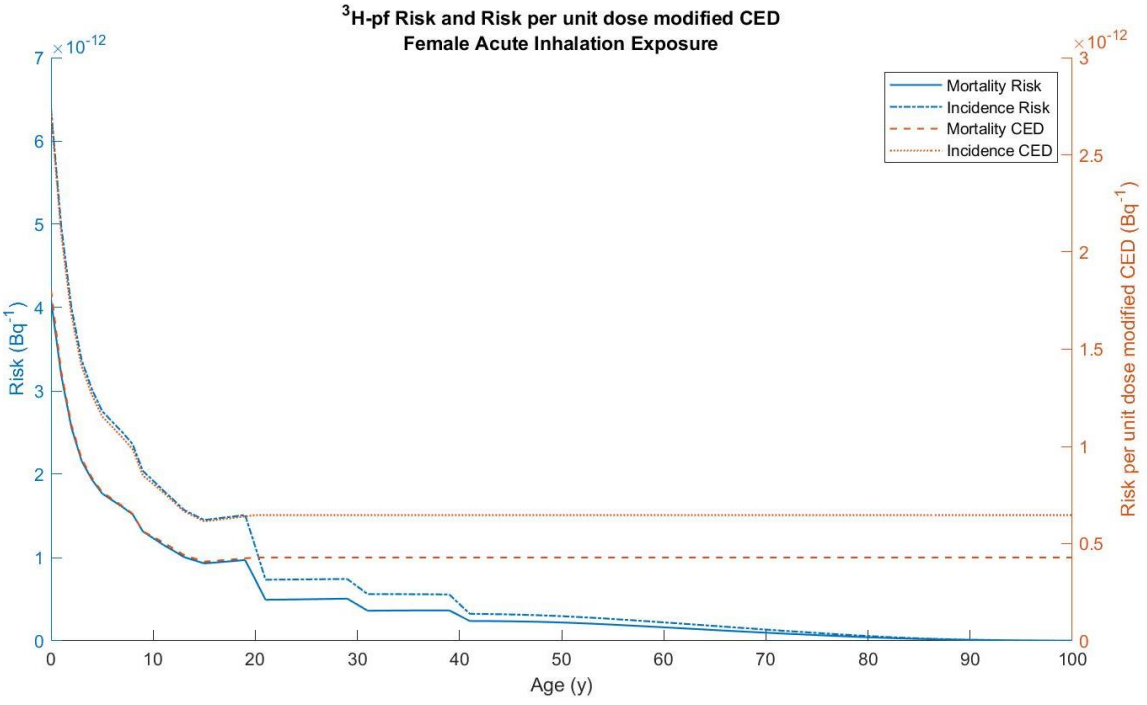

(a)

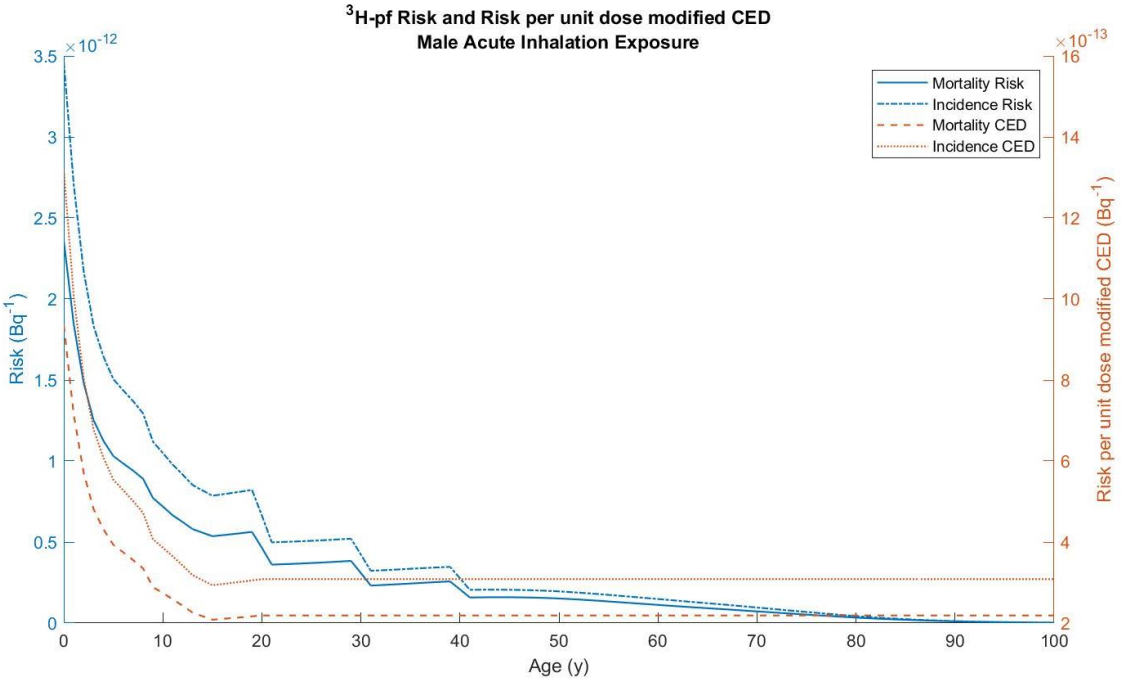

(b)

Figure 133. Risk and risk per unit dose modified CED for the whole body in (a) females and (b) males due to fast clearing tritium.

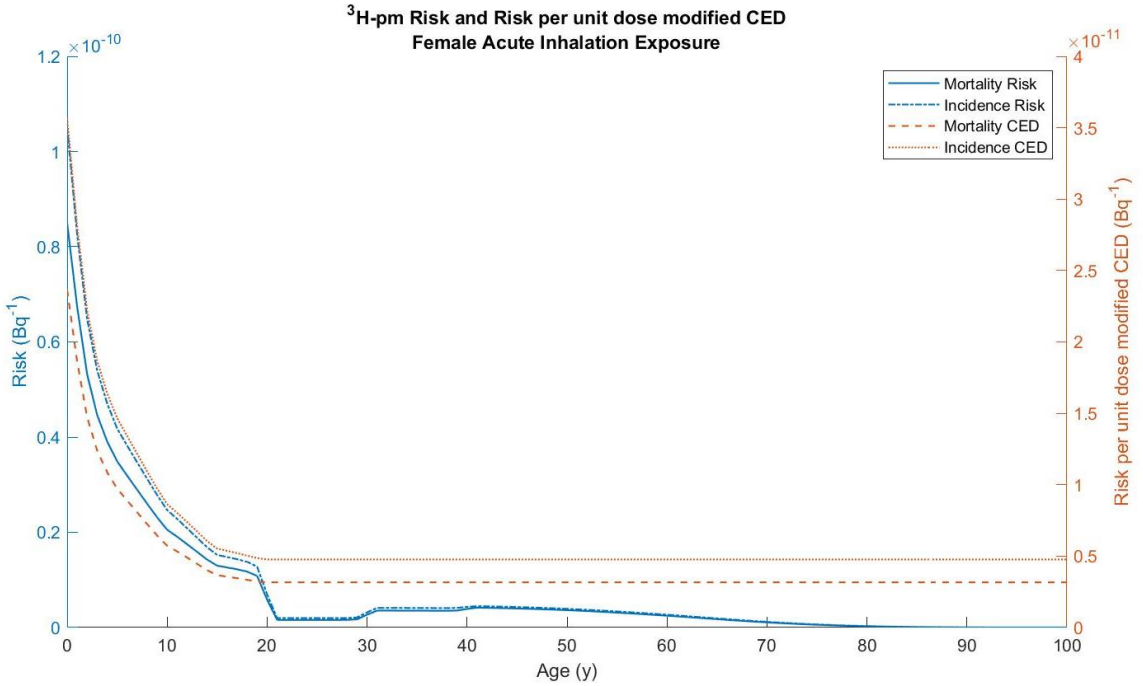

(a)

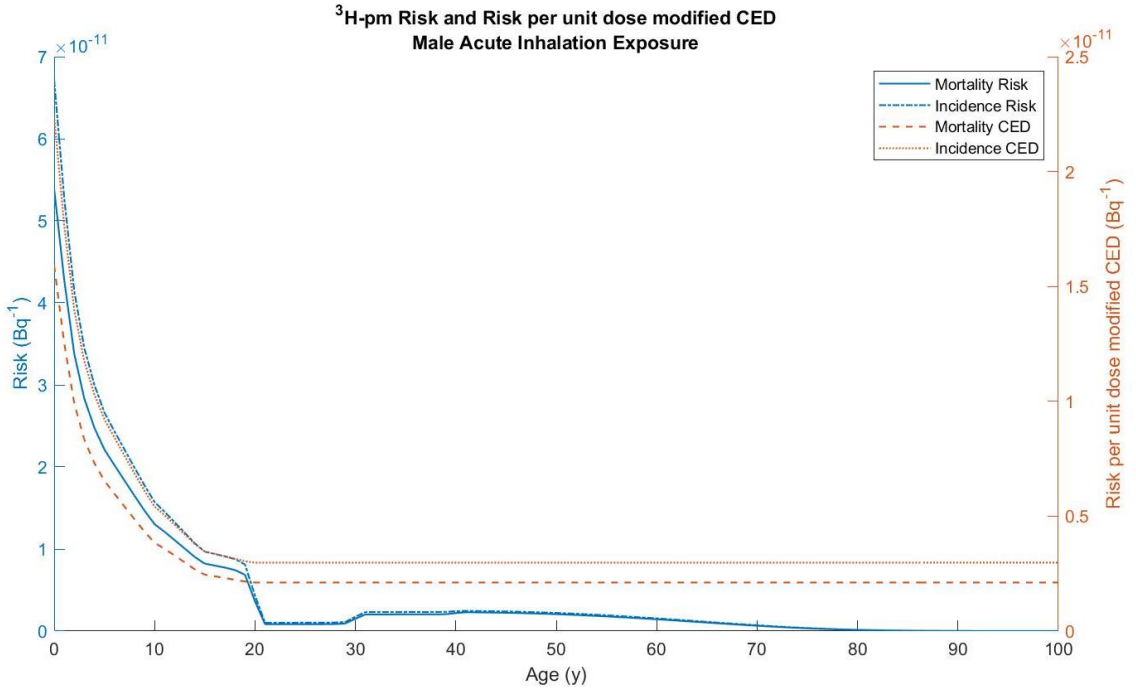

(b)

Figure 134. Risk and risk per unit dose modified CED for the whole body in (a) females and (b) males due to moderate clearing tritium.

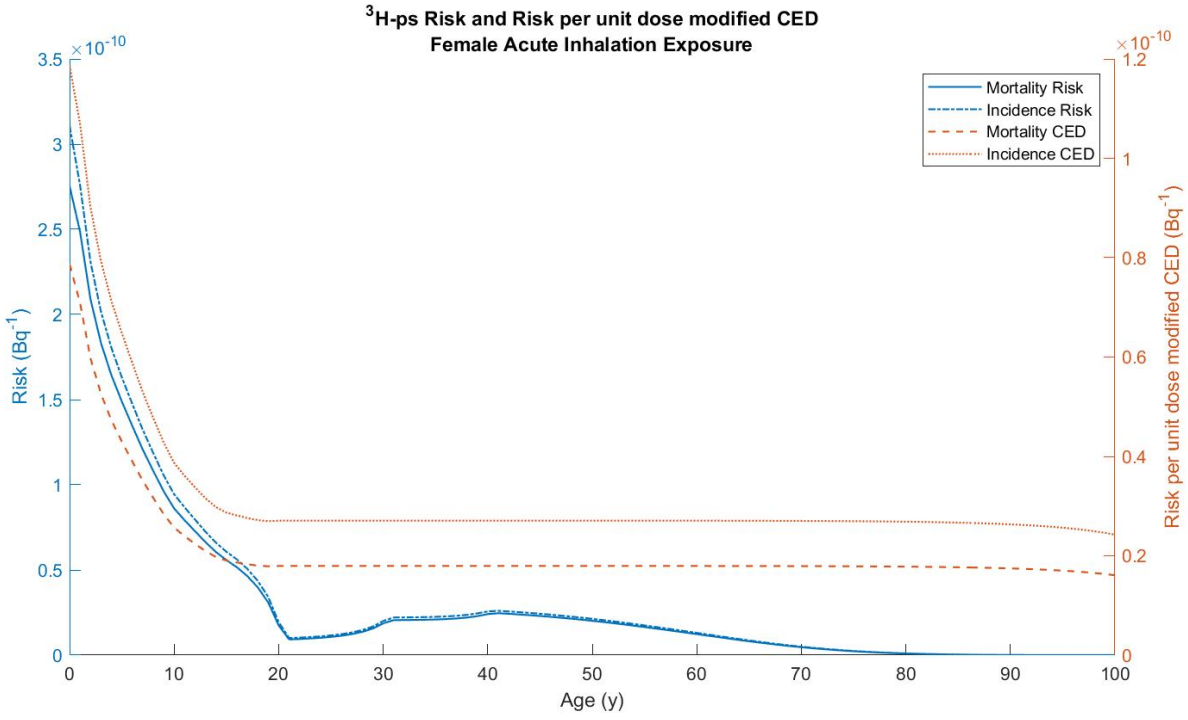

(a)

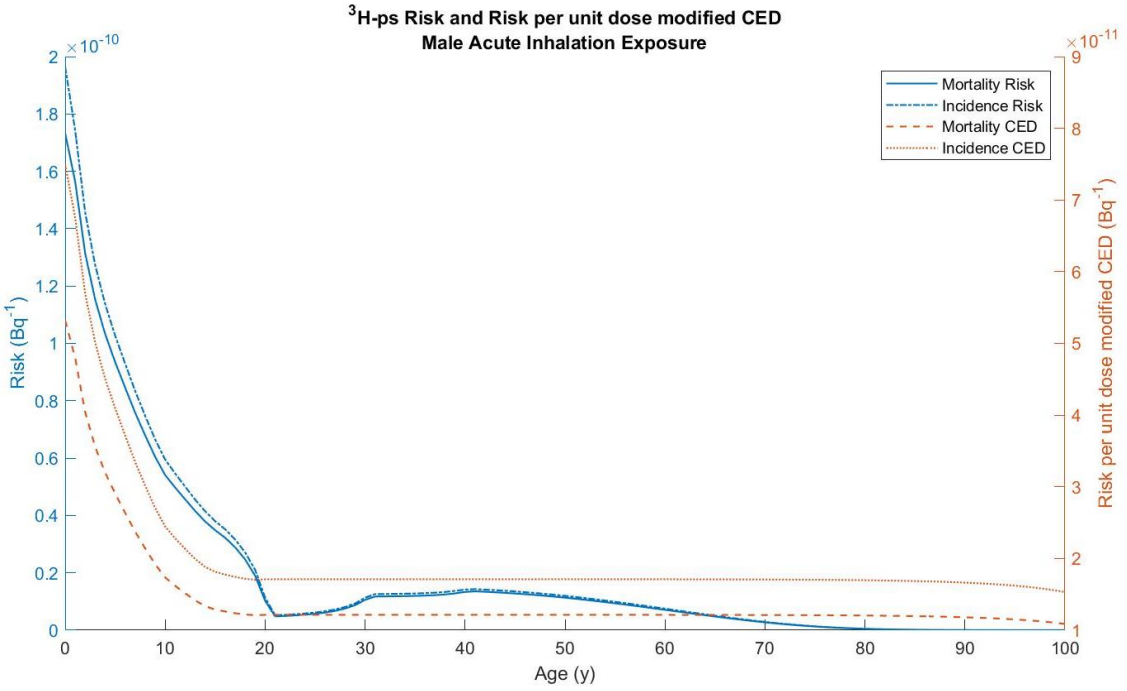

(b)

Figure 135. Risk and risk per unit dose modified CED for the whole body in (a) females and (b) males due to slow clearing tritium.

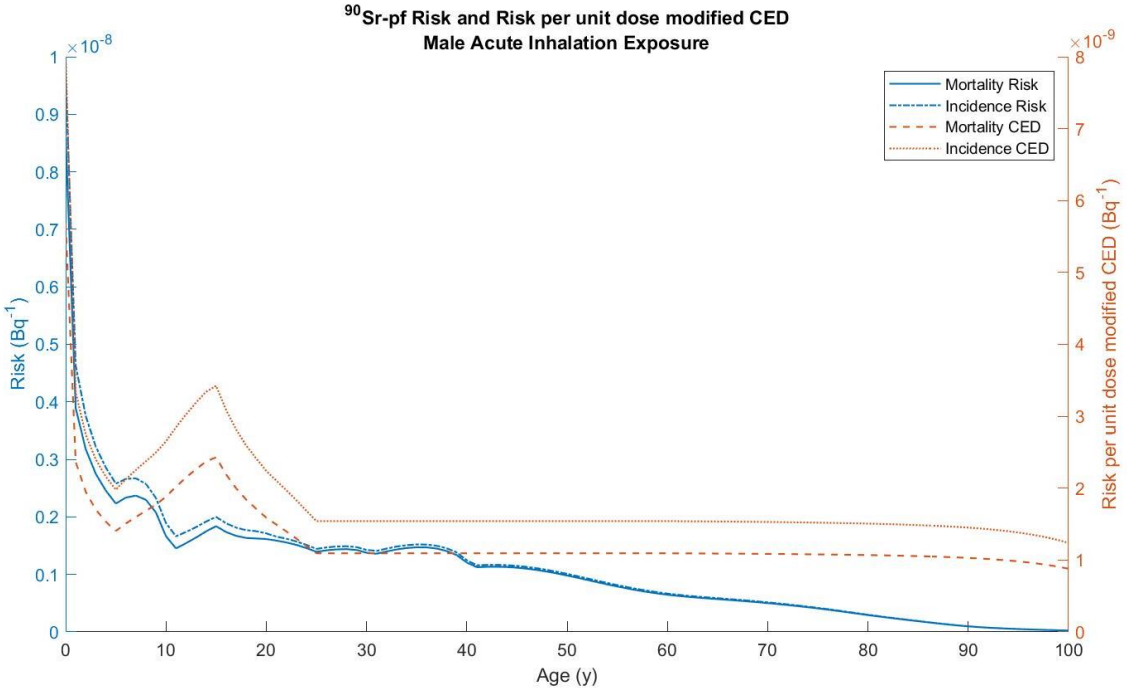

(a)

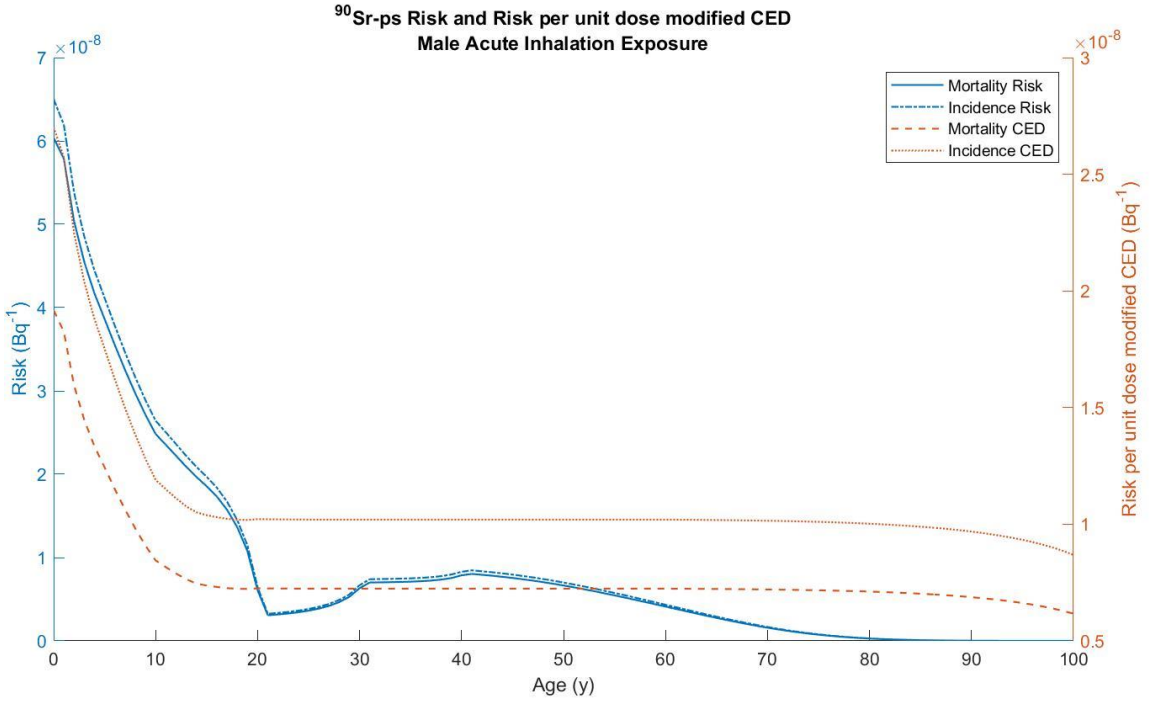

(b)

Figure 136. Risk and risk per unit dose modified CED for the whole body in males due to (a) fast-clearing and (b) slow-clearing ^{90}Sr.

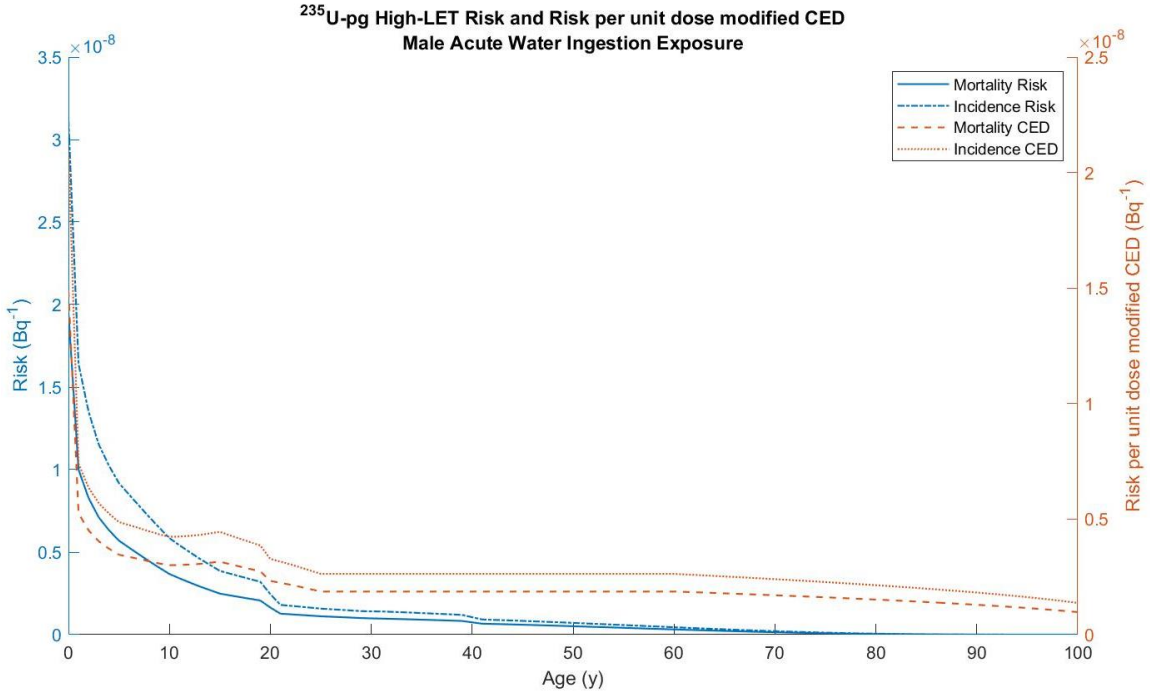

(a)

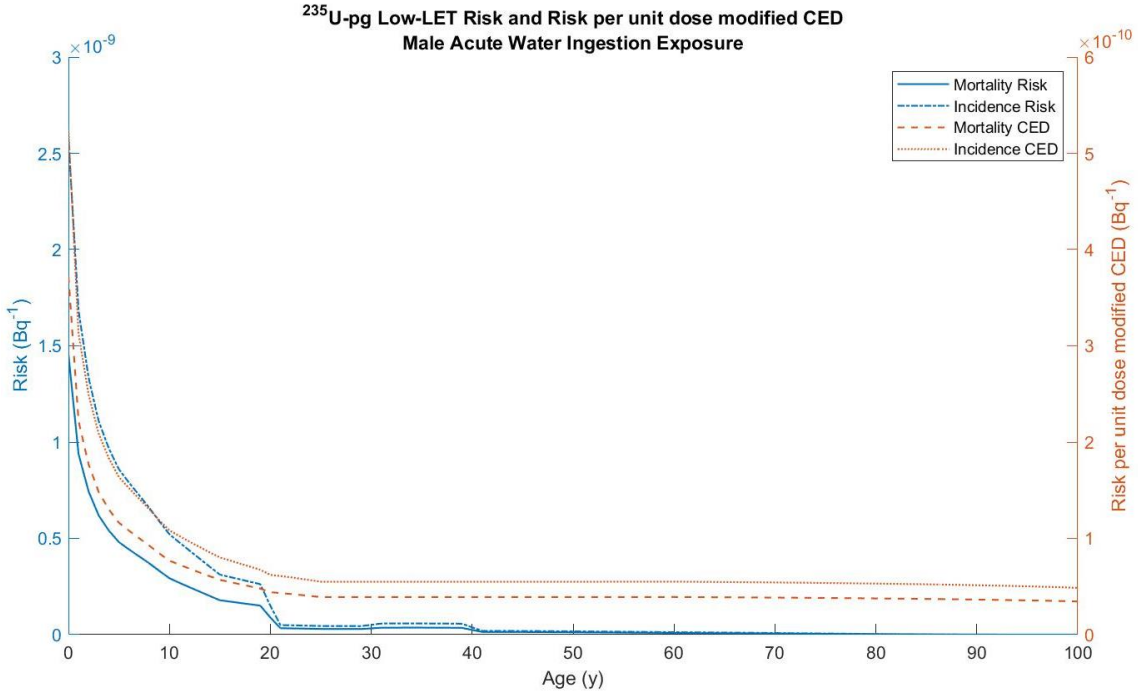

(b)

Figure 137. Risk and risk per unit dose modified CED for the whole body in males due to (a) the high-LET component and (b) low-LET component of tap water ingested ^{235}U.

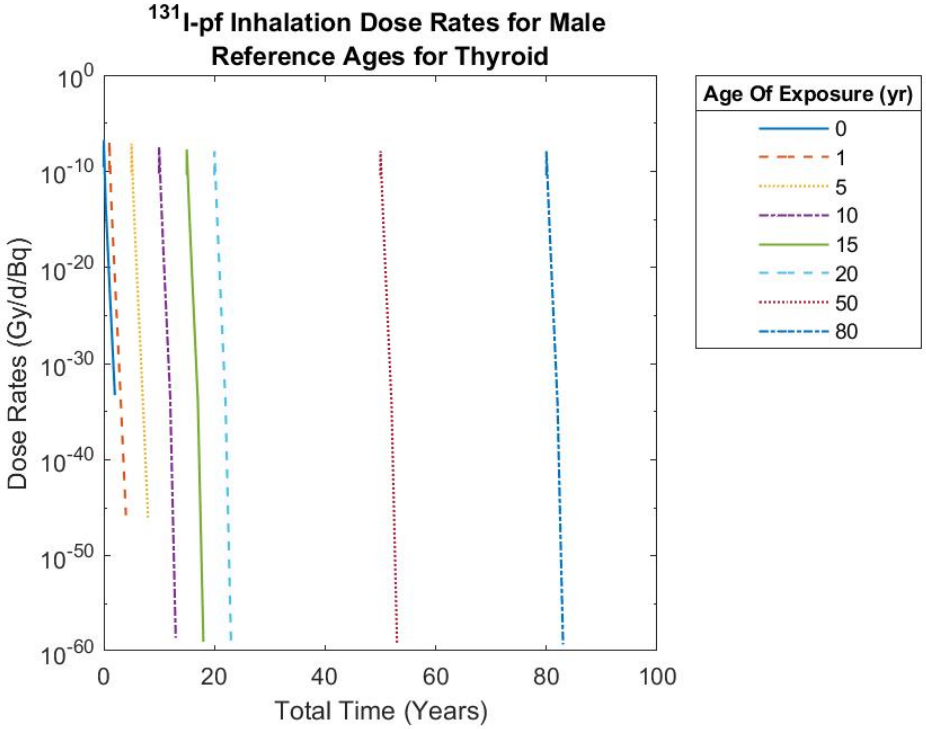

Figure 138. Dose rates to the male thyroid due to fast clearing ^{131}I.

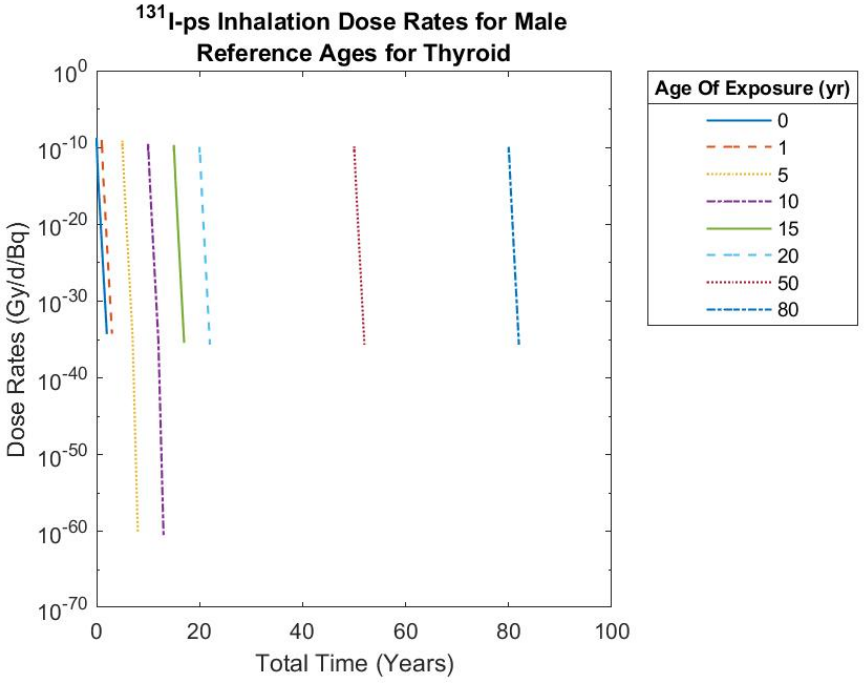

(a)

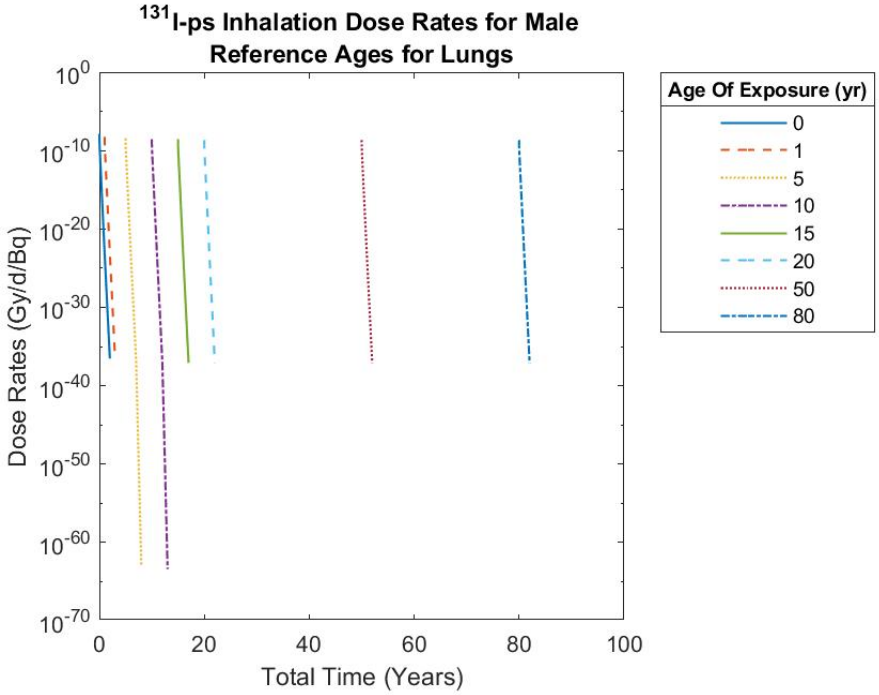

(b)

Figure 139. Dose rates to the (a) male thyroid and (b) male lungs due to slow-clearing ^{131}I.

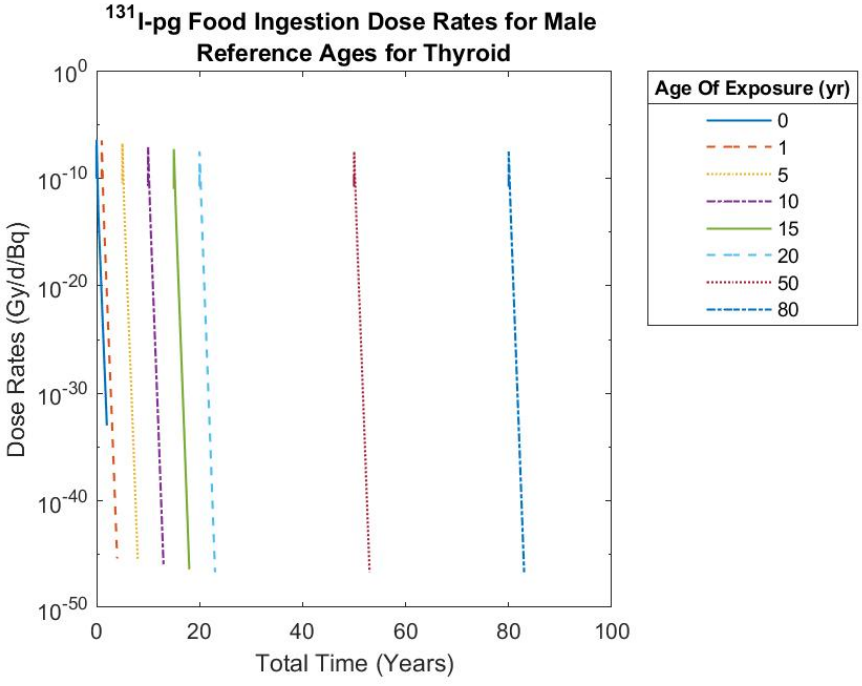

(a)

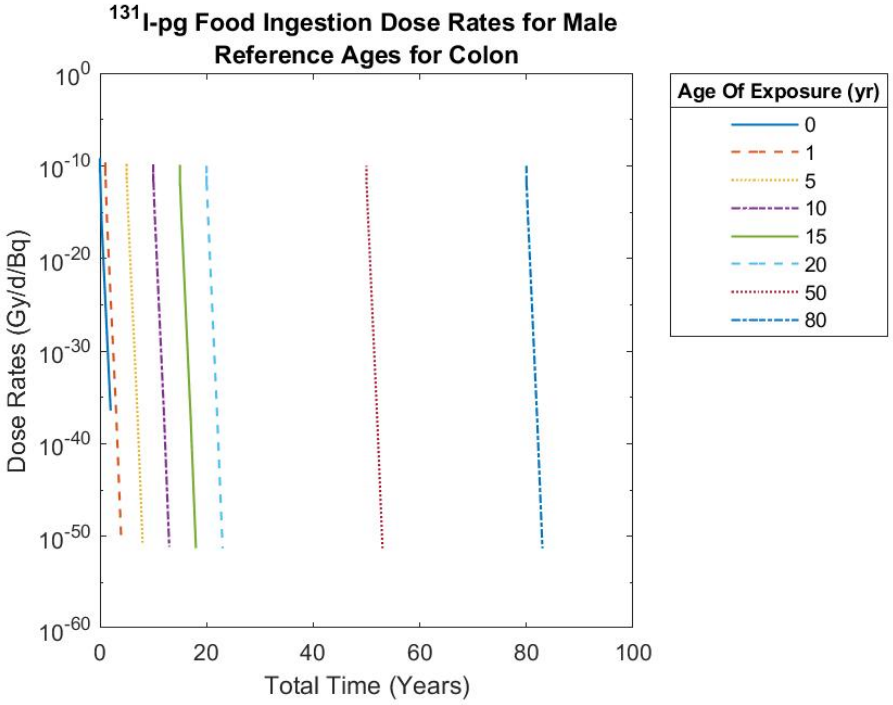

(b)

Figure 140. Dose rates to the (a) male thyroid and (b) male colon due to food ingested ^{131}I.

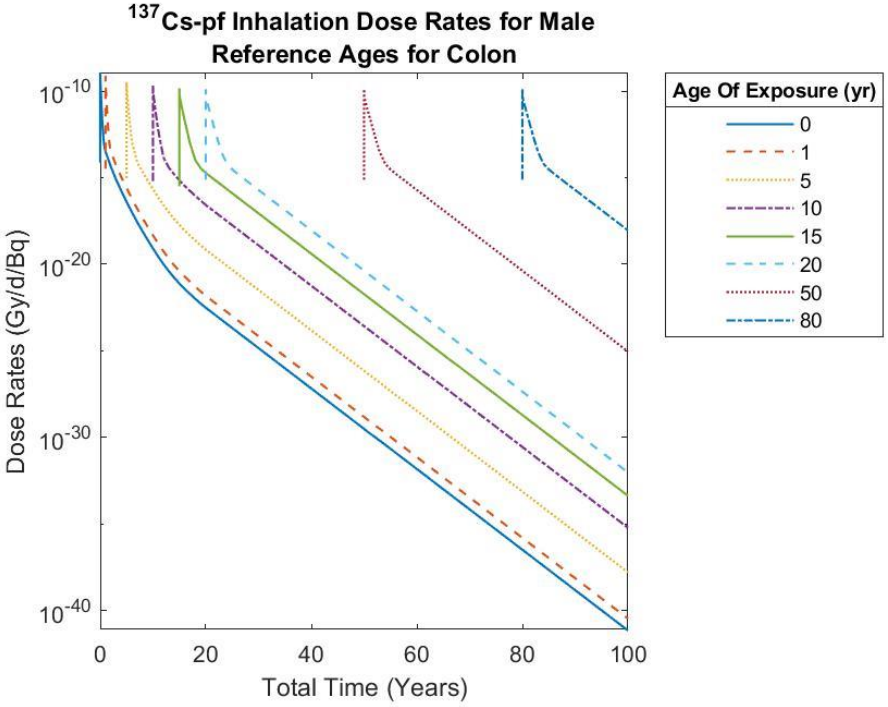

(a)

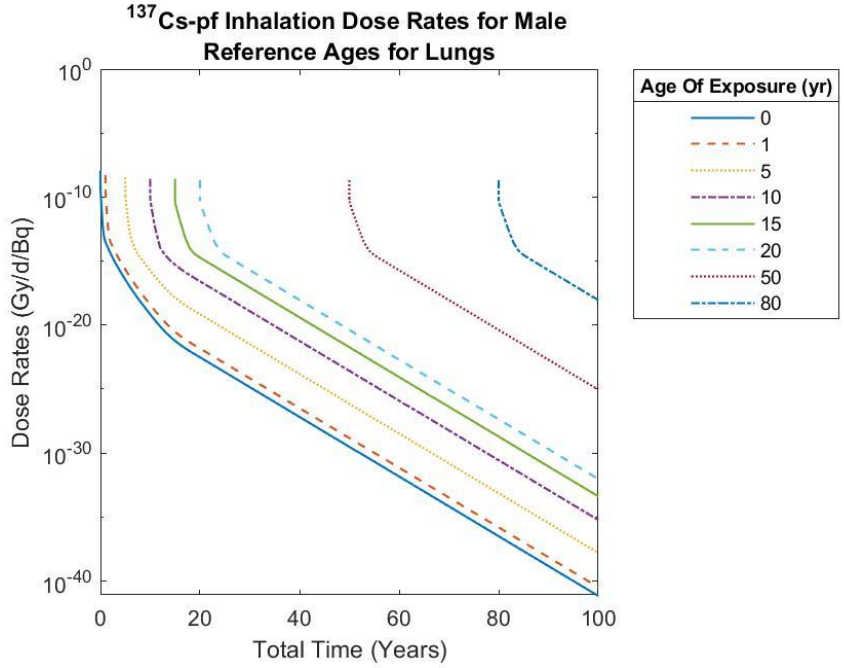

(b)

Figure 141. Dose rates to the (a) male colon and (b) male lungs due to fast-clearing ^{137}Cs.

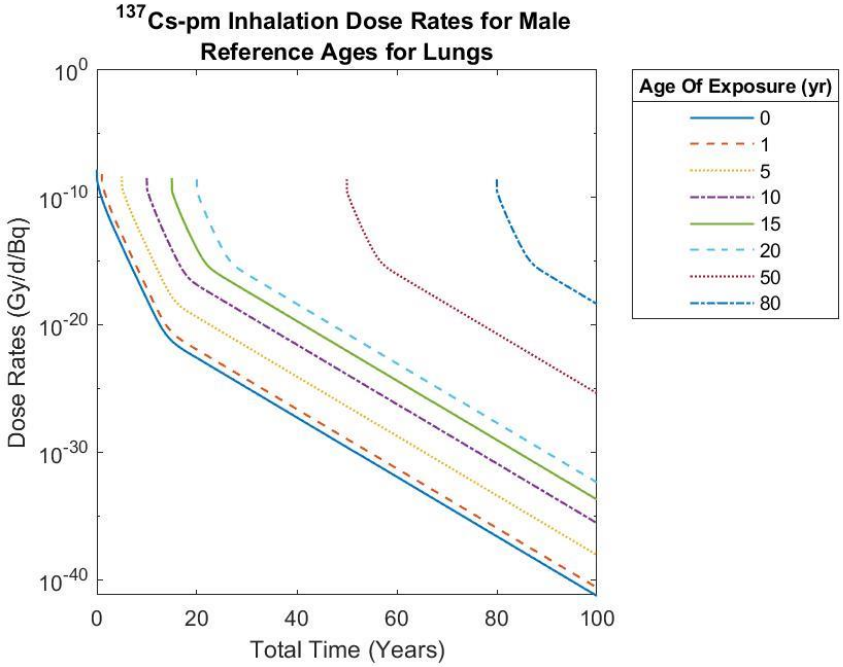

Figure 142. Dose rates to the male lungs due to moderate-clearing ^{137}Cs.

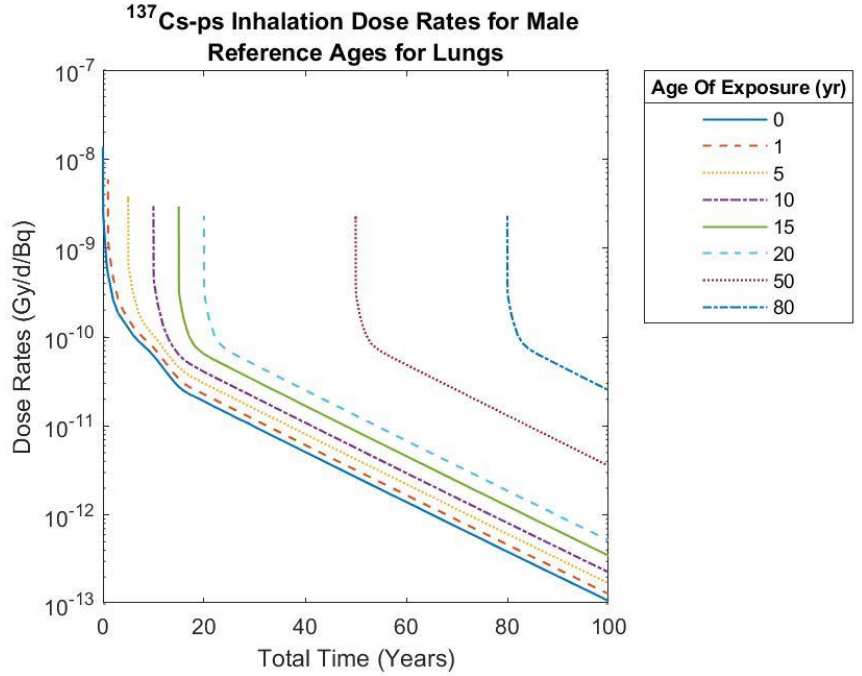

(a)

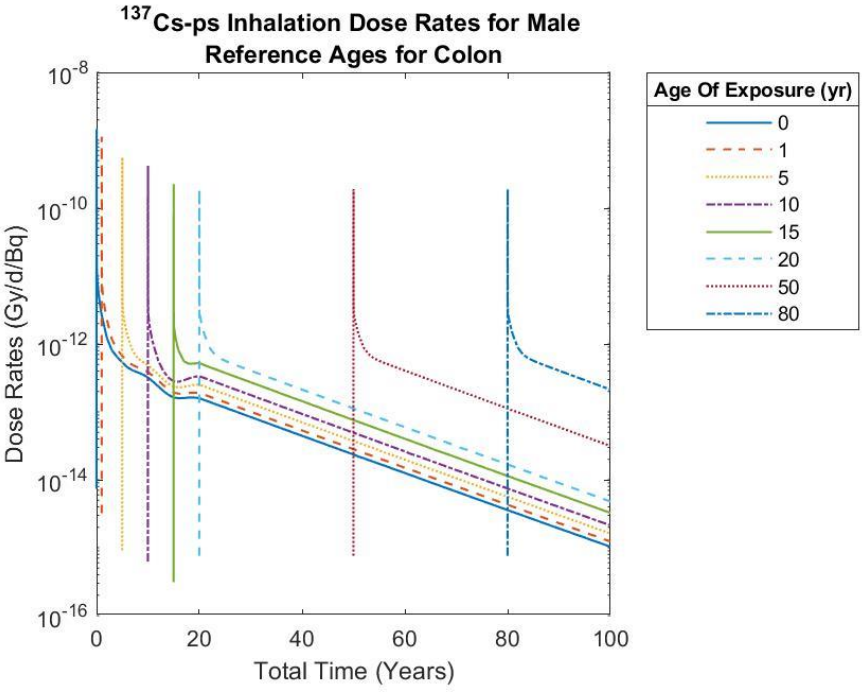

(b)

Figure 143. Dose rates to the (a) male lungs and (b) male colon due to slow-clearing ^{137}Cs.

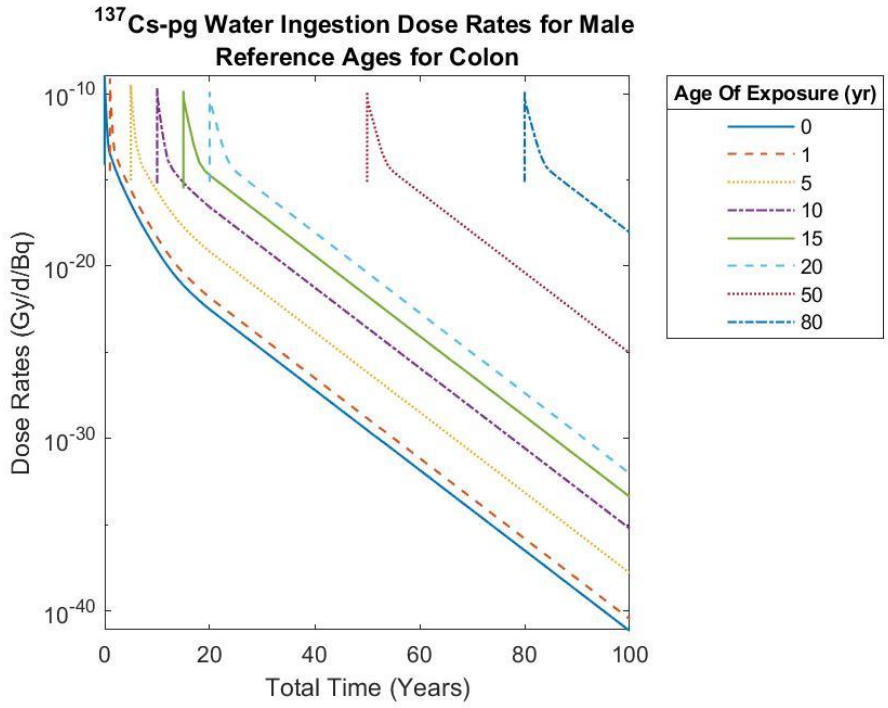

Figure 144. Dose rates to the male colon due to tap water ingested ^{137}Cs.

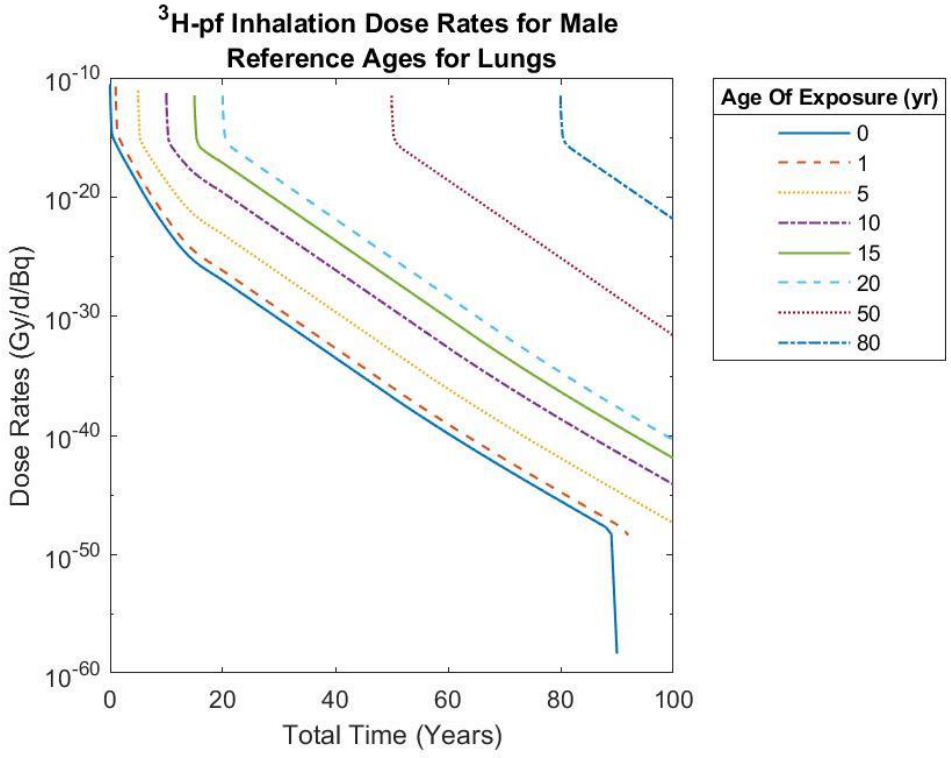

(a)

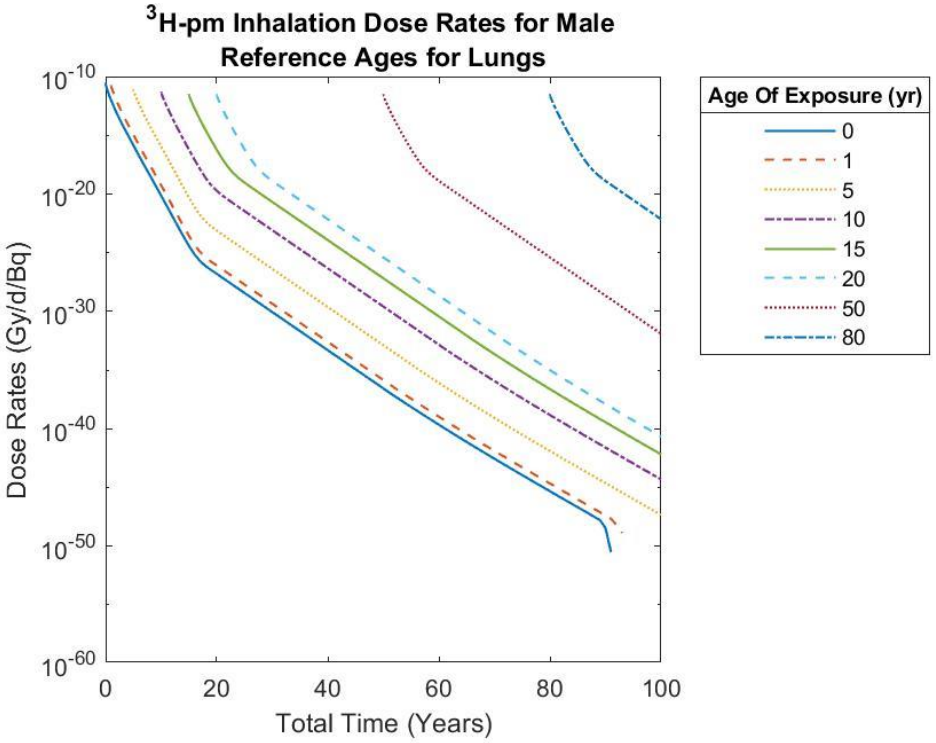
^{3}H-pm Inhalation Dose Rates for Male
Reference Ages for Lungs
Dose Rates (Gy/d/Bq)
Total Time (Years)
Age Of Exposure (yr)
0
1
5
10
15
20
50
80

(b)

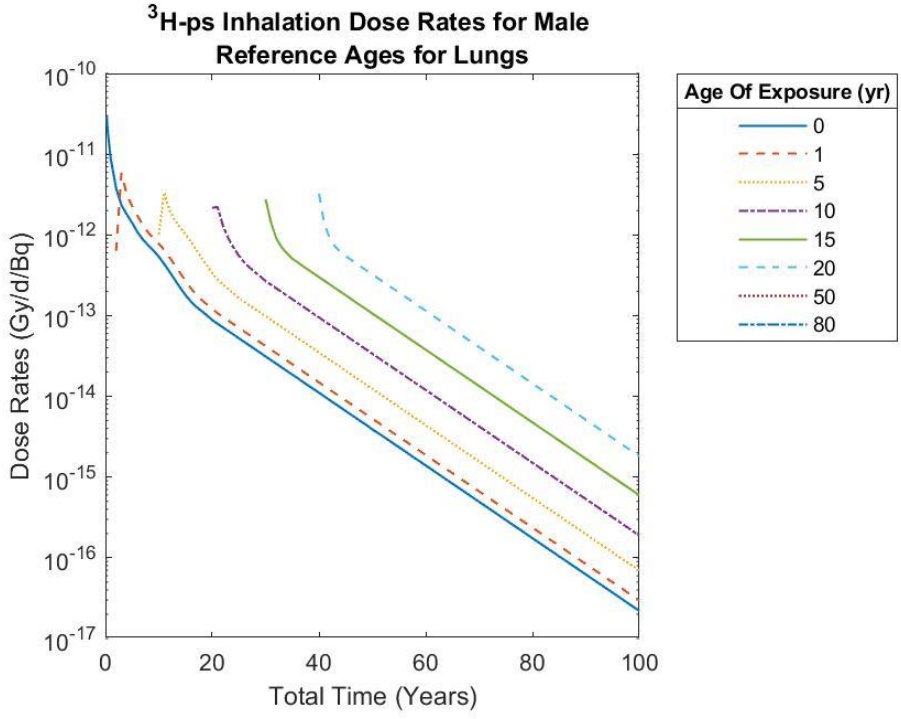
^{3}H-ps Inhalation Dose Rates for Male
Reference Ages for Lungs
Dose Rates (Gy/d/Bq)
Total Time (Years)
Age Of Exposure (yr)
0
1
5
10
15
20
50
80

(c)

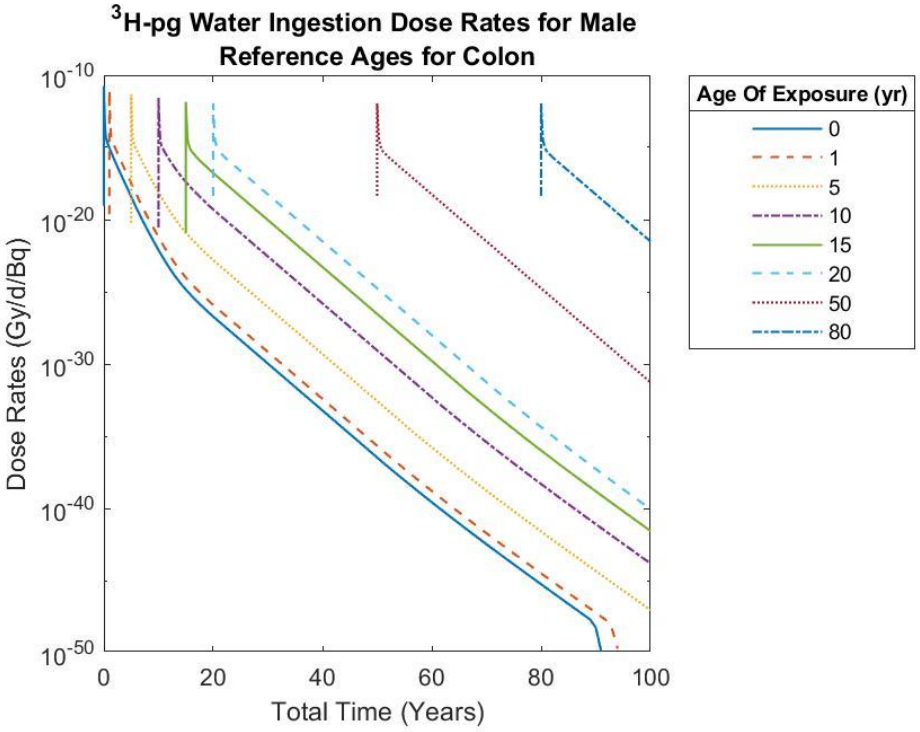

(d)

Figure 145. Dose rates to the (a) male lungs due to fast-clearing tritium, (b) to the male lung due to moderate-clearing tritium, (c) to the male lung due to slow-clearing tritium, and (d) to the male colon due to tap water ingested tritium.

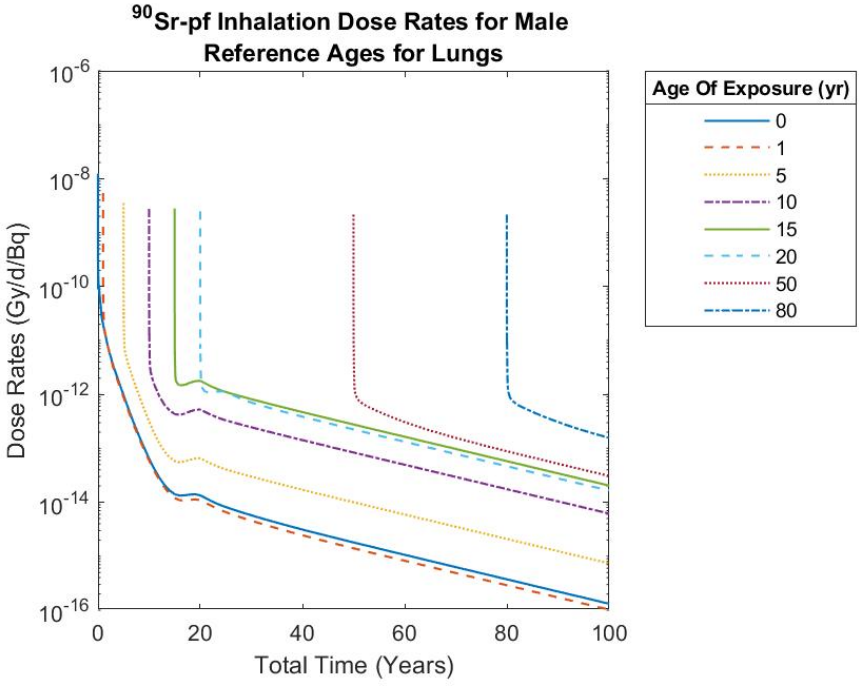

(a)

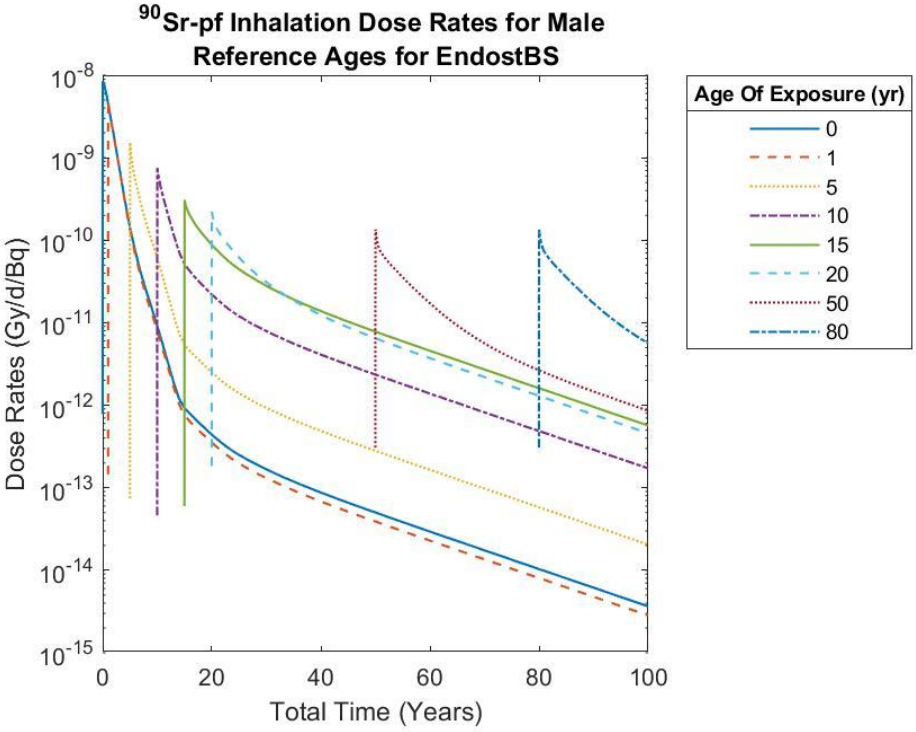

(b)

Figure 146. Dose rates in the (a) male lungs and (b) male bone surface due to fast-clearing ^{90}Sr.

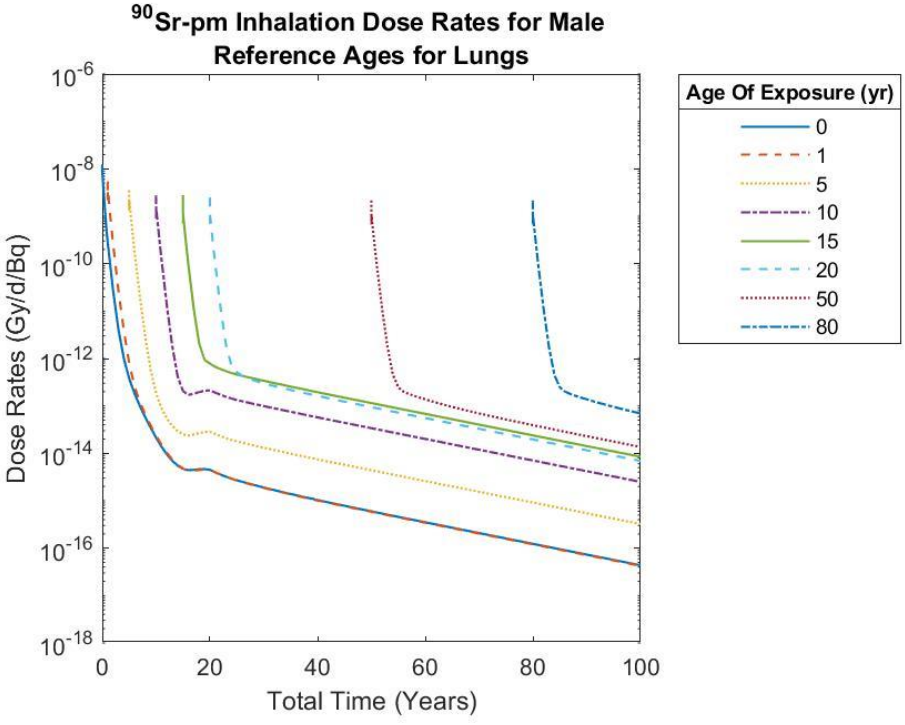

(a)

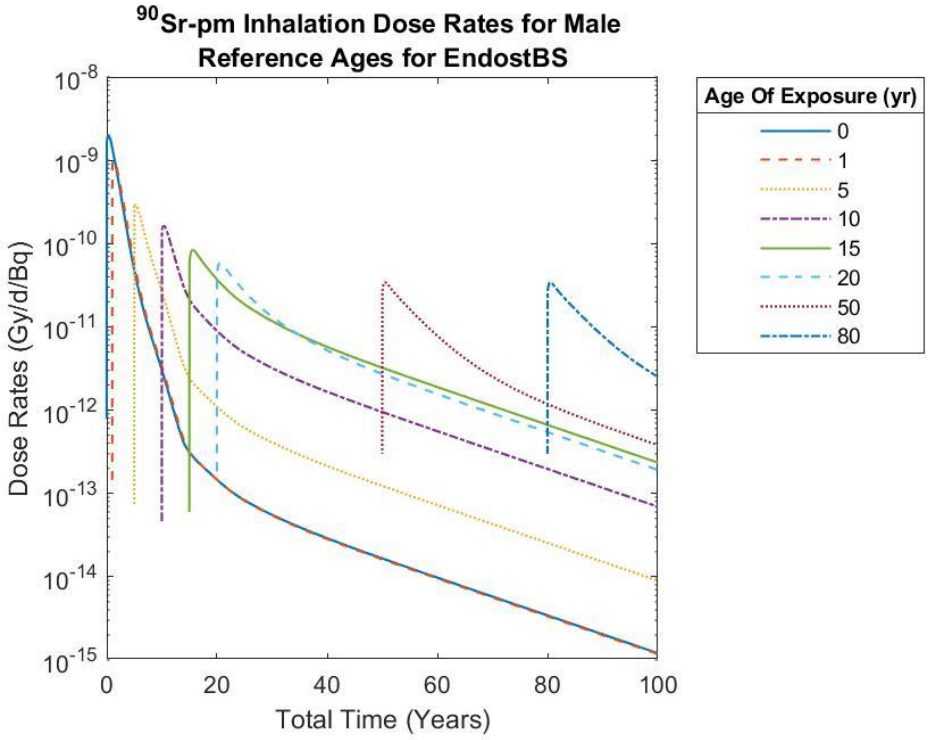

(b)

Figure 147. Dose rates in the (a) male lungs and (b) male bone surface due to moderate-clearing ^{90}Sr.

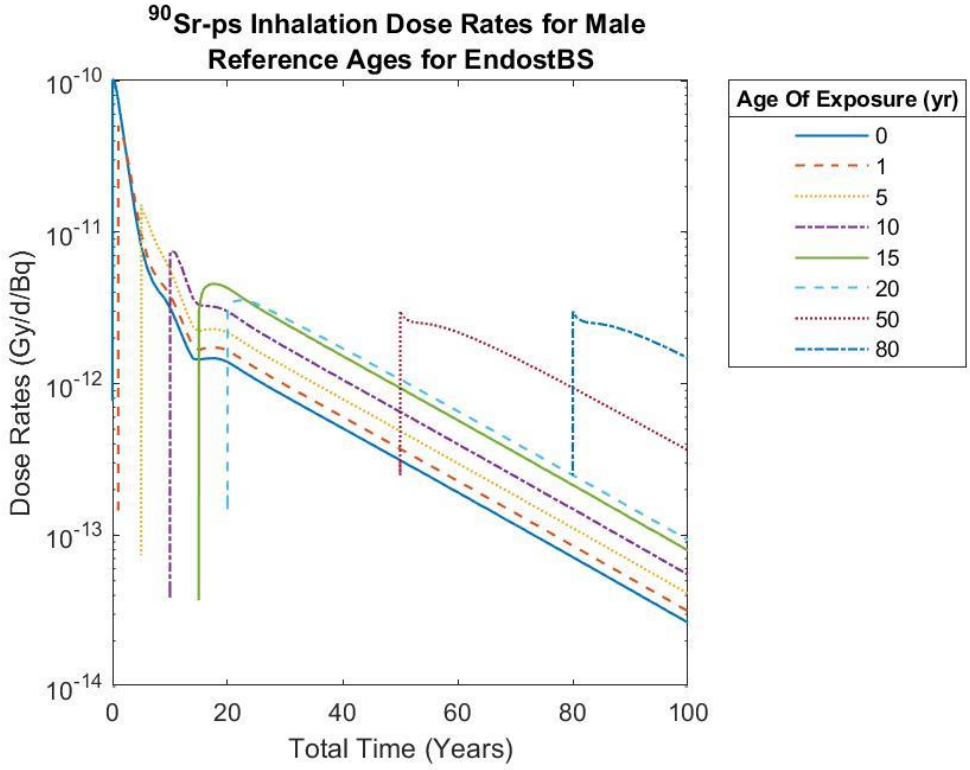

(a)

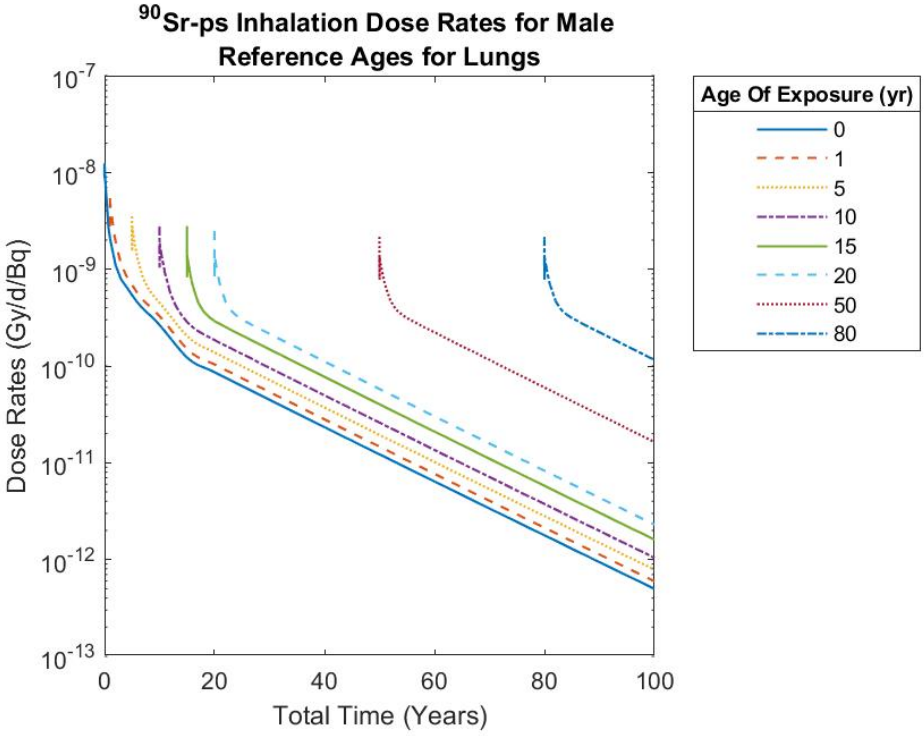

(b)

Figure 148. Dose rates in the (a) male bone surface and (b) male lungs due to slow-clearing ^{90}Sr.

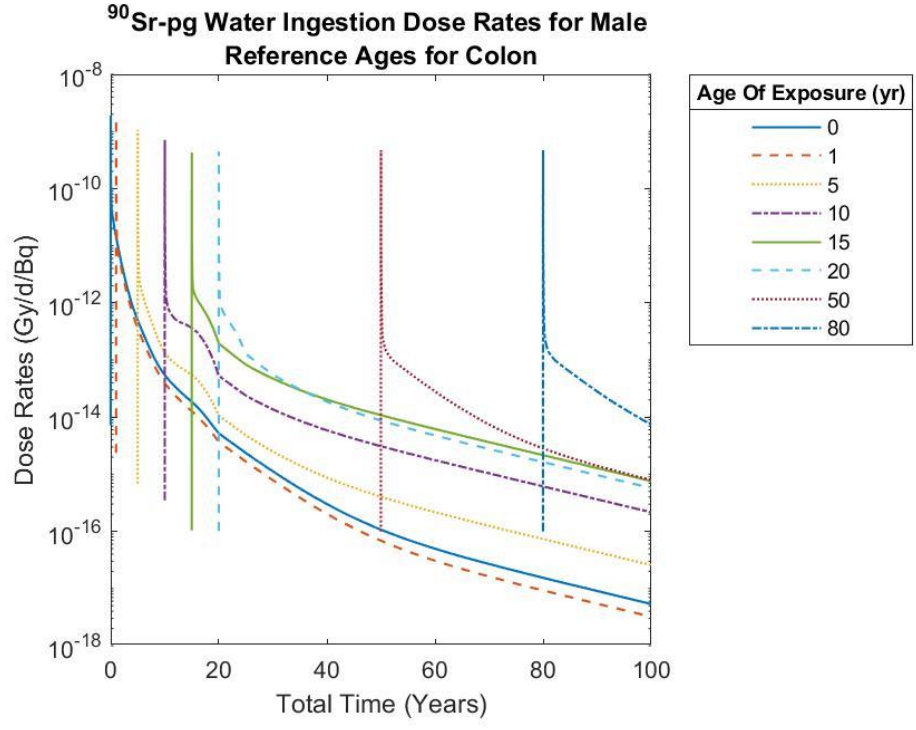

(a)

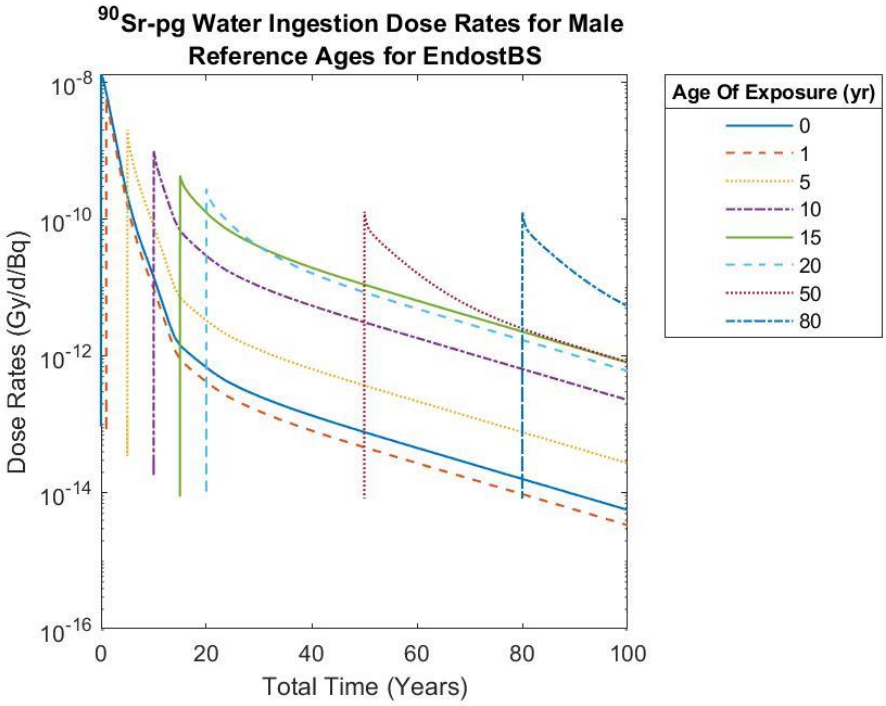

(b)

Figure 149. Dose rates in the (a) male colon and (b) male bone surface due to tap water ingested ^{90}Sr.

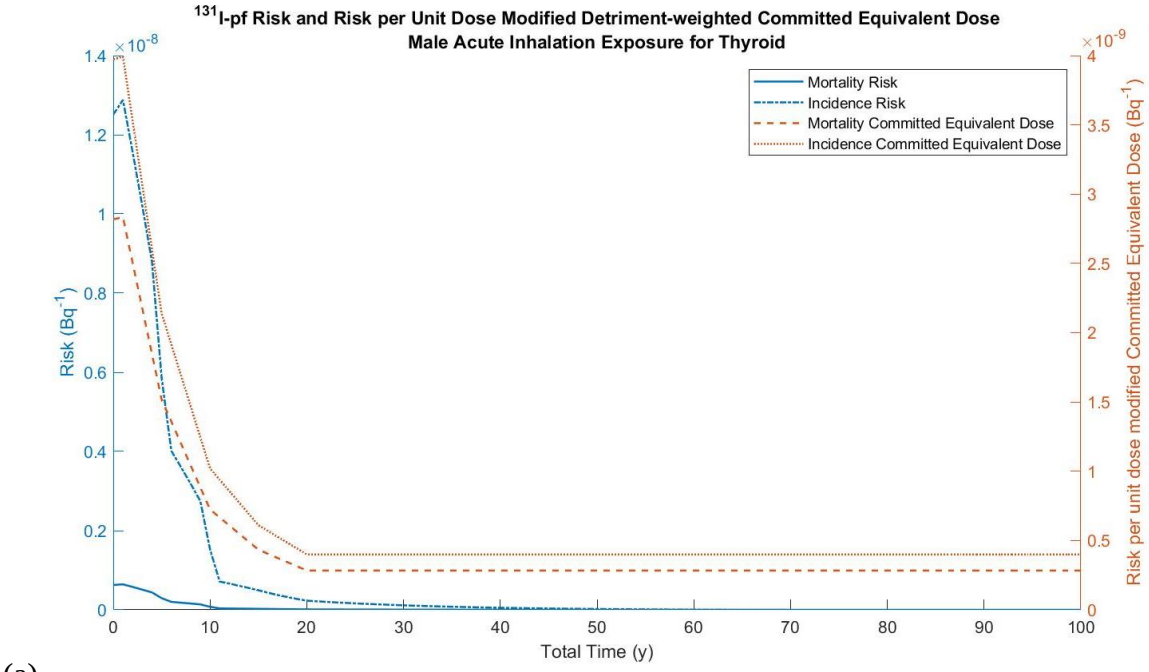

(a)

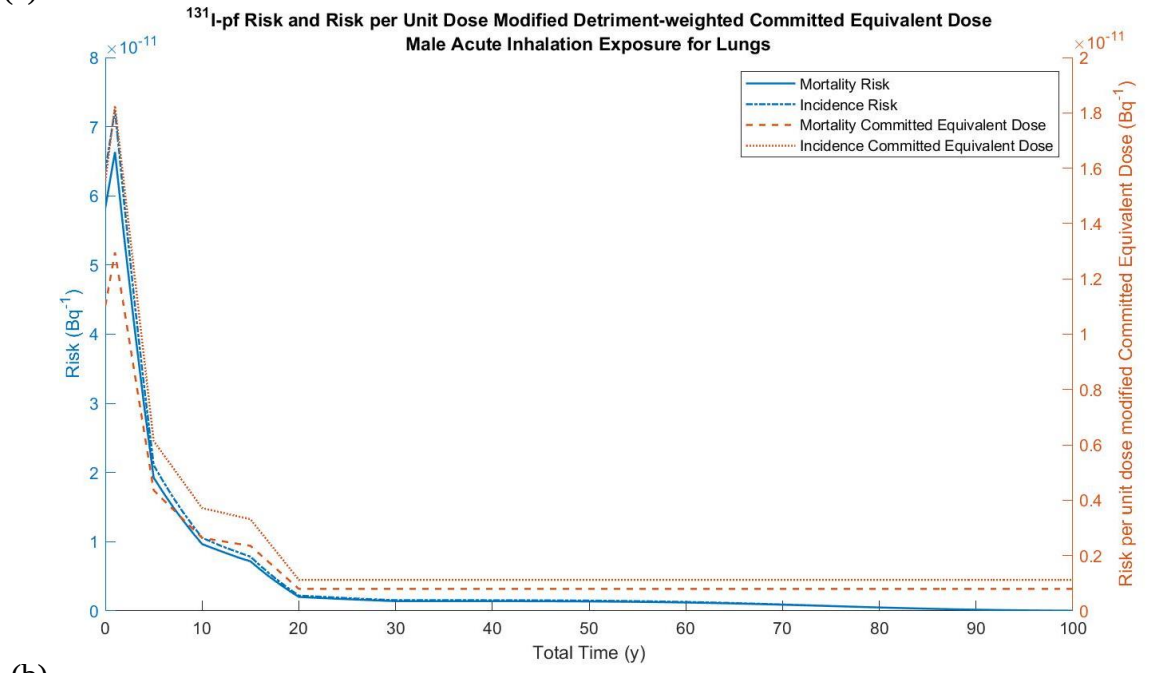

(b)

Figure 150. Risk and risk per unit dose modified detriment-weighted committed equivalent dose to the (a) male thyroid and (b) male lungs due to fast-clearing ^{131}I.

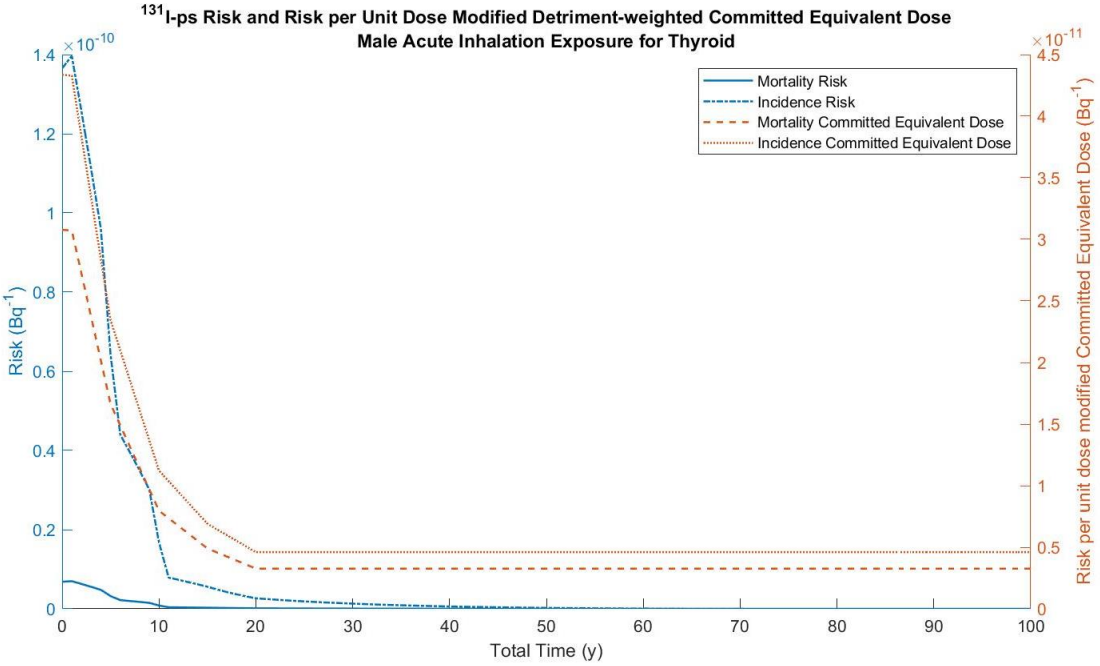

(a)

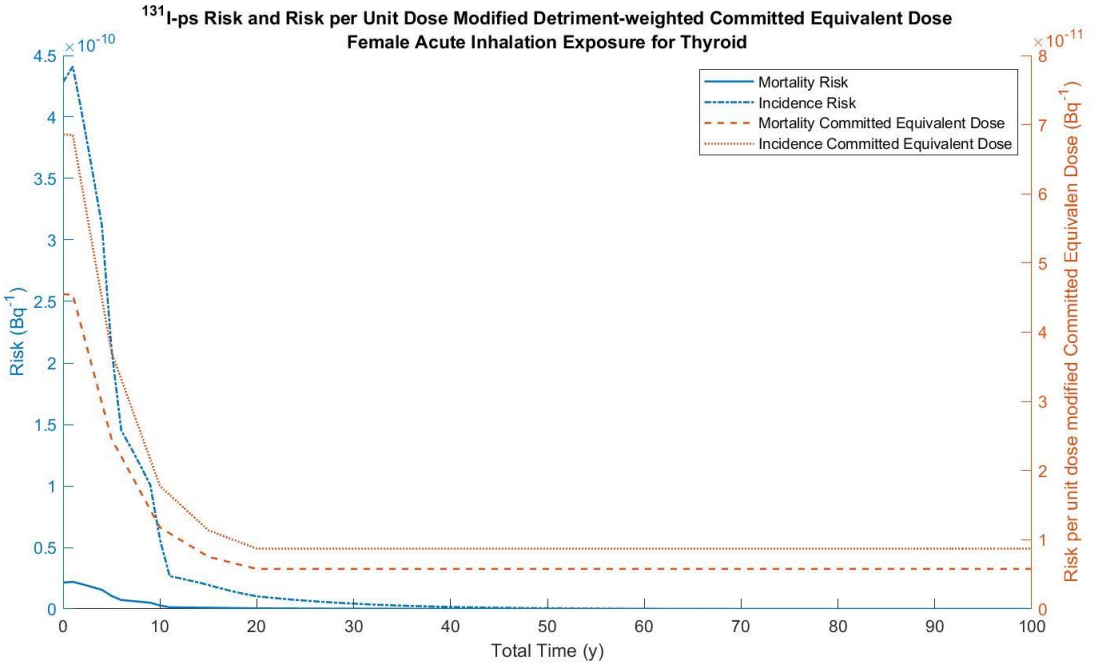

(b)

Figure 151. Risk and risk per unit dose modified detriment-weighted committed equivalent dose to the (a) male thyroid and (b) female thyroid due to slow-clearing ^{131}I.

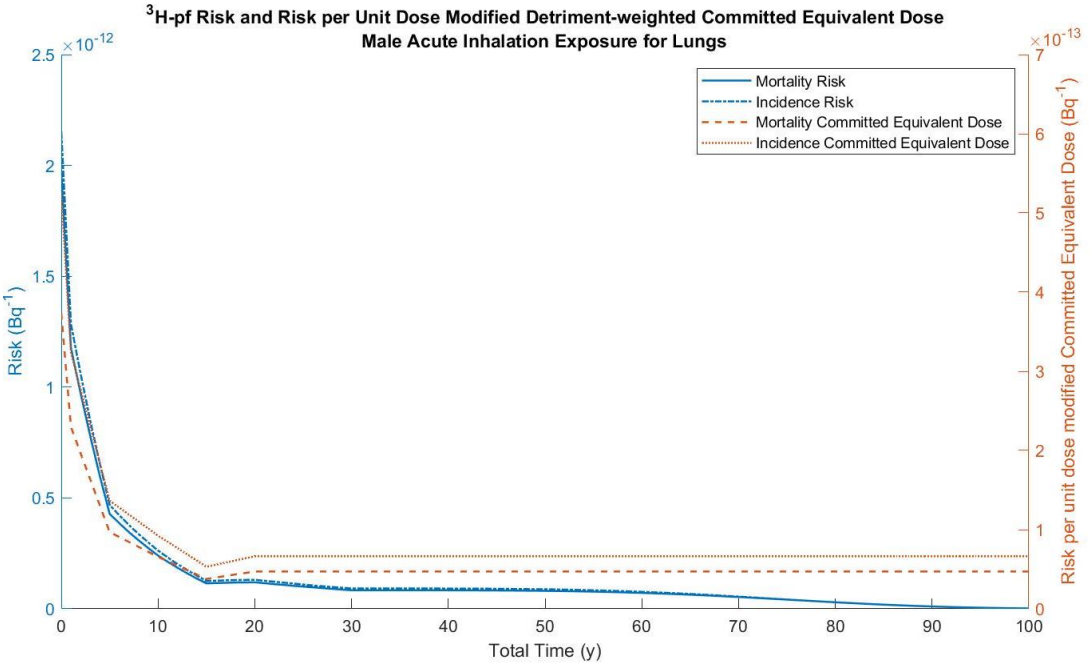

(a)

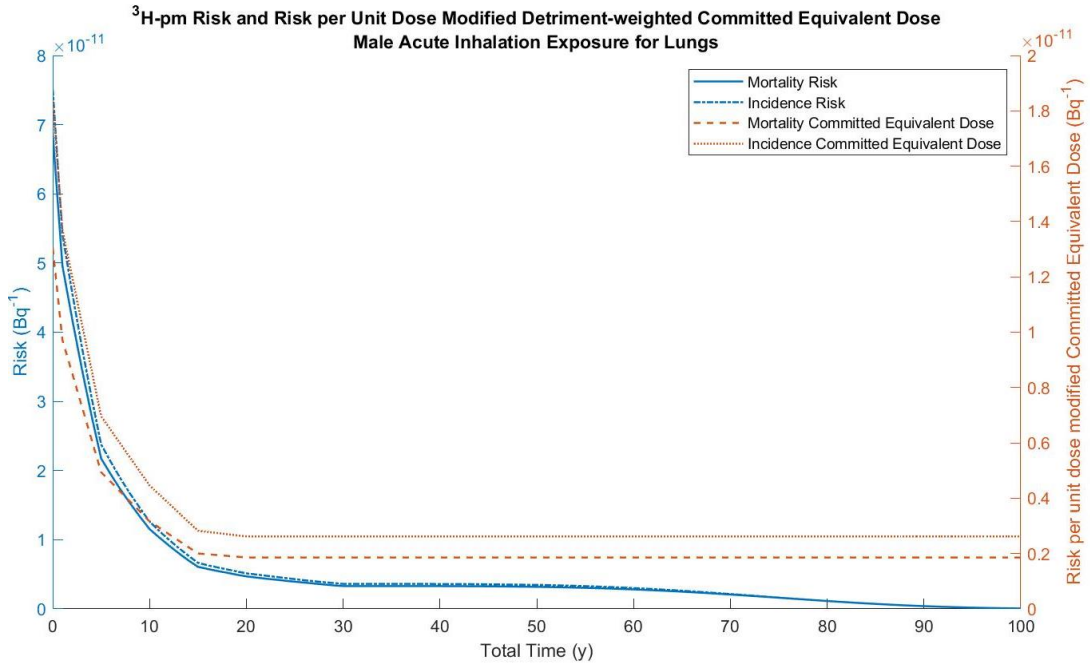

(b)

Figure 152. Risk and risk per unit dose modified detriment-weighted committed equivalent dose to the male lungs for (a) fast-clearing and (b) moderate-clearing tritium.

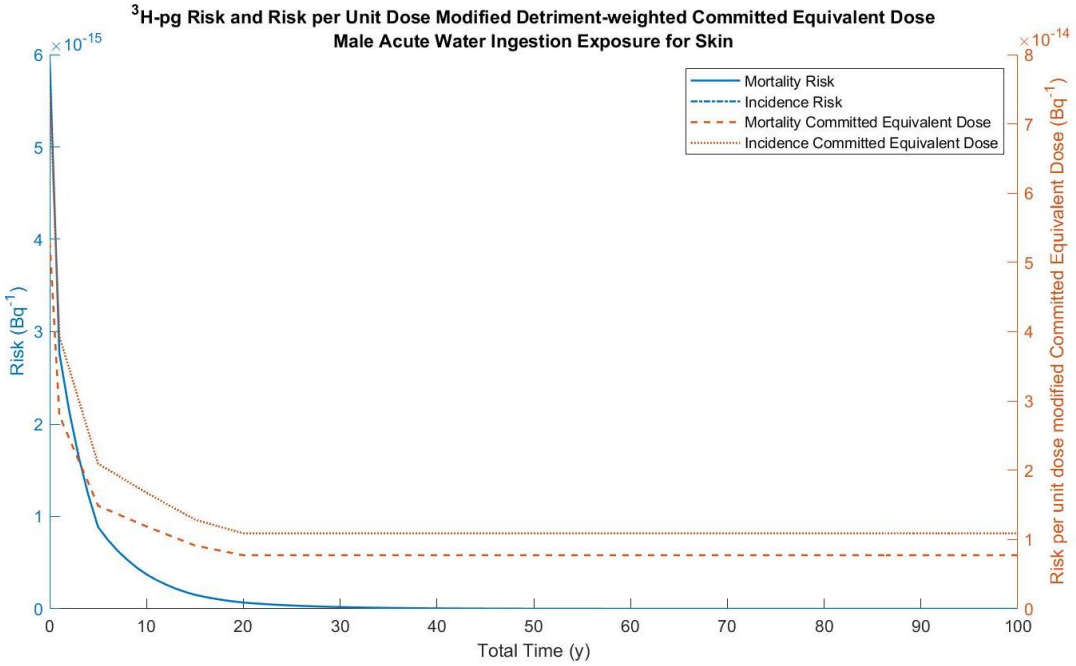

(a)

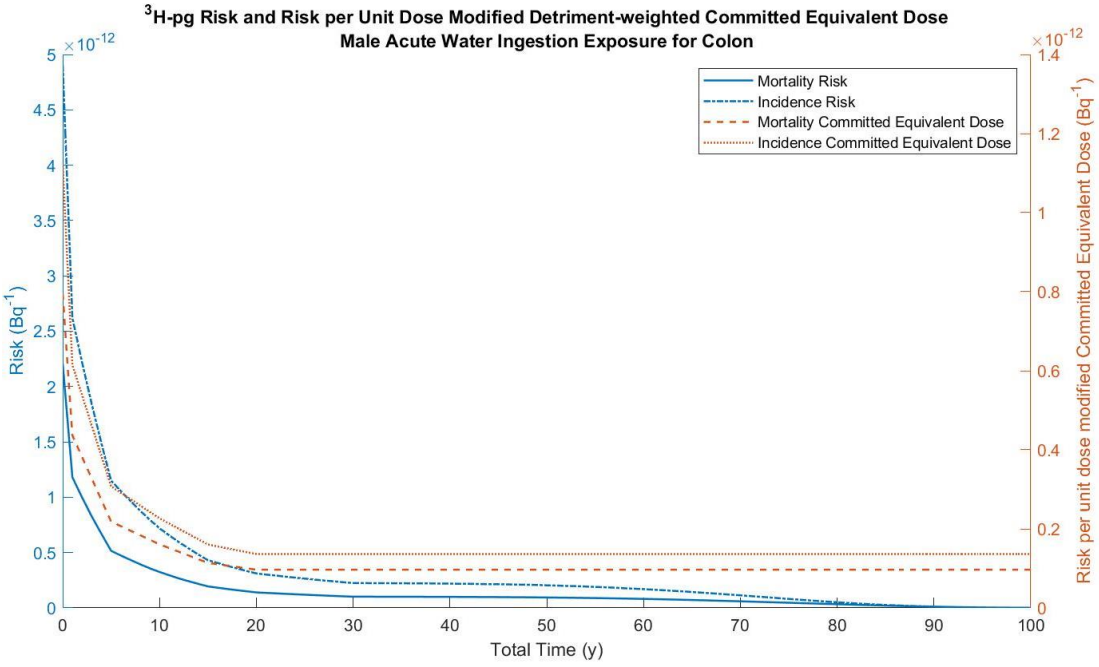

(b)

Figure 153. Risk and risk per unit dose modified detriment-weighted committed equivalent dose to the (a) male skin and (b) male colon due to tap water ingested tritium.

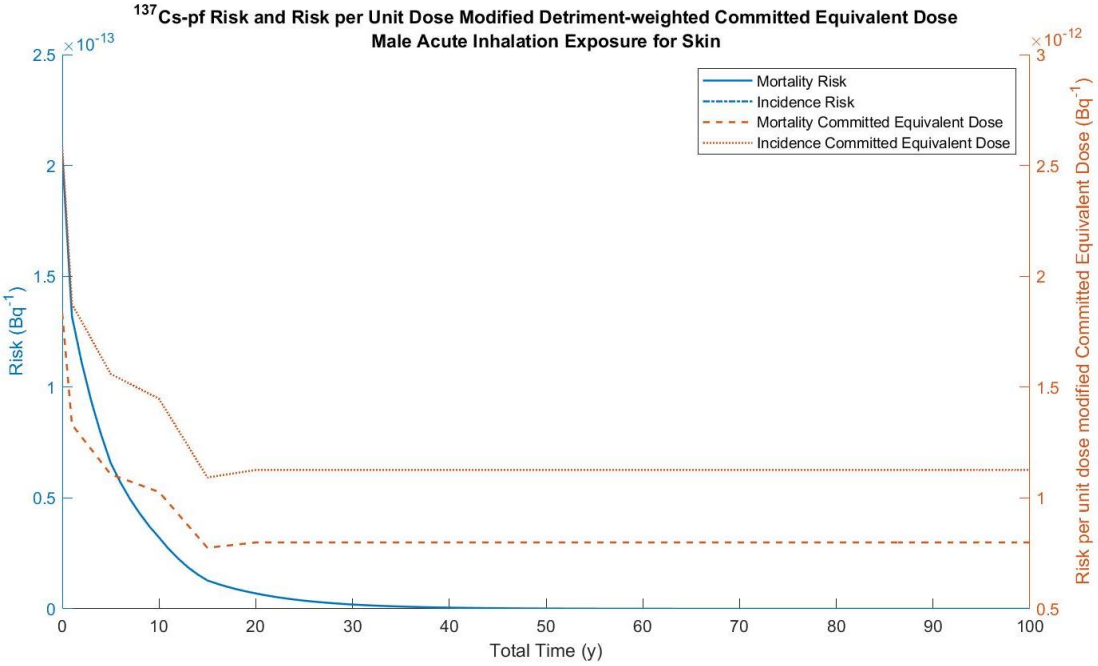
137Cs-pf Risk and Risk per Unit Dose Modified Detriment-weighted Committed Equivalent Dose
Male Acute Inhalation Exposure for Skin
×10-13
×10-12
Mortality Risk
Incidence Risk
Mortality Committed Equivalent Dose
Incidence Committed Equivalent Dose
Risk (Bq-1)
Risk per unit dose modified Committed Equivalent Dose (Bq-1)
Total Time (y)

(a)

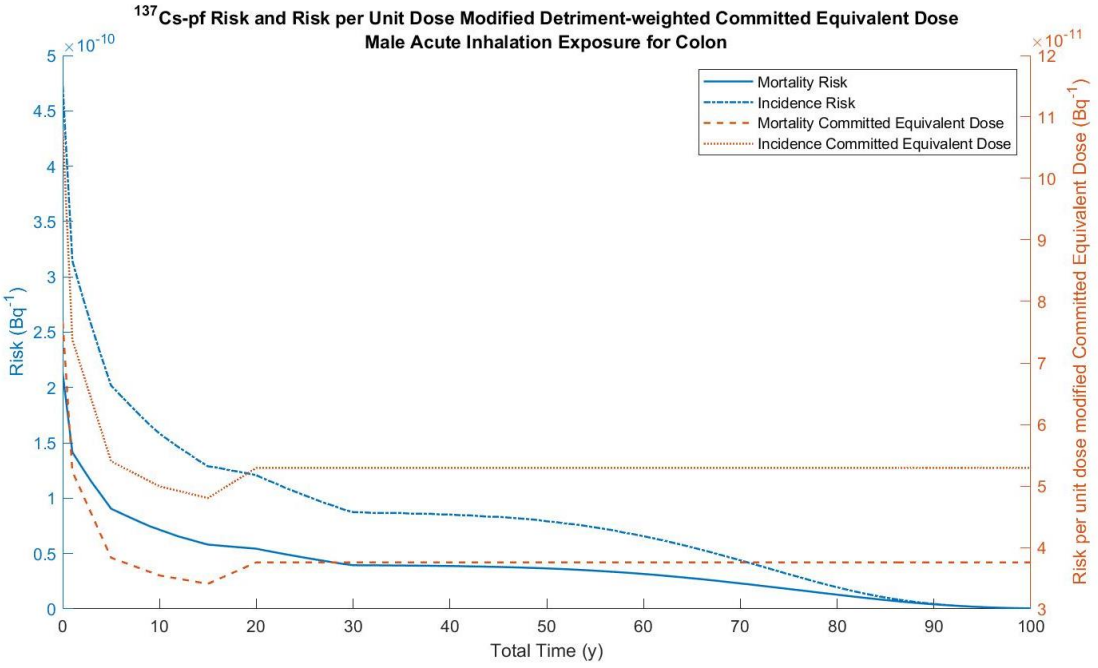
137Cs-pf Risk and Risk per Unit Dose Modified Detriment-weighted Committed Equivalent Dose
Male Acute Inhalation Exposure for Colon
×10-10
×10-11
Mortality Risk
Incidence Risk
Mortality Committed Equivalent Dose
Incidence Committed Equivalent Dose
Risk (Bq-1)
Risk per unit dose modified Committed Equivalent Dose (Bq-1)
Total Time (y)

(b)

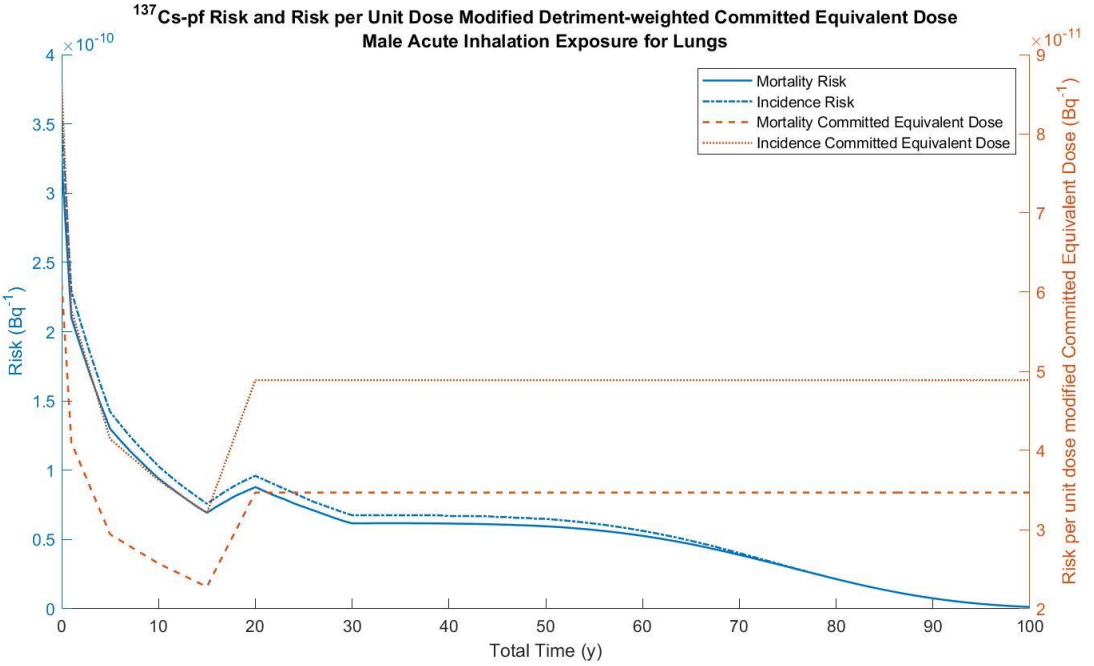

(c)

Figure 154.Risk and risk per unit dose modified detriment-weighted committed equivalent dose to the (a) male skin, (b) male colon, and (c) male lungs duet to fast-clearing ^{137}Cs.

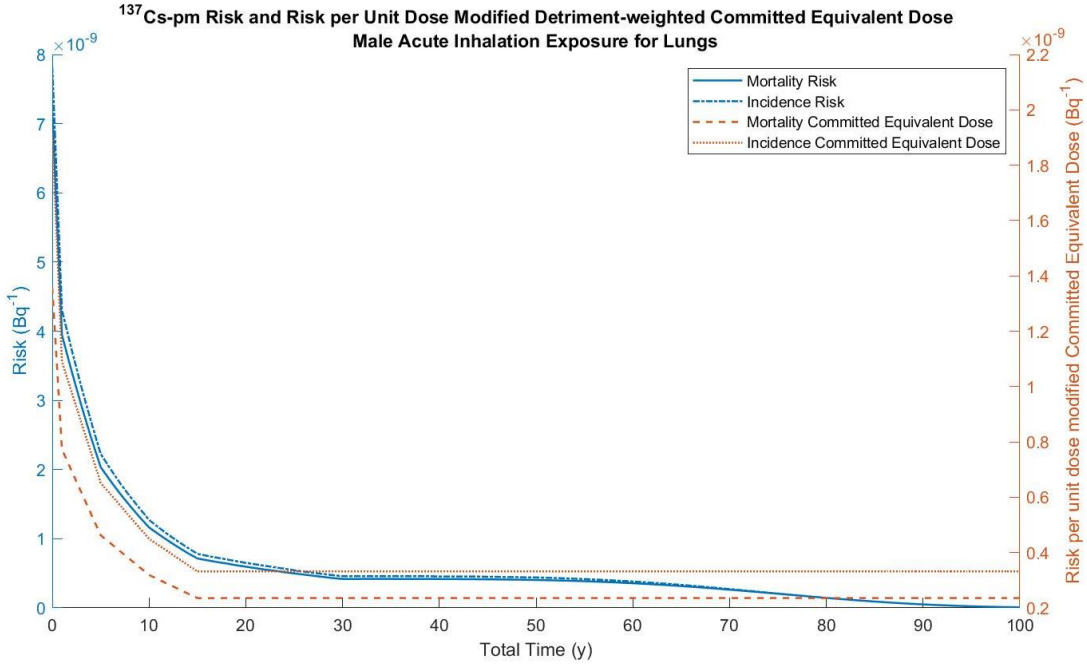

(a)

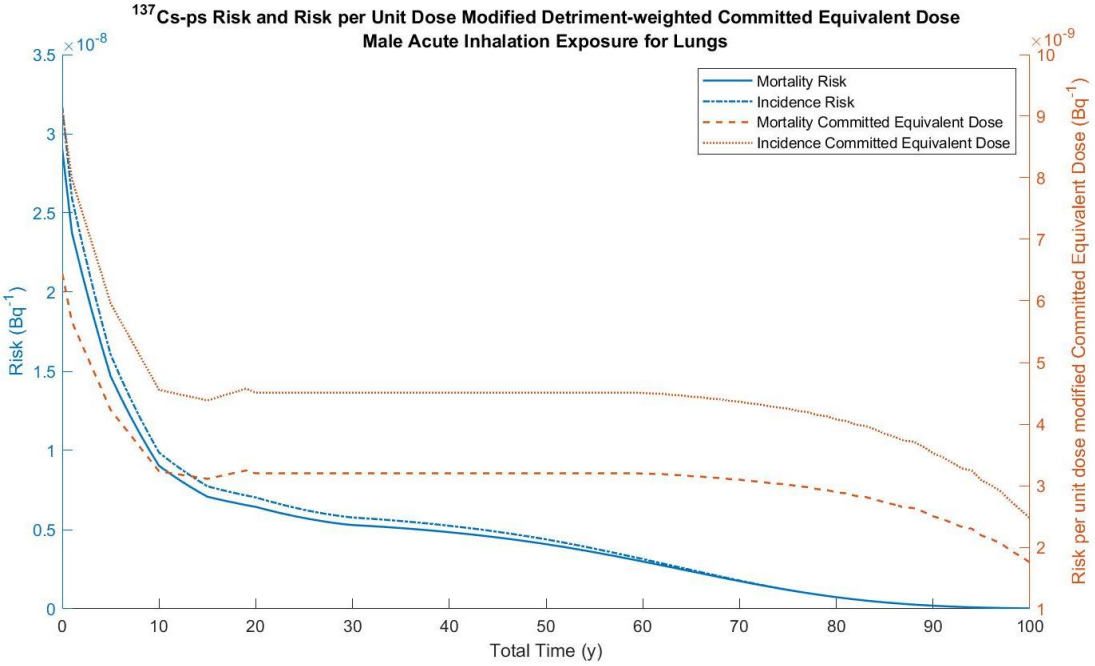

(b)

Figure 155. Risk and risk per unit dose modified detriment-weighted committed equivalent dose to the male lungs due to (a) moderate-clearing and (b) slow-clearing ^{137}Cs.

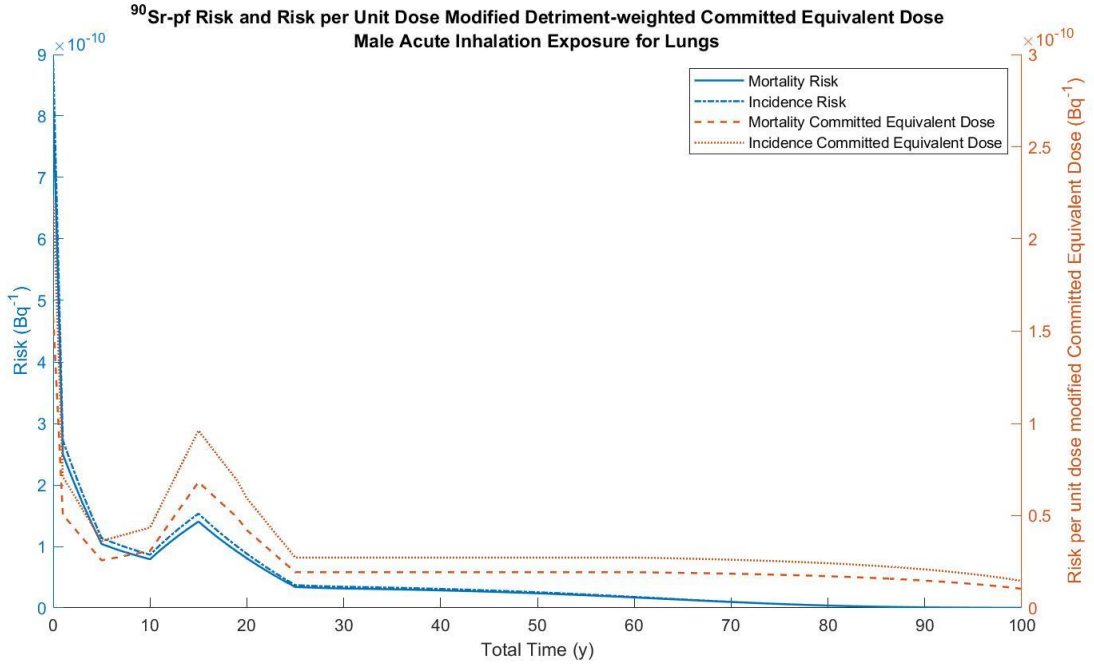

(a)

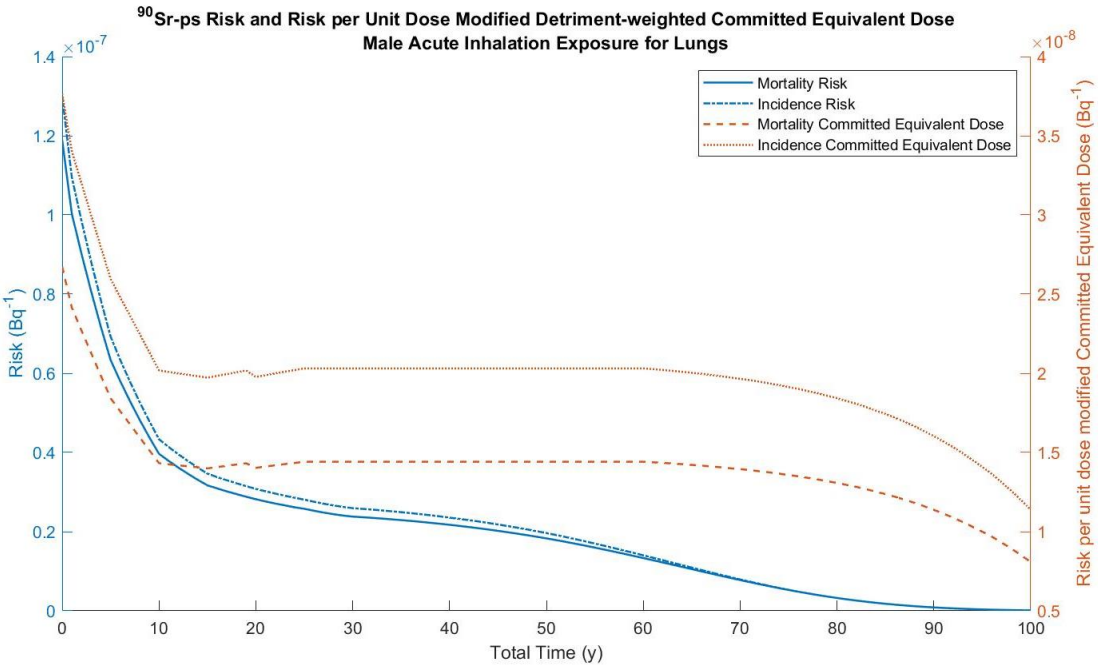

(b)

Figure 156. Risk and risk per unit dose modified detriment-weighted committed equivalent dose to the male lungs due to (a) moderate-clearing and (b) slow-clearing ^{90}Sr.

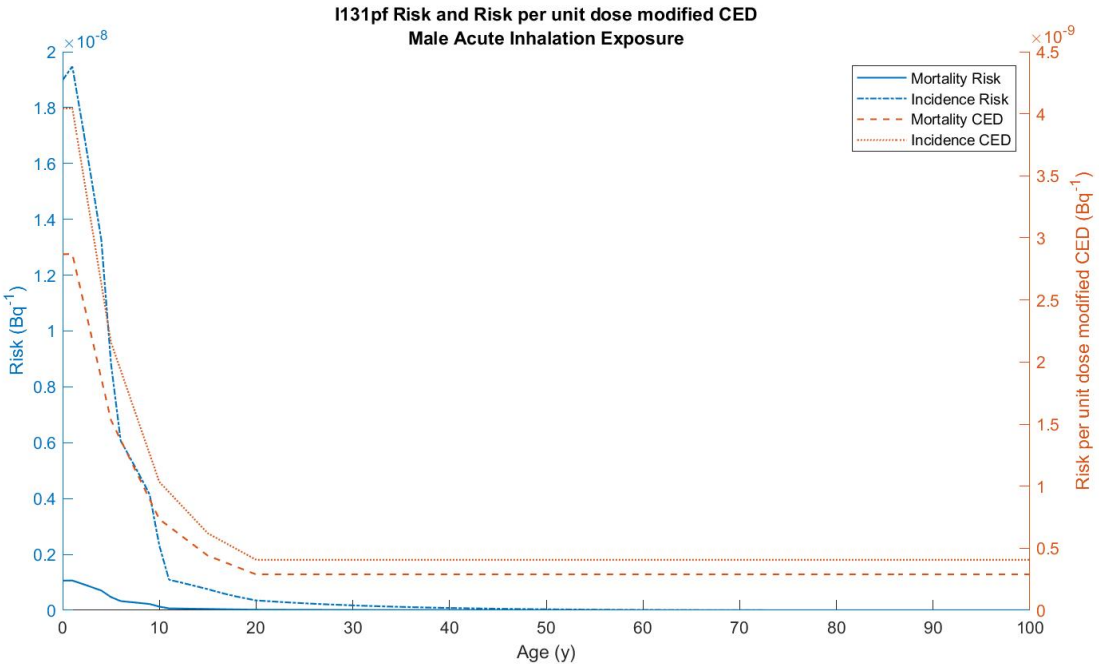

(a)

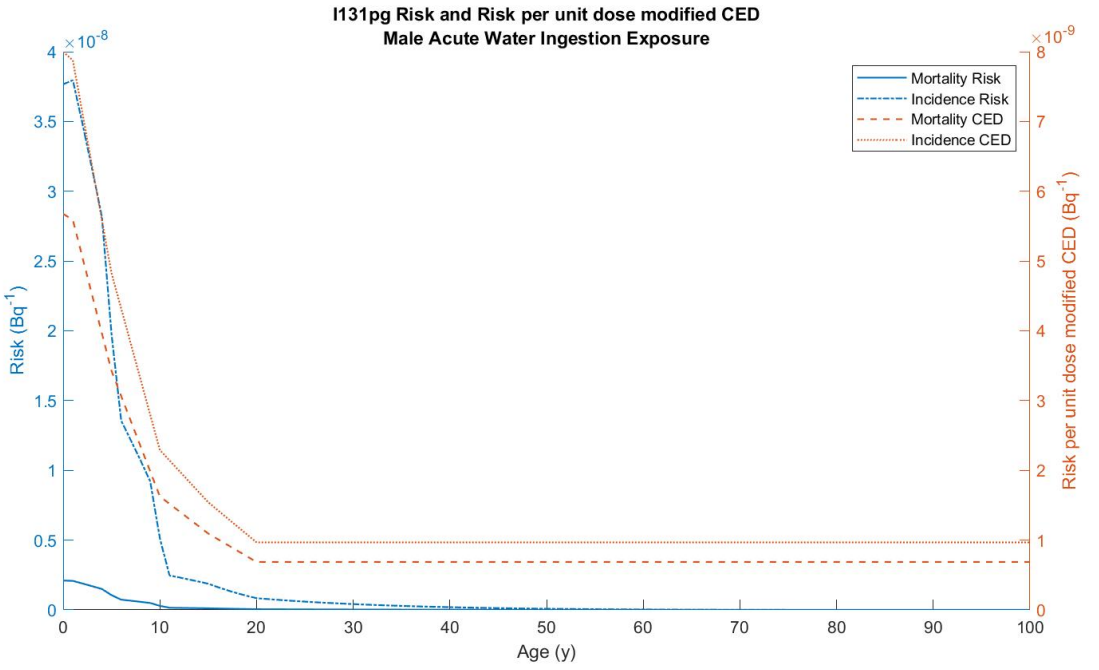

(b)

Figure 157. Risk and risk per unit dose modified CED for males due to (a) fast-clearing and (b) tap water ingested ^{131}I.

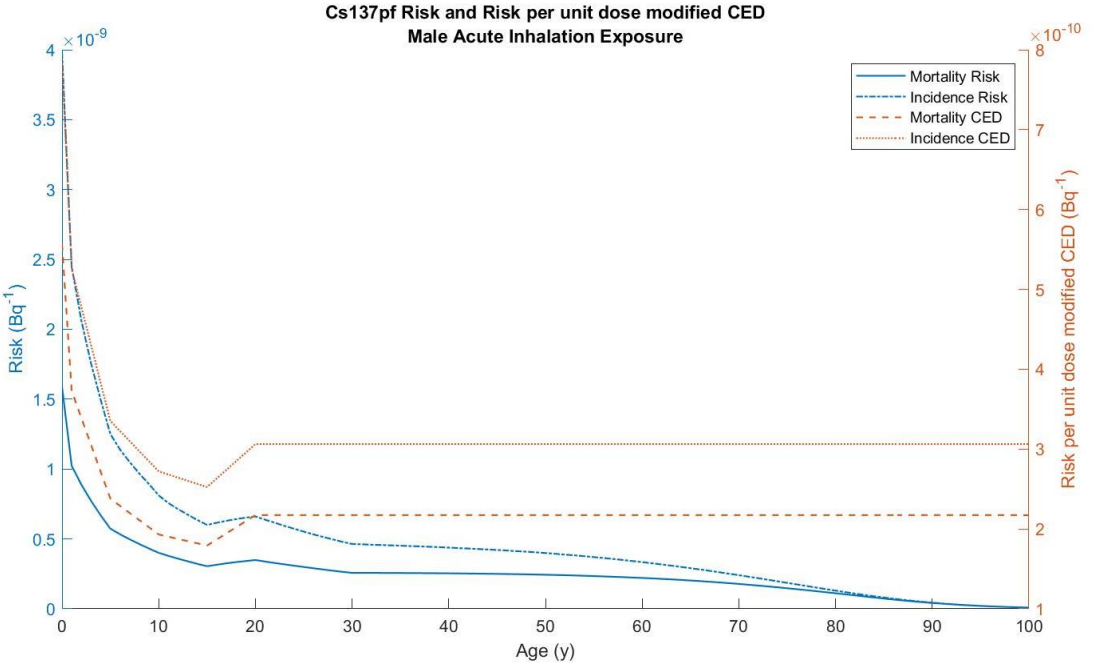
Cs137pf Risk and Risk per unit dose modified CED
Male Acute Inhalation Exposure
Mortality Risk
Incidence Risk
Mortality CED
Incidence CED
Risk (Bq-1)
Risk per unit dose modified CED (Bq-1)
Age (y)

(a)

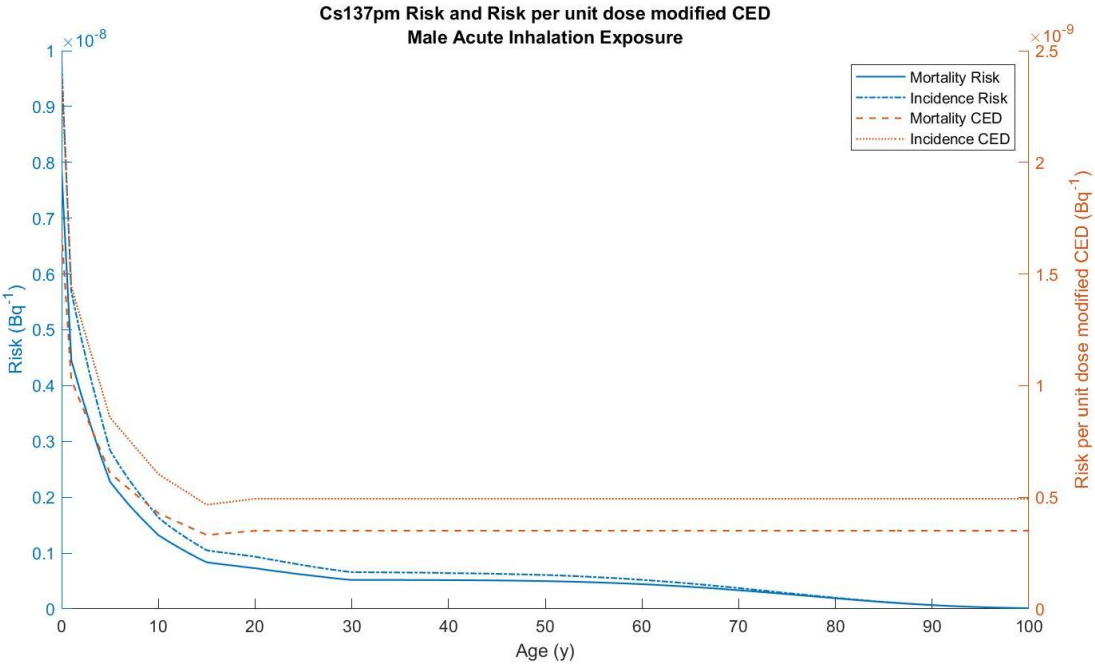
Cs137pm Risk and Risk per unit dose modified CED
Male Acute Inhalation Exposure
Mortality Risk
Incidence Risk
Mortality CED
Incidence CED
Risk (Bq-1)
Risk per unit dose modified CED (Bq-1)
Age (y)

(b)

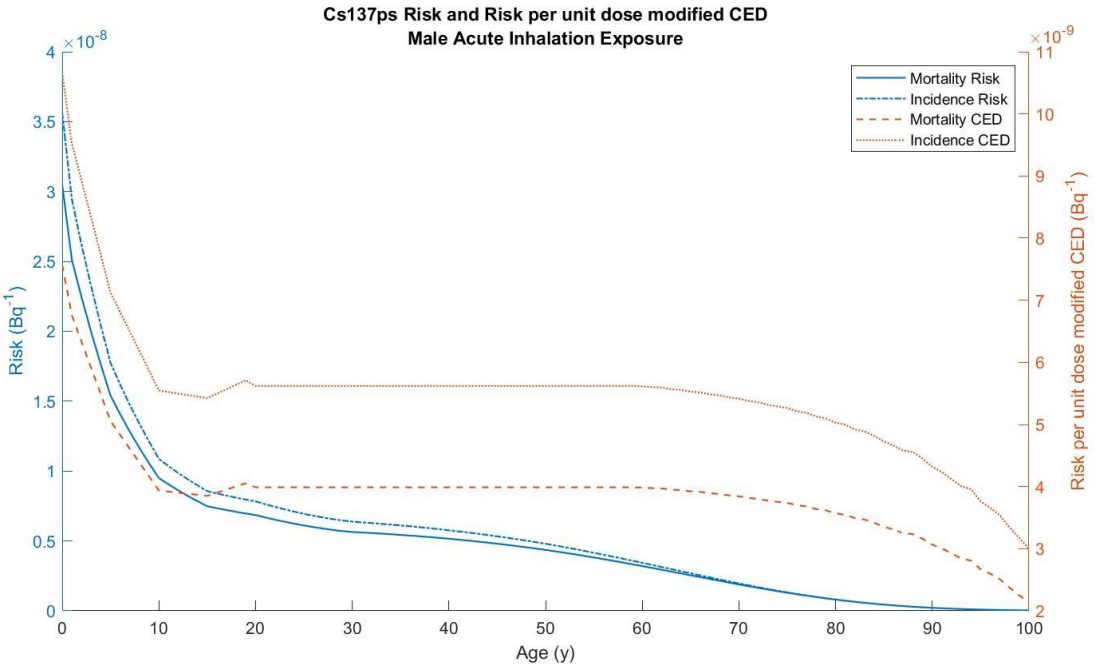

(c)

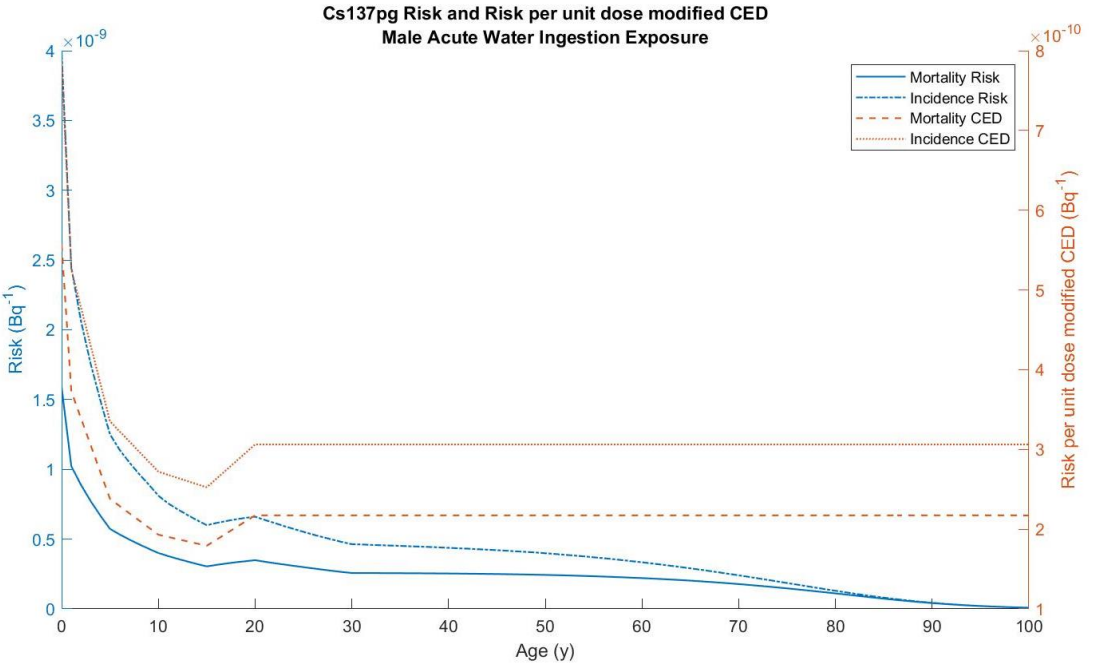

(d)

Figure 158. Risk and risk per unit dose modified CED for males due to (a) fast-clearing, (b) moderate-clearing, (c) slow-clearing, and (d) tap water ingested ^{137}Cs.

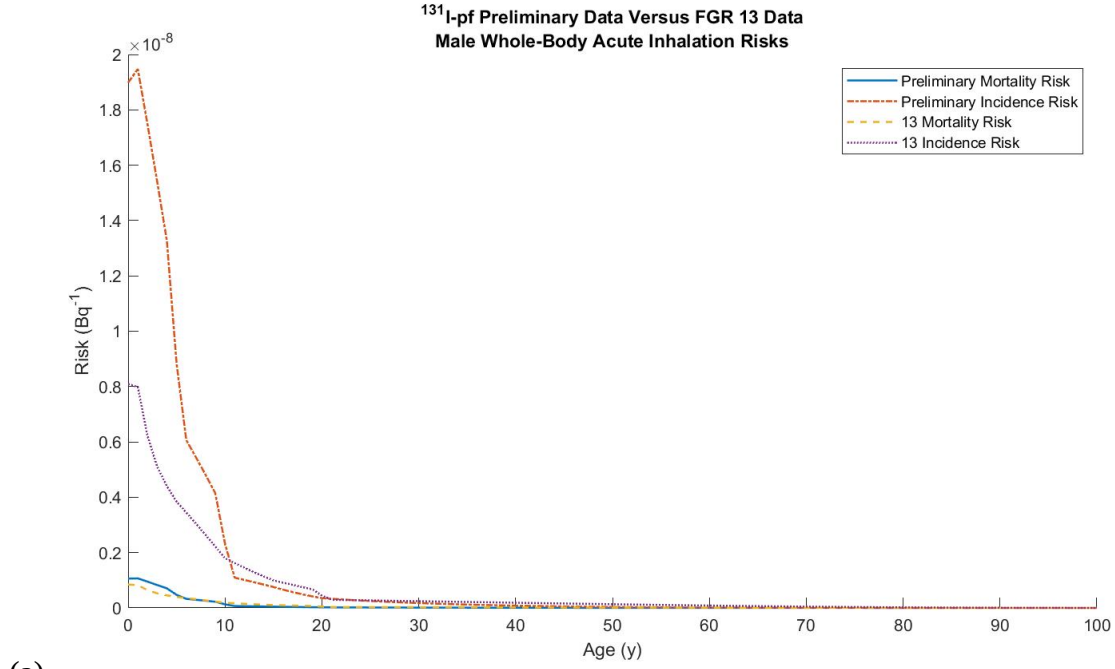

(a)

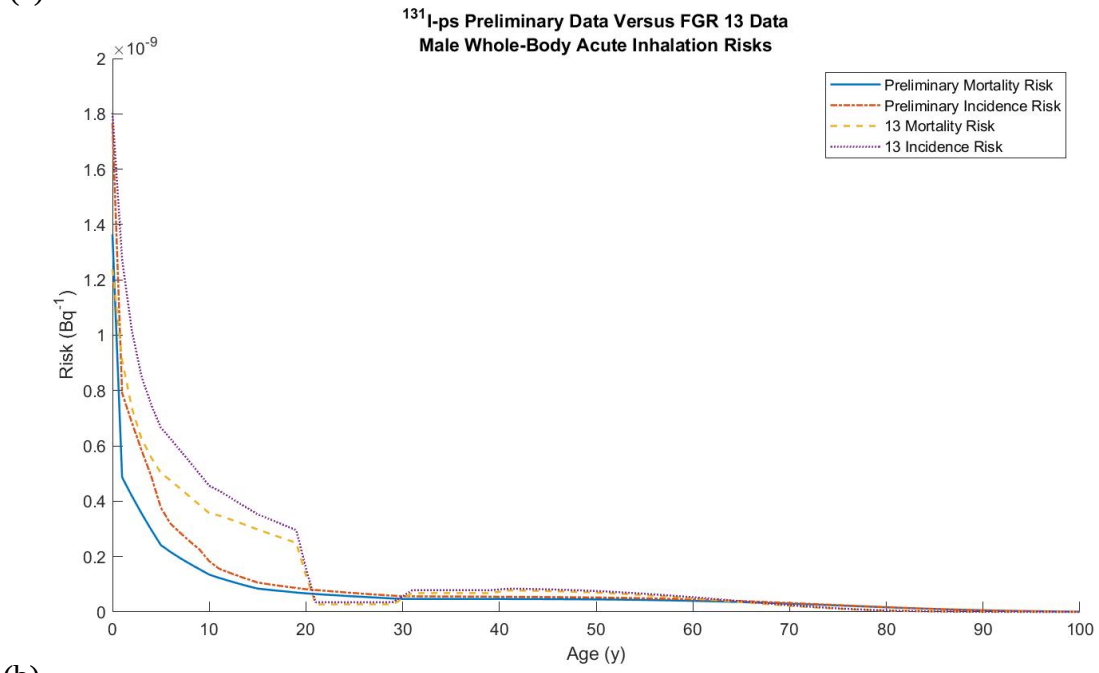

(b)

Figure 159. Comparison of FGR 13 and ICRP 103 informed data for male risks due to (a) fast-clearing and (b) slow-clearing ^{131}I.

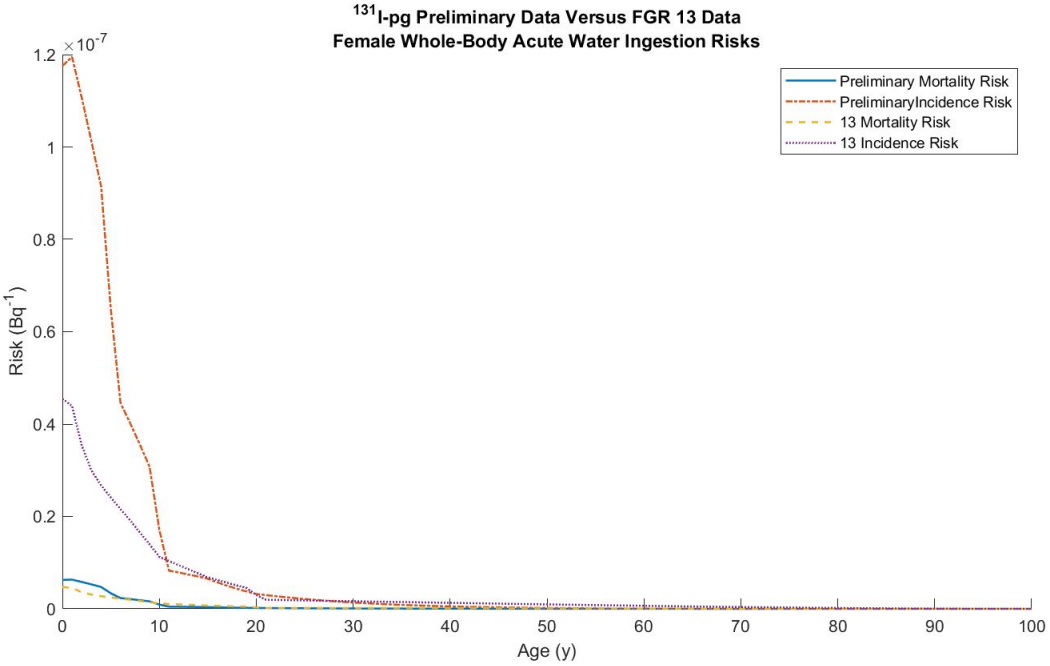

(a)

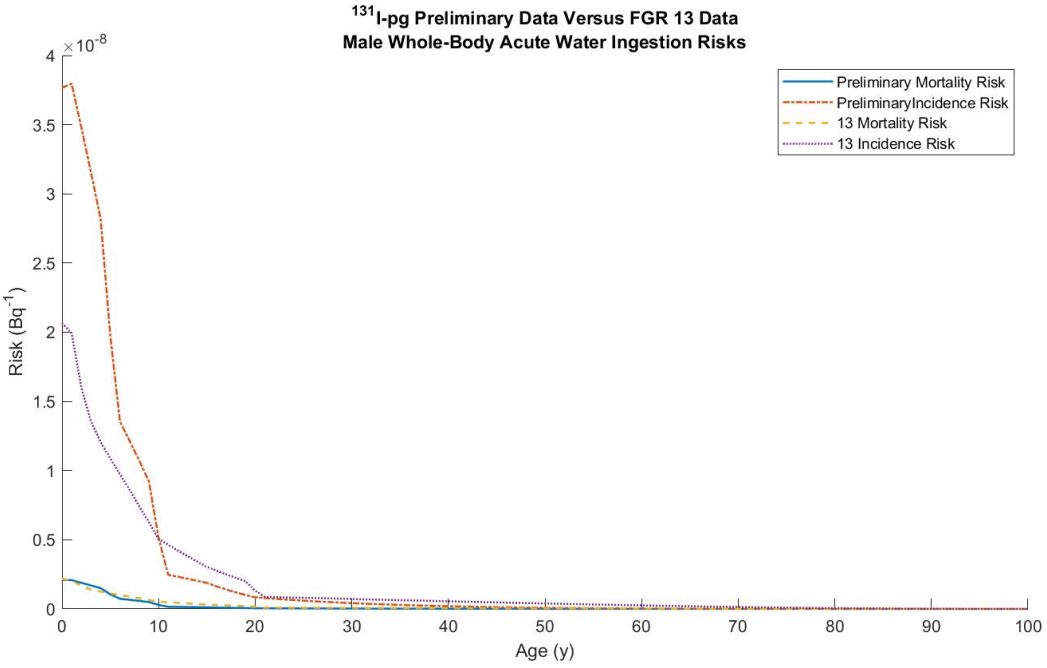

(b)

Figure 160. Comparison of FGR 13 and ICRP 103 informed data for (a) female risks and (b) male risks due to tap water ingested ^{131}I.

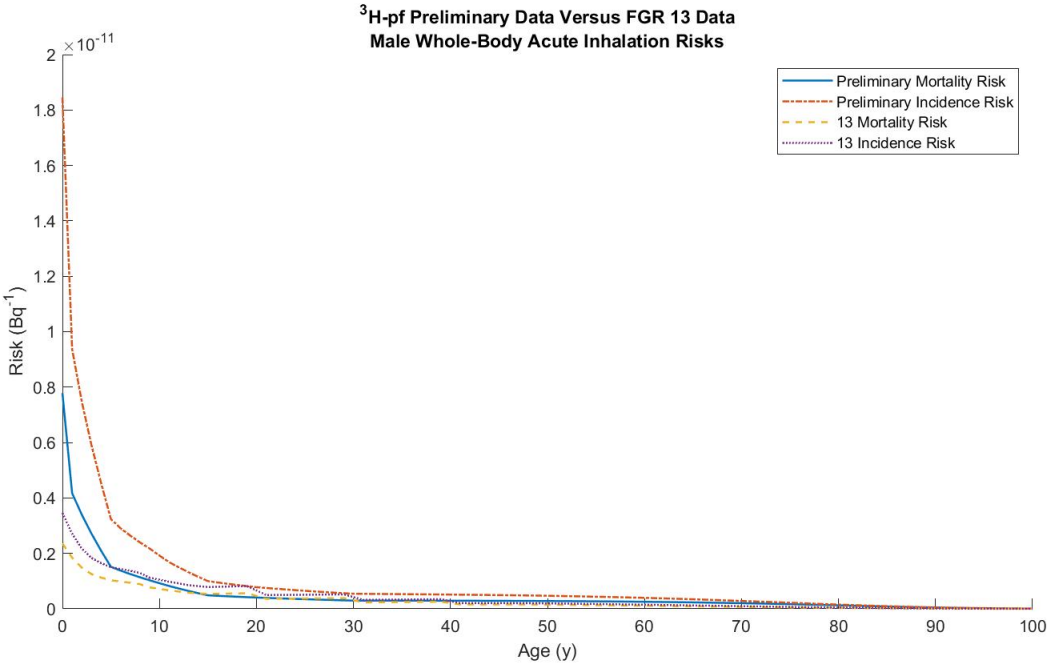
^{3}H-pf Preliminary Data Versus FGR 13 Data
Male Whole-Body Acute Inhalation Risks
Preliminary Mortality Risk
Preliminary Incidence Risk
13 Mortality Risk
13 Incidence Risk
×10^-11
Risk (Bq^-1)
Age (y)

(a)

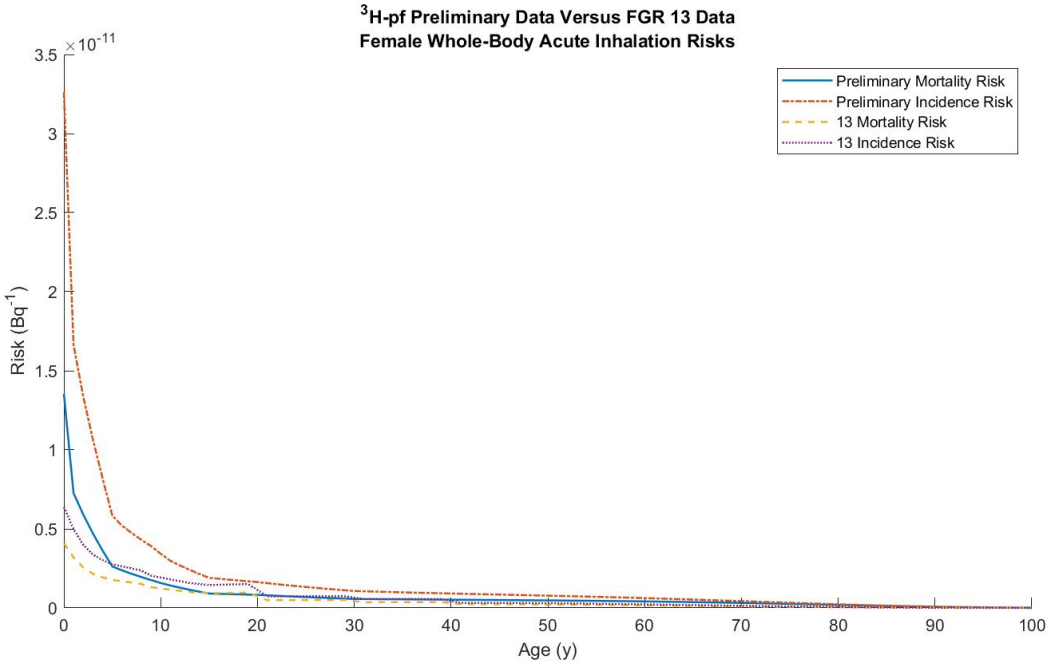
^{3}H-pf Preliminary Data Versus FGR 13 Data
Female Whole-Body Acute Inhalation Risks
Preliminary Mortality Risk
Preliminary Incidence Risk
13 Mortality Risk
13 Incidence Risk
×10^-11
Risk (Bq^-1)
Age (y)

(b)

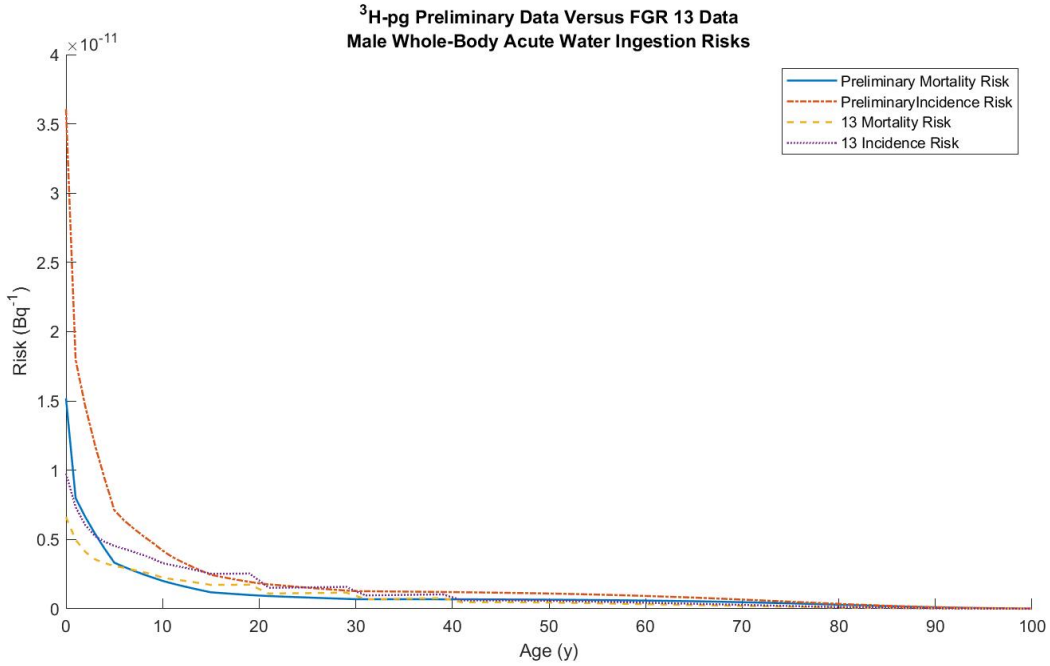

(c)

Figure 161. Comparison of FGR 13 and ICRP 103 informed data for (a) male risk due to fast-clearing tritium, (b) female risks due to tap water ingested tritium, and (c) male risk due to tap water ingested tritium.

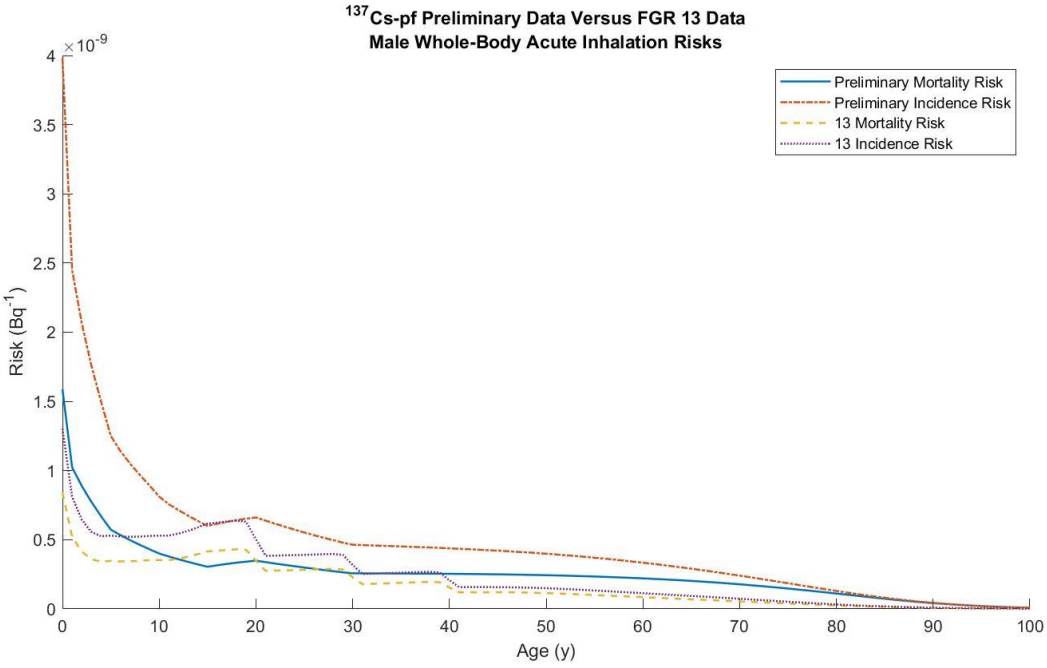

(a)

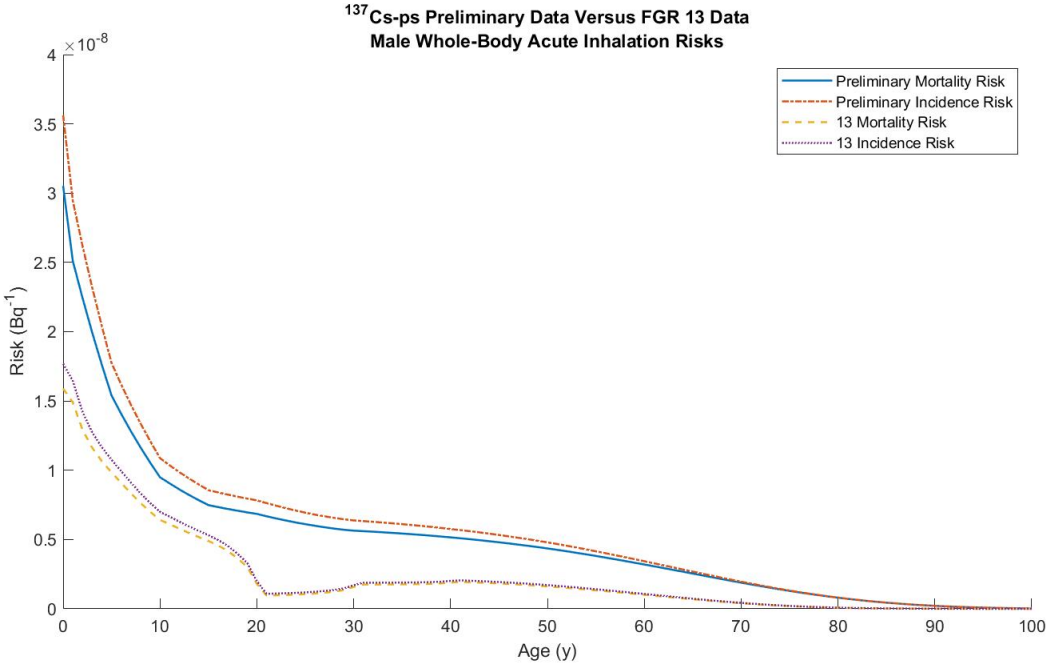

(b)

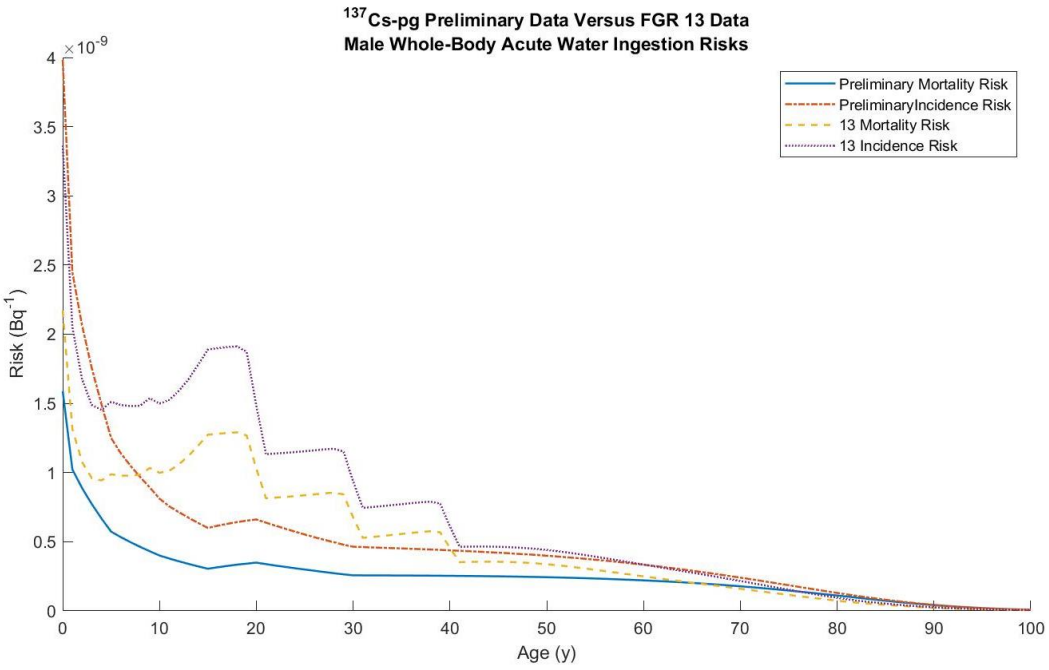

(c)

Figure 162. Comparison of FGR 13 and ICRP 103 informed data for male risks due to (a) fast-clearing, (b) slow-clearing, and (c) tap water ingested ^{137}Cs.

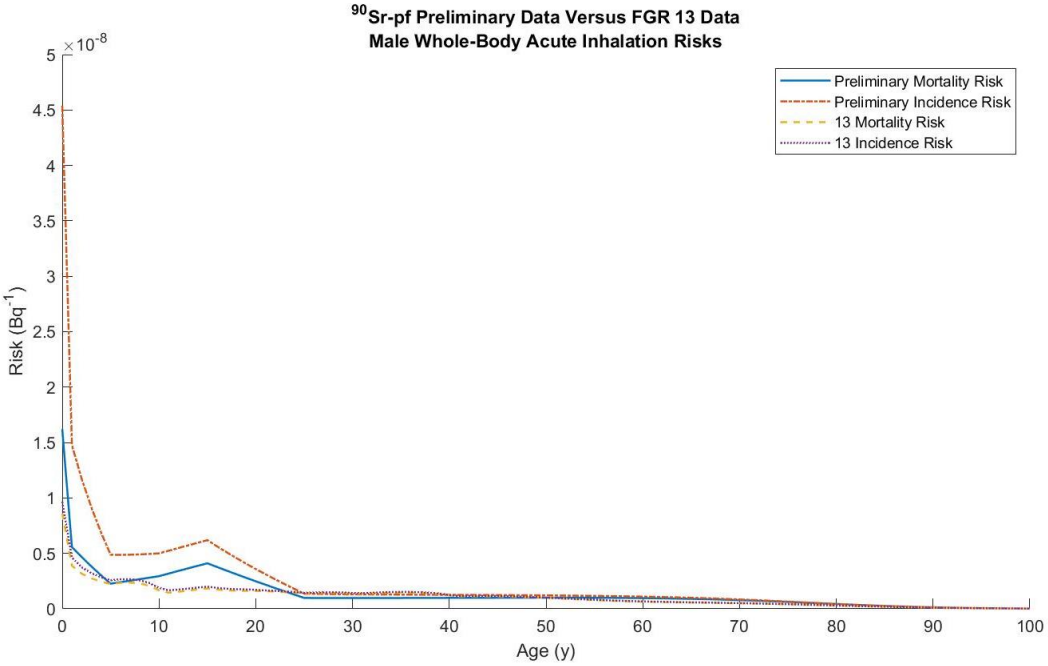

(a)

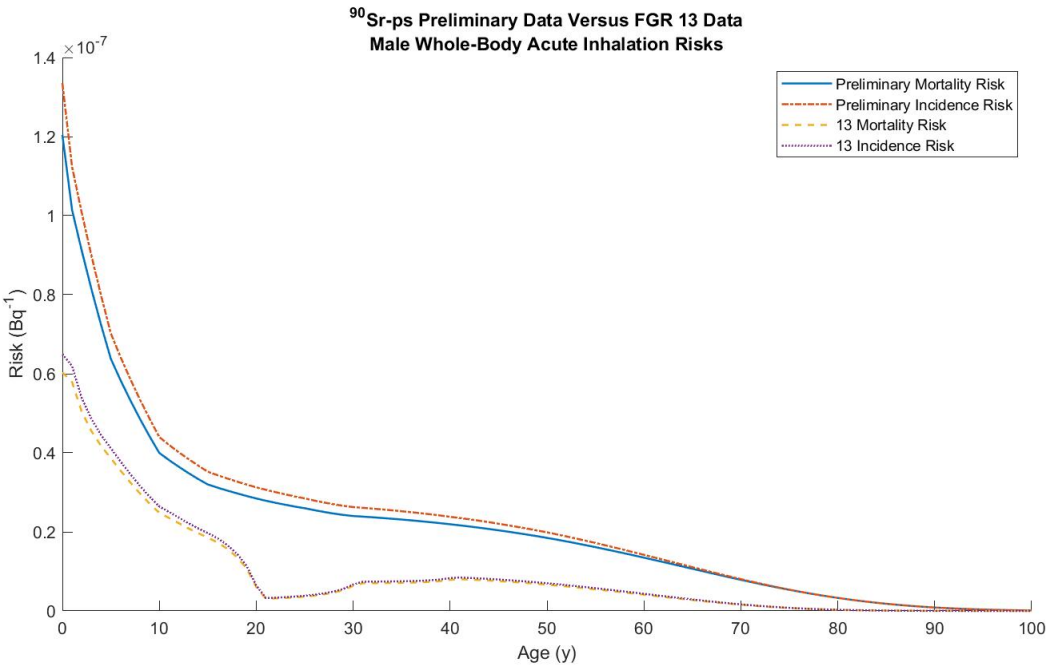

(b)

Figure 163. Comparison of FGR 13 and ICRP 103 informed data for male risks due to (a) fast-clearing, (b) and slow-clearing ^{90}Sr.

APPENDIX I: DATA GENERATION CED COMPARISON

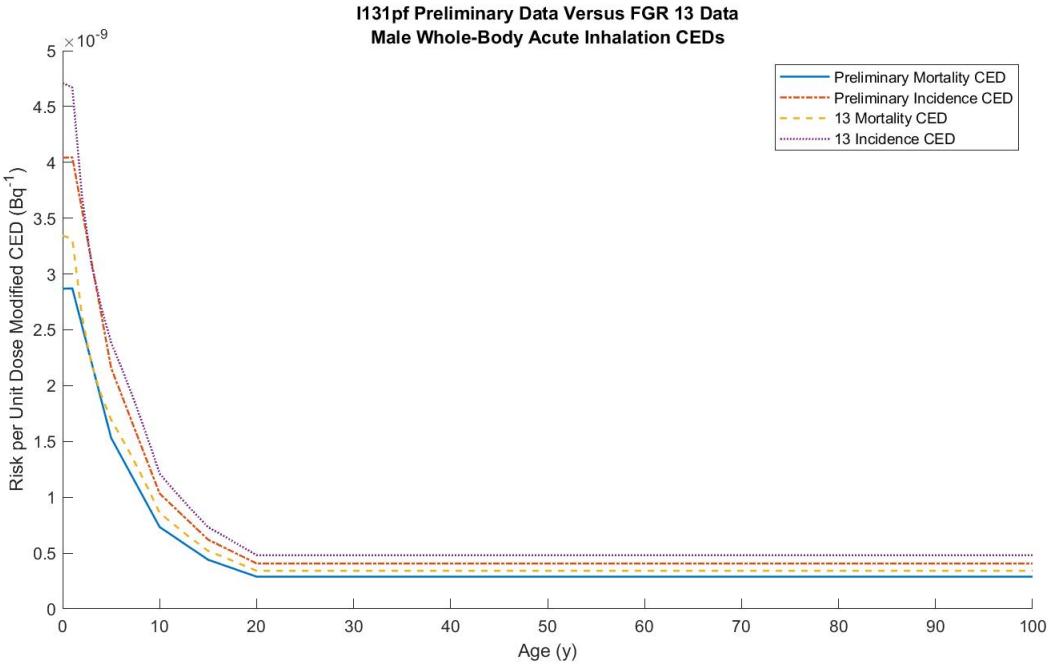

(a)

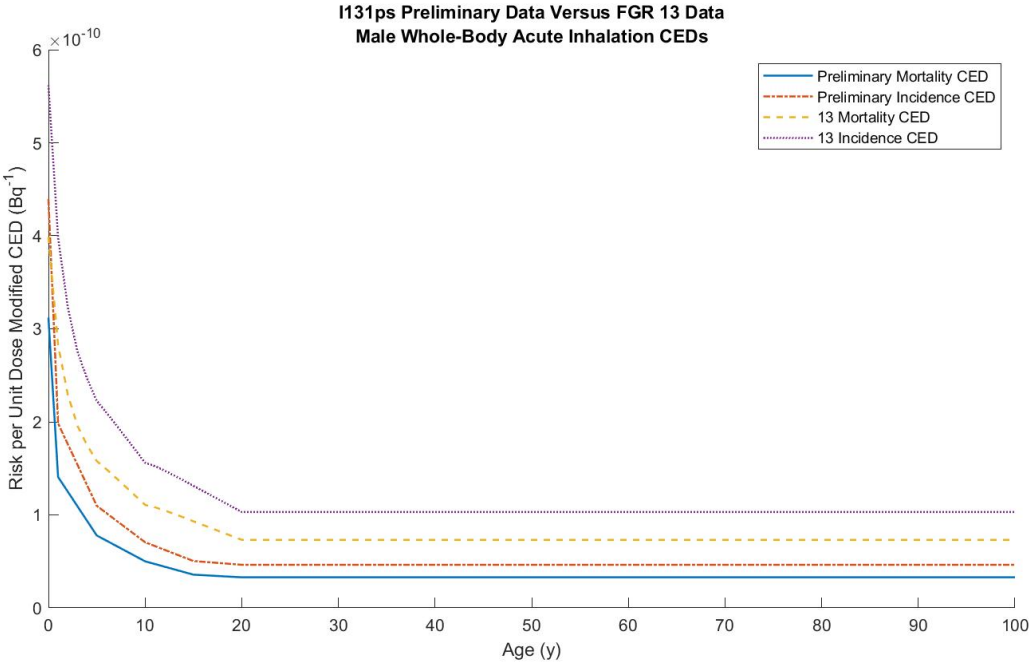

(b)

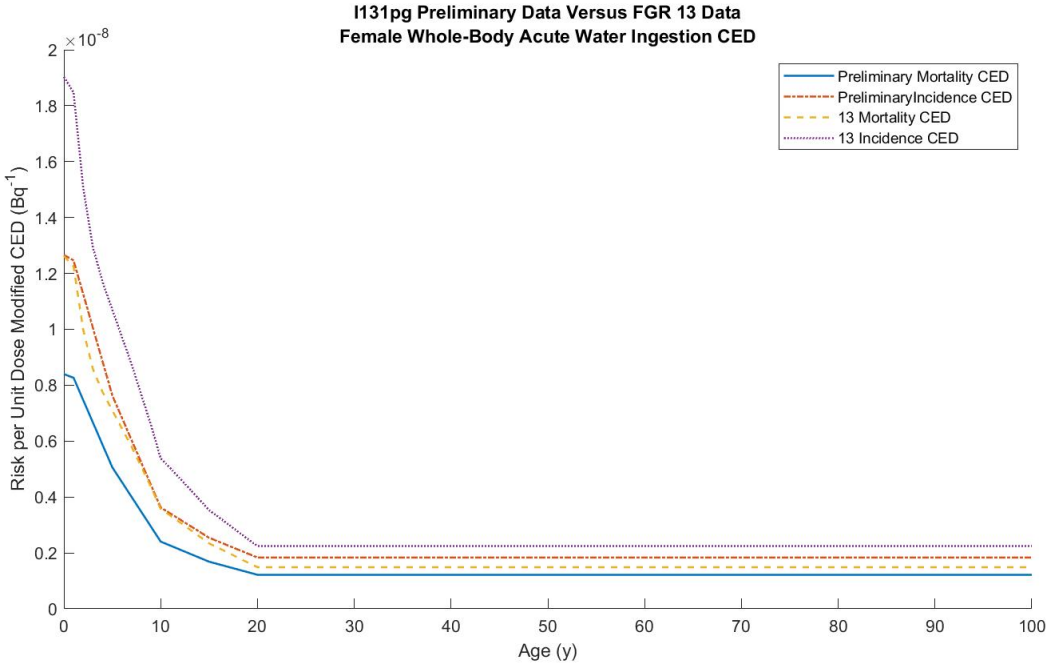

(c)

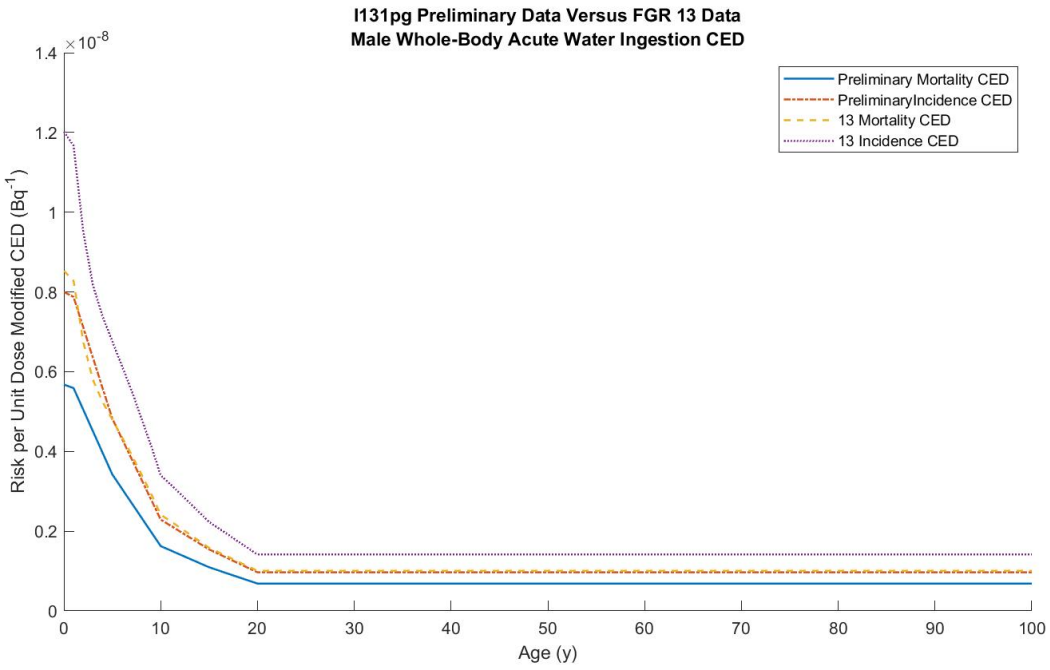

(d)

Figure 164. Comparison of FGR 13 and ICRP 103 informed data for (a) male CED due to fast-clearing ^{131}I, (b) male CED due to slow-clearing ^{131}I, (c) female CED due to tap water ingested ^{131}I, and (d) male risk due to tap water ingested ^{131}I.

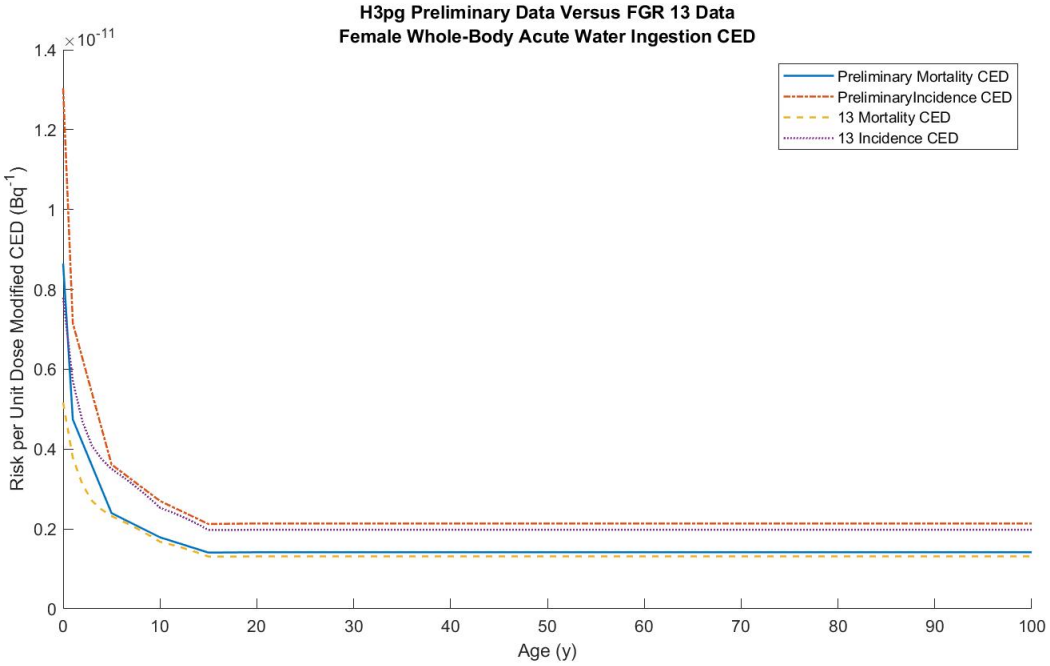
H3pg Preliminary Data Versus FGR 13 Data
Female Whole-Body Acute Water Ingestion CED
×10^-11
Preliminary Mortality CED
PreliminaryIncidence CED
13 Mortality CED
13 Incidence CED
Risk per Unit Dose Modified CED (Bq^-1)
Age (y)

(a)

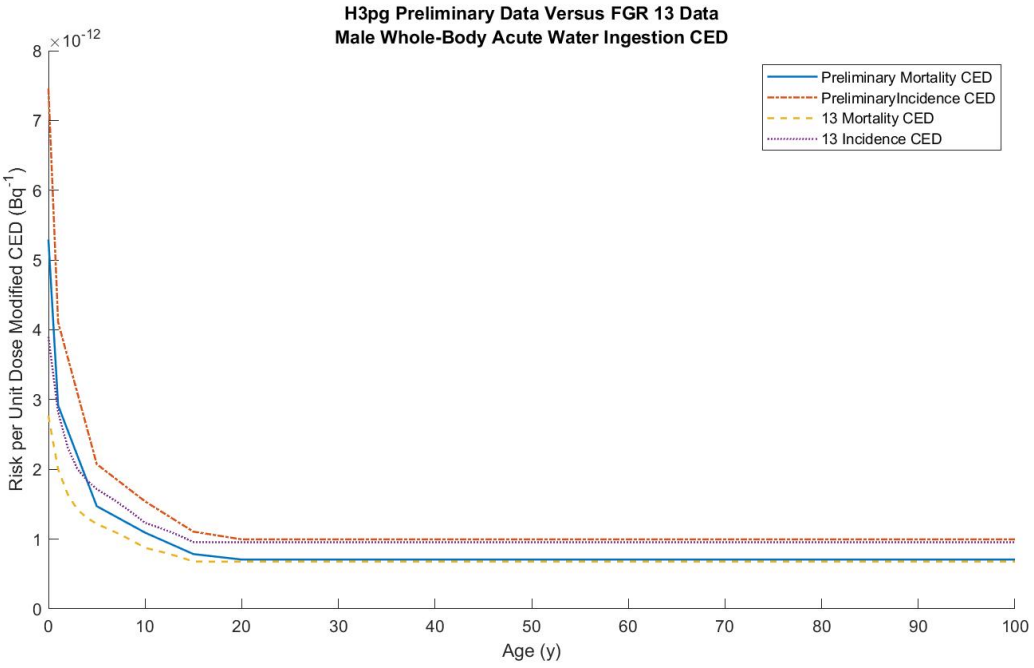
H3pg Preliminary Data Versus FGR 13 Data
Male Whole-Body Acute Water Ingestion CED
×10^-12
Preliminary Mortality CED
PreliminaryIncidence CED
13 Mortality CED
13 Incidence CED
Risk per Unit Dose Modified CED (Bq^-1)
Age (y)

(b)

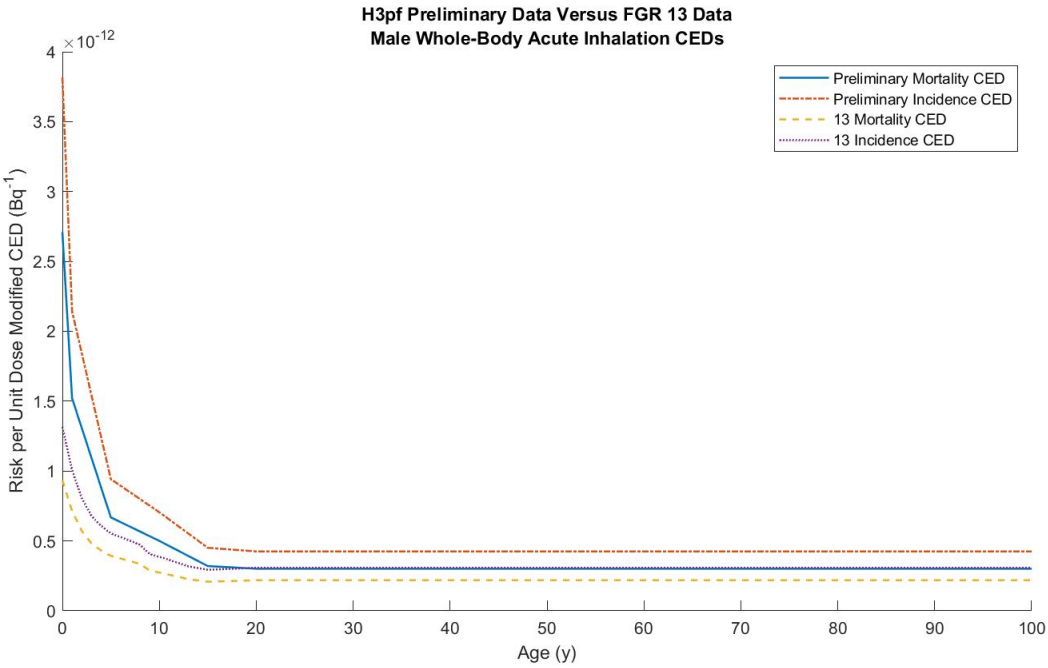

(c)

Figure 165. Comparison of FGR 13 and ICRP 103 informed data for (a) female CED due to tap water ingested tritium, (b) male CED due to tap water ingested tritium, (c) male CED due to fast-clearing tritium.

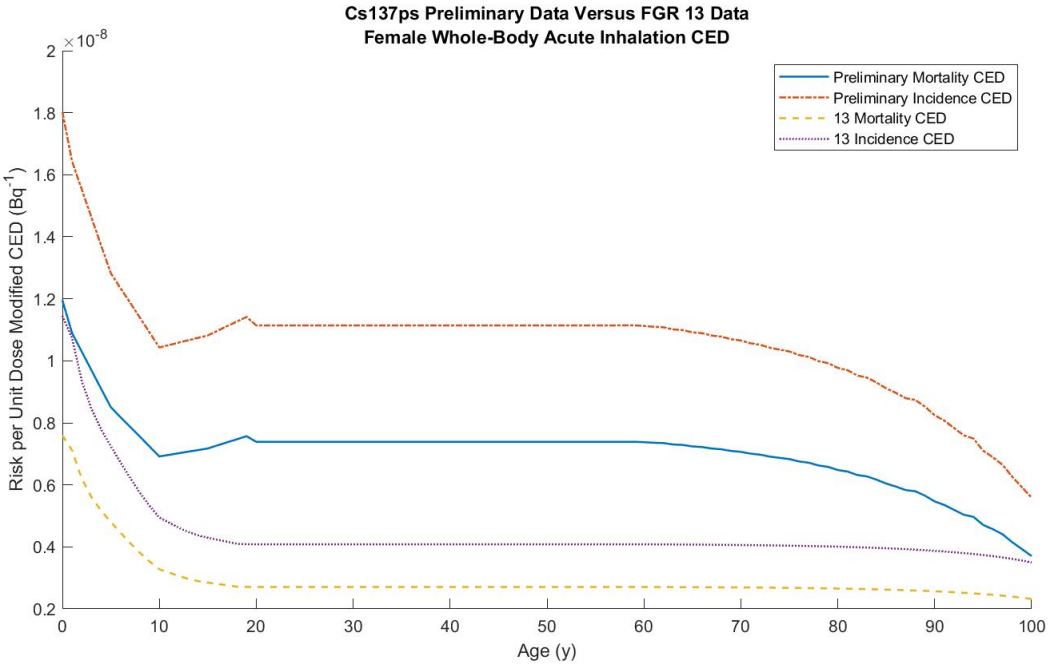

(a)

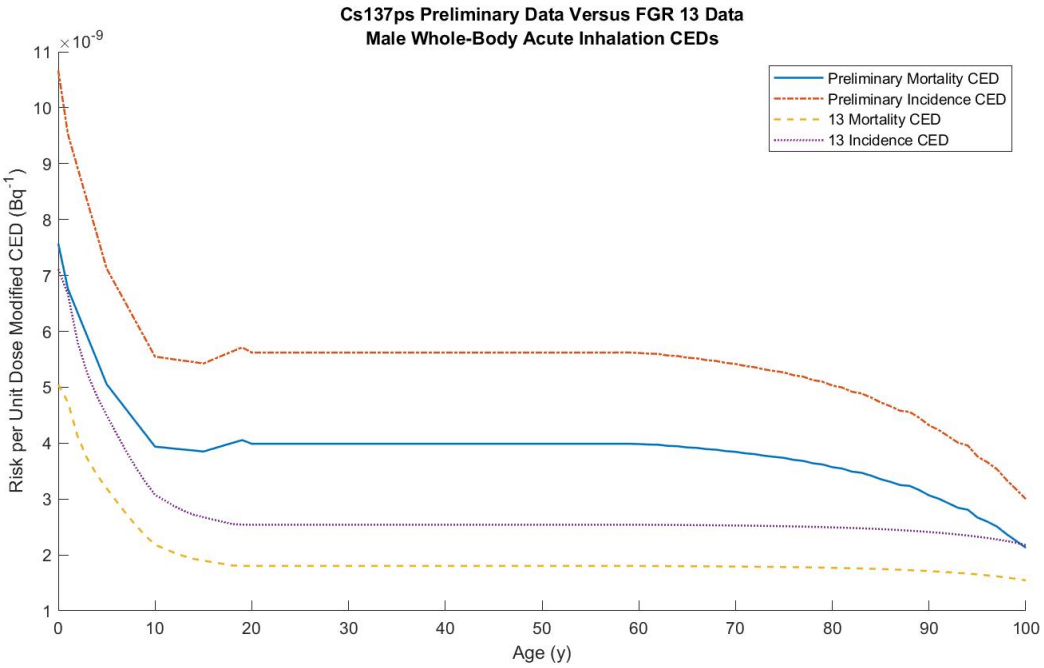
Cs137ps Preliminary Data Versus FGR 13 Data
Male Whole-Body Acute Inhalation CEDs
Preliminary Mortality CED
Preliminary Incidence CED
13 Mortality CED
13 Incidence CED
Risk per Unit Dose Modified CED (Bq-1)
Age (y)

(b)

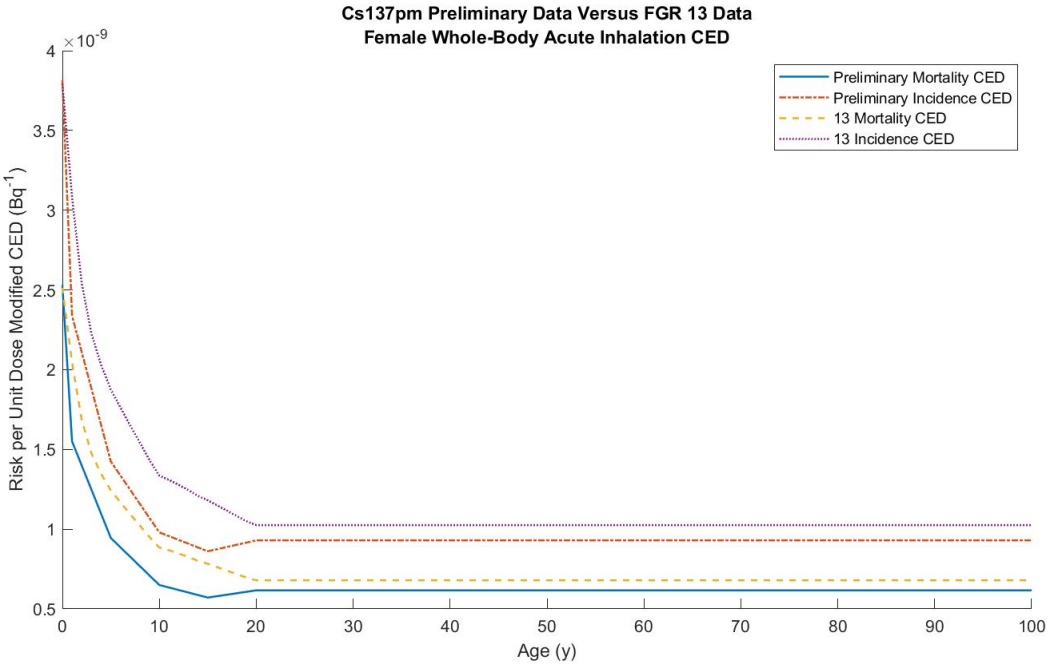
Cs137pm Preliminary Data Versus FGR 13 Data
Female Whole-Body Acute Inhalation CED
Preliminary Mortality CED
Preliminary Incidence CED
13 Mortality CED
13 Incidence CED
Risk per Unit Dose Modified CED (Bq-1)
Age (y)

(c)

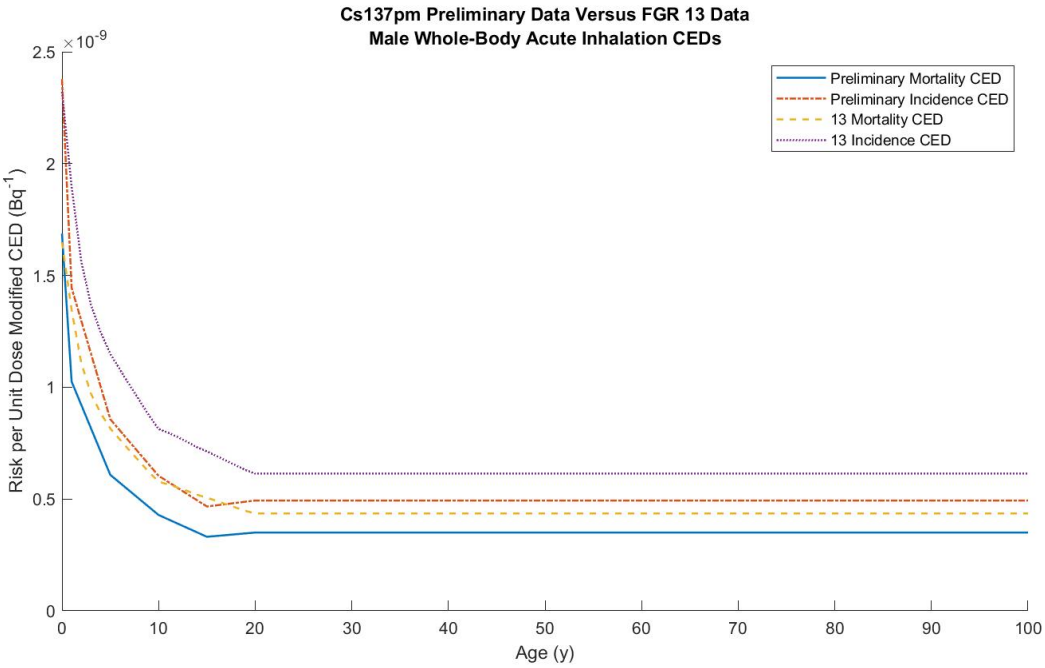

(d)

Figure 166. Comparison of FGR 13 and ICRP 103 informed data for (a) female CED and (b) male CED for moderate-clearing ^{137}Cs and (c) female CED and (d) male CED for slow-clearing ^{137}Cs.

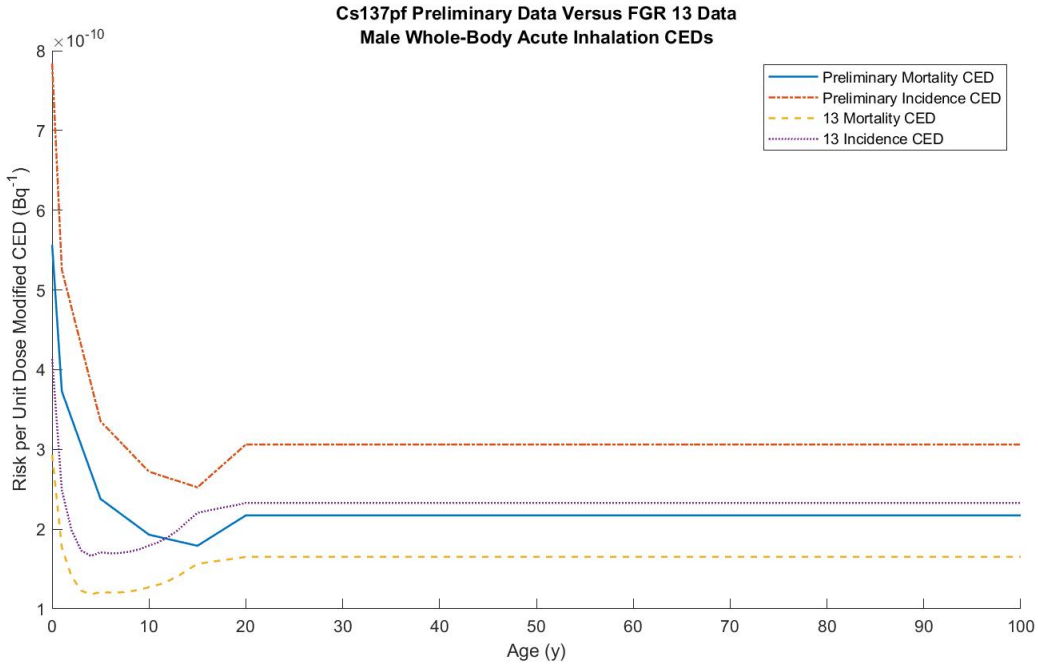

(a)

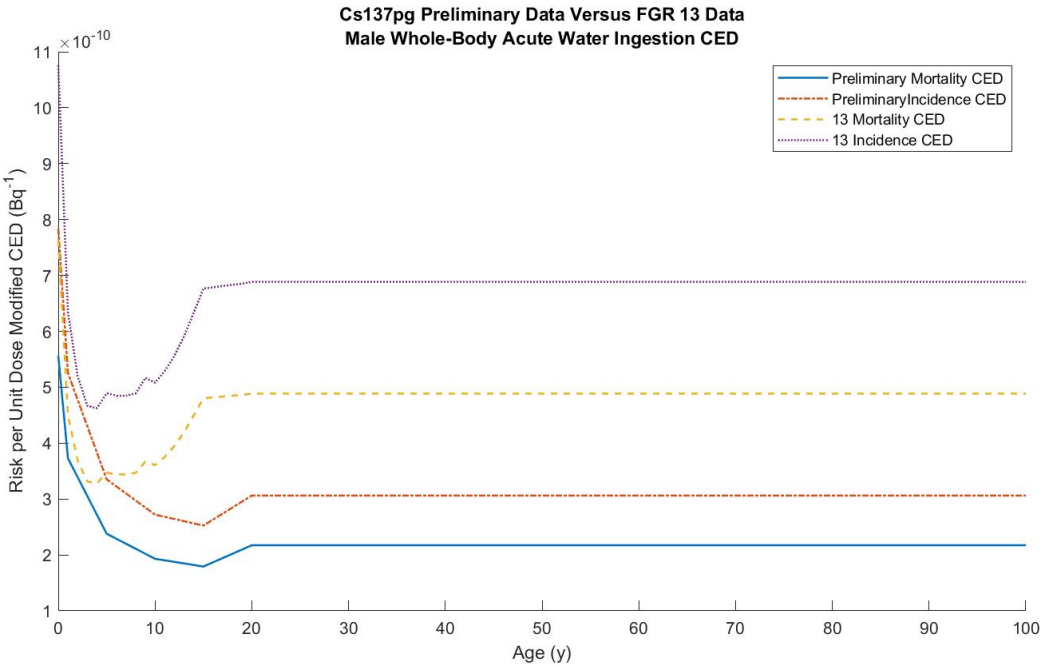

(b)

Figure 167. Comparison of FGR 13 and ICRP 103 informed CED data for males due to (a) fast-clearing and (b) tap water ingested ^{137}Cs.

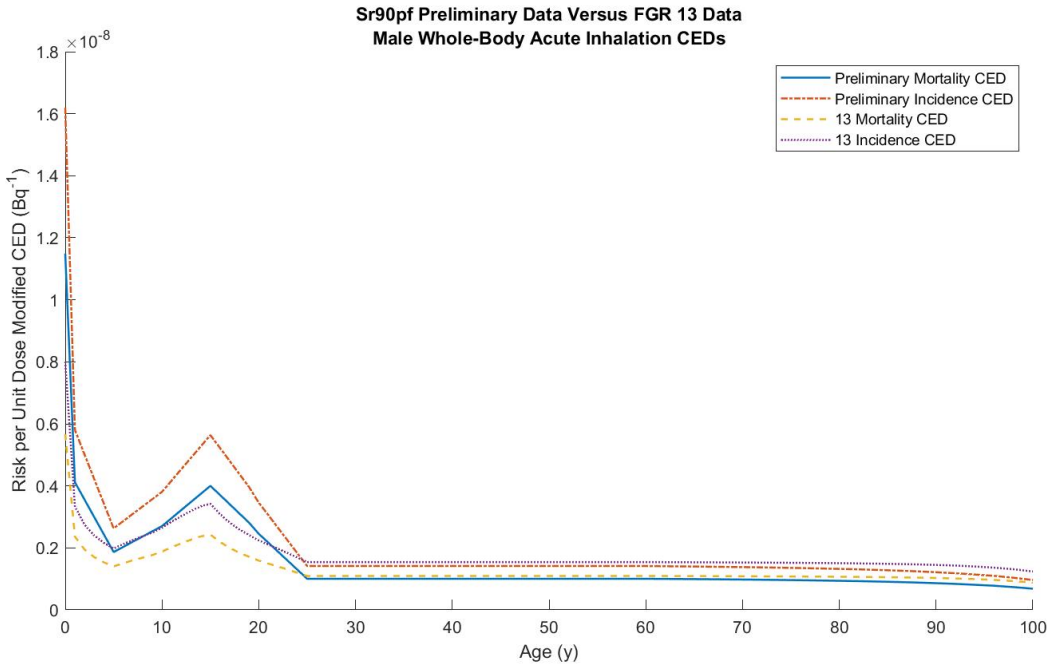

(a)

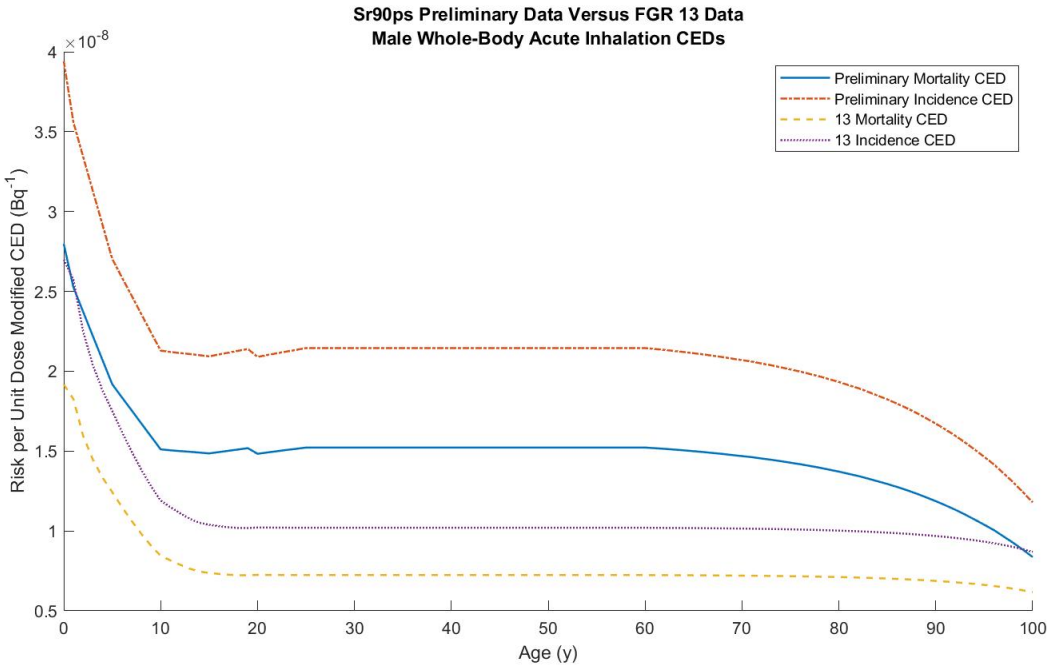

(b)

Figure 168. Comparison of FGR 13 and ICRP 103 informed CED data for males due to (a) fast-clearing, (b) and slow-clearing ^{90}Sr.